UNIVERSITY OF BIRMINGHAM

Chiral Perylene Diimide Containing Macrocycles and Rotaxanes

by

Angus Yeung

A thesis submitted to the University of Birmingham for the degree of DOCTOR OF PHILOSOPHY

School of Chemistry

College of Physical Sciences and Engineering

The University of Birmingham

August 2024

ABSTRACT

This thesis describes an investigation into a class of chiral organic dyes, perylene diimides (PDIs). Specifically, configurationally stable PDI dyes are targeted through the design, synthesis and analysis of PDI-based macrocycles and rotaxanes.

Chapter One introduces PDIs and outlines how the synthetic diversity of PDI derivatives impacts their photophysical, redox, supramolecular and chiral properties, with a particular focus on the integration of PDIs into macrocycles and rotaxanes.

Chapter Two describes the design and synthesis of a series of novel chirally-locked PDI-based macrocycles, including an investigation into kinetic templation in the macrocyclisation reaction. The successful synthesis of PDI-based macrocycles with π-electron donors in the macrocycle linkers evidences the importance of π-π donor-acceptor interactions.

Chapter Three explores kinetic templation in PDI-based macrocycles containing a second chiral aromatic component. Here, the diastereoselective synthesis of a PDI-based macrocycle is realised, in which templating non-covalent interactions between the aromatic units that direct the outcome of the dynamic kinetic resolution are discussed.

Chapter Four describes the progress towards a configurationally stable chiral PDI through mechanical bonding by the synthesis of a novel [3]rotaxane containing a PDI-based axle and two macrocycle components. When positioned in close proximity to the chiral PDI, the macrocycles are shown to slow down PDI atropisomer interconversion. The pH-induced molecular shuttling of these macrocycles is also presented.

Chapter Five describes the experimental procedures used throughout this work and details the characterisation of novel compounds.

Chapter Six provides a summary of the major conclusions from the research described in this thesis.

Supplementary information relating to collaborative work, such as computational methodologies and crystallographic data are provided in the Appendices.

ACKNOWLEDGEMENTS

First, I would like to thank my supervisor Dr. Tim Barendt. I truly appreciated his invaluable guidance throughout the past four years. I am also grateful for opportunity to learn and carry out the projects in this degree, where I had the freedom to design the macrocycles in this thesis, as well as synthetic attempts for some of my more realistic (but still crazy) ideas. I could not ask for a better supervisor.

I would also like to extend a heartfelt thank you to the members of the TAB lab, past and present, for their camaraderie and insightful discussions both in the lab and beyond. Special thanks to my fellow cat enthusiast, Mya, fellow weird music aficionado, Tom, and “Hips Don’t Lie” fan, Sam, for making the lab an enjoyable and lively place to be.

To my friends at the University, your companionship has been invaluable during this challenging journey. Sena and Aldrich, thank you for the laughter, banter, and boardgames that provided a much-needed escape. A special mention goes to Steven Coulthard, whose warm and welcoming presence has been a constant source of comfort and sanity. I am also immensely grateful to my ‘rant buddy’ Emma Jordan, with whom I could always share the frustrations that inevitably arise from the obstacles in chemistry.

I would also like to thank the technical staff who keeps the School of Chemistry and its facilities running. In particular, special mentions go to Cécile Le Duff, who singlehanded keeps the NMR facilities alive, as well as training provided for manual NMR spectroscopy. More importantly, her warm hugs and passionate chats always brighten up my day, for which I am glad to have her as a friend. Trevor Hardy must also be thanked, who not only keeps all the synthetic labs functional, but also seems to be omnipotent, as he is able to fix most lab equipment such as pumps and rotavaps,

responsible for the day-to-day health and safety in the lab, and also trained me on UV/vis, fluorescence, CD, and microwave synthesiser machines. Other members of the facilities have also been invaluable throughout my PhD: Chris Wiliams and Lianne Hill for mass spectrometry, Allen Bowden (and later Kamran Hussain) for HPLC, and also Bavlina Shafkalis for her help and chats.

Away from the University I would like to thank my friends and family, who may not understand what I actually do, but are unconditionally loving and supporting in my pursuit of a PhD. A special thanks to my cat, Freya, for keeping my keyboard warm and for contributing a few unexpected pages to this thesis whenever I left the room.

I thank the EPSRC and the School of Chemistry for funding.

And finally, I must thank Aaron for his loving support.

TABLE OF CONTENTS

ABBREVIATIONS

*	excited state
Δ	change in (a measurement)
A^-	anion
$A^{\cdot -}$	radial anion
abs	absorption
ACQ	aggregation caused quenching
aq.	aqueous
Ar	aromatic
AU	arbitrary unit
Boc	tert-butoxycarbonyl protecting group
br	broad
Br_2	bromine
Bu	butyl
C_2	2-fold rotational symmetry
cat.	catalytic
CD	circular dichroism
$CDCl_3$	deuterated chloroform
$CHCl_3$	chloroform
conc.	concentrated
COSY	correlated spectroscopy
CuAAC	copper (I)-catalysed azide-alkyne cycloaddition
d	doublet
DCM	dichloromethane
dd	doublet of doublets
DHN	1,5-dihydroxy naphthalene
DMF	dimethylformamide
DNA	deoxyribonucleic acid
ee	enantiomeric excess
EPR	electron paramagnetic resonance
eq., equiv.	equivalents
ESI	electrospray ionisation

Et	ethyl
Et_2O	diethyl ether
Et_3N	triethylamine
EtOAc	ethyl acetate
EtOH	ethanol
Ex	excitation
G	Gibbs free energy
Grubbs' II	Grubbs' second generation catalyst
h	Planck's constant
HMBC	heteronuclear multiple bond correlation
HOMO	highest occupied molecule orbital
HPLC	high performance liquid chromatography
HQ	hydroquinone
HSQC	heteronuclear single quantum correlation
^{i}	iso
i	point of interconversion
IPA	isopropanol
IR	infrared
ISC	intersystem crossing
J	coupling constant
k	kilo
LUMO	lowest un-occupied molecule orbital
m/z	mass to charge ratio
Me	methyl
MeCN	acetonitrile
MeOH	methanol
MS	mass spectrometry
NaN_3	sodium azide
NMR	nuclear magnetic resonance
NOE	nuclear Overhauser effect
NOESY	NOE spectroscopy
o/n	overnight
OAc	acetate
OLED	organic light-emitting diode

OPV	oligo(p-phenylene vinylene)
PDI	perylene diimide
PET	photoinduced electron transfer
pH	$-\log_{10}[H^+]$
Ph	phenyl
ppm	parts per million
Pr	propyl
Py	pyridinium
q	quartet
quin.	quintet
R	chemical substituent
RCM	ring closing metathesis
rt	room temperature
s	singlet
S_0	singlet ground state
S_1	first singlet excited state
SCE	saturated calomel electrode
SiO_2	silicon oxide
S_NAr	nucleophilic aromatic substitution
t	triplet
^{t}, *t*, *tert*	tert
T_1	triplet state
TBTA	tris[(1-benzyl-1H-1,2,3-triazol-4-yl)methyl]amine
THF	tetrahydrofuran
THPTA	tris((1-hydroxy-propyl-1H-1,2,3-triazol-4-yl)methyl)amine
TLC	thin layer chromatography
TMS	trimethylsilyl
trz	triazole
trz^+	triazolium
Ts, tosyl	*para*-toluenesulfuonyl chloride
UV/vis	ultraviolet/visible
v/v %	volume/volume percent
VT	variable temperature
wt.	weight

X	halogen atom
δ	chemical shift
λ	wavelength
σ	plane of symmetry

1. Introduction

1.1 Supramolecular Chemistry

Supramolecular chemistry could be found in numerous biological processes in nature, such as the replication of DNA,[1] the assembly and folding of proteins,[2] and the detection of pathogens.[3] Over the past century, supramolecular chemistry has advanced and expanded enormously to include concepts such as molecular self-assembly,[4] molecular recognition,[5] host-guest chemistry[6] and mechanically-interlocked molecular architectures.[7] Additionally, supramolecular chemistry is important in materials chemistry, where it can be used to direct the organisation of molecules in materials.[8]

Whilst traditional chemistry focuses on the formation and destruction of covalent bonds, supramolecular chemistry focuses on the non-covalent interactions between molecules (Figure 1.1).[9] These interactions include electrostatics, hydrophobic forces, hydrogen bonding and π-π interactions. Despite these individual forces being significantly weaker than a traditional covalent bond, the impact of these interactions cannot be overstated, especially when used in concert and in preorganised molecules such as macrocycles. The understanding of these non-covalent interactions has been vital in the development and discovery of drugs,[10] construction of rotaxanes (Section 1.6) and catenanes,[11] and the development of organic light-emitting diode (OLED) materials.[12]

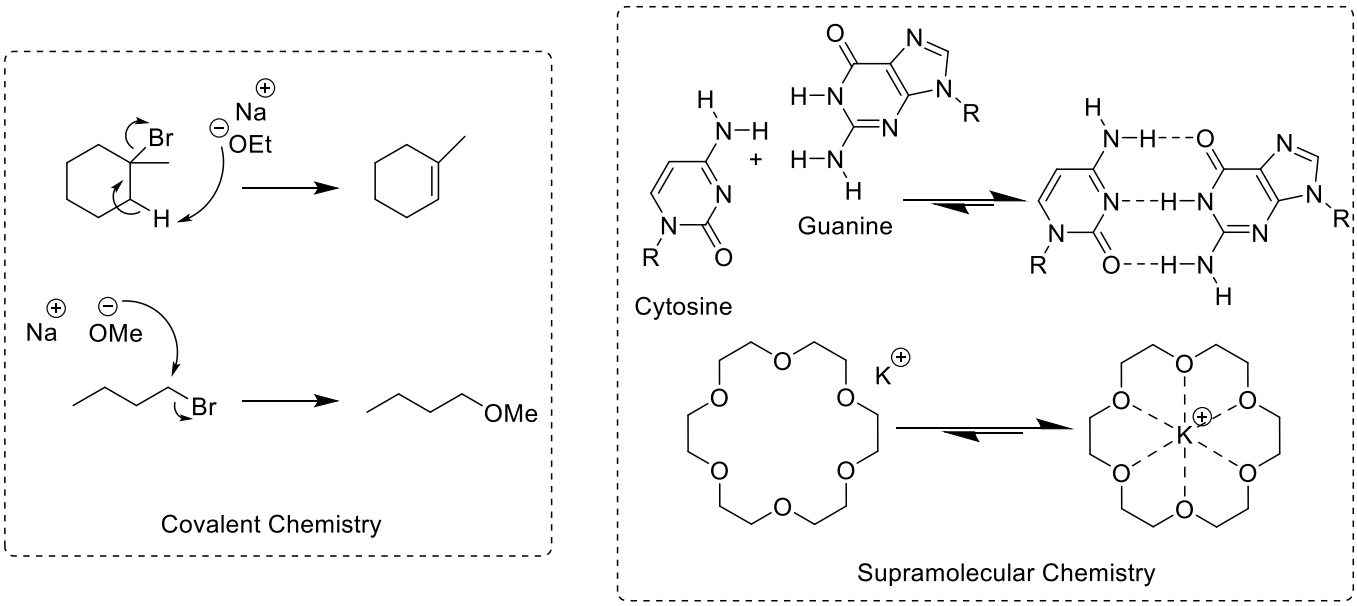

Figure 1.1. Examples of covalent chemistry and supramolecular chemistry.

1.2 Macrocycles

A central class of molecules that exemplifies the principles of supramolecular chemistry are macrocycles. Macrocycles are molecules with at least one large ring composed of twelve or more atoms. Macrocycles are inherently less flexible than their acyclic analogues, and thus are more conformationally restricted. Their conformational rigidity and ability to interact with challenging biological targets make them suitable for modulating protein-protein interactions and other difficult-to-drug sites, as well as potential for increased selective binding compared to acyclic drugs.[13] The cavity of macrocycles have also been utilised in host-guest chemistry. Macrocyclic ligands such as crown ethers and porphyrins exhibit a high affinity for metal ions, a phenomenon known as the "macrocyclic effect." This effect is attributed to the preorganized structure of macrocycles, which enhances their binding affinity compared to acyclic ligands.[14] These properties allows them to act as supramolecular catalysis by influencing substrate conformation and stabilising reactive metal centres.[15] Macrocycles are also a key component of

mechanically interlocked molecules[16] such as catenanes and rotaxanes (Section 1.6), which can be used to develop molecular machines and sensors.[17]

1.2.1 Macrocycle Synthesis

Macrocycles are challenging to synthesise due to the large entropic cost associated with macrocyclisation,[16] often leading to low yields and the formation of unwanted side products such as oligomers. One method to alleviate this problem is for the macrocyclisation reaction to occur under high dilution conditions,[18] whereby the rate of intermolecular reactions are retarded. The major drawback to this method is the slow reaction time and the large volume of solvent needed.

An alternative method for improving the yield of a macrocyclisation reaction is by supramolecular templation.[19] This is achieved by the use of templating non-covalent interactions, which may occur between the reacting macrocycle precursor(s) or through the use of a templating guest which coordinates to the macrocyclic precursor(s). Under kinetic (i.e., irreversible) conditions, templation typically works in tandem with preorganisation,[20] whereby the templating non-covalent interactions direct the macrocyclic precursor into a specific conformation that favours the ring-closing reaction. An example of this is the synthesis of cyclobis(paraquat-p-phenylene) macrocycle **1** (known as the “Blue Box”) by Stoddart and coworkers. Here, a π-electron rich dialkoxynaphthalene template **2** forms π-π donor-acceptor interactions with the macrocycle precursor **3,** which is a viologen-based π-electron deficient aromatic compound, to template the macrocyclisation reaction (Figure 1.2)[21]

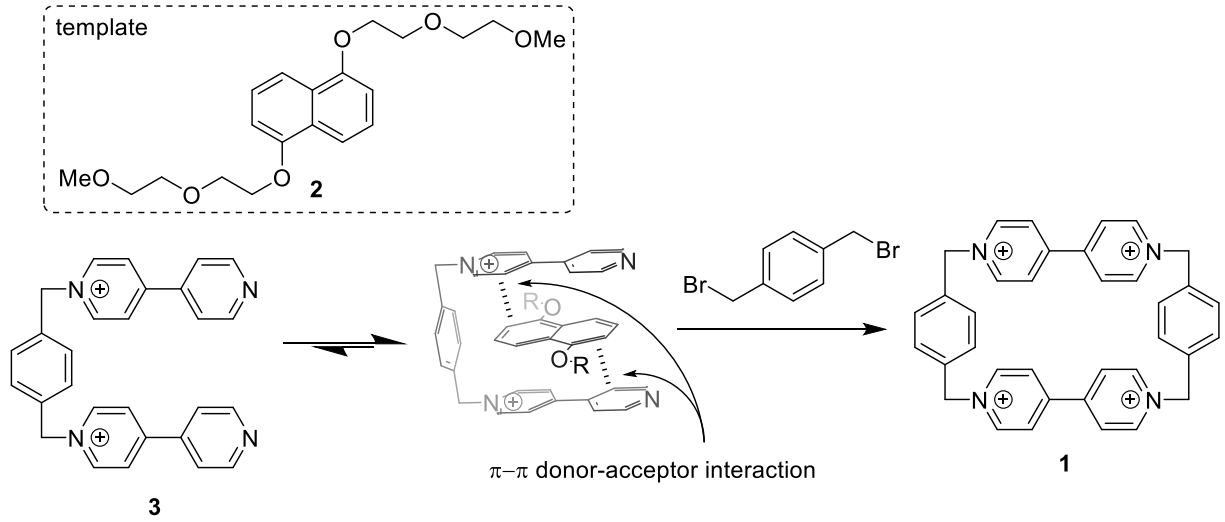

Figure 1.2. Stoddart and coworkers' templated macrocyclisation.

1.3 Perylene Diimides

Perylene-3,4:9,10-bis(dicarboximides)s, commonly abbreviated as PDIs, are compounds of interest, due to their properties and ease of synthetic functionalisation. They are brightly coloured and highly fluorescent dyes (nearing unity quantum yield), with high photothermal and chemical stability. This, together with the supramolecular properties of PDIs, has led to extensive research over the last century for their use in photoactive,[22] electronic[22-23] and optoelectronic materials.[24] Initial research focused on the imide substituents to ease its solubility, with limited effect on electronic properties.[25] To tune these properties, the relatively π-electron deficient perylene core must be functionalised (via the bay or ortho positions) and this has resulted in many applications such as biomolecular imaging, OLEDs and transistors (Figure 1.3).[26]

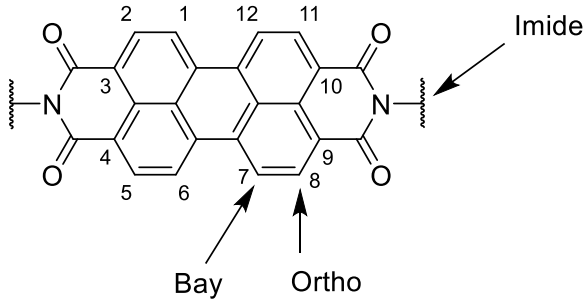

Figure 1.3. A generic perylene-3,4:9,10-bis(dicarboximides) (PDI), highlighting positions of imide, bay and ortho substituents.

1.3.1 Supramolecular Chemistry of Perylene Diimides

1.3.1.1 Self-Assembly of Perylene Diimides

The large flat π-surfaces of the PDI facilitates intermolecular π-π stacking of PDIs into large columnar aggregates in solution.[27] These aggregates can lead to desirable material properties, such as charge transport[28] or chiral enhancement (*vide infra*),[29] but can also lead to undesirable properties, such as poor solubility or aggregation caused quenching (ACQ).

The free energy of aggregation can be tuned by solvents,[30] where Würthner and coworkers found that the intermolecular π-π stacking interactions are dominated by different contributions in different solvents. While electrostatic forces are of most importance in nonpolar/aliphatic solvents, solvophobic effects govern PDI aggregation in polar protic solvents, since here the free energy of aggregation increases with increasing solvent polarity (Figure 1.4).[30]

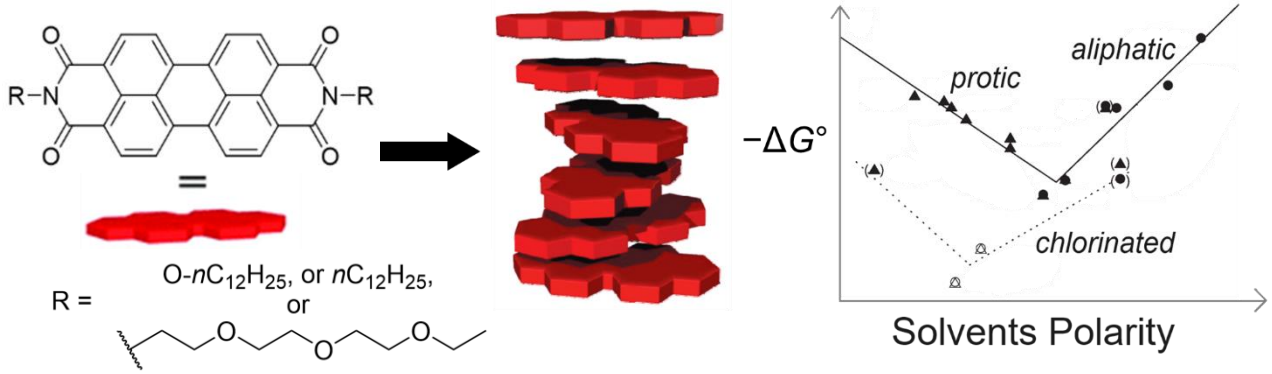

Figure 1.4. Left: Model of PDI columnar aggregates in solution. Right: graph of aggregation constants against solvent polarity. Reproduced from Ref. 30 with permission from the Royal Society of Chemistry.

Aggregation can also be disrupted by functionalisation at the imide, ortho and bay positions, where large or branched functional groups are situated above or below the PDI plane and so disrupt π-π stacking (Figure 1.5a). In particular, the steric clash between bay positions (X and Y in Figure 1.5b, left) leads to twisting of the perylene core away from

planarity, effectively forming two naphthalimide subunits, which also reduces the ability of PDIs to π-stack with itself (Figure 1.5b).[31]

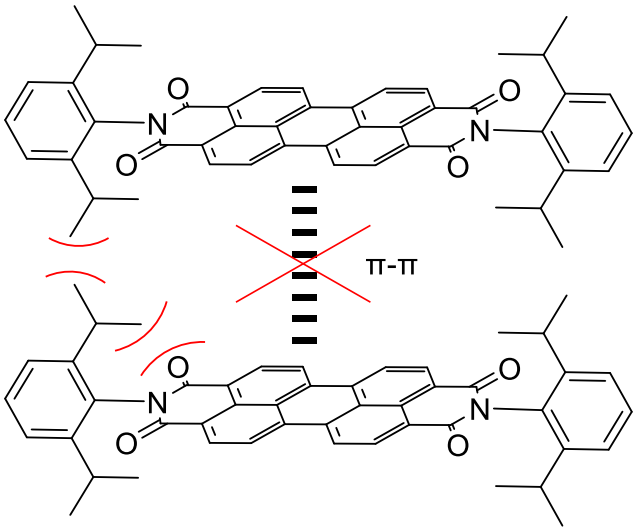

Figure 1.5a. Diisoopropyl aniline substituted PDIs, highlighting steric interaction of methyl groups and oxygen atom of the imide, which inhibits intermolecular π-stack and aggregate of PDI molecules.

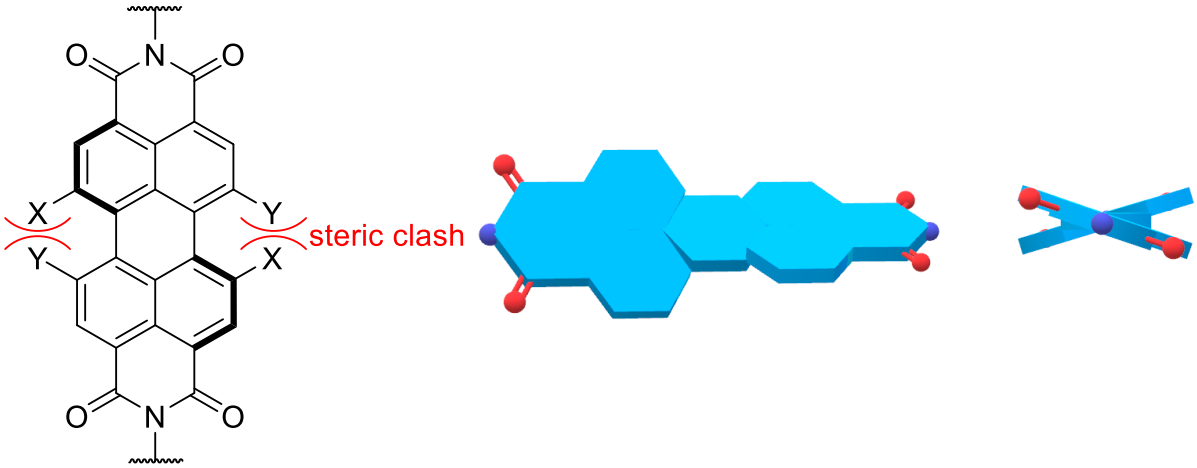

Figure 1.5b. Left: illustration of the steric clash between bay substituents, resulting in the twisted perylene core. Right: illustration of the twist of PDI perylene core (bay substituents not shown).

Another factor that affects aggregation is temperature. When aggregation is under thermodynamic control, increasing the temperature, which also increases entropy, will typically shift the equilibrium towards smaller aggregates. Thus, increasing the temperature decreases the number of PDI units per aggregate. An example is PDI **4** from the Würthner group, which, at -10 °C, self-assembles into a helical superstructure with an

average aggregation number greater than 50. However, at 90 °C PDI **4** exists mostly as dimers (Figure 1.6).[32]

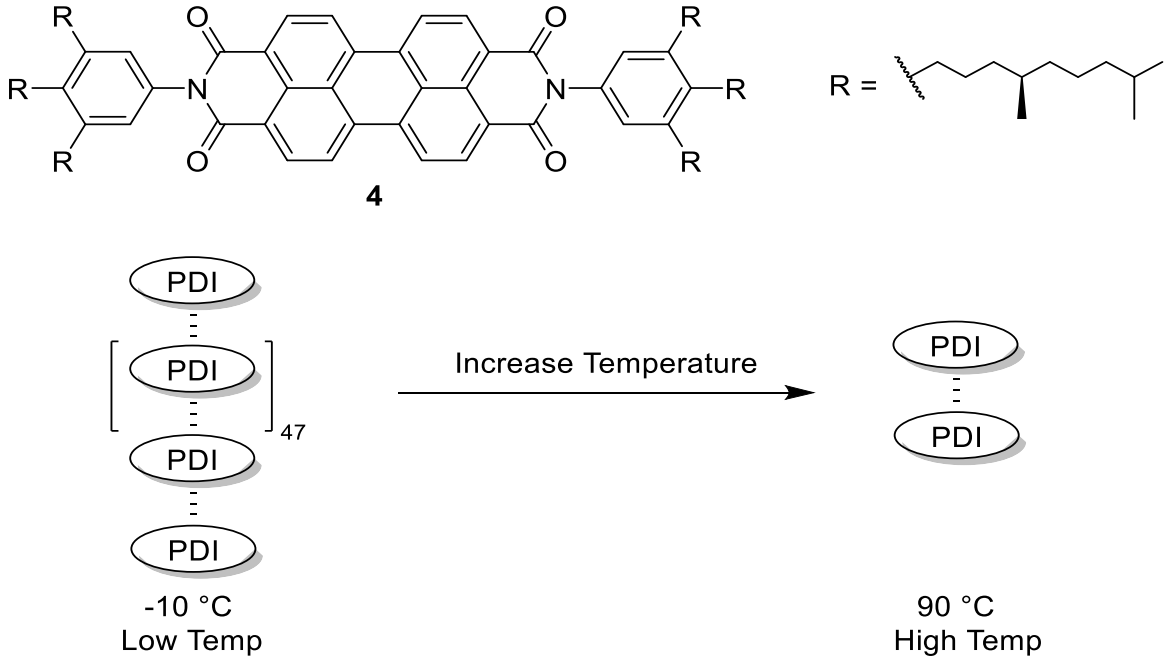

Figure 1.6. Dehm's PDI **4**, with large columnar aggregates at low temperatures and mostly dimers at high temperatures.

1.3.1.2 Non-covalent interactions with of Perylene Diimides

The π-electron deficient nature of PDIs enables their interaction with π-electron rich aromatic molecules through donor-acceptor π-π interactions. This property has been utilised in host-guest systems, where the PDI may can act as a guest or a host.

An example of PDI acting as a host is Zhang and coworkers' bis-PDI metallacage (host), which form host-guest complexes with electron-rich polycyclic aromatic hydrocarbons (e.g., pyrene, triphenylene, and perylene) due to donor-acceptor π-π interactions. The different guests were able to tune the photophysical properties of the PDI host, which has the potential for applications in adaptive emissive materials (Figure 1.7).[33]

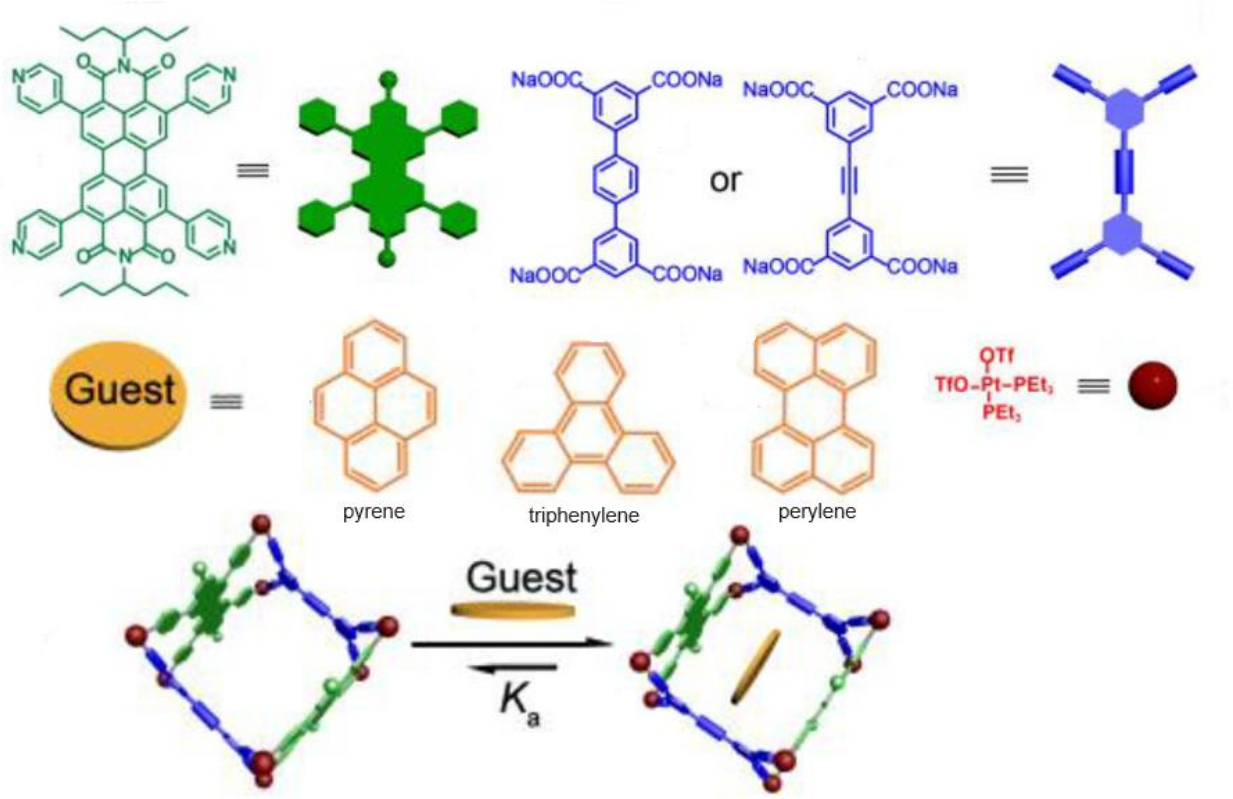

Figure 1.7. Zhang and coworkers' host-guest complexes with bis-PDI metallacage (host), and polycyclic aromatic hydrocarbons (pyrene, triphenylene, and perylene) (guests). Reproduced with permission from *J. Am. Chem. Soc. 2020, 142, 44, 18763–18768*. Copyright 2020 American Chemical Society.

1.3.2 Photophysical Properties of Perylene Diimides

As mentioned in Section 1.3.1, PDIs are highly fluorescent dyes, which results in applications such as biomolecular imaging,[26b] single molecule spectroscopy[26b, 34] and photonics.[35] The high fluorescence quantum yield arises from the PDI's rigid and planar structure, as well as negligible $S_1 \rightarrow T_1$ intersystem crossing due to its low-lying triplet.[36] However, the quantum yield is commonly observed to decrease with increasing PDI concentration, due to aggregation caused quenching (ACQ), due to nonradiative decay induced by strong intermolecular π-π interactions between the stacked PDIs. This is typically combated by installing large functional groups at the imide positions, rather than

the bay or ortho positions, since imide-based substituents can inhibit aggregation without impacting the photophysics of the PDI chromophore.[37] Common imide groups include 2,6-diisopropylaniline, pentan-3-amine, and undecane-6-amine (Figure 1.8).[38]

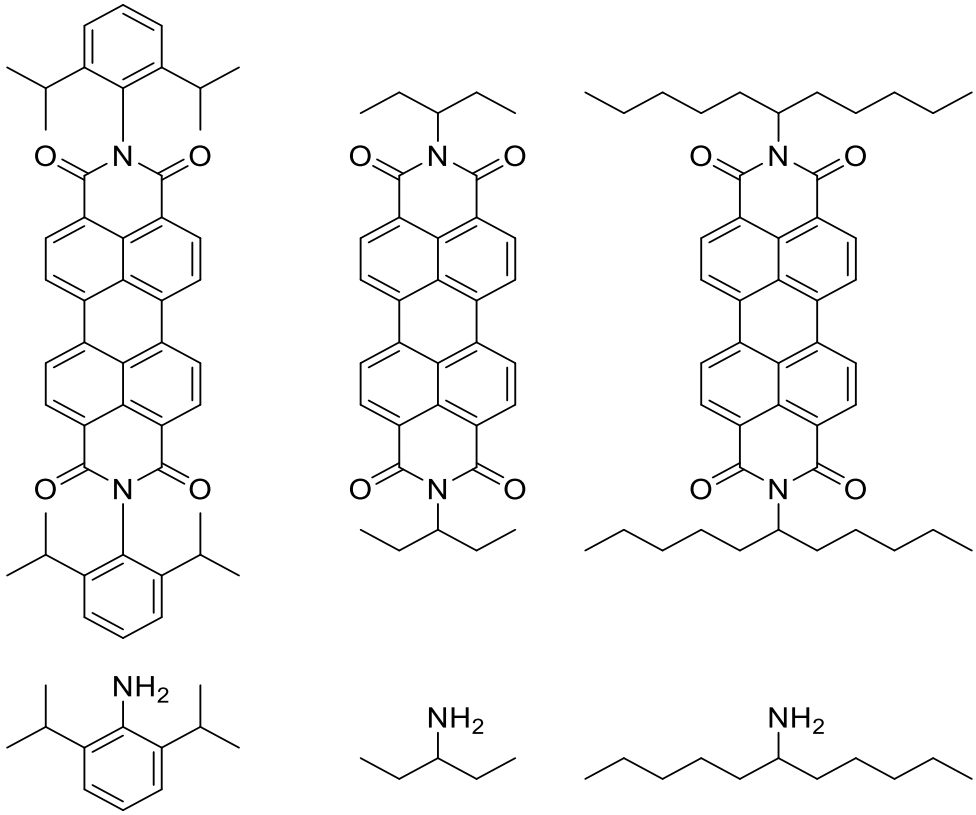

Figure 1.8. PDIs with 2,6-diisopropylaniline, pentan-3-amine, and undecane-6-amine imide groups.

For the parent PDI (i.e. core unsubstituted), a typical monomeric chromophore displays a main absorption band in the visible region for the $S_0 \rightarrow S_1$ transition. Due to the rigidity of the perylene core, this absorption band contains a vibronic progression, with the 0–0 and 0-1 vibronic transitions centred around 525 nm and 500 nm, respectively.

As substituents at the bay positions of the PDI induces a twist in the perylene core, this reduces conjugation between the two naphthalimide subunits, with larger twists leading to larger hypochromic shifts.[39] However, it is more common to observe a bathochromic shift

of the main PDI absorption band ($S_0 \rightarrow S_1$) due to inductive and/or mesomeric effects from the new substituent being dominant.[40]

1.3.3 Redox properties of Perylene Diimides

PDIs exhibit excellent redox properties, which has enabled their use as electron transport materials.[26c] The PDI LUMO levels could be tuned by substitution of the ortho or bay positions of the PDI core, a feature that has been utilised to make PDI-based organic solar cells with a power conversion efficiency of more than 10%.[41]

Cyclic voltammetry of PDIs without electron donating substituents typically show two reversible reductions ($PDI/PDI^{-} \approx -0.5$ and $PDI^{-}/PDI^{2-} \approx -0.7$ V *vs.* saturated calomel electrode (SCE)) and one reversible oxidation ($PDI/PDI^{+} \approx +1.5$ V *vs.* SCE), meaning they are easy to reduce and difficult to oxidise, evidencing their electron deficiency.[26a, 27] This electron deficiency also allows for greater photochemical stability, due to disfavoured decomposition upon excitation, where this property has been used as air stable electron transport materials.[42]

On the other hand, photoexcited PDIs become strong oxidants ($PDI^{*}/PDI^{\bullet-} = +1.97$ V *vs.* SCE),[43] where this property has been exploited for photocatalysis,[44] such as the oxidation of sulfides to sulfoxides in the presence of oxygen (Scheme 1.1a).[45] The PDI radical anion can also be generated in the presence of an electron donor (NEt_3) by photoinduced electron transfer (PET).[46] Here, its reduction potential ($PDI/PDI^{\bullet-} = -0.37$ V *vs.* SCE)[45] can be used for the reduction of aryl halides (Scheme 1.1b).[47] The mechanism of this reaction is currently debated,[43, 44b, 47a, 48] since an alternative mechanism includes photoexcitation of the PDI radical anion to form $PDI^{\bullet-*}$, which is a stronger reducing agent ($PDI^{\bullet-*}/PDI = -1.87$ V *vs* SCE).

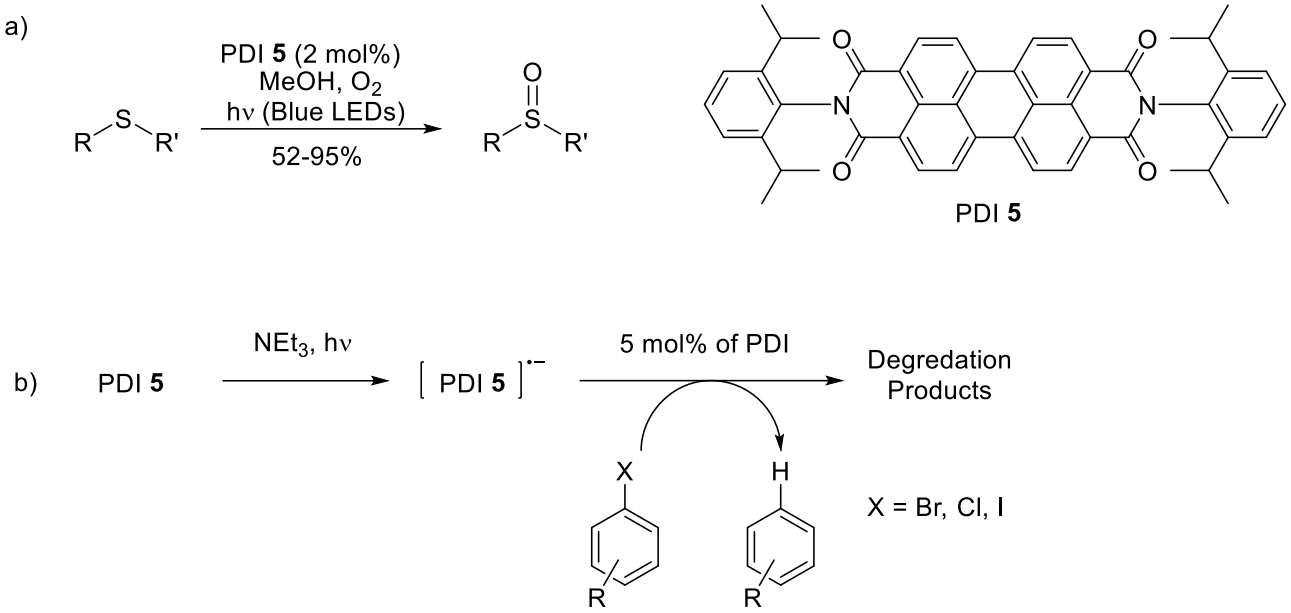

Scheme 1.1. The ability of PDI **5** to act as a photocatalyst in a) the oxidation of sulfides, and b) the reduction of aryl halides.

1.3.4 Synthesis of Perylene Diimides

Overall, the tuning of PDI properties is typically done by the synthesis of PDIs with different substituents at the imide, ortho, or bay positions. Imide substituents, often utilised to reduce aggregation (increase solubility), are typically installed by stirring perylene dianhydride (PDA) and the desired amine in molten imidazole at 140 °C, catalysed by the Lewis acid Zn(II) (Scheme 1.2).[49]

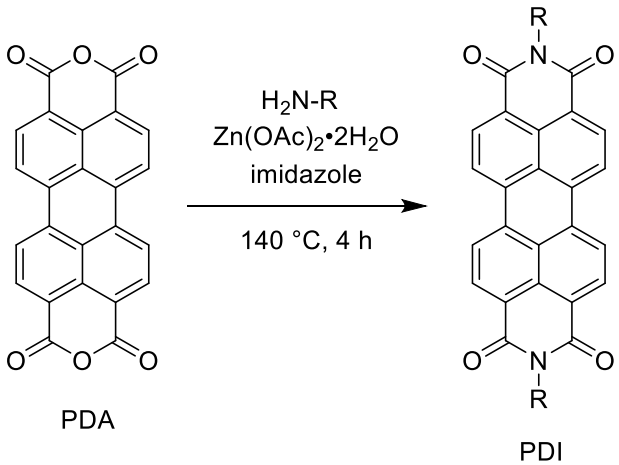

Scheme 1.2. Imidisation of PDA into PDI.

The ortho and bay positions are of more synthetic interest and importance due to their ability to tune the electronics of the PDI chromophore and, in the latter case, its twist away from planarity. The vast diversity and amount of S_NAr and coupling reactions (e.g. Suzuki coupling, Sonagashira coupling) in the literature makes halogenated PDIs a desirable precursor to many functional PDI derivatives. Halogenated PDIs can be prepared by either imidisation followed by halogenation, or vice versa. Indeed, PDA can be tetrachlorinated in high yields (99%) by treatment with chlorosulfonic acid and a catalytic amount of iodine at 66 °C for 18 hours.[50] The analogous tetrabromination is commonly achieved by stirring PDA with 4.2 equivalents of bromine and a catalytic amount of iodine in sulfuric acid at 100 °C over five days (Scheme 1.3).[51]

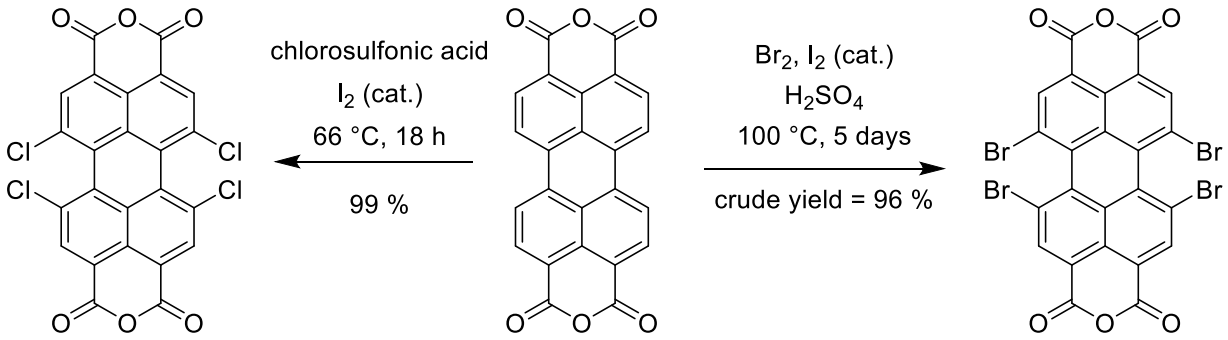

Scheme 1.3. Tetrachloronation and tetrabromonation of PDA.

Dibrominated PDIs ($PDIBr_2$) are prepared in a similar fashion yet importantly these conditions will yield a 3:1 regioisomeric mixture of 1,7- and 1,6-dibrominated PDAs (Scheme 1.4).[52] These PDAs are insoluble in any organic solvents, requiring imidisation to $PDIBr_2$ before further purification and characterisation is possible. For $PDIBr_2$, the 1,7- and 1,6- regioisomers are typically inseparable[52-53] without the aid of specialist HPLC[54] or, in cases where the imide substituents do not significantly inhibit intermolecular π-π stacking, they can also be separated by repeated recrystallisations.[52]

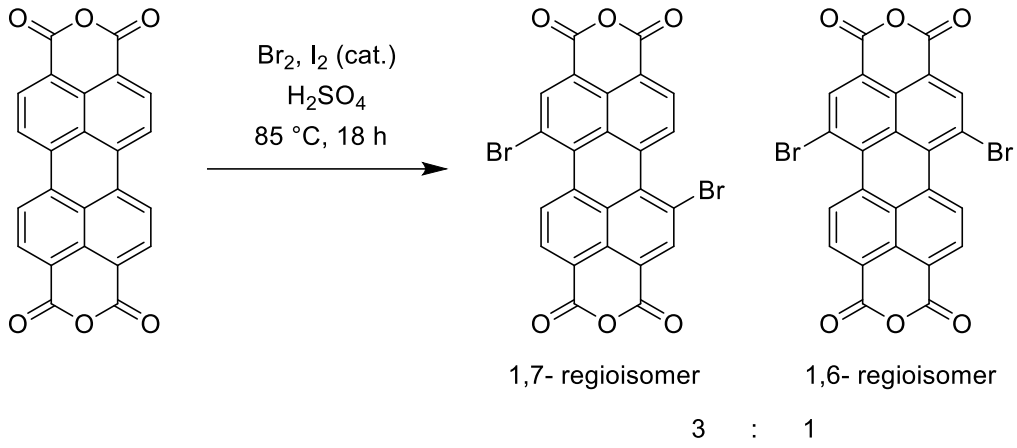

Scheme 1.4. Dibromination of PDA.

This regioisomeric ratio can be improved by milder bromination conditions, though this can only be achieved by imidisation followed by bromination due to the much superior solubility of PDI compared to $PDABr_2$. However, in cases where the imide group is susceptible to bromination, such as aromatic substituents like 2,6-diisopropyl aniline, 1,7-$PDIBr_2$ must be achieved by bromination under harsher conditions (due to low solubility of PDI) followed by imidisation (Scheme 1.5).

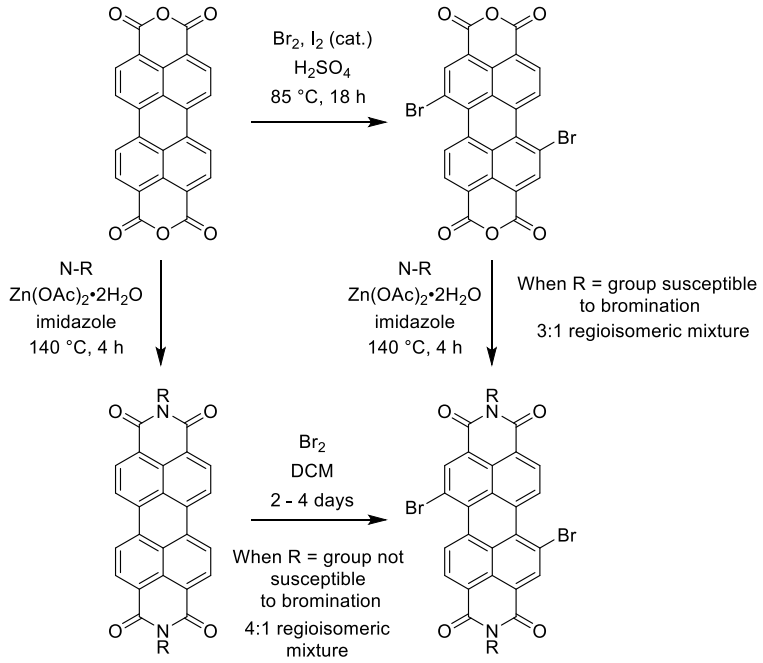

Scheme 1.5. Bromination and imidisation of PDA to $PDIBr_2$, where when using an imide group that is susceptible to bromination requires hasher bromination conditions, resulting in a worse regiosiomeric mixture (3:1 *cf.* 4:1)

These halogenated PDIs can then be derivatised into amino PDIs such as dipiperidinlyl-PDI,[55] dipyrrolidinyl-PDI,[56] and dimethylamino-PDI;[57] oxy PDIs such as 2,4-di-*tert*-butylphenoxy-PDI,[56] 2,6-di-*tert*-butylphenol-PDI,[58] and di-butyloxy-PDI;[59] thiol PDIs,[60] cyano PDIs,[61] fluoroalkyl PDIs.[62] Additionally, they can also undergo coupling reactions, such as Suzuki coupling[63] and Sonogashira coupling (Figure 1.9).[63b, 64]

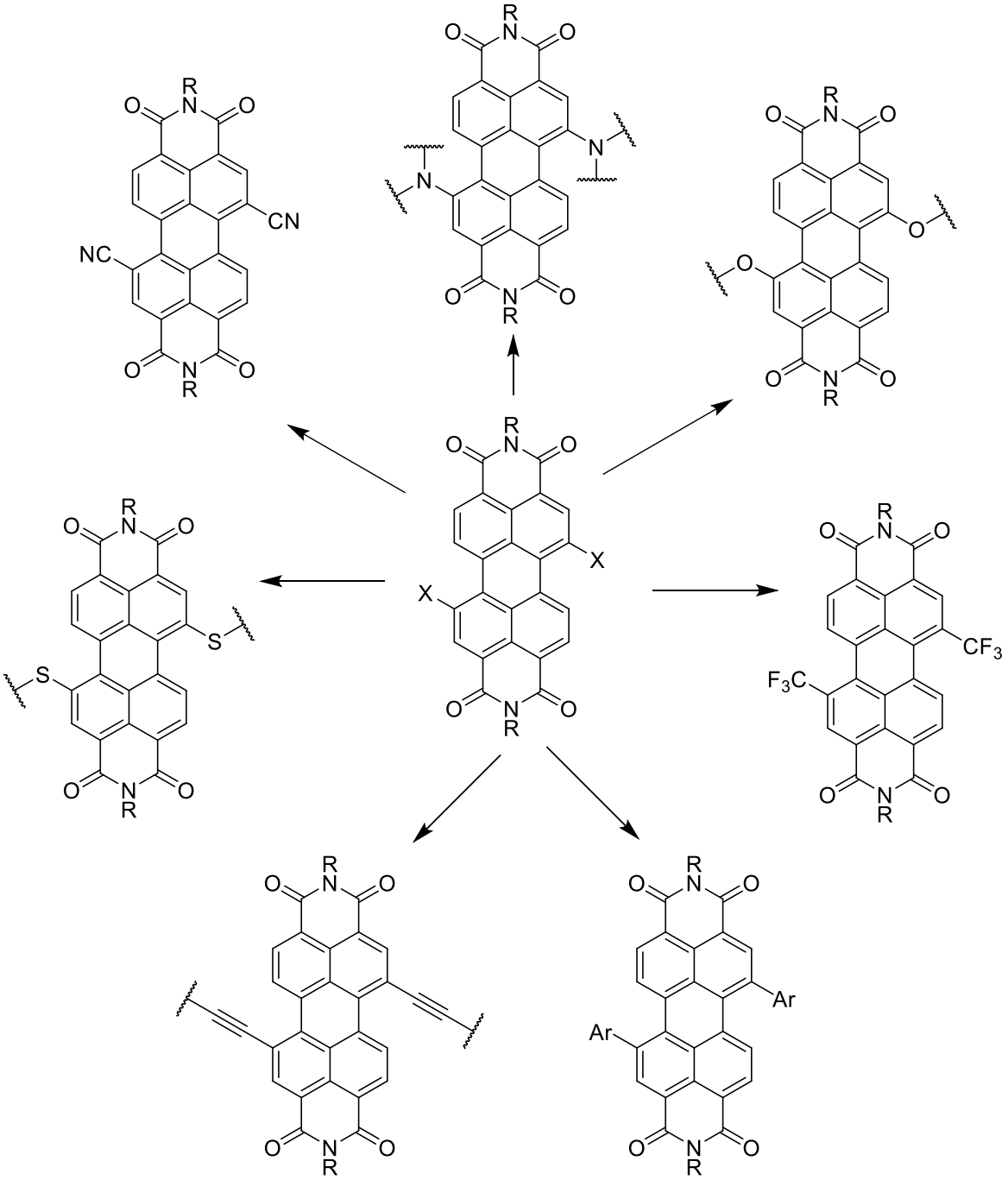

Figure 1.9. Halogenated PDI as a diverse building block to many PDI products.

Here, the derivatisation into PDI bis-alkynes via Sonagashira coupling[64] must be highlighted due to the synthetic diversity of alkynes.[63b, 64-65] In particular, the resulting PDI bis-alkyne can be coupled with any primary alkynes by Glaser coupling, which could be used in the synthesis of oligomers.[63b] Also, PDI bis-alkynes could be reacted with any

organic azide via the facile and high yielding copper-catalysed azide–alkyne cycloaddition (CuAAC),[65c] forming PDI bis-triazoles, which can also be used to tune the solubility and optical properties of the PDI core (Figure 1.10).[66]

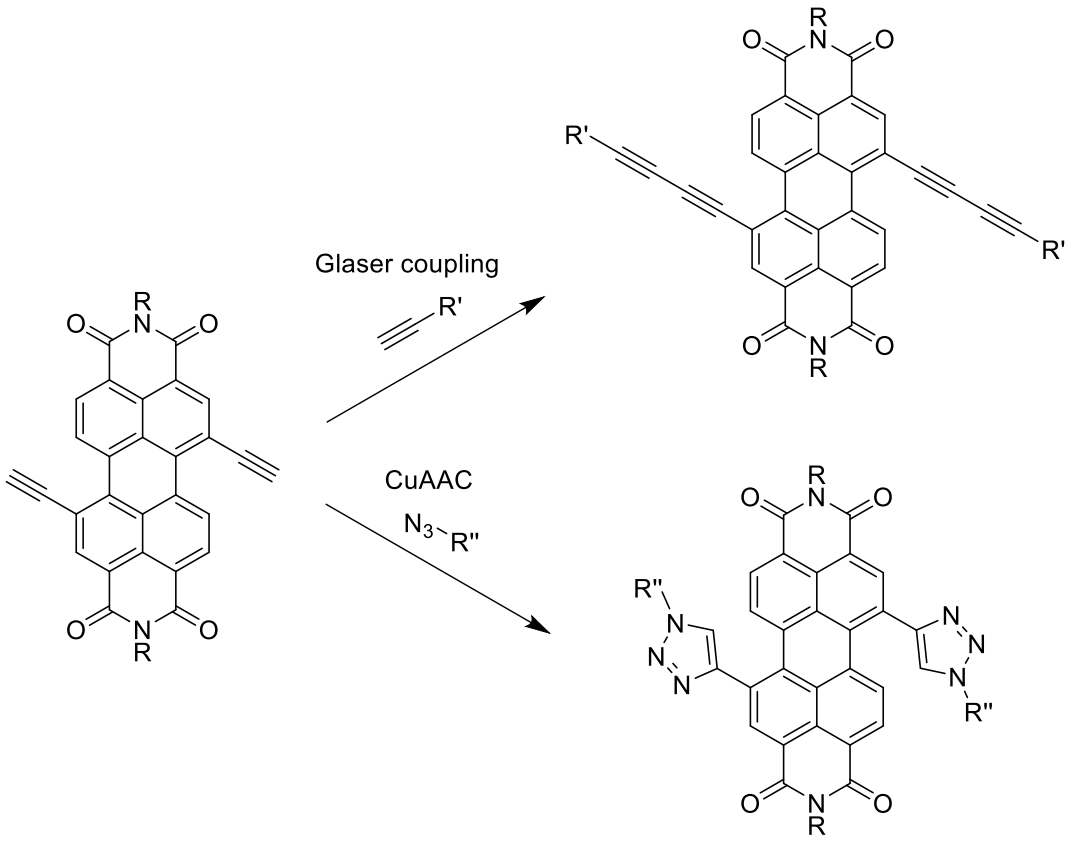

Figure 1.10. Glaser coupling and copper-catalysed azide–alkyne cycloaddition (CuAAC) of PDI bisalkyne.

1.4 Stereoisomers

Stereoisomers are isomers that differ in the spatial arrangement of atoms. Stereoisomerism not only affects physical and chemical properties of molecules, but also dictates its interactions in supramolecular assemblies. Stereoisomers are known as enantiomers if the two stereoisomers are mirror images and cannot be superimposed onto each other. Enantiomers will exhibit identical physical properties and spectra collected using achiral electromagnetic radiation (e.g. ^{1}H NMR spectra), meaning that they can only be distinguished by their interaction with polarised light or with enantiomers of other

compounds. Therefore, enantiomers can be characterised by circular dichroism (CD) spectroscopy, exhibiting mirror image CD spectra, and may be separated by chiral chromatography. All other stereoisomers are known as diastereomers. These do not exhibit identical ^{1}H NMR spectra and can often be separated by conventional, achiral chromatography techniques.

Amongst other sources of chirality, stereoisomerism can arise from point, axial and planar chiral groups (Figure 1.11). Based on the Cahn–Ingold–Prelog priority rules, the stereochemical labels of ***R*** and ***S*** are widely used for groups with point chirality, $\boldsymbol{R_a}$ and $\boldsymbol{S_a}$ for groups with axial chirality, and $\boldsymbol{R_p}$ and $\boldsymbol{S_p}$ for groups with planar chirality, an example of which is pillar[n]arenes (Figure 1.11, right). Rotamers are stereoisomers that interconvert through the rotation about an axis, typically a single bond, and hence are a type of axially chirality. When the barrier to rotation is significant enough for the resolution of the rotamers, these stereoisomers are called atropisomers, an example of which is 1,1′-bi-2-naphthol (BINOL, Figure 1.11, middle).

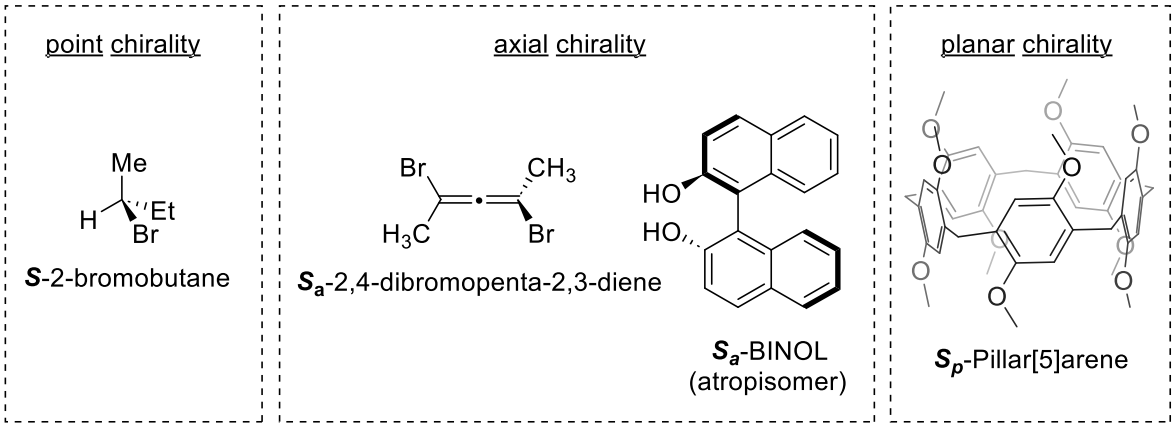

Figure 1.11. Point, axial and planar chiral groups.

Molecules with a helical, propeller, or screw-shaped geometry can be described as having helical chirality ([7]helicene, Figure 1.12, top). Furthermore, it is useful to describe assemblies of molecules in the context of helical chirality, such as the helical aggregates of PDIs.[67] This helicity is typically denoted with ***P*** or ***M***, where they respectively notate a left or right-handed helix. This ***P/M*** nomenclature can also be extended to molecular structures with axial chirality such as BINOL, which is labelled using the Cahn–Ingold–Prelog group rankings of the front groups in relation to the back groups when viewed along the axis of the restricted bond (Figure 1.12).

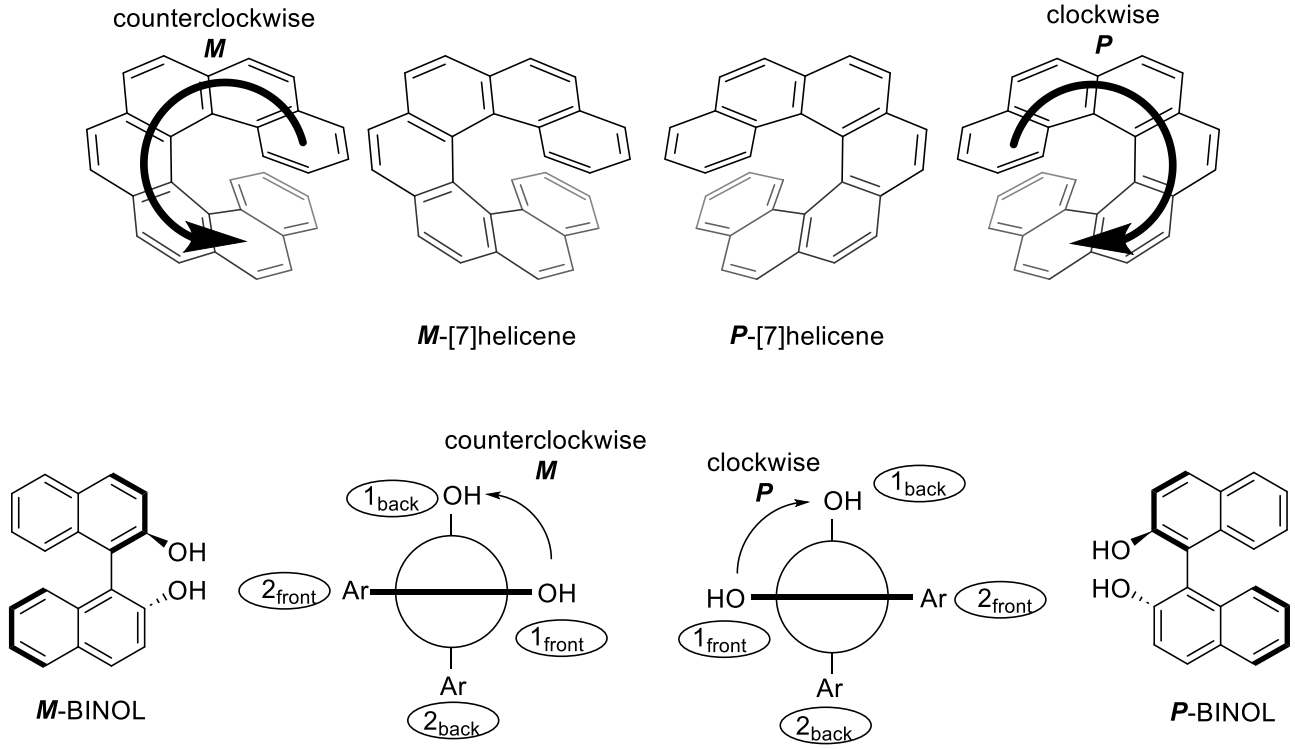

Figure 1.12. Top: the two enantiomers of [7]helicene, displaying its ***P***/***M*** helical chiral labelling. Bottom: the two enantiomers BINOL, displaying its ***P***/***M*** axial chiral labelling.

It should be noted that the stereochemical labels for PDIs can vary in the literature.[68] This arises because PDIs can be considered as either helical or atropisomeric molecules, whereby a bis-bay substituted PDI displaying a ***P*** helix may be notated as ***M*** based on the above rules for labelling axial chirality (Figure 1.13).[68a] Since aspects of this thesis are concerned with comparisons between the chirality of PDI and the axial chirality of BINOL

(see Chapter 3), the ***P***/***M*** nomenclature for disubstituted PDIs will be based on axial chirality labels throughout this thesis.

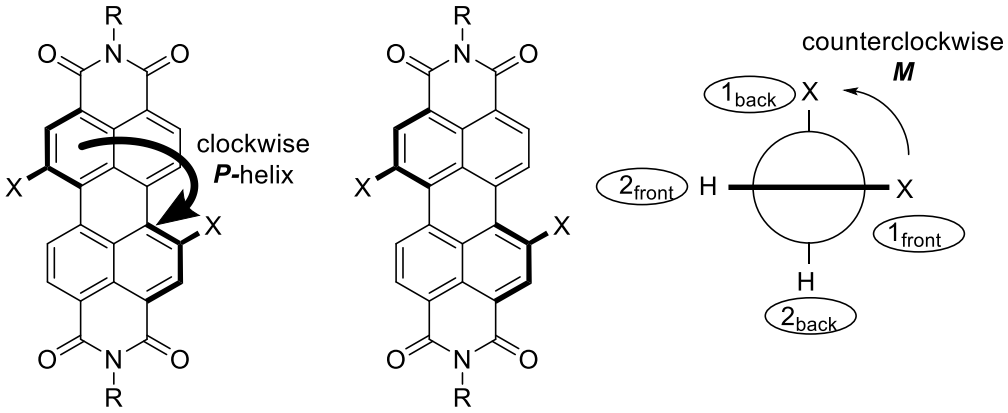

Figure 1.13. Inconsistency in the chiral nomenclature of ***P***/***M*** for PDIs due to its helical and axial chirality.

1.4.1 Stereoselectivity

The selectivity for synthesising one stereoisomer over another is challenging, since the conversion of a prochiral compound into a chiral compound requires a specific chiral auxiliary (e.g. anion, solvent),[69] a chiral reagent,[70] or a chiral catalyst.[71] An enantioselective synthesis is one where one of the possible enantiomers is formed preferentially over the other from an achiral substrate. Similarly, a diastereoselective synthesis is one in which the formation of one diastereomer is formed preferentially over the other(s). The latter is typically achieved when one substrate already contains a stereogenic centre, which then directs the chemical reaction to form their diastereomers in unequal amounts. The more general term of stereoselectivity encompasses both terms.

The importance of stereoselectivity cannot be overstated, particularly in the field of pharmaceuticals.[72] Here, an infamous example is thalidomide, a drug which was sold as a racemic mixture, yet unfortunately the ***S***-enantiomer was responsible for the severe harm of over 10000 infants.[73] Stereoselective syntheses are also important in chemical sensing, [74] and chiroptical (the absorption or emission of circularly polarised light) materials.[75] The

former could be used to determine the enantiomeric composition of reactions in real time, allowing high throughput screening of chiral catalysts and reagents.[76] The latter could be used in bioimaging, optical communication, and encryption.[75d]

Supramolecular chemistry can also be used to tune non-covalent interactions between molecules and thus may play an important role in directing the stereochemical outcome of a chemical reaction.[77] For example, Aguirre and coworkers realised the stereoselective synthesis of 1,2-diarylethylamines through the use of stabilising donor–acceptor π-π interactions between the aromatic rings joined to the carbanionic centre and the iminic carbon atom, where the other diastereomer is not realised due to electronic repulsion (Figure 1.14).[78]

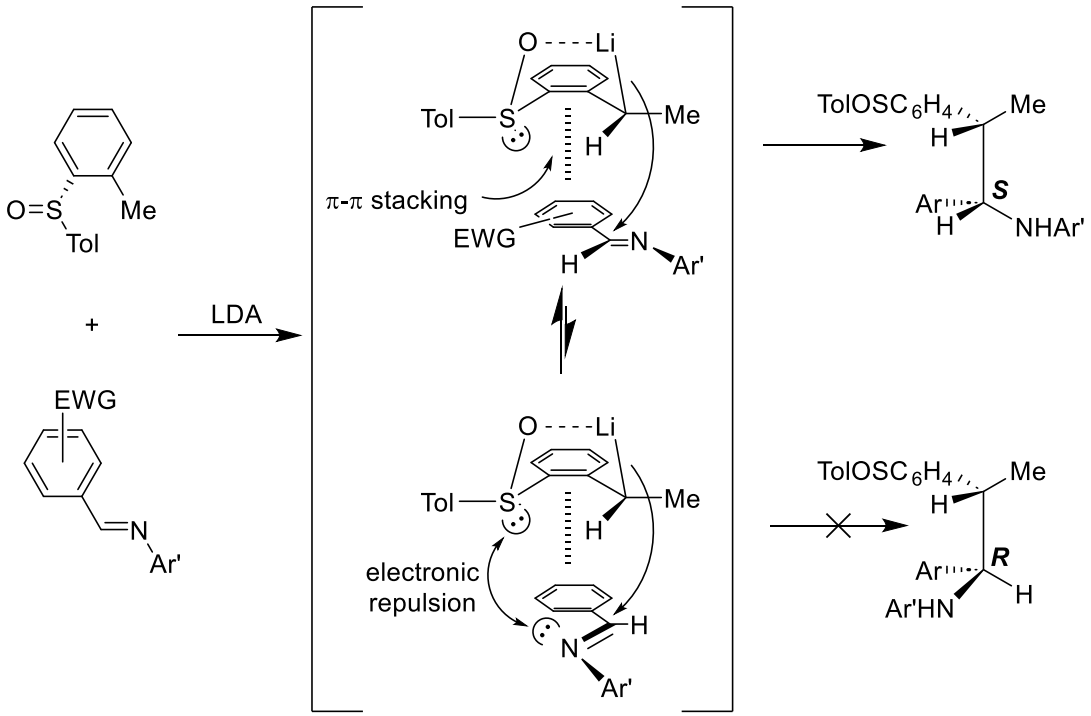

Figure 1.14. Aguirre and coworkers' stereoselective synthesis of ***R***-1,2-diarylethylamines.

1.5 Stereoisomerism of Perylene Diimides

Having highlighted the versatile and amazing properties of PDIs in Section 1.3, as well as the importance of stereoisomerism in Section 1.4. It is of interest to chemists to incorporate

stereoisomerism into PDI containing molecules. This can be accomplished by either self-assembly of PDIs (Section 1.5.1), or twisting the core of the PDI (Section 1.5.2). Both methods have major shortcomings. The former require the formation of a supramolecular assembly, limiting their potential use in drugs, materials and catalysts, as well as being less stable and scalable. The latter is often not stable to racemisation, where it is of current challenge to achieve a configurationally stable core-twisted PDI (See Section 1.5.2 and 1.5.3).

1.5.1 Chirality arising from PDI self-assembly

There are many examples of PDI derivatives containing point chiral substituents at one or more of the imide position(s). However, as monomers, these dyes rarely exhibit a CD spectrum since the chiral imide group does not influence the central perylene core which is the chromophore responsible for the absorption spectrum. Instead, these chiral substituents may direct the self-assembly of the PDI monomers into chiral aggregates which can lead to a strong CD signal in the visible region.[79] For example, Meijer and coworkers' oligo(p-phenylene vinylene) and phenyl derived triads **6-OPV** and **6-Ph** aggregate into a chiral dimer with a CD signal in the visible region in organic solvents such as chloroform and toluene. However, in THF or at higher temperatures (60 °C in toluene), the PDIs are monomeric in solution since intermolecular hydrogen bonding and π-stacking interactions between the monomers are disrupted leading to the loss of the CD signal (Figure 1.15).[29]

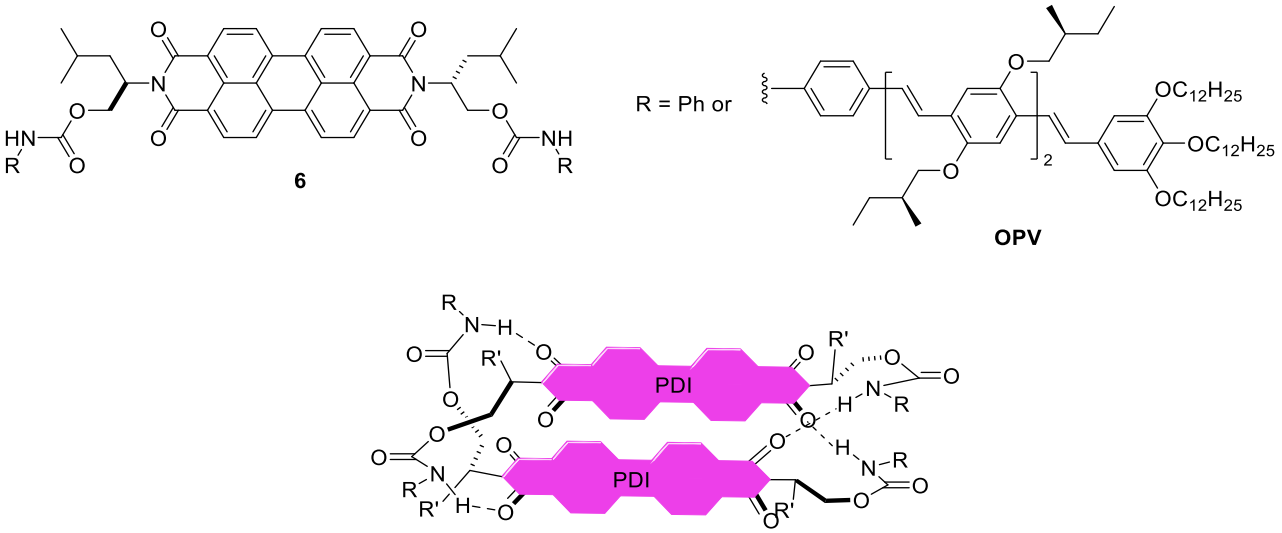

Figure 1.15. Top: Meijer and coworkers' triads **6.** Bottom: illustration of hydrogen bonded and π-stacked dimer of **6**.

1.5.2 PDI chirality arising from core twisting

Whilst unsubstituted PDIs are planar, the introduction of one or more bay substituent(s) leads to the twisting of PDI core along its long axis. However, the majority of bay-substituted PDIs are known to have a low racemisation barrier and so are not configurationally stable and will exist as racemates in solution. An investigation into the dynamic chirality of core twisted PDIs by Würthner and coworkers[80] (Figure 1.16) indicates there is a linear relation between the free activation energy of atropisomer interconversion ($\Delta G^{\ddagger}$) and the steric overlap of bay substituents ($\sum r^{*}$). Those with small bay-substituent overlaps (such as tetrafluoride substituted, dibromo substituted and tetraaryloxy-substituted PDIs) cannot be resolved by chiral HPLC. However, for larger substituents, tetrachloro-substituted PDI ($PDICl_4$) can be separated into >90% ee (with a half-lifetime of 825 min at 293 K), and tetrabromo-substituted PDI ($PDIBr_4$) can be fully separated (stable at 293 K, half-lifetime of 36 min at 383 K).

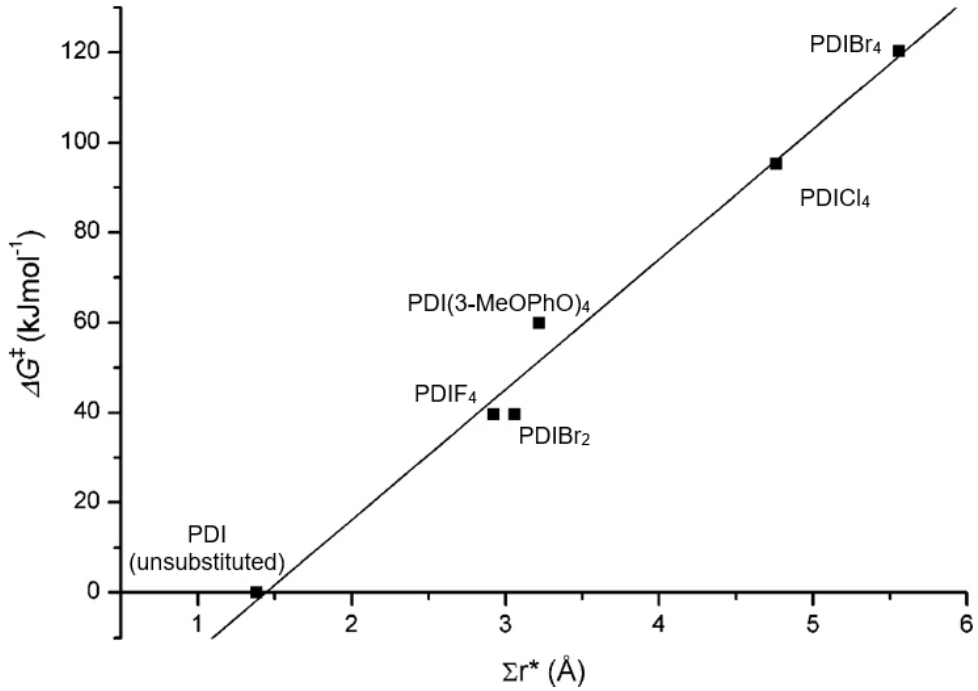

Figure 1.16. Dependence of the free activation enthalpy of racemization on the apparent overlap ∑*r** for PDIs. Reproduced with permission from *J. Am. Chem. Soc.* 2007, 129, 46, 14319–14326. Copyright 2007 American Chemical Society.

The correlation between bay substituents' steric overlap and the dihedral angle of the PDI twist is also found to be linear, except for the smallest and largest substituents (Figure 1.17). In the former case, the smaller substituents will bend away from the plane of the PDI rather than causing a core twist which disrupts π-orbital overlap in the perylene core. In the latter case, the twisting of PDI seems to have an upper limit (a dihedral angle of about 37°), and so the PDI undergoes different distortions to overcome the large steric repulsion.[80]

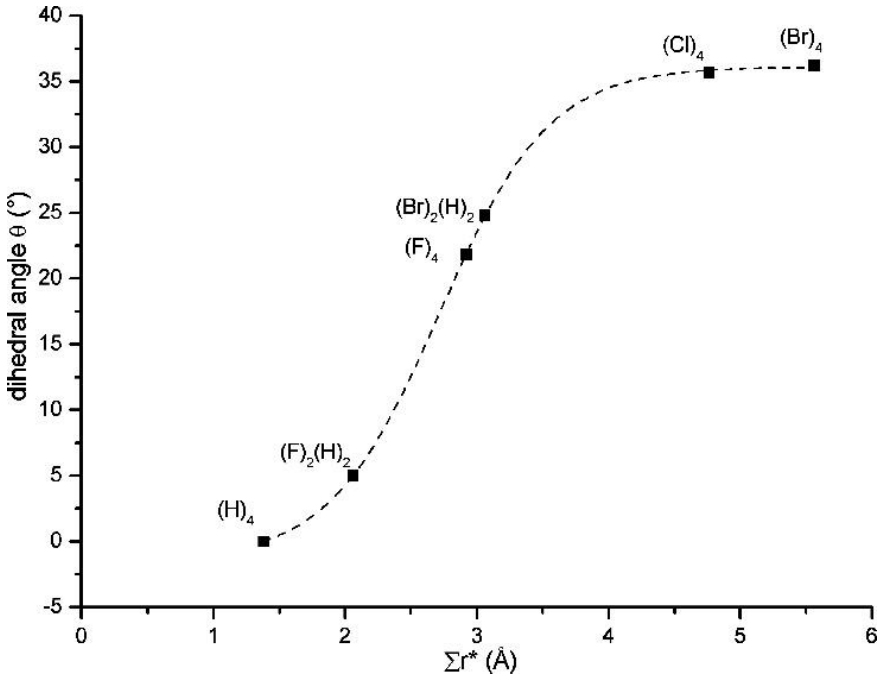

Figure 1.17. Dependence of the dihedral angle and the apparent overlap for different halogen-substituted perylene bisimides (substituents with numbers are given). Reproduced with permission from *J. Am. Chem. Soc.* 2007, 129, 46, 14319–14326. Copyright 2007 American Chemical Society.

Four bromine atoms are not the only substituents large enough to yield stable PDI ***P/M*** atropisomers stable at room temperature. Wüthner and coworkers' tetra-(n-butylthio)-substituted PDI **7** could also be resolved by chiral HPLC and is stable at room temperature, racemising at temperatures above 80 °C. The four thio-ethers allow coordination to soft metals, such as Ag^{+} and Pd^{2+} which can tune the electronics of the perylene core, turning the violet coloured compound to magenta and green respectively (Figure 1.18).[81]

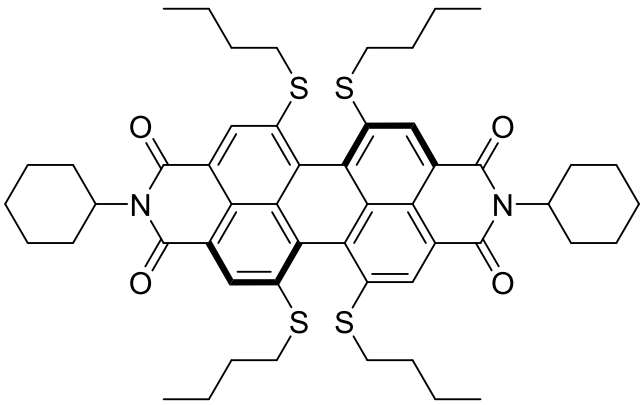

Figure 1.18. Wüthner and coworkers' tetra-(n-butylthio)-substituted PDI.

1.5.3 Stereoisomerism of PDI-based macrocycles

Macrocycles provide a preorganised architecture, ideal for investigating non-covalent interactions between functional groups in the ring (Section 1.2.1).[82] As such, chiral PDIs have been integrated into macrocycles,[39] to understand the impact of the interactions between PDI on their chiroptical properties.[83] The following sections will introduce such PDI-based examples, which have been categorised by their imide- or bay-connectivity. The latter is of particular interest since it provides a route to configurationally stable PDIs.[84]

1.5.3.1 Imide connectivity

The earliest example of a chiral imide-linked macrocycle was reported in 2003. Here, Janssen and coworkers synthesised ***S***-OPV-PDI macrocycle **7**, in which a CD signal in the visible region of the spectrum due to the PDI chromophore. Importantly, this CD signal does not arise from atropisomerism of the PDI, since the dye will be planar due to the absence of bay substituents (Section 1.3.1). Instead, the CD signal is due to the ***P***-helical stacking between the π-electron rich OPV component and the π-electron poor PDI. This demonstrates the importance of a macrocyclic motif in the chiral induction between a chiral π-donor (OPV) and achiral π-acceptor motifs, with their interaction further evidenced by a red-shift in the UV-vis absorption spectrum (Figure 1.19).[85]

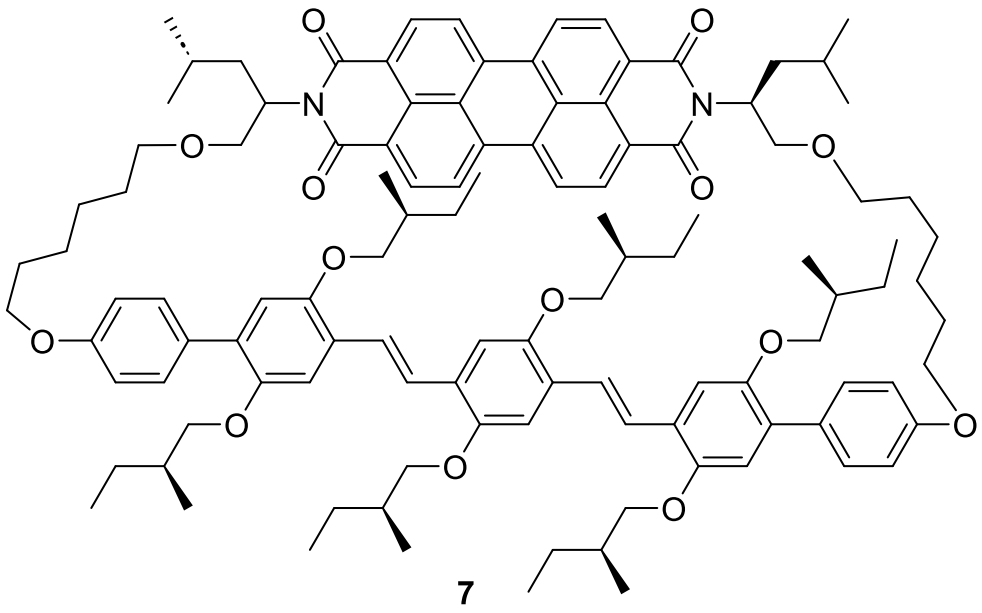

7

Figure 1.19. Janssen and coworkers' ***S***-OPV-PDI macrocycle **7**.

The macrocyclisation of $PDICl_4$ **8** into imide-connected bis-PDI macrocycle **9** by Li and coworkers[86] highlights the significance of chiral π-π interactions between twisted, yet dynamically chiral, PDIs. With all four bay positions occupied by large Cl atoms, $PDICl_4$ is highly twisted and, while not configurationally stable, the barrier to atropisomer interconversion is sufficiently large to enable their analysis by chiral HPLC (i.e., atropsiomer half-life = 14 hours at 20 °C). This analysis revealed that $PDICl_4$ monomer **8** forms the homochiral π-stack **8-Homo** (***PP*** or ***MM***), which then quickly reacts to form the macrocyclic dimer **9**, which is exclusively homochiral (***PP*** or ***MM***). However, the heterochiral π-π stacking of monomers in **8-Hetero** (***PM***) disfavours the orientation of the thiol groups for macrocyclisation, thus only reacts on one end to form the linear heterodimer intermediate **10-Hetero**. This intermediate then equilibrates into its homochiral equivalent **10-Homo** and so can quickly react to form the cyclic dimer **9**, which is exclusively homochiral. Whilst this macrocyclisation reaction demonstrates diastereoselectivity, the bis-PDI dimer product is not chirally locked since the homochiral macrocycle equilibrates to a 1:1 ratio of homo and heterochiral species over 24 hours. The

preference for homochiral over heterochiral π-π stacking is also revealed upon studying the folding of linear dimers of **11** upon increasing solvent polarity.[86] Here, selectivity for the homochiral foldamer is found due to the complementary folded structure being lower in energy (Figure 1.20).

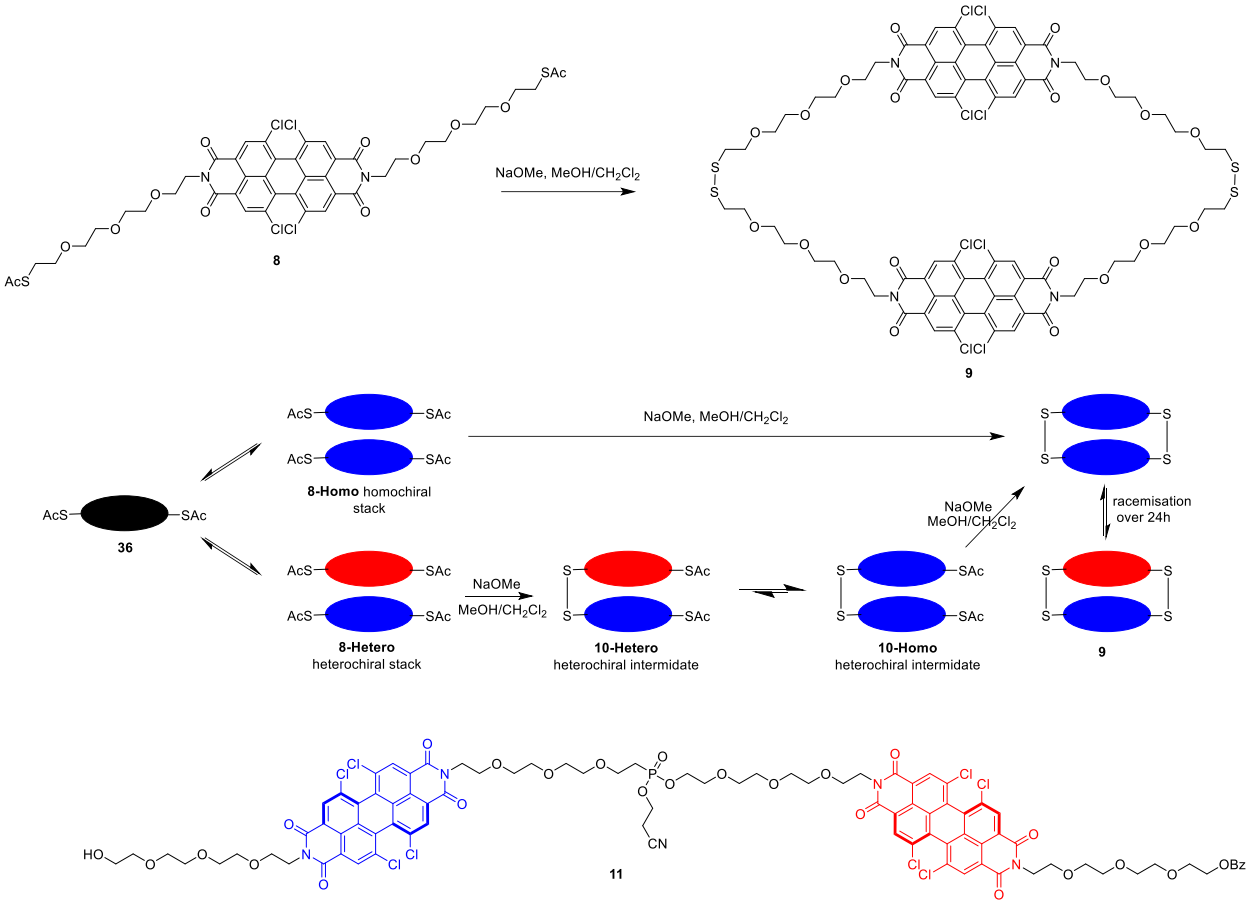

Figure 1.20. top: Li and coworkers' PDI **8** forming macrocycle **9**. Middle: Mechanism of macrocyclization, where **9-Homo** is the only major product in the reaction. Bottom: linear dimer **11** that folds depending on solvent polarity.

1.5.3.2 Bay connectivity

Bay substituted PDIs typically have a low interconversion barrier such that their atropisomers rapidly interconvert at room temperature (Section 1.3.1). In 2007, Würthner and coworkers[87] were the first to isolate an atropisomerically pure PDI by strapping the diagonal bay positions to form macrocycle **12**, which makes the interconversion between ***P*** and ***M*** atropisomers geometrically impossible. Here, in contrast to the imide linked

macrocycle **7** (Section 1.5.3.1), the strong CD spectrum exhibited by macrocycle **12** is due to the chiral twist of the PDI core. It should be noted that this PDI-based macrocycle does also contain chiral imide groups, but the rationale for their inclusion is to afford diastereotopic splitting in the ^{1}H NMR spectrum, which enables the configurational stability of the twisted PDI to be characterised. Interestingly, when the PDI is strapped adjacently (i.e., via 1,12- and 6,7- positions), the flexibility of the glycol strap does not increase the atropoisomerism barrier, since temperature dependent ^{1}H NMR spectroscopy studies showed similar racemisation rates for adjacently strapped PDI **13** and unstrapped PDI **14** (Figure 1.21).

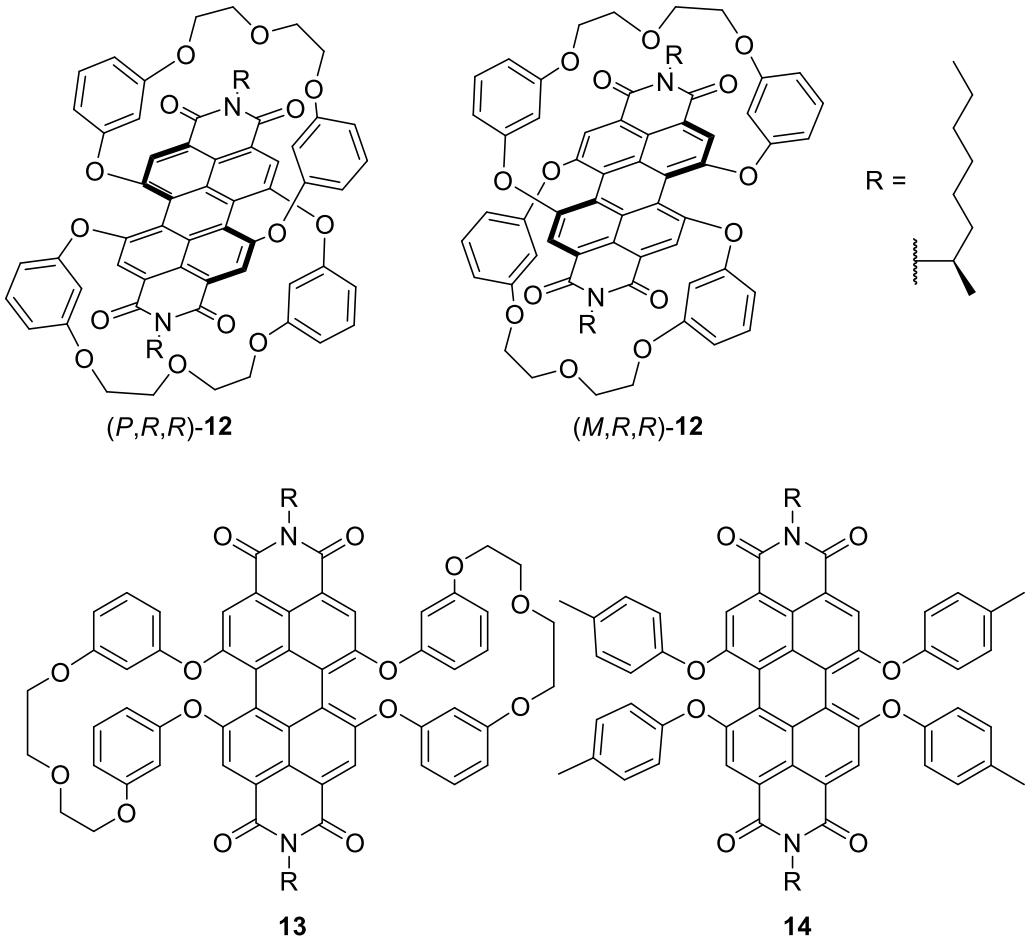

Figure 1.21. Würthner and coworkers' bay strapped PDI macrocycles **12** and **13**, and acyclic **14**.

Further work by Würthner and coworkers[88] has since achieved chirally-locked PDIs **15**-**17** from a tetrachloro-substituted PDI by linking the adjacent (1,12-) bay areas with a rigid 2'2-biphenol bridge, rendering it stable enough for resolution at room temperature. Compared to the 'broken-bridge' variant **18**, the rigidity of PDIs **15**-**17** is evidenced by hypochromic shifts with enhanced vibronic fine structure and a reduced Stoke's shift. The free energy barrier to racemisation ($\Delta G^{\ddagger}$), as determined by time-dependent HPLC at temperatures 40 – 60 °C, is roughly the same for all these PDI derivatives (~99 kJ mol^{-1}). This barrier is significantly higher than the tetraphenoxy-substituted PDI **18** (60 kJ mol^{-1}) (Figure 1.22).

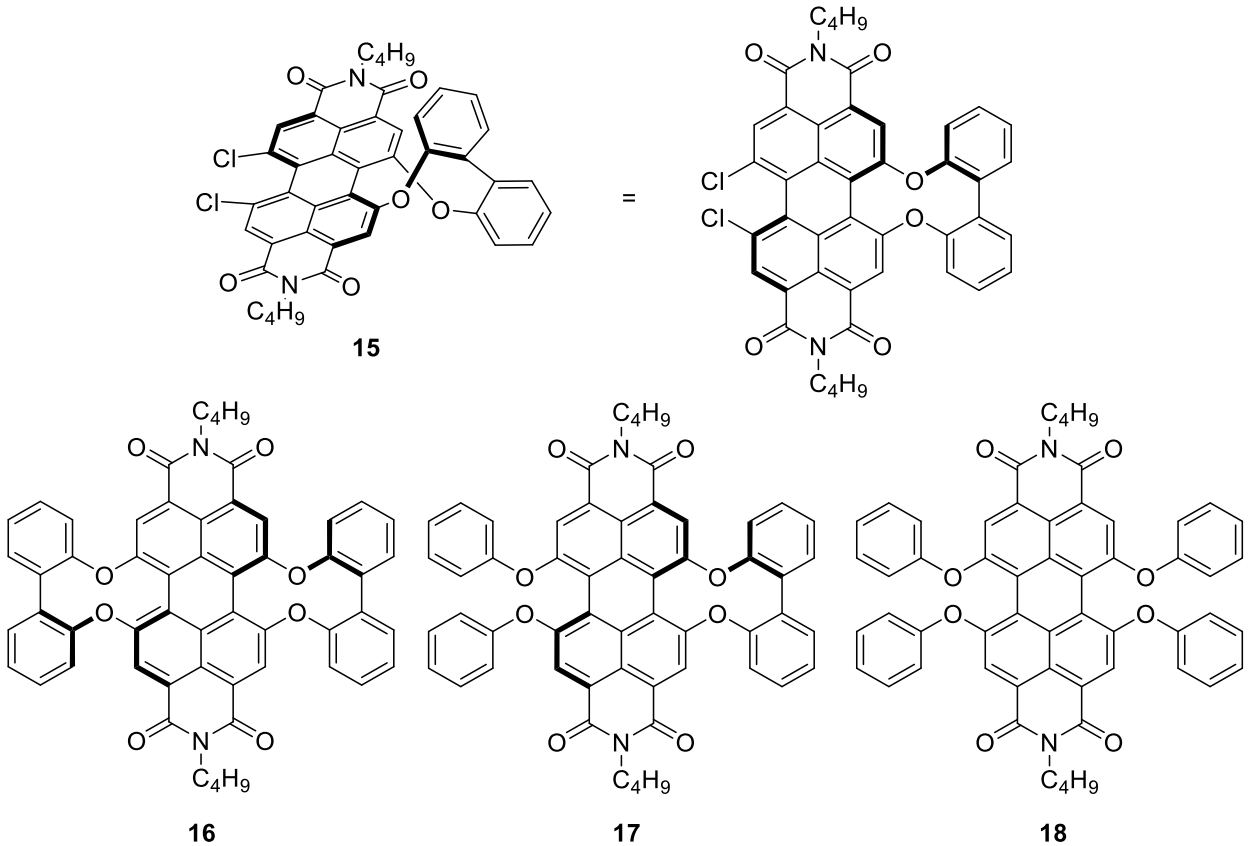

Figure 1.22. Würthner and coworkers' adjacently linked configurationally stable chiral PDIs **15-17** and 'broken-bridge' variant **18**.

Using a disubstituted chiral PDI, the same group also prepared the singly (1,7-) bay-strapped PDI macrocycle **19**, for which the ***M*** and ***P*** atropisomers can be resolved by chiral HPLC. This macrocycle can undergo supramolecular π-π self-assembly. Importantly, the

bridge of the (1,7-) bay-strapped PDI **19** blocks one face of the PDI, preventing its self-assembly into large columnar aggregates, and so PDI dimers are formed.[89] In line with the findings of Li and coworkers (Figure 1.20), the self-assembly of macrocycle **19** reveals a preference for homochiral over heterochiral π-stacked dimers.[90] The length of the strap of **19** determines the rigidity and angle of the PDI twist, whereby PDIs with a longer strap (less strained) are more conformationally flexible. Interestingly, this weakens the chiral self-recognition (i.e. less selectivity for homochiral dimers) but improves the strength of PDI–PDI binding, since the PDI core has increased freedom to twist into a conformation to optimise π-overlap, i.e., induced-fit (Figure 1.23).[91] Notably, the blue shifts in the absorbance spectra of the shorter strapped PDI macrocycles are due to the larger angle of the PDI twist, which reduces conjugation between the two naphthalimide subunits (Section 1.23).

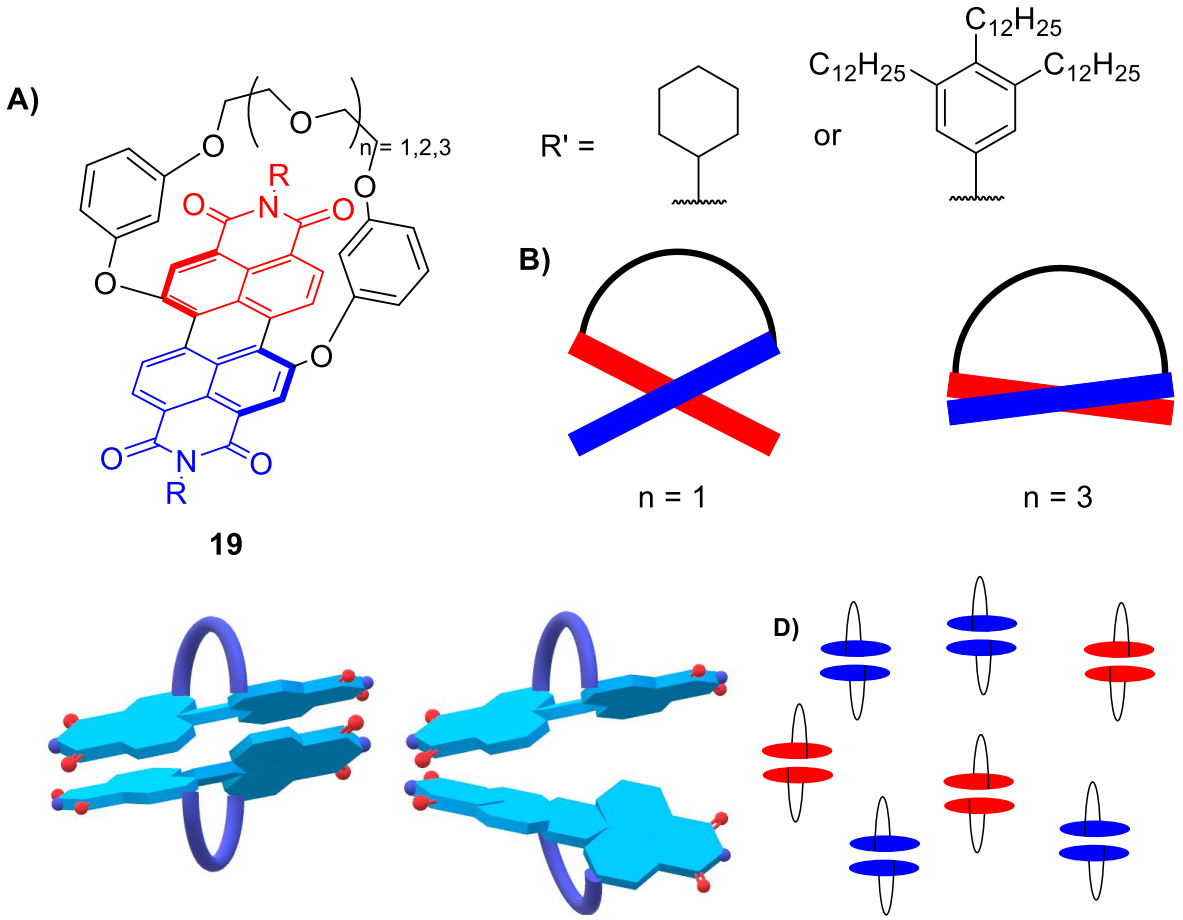

Figure 1.23. A) Würthner and coworkers' singly bay strapped PDI macrocycles **19**. B) Illustration of the effect where longer strap decreases rigidity and twist angle of the PDI. C) Illustration of the π-stacking of homochiral and heterochiral dimers, where homochiral dimer (left) is shown to more tightly stack with a larger π-contact. D) Illustration of a racemic aggregation of **19**, where only homochiral dimers are formed.

Nuckolls and coworkers have pioneered the development of chiral macrocycles containing two PDI units, including macrocycle **20**[92] which consists of two twisted PDI units connected through their bay positions by 2,2'-bithiophene linkers. Therefore, this macrocycle has stereoisomers that are categorised as either homochiral enantiomers (***PP*** or ***MM***) or a mesomeric diastereomer (***PM***). Once again it was found that the homochiral arrangement is favour over the heterochiral mesomer, with a 6:1 ratio at 87 °C. However, in contrast with the previous preference for homochirality due to π-π stacking, the preference for homochirality in **20** is likely due to the geometry of the strained macrocycle,

as the rigidity of the 2,2'-bithiophene linkers prevents through-space communication between the PDI units (Figure 1.24).

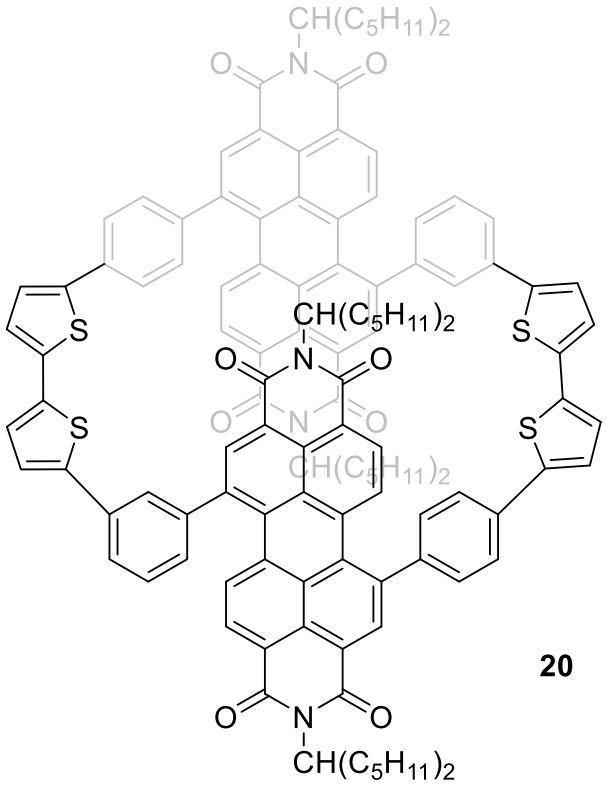

Figure 1.24. Nuckoll and coworkers' donor-acceptor-donor-acceptor (DADA) macrocycle **20**.

Whilst the stereoisomers of **20** can be separated by chiral HPLC, homochiral ***PP*-20** racemises within two hours at room temperature. Importantly, interconversion between enantiomers is shown to occur via the heterochiral meso isomer ***PM*-20**. Therefore, the mechanism of interconversion between stereoisomers in bay-connected PDI macrocycles relies upon an 'intramolecular somersault', whereby a PDI unit rotates 180° around its (1,7)-bay axis through the macrocycle cavity (Figure 1.25). While this mechanism is in action in the bis-PDI macrocycle **20**, it cannot occur in the previous smaller macrocycles of the Würthner group (e.g., **12**, Figure 1.21; and **19**, Figure 1.23) since their short strap inhibits the somersaulting motion.

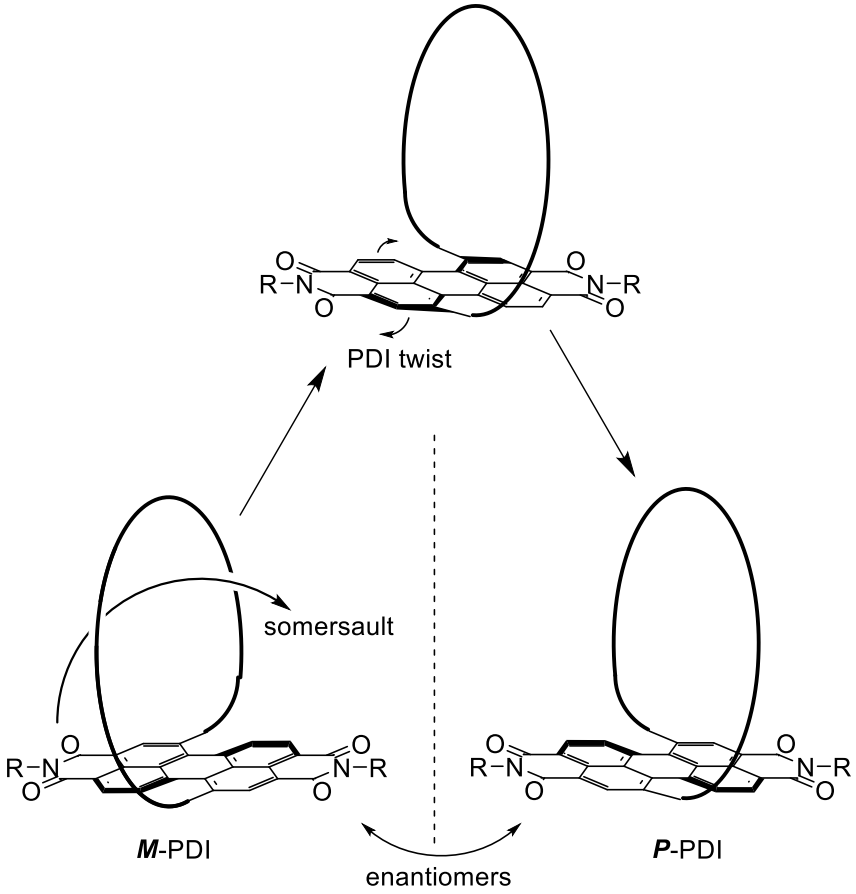

Figure 1.25. Illustration of racemisation of PDI macrocycle by 'intramolecular somersault'.

1.6 Rotaxanes

A [n]rotaxane, from Latin rota and axis (wheel and axle), is a molecule consisting of one or more macrocycle(s) (wheel), threaded onto one or more axle component(s), with large, sterically hindering stopper groups at both ends to stop the macrocycle from sliding off.[93] As such, these components are not covalently bonded together, but are held together mechanically (mechanical bond),[94] as covalent bonds are unable to pass through one another. The 'n' in [n]rotaxane refers to the number of interlocked molecular compounds (e.g. one macrocycle interlocked onto one axle gives a [2]rotaxane).[95]

The axle in a rotaxane can have binding interactions with the macrocycle at various locations, leading to the positioning of the macrocycle at these different binding sites. Moreover, the strength of the binding interactions at these sites can be modified in response to different physical stimuli

(e.g., solvent, temperature, light), whereby the macrocycle will shuttle to the most favourable binding site.[96] This stimuli-responsive molecular shuttling allows [n]rotaxanes to be used as molecular switches,[97] logic gates,[98] sensors[99] and valves[99b] (Figure 1.26).

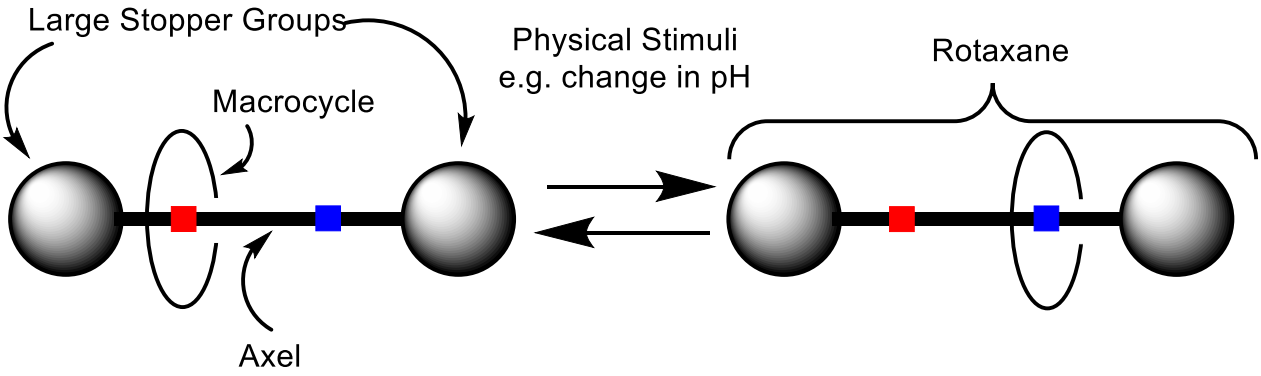

Figure 1.26. A [2]rotaxane, displaying its macrocycle, axle, and large stopper groups.

1.6.1 PDI-based Rotaxanes

The supramolecular and photophysical properties of PDIs make them attractive components to integrate into rotaxanes.[100] Early work by Champness and coworkers reported an early PDI-based [2]rotaxane by exploiting the π-π templation between a π-electron rich 1,5-dihydroxynaphthalene (DHN) based macrocycle with the π-electron deficient PDI-containing axle. They discovered that electrochemical reduction of the PDI leads to de-threading of the macrocycle due to electrostatic repulsion between the components. The same group have since developed a [4]rotaxane in which two additional pillar[5]arene macrocycles are threaded onto the axle near the stopper groups, which prevents de-threading upon electrochemical reduction (Figure 1.27). However, despite the locking of the pillar[5]arene's planar chirality that will occur upon mechanical interlocking, the chirality of this system has yet to be explored.

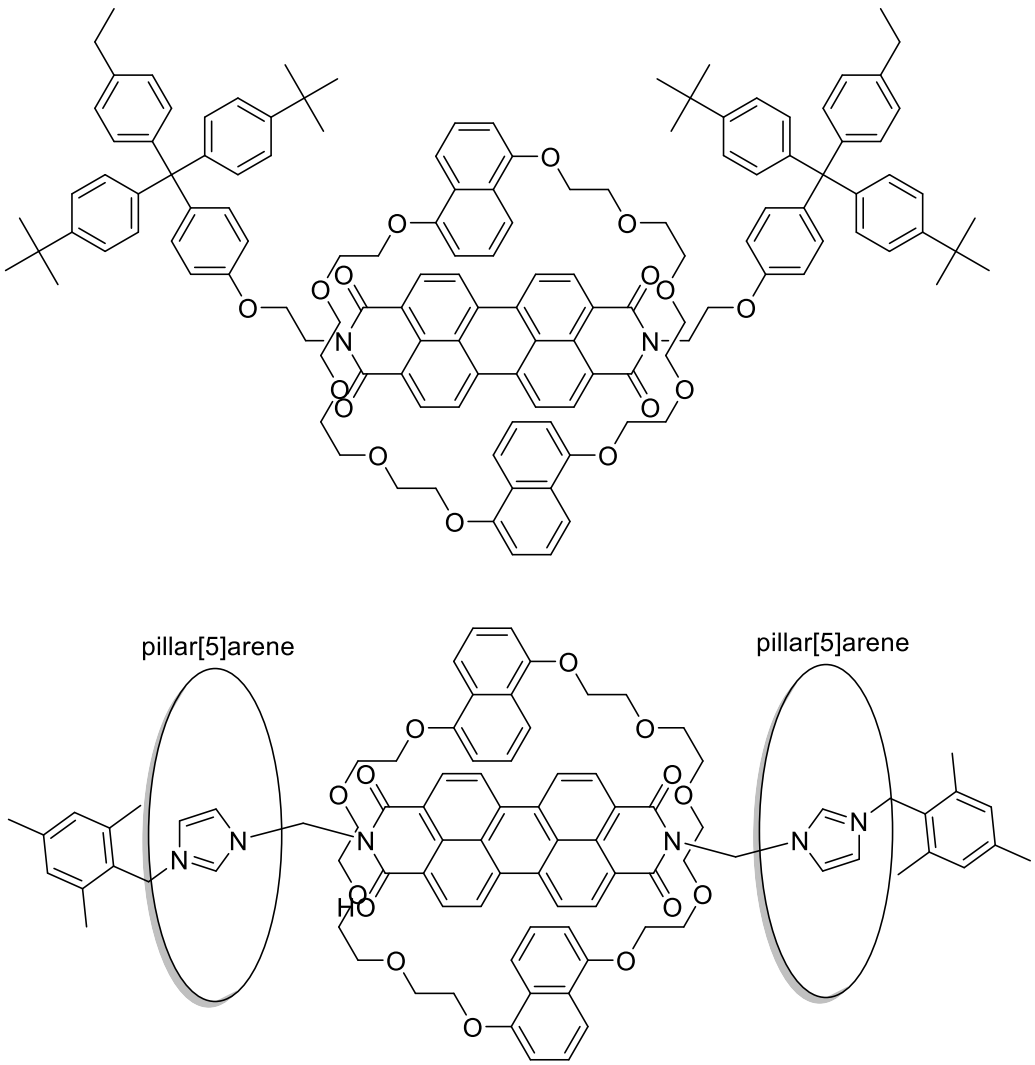

Figure 1.27. Champness and coworkers' PDI [2]rotaxane (top) and PDI [4]rotaxane (bottom), π-electron rich di-DHN based macrocycle π-stacks withboth sides of the π-electron poor PDI axle.

1.6.2 Chiral Rotaxanes

Recent research has seen the development of a plethora of chiral rotaxanes.[101] In the context of chiroptical properties, Leigh and coworkers have reported a two station [2]rotaxane in which a macrocycle is triggered by photoisomerization of the olefin station to shuttle along the axle to hydrogen bond with a chiral peptide station. This induces a strong CD signal, thus making the [2]rotaxane a chiroptical switch (Figure 1.28).[102] More recently, Blanco and coworkers developed a similar [2]rotaxane, whereby a luminescent 2,2'bipyrene macrocycle is stimulated to shuttle to a chiral peptide station by a change in

pH, which causes a switching on of the circularly polarised luminescence (CPL) emission (Figure 1.29).[103]

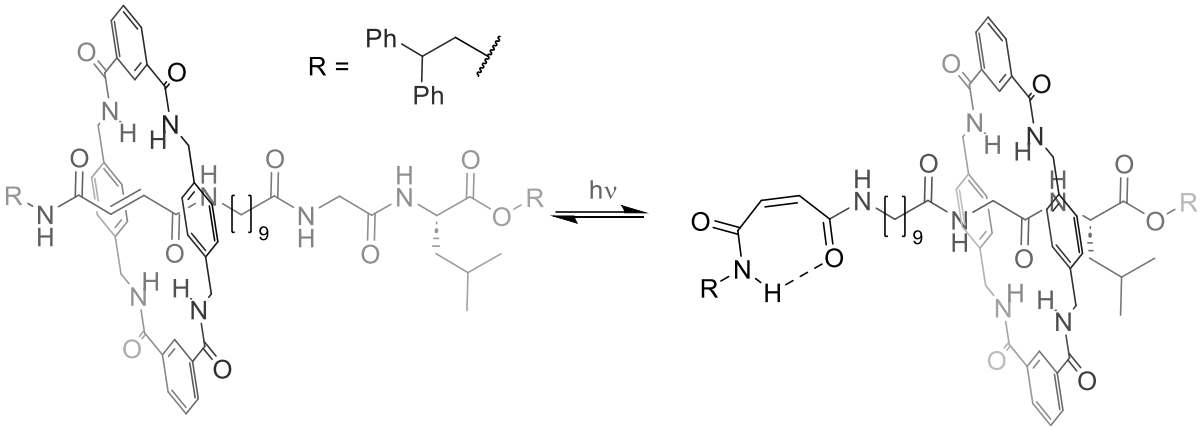

Figure 1.28. Leigh and coworkers' two station [2]rotaxane, shuttling to a chiral peptide station upon stimuli (light), inducing a strong CD signal.

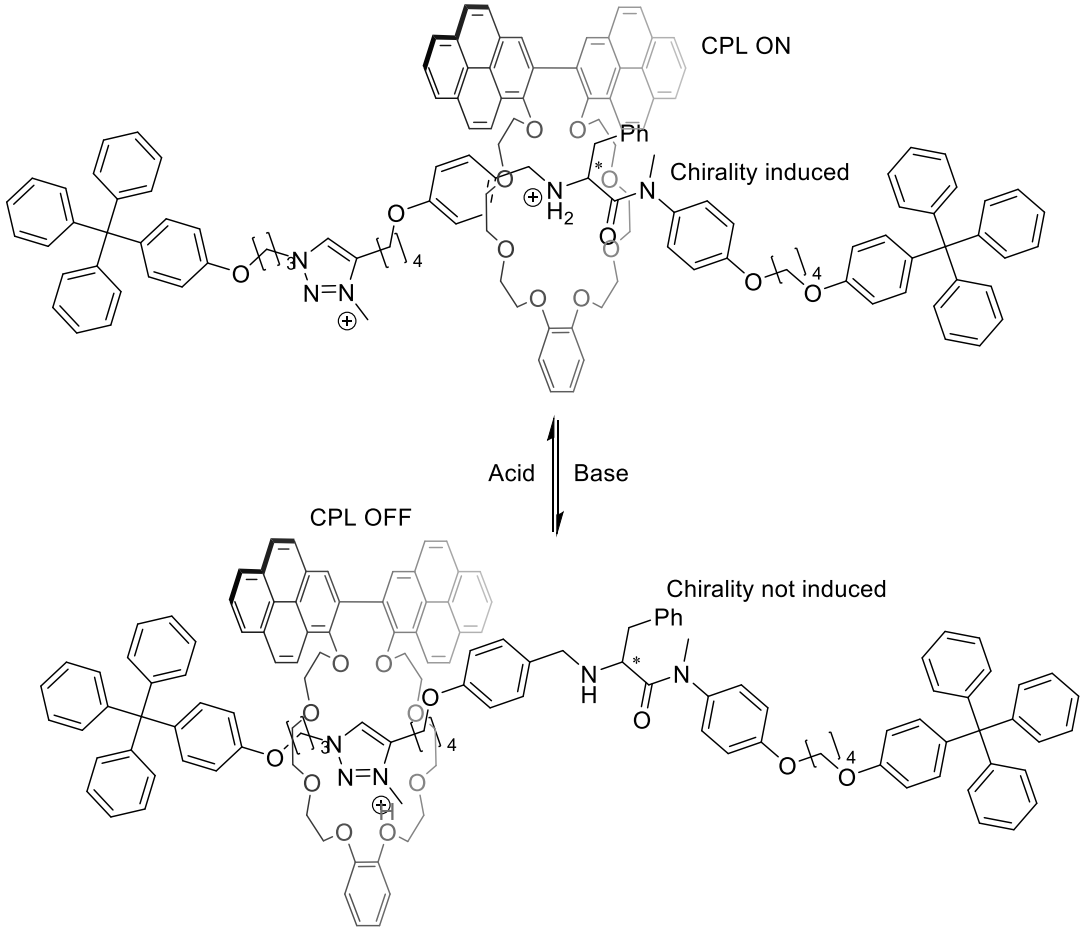

Figure 1.29. Blanco and coworkers' [2]rotaxane with luminescent 2,2'bipyrene macrocycle that shuttles to the ammonium station upon protonation of the secondary amine, emitting CPL.

1.7 Project Aims

The overall goal of the research in this thesis is to develop new strategies for generating configurationally stable and functional chiral perylene diimide dyes. Two methods are envisaged to accomplish this; firstly the integration of chiral PDIs into macrocycles will be expanded upon (Figure 1.30a) and secondly a novel strategy involving mechanical bonding in rotaxanes will be developed (Figure 1.30b). The former will be realised by macrocyclic strapping of the bay positions of the PDI, in which the linker also contains an aromatic functional group that is able to interact with the PDI unit (Figure 1.30a). The latter will be attempted by increasing the steric bulk at the PDI's bay positions by its incorporation into the axle component of a [3]rotaxane, such that the macrocyclic rings interact with the bay-substituted PDI (Figure 1.30b). A variety of analytical techniques will be used to characterise the PDI-based non-covalent interactions present in these systems.

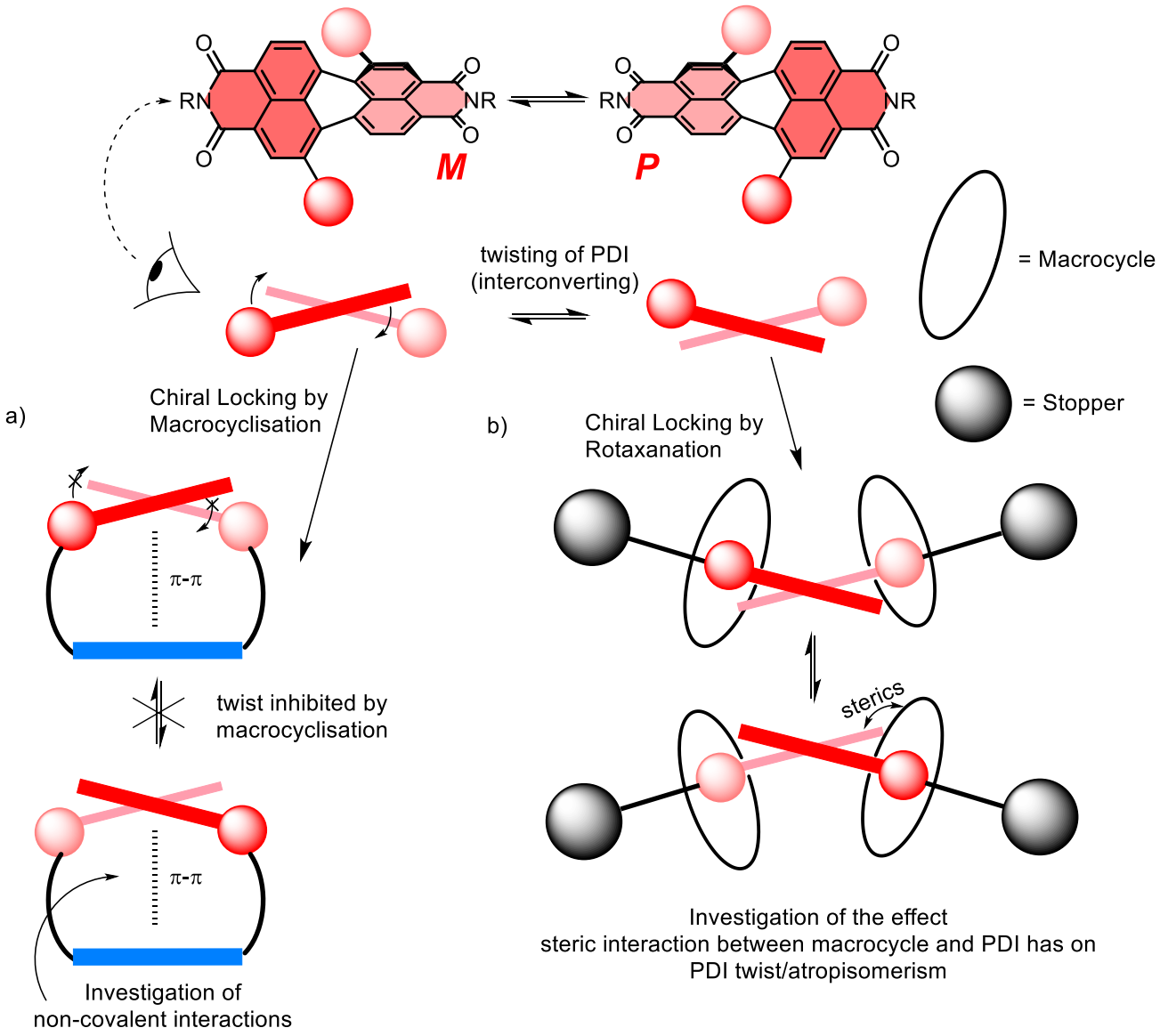

Figure 1.30. Illustration displaying the (a) chiral locking of PDI molecules by macrocyclisation and (b) the effect of a [3]rotaxane on PDI atropisomer interconversion

There are only a limited number of chirally-locked PDI macrocycles, and their macrocyclisation yields are often low.[84, 104] Therefore, Chapter Two aims to diversify this library by developing new synthetic strategies, most notably exploring the use of donor-acceptor π-π interactions between the PDI and an aromatic-based linker to template the synthesis of chiral and configurationally stable macrocycles in good yields (Figure 1.30a).

Building on the realisation of intramolecular π-π interactions within PDI-based macrocycles, Chapter Three aims to achieve the stereoselective synthesis of twisted PDIs (Figure 1.31). It was envisaged that this will overcome the need for specialist techniques such as chiral HPLC for the chiral resolution of PDIs, as well as improving atom economy of the synthesis of chirally locked PDIs. This challenge will be addressed through strapping the PDI with a second chiral unit, including both dynamically chiral and chirally locked species.

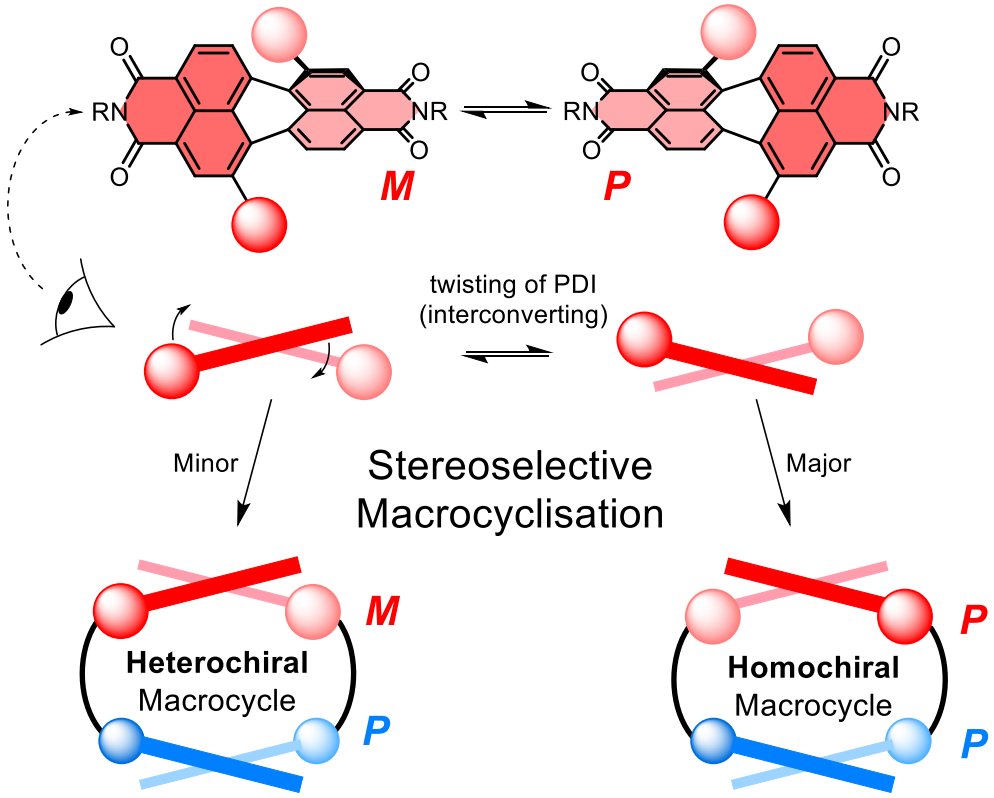

Figure 1.31. Illustration displaying a stereoselective macrocyclization reaction

The strategy of locking the chirality of a twisted PDI by its integration into a rotaxane is explored in Chapter Four. Here, a [3]rotaxane is developed in which two macrocycles are positioned either side of a bay-substituted PDI in the axle component, a novel method for increasing the free energy barrier to PDI atropisomer interconversion (Figure 1.30b).

2 Chiral locking of Perylene Diimides in Macrocycles

Some of the work in this chapter has been published as an edge article in the journal Chemical Science: A. Yeung, M. A. Zwijnenburg, G. R. F. Orton, J. H. Robertson, T. A. Barendt, Chem. Sci., 2024. DOI: 10.1039/D3SC05715A.

The DFT calculations that appear in this chapter were performed by Prof Martijn Zwijnenburg from University College London.

2.1 Introduction

2.1.1 Chirally locked macrocycles

As outlined in Section 1.3, PDIs are compounds of interest due to their use in sensors, photovoltaics and photonics;[35] which results in many applications such as imaging of biological systems,[75d] OLEDs and transistors.[26] The inherent twist, and thus potential for chirality, of the PDI core in bay-substituted PDIs further enhances their diversity in applications, where they could be used in chiral catalysis, chiral recognition and chiral sensing. One of such uses would be as luminescent materials for imaging of biological systems in medical applications, where the NIR circularly polarised emission of PDIs would be ideal to produce high quality images, with improved signal to noise and minimal damage to tissues.[105] However, one fundamental challenge is the low racemisation barrier as a simple twist between the two naphthalene units would convert one enantiomer to the other. To solve this problem, PDIs can be strapped via the bay positions to form chirally locked macrocycles.[87] Bay-strapped PDI macrocycles in literature are uncommon[84, 104] and many are too large (typically bis-PDI macrocycles), such that the PDI can racemise by 'somersaulting' (Figure 1.25, Section 1.5.3.2).[92]

The first configurationally stable mono-PDI macrocycle was the aforementioned doubly strapped macrocycle **12** Würthner and coworkers in 2007 (Section 1.5.3.2),[87] who

synthesised and isolated by with 0.35% overall yield over six steps from tetrachloroperylene dianhydride $PDACl_4$. Their synthesis required the switching of imide groups to a point chiral imide group, which while has no effect on the chiral twist of the PDI core, generated diastereoisomers which provided a handle for investigation into PDI chirality by NMR spectroscopy. Together with macrocycle strapping of both faces of the PDI core, this approach greatly lowers the synthetic yield of the macrocycle (Figure 2.1).

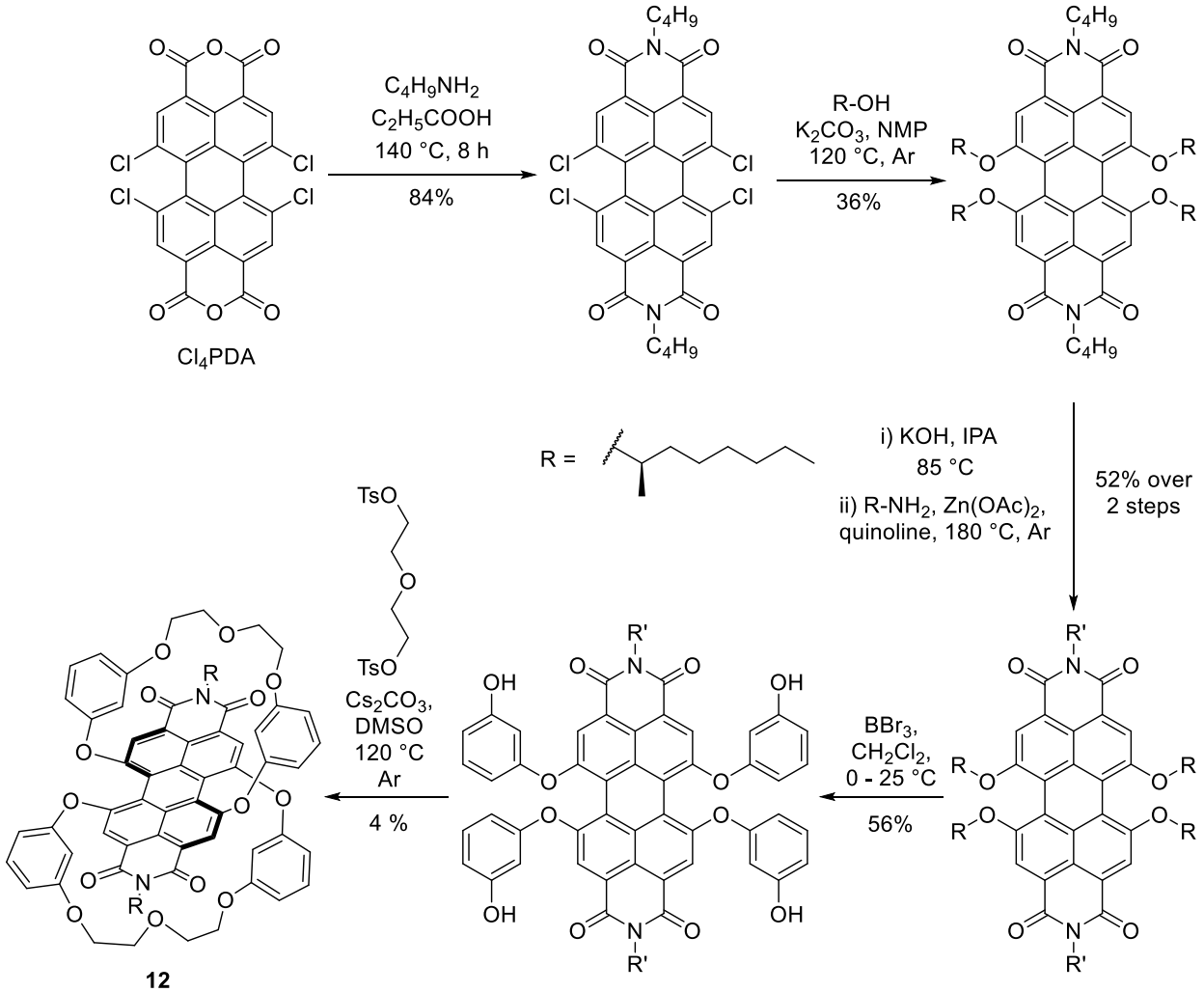

Figure 2.1. Synthesis of Würthner and coworkers' bay strapped PDI macrocycle **12**.

The synthesis of a chirally-locked macrocycle in this work is described in detail below in sections 2.1.3 – 2.2.4, where contrasting with previous PDI macrocycles**,** an imide group which can also probe the chirality could be more simply synthesised, with only one face of the PDI strapped to improve yield, and with different lengths and properties of the strap to

tune the PDI configuration, as well as any potential interactions between the strap and the PDI core.

2.1.2 Chapter Objectives

This chapter describes efforts to diversify the synthetic chemistry of configurationally stable PDI macrocycles, paving the way for the diastereoselective synthesis of PDI macrocycles (Chapter Three).

2.1.3 Macrocycle Design

To make a configurationally stable PDI macrocycle, several aspects of design were considered: the imide group of the PDI, the properties of the strap, how to attach the strap to the PDI, and the length of the strap (Figure 2.2).

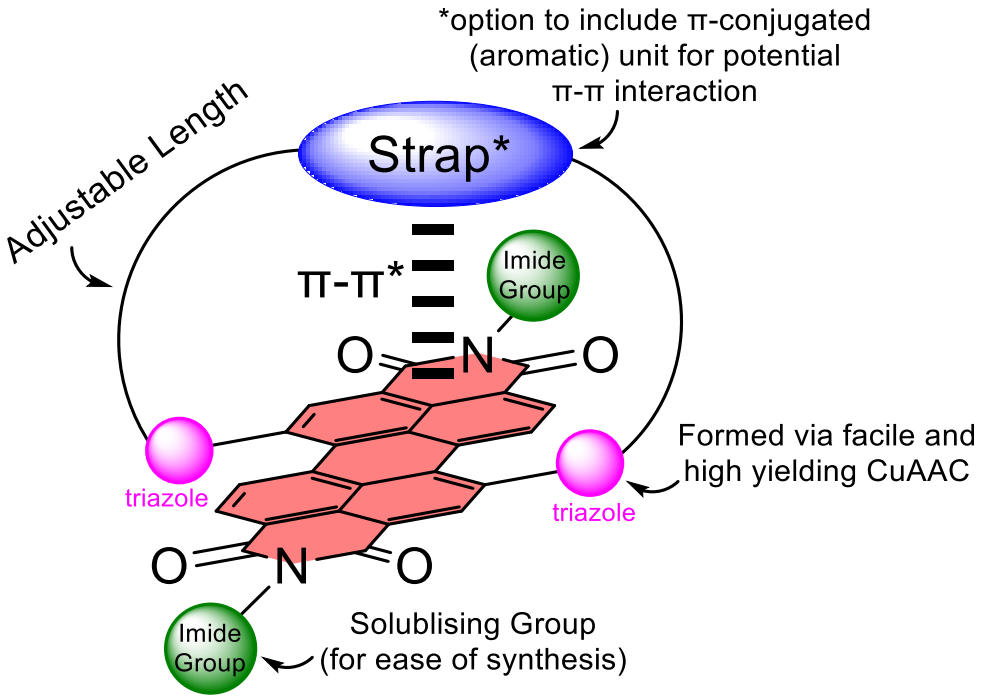

Figure 2.2. Design of PDI macrocycle.

Firstly, aforementioned in Chapter One, the imide group does not greatly interfere with the electronic properties of the PDI core. Thus, with the high affinity for PDIs to π-stack and aggregate,[27] diisopropyl phenyl groups were envisaged to be used as the imide group for enhanced solubility and ease of synthesis. The methyl groups disrupt π-stacking (and thus aggregation) as they are positioned over the top of the PDI core to avoid a steric clash with the carbonyl groups of the PDI (Figure 2.3).

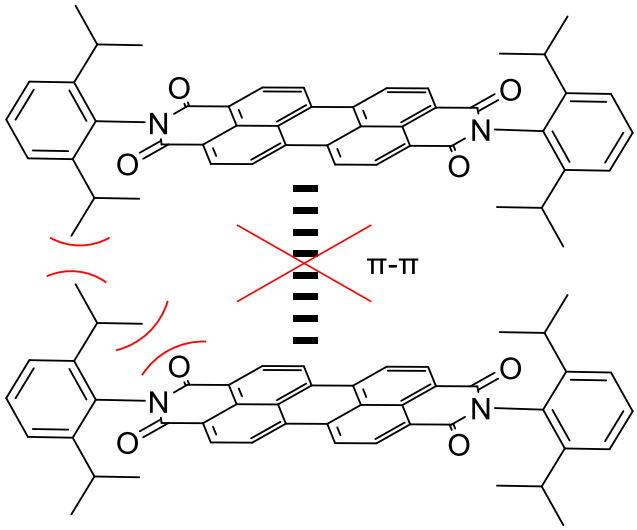

Figure 2.3. Diisoopropyl aniline substituted PDIs, highlighting steric interaction of methyl groups and oxygen atom of the imide, which inhibits intermolecular π-stack and aggregate of PDI molecules.

This imide group was also chosen due to their sensitivity for the chirality of the PDI. The helical twist of the PDI enhances the difference between the two diastereotopic environments of the two methyl groups of the isopropyl unit in the imide group, where this twist, and thus chirality, can be probed by ^{1}H NMR spectroscopy. As seen below in Figure 2.4, the blue and red methyl groups in the isopropyl units are closer to the respective blue and red planes of the PDI, leading to them being inequivalent by ^{1}H NMR spectroscopy. Note that in molecules with low interconversion barrier, the PDI rapidly twists between the two conformers and thus can be considered planar, such that these methyl groups do not show diastereotopic splitting.[31]

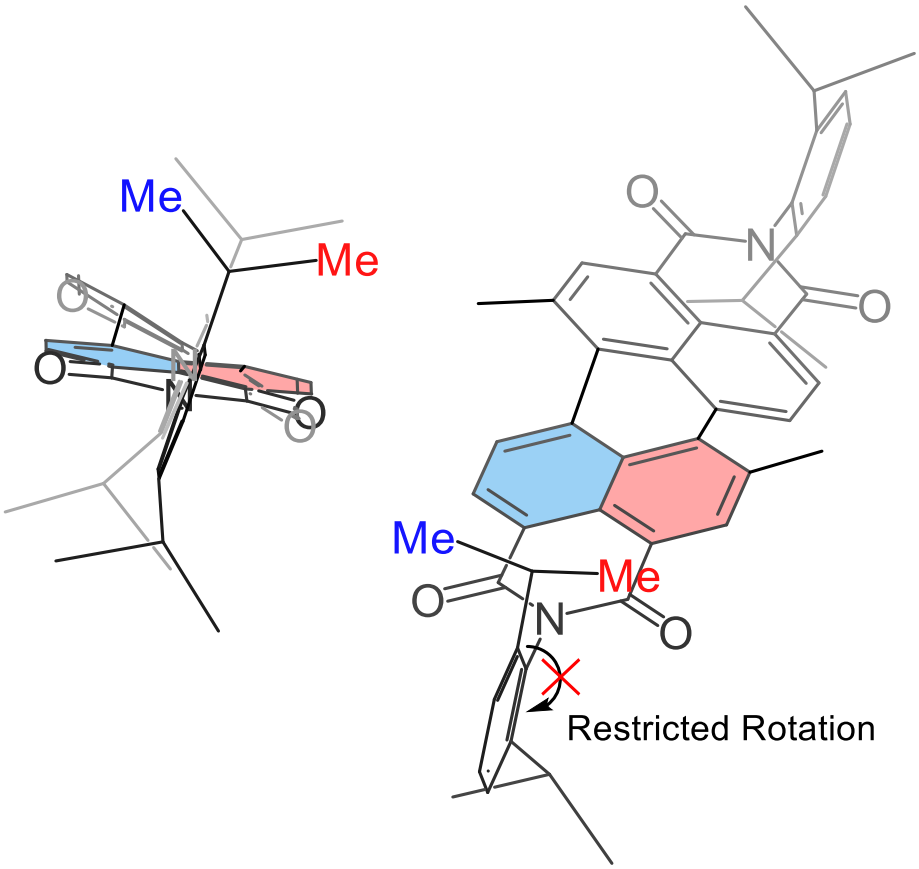

Figure 2.4. The two diastereotopic methyl groups in the isopropyl unit of the imide group.

The largest disadvantage of this imide group compared to other commonly used groups such as pentan-3-amine or undecan-6-amine is the ratio of 1,7- and 1,6- regioisomers when synthesising bis-brominated PDI. Those imide groups are not susceptible to bromination and thus can be substituted onto the PDA prior to bromination, making the PDI more soluble, which allows for milder bromination conditions (gentle heating with 70 equivalents of Br_2 in DCM), achieving a 4:1 ratio of desired 1,7- to undesired 1,6-regioisomer. Diisopropyl aniline substituted bis-brominated PDI, however, must be synthesised by bromination of PDA first before imidisation, where the bromination requires harsher conditions for solubility (heating to 80 °C in concentrated H_2SO_4), instead leading to a 2:1 ratio of 1,7- to 1,6- regioisomers (*vide supra*, Scheme 1.5). Despite this shortcoming, the advantages of using this imide group far outweighs the loss of atom economy, as not only can this group be used to probe the chirality of the PDI, it is also

superior in solubility. This allows further reactions to be reacted in higher concentration, which speeds up reaction time, allows for milder conditions, allows for larger scale reactions, uses much less solvent, and increases the diversity of usable solvents.

Next, it was envisioned to form a triazole at the bay position, which can also be used to tune optical and electronic properties of the PDI core, such as the binding of different anions or further alkylation. This would be achieved by a copper-catalysed azide-alkyne cycloaddition (CuAAC) reaction as it is known to be facile and high yielding,[66] and both precursors are synthetically achievable (Section 1.3.4). The synthesis of a PDI bisalkyne has been reported in literature,[106] and synthesis of azides could be accomplished by substitution of common leaving groups with NaN_3.

To form the macrocycle, three strategies were considered. First, macrocyclation could be accomplished via Grubb's Ring-Closing Metathesis (RCM) – a widely used and insensitive reaction that has been used for the past 30 years (Figure 2.5A). Second, amide condensation could be used instead, where after functionalising the PDI with amines, various commercially available acid chloride or carboxylic acids can be used to form a library of macrocycles (Figure 2.5B). Lastly, the ring can be closed directly by CuAAC of PDI bisalkyne with a bisazide, where various linkers could be converted into a bisazide to form a different library of macrocycles (Figure 2.5C).

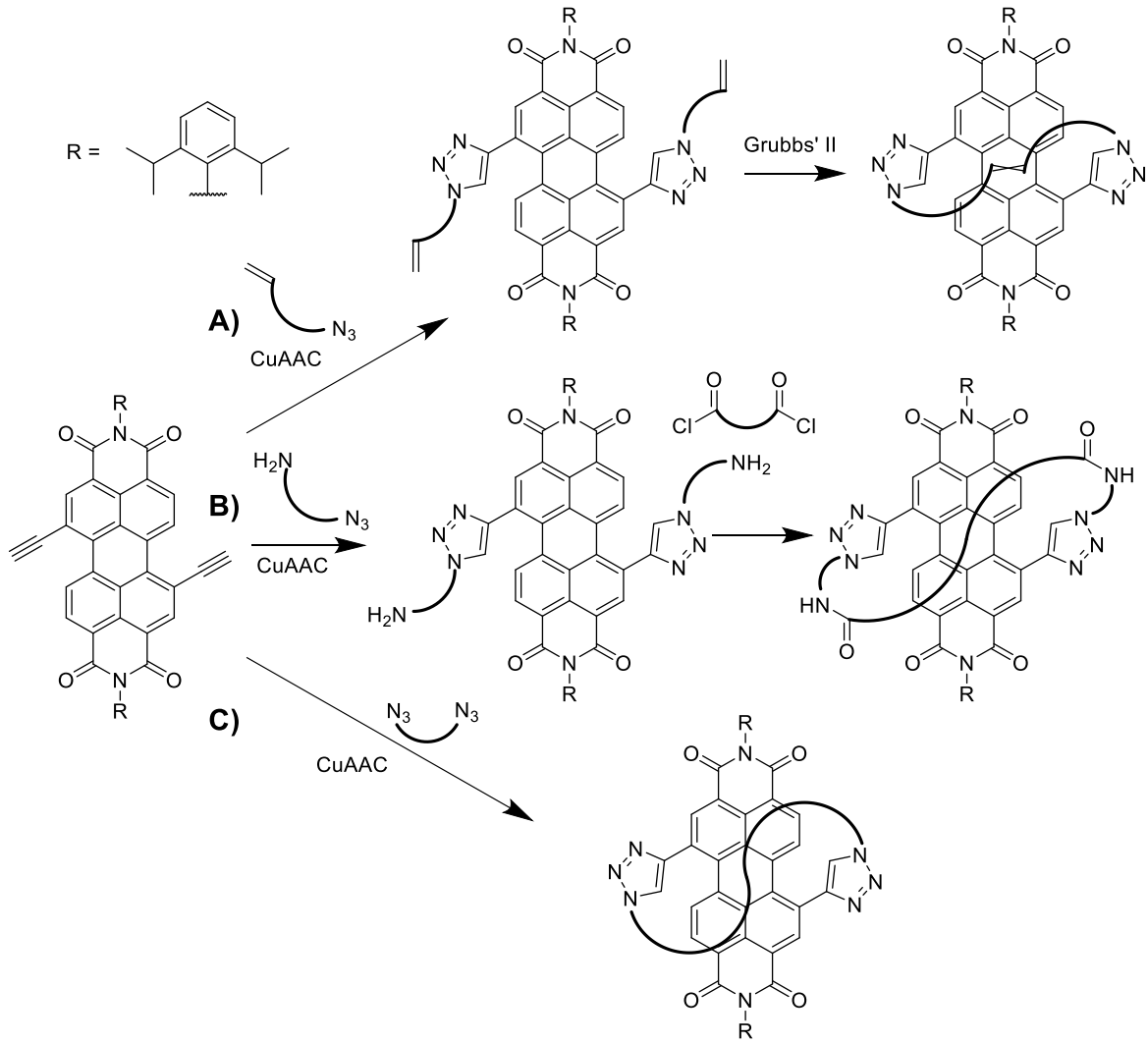

Figure 2.5. The three strategies to form a chirally locked macrocycle.

For each strategy, the strap could contain functional groups with potential to form interesting non-covalent interactions with the PDI, including aromatic units which can π-stack with the PDI. Here, the macrocycle provides a scaffold to preorganise these functional groups and so facilitate intramolecular non-covalent interactions. Finally, the length of the strap should also be considered. Too short of a strap, macrocycle would not form due to ring strain. Too long, however, and the PDI will interconvert via a 'somersault'.

2.2 Synthesis of Chirally-locked Macrocycles

2.2.1 Synthesis of PDI bisalkyne

All three strategies share the common precursor PDI bisalkyne, which could be synthesised from commercially available perylene-3,4,9,10-tetracarboxylic dianhydride (PDA) in four steps. Typically, PDA is brominated by reacting with 2.2 equiv of bromine and catalytic amount of iodine in sulfuric acid in a sealed pressure flask at 85 °C over 18 h.[51, 107] A problem with this reaction is the use toxic and highly reactive Br_2, where the reaction must be done in pressure flask to avoid the leakage of Br_2 gas. Therefore, a new methodology was developed were *N*-bromosuccinimide (NBS) was instead used. The NBS is a lot less hazardous to work with, and can also be easily weighed out. Additionally, it did not require the use of a pressure flask, which means that it can be upscaled without the need for large and expensive pressured flasks.

Both methods gave the same crude mixture of mono-, bis-, tris- and tetra-brominated PDA, which was determined by MALDI mass spectrometry and ^{1}H NMR spectroscopy after the imidisation reaction. Its poor solubility at this stage in any solvent left it unable to be characterised by mass spectroscopy or NMR spectroscopy, and thus, without further purification, it was subjected to an imidisation reaction with commercially available 2,6-diisopropylaniline.[107] After purification by silica gel flash column chromatography, this furnished a 2:1 mixture of 1,7 and 1,6 bis-brominated PDI **21** in 39% yield over two steps. Aforementioned in Section 1.3.4, such PDI regioisomers are inseparable by conventional silica chromatography methods, thus for simplicity and clarity, unless otherwise stated, all mentions of non-macrocyclic di-substituted PDI in this thesis are used as a mixture of regioisomers in this ratio.

Following this, $PDIBr_2$ **21** was subjected to Sonogashira coupling with trimethylsilylacetylene at 60 °C overnight to furnish TMS protected PDI bisalkyne **22** in 99% yield, which was deprotected quantitatively to the PDI bisalkyne **23** with K_2CO_3 in a mixture of DCM/MeOH (1:1 v/v). This solvent mixture was chosen as the starting materials were not able to be dissolved in pure MeOH (Scheme 2.1).[106]

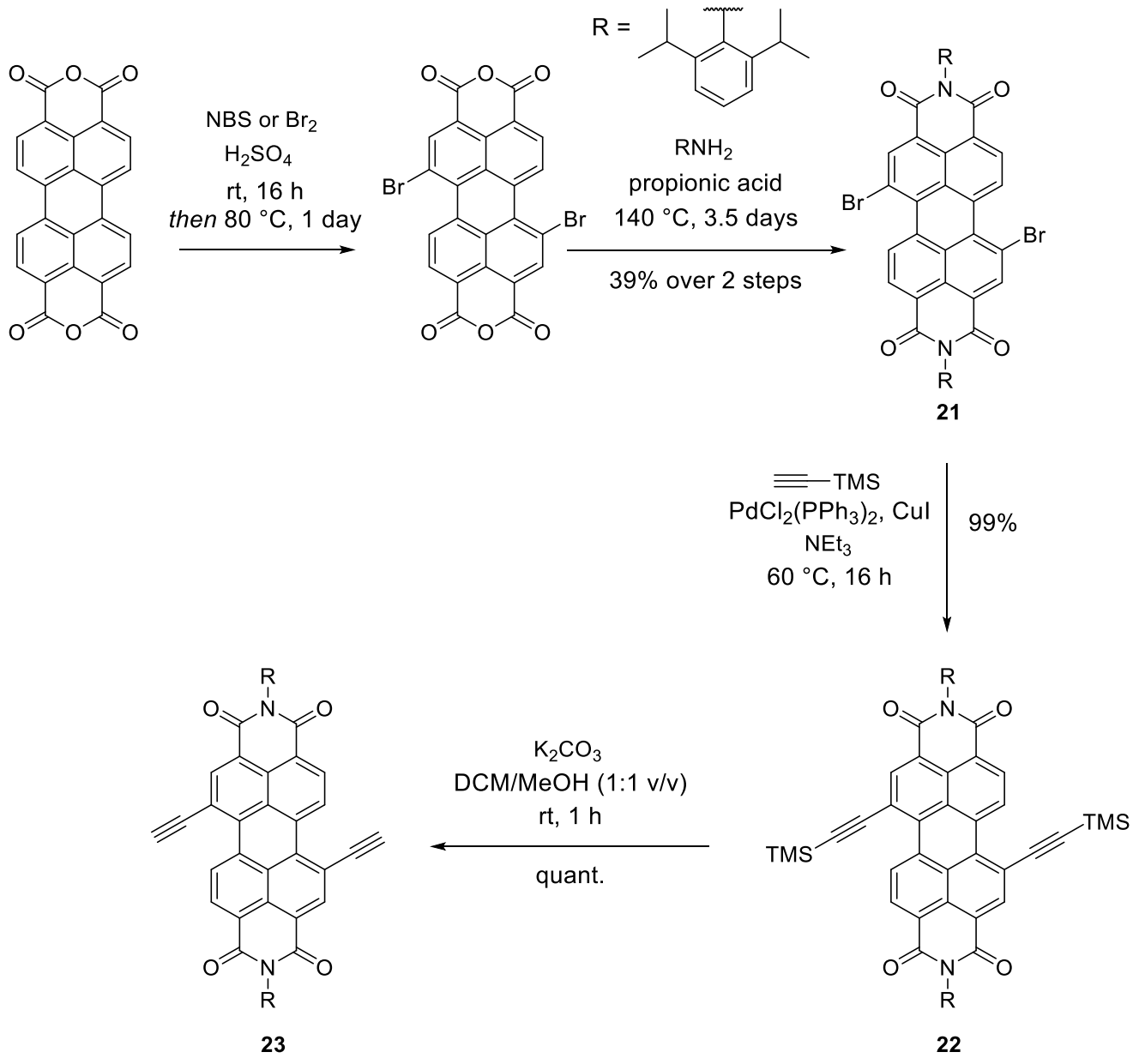

Scheme 2.1. Synthesis of PDI bisalkyne **23**.

Interestingly, PDI bisalkyne **23** is highly stable, even when left in solution in $CHCl_3$ at 60 °C for multiple days, whereas previous work in the group has shown that the same PDI bisalkyne with branched alkane imide groups instead **24** and **25** decomposes over this time, highlighting another advantage of the diisopropyl phenyl imide group (Figure 2.6).

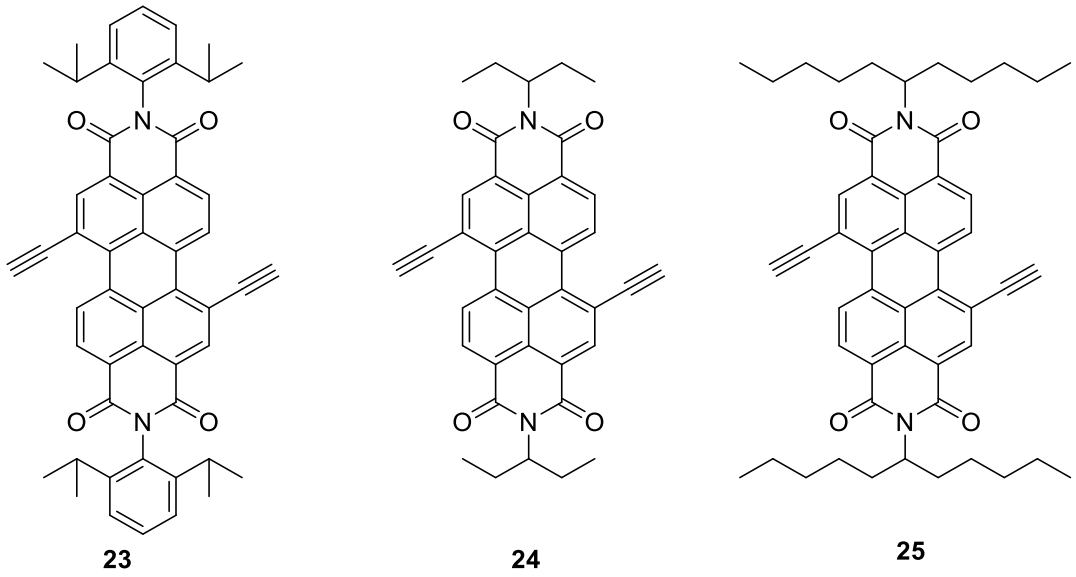

Figure 2.6. PDI bisalkynes with different imide groups **23**, **24** and **25**.

2.2.2 PDI Macrocycle Synthesis: Strategy A – Grubbs' catalysed RCM

With PDI bisalkyne **23** in hand, focus turned to strapping the PDI core to form the macrocycle. Initially, it was envisaged that the macrocyclisation could be accomplished by Grubbs' ring closing metathesis. Therefore, commercially available 2-(allyloxy)ethan-1-ol was tosylated overnight with tosyl chloride, catalytic amount of 4-dimethylaminopyridine (DMAP), and triethylamine (NEt_3) in DCM, to furnish **26** in 73% yield. The tosyl group was then substituted with an azide group by heating with NaN_3 in DMF at 75 °C overnight to achieve **27** in 89% yield (Scheme 2.2).

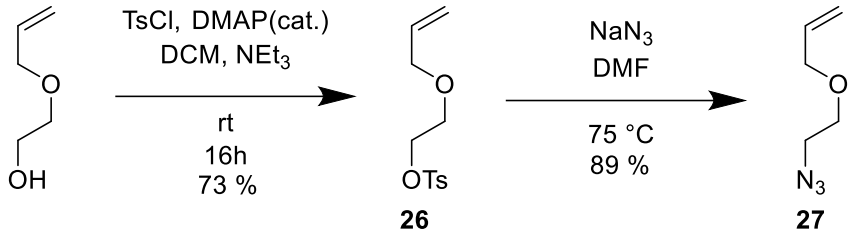

Scheme 2.2. Synthesis of azide **27.**

With both azide **27** and PDI bisalkyne **23** in hand, copper-catalysed azide-alkyne cycloaddition (CuAAC) proceeded by first dissolving both compounds in dry DCM. Then, under an inert atmosphere of N_2, was sequentially added TBTA and catalytic $Cu(MeCN)_4{\bullet}PF_6$, forming bisalkene **28** in 72% yield (Scheme 2.3).

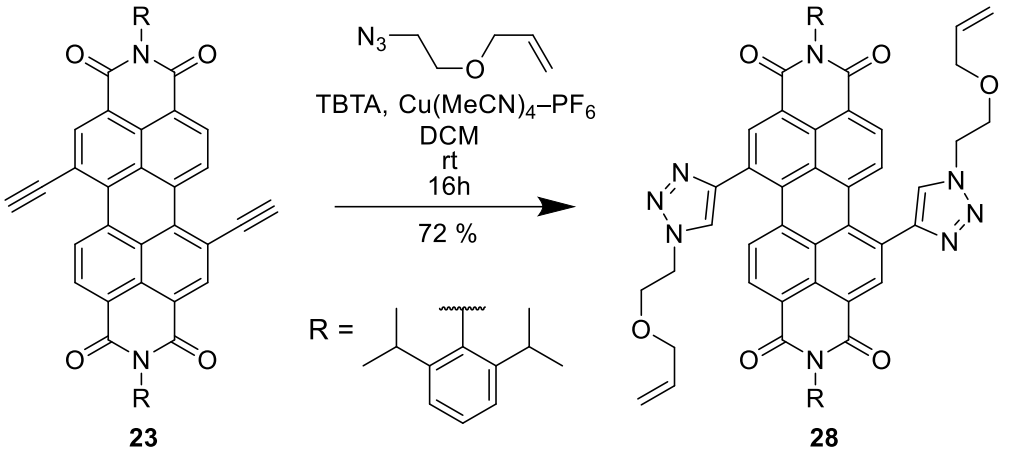

Scheme 2.3. Synthesis of PDI bisalkene **28.**

To encourage the formation of [1+1] macrocycle over larger macrocycles or oligomers, high dilution conditions were necessary to favour intramolecular macrocyclisation reaction over intermolecular alkene metathesis. As such, under high dilution conditions, PDI bisalkene **28** was stirred with 10% w/w Grubbs' II RCM catalyst in dry DCM at a relatively low concentration of 0.0004M, and the reaction was montitored by TLC. Unfortunately, no product could be observed by neither MALDI nor ESI mass spectroscopy after four days, and instead, the TLC showed mainly starting materials. Over time, TLC showed the slow formation of highly polar compounds that barely moved from the baseline, which suggests that these compounds contain multiple polar triazole units, i.e. large macrocycles or

oligomers. Additionally, visual inspection identified insoluble precipitate, which was also presumed to be oligomeric side products (Scheme 2.4).

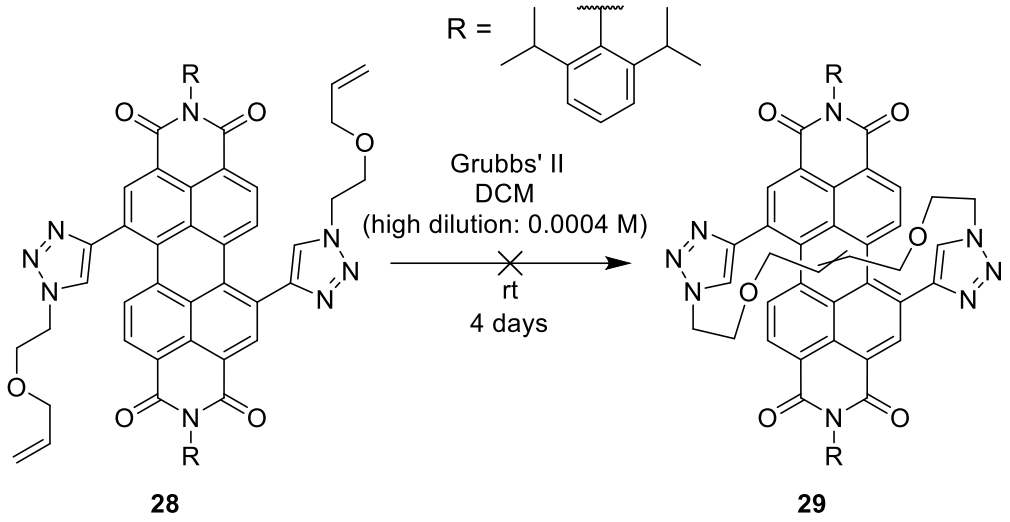

Scheme 2.4. Attempted synthesis of PDI macrocycle **28.**

Further attempts via Grubbs' RCM, including a higher catalytic load of 20% w/w Grubbs' II catalyst, heating to 40 °C, and for longer duration of one week were all also unsuccessful in generating a macrocycle. Additionally, other members in the group have attempted Grubbs RCM with different PDIs and linkers also yielded no macrocycle. There exists no literature precedent of a PDI macrocycle synthesised by Grubbs RCM, in which the imide functional groups are present. This led to the pursuit of an alternative strategy, amide condensation.

2.2.3 PDI Macrocycle Synthesis: Strategy B – Amide Condensation

It was envisaged that formation of the macrocycle could be achieved by an amide condensation reaction. This could be achieved by functionalising the PDI with an amine group and reacting with acid chlorides. Acid chlorides were chosen instead of carboxylic acids due to their higher electrophilicity, with Cl^- an excellent leaving group, in addition to improving solubility in organic solvents. It was also envisaged that a xylyl spacer could be

added to the PDI, with its rigidity decreasing the entropic cost in macrocyclisation, and also avoiding the formation of explosive low C/N ratio azides. Therefore, commercially available 1,4-bis(chloromethyl)benzene **30** was reacted with NaN_3 in DMF at 70 °C overnight to form bisazide **31** in quantitative yield. After which, a Staudinger reduction was performed by a slow dropwise addition of PPh_3 in EtOAc to a vigorously stirring mixture of bisazide **31** in Et_2O and 2.5M $HCl_{(aq)}$ at 0 °C, which was left to stir at room temperature overnight. This formed the mono-reduced xylene **32** after an aqueous workup and basifying with 1M $NaOH_{(aq)}$. Flash silica gel column chromatography with a 20:1 DCM:MeOH eluent mixture isolated pure **32** in 40% yield. Next, the primary amine must be protected prior to CuAAC reaction to avoid both coordination and thus poisoning of Cu(I) catalyst, and the unwanted nucleophilic attack of the Cu(I) activated alkyne. Thus, amine **32** was then quantitively protected by a tert-butyloxycarbonyl (Boc) protecting group by reaction with Boc_2O in NEt_3 and DCM overnight to achieve **33** in 87% yield. This, combined with PDI bisalkyne **23**, underwent CuAAC, and a simple deprotection with TFA in DCM to furnish **34** in 48% yield over 2 steps (Scheme 2.5).

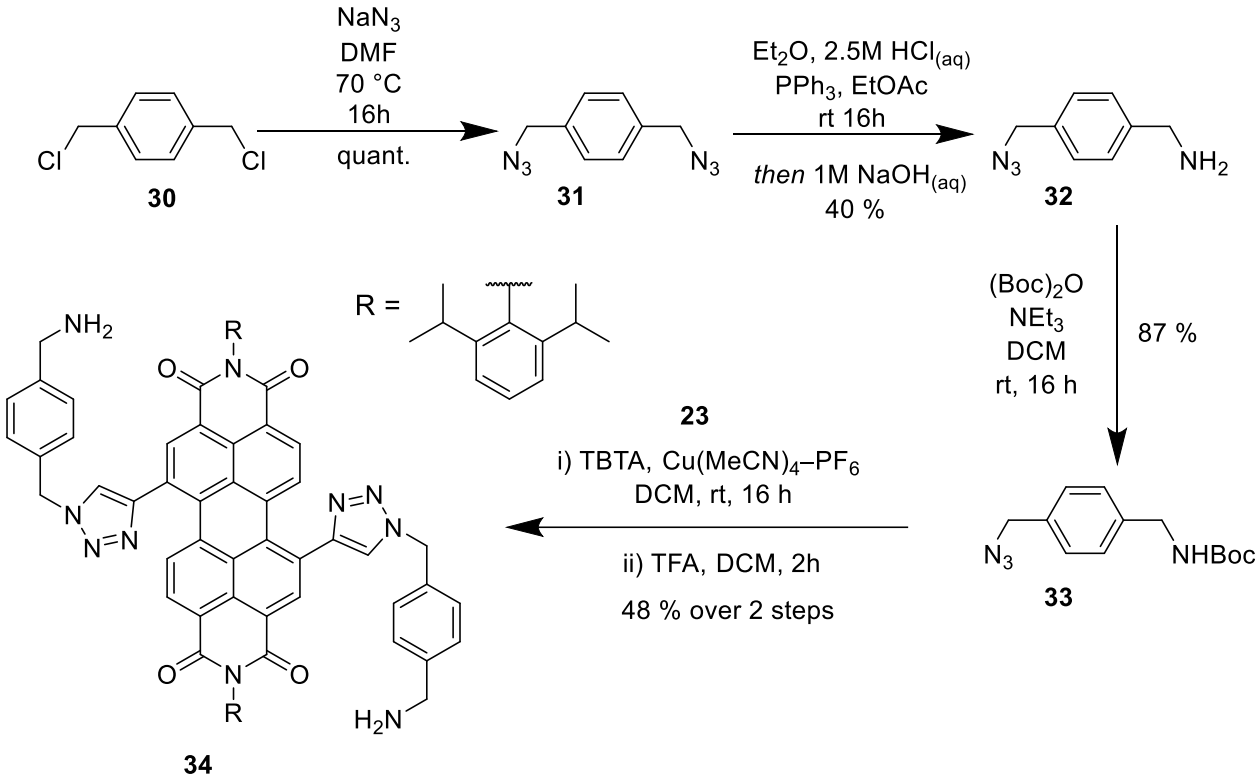

Scheme 2.5. Synthesis of PDI bisamine **34**.

Having isolated amine **34**, a test reaction was first performed with propionyl chloride in NEt_3 and DCM under relatively high dilution conditions (0.001M), which successfully achieved **35** overnight in quantitative yield. This shows that reaction of acid chloride and amine is facile in the presence of PDI in such low concentrations, and that both starting material and products are stable under these conditions (Scheme 2.6).

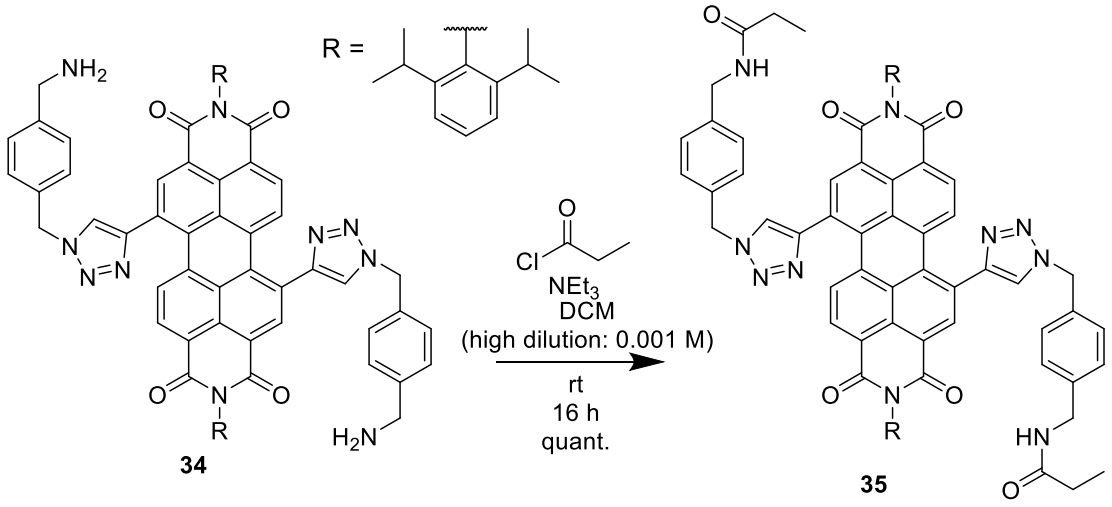

Scheme 2.6. Synthesis of **35**.

To prepare the bisacid chloride straps, decanedioic acid was added to oxalyl chloride in a mixture of DCM and DMF and stirred at 42 °C for four hours to quantitively yield decanedioyl dichloride **36**. Under high dilution conditions (0.0005 M), this was added to bisamine **34** in NEt_3 and DCM, which, after four days, did not yield the intended [1+1] macrocycle. Instead, the larger [2+2] macrocycle was confirmed to be formed by MALDI mass spectrometry, with other polar side products that may include [3+3] or larger macrocycles or oligomers (Scheme 2.7). These were not isolated since a [1+1] macrocycle was the target due to its potential for chiral locking.

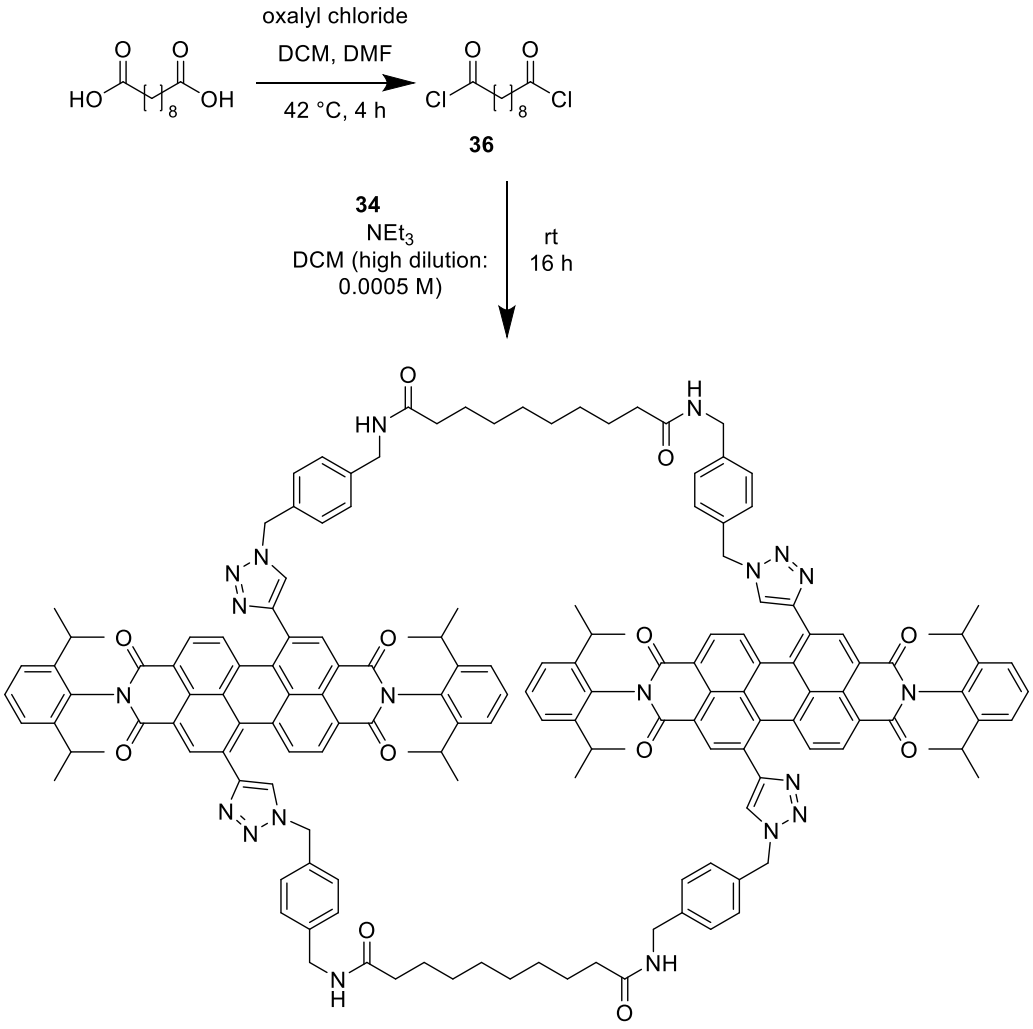

Scheme 2.7. Synthesis of **36**, and its macrocyclisation reaction leading to formation of the [2+2] macrocycle.

It was hypothesised that the decanediol dichloride may be too flexible to form the desired [1+1] macrocycle, and so, a rigid derivative of the strap **37**, similarly synthesized, was also reacted with amine **34** under identical conditions. It was envisaged that the rigidity of the aryl groups on **37**, in addition to the rigidity of bisamine PDI **34**, may provide favourable preorganisation to form the [1+1] macrocycle, akin to putting a lid on a box. Unfortunately, this reaction also only led to [2+2] or larger macrocycles as identified by MALDI mass spectrometry (Scheme 2.8).

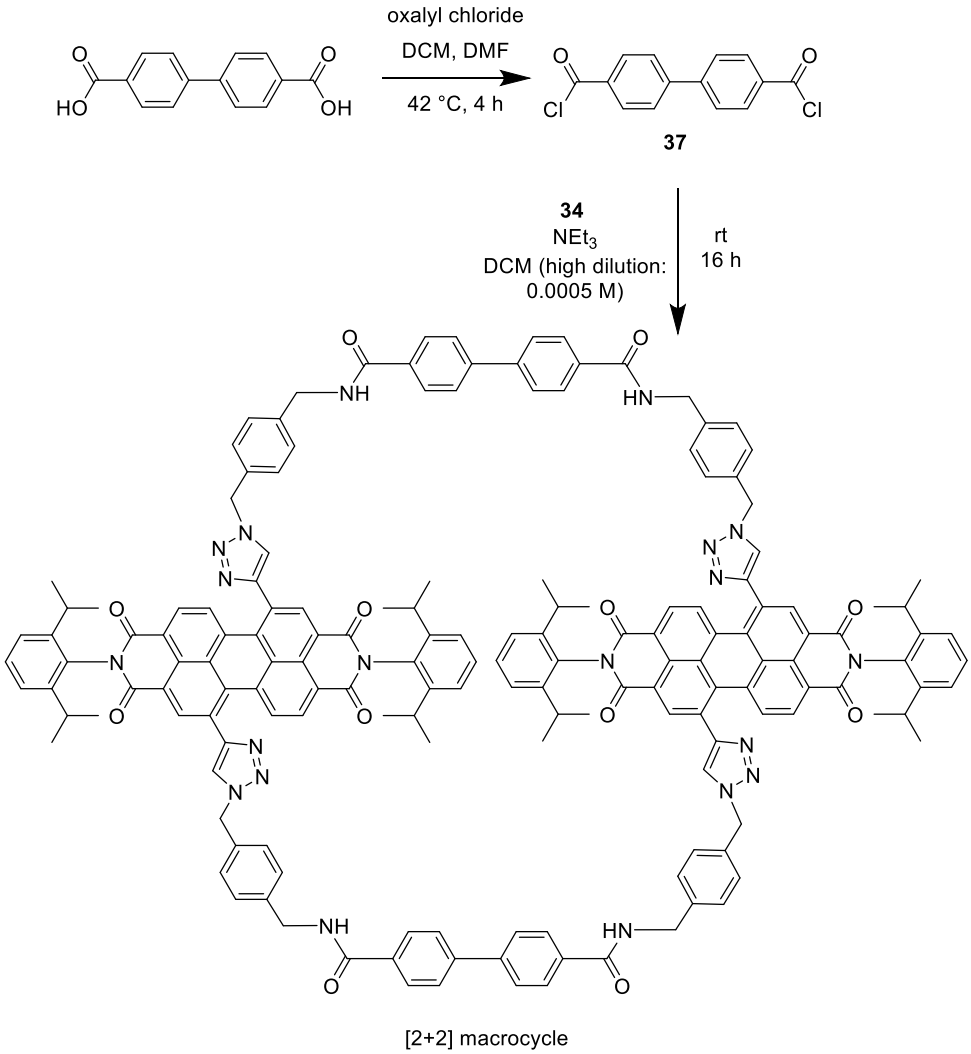

Scheme 2.8. Synthesis of **37**, and its macrocyclisation reaction leading to formation of the [2+2] macrocycle.

2.2.4 PDI Macrocycle Synthesis: Strategy C – Direct CuAAC

It was hypothesised that [2+2] or larger macrocycles are more energetically favourable to be formed relative to a smaller [1+1] macrocycle, as the latter will have a high ring strain. The rate determining step of a [1+1] macrocyclisation reaction is likely to be the second reaction (i.e. the formation of the macrocycle itself), and such in the amide condensation strategy above, there is no intramolecular interaction to lower the energetic cost. Thus, it was hypothesised that incorporating a π-electron rich aromatic unit would make it more favourable for the strap to pass over the PDI, and form a [1+1] macrocycle.

Aforementioned, CuAAC is a well known and facile reaction. And so, a strategy was developed to directly achieve macrocyclization via CuAAC. Three electron rich linkers were initially chosen in this strategy – a glycol chain (PEG_2), 1,5-dihydroxy naphthalene (DHN), and hydroquinone (HQ). These linkers can help understand the variables needed to form a [1+1] macrocycle, as well as the possible donor-acceptor interactions between the strap and the PDI core, including π-interactions (PEG cf. other two), and the size of the π-surface (DHN cf. HQ). The length of all three straps are comparable, where this length was initially chosen such that they are short enough to geometrically prevent the final PDI macrocycle from racemising by ‘somersault’ (*vide infra*), yet long enough to form the [1+1] macrocycle without a large ring strain. Additionally, a HQ linker with a longer

strap length was also targeted to investigate the effects of linker length on the yield and interactions between the strap and the PDI core (Figure 2.7).

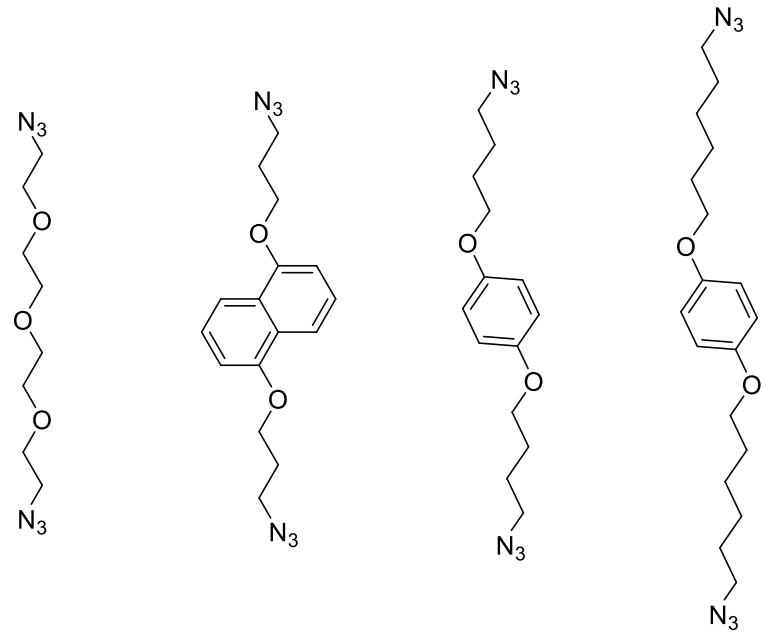

Figure 2.7. Four electron rich straps for the CuAAC macrocyclisation of PDIs – glycol chain (PEG_2) **38**, 1,5-dihydroxy naphthalene (DHN) **39**, and two hydroquinone linkers of different lengths (HQ-4 and HQ-6) **40** and **41.**

To synthesise the flexible PEG_2 linker, commercially available tetraethylene glycol was tosylated with tosyl chloride and catalytic DMAP in NEt_3 and DCM overnight to yield **42**. Reaction with NaN_3 then gave the azide strap **38** (Scheme 2.9).

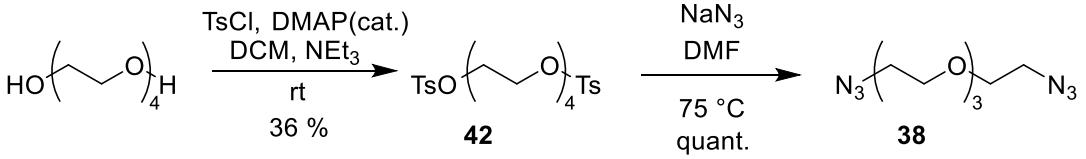

Scheme 2.9. Synthesis of azide straps **38.**

The higher rigidity straps **39**, **40** and **41** were synthesised next. Commercially available 1,5-dihydroxy naphthalene (DHN) was alkylated with an excess of 1,3-dibromo propane and K_2CO_3 in acetone at 60 °C over three days to furnish **43** after purification by flash

column chromatography. After which, reaction with NaN_3 quantitively yielded the bis-azide strap **39** (Scheme 2.10).

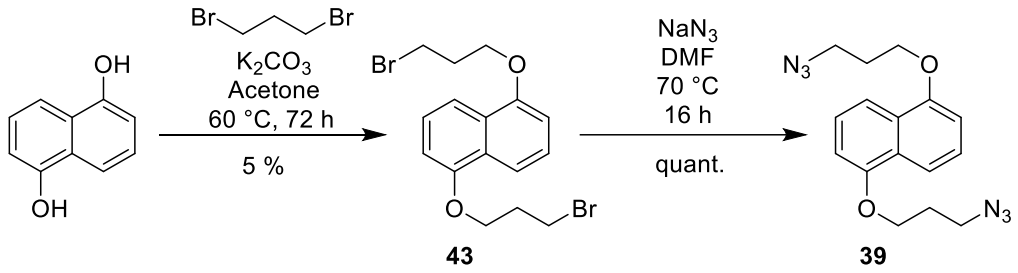

Scheme 2.10. Synthesis of bis-azide straps **39.**

Using the same methodology to synthesise DHN strap **39**, hydroquinone was alkylated with excess 1,4-dibromo butane and K_2CO_3 in acetone at 60 °C over three days to give **44** in 25% yield after purification. Reaction with NaN_3 quantitively yielded the azide strap **40**. A longer strap was also synthesised in the same manner using 1,6-dibromo hexane instead of 1,4-dibromobutane to furnish **45** then **41** in 79% and quantitative yields respectively (Scheme 2.11).

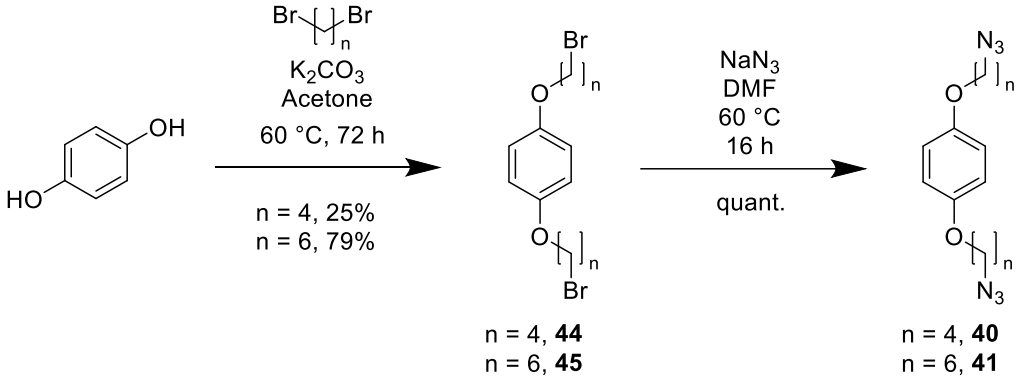

Scheme 2.11. Synthesis of HQ straps **40** and **41**.

Having successfully synthesised all four bis-azide straps, macrocyclisation proceeded via CuAAC by reacting each strap with **23** under high dilution (0.0005 M). The polyethylene glycol strap **38** once again only yielded [2+2] or larger macrocycles, whilst the other three π-donating straps **39** (DHN), **40** (HQ-4) and **41** (HQ-6) formed the desired [1+1] macrocycles **46**, **47**, and **48** in 24%, 16% and 23% yields respectively. This suggests that non-covalent aromatic interactions, such as π−π and CH−π interactions, between the π-electron rich strap and the π-electron poor PDI may be important in the formation of such

strained macrocycles. For valuable comparisons with the [1+1] macrocycles, acyclic control compounds **49** and **50** were also synthesised by this method but instead reacted at a much higher concentration and a large excess of strap (Scheme 2.12).

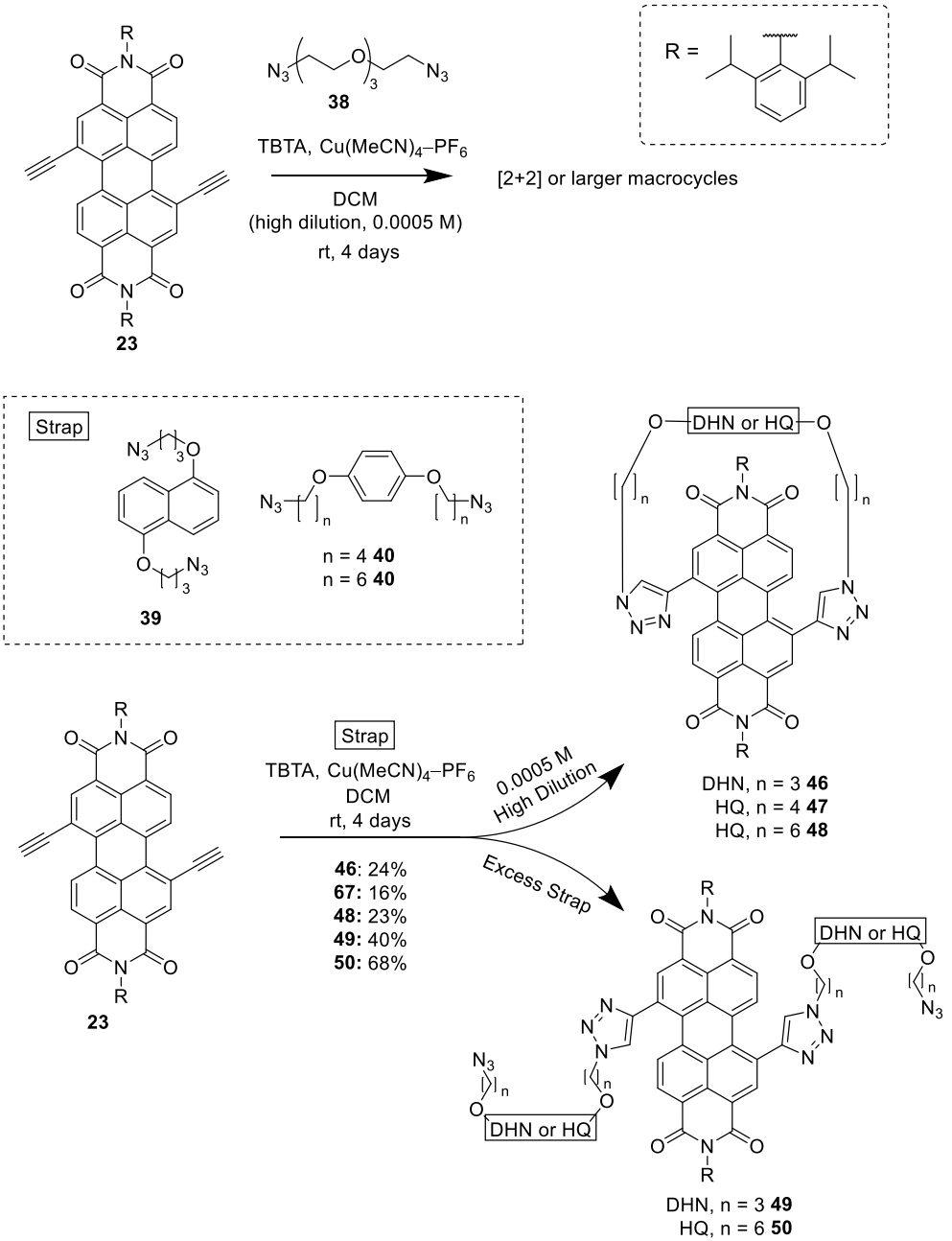

Scheme 2.12. Top: CuAAC of PEG_2 strap **38** with PDI **23**. Bottom: CuAAC of strap **39** (DHN), **40** (HQ-4), and **41** (HQ-6), with PDI **23** to form macrocycles **46**, **47** and **48,** and acyclic compounds **49** and **50**.

An bis-triazole acyclic control compound without any aromatic groups in the linkers was also prepared for later comparisons with the [1+1] macrocycles. Here, CuAAC of 1-bromohexane and PDI bisalkyne gave **51** in 67% yield after purification by silica gel flash column chromatography (Scheme 2.13). The investigation of the non-covalent interactions in [1+1] macrocycles will be aided by comparison against all these acyclic control compounds, and will be discussed in detail in Section 2.3.

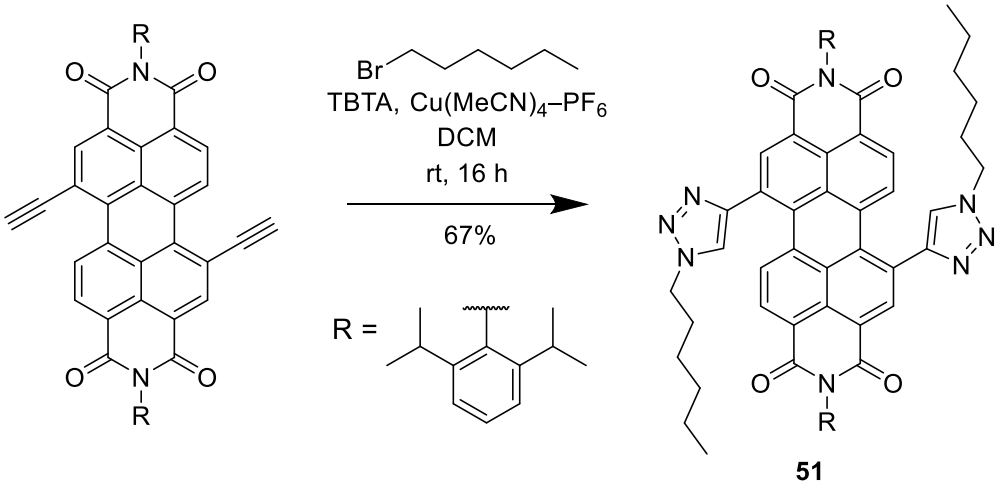

Scheme 2.13. Synthesis of acyclic control compound **51**.

2.3 Characterisation of [1+1] Macrocycles

For the macrocycles, only the 1,7-regioisomers were isolated by traditional silica gel column chromatography, mean either the yield of the [1+1] 1,6-regioisomer is too small to be isolated, or the 1,6-regioisomer [1+1] is not formed at all. It was important to determine that the isolated product is indeed the desired 1,7-regioisomer and not the 1,6-regioisomer. Note that whilst the number of quaternary carbon environments are different in the two regioisomers, and thus the number of these signals would be different in their ^{13}C NMR spectra, it was difficult to determine the number of these carbon signals as they are weak and may be overlapping. Thus, $^{1}H–^{13}C$ HMBC NMR spectroscopy was performed. In the 1,7-regioisomer, two protons on the ortho position of the PDI core (H_a, singlet, red; and H_b, doublet, blue) are both three atoms away from the carbon (orange), thus both should

exhibit a $^{1}H-^{13}C$ HMBC NMR signal to that same carbon. However, in a 1,6-regioisomer, the same protons are too distant to exhibit $^{1}H-^{13}C$ HMBC NMR signal to any of the same carbon nuclei. It is also important to note that the two doublet protons on the bay (H_c, black) and ortho (H_b, blue) positions of the PDI were distinguished based on the ortho protons H_b exhibiting a $^{1}H-^{13}C$ HMBC NMR signal to a very downfield shifted carbonyl (amide) carbon, whereas the bay protons H_c do not (Figure 2.8). This analysis was performed to characterise and confirm all 1,7-regioisomers in this thesis.

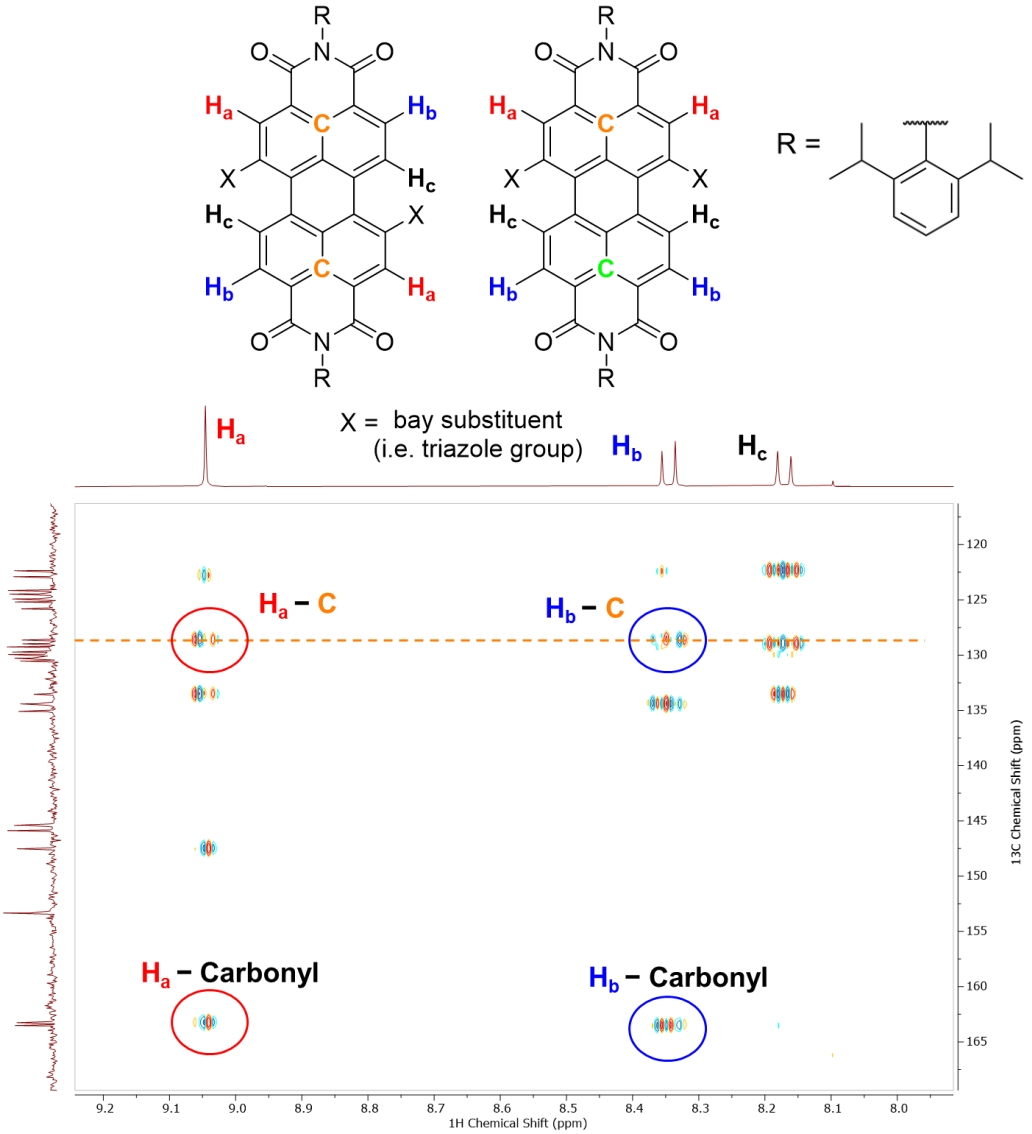

Figure 2.8. Top) 1,7- (left) and 1,6- (right) regioisomers of PDIs. Bottom) $^{1}H-^{13}C$ HMBC NMR spectrum of macrocycle **46** ($CDCl_3$, 298 K, 400 MHz (^{1}H), 101 MHz (^{13}C)).

For the acyclic variants **51**, **49** and **50**, the 1,7- and 1,6-regioisomers could not be separated by traditional silica gel flash column chromatography. It was important to determine if the presence of the 1,6- regioisomer in the acyclic has any impact on the later spectroscopic analysis performed. As such, **51** and **50** were subjected to high-performance liquid chromatography (HPLC) using a COSMOSIL Buckyprep Packed Column to separate the regioisomers. The conditions used were initially based on those used for chiral HPLC described in Section 2.5, where after several optimisation the 1,7-regioisomer were successfully isolated by elution with a 0.1:39.9:60.0 n-hexane:CH_2Cl_2:IPA mixture. The pure 1,7-regioisomer enabled direct comparisons with the regioisomeric mixtures. There was no impact on ^{1}H NMR, ^{13}C NMR, or UV-vis absorption spectra from the presence of the 1,6-regioisomer. Therefore acyclic were used as a mixture for time and solvent efficiency.

2.4 Macrocycle Conformational Analysis

As discussed above, non-covalent π interactions, such as π−π and CH−π interactions, between the π-electron rich strap and the π-electron deficient PDI may be important in the formation of strained [1+1] macrocycles. By characterising the macrocycle conformation, it was hoped to understand such interactions in their potential role of templating, by comparing the prevalence of these interactions in macrocycle against acyclic controls, including π-surface size (DHN cf. HQ-4), and linker length (HQ-6 cf. HQ-4). First, it is important to show that these interactions may be characterised by spectroscopic techniques.

2.4.1 Conformation in Solid State – Single Crystal XRD

Crystals of HQ macrocycle **47**, suitable for single crystal X-ray diffraction, were grown from a solution of **47** dissolved in $CHCl_3$, with slow diffusion of n-hexane (antisolvent). These crystals were subjected to single crystal X-ray diffraction in collaboration with members of

the Champness group, where Jennifer Robertson mounted and performed the crystallography, and Georgia R. F. Orton processed and solved the crystallographic data. The crystal structure displays a π–π interaction (d(π–π) = 3.7 Å) between the π-electron rich hydroquinone group and the π-electron deficient PDI group. Unfortunately, crystals of other macrocycles were unable to be grown (Figure 2.9, top). This provides strong evidence that **47** adopts a conformation where donor-acceptor π–π interaction is prevalent in the solid state. The crystal structure also shows that the PDI is twisted with a dihedral angle of 16°, with the triazoles pointed in the direction of the macrocyclic cavity to minimise ring strain, unlike bis-PDI macrocycles ([2+2]) synthesised by the group which shows triazoles are directed away to maximise π–π interaction between the PDIs (Figure 2.9, bottom). This suggests that ring strain is an important factor when considering the formation of a [1+1] macrocycle.

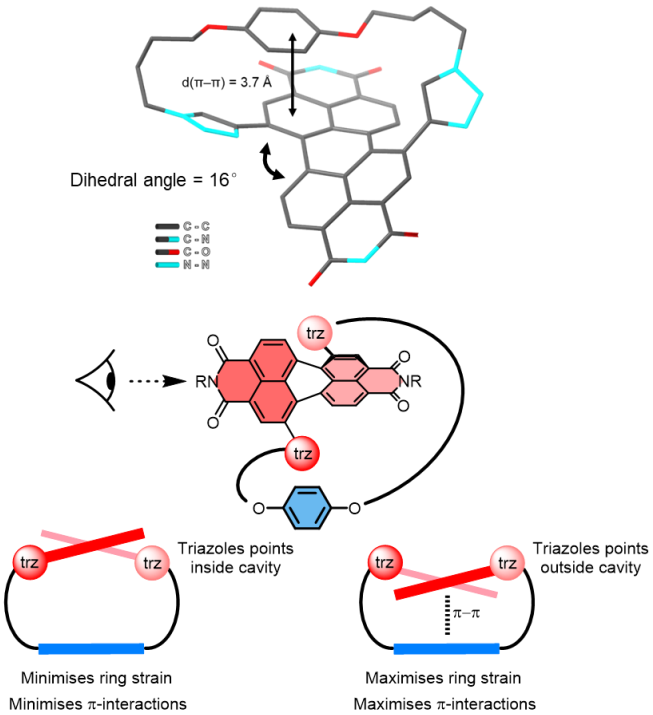

Figure 2.9. Top: X-ray crystal structure of macrocycle **47**. For clarity, hydrogen atoms and the 2,6-diisopropylphenyl imide substituents have been removed from the structure. Bottom: diagram displaying the different conformations of PDI macrocycles, where one minimises ring strain but minimises π-π interactions (left) and the other maximises ring strain but also maximises π-π interactions (right).

2.4.2 Conformation in Solution – NMR Spectroscopy and Photophysics

Next, it was important to provide evidence that this π–π interaction observed in the solid state confirmation is also present in the confirmation when in solution, which could be achieved by ^{1}H NMR, UV-vis and fluorescence spectroscopy.

2.4.2.1 ^{1}H NMR Spectroscopy

Comparing the ^{1}H NMR spectra in $CDCl_3$ of HQ macrocycles **47** (Figure 2.10d) and **48** (Figure 2.10c) against those of acyclic control compounds **51** (Figure 2.10a) and **50** (Figure 2.10b), the PDI protons $H_{a\text{-}c}$ of the macrocycles are shifted downfield, whilst HQ protons $H_{d,d'}$ are shifted upfield, indicating the proximity and π-π interaction between the HQ and the PDI core.[108] Note that the chemical shifts are much more significant in the shorter **47** macrocycle (Figure 2.10d), which indicates that the HQ unit is closer and thus interacting more strongly to the PDI core in the shorter length macrocycle.

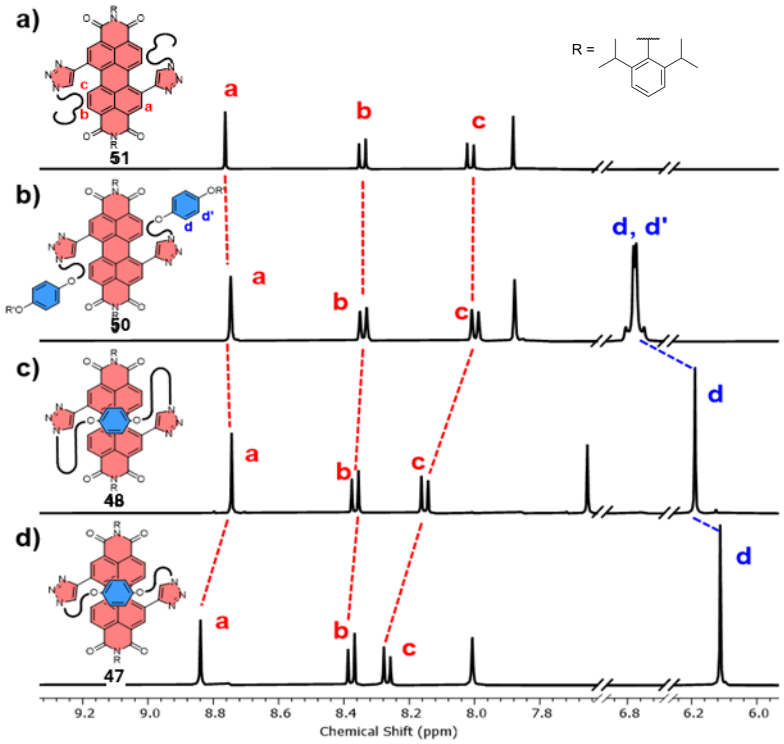

Figure 2.10. Stacked ^{1}H NMR spectra of a) acyclic bis-triazole PDI **51**, b) acyclic bis-HQ PDI **50**, c) HQ–PDI macrocycles **48** and, d) **47** ($CDCl_3$, 298 K, 400 MHz).

The ^{1}H NMR spectra of acyclic control compounds **51** and **50** (Figure 2.10a,b) show identical shifts of the PDI core, suggesting that there is no interaction between the π-electron rich HQ group and the π-electron deficient PDI core. Therefore, the macrocyclic framework preorganises the π-conjugated units in solution and is key to a donor-acceptor π-π interaction between the aromatic linker and the PDI. It is possible that, in the rate determining step (2nd CuAAC step – i.e. formation of the macrocycle) of the macrocyclic synthesis, where the transition state is akin to that of the macrocycle, there also exists a donor-acceptor π-π interaction. This templating interaction may reduce the enthalpic cost arising from ring strain. In other words, the presence of a π-donating HQ group may template macrocyclisation in the transition state by an intramolecular donor-acceptor π-π interaction (Figure 2.11).

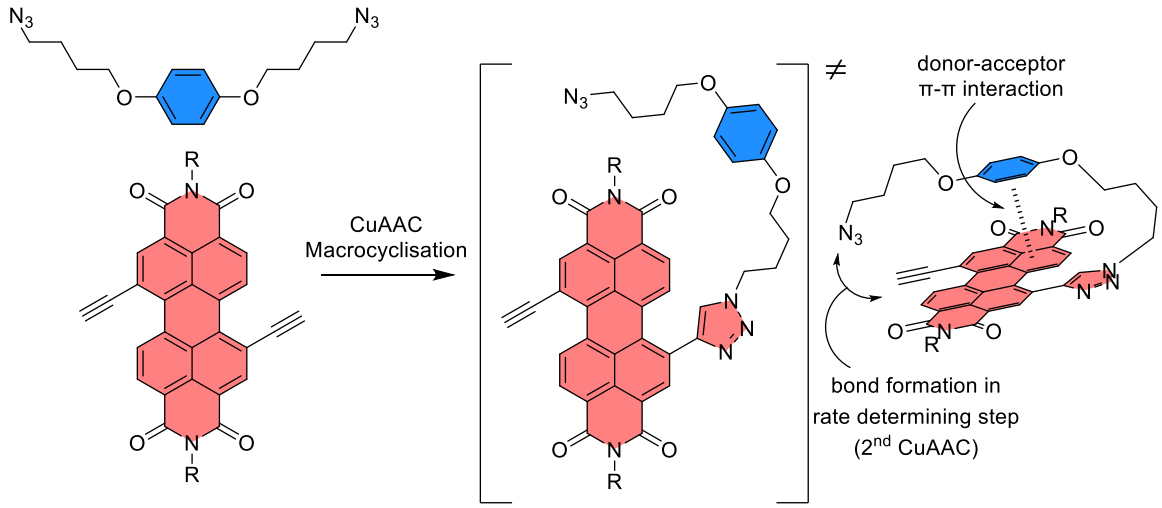

Figure 2.11. Potential donor-acceptor π-π interaction between the aromatic linker (blue) and the PDI (red) in the rate determining transition state of the macrocyclisation reaction.

In the ^{1}H NMR spectrum of the DHN macrocycle **46**, signals are also shifted in the similar way compared to acyclic control compounds **51** and **49**, with protons $H_{a\text{-}c}$ shifted downfield and $H_{d\text{-}f}$ shifted upfield (Figure 2.12). This shows that DHN, with a larger π-surface, behaves similarly to that of HQ in terms of potential for macrocycle synthesis templation.

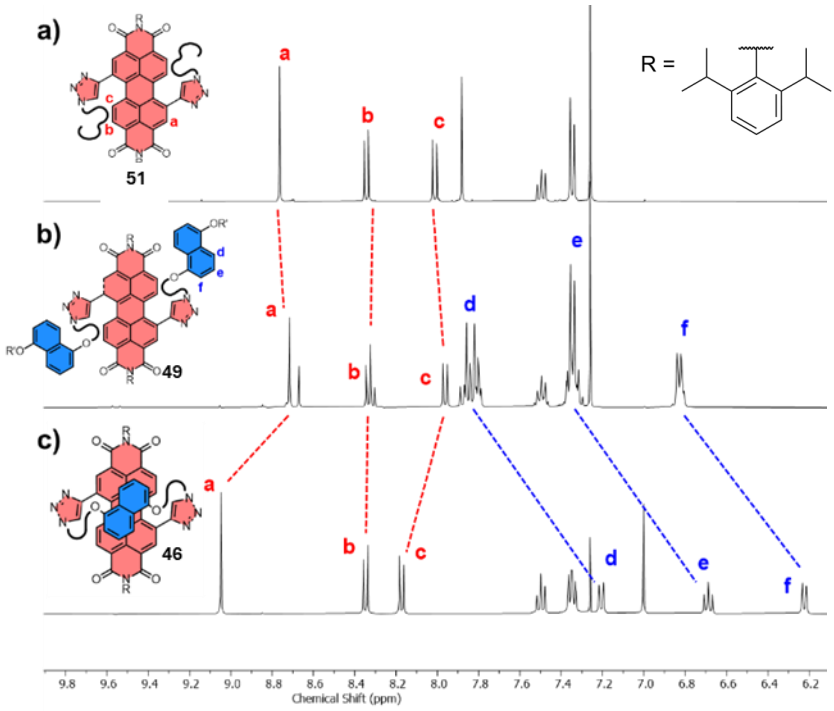

Figure 2.12. Stacked ^{1}H NMR spectra of a) acyclic bis-triazole PDI **51**, b) acyclic bis-DHN PDI **49**, c) DHN–PDI macrocycles **46** ($CDCl_3$, 298 K, 400 MHz).

2.4.2.2 Photophysics

A conformation of the macrocycle that facilitate intramolecular π-π interactions between π-donor and π-acceptor was also assessed by UV-vis and fluorescence spectroscopy. Here it is important to clarify that π–π interactions primarily consist of electrostatic and van der Waals contributions,[109] with the former readily probed by UV-vis absorption spectroscopy since red-shifted charge transfer absorbances can be a consequence of donor–acceptor interactions.[110] A clear red shift (Δλ = 12-14 nm) in the UV-vis absorption spectrum of the main PDI absorption band (S_0-S_1) can be seen in macrocycles **47** and **46** compared to acyclic compound **51** (Figure 2.13a) in $CHCl_3$, suggesting donor-acceptor π-π interactions are present between the electron rich aromatic donor (DHN or HQ) and the electron poor aromatic acceptor (PDI). Note that the acyclic HQ or DHN compounds **50** and **49** are not red shifted compared to acyclic compound **51** (Figure 2.13b). This supports the conclusions derived in ^{1}H NMR spectroscopy, where the macrocyclic framework preorganises the π-conjugated units in solution and is key to a donor-acceptor π-π

interaction observed in the solid state. A control experiment was performed in which 1000 equivalents of hydroquinone were added to acyclic **51**, where there was no change to UV-vis absorption spectra, further suggesting that donor-acceptor π-π interactions are intramolecular in nature and require the macrocyclic architecture. Additionally, the absence of a red shift in the longer strapped HQ macrocycle **48** compared to the acyclic compounds indicates that this donor acceptor interaction is significantly weaker with longer straps, suggesting that the macrocycle will adopt a conformer that minimises ring strain if possible, which increases the distance between donor and acceptor units (Figures 2.9 and 2.13c).

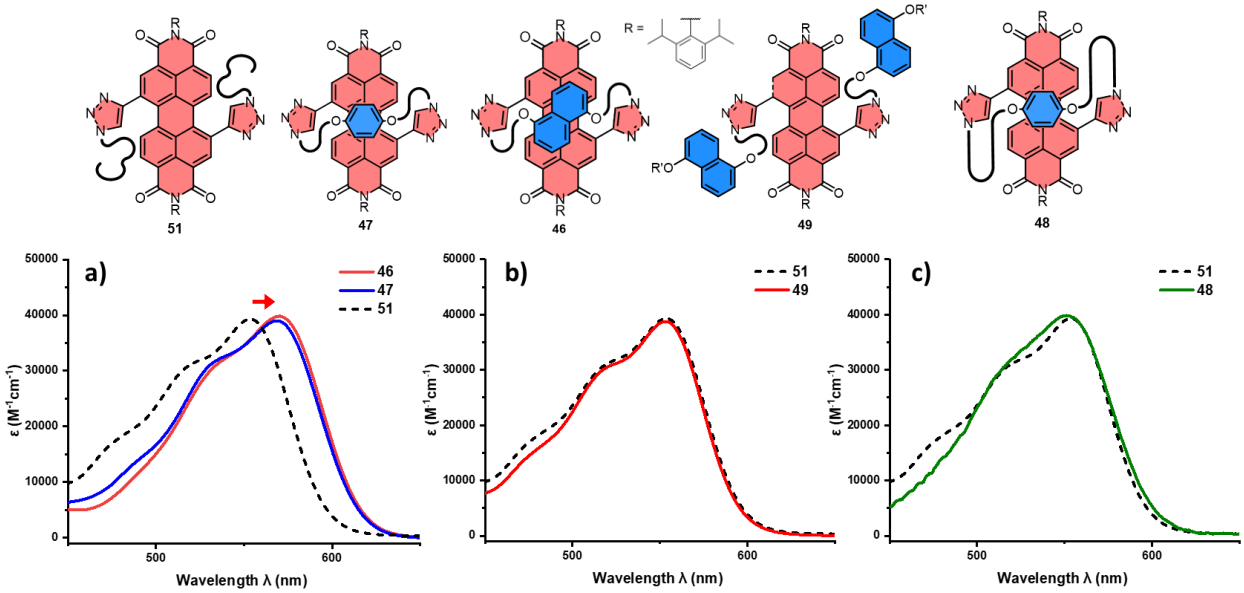

Figure 2.13. UV-vis absorption spectra of compounds a) **46** (red), **47** (blue), and **51** (black, dotted); b) **49** (red) and **51** (black, dotted); c) **48** (green) and **51** (black, dotted). All spectra were recorded in $CHCl_3$ at a concentration of 26 μM in a quartz cuvette with 1 cm path length.

Fluorescence spectroscopy supports the findings from UV-vis absorption spectroscopy, with compounds exhibiting similar red shifts in the emission spectra. Relative to the acyclic **51**, macrocycles **46** and **47** are both redshifted (Figure 2.14a). The acyclic DHN compound **49** is not redshifted (Figure 2.14b), and longer strapped HQ-PDI macrocycle **48** is slightly red shifted (Figure 2.14c). The Stokes shifts of the macrocyclic compounds (λ = 47-56 nm) are comparable, though slightly larger, to that of the acyclic compounds (λ = 45 nm), and

that there is no significant difference in the broadness of the emission spectra, which suggests that exciplex molecules are not formed.[111]

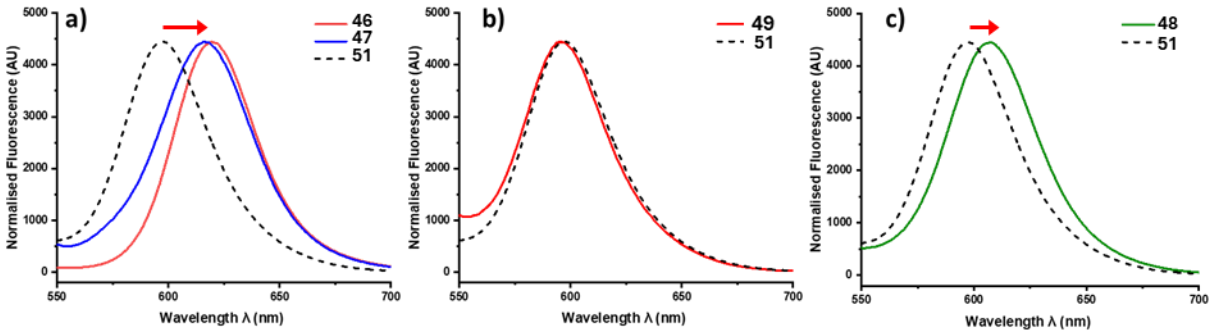

Figure 2.14. Normalised (to 45000) fluorescence spectra of compounds a) **46** (red), **47** (blue), and **51** (black, dotted); b) **49** (red) and **51** (black, dotted); c) **48** (green) and **51** (black, dotted). All spectra were recorded in $CHCl_3$ at a concentration of 26 μM in a quartz cuvette with 1 cm path length and excitation wavelength of 400 nm.

The donor acceptor π-interactions were also shown to be relatively independent of solvent when these solution studies were repeated in toluene (Appendix A). For example, ^{1}H NMR spectroscopy in toluene-d_8 shows a similar trend: comparing HQ macrocycles **47** and **48**, the shorter length **47** has PDI protons $H_{a\text{-}c}$ more shifted downfield and HQ protons $H_{d,d'}$ more shifted upfield. The lack of solvent dependency suggests that any π-π templation may also operate in other organic solvents of similar polarities.

2.4 Configurational Stability

To investigate the chiral locking (*i.e.* configurational stability) of macrocycles, DHN-PDI macrocycle **46** and both HQ-PDI macrocycle **47** and **48** were subjected to analysis by HPLC with a i-Amylose-1 chiral column from Phenomenex. A number of conditions were attempted in order to optimise the conditions (Table 2.1), where ideally, the two **P**/**M** enantiomers would elute without overlap of as quickly as possible (ideal total run time < 10 mins) to minimise time and solvent. Initially, a 50:50 n-hexane:CH_2Cl_2 ratio was attempted, where the two enantiomers, as confirmed by CD spectroscopy (*vide infra*,

Figure 2.16), were eluted after four and five minutes respectively, giving a large overlap between the elution times (Entry A). This was obviously not ideal, and so, the ratio was adjusted to an 80:20 n-hexane:CH_2Cl_2 ratio (Entry B). This new ratio was too apolar such that the macrocycles remained in the stationary phase after 30 mins. More polar eluent systems were attempted, where 70:30 and 60:40 n-hexane:CH_2Cl_2 ratio gave good separation between the enantiomers, but with long run times (Entry C, D). Next, a 55:45 n-hexane:CH_2Cl_2 ratio was attempted which needed a decent run time of 10 mins, but unfortunately had overlapping peaks (Entry E). As ratio of purely n-hexane and CH_2Cl_2 was unable to achieve separate enantiomers with a low total run time, a third solvent (isopropanol (IPA)) was added into the mix. A ratio of 70:29.5:0.5 n-hexane:CH_2Cl_2:IPA was attempted (the ratio of apolar n-hexane being increased to account for the highly polar IPA), which gave a run time of 20 mins (Entry F). Interestingly, the addition of the small amount of IPA sharpened the peaks, increasing the separation between the two enantiomers. Finally, optimal ratios of 60:39:1 and 60:38:2 n-hexane:CH_2Cl_2:IPA both gave good separation of enantiomers, with a total run time of less than 10 mins (Entry G,H). Therefore, **46**, **47**, and **48** were able to be separated into their ***P***/***M*** enantiomers by elution with 60:39:1 (**46**) or 60:38:2 (**47**, **48**) n-hexane:CH_2Cl_2:IPA (Figure 2.15). Integration of the chromatogram shows a 1:1 ratio of products was separated, indicative that these macrocycles were synthesised as a racemic mixture, as would be expected in the absence of chiral reagents.

Entry	Eluent Ratio			Enantiomer 1 Elution Time (min)	Enantiomer 2 Elution Time (min)	Total Run Time Needed (min)	Overlap?
	n-hexane	CH_2Cl_2	IPA				
A	50	50	0	4	5	8	Yes
B	80	20	0	N/A	N/A	>30	N/A
C	70	30	0	18	20	25	Yes
D	60	40	0	9	11	15	No
E	55	45	0	6	7	10	Yes
F	70	29.5	0.5	14	16	20	No
G	60	39	1	6	7	10	No
H	60	38	2	5.5	7	10	No

Table 2.1. Chiral HPLC conditions attempted to optimise conditions for macrocycle **46**.

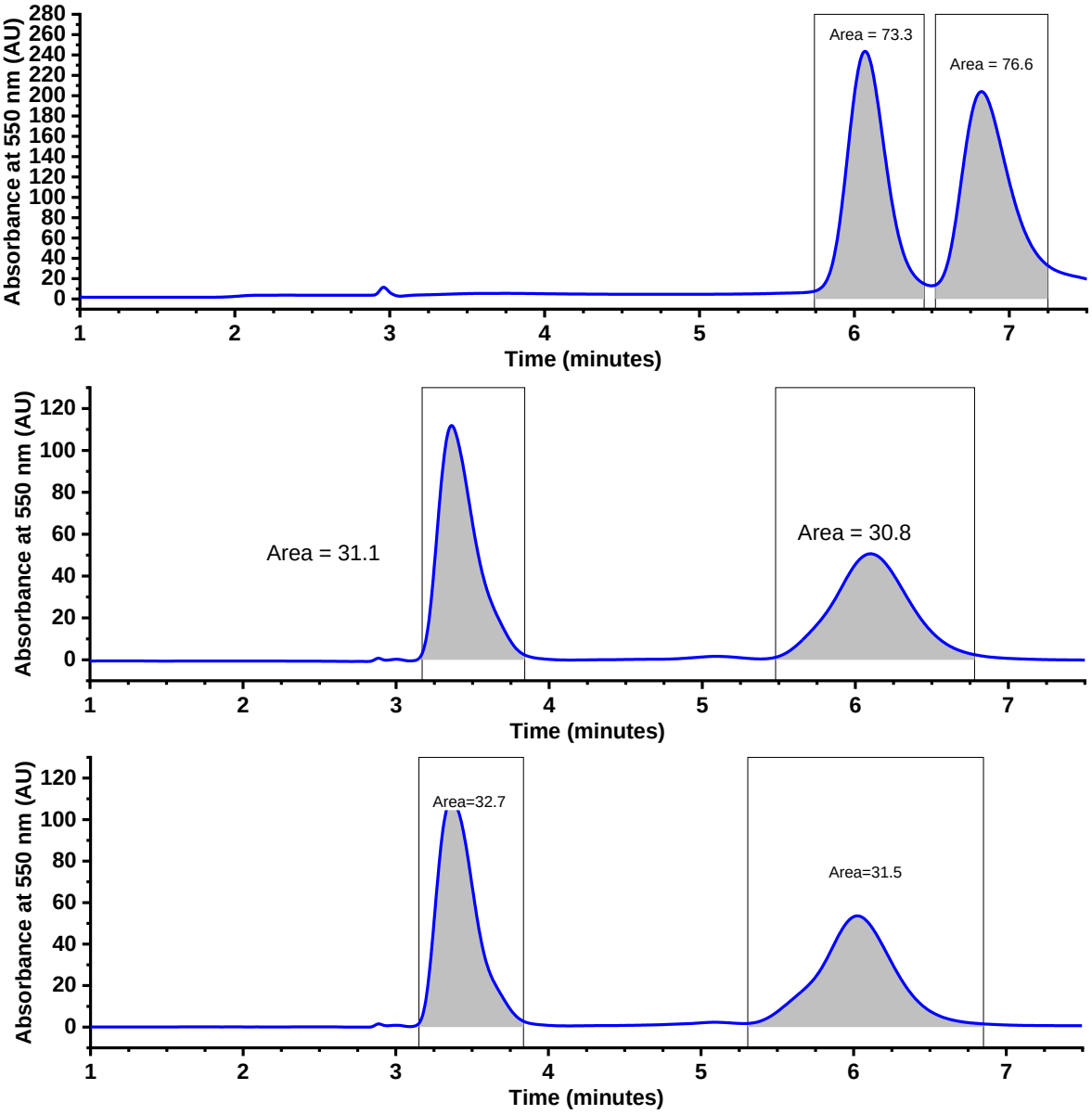

Figure 2.15. Chiral HPLC chromatogram of compounds **46** (top), **47** (middle) and **48** (bottom).

The isolated products were analysed by CD spectroscopy, where mirror image spectra confirmed the isolated products are indeed enantiomers (Figure 2.16). The CD spectra, in combination with time dependent density functional theory (TD-DFT) calculations of **47** were used the assign the chirality of these enantiomers. The computational studies were investigated by Prof Martijn Zwijnenburg from University College London, who performed conformer searches using the CREST code[112] and the GFN2-xTB tight-binding DFT

method,[113] followed by simulated absorption and CD spectra. This approach is supported by the fact that the predicted lowest energy conformer of macrocycle **47** is in agreement with the experimental X-ray crystal structure (Figure 2.9).

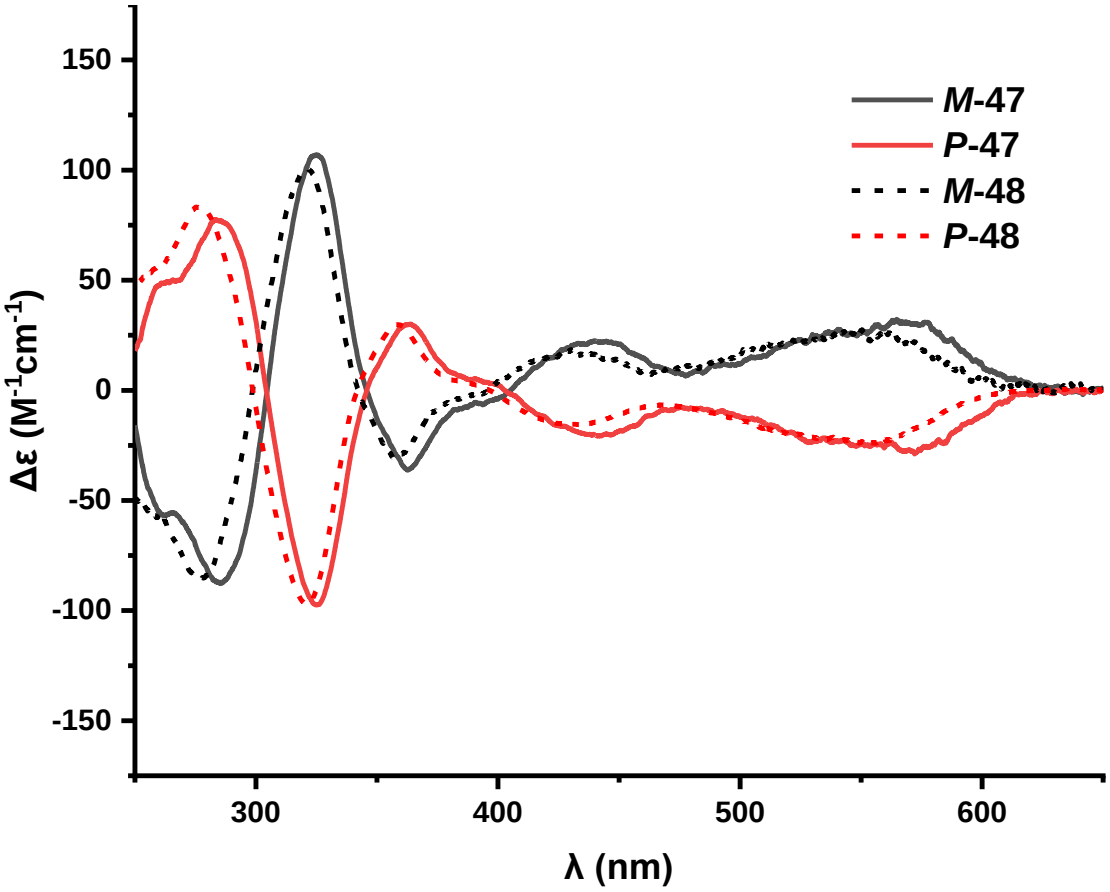

Figure 2.16. CD spectrum of **47** and **48**.

The isolated enantiomers of **46** were re-measured by CD spectroscopy, and also resubjected to identical HPLC conditions after one week. The enantiomers remained optically pure without racemisation, thus these macrocycles are shown to be configurationally stable at 25 °C.

The diisopropyl aniline imide group also displays evidence of chiral configurational stability in the ^{1}H NMR spectroscopy. As discussed earlier (Section 2.1.3), the methyl groups will clash with the PDI carbonyl O atoms, leaving the methyl groups situated above the PDI

core and also hindering rotation of the Ar—N bond. In the most simple case where the PDI core is not functionalised, all methyl groups on the diisoproyl aniline imide substituents are equivalent, and thus only one ^{1}H NMR signal is observed for these protons (Figure 2.17a). A chirally locked PDI, where all four bay-substituents are identical (Figure 2.17c), would desymmetrise the molecule such that the two methyl groups on the same diisoproyl group are in a diastereotopic relationship, and thus two ^{1}H NMR signals are observed. In other words, one methyl group (blue) is closer to the side twisted up, whereas the other methyl group (red) is further from the side twisted up, and thus are in different environments (Figure 2.17c). A chirally locked PDI where the 1,7- and 2,6- bay substituents are different, such as 1,7- substituted PDI (Figure 2.17d), would lead to the methyl groups on the top face (closer to 2,6- positions) being in a different environment to the bottom face (closer to 1,7- positions). In combination with the splitting of environments due to the twist, four ^{1}H NMR signals would be expected (Figure 2.17d). However, in PDIs with a low interconversion barrier, the PDI rapidly twists between the two conformers, and thus can be considered planar. Additionally, due to the pseudo-planarity of the PDI, the functionalised bay positions are far enough away from the methyl groups such that there is no influence to the environment of the diastereotopic methyl pair, and thus only one ^{1}H NMR signal is observed (Figure 2.17b).

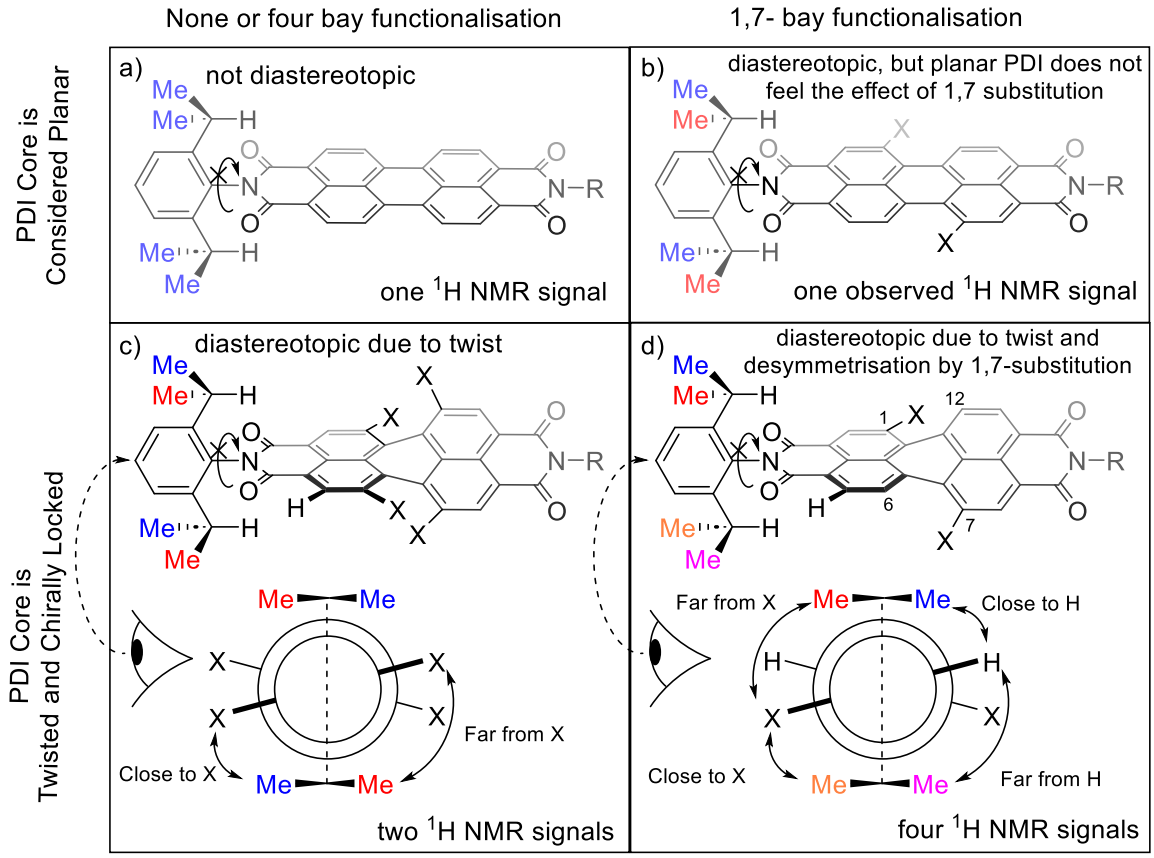

Figure 2.17. Diisopropyl analine imide group displaying different number of ^{1}H NMR signals based on the twist and substitution of the PDI core.

In chirally locked PDI macrocycles, the bay-strap renders the molecule unable to interconvert to its opposite enantiomer and thus, for ^{1}H NMR spectroscopy, all four methyl groups on one end of the PDI would be in different enviorments (*i.e.* four ^{1}H NMR signals). These four environments arise from diastereotopic splitting enhanced by the PDI twist (blue vs red; and orange vs magenta, Figure 2.18), in the same way as Figure 2.17c,d above. Since one face of the PDI core is strapped, the methyl groups on the top face are in a different environment to the bottom face, akin to Figure 2.17d above (note that Ar—N is hindered) (Figure 2.18).

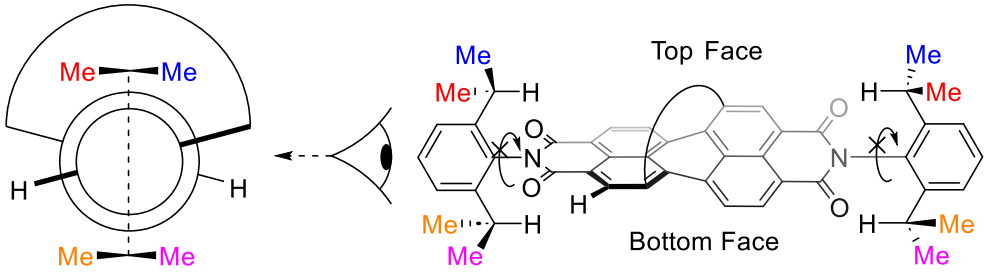

Figure 2.18. The four different environments (red, blue, orange, pink) of methyl group present in diisopropyl aniline imide group, should it be chirally locked in a macrocycle

Another way to rationalise this is to consider symmetry elements. In molecules with low interconversion barrier, where the PDI rapidly twists between the two enantiomers and so is considered planar, there exists three symmetry operations, such that all methyl groups are equivalent: 1) C_2 rotation about the centre of the perylene core that is orthogonal to the plane of the perylene core, 2) point of inversion, and 3) plane of symmetry in the plane of the aryl imide group. Once again, in 1,7-substituted PDI molecules, as the functionalised bay position are far enough away from the methyl groups to not influence the environment of the diastereotopic methyl pair, there can be considered a plane of symmetry in the plane of the aryl imide group for these molecules. This means that in a PDI where the PDI core are considered planar, the diisopropyl methyl groups will display only one ^{1}H NMR signal (Figure 2.19a). In a twisted acyclic PDI, the plane of symmetry no longer exists, thus the diisopropyl methyl displays two ^{1}H NMR signals (Figure 2.19b). In a chirally locked PDI macrocycle, the point of inversion also no longer exists, thus the diisopropyl methyl displays four ^{1}H NMR signals (Figure 2.19c).

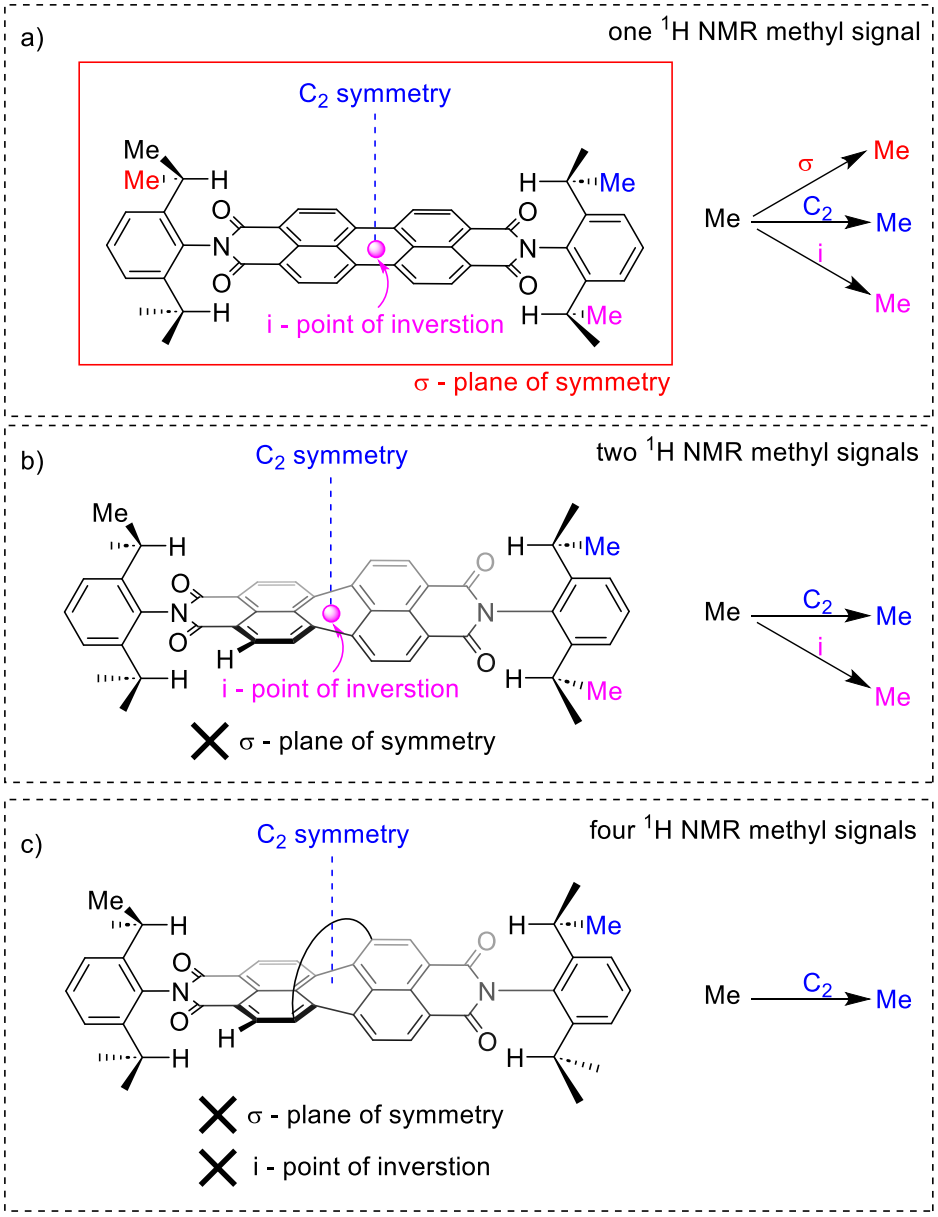

Figure 2.19. Diisopropyl analine imide group displaying different number of ^{1}H NMR signals based on the twist and substitution of the PDI core due to their symmetry elements.

If the PDI macrocycle is not chirally locked, such that the PDI core is able to perform an intramolecular 'somersault' through the macrocyclic cavity, the 'somersault' would result in achieving the other enantiomer, where the methyl groups that were on the top face of one enantiomer would end up on the bottom face of the other enantiomer (Figure 2.20). As NMR is a spectroscopic technique that is blind to chirality, the blue and magenta methyl groups, as well as the red and orange methyl groups, would be equivalent. This means

that a PDI macrocycle that is not configurationally stable would display only two sets of ^{1}H NMR signals with their diisopropyl aniline imide groups (Figure 2.20). It should be noted that these signals will appear as doublets due to coupling with C-*H*.

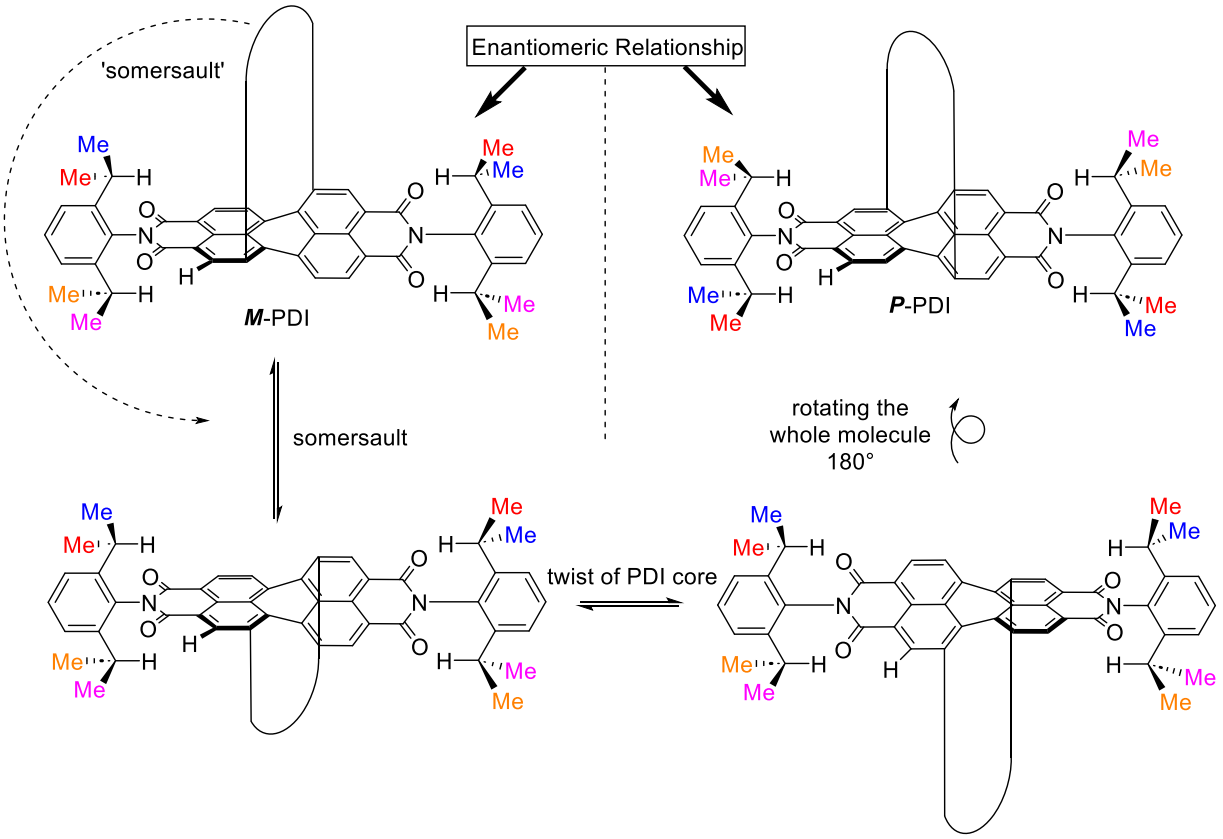

Figure 2.20. Chirally dynamic PDI macrocycle, showing its interconversion into its enantiomer by 'somersault' and twist.

Indeed, ^{1}H NMR spectroscopy of acyclic compounds **51**, **49** and **50** all show that the diastereotopic methyl protons exhibit only one doublet (Figure 2.21). Therefore, the rate of PDI atropisomer interconversion at 25 °C is faster than the chemical shift timescale of the ^{1}H NMR experiment (*i.e.* in fast exchange), and are considered planar in this timescale, a low barrier interconversion of the twist PDI.

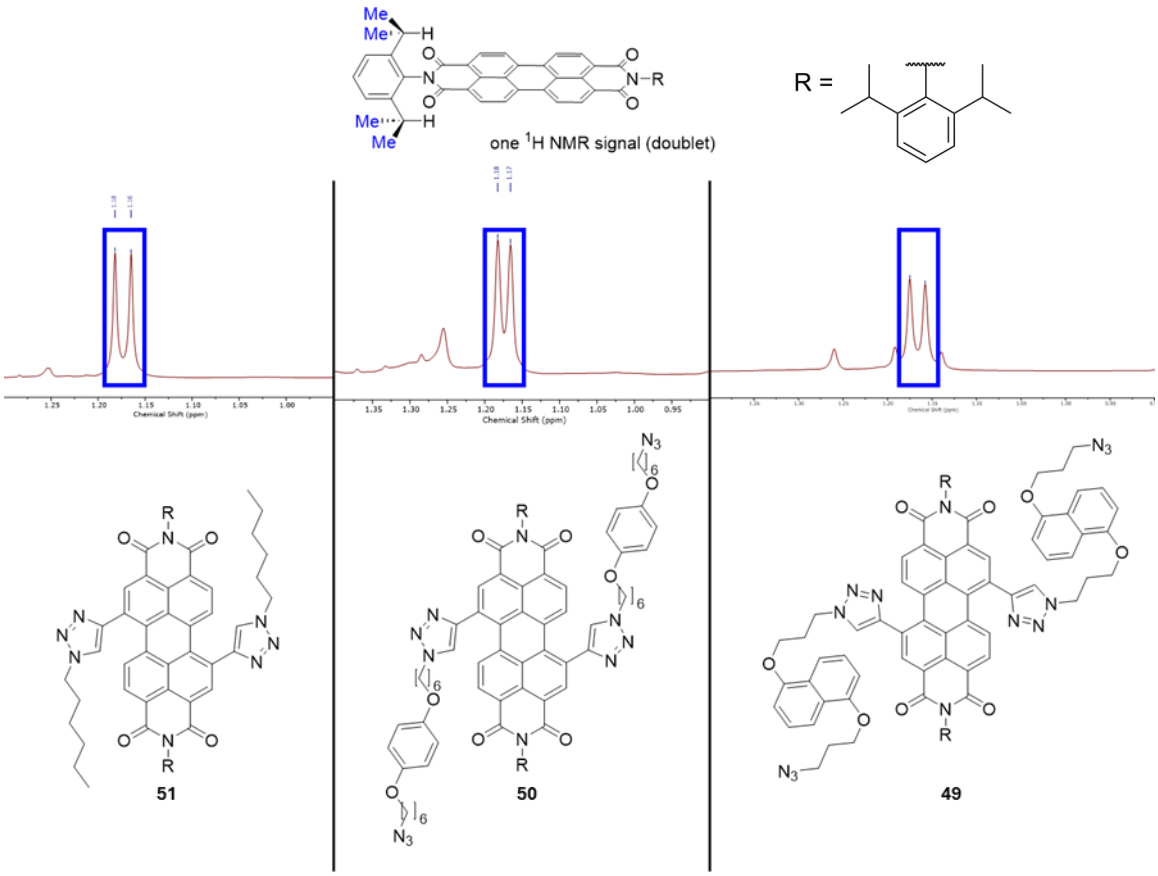

Figure 2.21. ^{1}H NMR spectra of acyclic PDIs **51**, **49** and **50**, displaying a single set of doublets for methyl groups**,** displaying no diastereotopic splitting as PDI atropoisomers are in fast exchange ($CDCl_3$, 298 K, 400 MHz).

The ^{1}H NMR spectra of PDI macrocycles **46**, **47**, and **48** all show the diastereotopic methyl protons are split into four sets of doublets, meaning that they are chirally locked (Figure 2.22). Therefore, the rate of PDI atropisomer interconversion is much slower than the chemical shift timescale of the ^{1}H NMR experiment (slow exchange at 25 °C). This means that the PDI interconversion barrier at 25 °C is high and thus these macrocycles can be configurationally stable, in agreement with CD and chiral HPLC analysis.

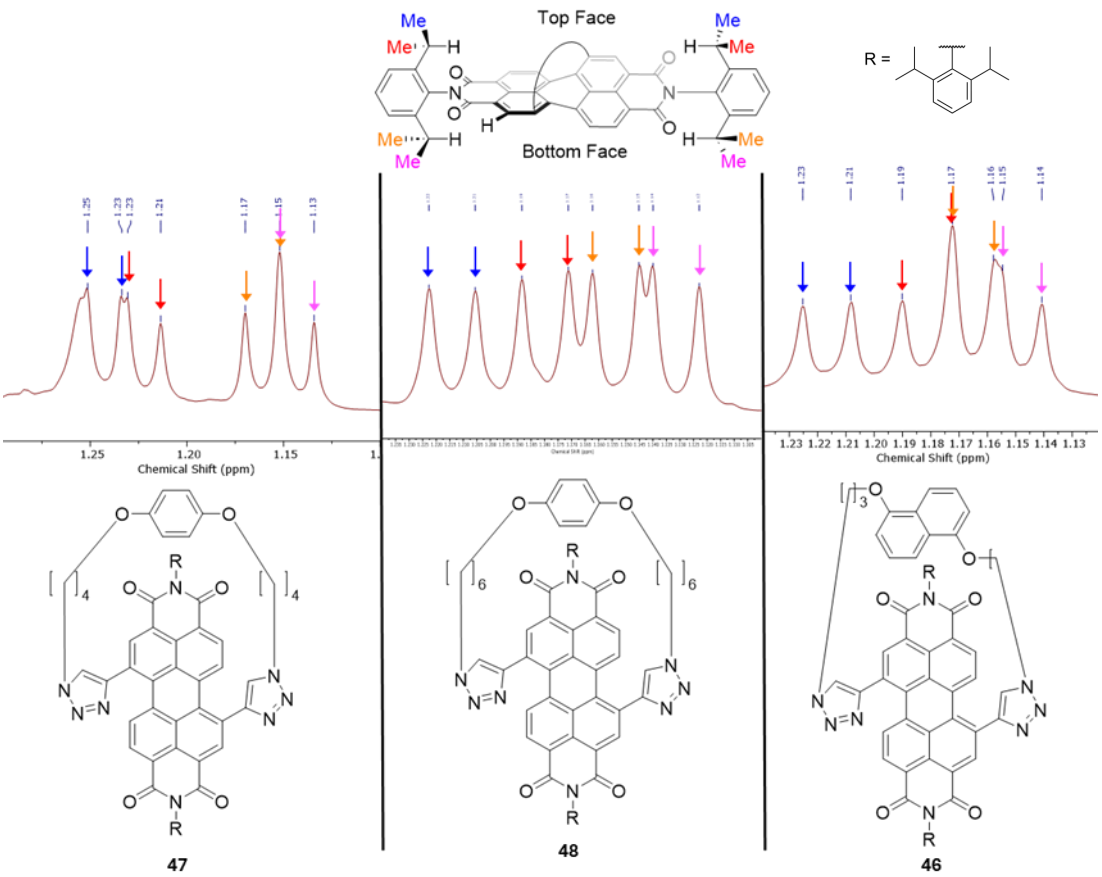

Figure 2.22. ^{1}H NMR spectra of PDI macrocycles **46**, **47**, and **48**, displaying four sets of doublets for methyl groups due to diastereotopic splitting arising from chiral locking of the PDI ($CDCl_3$, 298 K, 400 MHz). Note that the assignment of methyl groups are not confirmed.

2.5 Tuning the Donor-Acceptor Interaction

Having successfully isolated several chirally locked macrocycles, it was of interest to investigate the tunability of the π-π donor-acceptor through modification of the π-donor group in the strap or the PDI π-acceptor. Specifically, the HOMO-LUMO gap would be decreased by making the donor more electron rich, or LUMO lowered by making the PDI more electron poor. The former could be achieved by the use of a stronger electron donor, such as 1,5-diamino naphthalene (DAN) (redox potential E/V ≈ −0.2 *vs.* SCE),[114] which has the added benefit of being directly comparable to DHN (redox potential E/V ≈ 0.8 *vs.* SCE)[115] based macrocycle **46**, whilst he latter could be achieved by methylation of the triazole groups to give cationic triazolium groups.

2.5.1 Synthesis of DAN macrocycle

The synthesis of the 1,5-diamino naphthalene (DAN) based macrocycle proved to be a challenging synthesis that required significant optimisation. The table (Table 2.2) below outlines the attempts in alkylation of 1,5-diamino naphthalene, where, initial attempts following the same conditions as synthesis of DHN and HQ linkers were unsuccessful (acetone, K_2CO_3, 60 °C, 3 days), and led to a slow and incomplete reaction with significant evidence of decomposition by TLC (Entry A). Decreasing temperature led to no reaction (Entry B) and removal of inorganic base led to a slow reaction that was incomplete even after one week (Entry C). Changing the solvent to $CHCl_3$ with these conditions did not yield better results (Entry D, E). However, when organic base NEt_3 was used as base, the reaction, while slow, depleted all starting material after a week of stirring, generating DAN linker **52** (Entry F). After changing the solvent to MeCN, neither using no base nor using K_2CO_3 as a base yielded better results, even when heated (Entry G-I). Finally, the reaction was successful upon the use of NEt_3 as base in either MeCN or acetone as solvent (Entry K, L), where the former yielded a cleaner reaction with few side products (Table 2.2).

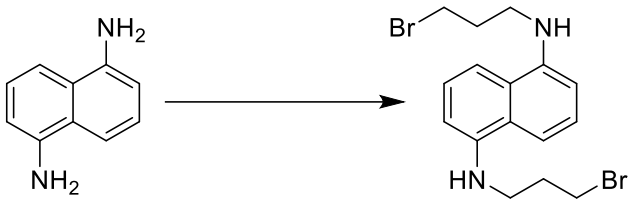

DAN **52**

Entry	Solvent	Base	Temperature °C	Duration	Reaction Notes
A	Acetone	K_2CO_3	60	3 days	Incomplete with decomposition
B	Acetone	K_2CO_3	20	2 days	No reaction
C	Acetone	None	20	2 days	Slow; incomplete after 1 week
D	$CHCl_3$	K_2CO_3	20	2 days	No reaction
E	$CHCl_3$	None	20	2 days	No reaction
F	$CHCl_3$	NEt_3	20	2 days	Slow but successful, where all starting material were consumed after 1 week
G	MeCN	K_2CO_3	20	2 days	No reaction
H	MeCN	None	20	2 days	Slow; incomplete after 1 week
I	MeCN	None	60	3 days	Incomplete with decomposition
J	MeCN	None	85	3 days	Incomplete with decomposition
K	MeCN	NEt_3	20	2 days	Successful (17% yield)
L	Acetone	NEt_3	20	2 days	Successful (5% yield)

Table 2.2. the alkylation of 1,5-diamino naphthalene (DAN) is outlined.

With the alkylated DAN **52** in hand, this was carried forward to react at 70 °C with NaN_3 in DMF overnight to form the azide **53** in 88% yield, which was subjected to CuAAC with PDI bisalkyne **23** to yield macrocycle **54** (high dilution) or acyclic variant **55** (excess linker) in 21% and 49% yields respectively (Scheme 2.14). The macrocycle and the acyclic analogue were synthesised using analogous conditions optimised from DHN macrocycle **46**.

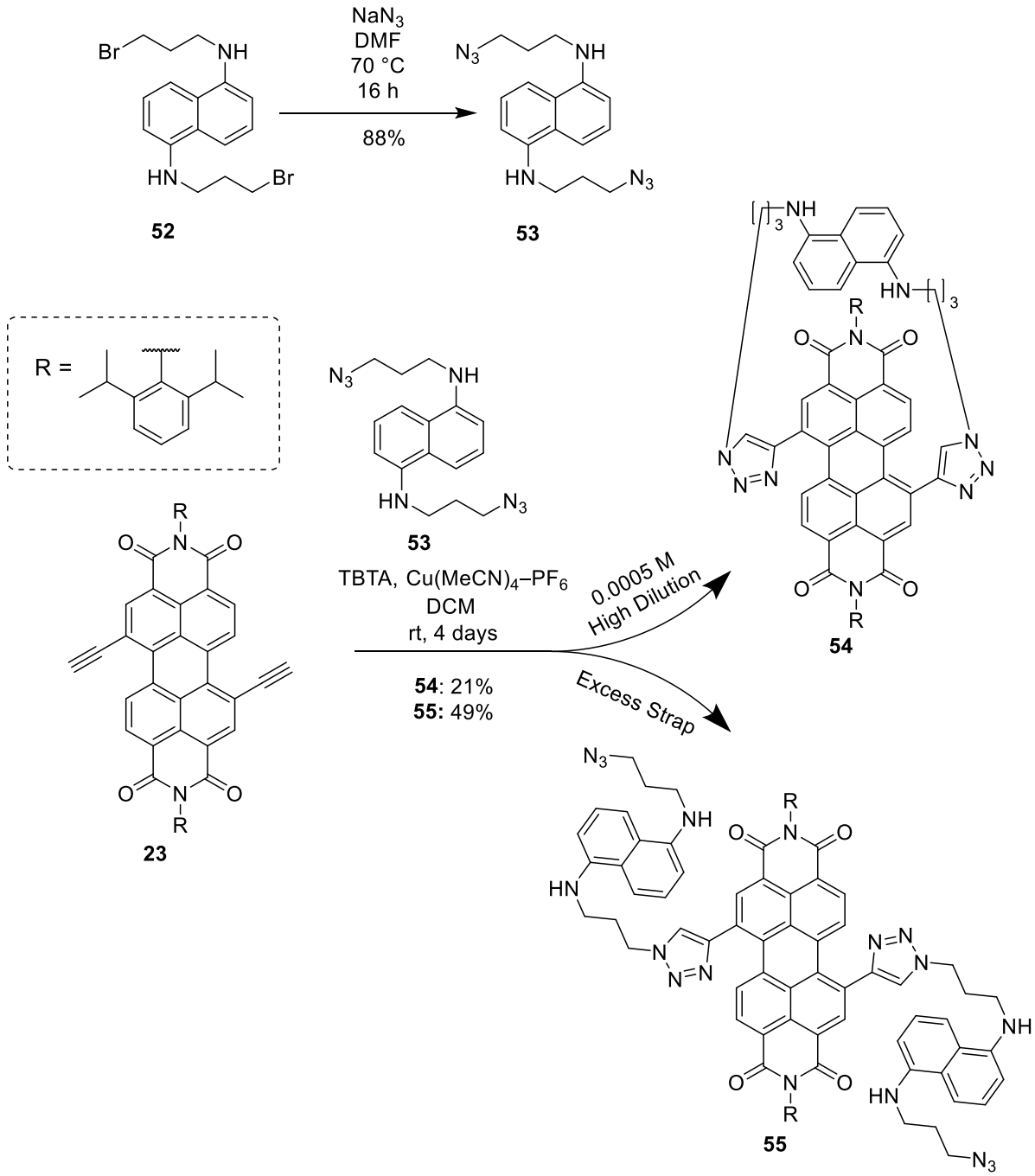

Scheme 2.14. Top: Synthesis of azide **53**. Bottom: CuAAC of DAN strap **53** and PDI **23** to form macrocycle **54** and acyclic compound **55**.

2.5.2 Characterisation of DAN-PDI macrocycle and comparison with DHN-PDI macrocycle

DAN-PDI macrocycle **54** as analysed by UV-vis, fluorescence and ^{1}H NMR spectroscopy. Interestingly, despite being a stronger electron donor, DAN-PDI macrocycle **54** gave similar results to DHN-macrocycle **46**. Both macrocycles have similar UV-vis absorption spectra (λ_{max} = 568 and 570 nm) (Figure 2.23a) with a λ_{max} of 619 nm by fluorescence spectroscopy (Figure 2.23b). These peaks are redshifted by the same amount compared to acyclic **51**. By ^{1}H NMR spectroscopy, the chemical shifts of DAN macrocycle **54** are very similar to that of DHN macrocycle **46**, with protons $H_{a\text{-}c}$ ($H_{e,f}$) in **54** only slightly more shifted downfield (upfield) relative to **46** (Figure 2.23c). This indicates that, despite DAN being a stronger π-electron donor, this donor may not be positioned any closer to the π-electron deficient PDI core to form a stronger donor-acceptor interaction, likely due to high ring strain.

Similar to acyclic DHN-PDI **49**, acyclic DAN-PDI **55** also does not show a red shift relative to acyclic control compound **51** in either UV-vis nor fluorescence spectroscopy (Figure 2.23d,e). Additionally, the ^{1}H NMR proton shifts are like those of acyclic DHN-PDI **49**. This suggests that the that the three acyclic compounds behave similarly, where there is no interaction between the π-electron rich DAN group and the π-electron deficient PDI core. Thus, even with a stronger electron donor, a macrocyclic framework that preorganises the π-conjugated units in solution is key to delivering a donor-acceptor π-π interaction. There were also no discernible differences in UV-vis absorption spectra when repeated with toluene as solvent (Appendix A).

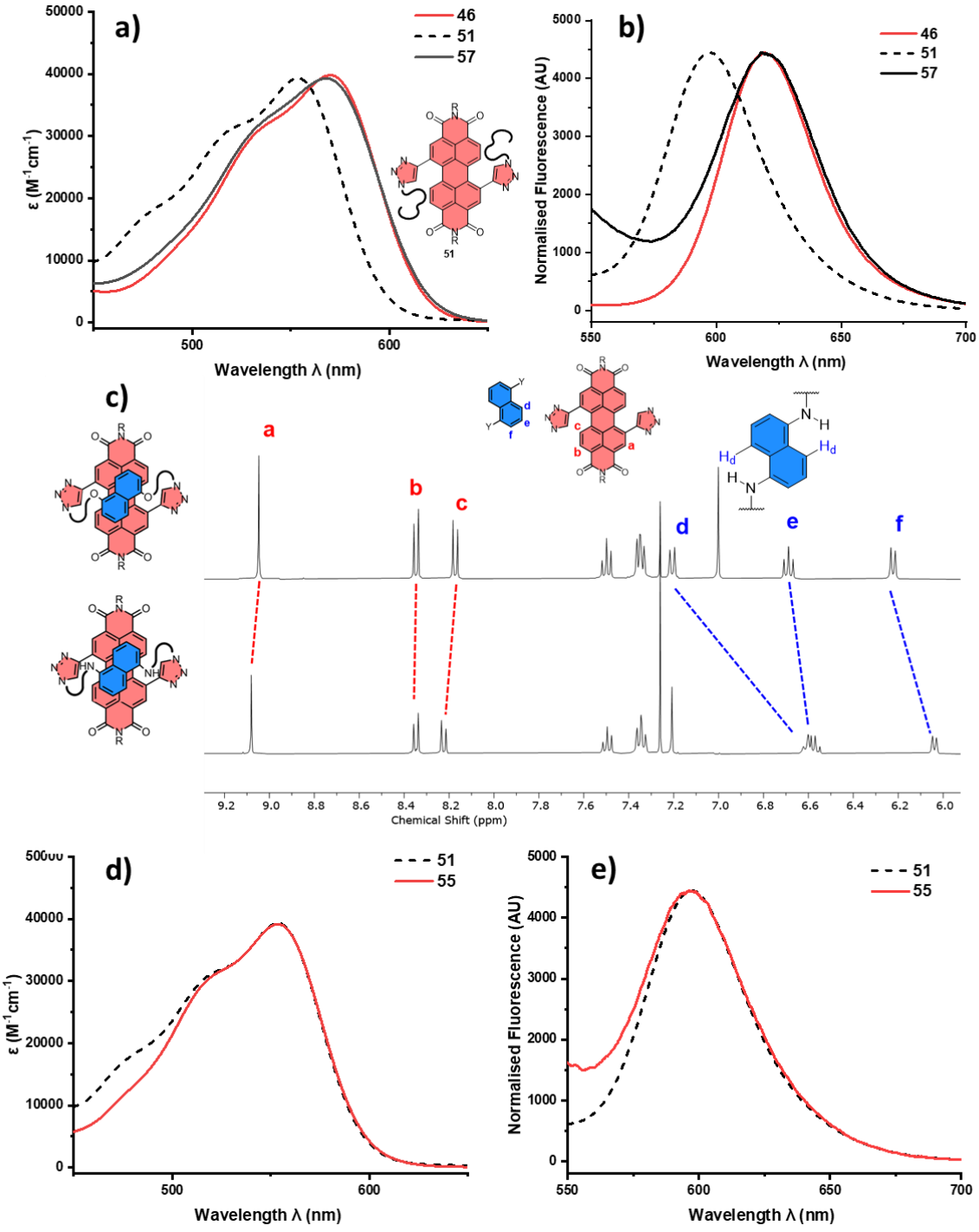

Figure 2.23. a) UV-vis spectra of DHN–PDI macrocycle **46** (red), DAN–PDI macrocycle **54** (black, solid), acyclic control **51** (black, dotted); b) Fluorescence spectra of DHN–PDI macrocycle **46** (red), DAN–PDI macrocycle **54** (black, solid), acyclic control **51** (black, dotted); c) Stacked ^{1}H NMR spectra of (top) DHN–PDI macrocycle **46** and (bottom) DAN–PDI macrocycle **54** ($CDCl_3$, 298 K, 400 MHz); d) UV-vis spectra of acyclic compounds **55** (red) and **51** (black, dotted); e) Fluorescence spectra of acyclic compounds **55** (red) and **51** (black, dotted). UV-vis and fluorescence spectra were recorded in $CHCl_3$ at a concentration of 26 µM in a quartz cuvette with 1 cm path length.

2.6 Methylation of PDI triazoles

As the DAN macrocycle **54** with its stronger π-electron donor has minimal effect on the π-π donor-acceptor interaction of PDI, attention turned to making the PDI π-acceptor more electron poor. One way in which this could be achieved was by methylation of triazole groups to give *N*-methyl triazolium groups, cationic heterocycles act as stronger electron withdrawing groups to strengthen donor-acceptor π-π interactions.

Several methylating reagents were identified to methylate the triazole groups: methyl triflate, trimethloxonium tetrafluoroborate, and methyl iodide (MeI). These have a range of methylating power based on the electrophilicity of the 'Me' group, where methyl triflate is the most powerful methylating reagent, and methyl iodide the weakest. Both methyl triflate and trimethloxonium tetrafluoroborate are extremely air sensitive and toxic, making these more challenging to work with. Methyl iodide, in addition to its stability in air, also has the advantages of being a good solvent and high affordability.

The methylation of bistriazole PDI compounds was challenging and required significant optimisation. Therefore, test reactions were performed with the acyclic bis-triazole PDI **51** ahead of using more precious macrocyclic compounds (Table 2.3). An initial attempt reacted **51** with an excess of methyl triflate in dry $CHCl_3$/MeCN (1:1 v/v) yielded full decomposition products. Despite previous systems not showing any light sensitivity, there is precedent from literature[66] that light can facilitate side-reactions between the triazole and PDI core to form a coronene derivative. Thus, this reaction (and all other reactions in this section) were performed in the dark. Repeating the same reaction in the dark, starting material was still observed by TLC after 24 hours along with some monomethylated product, which was identified by ESI mass spectrometry. The reaction was left for another 24 hours which yielded mainly monomethylated and decomposition products (Entry A). It was hypothesised that the monomethylated product was crashing out of solution, and thus

unable to further react to form the desired doubly methylated product. Therefore, since the positively charged monomethylated intermediate was discovered to be more soluble in higher polarity solvents, the reaction was repeated in 1:2 and 1:4 ratios of $CHCl_3$/MeCN (v/v) but yielded the same results (Entries B and C).

It was hypothesised that whilst the higher MeCN ratio does improve the solubility of the monomethylated intermediate, the high polarity is worse in solubilising the starting material **51**, and greatly slows down the first methylation. Therefore, increasing solvent polarity after first methylation had occurred was trialled, where additional MeCN was added after 24 h. A 2:1 and 4:1 ratio of $CHCl_3$/MeCN (v/v) was attempted in hopes of speeding up formation of monomethylated product, which crashed out of solution after 24 h. After which MeCN was added until the reaction was in solution and left for another 24 h but also yielded little product (Entry D, E). The reaction was then attempted in neat $CHCl_3$. Surprisingly, the compounds remained in solution throughout, thus $CHCl_3$ was shown to be a good solvent[30] for both starting material and methylated compounds. This successfully yielded bismethylated compound **56** in good (81%) yield after anion exchange to the PF_6^- salt using NH_4PF_6 (Entry F).

Initial attempts with the milder methyl iodide were slow and achieved mainly mono-methylated product, even with heating (Entry G, H). After further optimisation, **51** was also successfully methylated by dissolving in MeI and heated at 80 °C in a sealed pressure tube for 4 days, where the sealed pressure tube was needed in order to raise the pressure enough to heat the reaction mixture beyond the boiling point of MeI (Entry I).

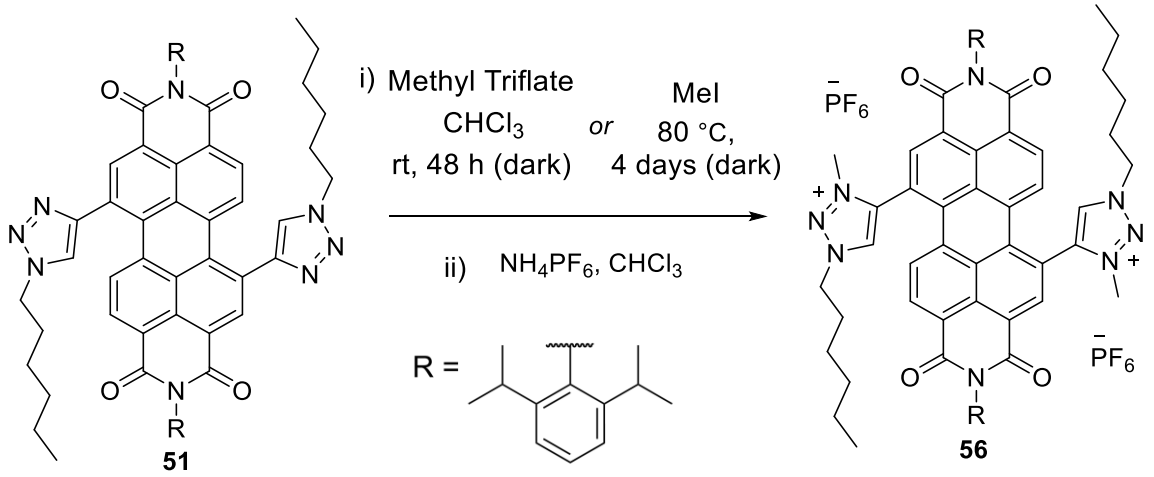

51 **56**

Entry	Methylating Agent	Solvent Ratio		Reaction notes after 24 h	Reaction notes after 48 h
		$CHCl_3$	MeCN		
A	Methyl Triflate	1	1	• Starting Material • Monomethylated • Decomposition	• Monomethylated • Decomposition
B	Methyl Triflate	1	2	• Starting Material • Monomethylated • Decomposition	• Monomethylated • Decomposition
C	Methyl Triflate	1	4	• Starting Material • Monomethylated • Decomposition	• Monomethylated • Decomposition
D	Methyl Triflate	2	1	• Monomethylated • Decomposition. • Monomethylated crash out of solution. • Additional MeCN added until double of total volume.	• Monomethylated • Decomposition
E	Methyl Triflate	4	1	• Monomethylated • Decomposition. • Monomethylated crash out of solution. • Additional MeCN added until double of total volume.	• Monomethylated • Decomposition
F	Methyl Triflate	1	0	• Bismethylated • Decomposition. • Isolated yield = 81%.	N/A
G	MeI	0	0	• Majority Starting material • Some monomethylated. • No significant change after 1 week.	
H	MeI at 42 °C	0	0	• Majority Starting material • Some monomethylated. • No significant change after 1 week.	
I	MeI at 80 °C	0	0	• Monomethylated • bismethylated. • Only bis methylated observed after 4 days.	

Table 2.3. Methylation of **51** to achieve **56**.

Methylation of DHN macrocycle **46** was attempted using the methyl triflate conditions optimised above (Entry F, table 2.3), but unfortunately the reaction proceeded much slower than the acyclic **51**, leading to a larger number of side products. The target macrocycle was unable to be purified or characterised. It is postulated that the macrocycle is more difficult to methylate due to steric shielding from the macrocycle's strap. Additionally, since the PDI is twisted, the hydrogen atoms on the unsubstituted bay positions may block the *N*-methylation site.

2.6.1 Photophysical Characterisation of Bis-triazolium PDI

Characterisation of the acyclic methylated compound **56** yielded interesting results. The UV-vis absorption spectrum of dicationic dye **56** displays a significant blue shift of 24 nm relative to the neutral counterpart **51**. This increases the twist of the PDI core, leading to less orbital overlap between the two naphthalene-imide units of the PDI core, leading to a hypsochromic shift (Figure 2.24). This effect can also be seen in literature,[104c] where the absorption spectra becomes more blue shifted as PDI becomes more twisted. This blue shift may also be indicative of the decreased orbital overlap between the triazolium and PDI core due to the aformentioned steric clash. The well defined and clear vibrational progression seen in the UV/Vis spetra of **56**, as well as its reduced stokes shift ($\Delta\lambda$ = 29 nm; cf. **51** $\Delta\lambda$ = 44 nm) and enhanced fluorescence, indicates the increased rigidity of the bis-triazolium PDI.

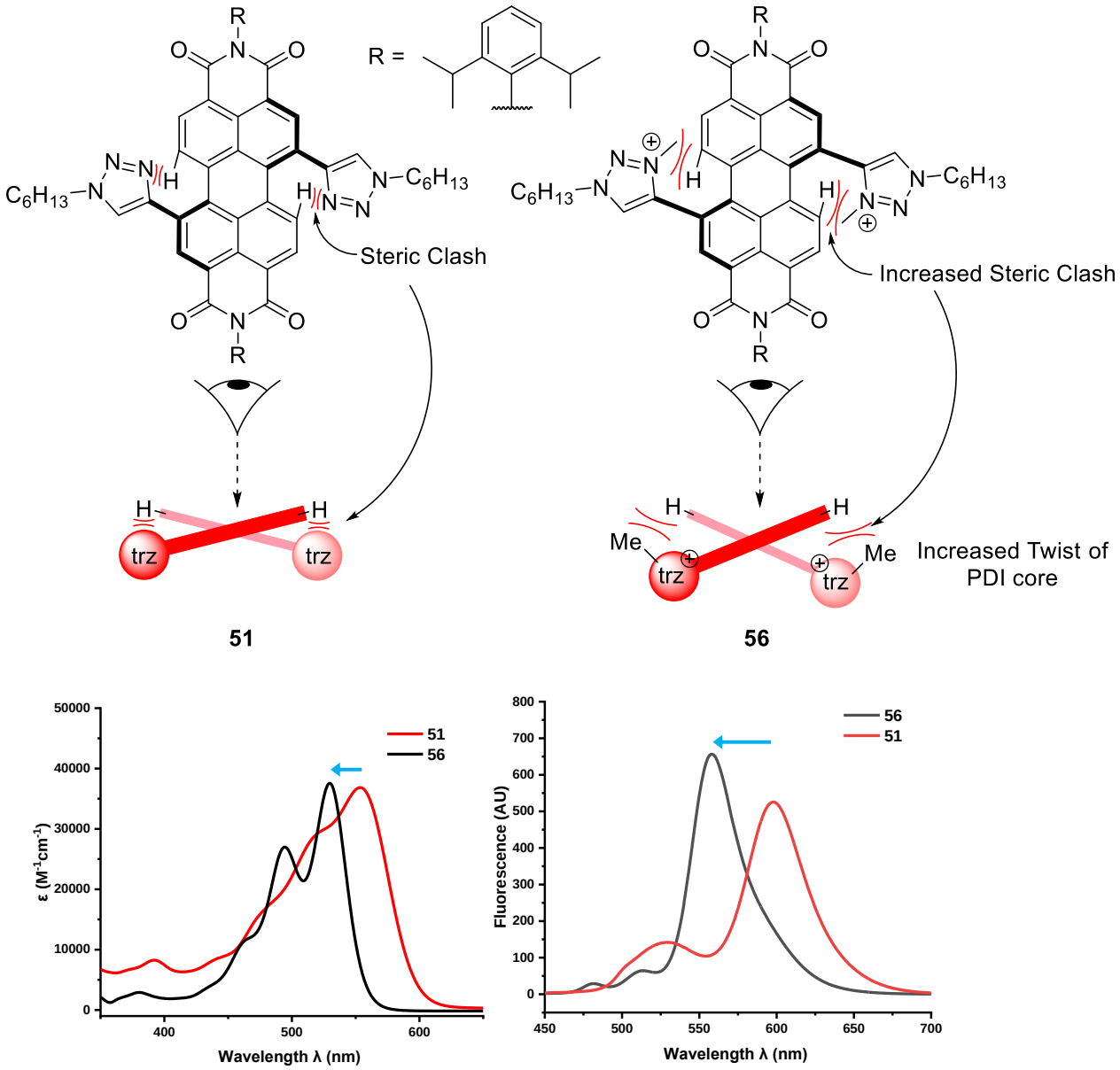

Figure 2.24. Top: Steric Clash between the triazole/triazolium and bay proton on PDI, where the increased steric clash of triazolium could increase greater twist of PDI core. Bottom: UV visible spectrum and fluorescence spectrum of triazole **51** and triazolium **56** in $CHCl_3$. All spectra were recorded in $CHCl_3$ at a concentration of 26 µM in a quartz cuvette with 1 cm path length and excitation wavelength of 400 nm.

PDIs have been reported to form radical anions in the presence of an electron donor (NEt_3) by photoinduced electron transfer (PET),[46] where this property has been exploited for photocatalysis.[44] Therefore, experiments were conducted with **56** to see if it could form radicals. Here, reduction of the 2^+ PDI will generate a radical cation (Figure 2.25). In comparison to the neutral PDIs reported in literature,[44, 46] **56** may result in a higher

oxidation power (*i.e.* be more easily reduced) and generate more stable radicals. It was anticipated that the introduction of two cationic electron withdrawing groups would make PDI more electron deficient and a candidate for photoredox chemistry. This would give it the potential to be a more potent photocatalyst for oxidation. The radical cation may facilitate reductions such as the reduction of aryl halides. The reduction of bis-triazolium PDIs will add to the evolving library of PDI radicals, which will assist in the understanding

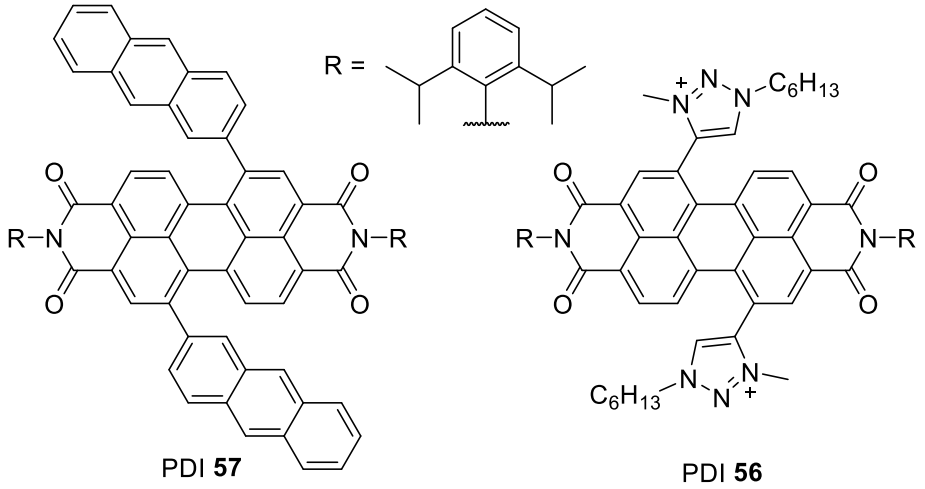

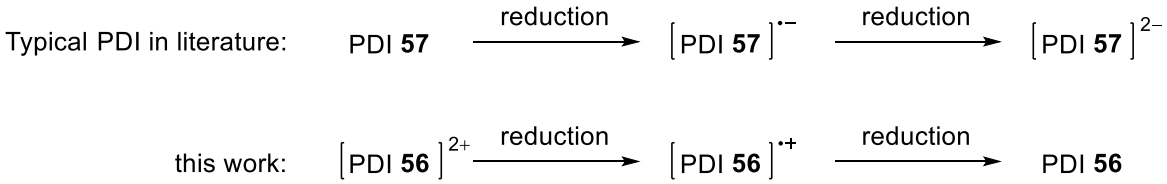

of these open shell species.

Figure 2.25. The same two stage reduction of PDIs where typical neutral PDIs in the literature it forms the radical anion and then doubly negatively charged anion, whereas in this work the doubly charged cation is reduced to the radical cation, then further reduced to the neutral species.

2.6.2 Photochemical reduction

The photochemical reduction of bis-triazolium PDI **56** was performed photochemically using NEt_3 as a sacrificial donor. A hundred-fold excess of NEt_3 was added to **56**, where no immediate change could be seen in its absorption spectra. However, upon exposure to ambient light for 1 min, the orange solution quickly turned colourless with a slight blue

tinge. This solution then slowly reverted back to an orange solution in air and in the dark after 25 h. It should be noted that no change can be seen upon irradiation of **56** without NEt_3, as the PDI is unable to be reduced by PET without an electron donor (NEt_3). UV-vis absorption spectroscopy of the colourless solution revealed significantly diminished absorption bands in the 400—600 nm region replaced by new bands at 700 nm, 800 nm and 950 nm, indication the formation of a new species (Figure 2.26). This new species matches that of the radical anion $PDI^{\bullet-}$ (**57**), suggesting that this new species is also a PDI radical, where in this case is a radical cation $\mathbf{56}^{\bullet+}$ due to reduction of a dicationic PDI. The reduction to the radical cation by NEt_3 and light and subsequent oxidation in air was repeated five times without significant decomposition, revealing the stability of this compound. It should be noted that $\mathbf{56}^{2+}$ did start to decompose after several weeks, though the exact conditions for this are unknown. Importantly, literature examples of generating $PDI^{\bullet-}$ (**57**) were less susceptible to reduction, as even after one hour of photoirradiation, the majority of PDI (**57**) is not converted to its radical anion $PDI^{\bullet-}$. However, there is full conversion after one minute of irradiation of $\mathbf{56}^{2+}$. Additionally, the $PDI^{\bullet-}$ (**57**) is often less stable in air, with the $PDI^{\bullet-}$ (**57**) rapidly oxidising back to closed shell species (**57**) within 30 minutes, whereas $\mathbf{56}^{\bullet+}$ required over 25 hours in air to revert to back $\mathbf{56}^{2+}$.[116]

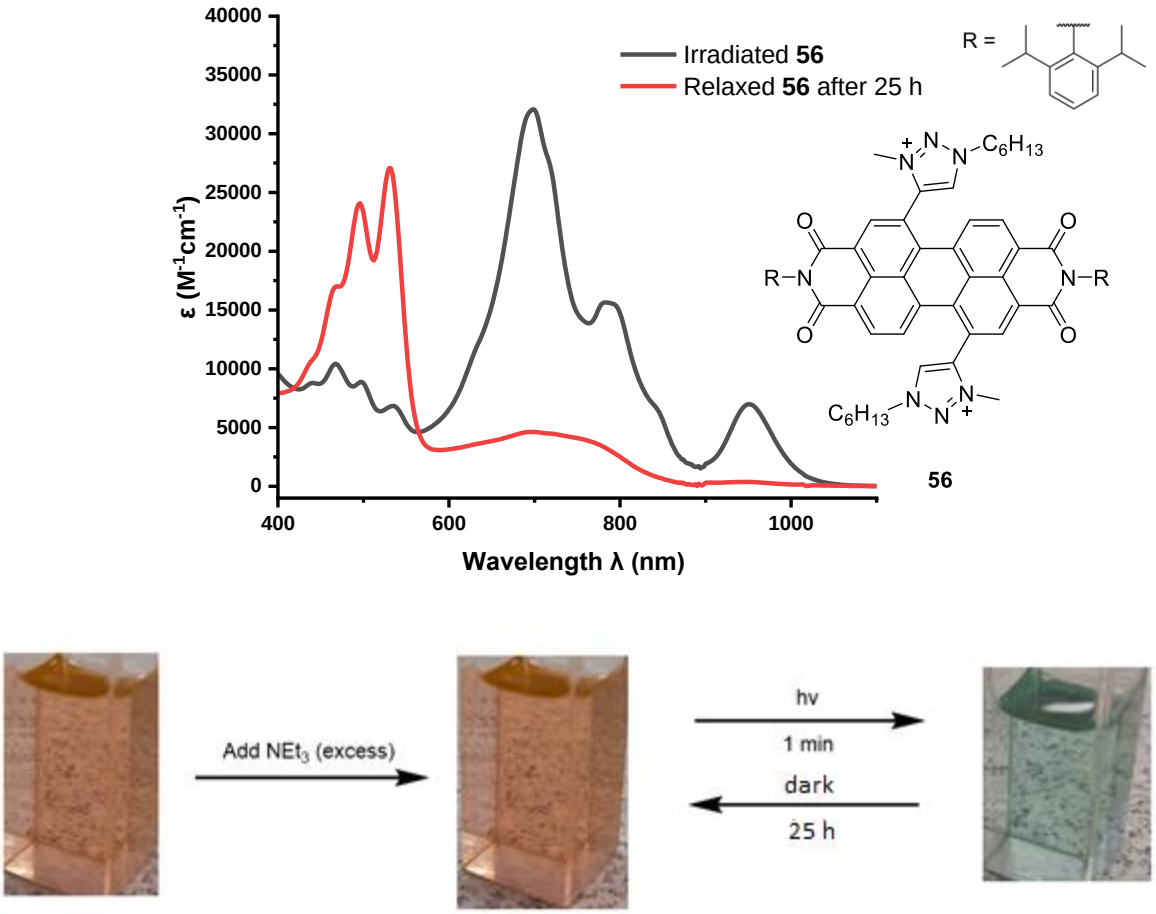

Figure 2.26. Top: UV visible spectrum o3, after irradiation (red) and relaxation back to ground state (black). Bottom: Colour change seen upon addition of NEt_3 to 56 and exposing it to light.

Interestingly, despite the photoirradiation of triazole bay-substituted PDIs being known to cyclise to a coronene,[66] this formation is not observed for the bis-triazolium PDI **56**. This may be due to the aforementioned steric clash between the triazolium unit and the PDI core, resulting in the lack of overlapping molecular orbitals.

2.6.3 Chemical Reduction

Where typically PDIs require photoexcitation to PDI* in order to raise the reduction potential enough to be reduced by electron donors such as NEt_3, Cobaltocene Cp_2Co is an extremely strong chemical reductant,[117] which is able to reduce PDIs without the need for photoirradiation. The reducing strength of Cp_2Co was used in an attempt to form the

neutral (doubly reduced) species. As such, Cp_2Co was slowly added and monitored by UV-vis absorption spectroscopy until the radical cation absorbance band reaches its maxima (complete consumption of **56**$^{2+}$) and the solution turns colourless (as all absorption bands are now situated in the NIR region and outside the visible region). The spectra of this colourless solution matches that of the radical cation formed by photoirradiation in the presence of NEt_3. Further addition of Cp_2Co reduces the bands at 700 nm, 800 nm and 950 nm, and new bands at 580 nm and 620 nm appear. The solution also turned dark blue and no further change was observed afterwards upon addition of Cp_2Co. Comparing against the doubly reduced anion PDI species PDI^{2-} (**57**),[116] it was found that the new dark blue species are similar in UV-vis spectra, suggesting that the doubly reduced neutral species is formed (Figure 2.27).

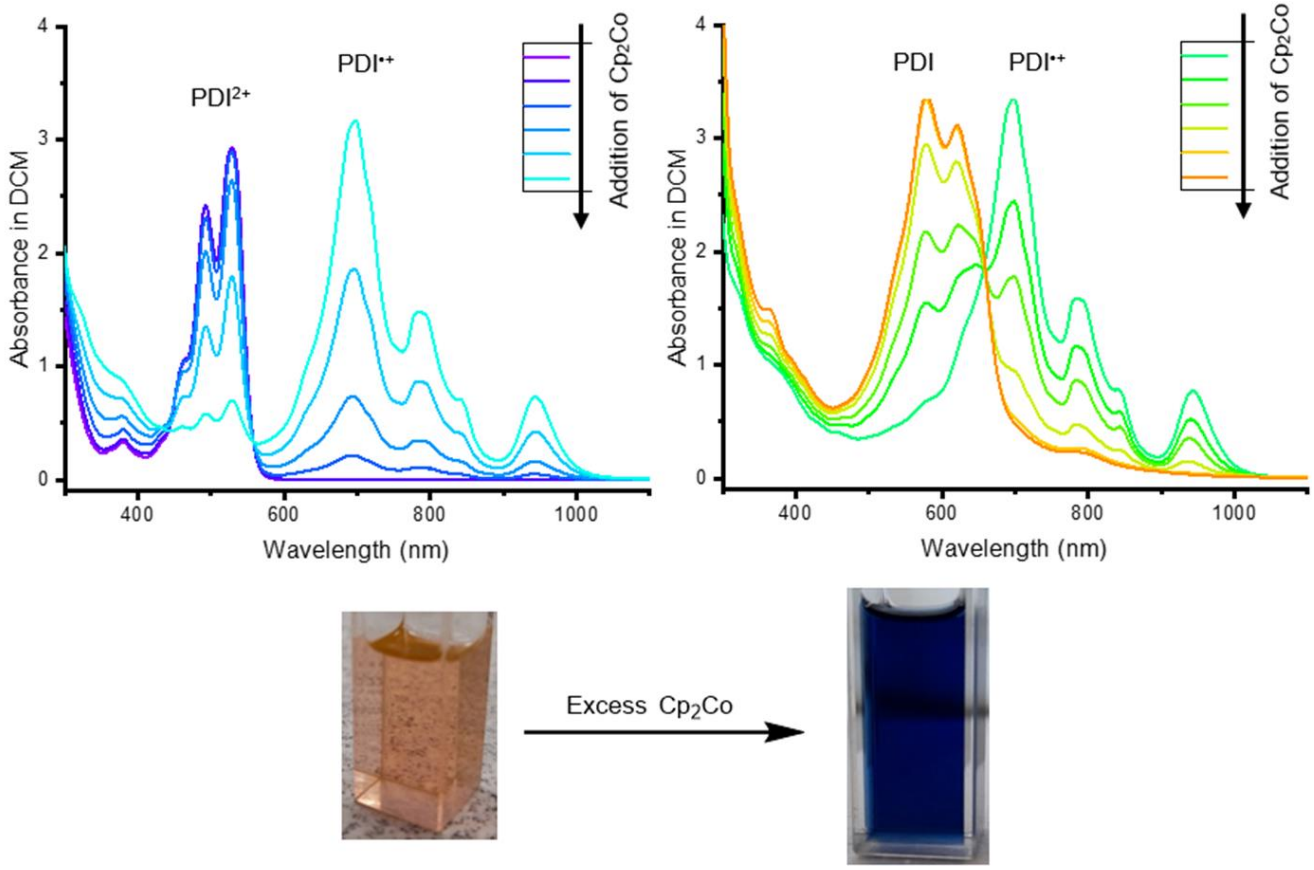

Figure 2.27. UV-vis absorption spectrum of triazolium **56** upon addition of Cp_2Co. Bottom: Colour change seen upon addition of Cp_2Co to 56.

These species are not only of interest due to their potential as photocatalysts,[44] their absorption in the near infrared (NIR) region of the spectrum brings applications in sensing,[74] while their colour change also allows applications in electrochromic/photochromic materials.[118]

2.7 Conclusions and future work

This chapter details the design of chirally locked macrocycles, and the synthetic strategies to these macrocycles. Various unsuccessful synthetic approaches revealed the potential importance of linker rigidity, length and ability to form non-covalent interactions, such as π-π interactions, in order the alleviate ring strain in small [1+1] macrocycles. The synthesis of novel PDI macrocycles **46**, **47**, **48**, and **54** were achieved from PDA in up to 9% yields over five steps using π-electron donating straps of DHN, HQ, and DAN. The synthesis of novel acyclic control compounds **51**, **49**, **50**, and **55** were achieved from PDA up to 26% yields over five steps.

These compounds evidenced the importance of macrocycle preorganisation to observe π-π donor-acceptor interactions between PDI and linkers. These interactions may also act as templating interactions during ring closing step. This was achieved by NMR, UV/vis and fluorescence spectroscopic techniques, where, compared to those of acyclic, a clear red shift could be seen in the photophysical spectroscopies of the macrocycles; and downfield (upfield) shifts could be seen in ^{1}H NMR spectra of PDI (HQ/DHN) protons of the macrocycles. The lack of π-π interactions observed in the acyclic variants indicates that the macrocyclic framework is key to the preorganisation of these donor-acceptor π-interactions. The dihedral angle of 16° between the two naphthalene units of the PDI found in the crystal structure of **47**, as well as the conformation it adopts (triazole pointing inside cavity), displays the high ring strain required for macrocyclisation. The longer strapped **50** was also found to decrease the donor-acceptor π-π interaction, while the use of a stronger

π-electron donor (DAN cf DHN) did not deliver more red-shifting, further evidence suggesting that the major cost of macrocyclisation is ring strain.

The configurational stability of these macrocycles was confirmed by chiral HPLC and CD spectroscopy, where resubmission after a week of the isolated enantiomers returned the pure enantiomers. The configurational stability could also be probed by ^{1}H NMR spectroscopy, specifically the methyl signals of the diisopropyl aniline imide group. The CD spectra also allowed the chirality of these enantiomers to be assigned by comparison with computational predictions (from collaborator Prof Martijn Zwijnenburg). This provides the basis and an understanding of systems involving PDI macrocycles that will be important in the discussion of Chapter 3, where a diastereoselective synthesis of PDI macrocycles will be described.

Further interest arose from the bis-triazolium PDI **56**, where upon photoirradiation of this novel dicationic dye in the presence of NEt_3, the orange compound forms a colourless radical cation as characterised by UV-vis absorption spectroscopy. The addition of stronger reducing agent Cp_2Co generated this radical cation chemically, and ultimately the doubly reduced neutral species which is blue.

An avenue of further research may include synthesis of longer strapped mono-PDI based macrocycles, where the length required for racemisation via the intramolecular somersault could be investigated (Figure 2.28a). The pH sensitivity of DAN macrocycles could also be investigated. Here, pH switching between π-electron poor and rich aromatic group lead to tunable π-π interactions between DAN and the PDI core, where, should the linker length allow, may also result in a tuneable macrocyclic cavity (Figure 2.28b).

Further research will also include characterisation of the radical by EPR spectroscopy. Attention then may turn to methylation of the PDI-based macrocycles, where the macrocyclic architecture may stabilise the radical cation after reduction.

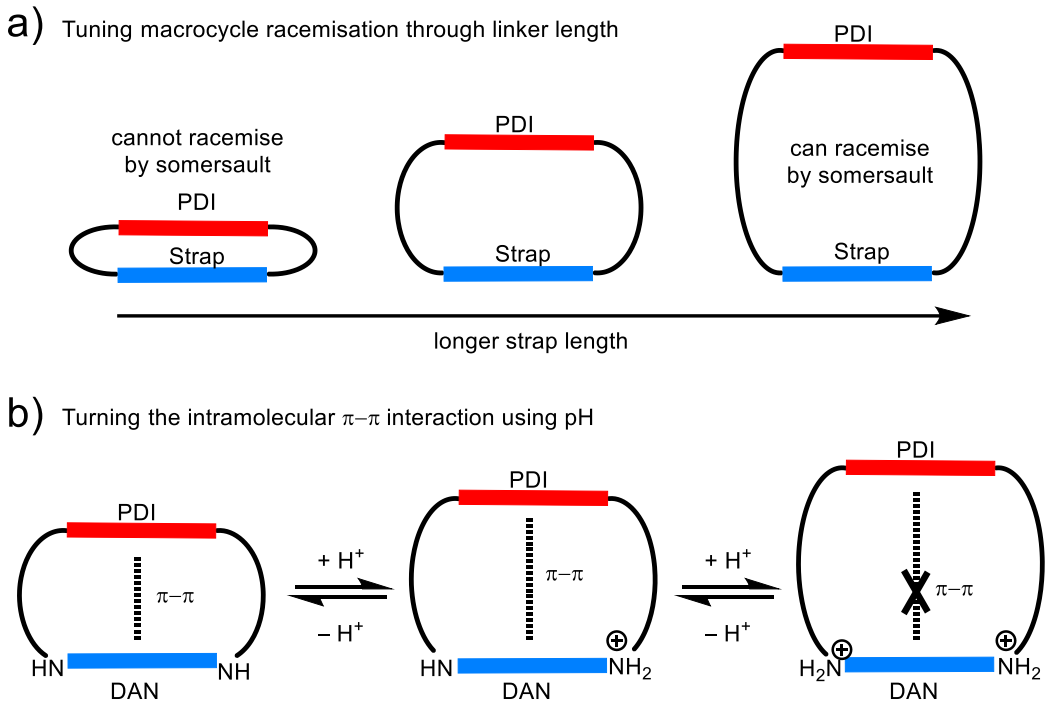

Figure 2.28. Avenues of further research to investigate a) longer straps, b) pH sensitivity of DAN macrocycles.

3 The Stereoselective Synthesis of PDIs

Some of the work in this chapter has been published in the journal Chemical Science: A. Yeung, M. A. Zwijnenburg, G. R. F. Orton, J. H. Robertson, T. A. Barendt, *Chem. Sci.*, 2024, **15**, 5516-5524.

The DFT calculations that appear in this chapter were performed by Prof Martijn Zwijnenburg from University College London.

3.1 Introduction

As described in Chapter 1, the role of supramolecular chemistry to tune non-covalent interactions between molecules can be used to direct the stereochemical outcome of a chemical reaction[77] or the self-assembly of a chiral material.[119] In the latter case, chiral self-assembly mainly operates under reversible conditions (i.e., thermodynamic control),[120] which means the selection for homochiral or heterochiral products is dictated by their relative energies.[121] However, the role of supramolecular chemistry in a dynamic kinetic resolution is not as well understood. This is essential for directing the stereochemical outcome of a reaction between interacting chiral molecules under irreversible conditions. In this chapter, PDI macrocycles with chiral or prochiral linkers will first be synthesised, which builds from the understanding of the kinetically controlled synthesis of chirally locked macrocycles described in Chapter 2. The analysis of the resulting dynamic kinetic resolution of stereoisomers will be of huge value to synthetic supramolecular chemistry.[122]

3.2 Chapter Aims

It was envisaged that PDI bisalkyne **23** could be strapped by CuAAC with a bisazide containing a dynamically chiral unit (prochiral or rapidly interconverting between its enantiomers). As discovered in Chapter 2, templation between the π-donor (strap) and π-acceptor (PDI) was key in such macrocyclic synthesis under irreversible conditions.

In a macrocyclisation reaction, the rate determining step is typically the one that forms the ring,[123] which here is the second ring-closing CuAAC 'click' reaction. Figure 3.1 illustrates chirally interconverting starting materials ("strap" and "PDI") reacting to form the singly clicked intermediate (grey box, Figure 3.1). The strap and PDI of the intermediate exist as two sets of enantiomers are still able to chirally interconvert. It was envisaged that one of these sets is able to exhibit π-π interactions between the "strap" and "PDI" and have a lower energy transition state to the macrocycle upon the second (irreversible) CuAAC reaction to form the ring. This second CuAAC reaction, which also twists and locks the chirality of the PDI unit, would induce chirality into the configurationally interconverting unit, thereby resulting in one set of enantiomers being formed more favourably over the other.

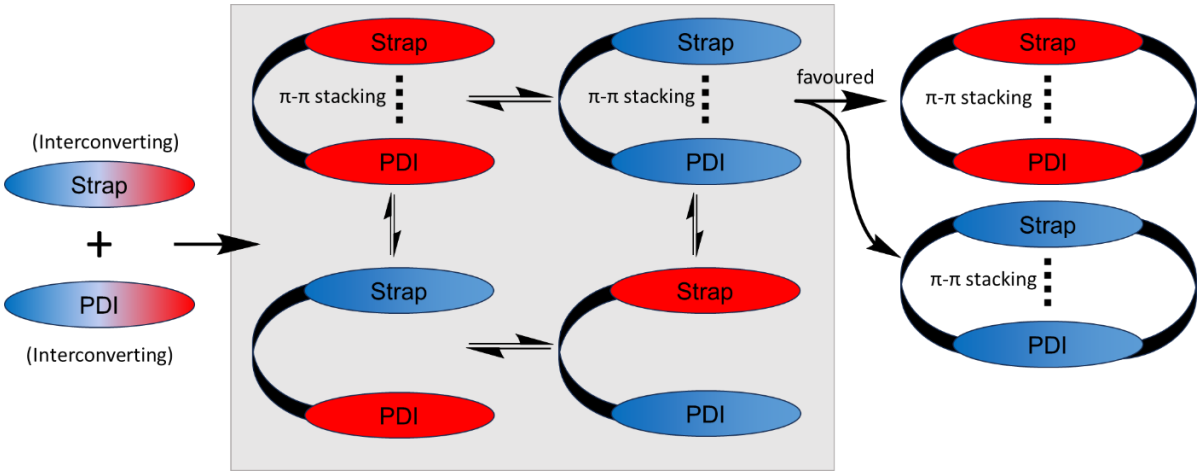

Figure 3.1. Envisaged reaction of PDI with dynamically chiral strap, resulting in a favoured set of enantiomers as a result of π-π stacking. The blue and red colours represent opposite enantiomers/handedness of the two components (strap and PDI).

In a similar sense, if the PDI is instead strapped with a configurationally stable chiral unit, this chirally locked unit may instead induce its chirality into the configurationally interconverting PDI, resulting in one diastereomer being formed in favour of the other (without formation of its enantiomers), thus achieving a stereoselective synthesis (Figure 3.2).

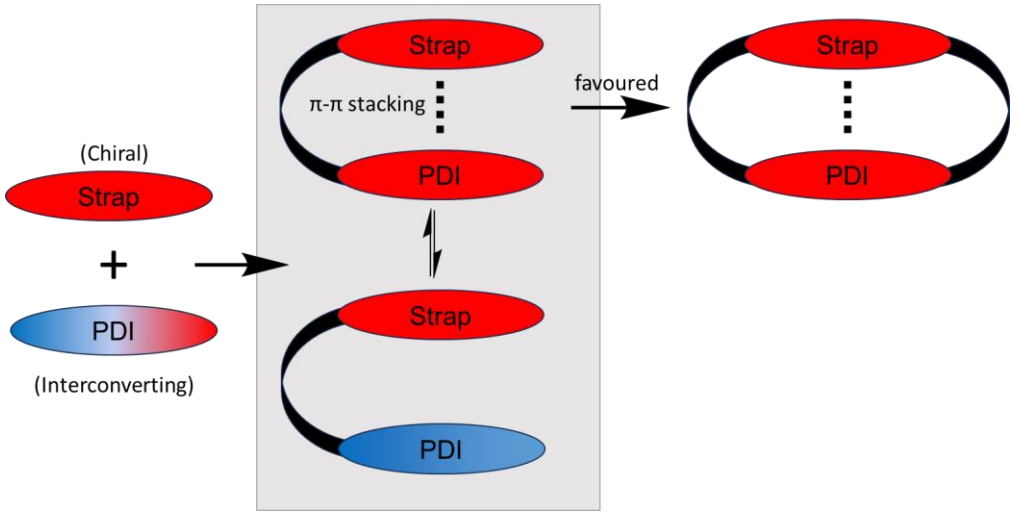

Figure 3.2. Envisaged reaction of PDI with configurationally stable chiral strap.

3.3 Synthesis of Macrocycles from Configurationally Interconverting Motifs

3.3.1 Bis-PDI Macrocycle

One source of dynamically chirality is the PDI unit. The connection of two PDIs via the bay positions was known to result in configurationally unstable PDIs, where these macrocycles typically relax into their thermodynamically most stable (homochiral) configuration via ‘somersaulting’ of the PDI units. It was decided to target a bis-PDI macrocycle in which one PDI was chirally locked while the other was not, in contrast to these previous bis-PDI macrocycles. This would be used to understand how the chirality of the locked PDI unit, which would be connected via the bay positions, impacted the chirality of the dynamic PDI, which would be connected via the imide positions.

3.3.1.1 Synthesis of Bis-PDI Macrocycles

To synthesise the target bis-PDI macrocycles, first, a flexible 1,4-dibromobutane linker, and a more rigid 1,4-bis(chloromethyl)benzene linker, were individually reacted with NaN_3 in DMF at 70 °C overnight to furnish bisazides **31** and **58** in quantitative yields. These bisazides were then each subjected to a Staudinger reduction by first dissolving in a suspension of Et_2O and 2.5M HCl(aq), before adding a stoichiometric amount of PPh_3 in EtOAc to achieve the mono-reduced amines **32** and **59** in 65% and 78% yields respectively (Scheme 3.1).

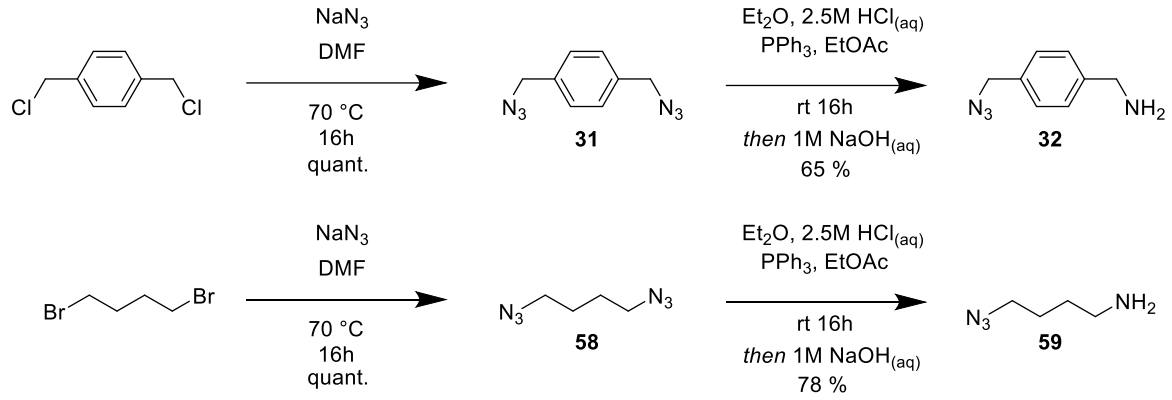

Scheme 3.1. Synthesis of **32** and **59**.

Having achieved amines **32** and **59**, imidisation of 1,6,7,12-tetrachloro perylene dianhydride ($PDACl_4$) (prepared by a previous group member) took place in molten imidazole at 140 °C, catalysed by the Lewis acid $Zn(OAc)_2•2H_2O$. Respectively, bisazide **60** was furnished in 58% yield after 4 h, and bisazide **61** was furnished in 33% yield after 16 h (as only one imide group was present by MALDI mass spectrometry after 4 h) (Scheme 3.2).

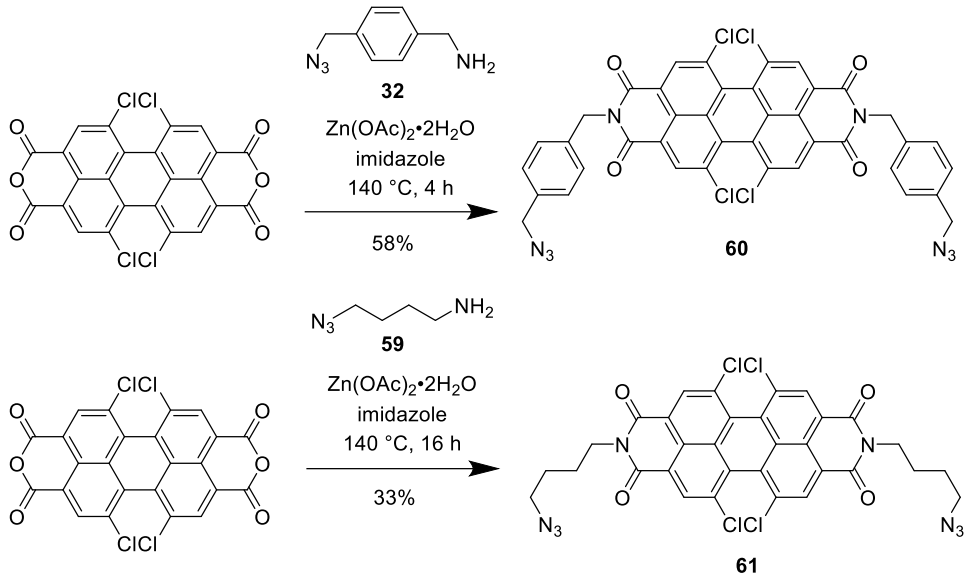

Scheme 3.2. Synthesis of **60** and **61**.

With the PDI bisazides **60** and **61** in hand, CuAAC with bisalkyne **23** in DCM, catalysed by $Cu(MeCN)_4$-PF_6 in the presence of TBTA proceeded under the high-diltuion macrocyclisation conditions optimised in Chapter 2. After a challenging purification, requiring both column chromatography and then preparative TLC, the macrocycles **62** and **63** were obtained in 5% and 21% isolated yields respectively (Scheme 3.3).

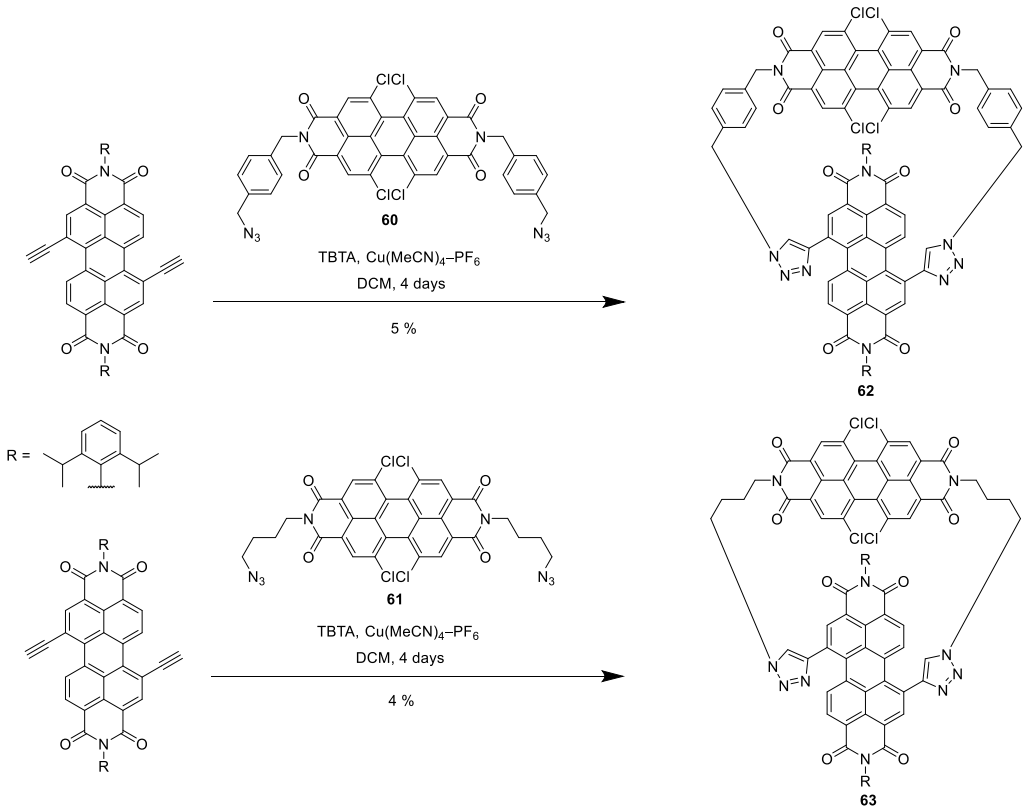

Scheme 3.3. Synthesis of **62** and **63**.

3.3.1.2 Macrocyclic Chirality

The bis-triazole PDI unit of these bis-PDI macrocycles was configurationally stable, since ^{1}H NMR spectra of **62** and **63** both show the diastereotopic methyl protons are split into four sets of doublets, and thus are in slow exchange at 25 °C (i.e., a high bis-triazole PDI interconversion barrier at 25 °C). Therefore, the rate of bis-triazole PDI atropisomer interconversion is much slower than the chemical shift timescale of the ^{1}H NMR spectroscopy experiment (Figure 3.3).[124]

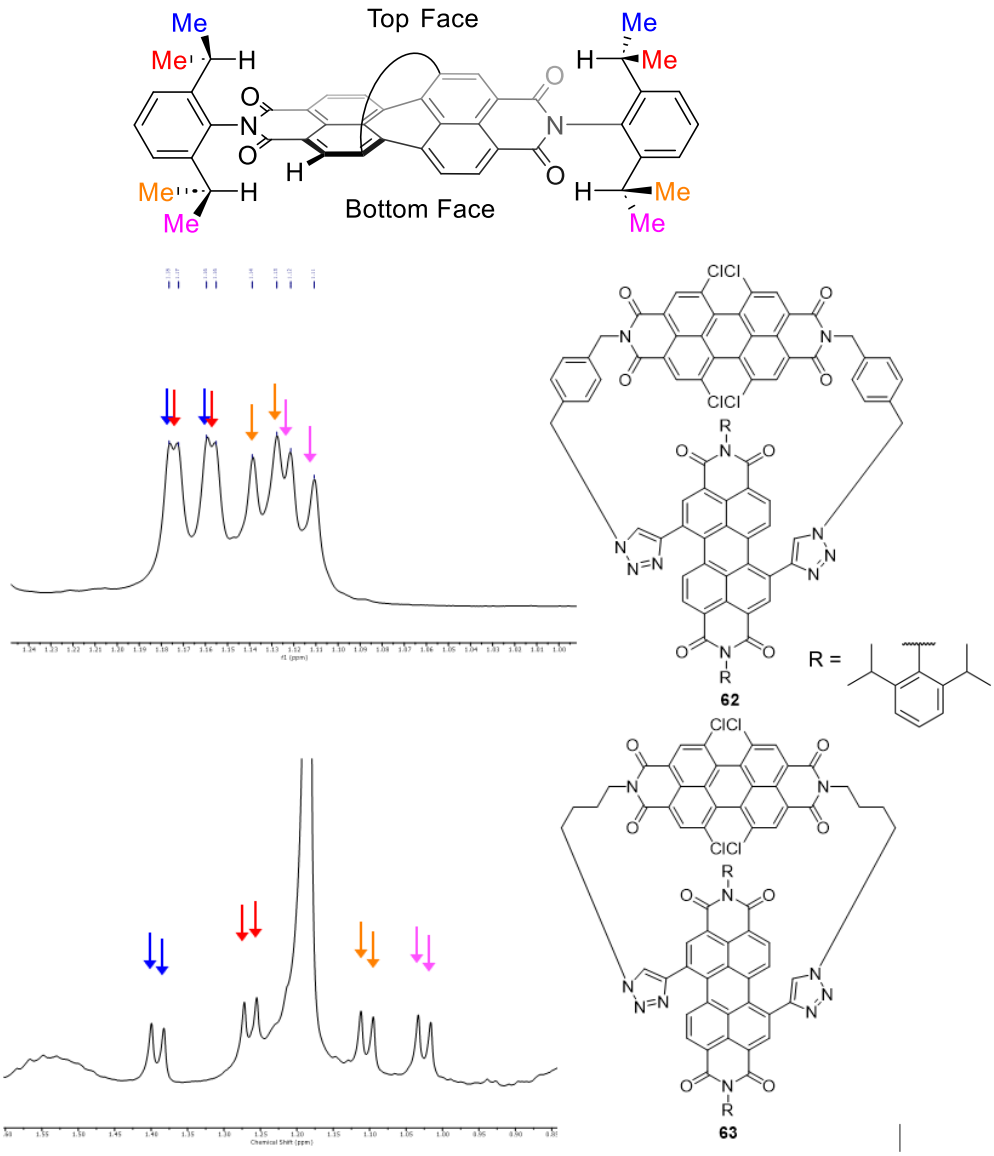

Figure 3.3. ^{1}H NMR spectra of PDI macrocycles **62** and **63**, displaying four sets of doublets for methyl groups due to diastereotopic splitting arising from chiral locking of the bay-connected PDI unit ($CDCl_3$, 298 K, 400 MHz). Note that the assignment of methyl groups are not confirmed.

The more flexible **63** was then subjected to ^{1}H NMR spectroscopy at 100 °C in TCE-d_2. Upon heating, the diastereotopic methyl protons remain split into four sets of doublets, with no significant broadening or shifting in any of the proton signals. This shows that the bis-triazole substituted PDI unit is configurationally stable at high temperatures.

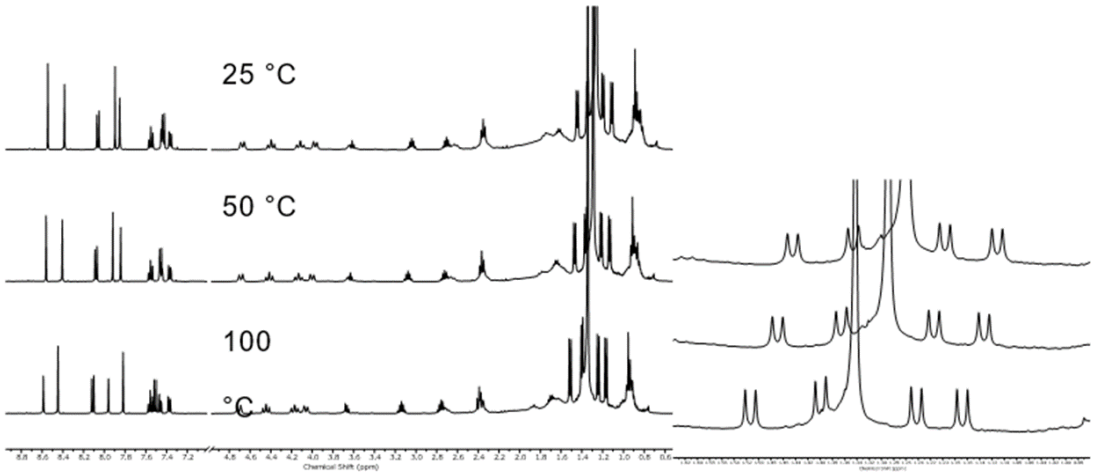

Figure 3.4. ^{1}H NMR spectra of PDI macrocycles **63** at 25 °C, 50 °C, and 100 °C, displaying four sets of doublets for methyl groups due to diastereotopic splitting arising from chiral locking of the PDI (TCE-d_2, 400 MHz).

As both the bis-triazole PDI (***PIM***) and the $PDICl_4$ (***PIM***) units will exhibit atropisomerism, two diastereomeric sets of enantiomers: ***PP*** and ***MM***; and ***PM*** and ***MP***, may be formed upon macrocyclisation. Since the bis-triazole PDI is chirally locked (Figure 3.3) and the barrier to $PDICl_4$ atropisomer interconversion is relatively high ($\Delta G^{\ddagger}$ = 97 kJ mol^{-1}),[31] one would expect to see two sets of signals in the ^{1}H NMR spectra of macrocycles **62** and **63**. These two sets of signals would arise from the diastereomeric relationship between the two sets of enantiomers (i.e. ***PP/MM*** vs ***PM/MP***). However, both bis-PDI macrocycles show only one set of ^{1}H NMR signals, meaning that only the most stable set of enantiomers is present (i.e. ***PP*** and ***MM*** only, or ***PM*** and ***MP*** only). This suggests that the free energy difference between the diastereomeric sets of enantiomers ($\Delta G°$) is large enough that the higher energy diastereomeric pair of enantiomers are not observed. Given the ^{1}H NMR spectra at 100 °C show a single set of peaks, indicative of a large diastereomeric ratio (> 95:5 dr, Figure 3.5), the difference

in free energy between the diastereomeric sets of enantiomers can be estimated to be $\Delta G° > -9.1$ kJ mol^{-1}.

However, determining which set of enantiomers (***PP*** and ***MM***, or ***PM*** and ***MP***) was present through CD spectroscopy was expected to prove very challenging. This is because the two PDI units have overlapping absorption bands in the UV-vis absorption spectrum which, following their resolution by chiral HPLC, would most likely prevent the individual assignment of PDI chirality by CD spectroscopy.

3.3.1.3 Pyrrolidine Substituted Bis-PDI Macrocycle

To address the challenge of PDI atropisomer assignment, it was attempted to use a pyrrolidine substituted PDI instead of $PDICl_4$, as it has a more bathochromically shifted absorbance,[125] and thus could be probed more easily by CD spectroscopy. To synthesise this macrocycle, $PDApy_2$ (prepared by a previous group member) underwent imidisation with **59** by refluxing in toluene over 4 days to achieve bisazide **60** in 84% yield (Scheme 3.4).

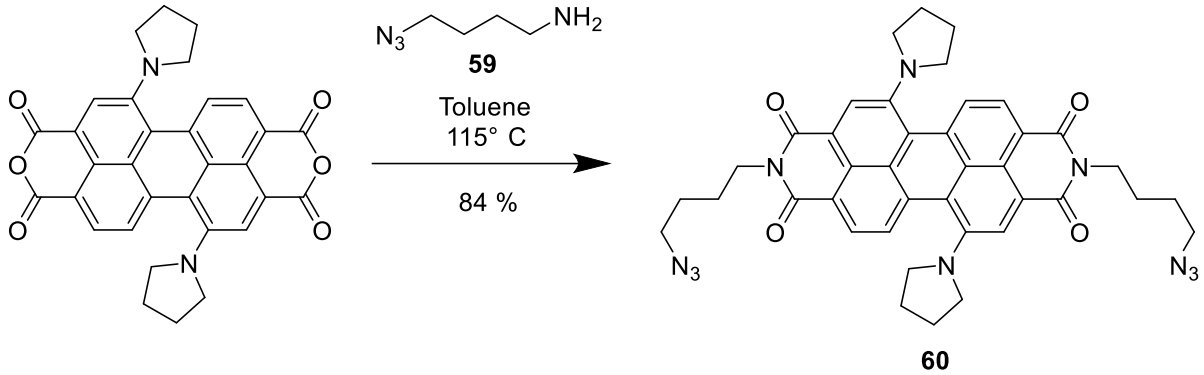

Scheme 3.4. Synthesis of **60**.

Under identical conditions as for the bis-PDI macrocycle above, a Cu(I) catalysed 'click' chemistry macrocyclisation reaction led to formation of the desired macrocycle, as confirmed by MALDI spectrometry. Unfortunately however, after column chromatography and then two successive preparative TLC plates, the macrocycle was unable to be obtained in high enough purity for its accurate characterisation. This may be due to the increased number of macrocycle isomers arising from the di-substituted

$PDIpy_2$, as a 1,7-substituted and a 6,12-substituted PDI would result in two distinct isomeric macrocycles. Additionally, if this macrocycle was configurationally stable, the pyrrolidine may be directed to point inside or outside the macrocycle's cavity, resulting in further isomers. Thus, this macrocycle may have formed four times the number of isomers compared to the $PDICl_4$ macrocycle **63** (Scheme 3.5).

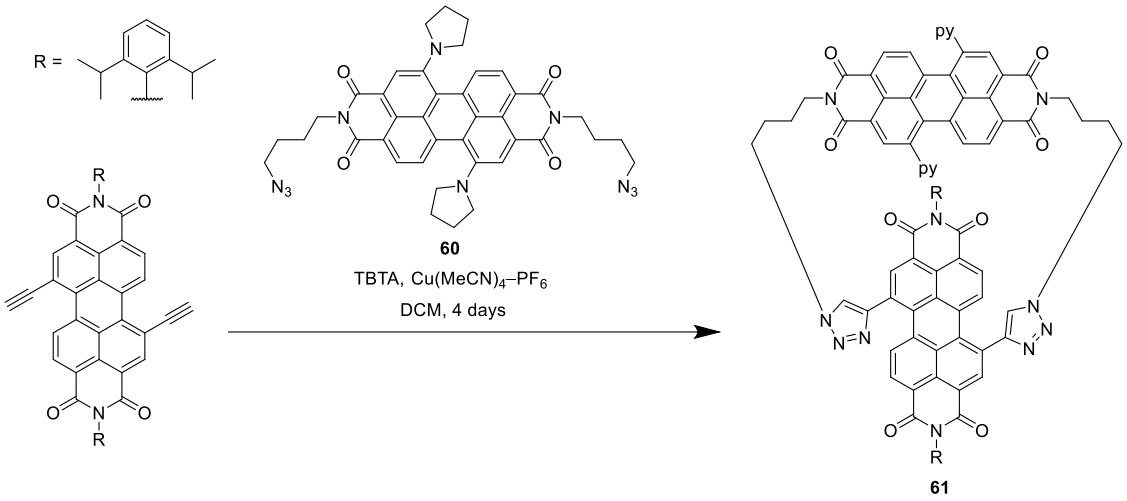

Scheme 3.5. Synthesis of **61**.

3.3.2 Pillar[5]arene Macrocycle

Another potential source of dynamic chirality are pillar[n]arenes, which are macrocycles composed of [n] dialkoxybenzene (or hydroquinone) units linked by methylene bridges via the para position (Figure 3.6). These compounds are of recent interest due to their electron rich cavity and planar chirality. They are configurationally unstable as they can interconvert between their enantiomers by the inversion of each of their phenyl units, an oxygen-through-the-annulus rotation. Therefore, the functionalisation of a phenyl unit with any large group that cannot fit through the pillarene cavity will inhibit stereoisomer interconversion and thus stop racemisation.

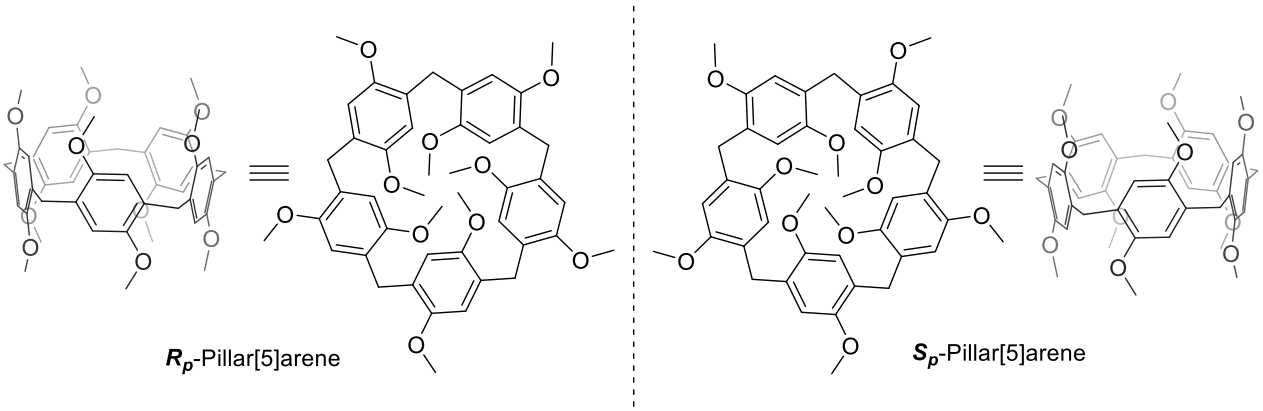

Figure 3.6. R_p- and S_p-Pillar[5]arene.

It was envisaged that that since HQ-PDI macrocycle **47** exhibits π-π interactions between the electron rich hydroquinone unit and the electron poor PDI unit in Chapter 2, a similar interaction may be seen between the pillar[5]arene unit and the PDI unit in a pillar[5]arene-PDI macrocycle. In other words, it could be thought that the pillar[5]arene unit is a 2,5-subsituted (or 3,6-substituted) hydroquinone unit, where these substituents form the pillar[5]arene ring (Figure 3.7).

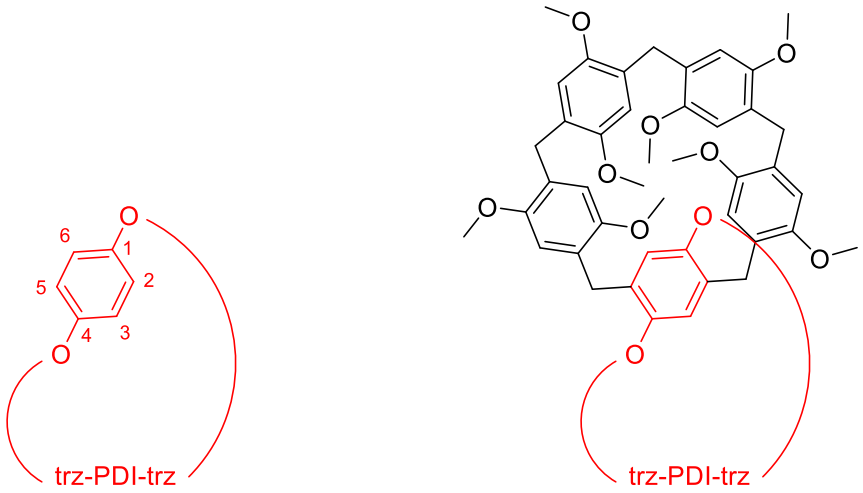

47

HQ-PDI macrocycle Pillar[5]arene-PDI macrocycle

Figure 3.7. HQ-PDI macrocycle **47** and pillar[5]arene-PDI macrocycle.

The twisted bis-alkyne PDI is also conformationally unstable prior to macrocyclisation (i.e., chirality is dynamic with $\Delta G^{\ddagger} < 39$ kJ mol^{-1})[126] and is therefore racemic (1:1 ***P***:***M***).[126b, 126c]. With both pillar[5]arene (***R**p**I**S**p***) and bis-alkyne PDI (***PIM***) being chirally dynamic, four stereoisomers could potentially be formed upon macrocyclisation, or two diastereomeric sets of enantiomers: ***PR**p*** and ***MS**p***; and ***PS**p*** and ***MR**p***. The confirmed

π-π interactions and proximity of hydroquinone-PDI macrocycle indicates that such a pillar[5]arene-PDI macrocycle may have similar π-π interactions and proximity in the ring-closing step to prefer one diastereomeric set over the other, thus achieving a diastereoselective synthesis. The important difference to previous bis-PDI macrocycles (**62**, **63**, and **60**) is that now both chiral units become configurationally stable upon macrocyclization. Furthermore, the well documented[127] chiral absorption of pillar[5]arene is at much lower wavelength (250 – 320 nm) compared to the main PDI absorption band (470 – 640 nm). Together, this should enable analysis of the stereochemical outcome of the reaction by CD spectroscopy.

3.3.2.1 Synthesis of Pillar[5]arene-PDI Macrocycle

Dibutyl alkylated pillar[5]arene **62**, synthesised and donated to the project by Dr. Pierce in Professor Champness' group, was reacted with NaN_3 in DMF at 60 °C overnight to quantitively yield azide **63**. This was then subjected to the CuAAC macrocyclisation conditions with PDI bis-alkyne **23** under identical high dilution conditions to furnish PDI-pillar[5]arene macrocycle **64** in 25% yield (Scheme 3.6).

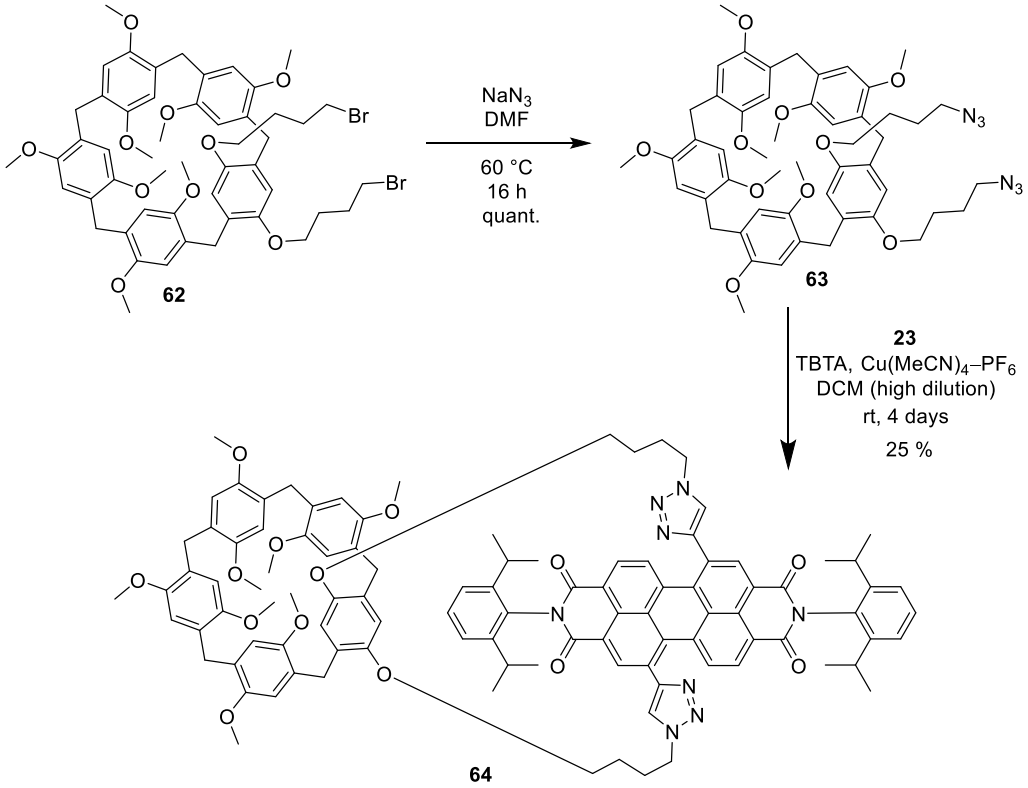

Scheme 3.6. Synthesis of pillar[5]arene-PDI macrocycle **64**.

Only one [1+1] macrocycle band was identified by TLC-mass spectrometry analysis. Upon isolation, this band only shows one set of signals by ^{1}H NMR spectroscopy. This suggests that only one diastereomeric set of enantiomers have been formed in this reaction, i.e. only ***PR$_p$*** and ***MS$_p$***, or only ***PS$_p$*** and ***MR$_p$***. Indeed, when subjected to chiral HPLC, two peaks of equal intensity were isolated under the optimised HPLC conditions from Chapter 2 (Figure 3.8). These stereoisomers of the macrocycle have exact mirror image CD spectra, demonstrating their identity as enantiomers.

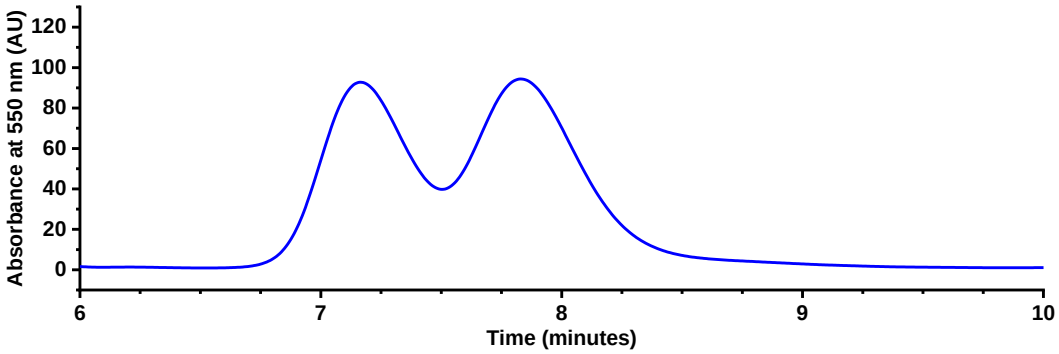

Figure 3.8. Chiral HPLC chromatogram of compound **64**.

3.3.2.2 Configurational Stability of PDI

As with other chirally locked macrocycles observed in Chapter 2, the methyl protons of the isopropyl groups on the imide group show diastereotopic splitting by ^{1}H NMR spectroscopy, indicating that this bis-triazole PDI units in the macrocycle is chirally locked (Figure 3.9).

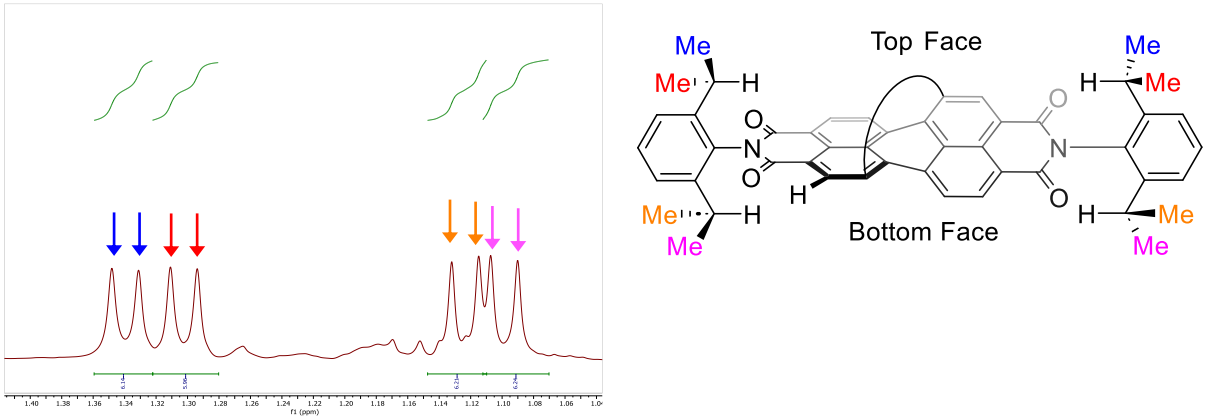

Figure 3.9. ^{1}H NMR spectra of PDI macrocycle **64**, displaying four sets of doublets for methyl groups due to diastereotopic splitting arising from chiral locking of the PDI ($CDCl_3$, 298 K, 400 MHz). Note that the assignment of methyl groups are not confirmed.

3.3.2.3 Interactions between Strap and PDI

Comparing the pillar[5]arene macrocycle **64** against the hydroquinone macrocycle **47**, ^{1}H NMR spectroscopy shows very similar shifts, with the triazole proton in **64** being slightly more deshielded (Δδ = 0.3 ppm). This suggests that both of these compounds are similar in the non-covalent interactions between the π-electron rich strap and the π-electron deficient PDI (Figure 3.10).

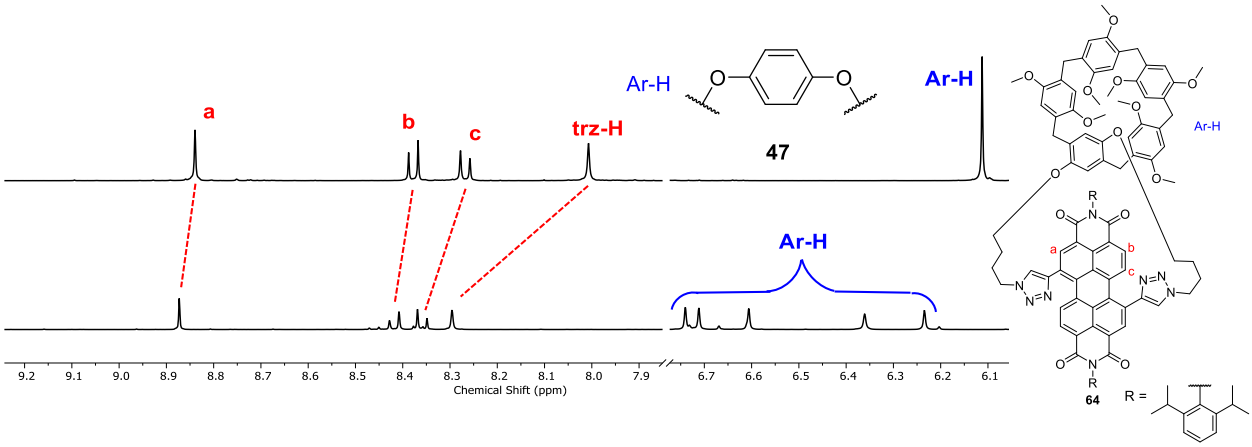

Figure 3.10. ^{1}H NMR spectra of PDI macrocycles **47** (top) and **64** (bottom) ($CDCl_3$, 298 K, 400 MHz).

Indeed, UV-vis absorption spectra of pillar[5]arene macrocycle **64** shows similar spectra compared to the hydroquinone counterpart **47**, with the former being slightly red shifted by 9 nm (Figure 3.11).

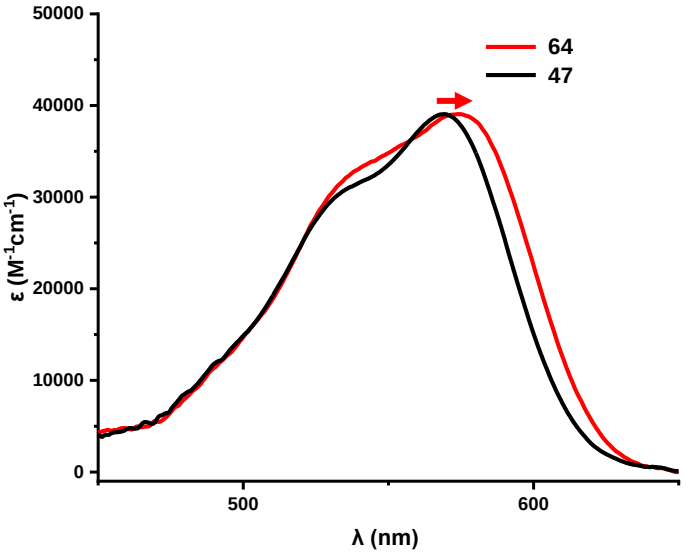

Figure 3.11. UV-vis absorption spectra of pillar[5]arene macrocycle (red), and HQ–PDI macrocycle **47** (black). All spectra were recorded in $CHCl_3$ at a concentration of 26 μM in a quartz cuvette with 1 cm path length.

3.3.2.4 Macrocyclic Chirality

To identify which of the diastereomeric sets are present in PDI-pillar[5]arene macrocycle **64**, the CD spectra were analysed in more detail. The chirality of the PDI unit (***P/M***) could be assigned by comparison against the hydroquinone macrocycle **47**, which was supported by literature and computational studies as described in Chapter 2. As such, the negative signals in the visible part of the CD spectrum (λ > 400 nm) were assigned to the ***P*** atropisomer of PDI, while the positive CD signals to ***M***-PDI (Figure 3.12).

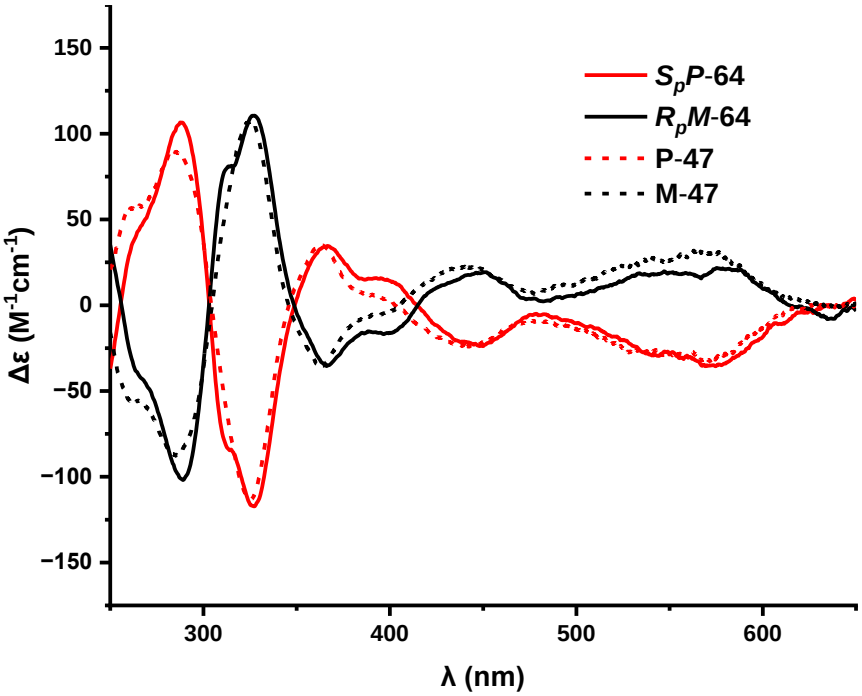

Figure 3.12. CD spectra of macrocycles **47** and **64**.

Yang and coworkers[127] have reported that pillar[5]arene has a CD active region between 250-330 nm, with positive/negative absorbances at 290 nm and 310 nm. A pillar[5]arene with $\boldsymbol{R_p}$ chiral conformation exhibits a negative signal at 290 nm and positive signals at 255nm and 310 nm, and vice versa for $\boldsymbol{S_p}$. Similarly, comparing the CD spectra of the pillar[5]arene PDI macrocycle **64** against the hydroquinone PDI **47**, a stronger negative CD signal is observed at 290 nm, and further positive absorptions at 255 and 310 nm. Indeed, there is a clear shoulder band at 310 nm, where the pillar[5]arene signal is most intense. This provides strong evidence for assigning the

chirality of the pillar[5]arene in macrocycle **64**. Therefore, in the absence of further computational studies, the isolated set of macrocycle enantiomers are ***P***-PDI with S_p-pillar[5]arene, and ***M***-PDI with R_p-pillar[5]arene (Figure 3.13).

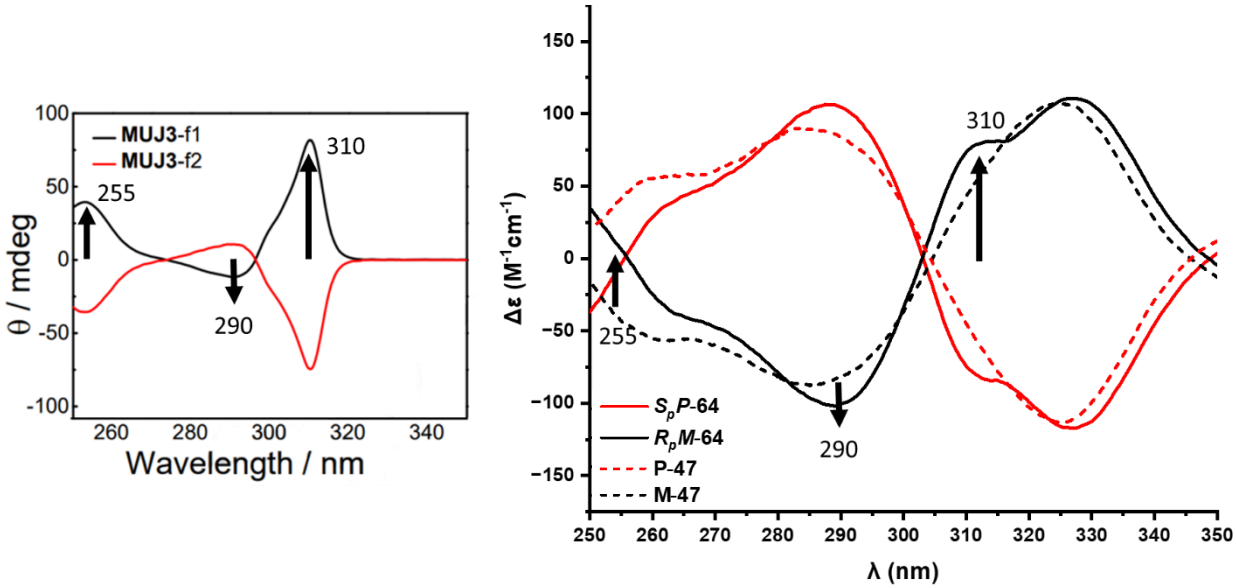

Figure 3.13. Left: CD spectra of pillar[5]arene by Yang and coworkers. Right: CD spectra of pillar[5]arene-PDI macrocycle **64**.

A preliminary investigation was conducted to try and explain why this diastereomeric set is favoured. Aforementioned, pillar[5]arene-PDI macrocycle can be thought of as a hydroquinone-PDI macrocycle that has been strapped into a pillar[5]arene at the 2,5- or 3,6- positions of the hydroquinone, which would give a pillar[5]arene of R_p or S_p chirality, respectively. Therefore, the crystal structure of HQ-macrocycle **47** was modified (using Chem3D software) by appending methyl groups at the 2,5- positions, and the 3,6- positions of the hydroquinone. These methyl groups, if cyclised into pillar[5]arenes, would respectively form R_p-pillar[5]arene and S_p-pillar[5]arene (Figure 3.14).

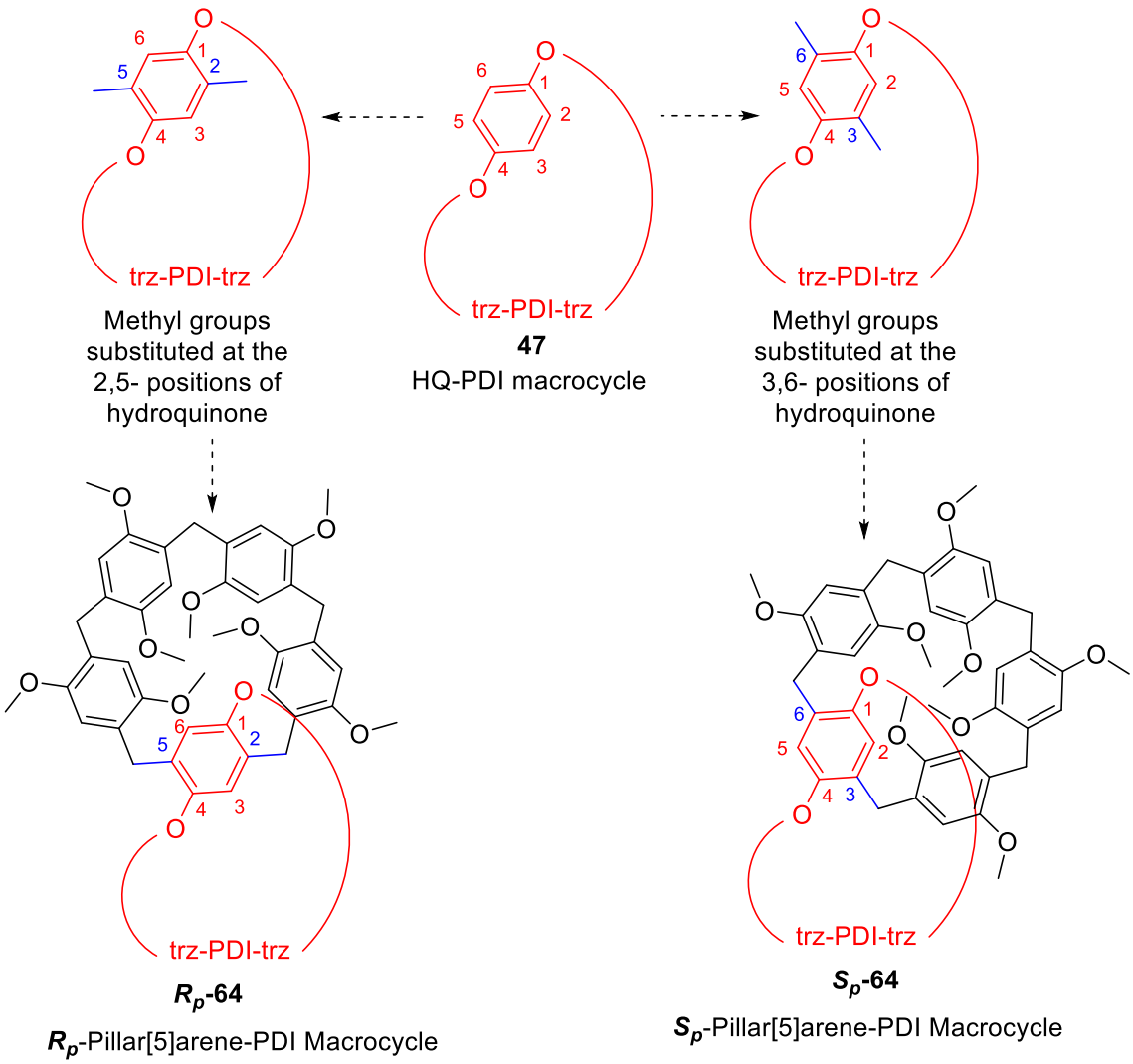

Figure 3.14. Methyl substituted PDI-HQ macrocycles, representing the two stereoisomers of pillar[5]arene-PDI macrocycles **64**.

It was discovered that a methylene group in ***R***$_p$-pillar[5]arene would sterically clash with the isopropyl group in the imide substituent of a ***P***-PDI unit, while another methylene group would also clash with a triazole heterocycle. These steric clashes are already significant without taking into account the hydrogen atoms on these groups. Indeed, the distances between the relevant carbon atoms is small (2.8 – 3.1 Å), less than the sum of van der Waals radii (Figure 3.15, left). These steric clashes, are, however, not present in the macrocycle of ***S***$_p$-Pillar[5]arene and ***P***-PDI as the methylene groups of the ***S***$_p$-Pillar[5]arene unit are situated much further away from both the isopropyl methyl and triazole groups, with longer carbon-carbon distances of 4.2 and 4.5 Å respectively

(Figure 3.15). These steric effects may help to explain why only ***PS*$_p$** and ***MR*$_p$** macrocycles were formed selectively in the reaction whereas ***MS*$_p$** and ***PR*$_p$** were not.

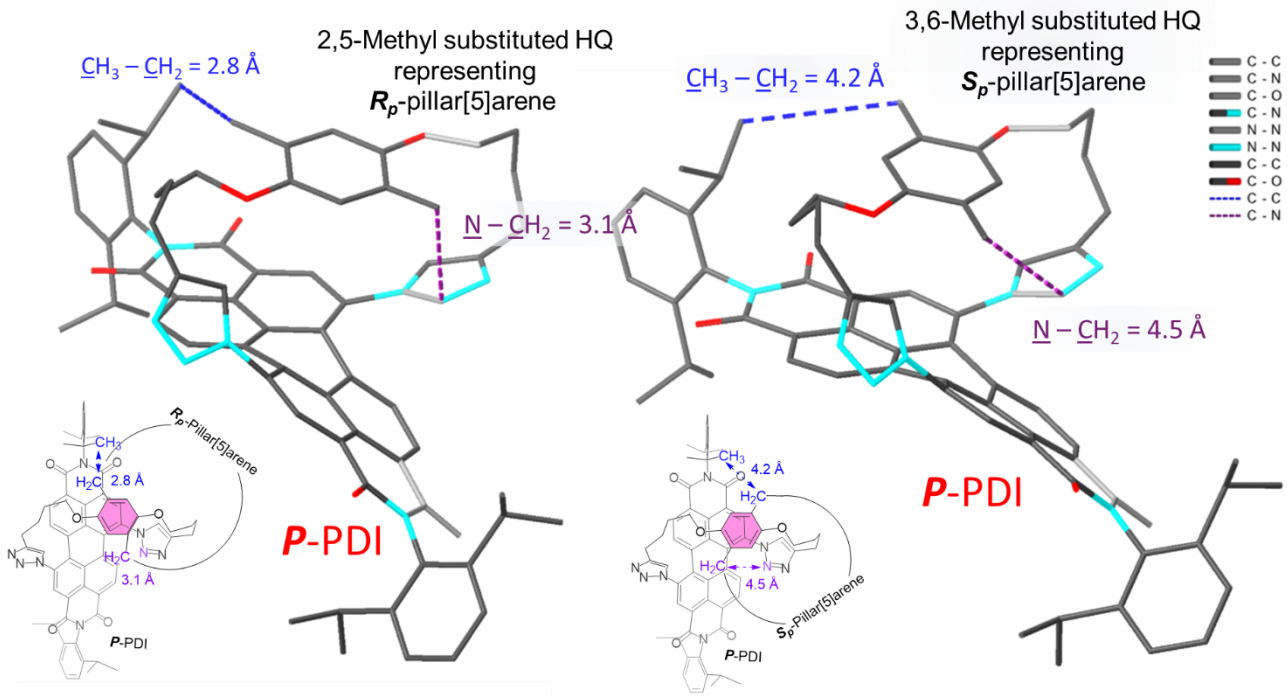

Figure 3.15. Constructed methyl substituted macrocycles representing both diastereomers of ***PS*$_p$** and ***PR*$_p$**-**64**, based on the crystal structure of HQ-PDI macrocycle **47** (HQ = hydroquinone)

It was shown in Chapter 2 that the PDI is configurationally stable in macrocycles of the design of **64**. The pillar[5]arene unit is also configurationally stable, since the large PDI unit cannot flip through the cavity of the pillar[5]arene. Indeed, smaller functional groups than PDI have been used to prevent the racemisation of pillar[5]arene, such as 4-(methoxycarbonyl)phenyl groups.[128] Thus, it can be concluded that macrocycle **64** is configurationally stable, meaning that diastereoselectivity must occur in the synthesis. Prior to cyclisation, it is likely that the four conformers of the mono-clicked macrocycle intermediate (***PS*$_p$**, ***MR*$_p$**, ***MS*$_p$**, and ***PR*$_p$**) are in thermodynamic equilibrium and able to rapidly interconvert, as both acyclic PDI ($\Delta G_{int}^{\ddagger}$ < 39 kJ mol^{-1}) and the parent pillar[5]arene ($\Delta G_{int}^{\ddagger}$ ≈ 57 kJ mol^{-1}, *cf.* 1,4-bis(heptyloxy)pillar[5]arene)[129] have low interconversion barriers. Furthermore, as no detectable interaction could be found between the HQ unit and the PDI unit in the acyclic HQ-PDI-HQ control compound **50** (*vide infra*, Section 2.4.2), it was likely that all four of these conformers mono-clicked

macrocycle intermediate (***PS*$_p$**, ***MR*$_p$**, ***MS*$_p$**, and ***PR*$_p$**) are in equal populations (i.e. of equal energies) prior to the second ring-closing CuAAC 'click' reaction. As such, it can be postulated that the diastereoselectivity arises from the difference in transition state energies between the experimentally isolated set of enantiomers (***PS*$_p$** and ***MR*$_p$**), and the unseen stereoisomers (***MS*$_p$**, and ***PR*$_p$**). This free energy difference may be due to the aforementioned steric clash between the methylene group in pillar[5]arene and the isopropyl group in the imide group of PDI seen in ***MS*$_p$**, and ***PR*$_p$** set of enantiomers, potentially weakening the π-π donor-acceptor interaction between the pillar[5]arene and PDI units (Figure 3.16).

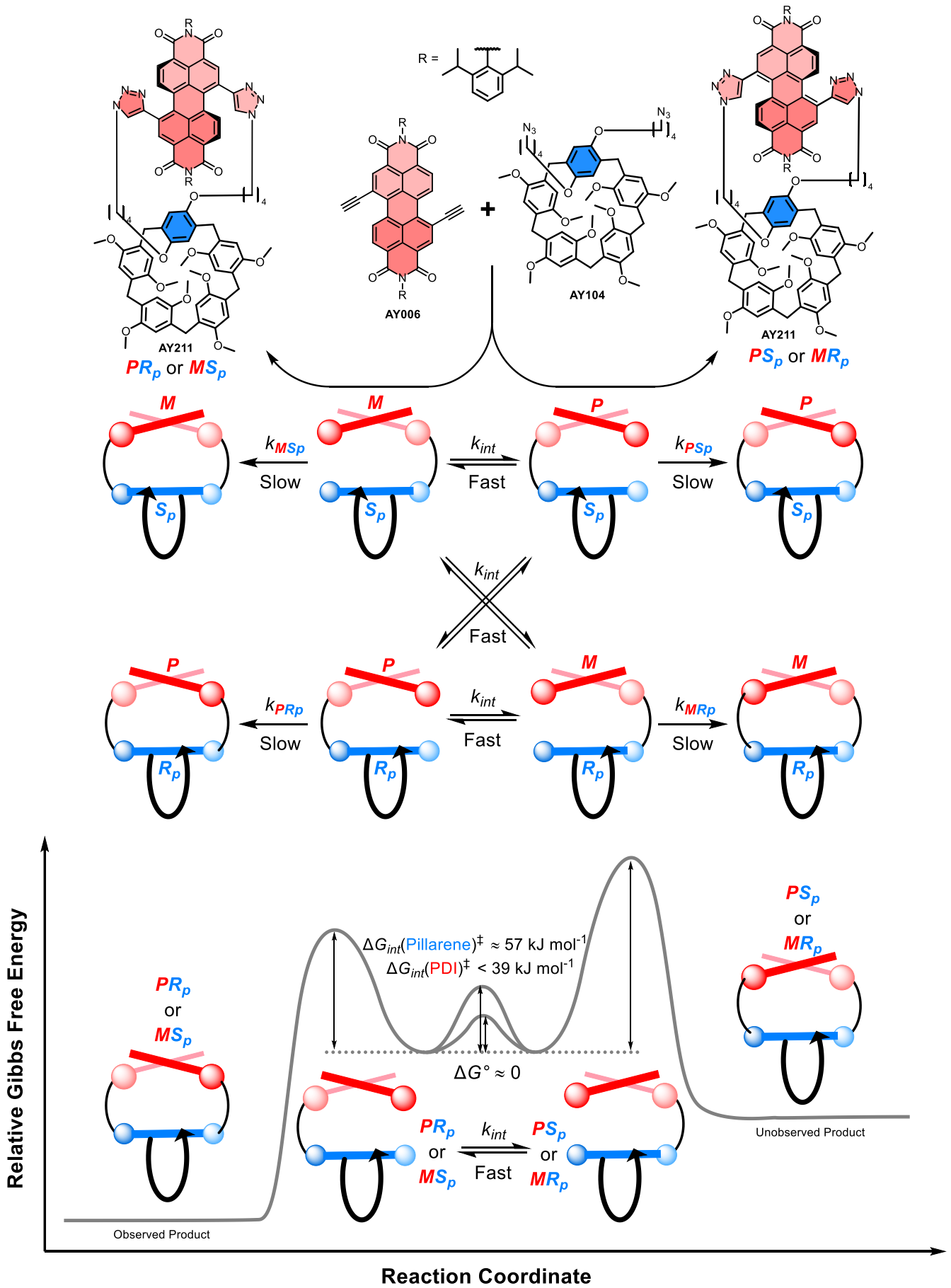

Figure 3.16. The energy profile diagram for the diastereoselective synthesis of macrocycle **64**.

3.4 Diastereoselective Synthesis with a Configurationally Stable Unit

With pillar[5]arene-PDI macrocycle **64**, it is shown that PDI macrocycles can be formed with a preference for one pair of enantiomers over the other. To further build upon this, it was of interest to see if a configurationally stable chiral unit would induce its chirality onto the PDI in the formation of the macrocycle, thereby limiting the number of stereoisomeric products to two diastereomeric [1+1] macrocyclic products (i.e., no enantiomers) (*vide supra*, Figure 3.2). This would enable configurationally stable PDI macrocycles to be prepared as a single stereoisomer without the need for specialist techniques such as chiral HPLC for resolution. This may also deepen our understanding of the role of supramolecular chemistry in a dynamic kinetic resolution for directing the stereochemical outcome of a reaction between interacting chiral molecules under irreversible conditions.

Several criteria for the configurationally stable unit must be met, namely chiral stability, affordability, ease of synthesis, ease of characterisation and a π-donating ability for aromatic interactions with PDI. 1,1'-Bi-2-naphthol (BINOL) fits all these criteria, being configurationally stable at room temperature ($\Delta G^{\ddagger}$ = 158 kJ mol^{-1})[130] and commercially available in high enantiopurity. Additionally, BINOL is made of two π-donating naphthalene units, which could form π-π interactions with the π-electron deficient naphthalene units of the PDI. Furthermore, BINOL and PDI exhibit axial chirality and thus may lead to the formation of a complimentary twisted homochiral macrocycle (***PP*/*MM***) and a non-complimentary twisted heterochiral macrocycle (***PM*/*MP***) (Figure 3.17).

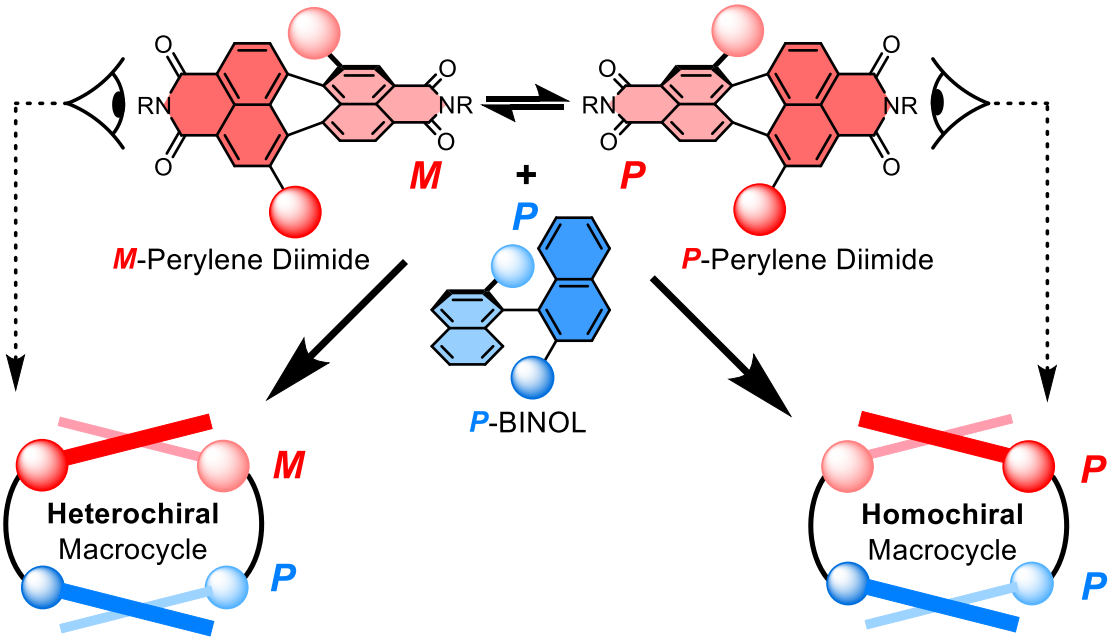

Figure 3.17. Synthesis of PDI and ***P***-BINOL macrocycle resulting in complimentary twisted homochiral macrocycle (***PP***) and non-complimentary twisted heterochiral macrocycle (***PM***).

3.4.1 Synthesis of BINOL Macrocycles

Synthesis of the BINOL linkers proceeded with similar conditions than that of DHN or HQ linkers described in Chapter 2. Commercially available ***P***-BINOL was alkylated with an excess of 1,3-dibromopropane or 1,4-dibromobutane in the presence of K_2CO_3 in acetone at 60 °C for three days, to respectively furnish **65-3** in 51% yield and **65-4** in 36% isolated yield (57% conversion). The major side product was identified to be the [1+1] macrocyclic adduct by ^{1}H NMR spectroscopy and ESI mass spectrometry. The bromides **65-3** and **65-4** were then reacted with NaN_3 in DMF and left to stir at 75 °C overnight to quantitively yield the bis-azides **66-3** and **66-4** respectively (Scheme 3.7).

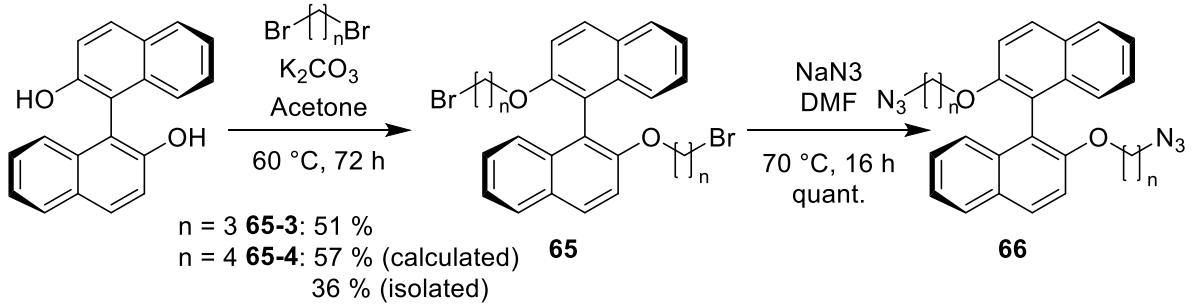

Scheme 3.7. Synthesis of **66**.

The bis-azides **66-3** and **66-4** were then reacted with PDI-bisalkyne **23**, with a catalytic amount of $Cu(MeCN)_4 \cdot PF_6$ and TBTA in DCM under high dilution conditions over six days, after which the reaction showed full consumption of starting materials by TLC. Whist reaction with the shortest linker **66-3** did not yield any [1+1] macrocyclic products, purification by silica flash column chromatography followed by preparative TLC of **67-4** gave two [1+1] macrocyclic products, each in a low yield, 2% (Scheme 3.8). These [1+1] macrocyclic products were characterised by TLC, ^{1}H NMR spectroscopy, and ESI mass spectrometry.

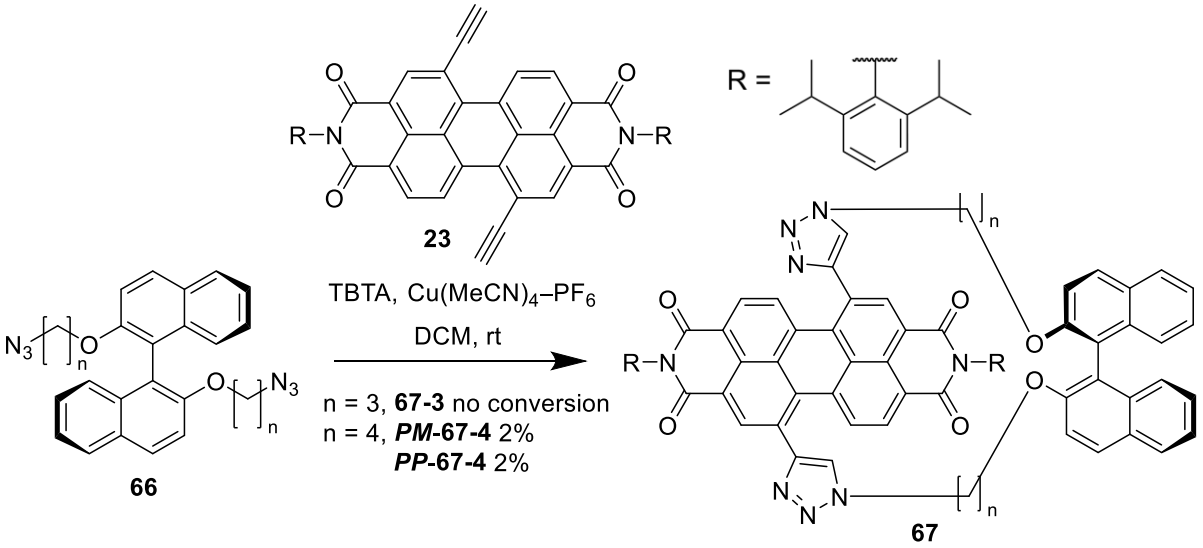

Scheme 3.8. Attempted synthesis of PDI-BINOL macrocycle **67-3** and synthesis of PDI-BINOL macrocycle **67-4**.

The lack of reaction of the shortest propyl linker **66-3** and the low yield of **67-4** were ascribed to the majority of starting materials reacting to form [2+2] or larger macrocycles or oligomers, since monitoring the reactions by TLC showed many concentrated spots of high polarity. ESI mass spectrometry also revealed the formation of these larger macrocycles.

It was hypothesised that the absence of the desired [1+1] macrocycle in **67-3** and the low yield of **67-4** was due to the high ring strain present in these macrocycles, where the second intramolecular CuAAC reaction is retarded to the point where intermolecular reaction with a second molecule becomes more likely. While the use of a longer linker may weaken the templating interaction with the PDI (Chapter 2, section 2.3.2), the

overall energetic cost may be lower as the macrocycle is less strained. Upon increasing the linker length further still, where ring strain is of much less significant, one may expect the yield to decrease again due to weaker non-covalent interactions between the linker and PDI and the potential increase in the entropic penalty, i.e. the linker is less preorganised.

Therefore, a longer dibromo hexyl **66-6** and an even longer dibromo octyl **66-8** linkers were synthesised using an analogous procedure to the butyl **66-4** above. Specifically, 1,6-dibromohexane and 1,8-dibromooctane were used to alkylate P-BINOL to yield **65-6** and **65-8** in 69% and 86% respectively. Once again, the major side product was identified to be the [1+1] macrocyclic adduct. It was interesting to see the effect of entropy on this reaction. When the shortest 1,3-dibromobutane was used, the entropic cost in the formation of the [1+1] macrocyclic side product was the lowest, thus more side product is formed in the reaction and the yield of the desired acyclic product was the lowest (51%). The longer 1,4-dibromohexane, 1,6-dibromohexane and 1,8-dibromooctane sequentially have higher entropic cost to form [1+1] macrocycles, thus the yields of the desired acyclic products were sequentially higher (57%, 69% and 86% respectively) (Scheme 3.9).

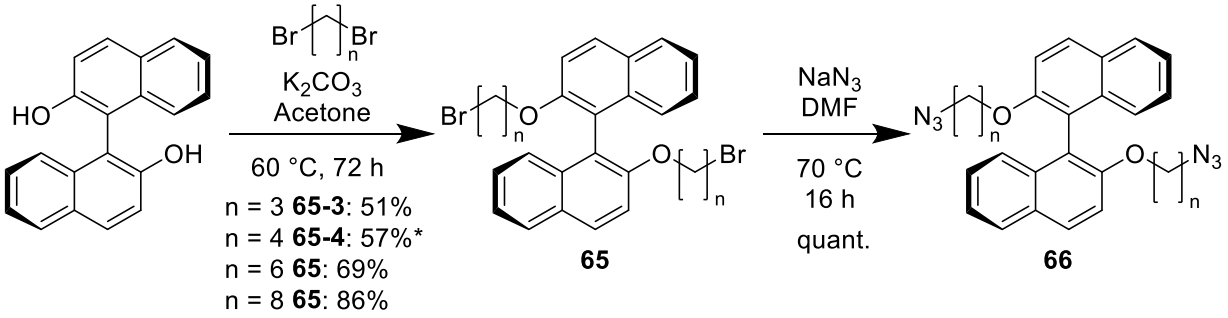

*calculated yield by ^{1}H NMR spectroscopy of crude mixture

Scheme 3.9. Synthesis of BINOL bisazide **66**.

Next, the resulting bis-bromo acyclic BINOL compounds **65-6** and **65-8** were each reacted with NaN_3 in DMF at 75 °C overnight to quantitively yield bis-azides **66-6** and **66-8**. These bis-azides **66-6** and **66-8** were subjected to identical CuAAC conditions as above with PDI-bisalkyne **23** to respectively furnish the BINOL-PDI macrocycles **67-6**

and **67-8**. The hexyl linked **67-6** was purified by silica flash column chromatography to yield two [1+1] macrocyclic species, the first of which did not require further purification and was isolated in a much improved yield of 42% yield; the second macrocyclic species required further purification by preparative TLC to and isolated in a 3% yield. The larger **67-8** was purified by preparative TLC to give two [1+1] macrocyclic products **67-8** in much lower isolated yields (1% for both). The presence and purity of these [1+1] macrocyclic products were once again confirmed by TLC, ^{1}H NMR spectroscopy, and ESI mass spectrometry. The major side products were [2+2] or larger macrocycles or oligomers, as confirmed by TLC and ESI mass spectrometry (Scheme 3.10).

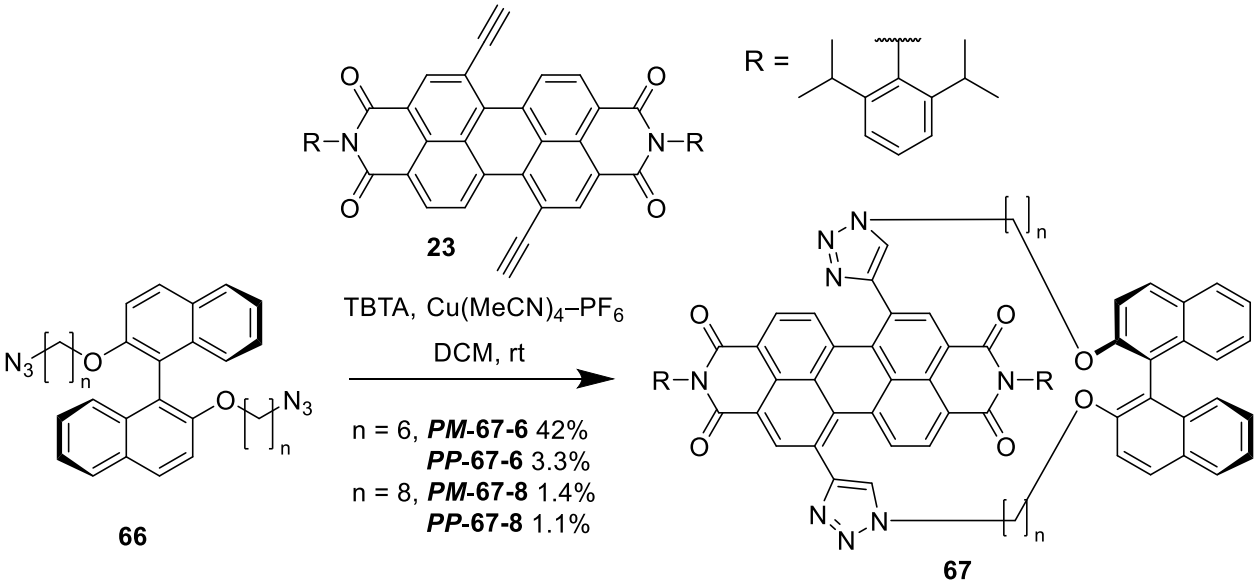

Scheme 3.10. Synthesis of PDI-BINOL macrocycle **67**.

As expected, upon swapping ***P***-BINOL for ***M***-BINOL in the synthesis of macrocycle **67-6**, the two macrocycle stereoisomers are obtained in the same ratio, with the first isolated stereoisomers having identical ^{1}H NMR spectra to each other, and second isolated stereoisomers having identical ^{1}H NMR spectra each other, as expected due to their enantiomeric relationship.

An acyclic control compound **68** was also synthesised by CuAAC of **23** and an excess of **66-6** at a higher concentration. This procedure mirrors the synthesis of the acyclic control compounds described in Chapter 2 (Scheme 3.11).

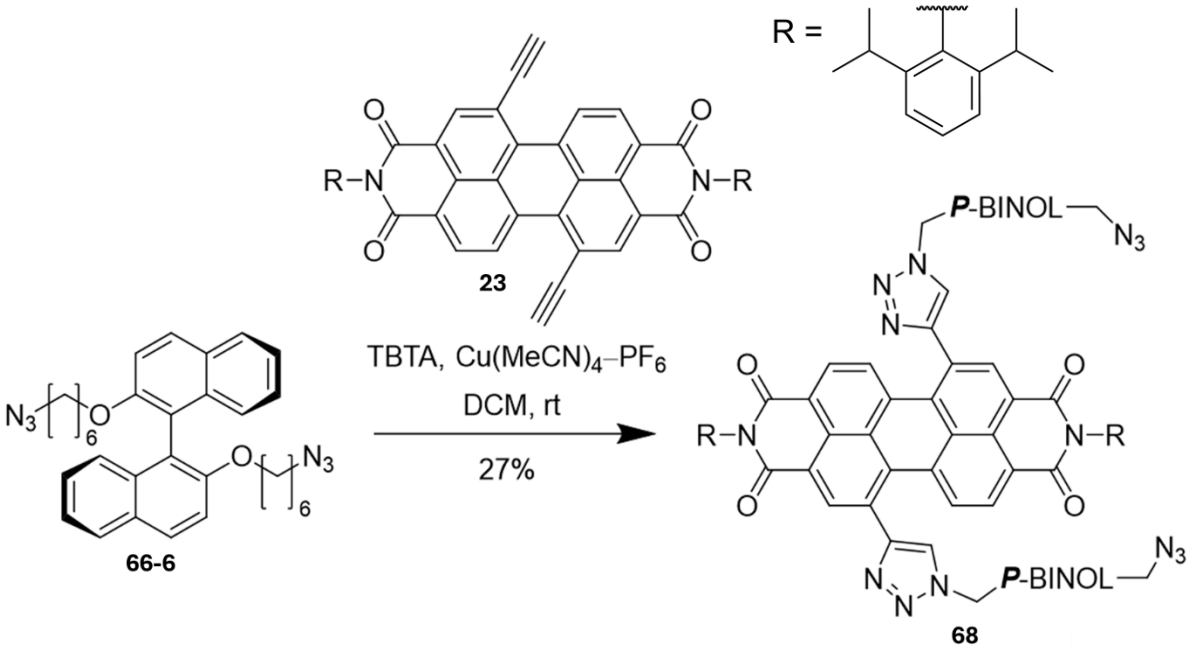

Scheme 3.11. Synthesis of acyclic BINOL-PDI-BINOL **68**.

To accurately quantify the diastereoselectivity (*vide infra*) of the macrocyclisation reaction for each linker length of **67**, the crude reaction mixture was subjected to ^{1}H NMR spectroscopy prior to purification. This eliminates the error arising from the loss of compound during the purification. Here, the integration of non-overlapping ^{1}H NMR signals of the same relative proton reveals that neither the shorter butyl **67-4** (Figure 3.18, top) or the longer octyl **67-8** (Figure 3.18, bottom) linkers exhibit any diastereoselectivity, whereas the medium length hexyl **67-6** displays a 4:1 diastereoselectivity (Figure 3.18, middle).

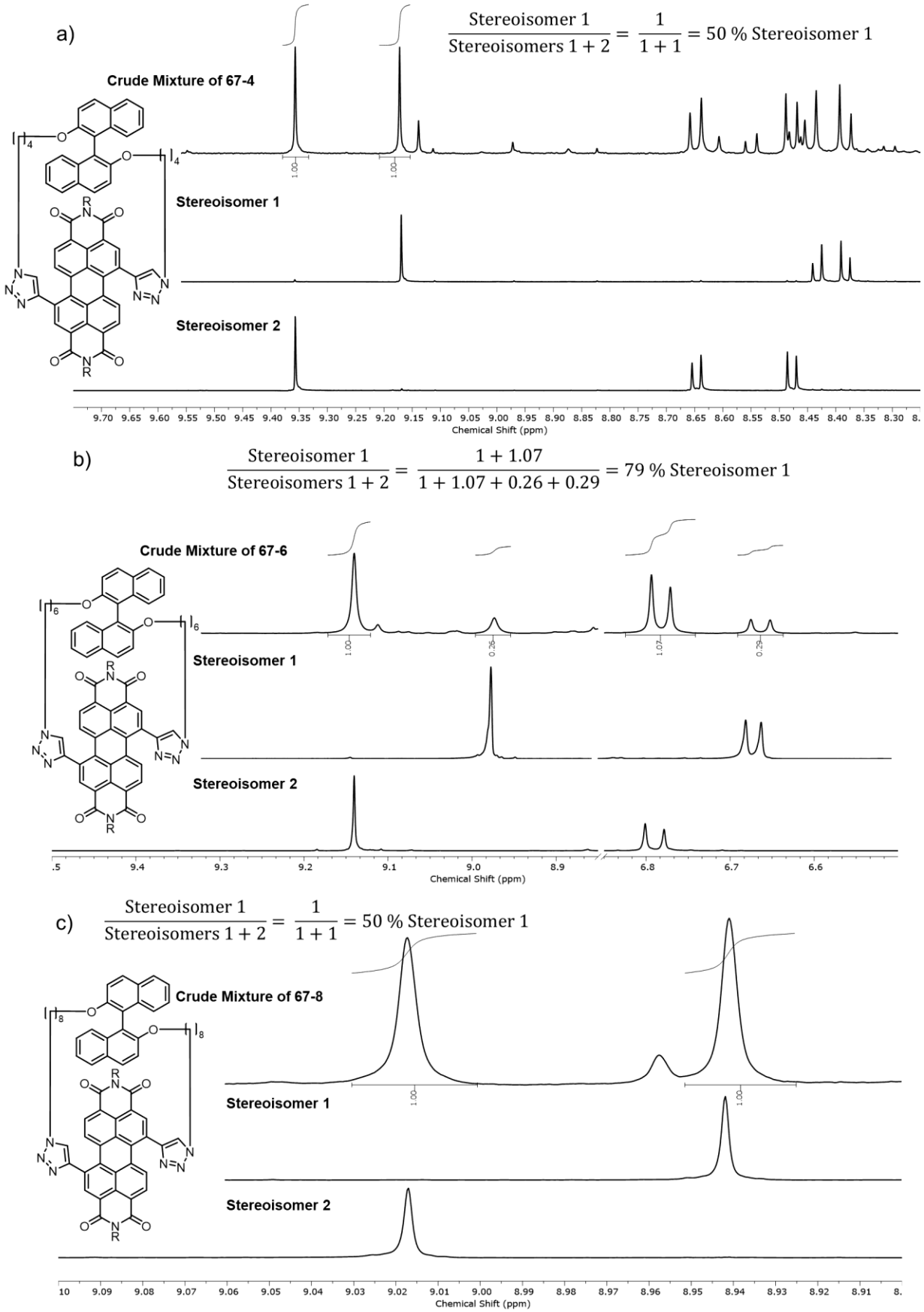

Figure 3.18. ^{1}H NMR of crude reaction mixture of macrocycle, and both purified stereoisomers of a) **67-4** b) **67-6** c) **67-8** (400 MHz, $CDCl_3$).

3.4.2 Macrocyclic Chirality

It was important to assign the stereoisomers of the BINOL–PDI macrocyclic products of **67**. As the stereoisomeric macrocyclic products found for each linker length of **67** were separable by silica gel chromatography, exhibit distinct ^{1}H NMR spectra (*vide infra*, Section 3.4.4), and also display a single peak in chiral HPLC (Figure 3.19), these stereoisomers are confirmed as diastereomers. As expected, there are no enantiomeric products due to the fixed axial chirality of the BINOL unit.

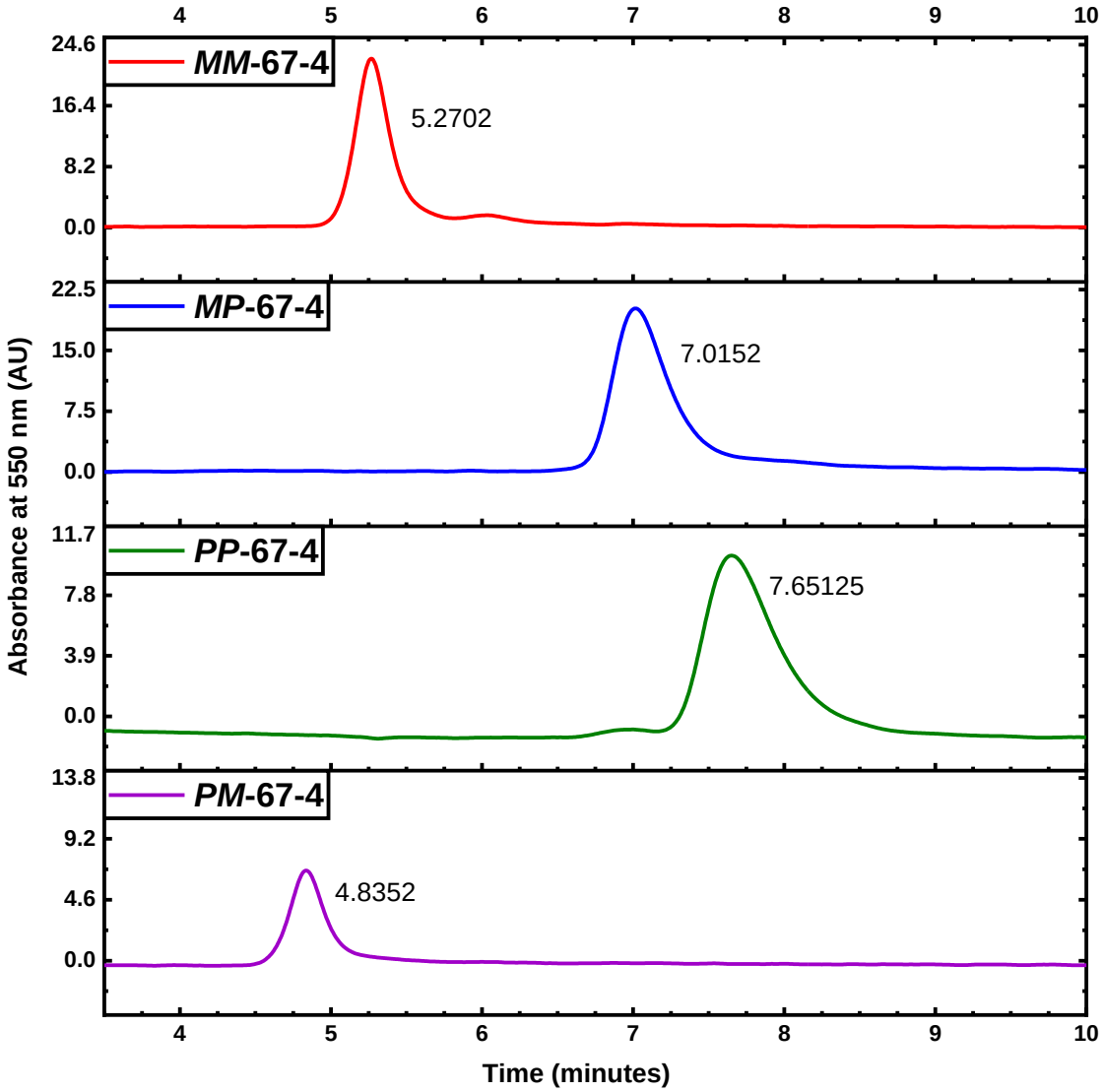

Figure 3.19. Chiral HPLC chromatogram of compounds **67-6** with chirality: ***MM*** (red), ***MP*** (blue), ***PP*** (green), and ***PM*** (purple), dissolved in DCM and eluted with 0.1:60:39.9 IPA:n-hexane:CH_2Cl_2. The flow rate was 1 mL/minute, and the detection wavelength was 500 nm. Retention times of each compound are shown next to the peaks. Chirality labels are assigned based on CD and DFT described below.

To assign the chirality of the two ***P***-BINOL–PDI macrocycle diastereomers, CD spectroscopy was performed. It should be noted that the CD spectrum of ***P***-BINOL is CD silent at wavelengths greater than λ = 400, showing that the CD signal seen in this region for **67** must arise purely from the PDI. Notably, the spectrum of acyclic control compound ***P***-BINOL-PDI-***P***-BINOL **68** matches that of ***P***-BINOL (but doubled in intensity as it contains two ***P***-BINOL units), with no signal in the PDI region, demonstrating that a macrocyclic motif is needed to induce chirality into the PDI unit. The two macrocyclic products exhibit almost opposite CD spectra but are not perfect mirror images due to being diastereomers. The opposite CD signals in the PDI-only region (λ = 350 – 600 nm) indicate the respective opposite twisting (***P***/***M***) of the PDI units (Figure 3.20).

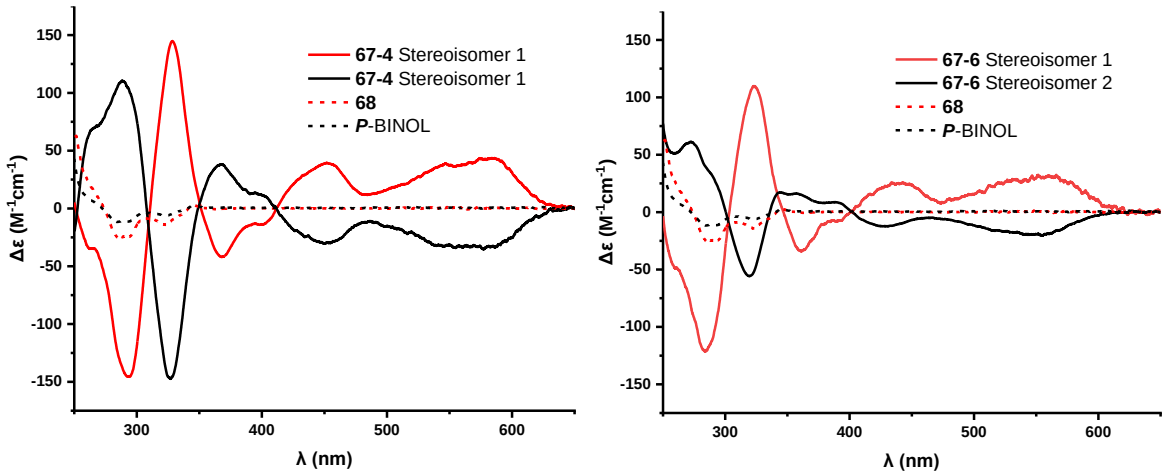

Figure 3.20. CD spectra of ***P***-BINOL (black, dotted); BINOL-PDI-BINOL **68** (red, dotted); stereoisomer 1 (red, solid) of **67-4** (left) and **67-6** (right); and stereoisomer 2 (black, solid) or **67-4** (left) and **67-6** (right).

The assignment of these macrocycle diastereomers was achieved by comparisons with DFT predicted CD spectra, as calculated by the same methodology previously described in Section 2.4. Here, it is important to note that the CD spectrum of the heterochiral diastereomer (**67-6**) was calculated using a structure that is not guaranteed to be the lowest energy structure because it is significantly higher in energy compared to the homochiral diastereomer structure (>20-30 kJ mol^{-1}). Further details of this computational work are provided in Section 5.7.

Comparing the calculated against the experimental CD spectra, the negative signals in the visible part of the CD spectrum (λ > 400 nm) can be assigned to the ***P*** atropisomer of PDI (i.e., ***PP*-67**), while the positive CD signals to ***M***-PDI (i.e., ***PM*-67**) (Figure 3.21). This revealed that the higher yielding diastereomer is the higher energy heterochiral macrocycle (***PM***) and the lower yielding diastereomer is the lower energy homochiral (***PP***), in a diastereomeric ratio of 4:1. This is intriguing because previous work on diastereomeric PDI-based macrocycles has found the major species to be homochiral.[131]

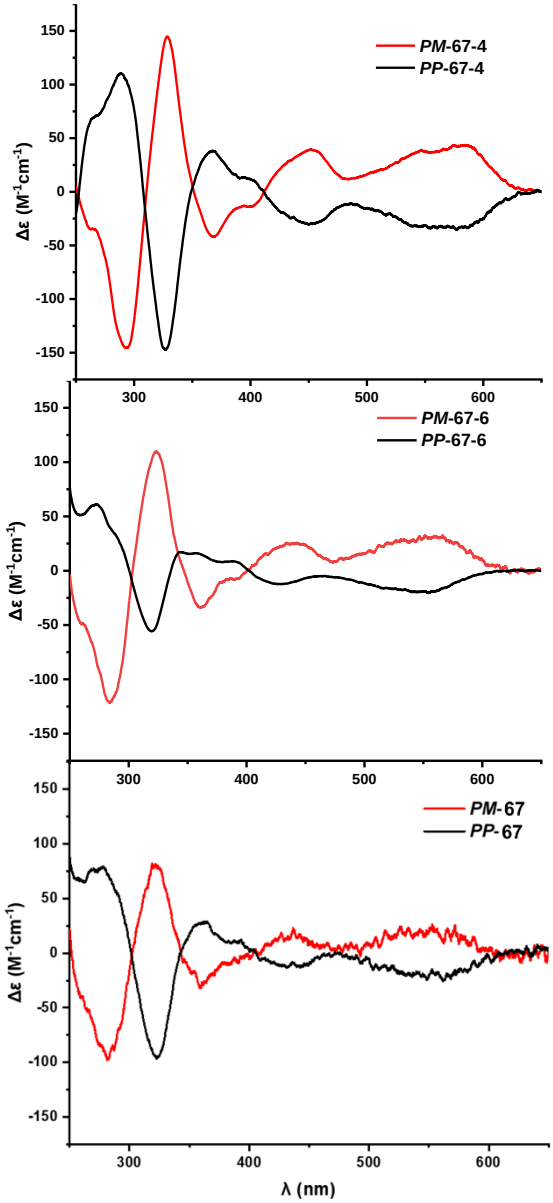

Figure 3.21. CD spectrum of BINOL-PDI macrocycles **67-4** (top), **67-6** (middle), and **67-8** (bottom), with chirality ***PM*** (red) and ***PP*** (black).

Interestingly, comparing the CD spectra of the three different linker lengths of **67**, the intensity of their CD signals increases as linker length decreases. This is indicative of smaller macrocycles placing more strain on the PDI, which in turn increases the PDI twist angle.[104c] Indeed, the DFT optimised structure of ***PP*-67-4** exhibit a larger twist angle (25°) compared to that of ***PP*-67-6** (23°). Additionally, the CD signal for heterochiral macrocycle ***PM*-67-6** is also stronger than homochiral ***PP*-67-6**, also in agreement with the PDI twist angles in the DFT optimised structures (Figure 3.22). This suggests that heterochiral ***PM*-67-6** is more strained than its homochiral counterpart (***PP***), a factor that will contribute to the former macrocycle being a higher energy structure, as predicted by DFT.[132]

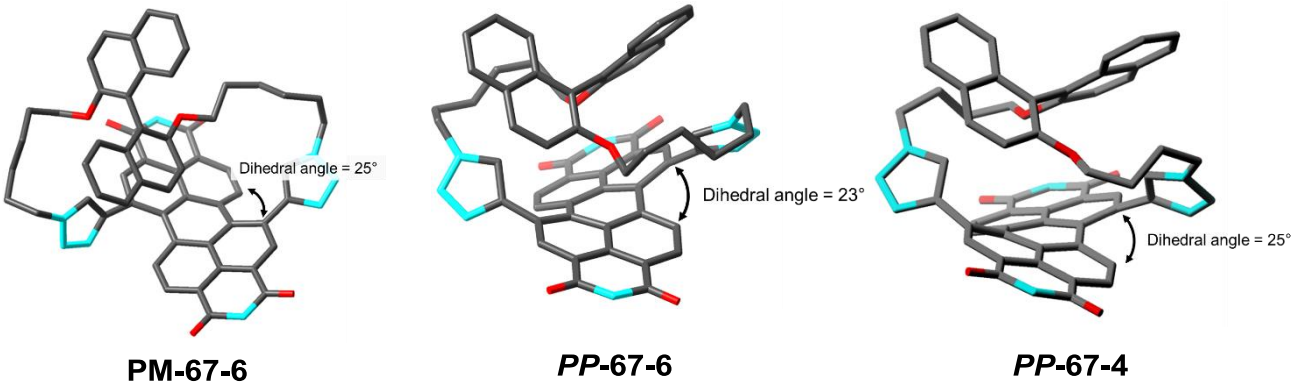

Figure 3.22. Calculated structures of ***PM*-67-6**, ***PP*-67-6**, and ***PP*-67-4**, displaying their PDI core twists of 25°, 23° and 25° respectively. For clarity, hydrogen atoms and the 2,6-diisopropylphenyl imide substituents have been removed from these structures.

Furthermore, the DFT optimised structure of macrocycle ***PP*-67-6** shows an additional intramolecular CH–O hydrogen bond (d = 2.5 Å) between the triazole unit and the

BINOL's O atom compared to ***PM*-67-6**, which will also contribute to the former being lower in energy. (Figure 3.23).

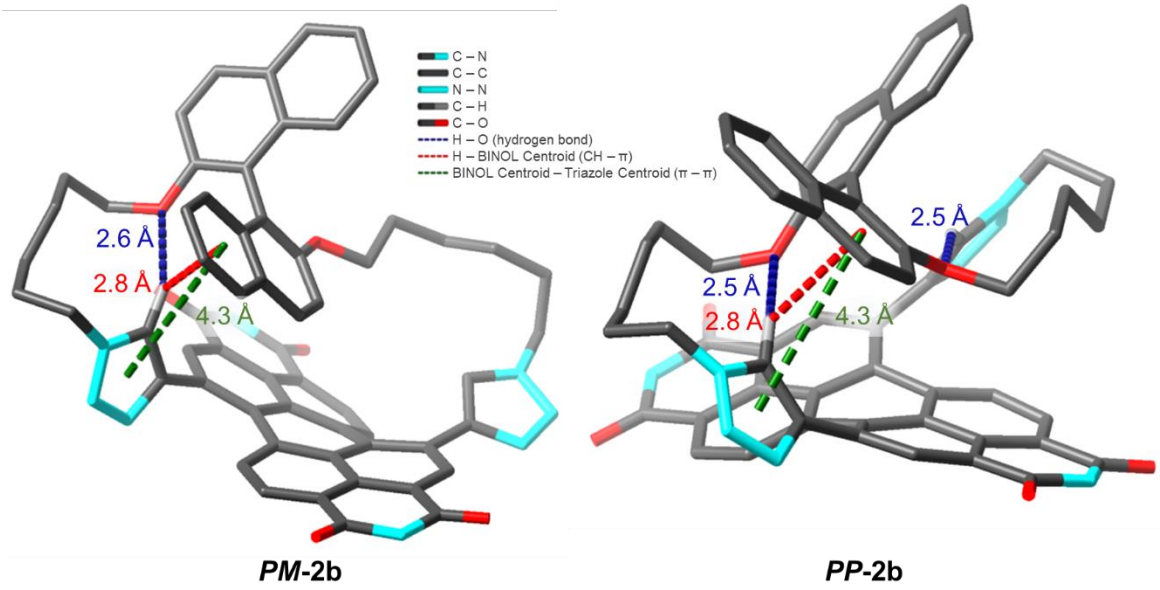

Figure 3.23. Calculated structures of ***PM*-67-6** and ***PP*-67-6** showing relevant non-covalent interactions (π–π, CH–π and CH–O hydrogen bonding). Note, the CH–π interactions are represented by close contacts between H and a BINOL centroid and π–π interactions are represented by close contacts between BINOL/PDI/triazole centroids. For clarity, hydrogen atoms and the 2,6-diisopropylphenyl imide substituents have been removed from these structures.

As expected, in macrocycle **67-6** where ***P***-BINOL was swapped for ***M***-BINOL, the major macrocyclic product was revealed to be the heterochiral ***MP*-67-6**, and the minor was homochiral ***MM*-67-6**. Both ^{1}H NMR and CD spectroscopy show that ***MM*-67-6** and ***MP*-67-6** are respectively enantiomeric to ***PP*-67-6** and ***PM*-67-6**, as displayed by their identical ^{1}H NMR spectra (Figure 3.25) and perfect mirror imager CD spectra (Figure 3.24).

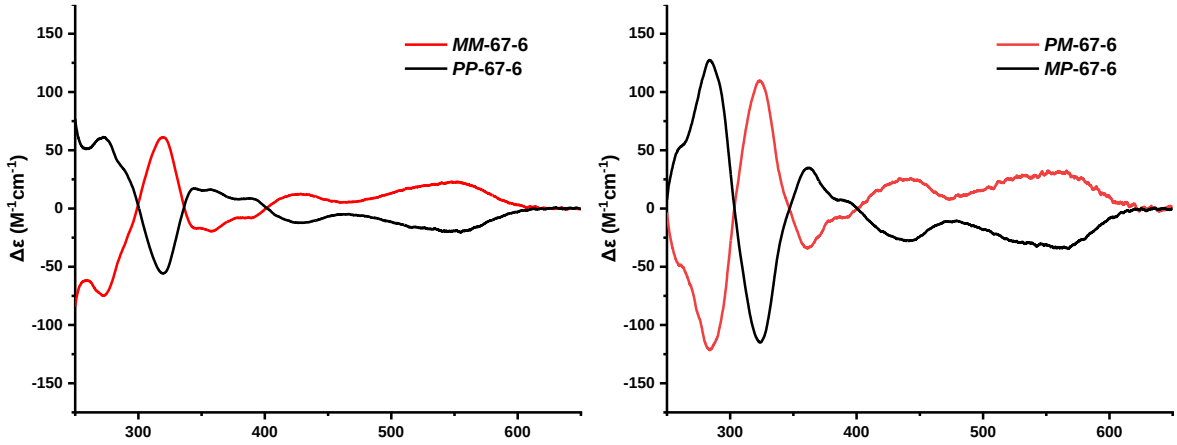

Figure 3.24. CD spectrum of ***PP*-67-6** (left, black), ***MM*-67-6** (left, red), ***MP*-67-6** (right, black), ***PM*-67-6** (right, red).

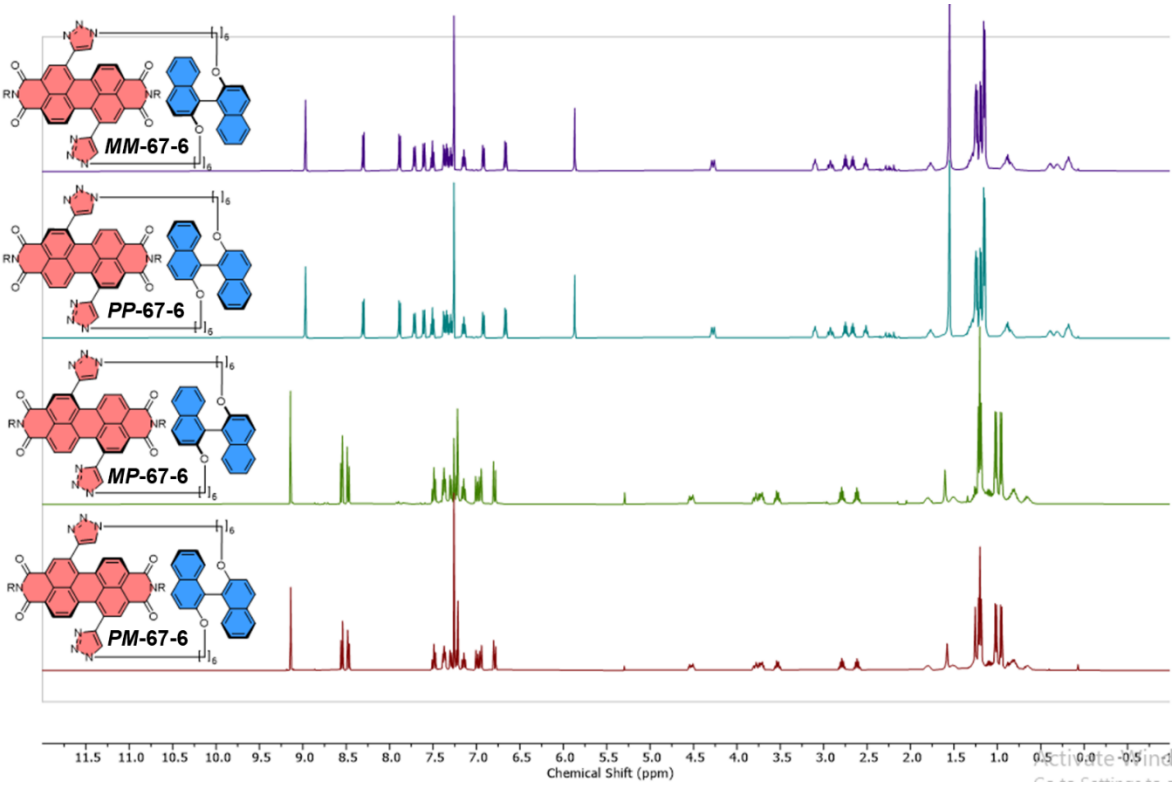

Figure 3.25. ^{1}H NMR of **67-6** (400 MHz, $CDCl_3$), displaying the identical spectra of macrocycles that have an enantiomeric relationship (e.g., ***MM*-67-6** and ***PP*-67-6**).

Compound	***PM*** isolated yield	***PP*** isolated yield	***PM*:*PP*** dr
67-3	0	0	N/A
67-4	2	2	1:1
67-6	42	3.3	4:1
67-8	1.4	1.1	1:1

Table 3.1. Table summarising yields and selectivity of compounds **67-3**, **67-4**, **67-6**, and **67-8**.

3.4.3 Curtin-Hammett Principle

According to DFT calculations, the heterochiral (***PM***) macrocycle is higher in energy than the homochiral (***PP***) stereoisomer, yet the former macrocycles is formed in higher yield. To understand the origin of this stereoselectivity, it is important to consider the Curtin-Hammett principle. This principle states that the outcome of a dynamic kinetic resolution is dependent on the relative free energy of the interconverting precursors (i.e., $\Delta G°$ in Figure 3.26) and the relative activation energies (i.e., $\Delta G_{PP}^{\ddagger} - \Delta G_{PM}^{\ddagger}$). Or in other words, the reaction outcome is solely dependent on the difference in transition state energies of the products ($\Delta\Delta G^{\ddagger}$, Figure 3.26).[133] Indeed, the Curtin-Hammett

principle explains the distribution of products in irreversible chemical transformations, including stereoselective reactions on dynamic heterocycles,[134] as well as understanding the interactions between conformationally flexible macrocycles and proteins[135] and, more recently, the operation of Brownian ratches in molecular machines.[136] While CuAAC chemistry is irreversible, for the synthesis of **67-6** to fulfil the criteria for Curtin-Hammett control, two further conditions must also be met. Firstly, the macrocycle products must be configurationally stable, and secondly, the diastereomers of the mono-clicked macrocycle intermediate (***PP*** and ***PM***, Figure 3.26) must be in thermodynamic equilibrium and able to rapidly interconvert.

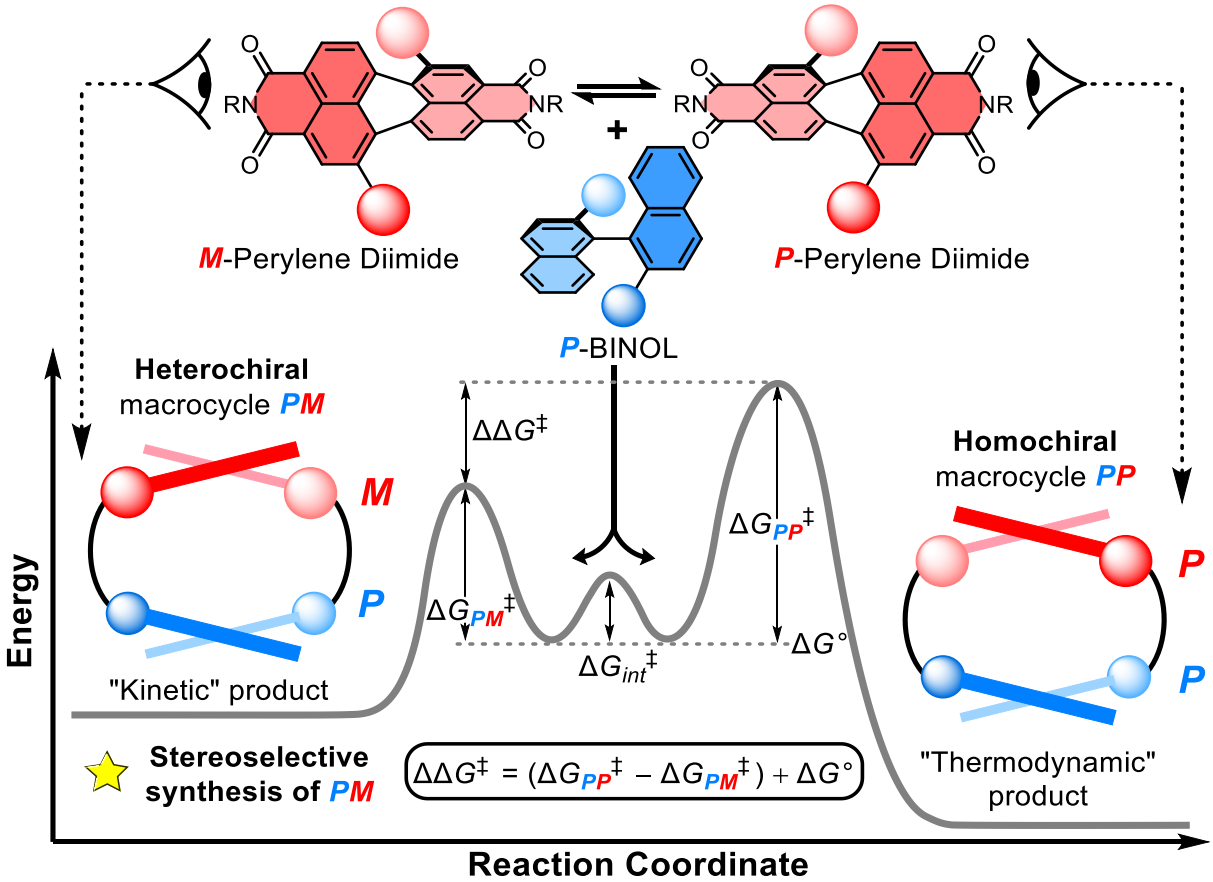

Figure 3.26. The diastereoselective synthesis of a heterochiral (***PM***) over a homochiral (***PP***) macrocycle under Curtin-Hammett control. Here, $\Delta\Delta G^{\ddagger} = (\Delta G_{PP}^{\ddagger} - \Delta G_{PM}^{\ddagger}) + \Delta G°$; $\Delta G_{PP/PM}^{\ddagger}$ = the activation energy of ***PP***/***MM*** macrocycles; $\Delta G°$ = the relative free energy of the interconverting precursors; and $\Delta G_{int}^{\ddagger}$ = the activation energy of this interconversion.

First, the configurational stability of the macrocyclic products was demonstrated. The ^{1}H NMR spectra of PDI macrocycles **67-6** show the diastereotopic methyl protons are split into four sets of doublets, and thus are in slow exchange at 25 °C (i.e., a high PDI

interconversion barrier at 25 °C). Therefore, the rate of PDI atropisomer interconversion is much slower than the chemical shift timescale of the ^{1}H NMR experiment (Figure 3.27).[124]

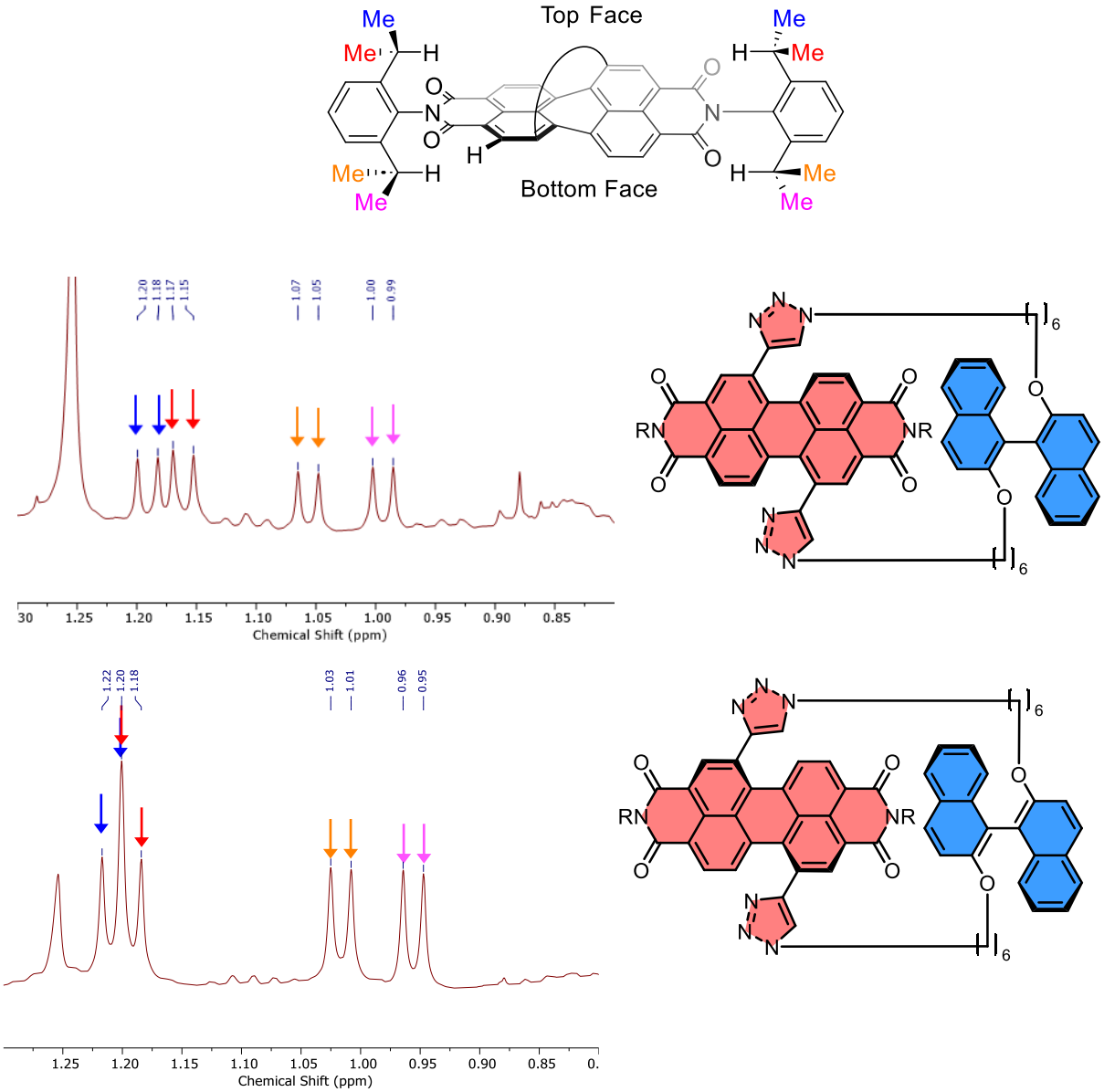

Figure 3.27. ^{1}H NMR spectra of both diastereomers of BINOL-PDI macrocycles **67-6**, displaying four sets of doublets for methyl groups due to diastereotopic splitting arising from chiral locking of the PDI ($CDCl_3$, 298 K, 400 MHz). Note that the assignment of methyl groups are not confirmed.

To further confirm their configurational stability, both diastereomers of macrocycle **67-6** were subjected to heating at 140 °C for 12 hours in 1,1,2,2-tetrachloroethane, with ^{1}H NMR spectra collected prior to and after heating. The identical ^{1}H NMR spectra

indicate that the PDI and BINOL atropisomers are configurationally stable in the macrocycles (Figure 3.28).

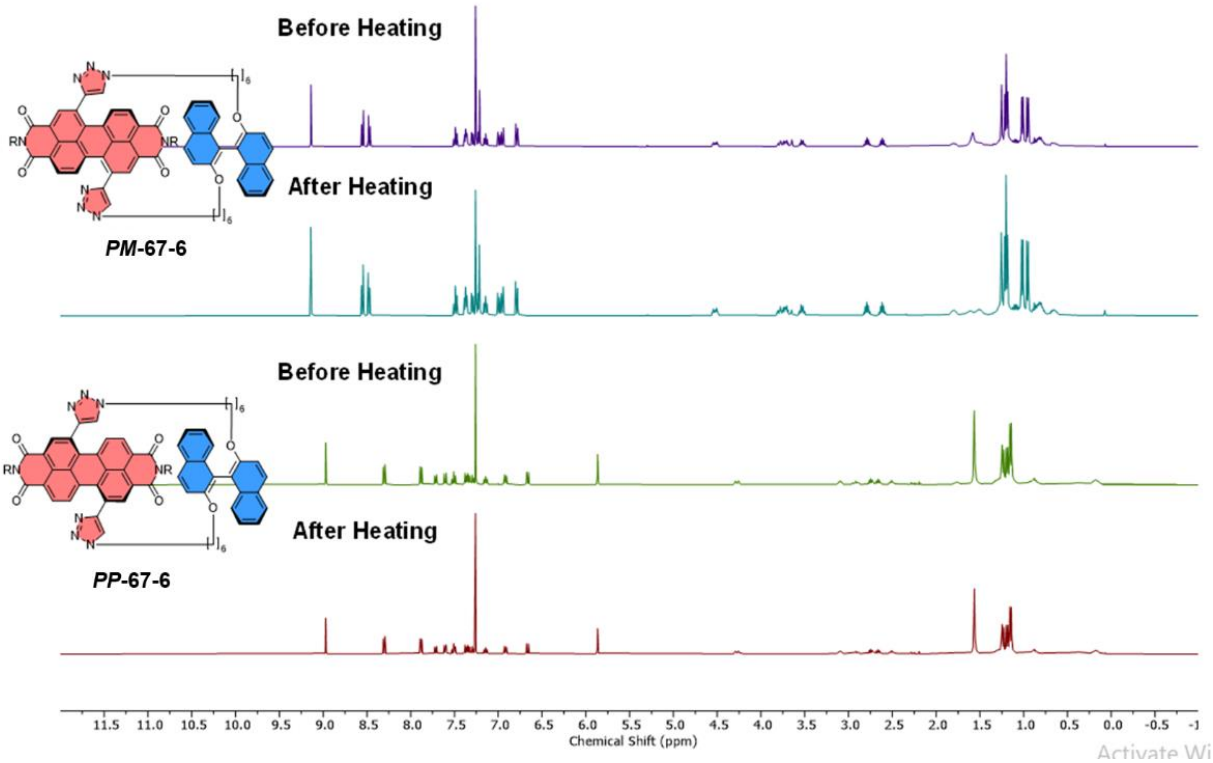

Figure 3.28. 1H NMR spectra of macrocycle **67-6** before and after heating ($CDCl_3$, 298 K, 400 MHz).

Furthermore, there is no change to the CD spectra of macrocycle **67-6** upon heating up to 180 °C, which is just below the isomerisation temperature of BINOL[137] (i.e., $\Delta G^{\ddagger} > 158$ kJ mol^{-1}, Figure 3.29). Therefore, this means that the first criterion for Curtin-Hammett control is fulfilled.

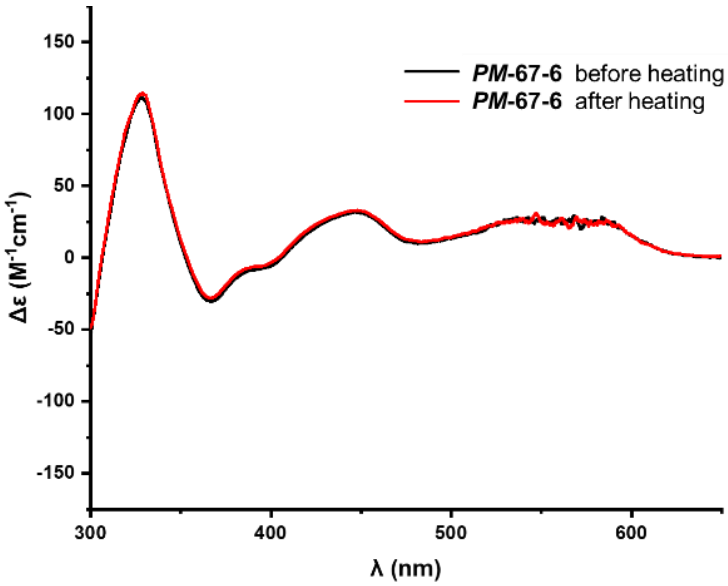

Figure 3.29. CD spectra for macrocycle ***PM*-67-6** (concentration = 26 μM) in 1,2-dichlorobenzene, prior and after heating to 180 °C for two hours.

Here, it is also important to note that the BINOL-PDI macrocycles containing the shorter (**67-4**) and longer (**67-8**) linkers also possess diastereotopic methyl protons split into four sets of doublets in their ^{1}H NMR spectra. Thus, these macrocycles are also chirally locked. This means that the 1:1 ***PM***:***PP*** diastereomeric ratio is as a result of an absence of diastereoselectivity in their synthesis and not a result of racemisation post-synthesis (Figure 3.30).

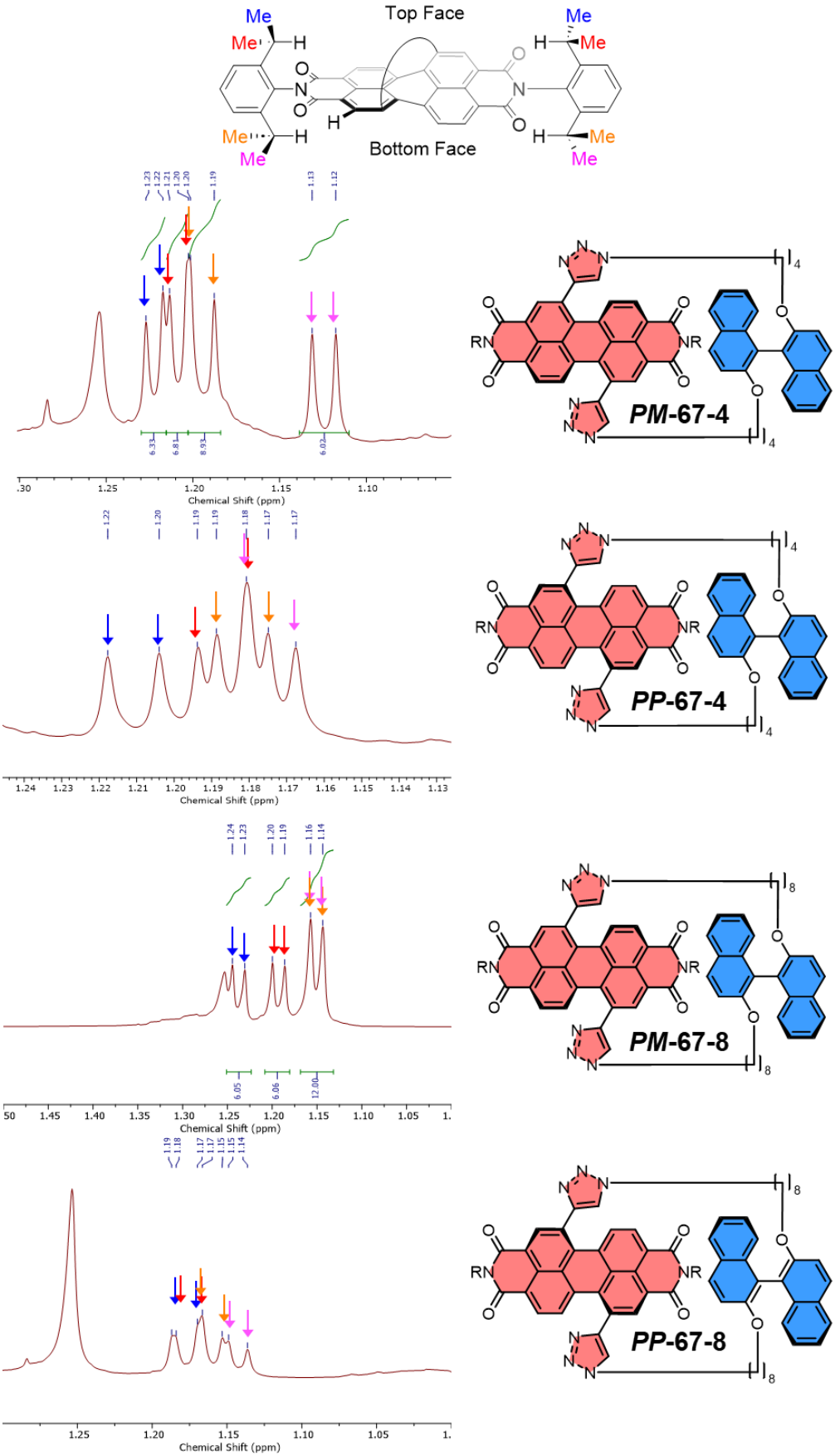

Figure 3.30. ^{1}H NMR spectra of PDI macrocycles **67-4** and **67-8**, displaying four sets of doublets for methyl groups due to diastereotopic splitting arising from chiral locking of the PDI ($CDCl_3$, 298 K, 400 MHz). Note that the assignment of methyl groups are not confirmed.

Next, the barrier to interconversion of the mono-clicked macrocycle intermediate was estimated using a method developed by Würthner and coworkers. The key to this method is that the barrier to PDI atropisomer interconversion is dependent on the apparent overlap parameter $\sum r^*$ of the bay substituent (Y) according to equation (1) below:

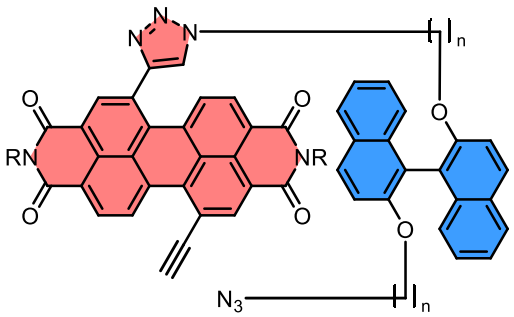

mono-clicked macrocycle intermediate

$$\Delta G^{\ddagger}\,(180\ \mathrm{K}) = 29.0 \sum r^* - 41.8 \qquad (1)$$

Given the C–H bond length and van der Waals radius of hydrogen, $\sum r^*$ can be calculated from equation (2):

$$\sum r^* = 2r_{vdW}(Y) + 2.40\ \text{Å} - 2\sqrt{(2.312\ \text{Å} - 0.5a)^2 + (-0.953\ \text{Å} + 0.866a)^2} \qquad (2)$$

Where:

$r_{vdW}(Y) =$ *van der Waals radius of Y* (bay substituent)

$a =$ *Bond length of C − Y*

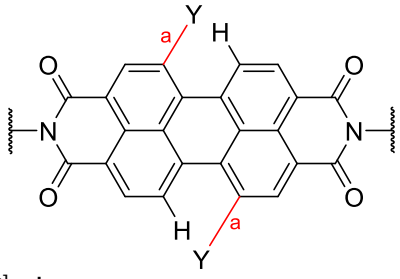

For a diethynyl substituted PDI, such as starting material **23**, Substituting $r_{vdW}(ethynyl) = 1.78$,[126a] and $a = 1.53$,[126a] gives:

$$\sum r^* = 2.78\ \text{Å}$$

Substituting into equation (1) gives:

$$\Delta G^{\ddagger}\,(180\ \mathrm{K}) = 38.8\ \mathrm{kJ/mol}$$

This gives an upper bound of $\Delta G^{\ddagger} < 39$ kJ mol^{-1}, and hence rate $k > 6 \times 10^5$ s^{-1}.

For a bis-triazole substituted PDI, such as acyclic BINOL-PDI-BINOL compound **68**, it was assumed that the triazole heterocycle must twist away from the plane of the PDI

to enable atropisomer interconversion, which gives an estimated value $r_{vdW}(triazole) = 1.77$.[126a]

Substituting this value into equation (2) and then (1) gives:

$$\sum r^* = 2.76\ \text{Å} \text{ and } \Delta G^{\ddagger}\ (180\ \text{K}) = 38.2\ \text{kJ/mol}$$

This gives an upper bound of $\Delta G^{\ddagger}$ < 39 kJ mol^{-1}, and hence rate k > 6 × 10^5 s^{-1}.

Therefore, for the mono-clicked macrocycle intermediate, where one bay substituent has formed the triazole heterocycle and the other remains as an ethynyl group, it can be concluded that the upper bound for atropisomer interconversion of $\Delta G^{\ddagger}$ < 39 kJ mol^{-1}(rate k > 6 × 10^5 s^{-1}) is also applicable.

For room-temperature stable atropisomers of PDIs, $\Delta G^{\ddagger}$ > 106 kJ mol^{-1}, meaning the apparent overlap $\sum r^*$ must be greater than 5.1 Å.[126a] This is clearly not the case for the mono-clicked macrocycle intermediate and so the PDI atropisomers are in thermodynamic equilibrium and rapidly interconvert at room temperature, the temperature at which the reaction was performed. Therefore, this means that the second criterion for Curtin-Hammett control is also fulfilled.

These calculations also explain why the diastereomers of the acyclic BINOL–PDI–BINOL control compound **68** (***PMP*** and ***PPP***) could not be isolated or observed by ^{1}H NMR spectroscopy due to their rapid exchange.[138] Indeed, the diastereotopic methyl protons

also exhibit only one doublet in the ^{1}H NMR spectrum of **68**, and thus are in fast exchange at 25 °C (Figure 3.31).

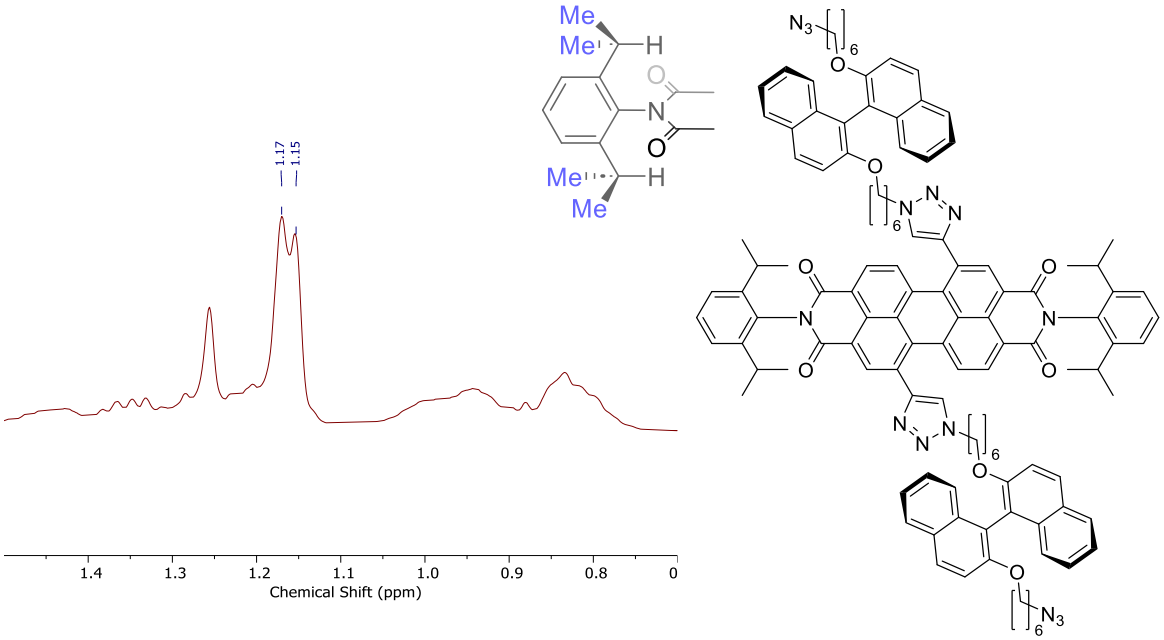

Figure 3.31. 1H NMR spectra of acyclic BINOL-PDI-BINOL **68**, displaying a single set of doublets for methyl groups, displaying no diastereotopic splitting as PDI atropoisomers are in fast exchange ($CDCl_3$, 298 K, 400 MHz).

Since the synthesis of **67-6** is confirmed to fulfil the criteria for Curtin-Hammett control, the macrocyclisation reaction was repeated at different temperatures. From analysis of the yields of the macrocycle diastereomers, it was discovered that diastereoselectivity decreases upon increasing the macrocyclisation reaction temperature, as expected for a reaction under Curtin-Hammett control. Here, 1,2-dichlorobenzene was used as solvent instead of dichloromethane due to its higher boiling point (Figure 3.32).

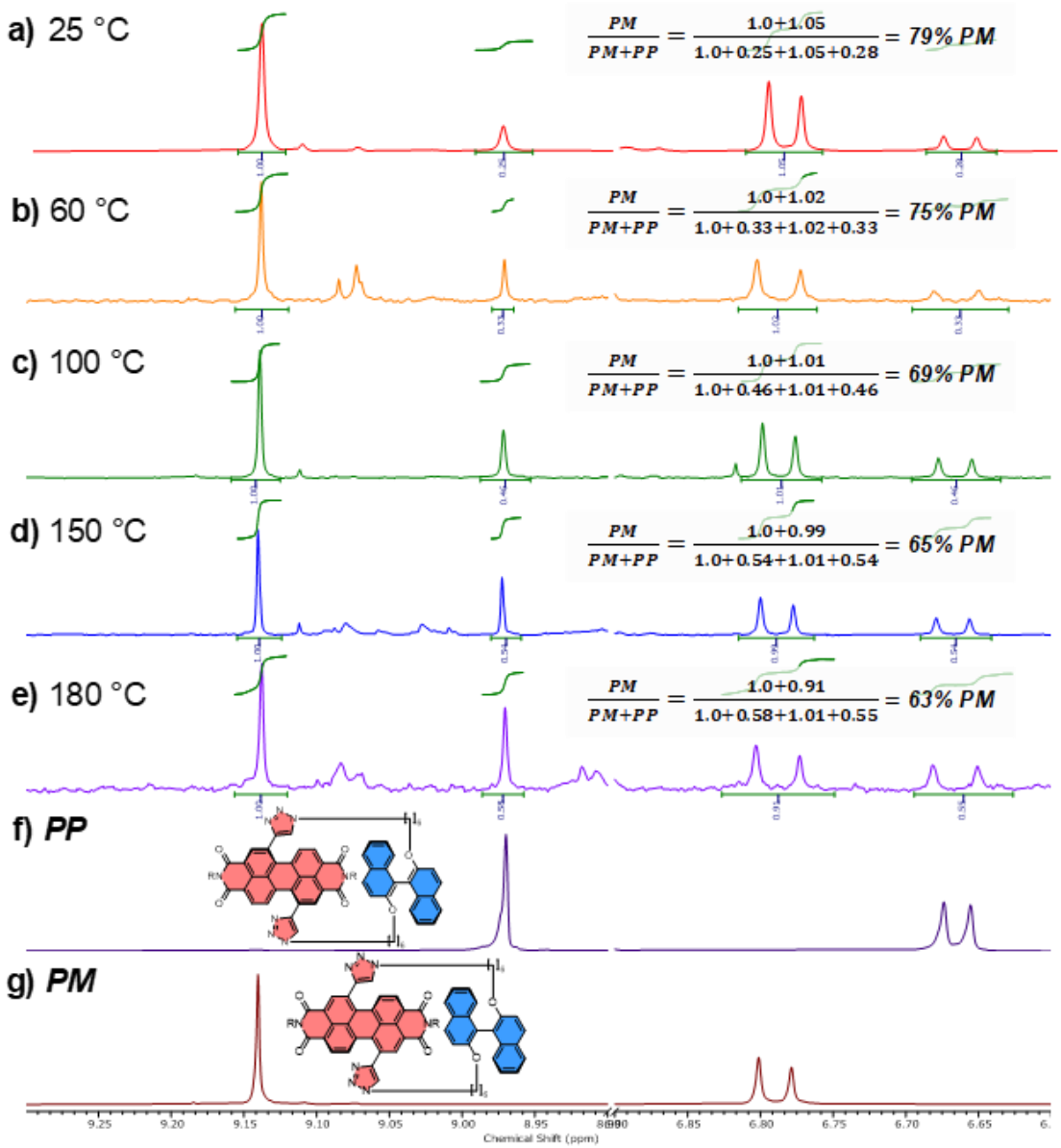

Figure 3.32. ^{1}H NMR spectra of: a)-e) crude reaction mixture of macrocycle **67-6** ($CDCl_3$, 298 K, 400 MHz), reacted at stated temperatures with 1,2-dichlorobenzene as solvent; and f)-g) purified **67-6**. The PM:PP diastereomeric ratio are: a) 79:21 at room temperature (25 °C), b) 75:25 at 60 °C, c) 69:31 at 100 °C, d) 65:35 at 150 °C, and e) 63:37 at 180 °C. These values are used to calculate the difference in standard Gibbs energies between the ***PP*-67-6** and ***PM*-67-6** transition states ($\Delta\Delta G^{\ddagger}$) following the Curtin-Hammett principle below.

From here, the Curtin-Hammett principle allows calculation of the difference in energy between the transition states ($\Delta\Delta G^{\ddagger}$) according to equation (3).

$$Product\ ratio = e^{-\Delta\Delta G\ddagger/\mathrm{RT}} \qquad (3)$$

Where, in context:

Product ratio = [***PM*-67-6**]/[***PP*-67-6**]

$\Delta\Delta G^{\ddagger}$ = free energy difference between transition states of the two products (i.e., ***PM*-67-6** and ***PP*-67-6**)

R = Ideal gas constant

T = Temperature

Rearranging (3) gives the following equation:

$$\ln(product\ ratio) = \frac{-\Delta\Delta G\ddagger}{RT} \qquad (4)$$

Using the product ratio calculated from the ^{1}H NMR spectra in Figure 3.32, ln(product ratio) was plotted against 1/T to give a slope of $-\Delta\Delta G^{\ddagger}/R$ (754 ± 53 J mol^{-1}, Figure 3.33). This gave a $\Delta\Delta G^{\ddagger}$ of −6.3 ± 0.4 kJ mol^{-1}.

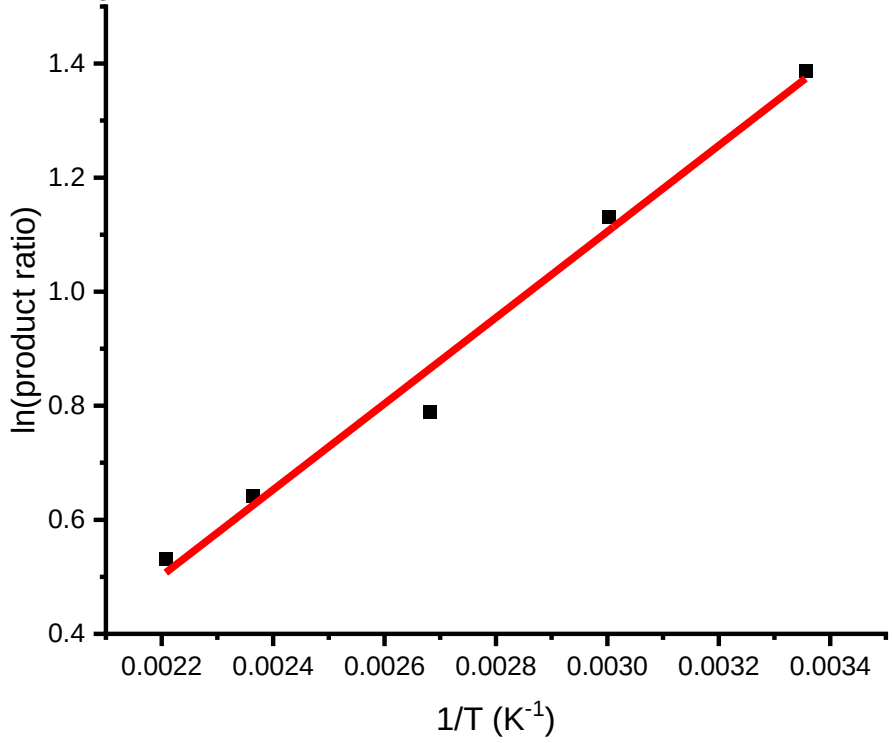

Figure 3.33. Curtin-Hammett plot of ln(product ratio) against 1/T.

This $\Delta\Delta G^{\ddagger}$ is dependent on the relative free energy of the interconverting intermediate ($\Delta G°$) and the relative activation energies ($\Delta G_{PP}^{\ddagger} - \Delta G_{PM}^{\ddagger}$). Since the acyclic BINOL–PDI–BINOL compound **68** does not exhibit a CD spectrum in the PDI-only region (Figure 3.20, Section 3.4.2), the mono-clicked ***PP*** and ***PM*** diastereomeric intermediates must be very close in energy prior to macrocyclisation, and hence $\Delta G° \approx 0$. Therefore, the difference in transition state energies $\Delta\Delta G^{\ddagger}$ (and hence the kinetic resolution of **67-6**) does not occur from any inherent stability of the heterochiral mono-clicked intermediate over the homochiral intermediate, $\Delta G°$, and instead arises purely on the difference in their activation energies, i.e. $\Delta G_{PP}^{\ddagger} - \Delta G_{PM}^{\ddagger}$ (Figure 3.34).

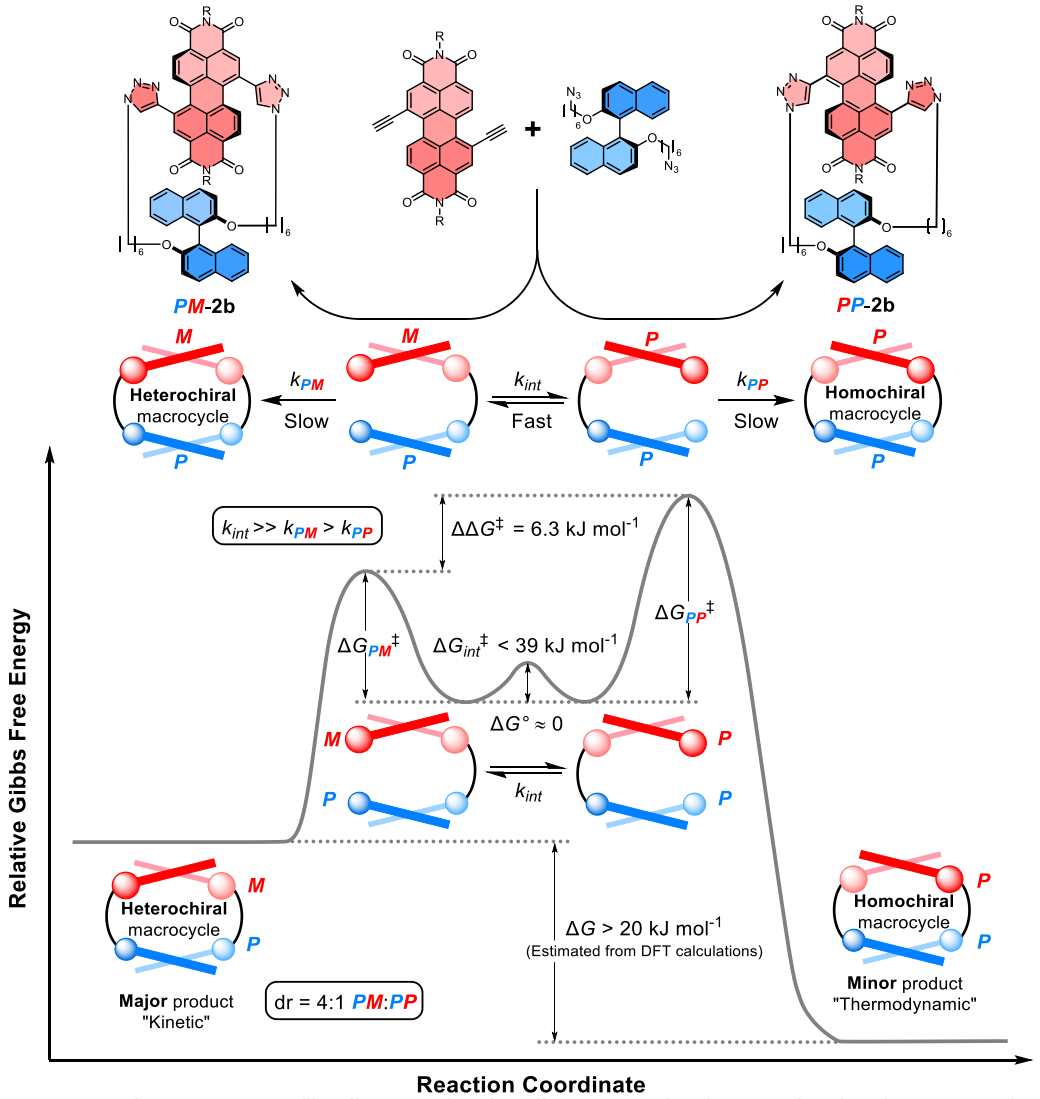

Figure 3.34. The energy profile diagram for the diastereoselective synthesis of macrocycle ***PM*-67-6** under Curtin-Hammett control. Values for the free energies $\Delta\Delta G^{\ddagger}$, $\Delta G°$ and $\Delta G_{int}^{\ddagger}$ have been determined experimentally, while the free energy difference between macrocycles ***PM*-67-6** and ***PP*-67-6** (ΔG) has been estimated computationally using the DFT (B973c) optimized geometries of the likely lowest energy conformer of macrocycles ***PM*-67-6** and ***PP*-67-6**, as found in the tight-binding DFT (GFN2-xTB) conformer searches.

3.4.4 Non-covalent templating interactions

As the PDI–BINOL macrocycles with shorter (*n*-butyl, **67-4**) and longer (*n*-octyl, **67-8**) strap lengths did not exhibit any diastereoselectivity (i.e., ***PP*:*PM*** = 1:1), stabilisation of the heterochiral transition state is unique to macrocycle **67-6** (n-hexyl). This suggests that the trend in diastereoselectivity does not correlate with the change in ring strain that would be anticipated upon changing the linker length. As such, in light of the evidence for intramolecular π–π stacking in previous HQ and DHN based macrocycles (Chapter 2), investigations turned to identify any connection between diastereoselectivity and the potential differences in electronic properties.

Evidence for intramolecular non-covalent interactions can be seen by ^{1}H NMR spectroscopy, by stacking the spectra of acyclic bis-triazole PDI **51**, acyclic bis-BINOL PDI **68**, and BINOL–PDI macrocycles **67**. Similar to the hydroquinone series in Chapter 2, the PDI proton signals $H_{a\text{-}c}$ become increasingly deshielded in the order of acyclic, octyl, hexyl, and butyl. This indicates that intramolecular non-covalent interactions between the aromatic units become stronger as the BINOL unit is brought closer to the PDI unit upon macrocyclisation or by shortening the strap of the macrocycle. Therefore, the macrocyclic framework preorganises the π-conjugated units in solution, providing the potential for intramolecular aromatic interactions, including π–π and CH–π interactions (Figure 3.35).

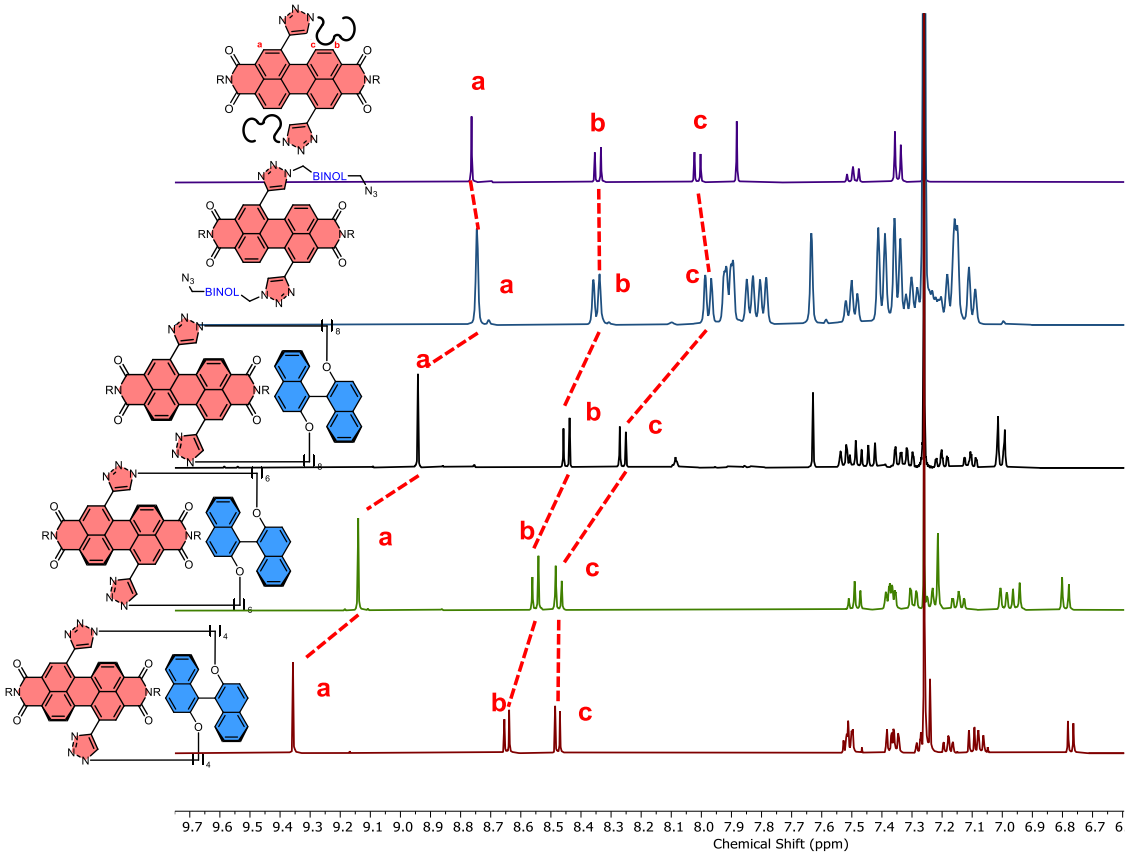

Figure 3.35 Stacked ^{1}H NMR spectra of acyclic bis-triazole PDI **51**, acyclic bis-BINOL PDI **68**, BINOL–PDI macrocycles **67-4**, **67-6**, and **67-8** ($CDCl_3$, 298 K, 400 MHz).

Moreover, NOESY NMR spectroscopy shows cross-peaks between PDI and ***P***-BINOL protons (Figure 3.36), confirming the proximity of these units in **67-6**.

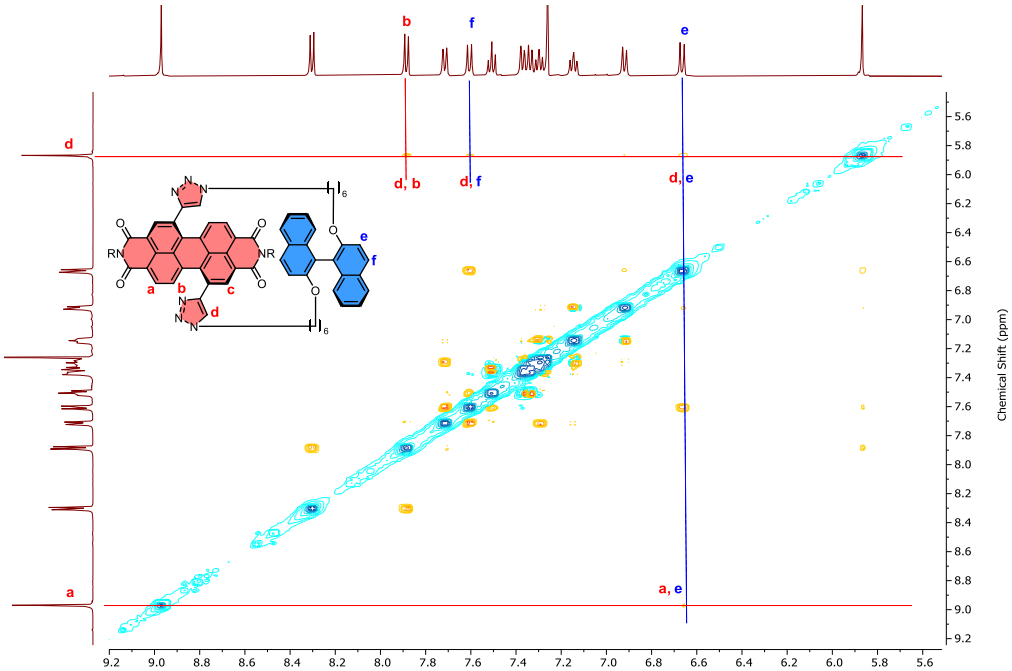

Figure 3.36. ^{1}H–^{1}H NOESY NMR spectrum of **PP-67-6** (500 MHz, $CDCl_3$), displaying nOe signals between protons $H_{d,f}$, $H_{d,e}$, and $H_{a,e}$, confirming the proximity of PDI and BINOL units in macrocycle **67-6**.

The aromatic-based non-covalent interactions between the PDI and the linker can also be characterised by UV-vis absorption spectroscopy. Here it is important to clarify that π–π interactions primarily consist of electrostatic and van der Waals contributions,[109] with the former readily probed by UV-vis absorption spectroscopy since red-shifted charge transfer absorbances can be a consequence of donor–acceptor interactions,[110] such as those between BINOL and PDI.

First, the UV-vis absorption absorption was plotted against concentration for both macrocycle diastereomers of **67-6**, where the resulting linear graphs shows Beer-Lambert behaviour. This importantly shows that at these concentrations, the interactions probed by UV-vis absorption spectroscopy are intramolecular and not intermolecular in origin (Figure 3.37).

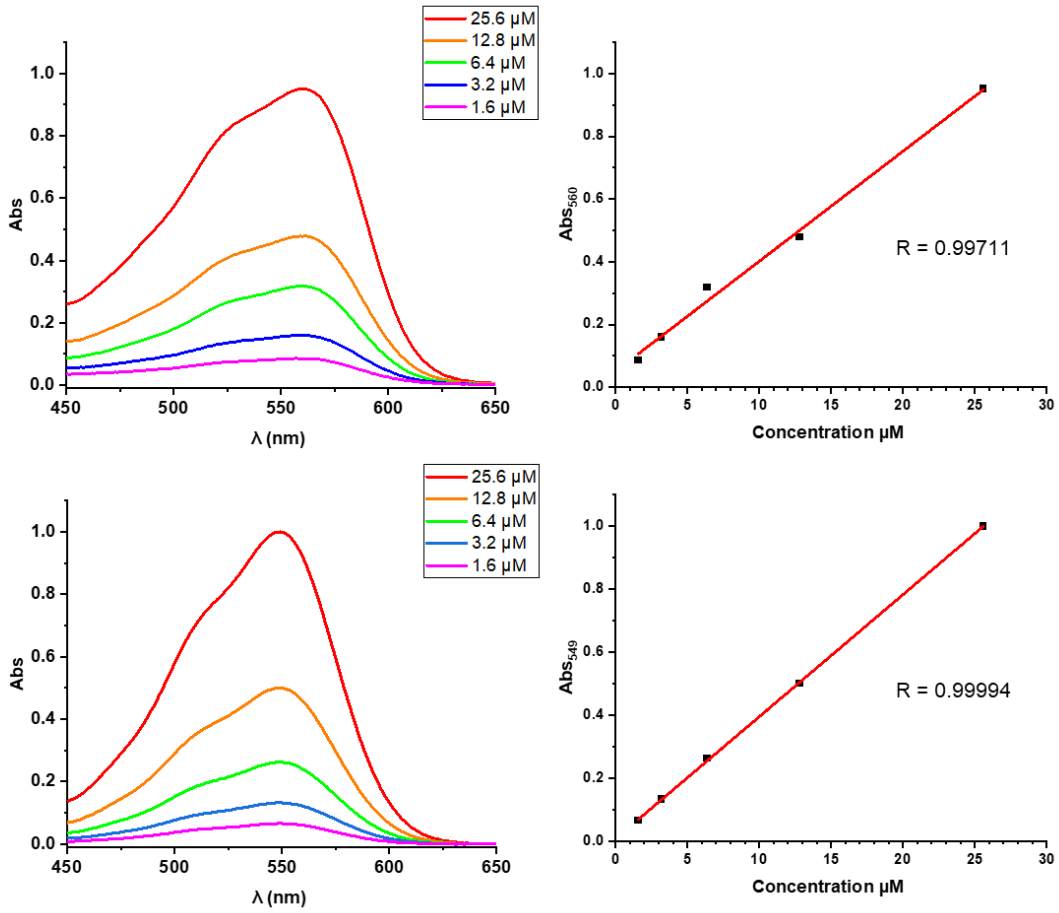

Figure 3.37. Left: absorption spectrum of macrocycles: ***PM*-67-6** (top) and ***PP*-67-6** (bottom) in $CHCl_3$ at different concentrations. Right: the dependence of absorption (λ_{max}) on concentration for these macrocycles: ***PM*-67-6** (top, λ_{max} = 560 nm), and ***PP*-67-6** (λ_{max} = 549 nm, bottom), in $CHCl_3$ is linear, showing Beer-Lambert behaviour.

While ^{1}H NMR spectroscopy indicated an absence of intramolecular interactions between BINOL and PDI in acyclic BINOL-PDI-BINOL **68**, this was also evident from UV-vis absorption spectroscopy since the absorption spectrum of **68** is identical to that of **51**. This also explains the absence of a CD spectrum in the PDI-only region of **68**. UV-vis absorption spectroscopy also shows that, similar to the hydroquinone series in Chapter 2, the main PDI absorption band (S_0–S_1) of heterochiral ***PM*-67** becomes increasingly red-shifted in the order of acyclic, octyl, hexyl, and butyl, demonstrating increasing donor–acceptor interactions between BINOL and PDI (Figure 3.38).

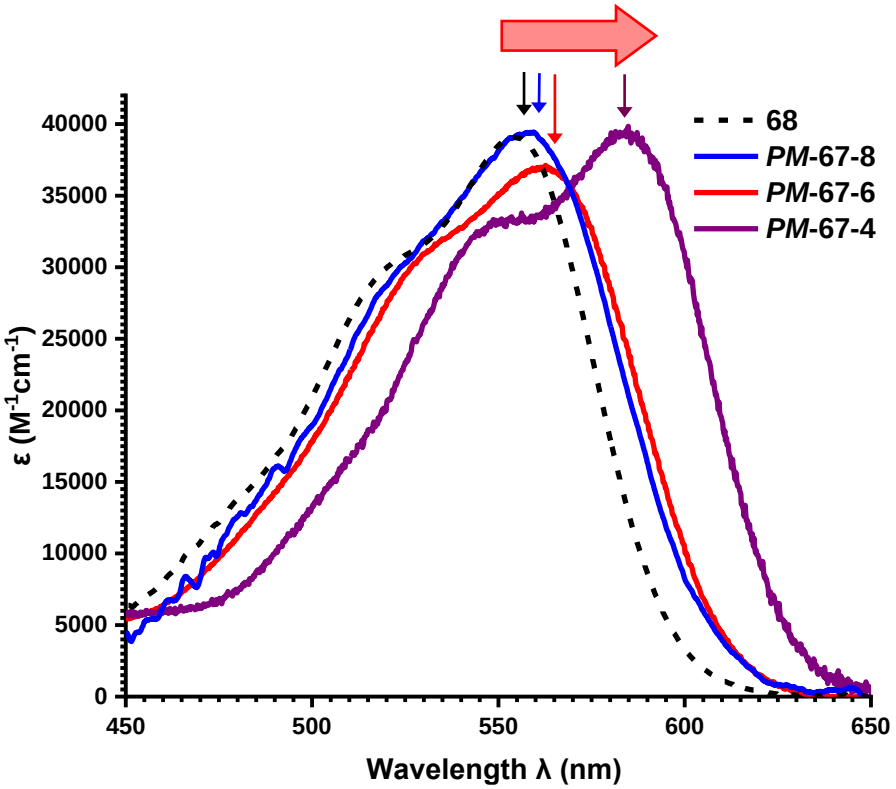

Figure 3.38. UV-vis absorption spectra of **68** (black, dotted), ***PM*-67-4** (purple), ***PM*-67-6** (red), and ***PM*-67-8** (blue), displaying a redshift in the order of acyclic, octyl, hexyl, and butyl. All spectra were recorded in $CHCl_3$ at a concentration of 26 µM in a quartz cuvette with 1 cm path length.

Most importantly, whilst ***PM*-67-6** is significantly red-shifted relative to the acyclic species ($\Delta\lambda$ = 10 nm), the absorption spectra of ***PP*-67-6** is relatively unchanged (Figure 3.39, middle), indicating any donor–acceptor π–π interactions in the homochiral macrocycle are significantly weaker than in the heterochiral macrocycle. This difference in the bathochromic shifts between the homochiral ***PP*** and heterochiral ***PM***

diastereomer is not present in the shorter (**67-4**) or longer (**67-8**) length macrocycles. Both diastereomers ***PP*-67-8** and ***PM*-67-8** have similarly red-shifted PDI absorption bands ($\Delta\Delta\lambda \approx 0$ nm, Figure 3.39, right), as do diastereomers with shorter linkers, ***PP*-67-4** and ***PM*-67-4** ($\Delta\Delta\lambda$ = 1 nm, Figure 3.39, left). Since these macrocycles also exhibit no diastereoselectivity, this points towards the importance of donor–acceptor π interactions in the stereoselective synthesis of **67-6**.

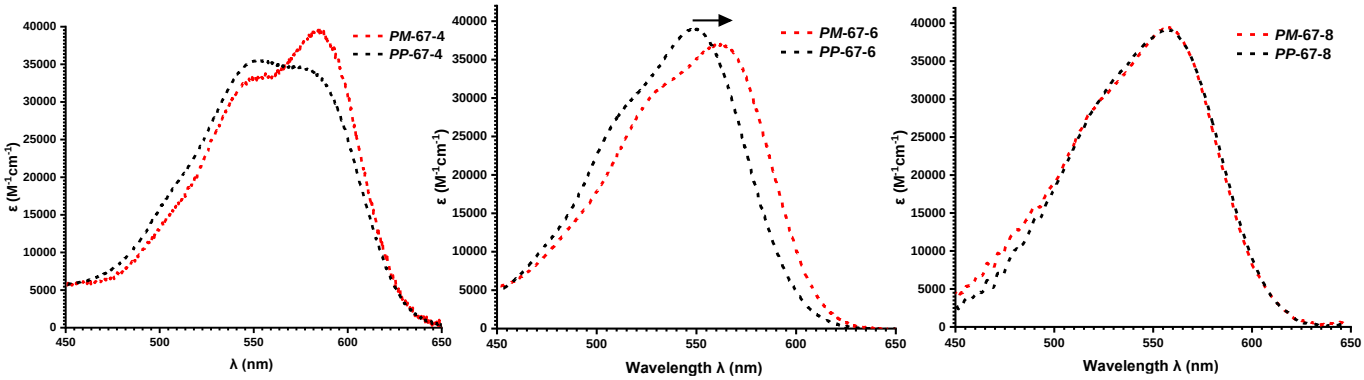

Figure 3.39. UV-vis absorption spectra of **67-4** (left), **67-6** (middle), ***PM*-67-8** (right), of chirality ***PP*** (black) and ***PM*** (red), where **67-6** is the only one that shows a red shift in ***PM*** relative to ***PP***. All spectra were recorded in $CHCl_3$ at a concentration of 26 μM in a quartz cuvette with 1 cm path length.

This explanation is also supported by further analysis by ^{1}H NMR spectroscopy. Indicative of π–π interactions, the heterochiral macrocycle ***PM*-67-6** exhibits a larger downfield shift of PDI protons relative to homochiral ***PP*-67-6** (for H_c, $\Delta\delta$ = 8.47 *vs.* 7.88 ppm, $\Delta\Delta\delta$ = 0.59 ppm, Figure 3.40a), while the difference between diastereomers is much smaller for macrocycles **67-4** and **67-8** ($\Delta\Delta\delta$ = 0.1 and 0.07 ppm respectively, Figure 3.40b,c)

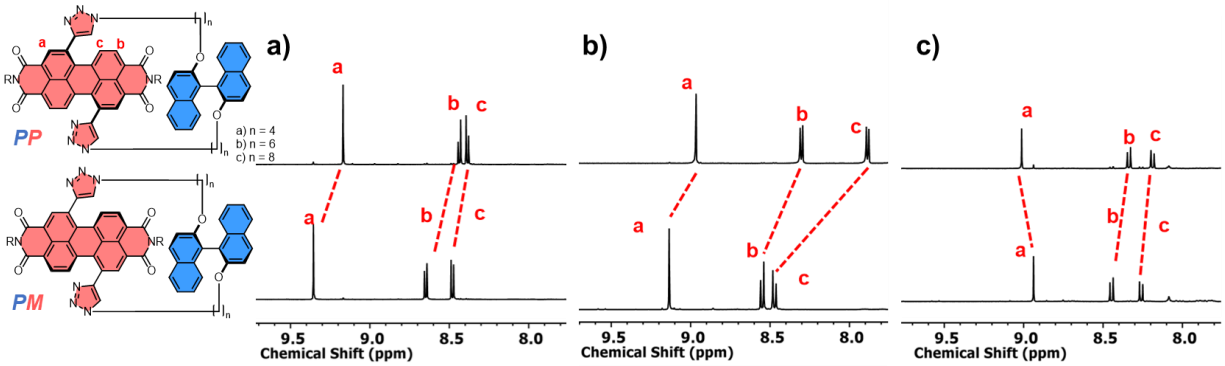

Figure 3.40. Stacked ^{1}H NMR spectra of a) ***PP*-67-6**, and ***PM*-67-6**; b) ***PP*-67-4**, and ***PM*-67-4**; c) ***PP*-67-8**, and ***PM*-67-8** ($CDCl_3$, 298 K, 400 MHz).

Finally, this is also supported by analysis of the DFT optimised structures of the heterochiral and homochiral macrocycles. The heterochiral macrocycle ***PM*-67-6** displays a shorter π-π distance (4.2 Å vs 4.8 Å), as well as shorter and more numerous CH–π interactions (2.7 Å and 3.0 Å, vs 3.5 Å), compared to ***PP*-67-6** (Figure 3.41, bottom).

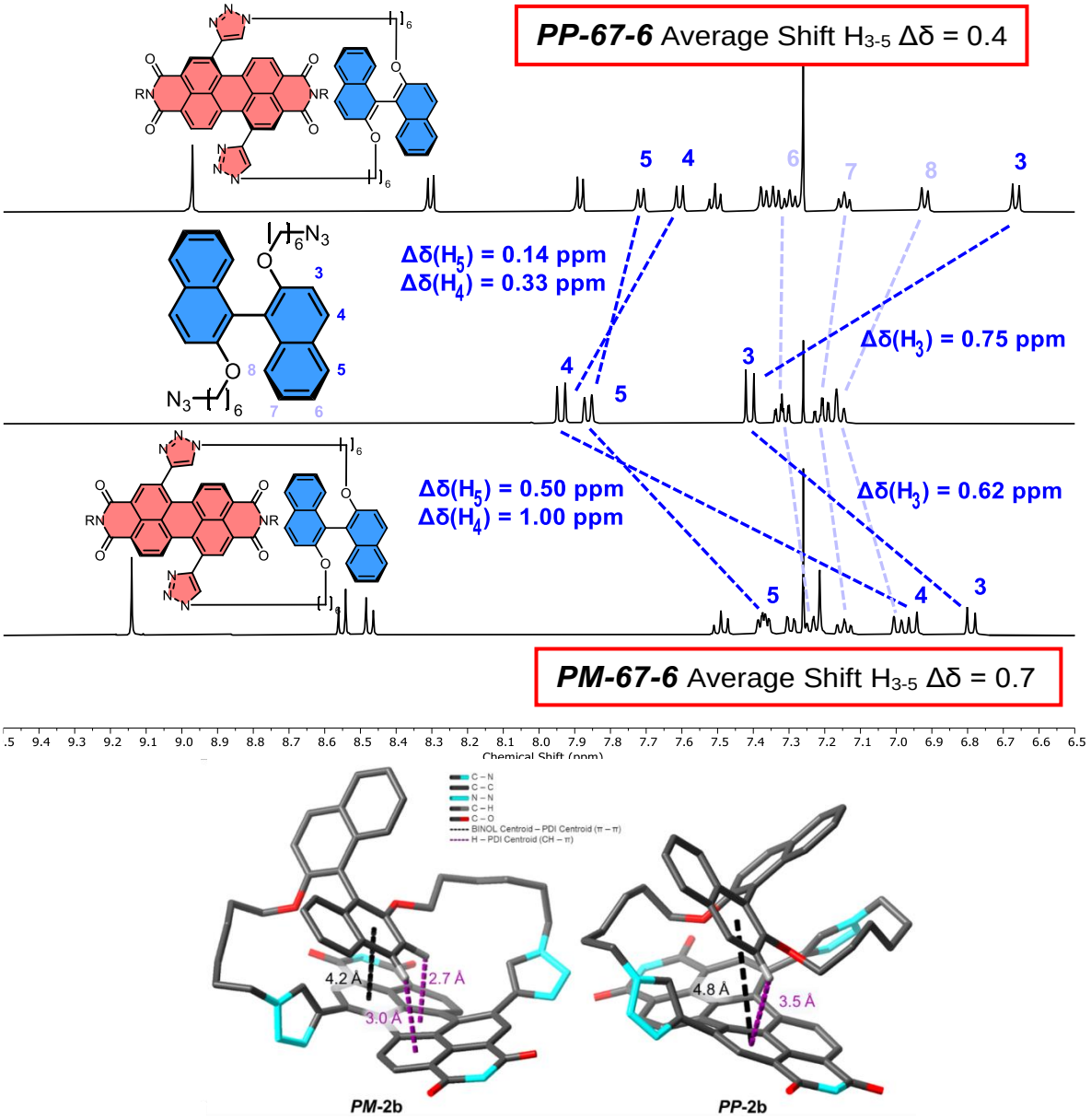

Figure 3.41 Top: Stacked ^{1}H NMR spectra ($CDCl_3$, 298 K, 400 MHz) of acyclic BINOL **67-6** against both homo and heterochiral BINOL–PDI macrocycles **67-6**, displaying a higher average upfield shift from $H_{3\text{-}5}$ in ***PM*-67-6** (0.7 vs 0.4). Bottom: Calculated structures of ***PM*-67-6** and ***PP*-67-6** showing relevant non-covalent interactions (π–π, CH–π and CH–O hydrogen bonding). Note, the CH–π interactions are represented by close contacts between H and a PDI centroid and π–π interactions are represented by close contacts between BINOL/PDI centroids. For clarity, hydrogen atoms and the 2,6-diisopropylphenyl imide substituents have been removed from these structures.

3.5 Conclusions and Future Work

This chapter details the stereoselective synthesis of various PDI-based macrocycles. Initial attempts with the use of a second dynamically chiral PDI unit in the macrocycle's strap successfully synthesised the bis-PDI macrocycles **62** and **63** in 3% and 1% respective yields over 3 steps. Here, one PDI unit is connected via the bay positions and other via the imide positions, the first of a kind for bis-PDI macrocycles. The bis-triazole substituted PDI is chirally locked, as evidenced by ^{1}H NMR spectroscopic analysis of the imide groups at 100 °C. Challenges in purification, characterisation and overlapping absorbance spectra meant that these bis-PDI macrocycles were unsuitable to investigating intramolecular aromatic non-covalent interactions, as desired to direct the outcome of a dynamic kinetic resolution (i.e. a diastereoselective synthesis).

Following this, the PDI bisalkyne was strapped with a chiral, yet configurationally unstable, pillar[5]arene unit to achieve macrocycle **64** in 25% yield. The chiral bis-triazole PDI unit in this pillar[5]arene-PDI macrocycle was shown to be chirally locked. Moreover, only one set of enantiomeric products were found. This indicates that, in this irreversible macrocyclisation reaction, both dynamically chiral PDI and dynamically chiral pillar[5]arene may influence each other in the reaction intermediate, which results in the formation of a single set of enantiomers. Preliminary basic molecular modelling revealed that the unseen set of enantiomers may sterically inhibit intramolecular π-stacking between the pillar[5]arene and the PDI, thereby hindering their kinetic templation in the synthesis.

Finally, to achieve a stereoselective synthesis, a racemic and dynamically chiral PDI dye (1:1 ***P***:***M***) is made configurationally stable by its strapping with an enantiopure ***P***-BINOL derivative under irreversible reaction conditions. Therefore, in contrast to previous diastereomeric PDI-based macrocycles,[131] both the macrocyclisation reaction and products are under kinetic control, enabling the facile isolation of

heterochiral and homochiral macrocycles in high enantiopurities without the need for chiral HPLC. Notably, instead of a 1:1 mixture of macrocycle diastereomers,[104a, 139] there is diastereoselectivity for the heterochiral (***PM*-67-6**) over homochiral (***PP*-67-6**) product (dr = 4:1).

Analogous BINOL-PDI macrocycles containing longer (67-8) or shorter (67-4) linkers exhibited no diastereoselectivity, indicating that diastereoselectivity does not appear to arise from macrocycle ring strain or steric effects. The Curtin-Hammett principle revealed the origin of diastereoselectivity in **67-6** is the lower transition state energy of the hetero- *vs.* homo-chiral macrocycle ($\Delta\Delta G^{\ddagger}$ = 6.3 kJ mol^{-1}), with experimental and computational studies revealing that stabilising π–π and CH–π interactions are predominant in ***PM*-67-6,** indicative of a kinetic template effect.[140] The use of aromatic non-covalent interactions to direct the synthesis of atropisomeric π-conjugated materials[131d, 141] under irreversible conditions is desirable for preparing preorganised chiral receptors[142] or persistent chiroptical materials[75] or, as found here, for tuning selectivity for a chiral product that may not be favoured under thermodynamically controlled conditions. Therefore, the stereoselective synthesis of other chiral polycyclic aromatic hydrocarbons, such as helicenes or twisted nanographenes, may be explored through this strategy. Here, the impact of chiral solvents could also be investigated, which may enable an enantioselective synthesis of chiral aromatic materials such as PDI-based macrocycles.

Another promising avenue for future research includes characterisation of the host-guest binding properties of the pillar[5]arene-PDI macrocycle **64**. Here, the binding of guests (e.g., lipophilic organic molecules) within the pillar[5]arene cavity may detected by the nearby PDI chromophore, including by circularly polarised luminescence due to the PDI's locked chirality. Pillar[5]arene is also ubiquitous as a macrocycle component in templated rotaxane syntheses. Therefore, a two-station rotaxane shuttle with

macrocycle **64** could be used to engineer a chiroptical switch, in which the circularly polarised luminescence from the pillar[5]arene-PDI macrocycle is turned on or off.

4 A Two Station Perylene Diimide [3]Rotaxane

4.1 Introduction

4.1.1 Chapter Aims

Whilst PDI-based rotaxanes and chiral switchable rotaxanes have been synthesised (Section 1.6.1), to date, a switchable chiral PDI-based rotaxane have yet to be reported in literature, in spite of the useful photo- and electro-chemical properties of PDIs. This is likely due to the low racemisation barrier of PDIs. As discussed in Section 1.5.2, the barrier to PDI atropoisomer interconversion is dependent on the steric overlap of the PDI bay substituents (Figure 4.1, top).[80] Thus, in a PDI where the bay substituent is extended into the axle for a rotaxane, it was envisaged that as a macrocycle is brought closer to the PDI, this would effectively increase the steric bulk of the bay substituent, thus inhibiting racemisation of the PDI (i.e. chiral locking). If such system is expanded as a two station rotaxane, the chiral locking of PDI could be switched on and off (Figure 4.1, bottom).

This work will exploit the mechanical bond to increase the energy barrier of atropisomer interconversion and as such tune the racemisation rate, with the ultimate aim of realising configurationally stable PDIs.

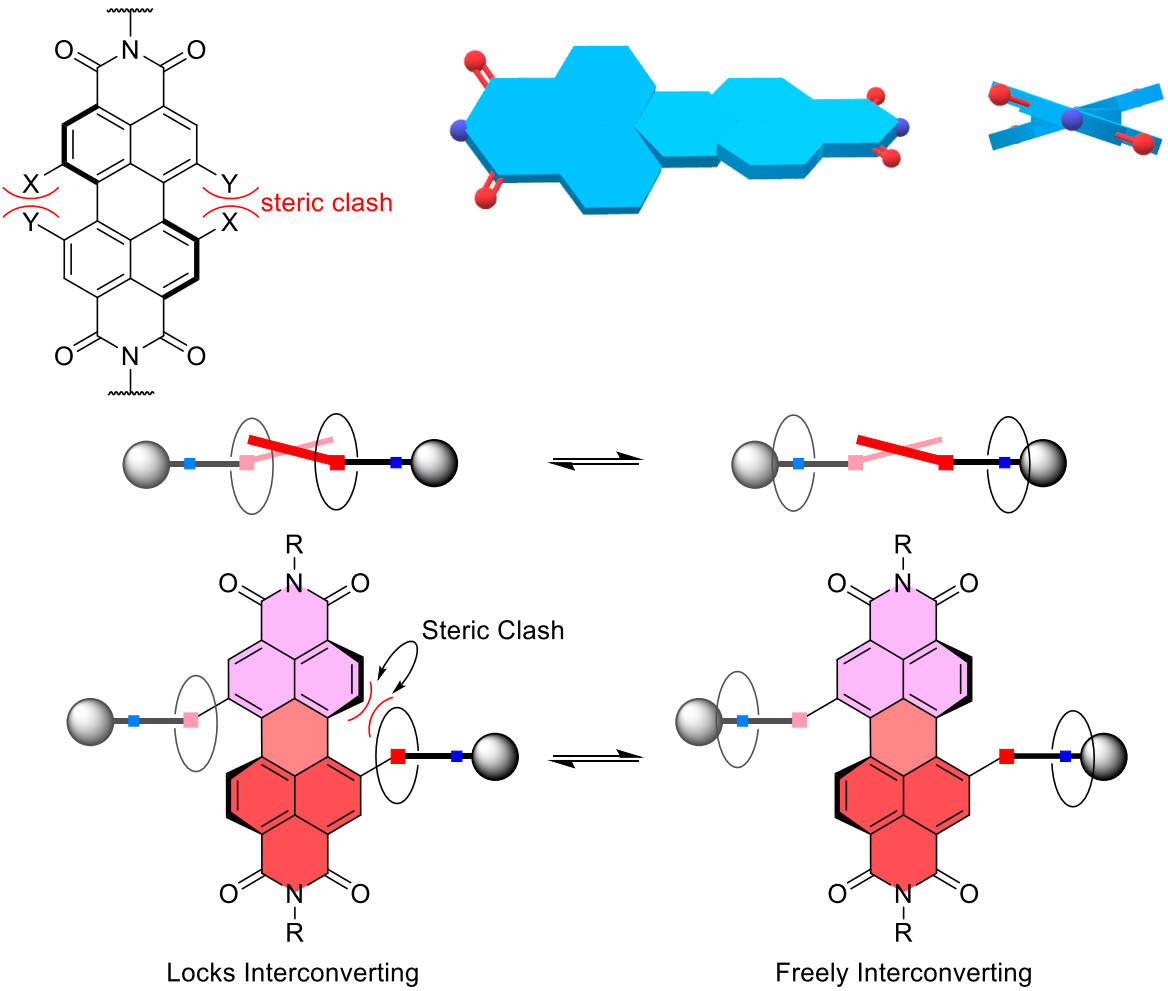

Figure 4.1. Top: steric clash of the bay substituents of a PDI, resulting in a twist away from planarity. Bottom: a two station PDI [3]rotaxane, where the station next to PDI would sterically clash with the bay position of the PDI to lock its chirality.

4.1.2 Synthetic Design

Several aspects of the design of a PDI-based two station rotaxane were considered. First, it was envisaged that the axle would incorporate a 1,7-bay-substituted PDI unit at the centre, with one macrocycle component interlocked onto either side of the PDI, creating a [3]rotaxane. This has advantages over the formation of a [2]rotaxane, in which one macrocycle would be interlocked onto a singly bay-substituted PDI axle. Compared to a mono bay-substituted PDI, a disubstituted PDI would enable a greater steric bulk to be assembled at the bay positions, courtesy of the additional macrocycle, thereby providing the potential for a larger barrier to PDI atropisomer interconversion. Additionally, the higher symmetry of the [3]rotaxane would simplify the characterisation of the product, and allow diastereotopic methyl groups situated on the imide group to potentially probe the chiral stability of the PDI.

Furthermore, it was envisaged that the PDI would be bay-substituted with triazole groups, since the variety of azide starting materials, access to bis-alkyne PDI **23** and ease of CuAAC "click" chemistry facile have been demonstrated in Chapters 2 and 3. This group is also a capable hydrogen bond donor, and can thus act as a station for a hydrogen bond accepting macrocycle in a rotaxane, such as a crown ether (Figure 4.2).

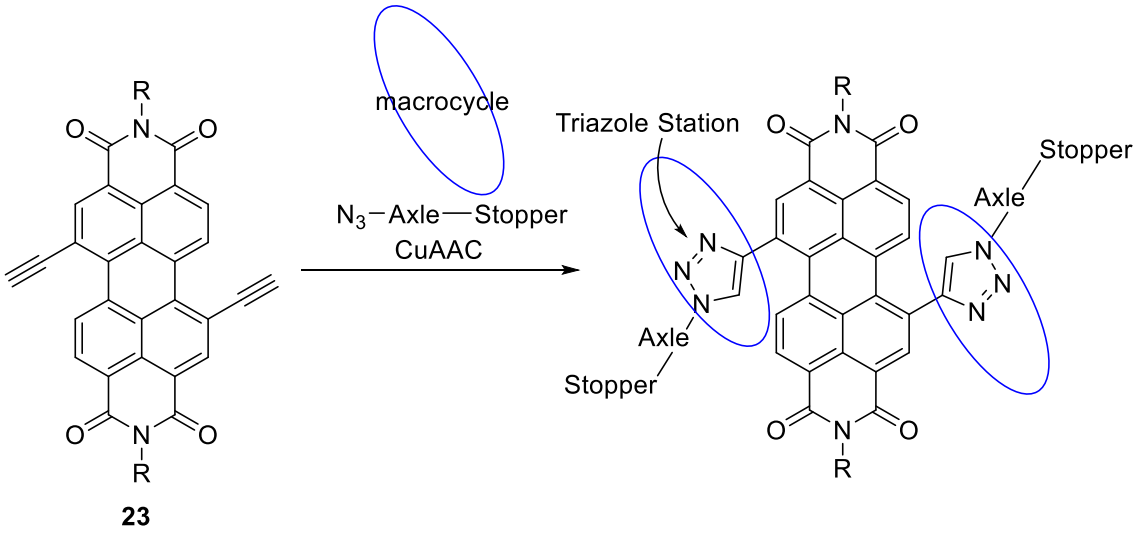

Figure 4.2. Envisioned formation of a [3]rotaxane via CuAAC.

The chosen crown ether macrocycle was dibenzo-24-crown-8 (DB24C8, Figure 4.3). As well interacting with triazole groups, this crown ether is also known to bind strongly to secondary ammonium functional groups through hydrogen bonding. Indeed, triazolium-ammonium-DB24C8 rotaxanes are a common type of pH sensitive two station rotaxane, in which the macrocycle can be switched between ammonium and triazolium stations upon deprotonation of the former. This is because the binding affinity of DB24C8 follows the order ammonium > triazolium > amine, as reflected by the hydrogen bond donating ability of these groups.[143] Additionally, DB24C8 is commercially available and contains π-electron rich aromatic rings which may be able to interact with the π-electron poor PDI through donor-acceptor π-stacking (Figure 4.3).[144]

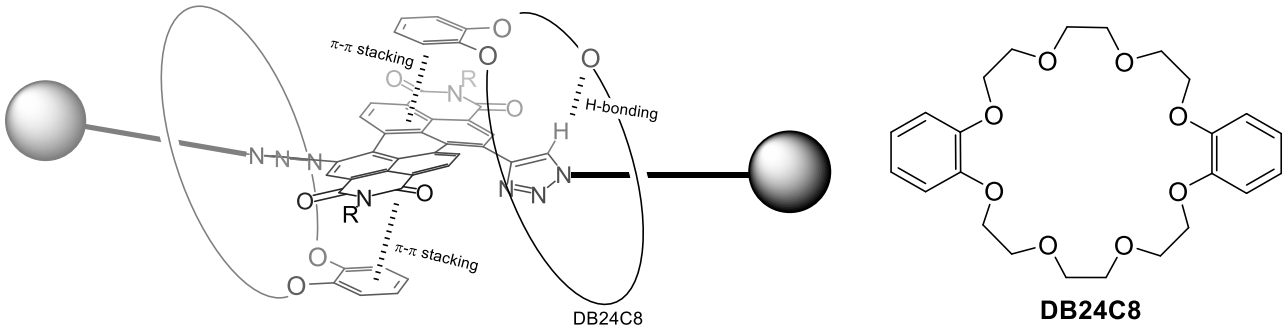

Figure 4.3. A PDI [3]rotaxane with crown ether macrocycle dibenzo-24-crown-8 (DB24C8), displaying hydrogen bonding and π-π stacking at the PDI bistriazole station. Parts of the macrocycle (aromatic ring and ethylene glycol chain) have been removed from the cartoon of the [3]rotaxane for clarity.

The use of 3,5-*tert*-butyl aniline as the stopper groups was envisaged due to its bulky *t*-Bu groups and its ease of synthesis into an organic azide rotaxane precursor,[144] through alkylation of the aniline to generate a secondary amine. The protonation of this secondary amine would generate an ammonium binding site for macrocycles such as DB24C8 (Figure 4.4).

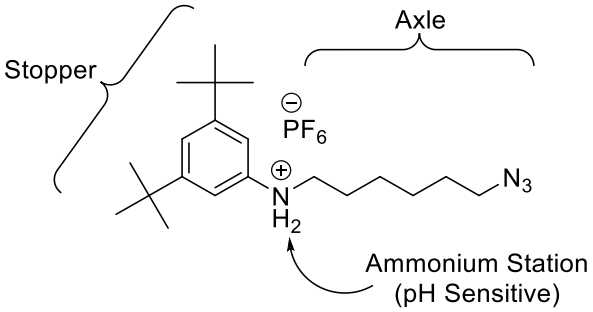

Figure 4.4. Envisioned stopper group for rotaxane

Putting this together, a two station rotaxane would be formed, containing a secondary amine, which is pH sensitive. At low pH, it was expected that the secondary amine would be protonated to generate an ammonium cation, whereby the macrocycle DB24C8 will shuttle to this station due to the formation of intramolecular charge-assisted hydrogen bonds. At high pH, it was expected that the free amine is regenerated, which is potentially a weaker hydrogen bond donor than the triazole heterocycles, thereby causing the macrocycle to move to the bis-triazole PDI station.

4.2 [3]Rotaxane Synthesis

The synthesis of bis-alkynyl PDI **23** has already been described in Chapter 2, and so synthesis began with the aniline-based mono-stoppered azide thread, required to prepare the axle component (Figure 4.4). First, commercially available 3,5-di-*tert*-butylbenzoic acid was dissolved in a suspension of $CHCl_3$ and H_2SO_4 and heated to 45 °C. Then NaN_3 was very slowly added to the reaction mixture behind a blast shield over the course of an hour, done in this way to prevent the formation of the highly explosive HN_3. After stirring for five hours at 45 °C, the reaction was worked up and basified with KOH to yield 3,5-*tert*-butyl aniline **69** in 79% yield (Scheme 4.1).

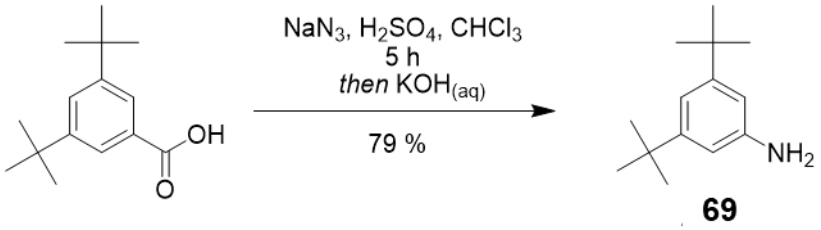

Scheme 4.1. Synthesis of 3,5-*tert*-butyl aniline **69**.

To the thread onto this stopper group, an excess of 1,6-dibromohexane was reacted with 3,5-*tert*-butyl aniline **69** in MeCN at 50 °C over two days to form amine **70** in 91% yield. It should be noted that temperature control plays an important role in this reaction, as the same reaction repeated at 80 °C resulted in double alkylated **71** (Scheme 4.2).

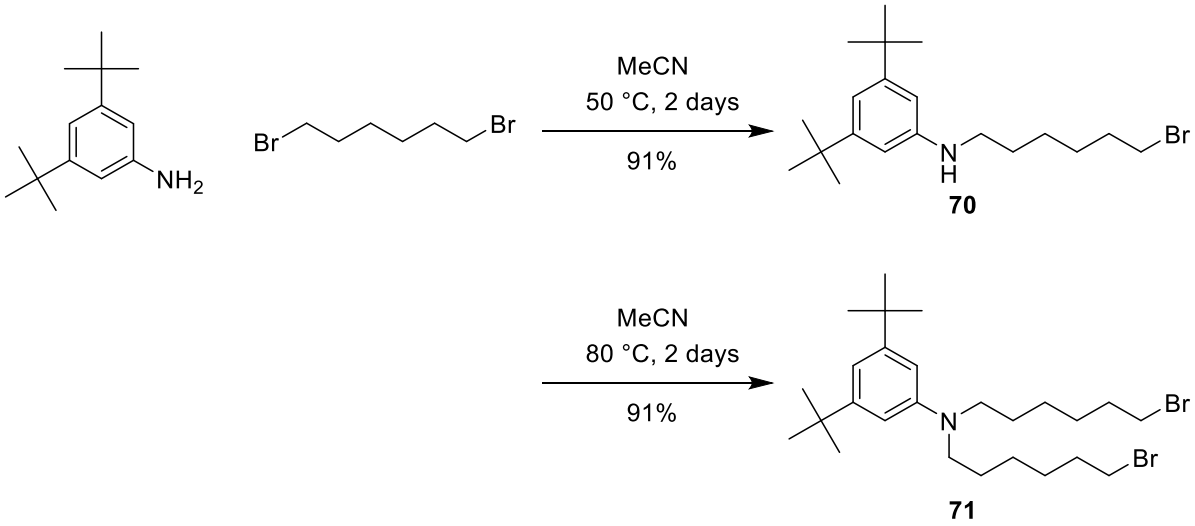

Scheme 4.2. Synthesis of **70** and **71**.

The singly alkylated **70** was then reacted with sodium azide in DMF at 70 °C over five hours to quantitively form the mono-stoppered azide **72**. In order to thread **72** through DB24C8, it was necessary to protonate the secondary amine group, thereby increasing the strength of the templating intermolecular hydrogen bond interactions. Therefore, **72** was dissolved in Et_2O, and stirred with 2M HCl in Et_2O over an hour, thereby generating the secondary ammonium station. To prevent poisoning of the Cu(I) catalyst by Cl^- anions, in the next step (CuAAC), this was subjected to ion exchange to form the weakly-coordinating PF_6^- ammonium salt. This was achieved by redissolving **73** in Et_2O and then vigorously stirring in a suspension with 0.5 M NH_4PF_6 in water, then further washing with 0.5 M $NH_4PF_{6(aq)}$ to achieve **73** in 93% yield (Scheme 4.3). Alternatively, vigorously washing four times with a saturated solution of NH_4PF_6(aq) and extracting with Et_2O, DCM or $CHCl_3$ yielded the same result, as both methods displayed one set of signals in their ^{31}P NMR and ^{19}F NMR spectra (Scheme 4.3).

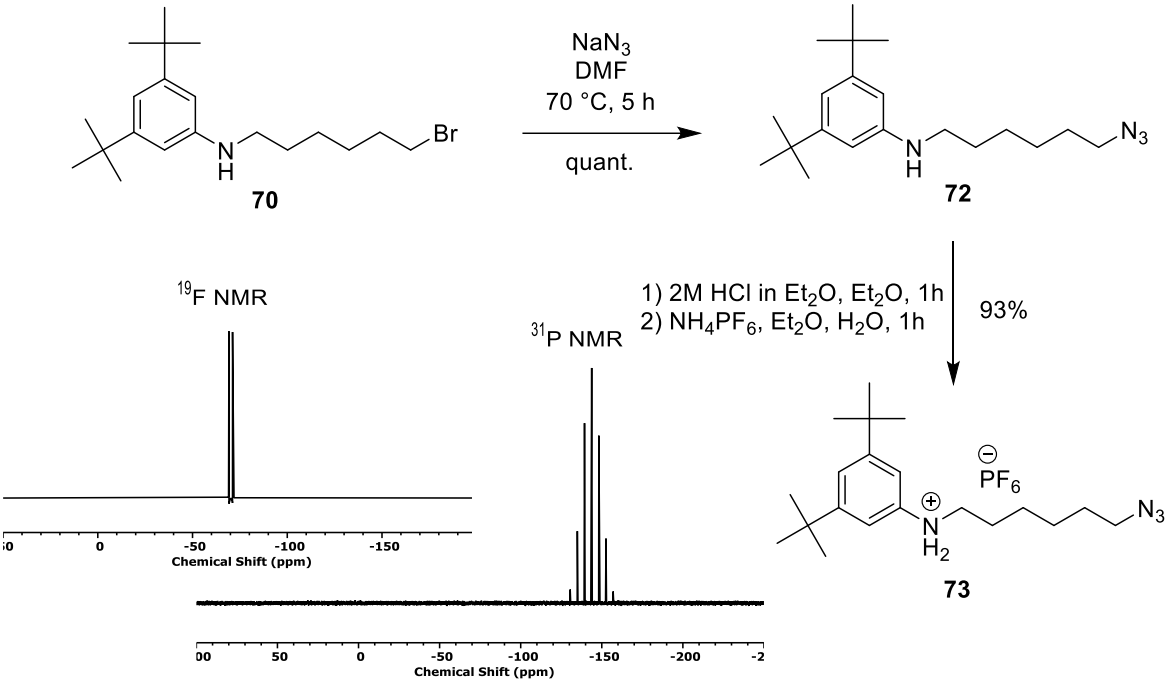

Scheme 4.3. Synthesis of rotaxane precursor **73** from 1,6-dibromohexane and 3,5-*tert*-butyl aniline. ^{31}P NMR and ^{19}F NMR spectra of **73** is displayed.

A threading study was first conducted to quantify the equivalents of macrocycle DB24C8 needed. As the threaded stopper and the de-threaded stopper is in constant equilibrium, favouring the threaded macrocycle due to stabilisation from hydrogen bonding between the

ammonium and the crown ether, the addition of more free macrocycle will shift the equilibrium to favour the threaded stopper more by Le Châtelier's principle. By ^{1}H NMR spectroscopy, addition of 2.5 eq of DB24C8 to 1 eq of stopper **73** lead deshielding of both H_f (CH_2 adjacent to NH_2^+) and H_g (Ar*H* on stopper) by 0.72 ppm and 0.03 ppm respectively. Further addition of DB24C8 did not significantly shift the signals, where upon addition of 5 eq of DB24C8, H_f and H_g only shifted by a further 0.04 ppm and 0.01 ppm respectively (Figure 4.5). Thus, 2.5 eq of DB24C8 to 1 eq stopper is sufficient to be used in the rotaxanation reaction.

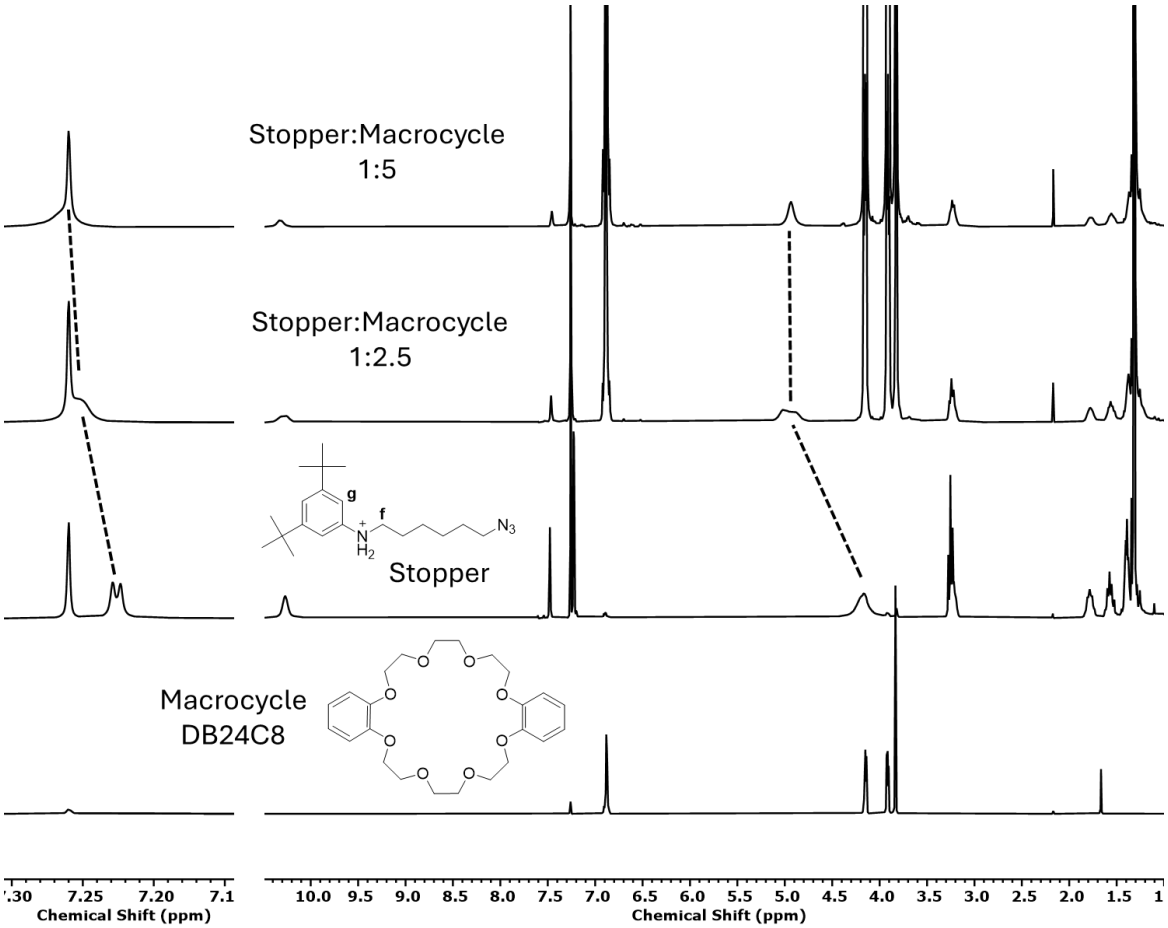

Figure 4.5. ^{1}H NMR threading study of stopper **73** and macrocycle DB24C8.

To prepare the target [3]rotaxane, bisalkynyl PDI **23** (1 eq), an excess of mono-stoppered ammonium-azide thread **73** (2.5 eq), and an even larger excess of crown ether macrocycle DB24C8 (6.25 eq) was subjected to a CuAAC reaction, catalysed by $Cu(MeCN)_4{-}PF_6$ in the presence of TBTA. This yielded [3]rotaxane **74** in approximately 20% yield. When the reaction was repeated in the absence of DB24C8, the axle component **75** was also formed in approximately 60% yield (Scheme 4.4).

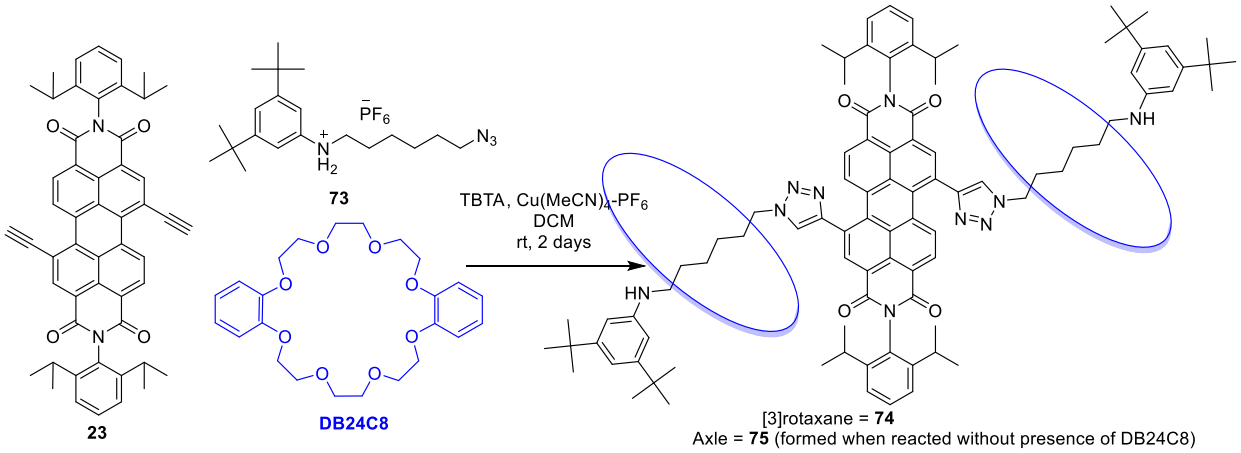

Scheme 4.4. Synthesis of [3]rotaxane **74** and its axle **75.**

Following a challenging purification (*vide infra*), the successful isolation of the target [3]rotaxane **74** and axle **75** were confirmed by mass spectrometry and ^{1}H NMR spectroscopy. In particular, in the ^{1}H NMR spectra, the desymmetrisation of macrocycle DB24C8 indicates the formation of the [3]rotaxane, and the symmetric signals of the PDI confirmed the formation of a [3]rotaxane (Figure 4.6).

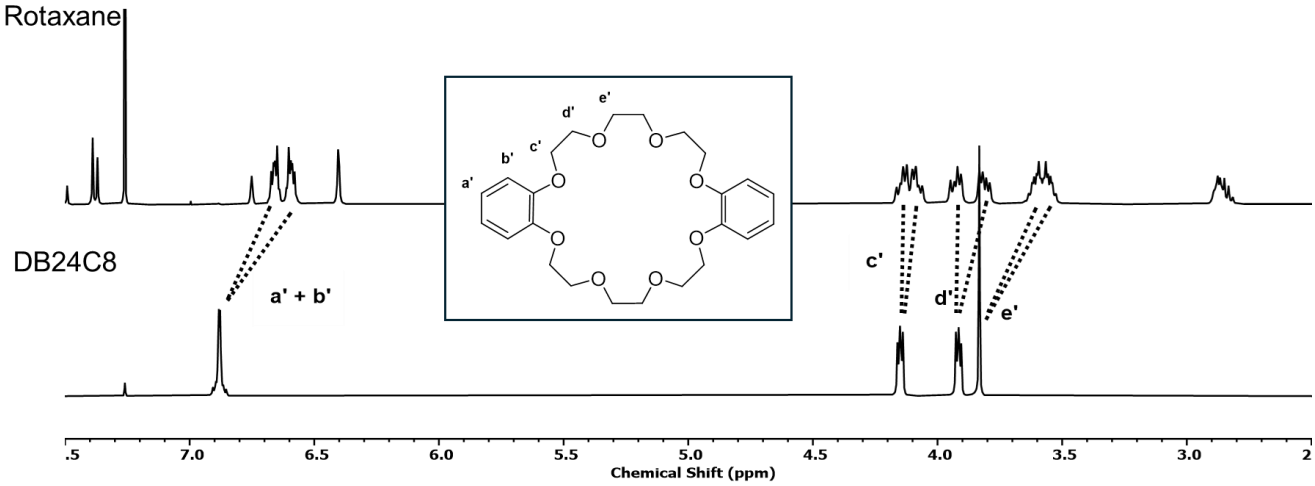

Figure 4.6. Stacked ^{1}H NMR spectra of rotaxane **74** (top) and free macrocycle DB24C8 (bottom) ($CDCl_3$, 298 K, 400 MHz). Note the doubling of macrocyclic signals arising from the decrease in symmetry (C2) in [3]rotaxane against free macrocycle.

The purification of the [3]rotaxane and axle compounds proved to be challenging. Silica gel flash chromatography was performed with the neutral materials (i.e., free amines) with an eluent system containing a small mixture of NEt_3 (**74:** DCM:MeOH:NEt_3 95:5:0.1; **75:** DCM:MeOH:NEt_3 99.5:0.5:0.1) to prevent re-protonation on the silica gel. This greatly improved the tightness of the product bands as they moved down the silica gel column. This method was able to isolate the [3]rotaxane from the excess stopper group, the [2]rotaxane,

and other unidentified side products. However, silica gel flash chromatography did not remove the excess DB24C8 or TBTA from the [3]rotaxane **74** or axle **75,** as evidenced by ^{1}H NMR spectroscopy. Moreover, this method of purification did not separate out the minor, and undesired**,** 1,6-regioisomeric PDI products.

The removal of these impurities (DB24C8, TBTA, and 1,6- PDI regioisomer) proved to be difficult. Whilst traditional chromatography techniques (column chromatography and preparative TLC) were able to remove each contaminant, the drop in isolated yield was deemed too significant for this purification to be done in conjunction. Figure 4.7 outlines these numerous purification attempts. Ultimately, it was discovered that the tris((1-hydroxy-propyl-1H-1,2,3-triazol-4-yl)methyl)amine (THPTA) could be used as a ligand instead of TBTA in the CuAAC rotaxanation, since this ligand can easily be removed by aqueous work up.

Furthermore, it was found that $PDIBr_2$ **21**, a precursor to PDI bisalkyne **23** (*vide supra*, Section 2.2.1), was able to be purified on scale by preparative HPLC using a COSMOSIL Buckyprep Packed Column. The 1,7- regioisomer was successfully separated from the 1,6-regioisomer by elution with 1:2:1 n-hexane:CH_2Cl_2:IPA mixture. This was then further reacted as described in Section 2.2.1 to achieve pure 1,7- PDI bisalkyne **23**, and then by CuAAC with THPTA and $Cu(MeCN)_4{-}PF_6$, to yield [3]rotaxane **74** and axle **75**.

Finally, to remove DB24C8, both [3]rotaxane **74** and axle **75** were able to be purified by two successive preparative TLCs (Figure 4.7c). Whilst the calculated yields (by ^{1}H NMR spectroscopy) of [3]rotaxane **74** and axle **75** were 20% and 59% respectively, the isolated yields after these preparative TLC plates were 0.4% and 0.5% respectively.

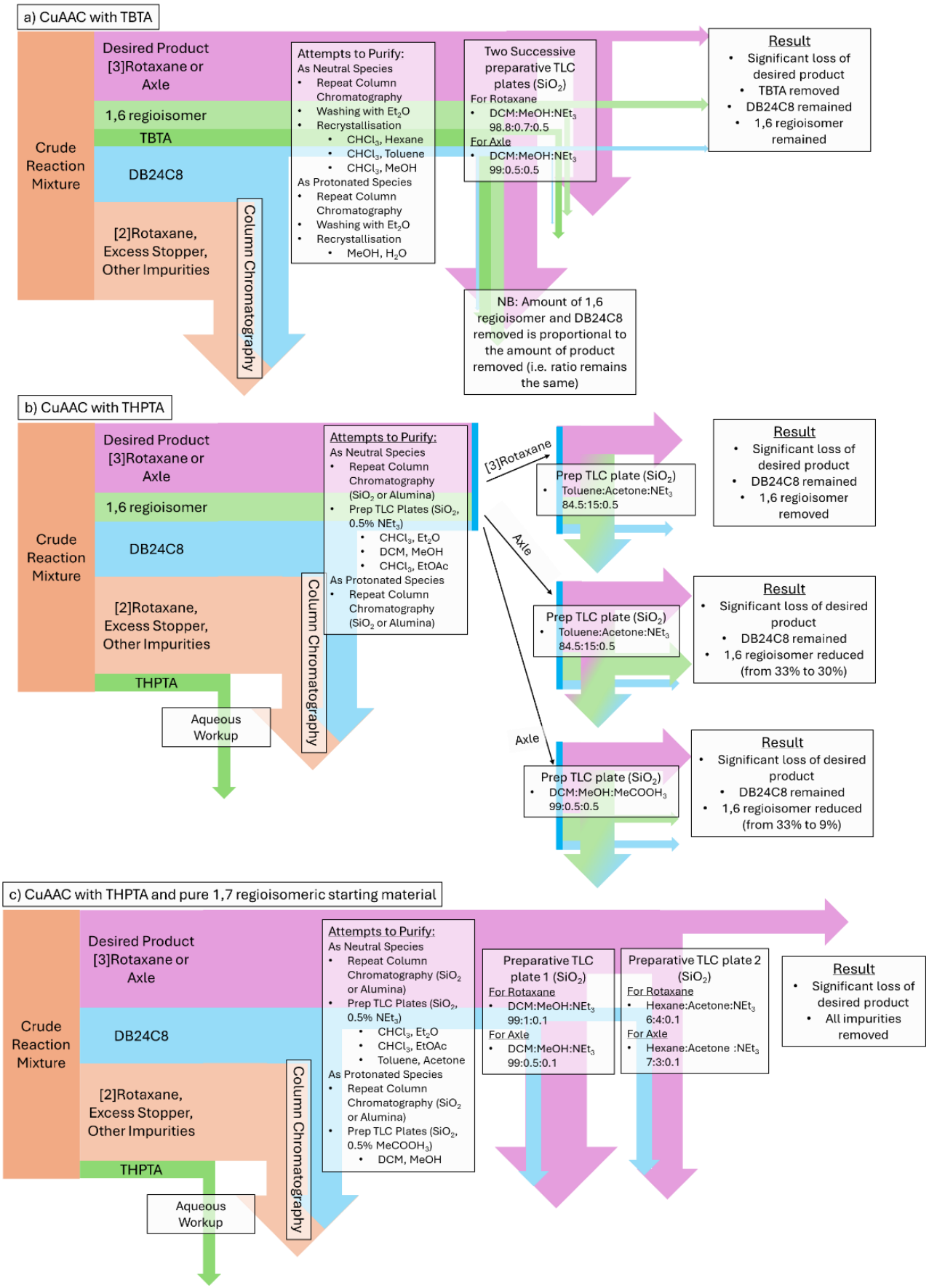

Figure 4.7. Purification of **75** and **74** after CuAAC with a) mixed 1,6- and 1,7- PDI regioisomeric starting material and TBTA, b) mixed 1,6- and 1,7- PDI regioisomeric starting material and

THPTA, and c) pure 1,7- PDI regioisomeric starting material and THPTA. Further details of these purification attempts have been outlined in Appendix C.

4.3 Co-conformational Switching in [3]rotaxane

The macrocycle shuttling between the two stations (secondary ammonium/amine and triazole) was initially investigated by preparing the neutral (i.e. free amine) and dicationic (i.e. ammonium) states of [3]rotaxane **75** and axle **74**. Rotaxane **74** and axle **75** contains a secondary amine, which can protonated or deprotonated by pH stimulus, where in the case of rotaxane **74**, the macrocycle would be switched between the two station. To protonate the secondary amines, the rotaxane and axle were each subjected to 2M HCl in Et_2O. To maximise inter-component hydrogen bonding, the protonated products were washed four times with saturated $NH_4PF_{6(aq)}$ to exchange their Cl^- anions with more weakly coordinating PF_6^- anions. This successfully achieved the dicationic [3]rotaxane **74·(PF$_6$)$_2$** and its corresponding axle **75·(PF$_6$)$_2$**. This process was easily reversed by addition of NEt_3, then a simple aqueous workup to return the neutral amines, [3]rotaxane **74** and axle **75** (Scheme 4.5).

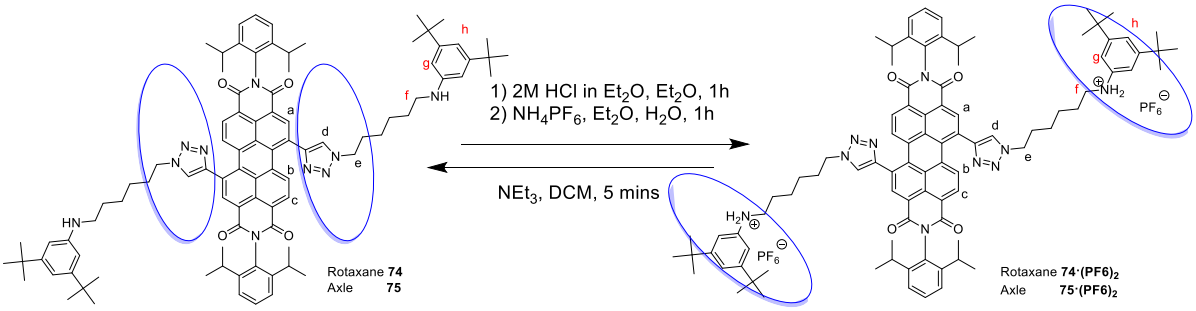

Scheme 4.5. Switching of protonation stages of **74** and **75** via base and acid wash.

4.3.1 Investigation of shuttling by ^{1}H NMR Spectroscopy

Evidence for macrocycle shuttling in [3]rotaxane **74** was observed by ^{1}H NMR spectroscopy. In the neutral [3]rotaxane, the free amines exhibit only weak interactions with DB24C8 and so the macrocycles reside at the triazole stations. This is evidenced by significant shifts of protons associated with this station ($H_{a\text{-}e}$ (red), Table 4.1) relative to the free axle **75**, while protons at the amine station ($H_{f\text{-}h}$ (black), Table 4.1) are relatively unchanged compared to axle **75**. The large downfield shift of H_d is indicative of hydrogen bonding to the oxygens in the macrocyclic cavity. It should be noted that in literature, the triazole station is typically methylated (to a *N*-

methyl triazolium group) to act as a station for a crown ether macrocycle. However, it appears that the electron-withdrawing nature of the PDI, which is conjugated to the triazole, increases the hydrogen bond donating ability of the triazole, so enabling the neutral heterocycle to act as a station for the macrocycle in this system. Furthermore, π-interactions between the π-electron rich dibenzo groups on DB24C8 and the π-electron deficient PDI may also make the triazole groups effective macrocycle recognition sites. Upon protonation of the amines, the ammonium groups outcompete the triazoles for recognition of DB24C8 due to stronger charge-assisted hydrogen bonding, thus the macrocycles in **74·(PF$_6$)$_2$** shuttle to the ammonium stations. This is evidenced by significant shifts of protons associated with this station ($H_{f\text{-}h}$ (black), Table 4.1) relative to the free axle **75·(PF$_6$)$_2$**, while protons at the amine station ($H_{a\text{-}e}$ (red), Table 4.1) are relatively unchanged compared to axle **75·(PF$_6$)$_2$** (Figure 4.8).

Proton (ppm)	**a**	**Δδ**	**b**	**Δδ**	**c**	**Δδ**	**d**	**Δδ**	**e**	**Δδ**	Mean |Δδ| ($H_{a\text{-}e}$)
75	8.77	0.38	8.01	-0.16	8.35	0.22	7.88	-1.07	4.53	-0.59	0.48
74	8.39		8.17		8.13		8.95		5.12		
74·(PF$_6$)$_2$	8.81	-0.04	8.05	-0.01	8.27	0.06	7.86	0.04	4.26	0.27	0.08
75·(PF$_6$)$_2$	8.77		8.04		8.33		7.90		4.53		

Proton (ppm)	**f**	**Δδ**	**g**	**Δδ**	**h**	**Δδ**	Mean |Δδ| ($H_{f\text{-}h}$)
75	3.50	0.62	6.77	0.02	6.46	0.06	0.23
74	2.88		6.75		6.40		
74·(PF$_6$)$_2$	4.17	-1.00	7.33	-0.46	7.33	-0.78	0.75
75·(PF$_6$)$_2$	3.17		6.87		6.55		

Table 4.1. ^{1}H NMR ($CDCl_3$, 400 Hz) shifts of axles **75**, **75·(PF$_6$)$_2$**, and rotaxanes **74**, **74·(PF$_6$)$_2$**.

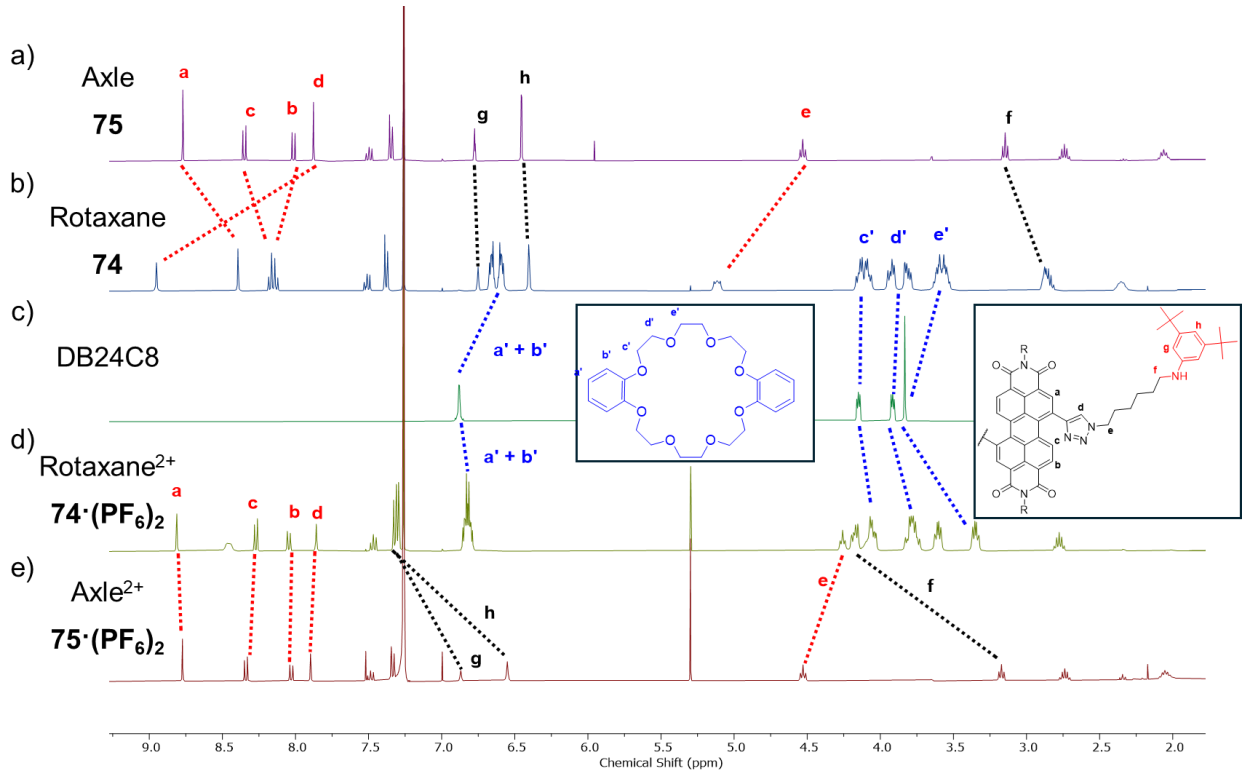

Figure 4.8. ^{1}H NMR ($CDCl_3$, 400 Hz) spectra of a) axle **75**, b) rotaxane **74**, c) macrocycle DB24C8, d) rotaxane **74·(PF$_6$)$_2$**, and e) axle **75·(PF$_6$)$_2$**.

4.3.2 Photophysical Investigation of Shuttling Behaviour

This macrocycle shuttling is also evident from the UV-vis absorption and fluorescence spectra of [3]rotaxanes **74** and **74·(PF$_6$)$_2$**, and axles **75** and **75·(PF$_6$)$_2$**. Firstly, the UV-vis absorption spectra of all four compounds were measured at different concentrations to confirm Beer-Lambert behaviour. Therefore, at these concentrations, the interactions probed by UV-vis spectroscopy are intramolecular and not intermolecular in origin (Figure 4.9).

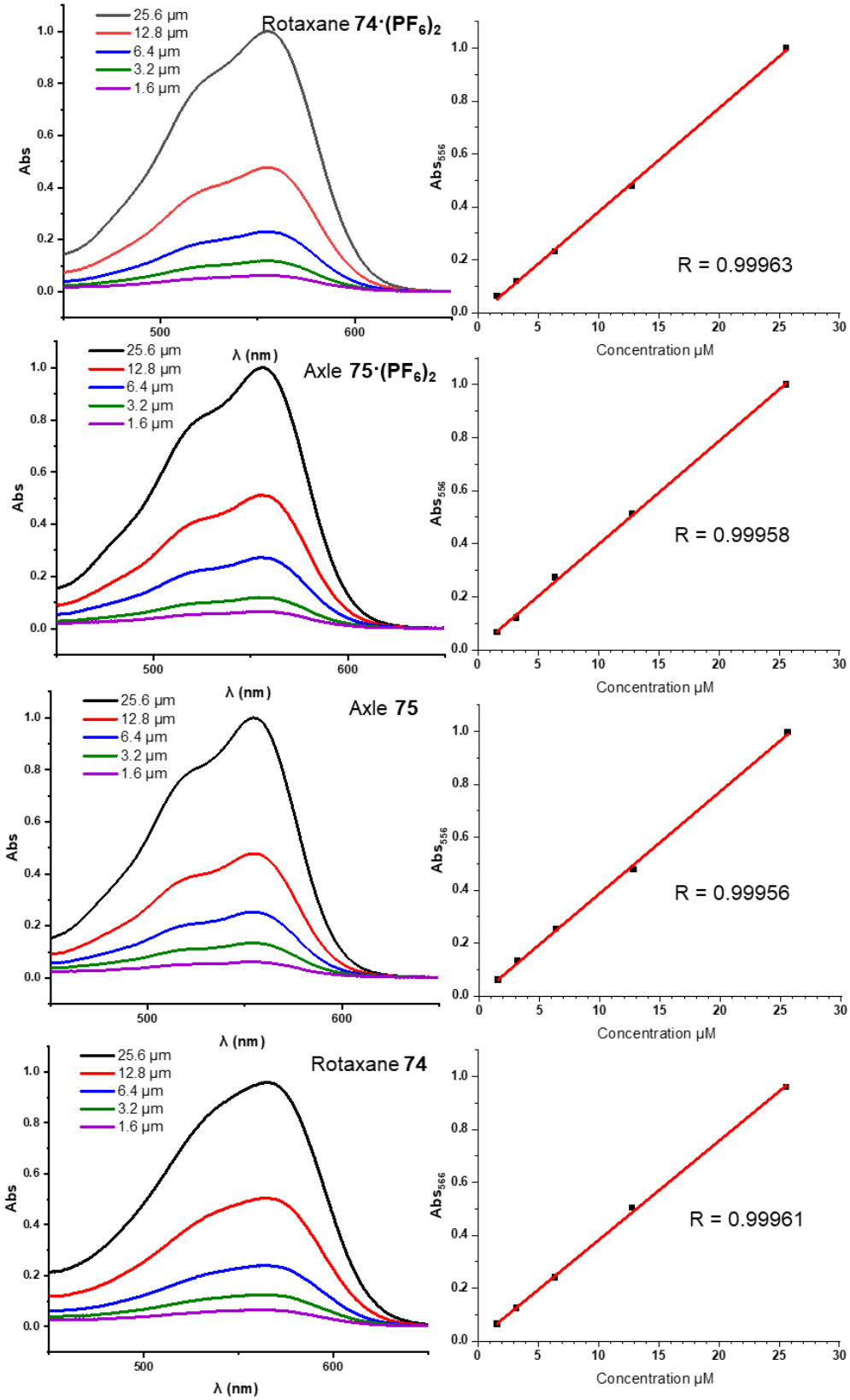

Figure 4.9. Left: UV-vis absorption spectra of: [3]rotaxanes **74** and **74·(PF$_6$)$_2$**, and axles **75** and **75·(PF$_6$)$_2$** in $CHCl_3$ at different concentrations. Right: the dependence of absorption (λ_{max}) on concentration for these compounds: [3]rotaxanes **74** (λ_{max} = 566 nm) and **74·(PF$_6$)$_2$** (λ_{max} = 556 nm), and axles **75** (λ_{max} = 556 nm) and **75·(PF$_6$)$_2$** (λ_{max} = 556 nm), in $CHCl_3$ is linear, showing Beer-Lambert behaviour.

Comparing the UV-vis absorption spectra of the neutral rotaxane **74** against the protonated rotaxane **74·(PF$_6$)$_2$**, the main PDI absorption band (S_0-S_1, λ_{max} = 556 nm) of **74** is red shifted by 10 nm (Figure 4.10, left). Importantly, this red shift is only observed in the rotaxanes and not in the axles **75,** since the PDI absorption band of unprotonated axle **75** is identical to that of the protonated axle **75·(PF$_6$)$_2$**. Therefore, the red-shift in the [3]rotaxane indicates new intramolecular non-covalent interactions as the macrocycles move to occupy the bis-triazole PDI stations. As well as hydrogen bonding between the crown ethers and the triazole groups, there may also be donor–acceptor π–π interactions from the π-electron rich dibenzo groups and the π-electron deficient PDI unit. Unsurprisingly, the UV-vis absorption spectrum of the protonated [3]rotaxane **74·(PF$_6$)$_2$** is identical to that of the axles **75** and **75·(PF$_6$)$_2$**, since under these conditions the DB24C8 macrocycles have vacated the bis-triazole PDI stations and reside at the ammonium stations further away from the chromophore.

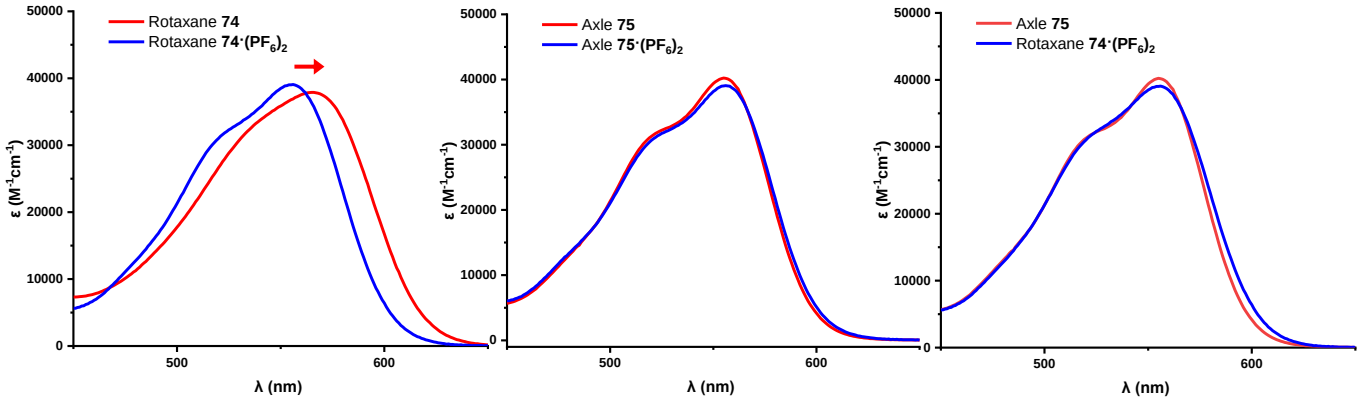

Figure 4.10. Left: UV-vis absorption spectra of rotaxanes **74** (red) and **74·(PF$_6$)$_2$** (blue). Middle: UV-vis absorption spectra of axles **75** (red) and **75·(PF$_6$)$_2$** (blue). Right: UV-vis absorption spectra of axle **75** (red) and rotaxane **74·(PF$_6$)$_2$** (blue). All spectra were recorded in $CHCl_3$ at a concentration of 26 μM in a quartz cuvette with 1 cm path length.

The co-conformational change is also evident by fluorescence spectroscopy. The fluorescence spectrum of neutral [3]rotaxane **74 is** significantly red-shifted (Δλ = 14 nm) and quenched in comparison to that of the dicationic [3]rotaxane **74·(PF$_6$)$_2$** (Figure 4.11, left). This fluorescence quenching is likely to arise from donor–acceptor charge transfer interactions between DB24C8 and the PDI, when the macrocycles reside at the triazole stations. It should be noted that a similar decrease in fluorescence emission intensity is observed upon deprotonation of the axle **75**, indicating that PDI

fluorescence quenching by photoinduced electron transfer quenching from the free amine is also occurring (Figure 4.11, middle). However, the emission spectrum of axle **75** is not red-shifted compared to that of the [3]rotaxane **74·(PF$_6$)$_2$** (Figure 4.11, right), a result in line with what was observed by UV-vis absorption spectroscopy, and so indicating the role of macrocycle shuttling in the photophysical response. Overall, the acid/base mediated changes in photophysical properties of the [3]rotaxane **74** are greater than the axle component alone (**75**), due to the former's change in co-conformation, and indeed are more clearly visible to the naked eye (Figure 4.12).

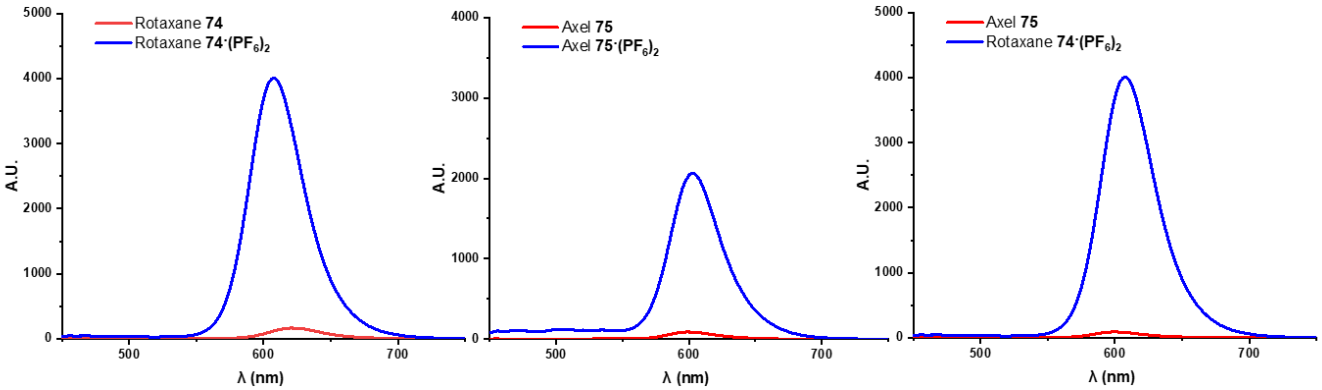

Figure 4.11: Left: Fluorescence emission spectra of rotaxanes **74** (red) and **74·(PF$_6$)$_2$** (blue). Middle: Fluorescence emission spectra of axles **75** (red) and **75·(PF$_6$)$_2$** (blue). Right: Fluorescence emission spectra of axle **75** (red) and rotaxane **74·(PF$_6$)$_2$** (blue).. All spectra were recorded in $CHCl_3$ at a concentration of 26 μM in a quartz cuvette with 1 cm path length.

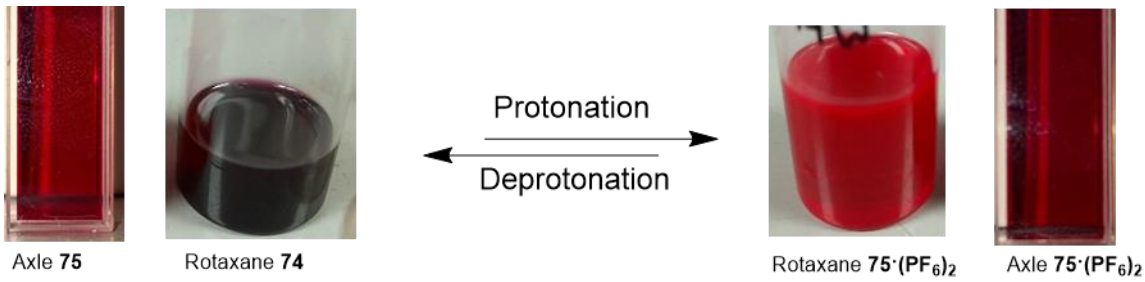

Figure 4.12: Images of [3]rotaxane **74** and axle **75** upon protonation and deprotonation, displaying significant visible change in [3]rotaxane **74**.

4.4 PDI Atropisomer Interconversion

Having demonstrated the shuttling of DB24C8 in rotaxane **74**, where these macrocycles switch between occupation of the ammonium and bis-triazole PDI stations, it was next of interest to understand the impact of this shuttling on the barrier to PDI atropisomerism. To achieve this, axle component **75** and [3]rotaxane **74** were

subjected to chiral HPLC at 5 °C. As expected, the chromatogram of axle **75** shows a single peak (Figure 4.13, top). This indicates that the ***P*** and ***M*** atropisomers are rapidly interconverting in the axle, which is in line with previous acyclic PDIs shown in Chapters 2 and 3. In contrast, the analogous chromatogram of neutral [3]rotaxane **74** exhibits two overlapping peaks (Figure 4.13, middle), assigned to the ***P*** and ***M*** atropisomers. Therefore, this suggests that the rate of PDI atropisomerism has decreased when the macrocycles are positioned either side of the PDI unit, meaning the barrier to interconversion ($\Delta G^{\ddagger}$) has increased. This is a notable result since it is the first time mechanical bonding has been used as a tool to impact PDI atropisomerism.

It should be noted that that the protonated rotaxane **74·(PF$_6$)$_2$** and axle **75·(PF$_6$)$_2$** were not subjected to HPLC due to the risk of them not being eluted due to their high polarity and so permanently damaging the chiral column.

In attempts to resolve the ***P*** and ***M*** enantiomers of the [3]rotaxane, the edges of each peak were collected, such that the areas in which the peaks overlap were discarded. However, upon reinjection of these samples on the chiral HPLC column within minutes of their isolation, it was discovered that they had equilibrated back into a racemic mixture. Furthermore, the samples did not exhibit a CD spectrum. This demonstrates that the interconversion barrier ($\Delta G^{\ddagger}$) was not raised significantly enough to enable resolution of the ***P*** and ***M*** atropsiomers of **74** at 5 °C (Figure 4.13, bottom).

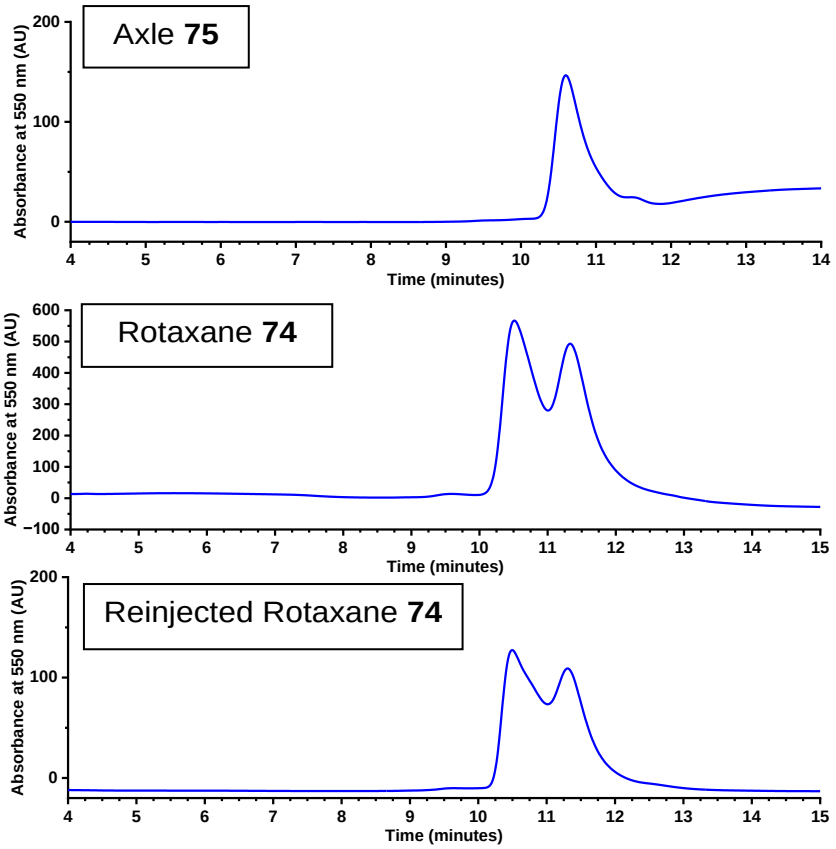

Figure 4.13. Chiral HPLC chromatograms of axle **75** (top), rotaxane **74** (middle)**,** and reinjected rotaxane **74** (bottom).

Indeed, ^{1}H NMR spectroscopy of the diastereotopic methyl protons, situated on the imide groups of the PDI, of both [3]rotaxane **74** and axle **75** exhibit only one doublet, which provides further evidence that the ***P*** and ***M*** PDI atropisomers are rapidly interconverting at 25 ° C (Figure 4.14).

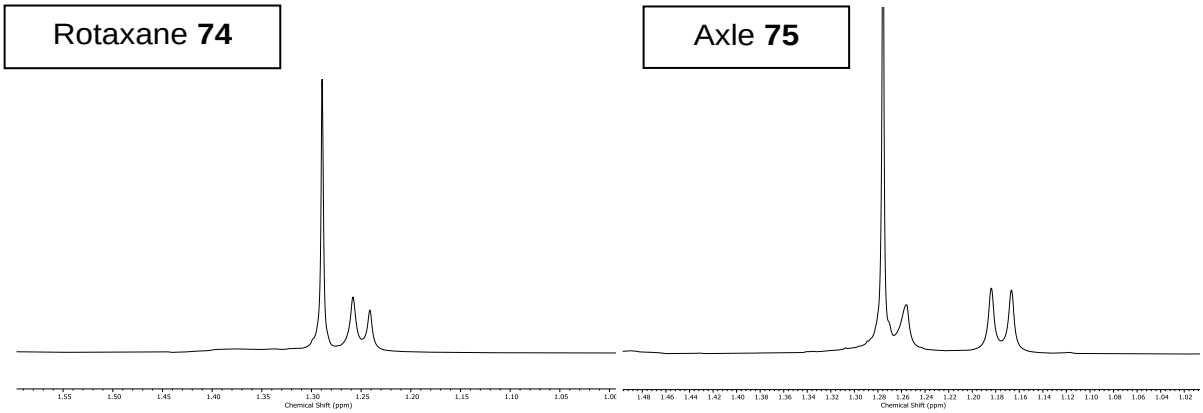

Figure 4.14. ^{1}H NMR spectra of rotaxane **74** (left), and axle **75** (right), displaying a single set of doublets for methyl groups, displaying no diastereotopic splitting as PDI atropoisomers are in fast exchange ($CDCl_3$, 298 K, 400 MHz).

4.5.1 Methylation of [3]rotaxane

It was envisaged that the methylation of the triazole stations of [3]rotaxane **74**, to generate a bis-triazolium PDI (see Section 2.6), would increase the strength of the hydrogen bonding interactions with the macrocycles at these positively charged stations. This increase in interaction strength may cement the macrocycles' position at the central PDI unit, thereby resulting in an increased barrier to PDI atropisomerism.

Therefore, [3]rotaxane **74·(PF$_6$)$_2$** was subjected to methylation by stirring in MeI at 80 °C in a sealed pressure tube for four days (Scheme 4.6). Here, the protonated [3]rotaxane **74·(PF$_6$)$_2$** was used to avoid the risk of methylating the free amine, and so preserving this station. Whilst ESI mass spectrometry indicated the formation of the methylated [3]rotaxane, the poor solubility of the crude product prevented its purification and characterisation.

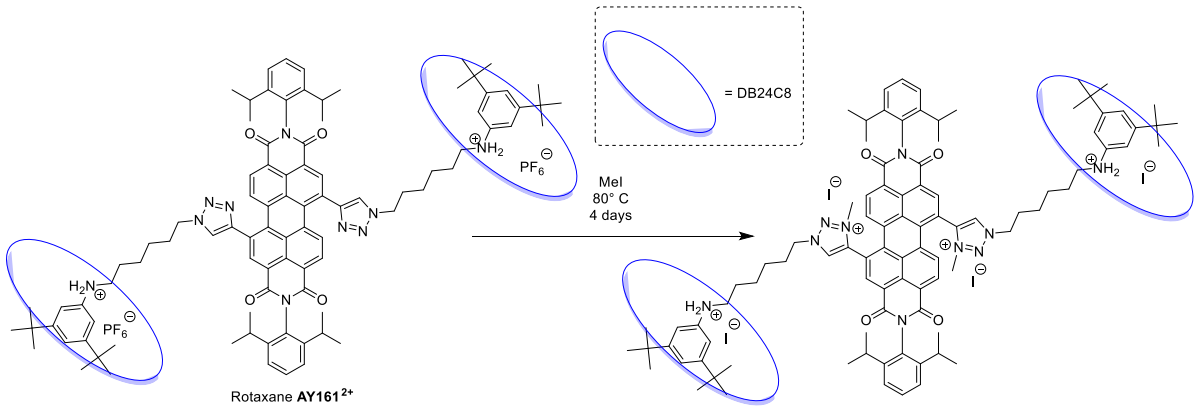

Scheme 4.6. Methylation of [3]rotaxane **74**.

4.5 Towards the Induction of Chirality in a PDI-based [3]Rotaxane

4.5.2 Chiral macrocycle

Since it was not possible to resolve the PDI atropsiomers of [3]rotaxane **74**, it was decided that PDI chirality might be induced through the mechanical bond by the interlocking of chiral macrocycles onto the bis-triazole PDI axle component. Since P/M-BINOL had been shown to be able to direct the stereoselective synthesis of PDI-based macrocycles through non-covalent aromatic interactions in Chapter 3, it was thought a

PP-diBINOL-28-crown-8 macrocycle (**76)** could be incorporated into the PDI [3]rotaxane. To prepare this chiral macrocycle, commercially available triethylene glycol was tosylated by stirring with tosyl chloride and KOH in DCM at 0° C for 3 h, which quantitively furnished ditosylated glycol **77** (Scheme 4.7).

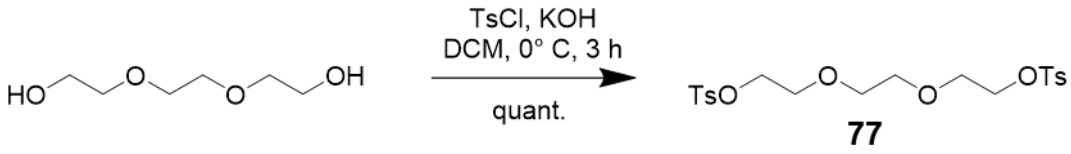

Scheme 4.7. Synthesis of glycol **77**.

An initial attempt to synthesise the macrocycle used an adapted literature procedure for preparing DB24C8.[145] Ditosylated glycol **77** was added to ***P***-BINOL in equal stoichiometry, where they were stirred together in the presence of KPF_6 and K_2CO_3 in MeCN at 90 °C for one week. Unfortunately, this reaction did not yield any [2+2] macrocycle, as only starting materials and short oligomers were detected by ESI mass spectrometry, suggesting that the reaction was too slow. To increase the rate of reaction, an alternative literature procedure was adapted, which use a stronger base (^{t}BuOK) and a different solvent (THF), which successfully yielded macrocycle **76** after purification in 5% yield.[146] Here, it is likely that the potassium cations present in the reaction will template the formation of a [2+2] crown ether macrocycle (Scheme 4.8).

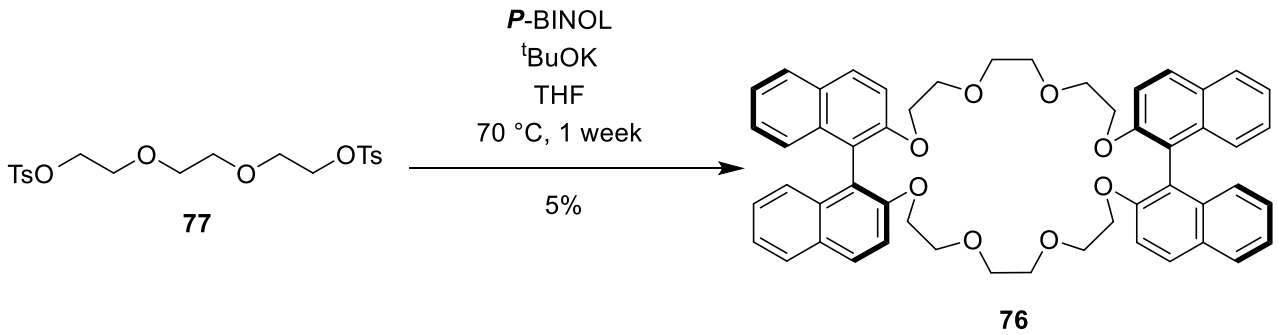

Scheme 4.8. Synthesis of macrocycle **76**.

The synthesis of the [3]rotaxane using this chiral macrocycle was then attempted using the same conditions as for the DB24C8-containing [3]rotaxane **74**. Regioisomerically pure 1,7-bisalkynyl PDI **23** (1 eq), an mono-stoppered azide **73** (2.5 eq), and an excess of macrocycle **76** (6.25 eq) was subjected to CuAAC reaction conditions, catalysed by

$Cu(MeCN)_4{-}PF_6$ and in the presence of THPTA (Scheme 4.9). Unfortunately, ^{1}H NMR spectroscopy analysis of the crude reaction mixture revealed only free axle and macrocycle and no [3]rotaxane. This is because the ^{1}H NMR sprectrum of the crude reaction mixture is a superposition of the axle **75** and macrocycle **76** ^{1}H NMR spectra.

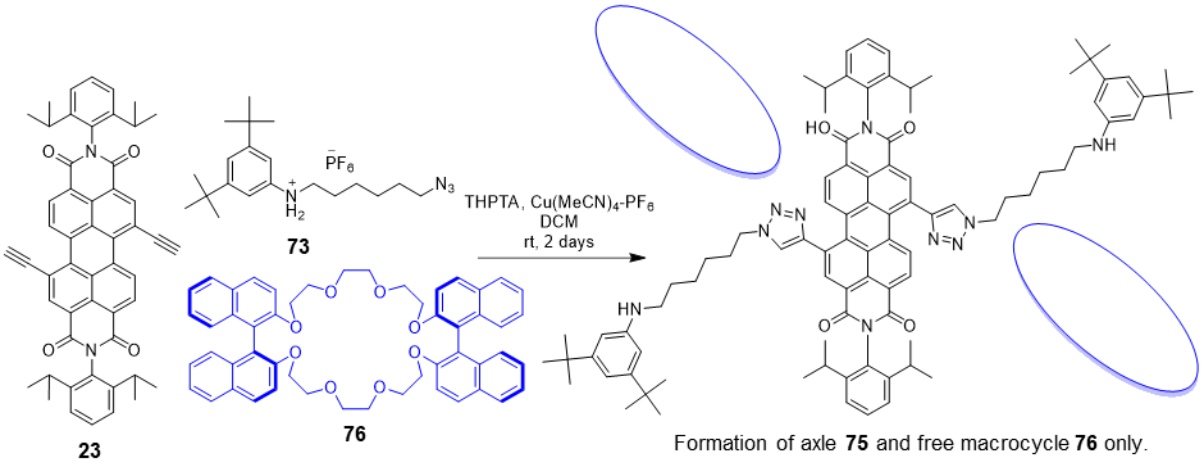

Scheme 4.9. Attempted rotaxanation with **23**, **73**, and **76**.

4.6 Conclusions and Future Work

This chapter details the synthesis of a novel two station PDI [3]rotaxane **74** and its axle **75**, where the DB24C8 macrocycles in **74** shuttle to and from the triazole stations and the ammonium/amine stations in response to pH stimuli. The [3]rotaxane **74** and corresponding axle **75** were prepared in 20% and 59% calculated yields respectively (by ^{1}H NMR spectroscopy analysis), and isolated in yields of 0.4% and 0.5% due to lengthy purification procedures. The synthesis of a [3]rotaxane with a chiral macrocycle (PP-diBINOL-28-crown 8) **76** was also attempted but, without optimization of the reaction, only resulted in the formation of the axle component **75**, without any rotaxane products.

Initial purification of [3]rotaxane **74** and axle **75** was difficult as the product was contaminated with TBTA, its 1,6-regioisomer, and excess macrocycle DB24C8. Whilst traditional chromatography techniques (column chromatography and preparative TLC) were able to remove each contaminant, the drop in isolated yield is deemed too significant for this purification to be done in conjunction. Instead, the synthesis was adapted such that THPTA could be used as a water soluble ligand instead of TBTA, and it was discovered that 1,7-$PDIBr_2$

could be separated from its 1,6-regioisomer to achieve pure 1,7-PDIBr2, which was then used to synthesise the PDI bisalkyne starting material **23** needed for rotaxanation.

The secondary amine stations of the [3]rotaxane could be protonated by acids (HCl) and deprotonated by base (NEt_3) to afford co-conformational change. Upon protonation, ^{1}H NMR spectroscopy revealed that the DB24C8 macrocycles reside at the ammonium stations. Whereas upon deprotonation, ^{1}H NMR spectroscopy evidenced shuttling of these macrocycles to the PDI-triazole stations, thereby affording a two-station [3]rotaxane switch. Photophysical studies by UV-vis and fluorescence spectroscopy underpinned this dynamic behaviour. The protonated [3]rotaxane **74·$(PF_6)_2$** shows near identical spectra to axles **75** and **75·$(PF_6)_2$**. However, the deprotonated [3]rotaxane **74** was unique in exhibiting a significant redshift in both the UV-vis and fluorescence spectra, indicative of new hydrogen bonding and/or donor–acceptor π–π interactions between the crown ether macrocycles and the bis-triazole PDI.

Chiral HPLC analysis revealed that the [3]rotaxane **74** exhibits two peaks for the two PDI atropisomers (***M*** and ***P***), while the axle component alone contains only a single peak. Therefore, the mechanical bonding in the [3]rotaxane appears to be slowing down PDI atropisomer interconversion. Whilst the interconversion barrier was not high enough to enable isolation and chiroptical analysis of the enantiomers, the dynamic properties of the macrocycle in [3]rotaxane **74** have enabled characterisation of the positioning of a mechanically bonded macrocycle proximal to a chiral PDI, demonstrating their potential to impact PDI atropisomer interconversion.

However, this current [3]rotaxane design is not sufficient to enable atropisomer resolution, perhaps because the macrocycles have too much freedom to move along the axle. Therefore, future research may target a much shorter axle component, containing only the bis-triazole PDI for the macrocycle to reside at. This is designed to restrict translational molecular motion,

anchoring the macrocycles either side of the twisted PDI and potentially increasing the barrier to atropisomer interconversion further than in **74**.

5. Experimental

5.1 Materials and Techniques

All commercial solvents and reagents were used as purchased, unless otherwise stated. Anhydrous solvents were degassed with N_2 and dried using an Innovative Technology PureSolv MD 5 solvent purification system. $Cu(MeCN)_4 \cdot PF_6$ was stored in a desiccator. 1-Azidohexane,[147] tris((1-benzyl-4-triazolyl)methyl)amine (TBTA),[148] and tris-hydroxypropyltriazolylmethylamine (THPTA)[149] were prepared following literature procedures. Water was distilled and microfiltered using an ELGA DV 35 Purelab water purification system. Chromatography was undertaken using silica gel (particle size: 40-63 μm) or preparative TLC plates (20 × 20 cm, 1 cm silica thickness).

All NMR spectra (1D: ^1H, ^{13}C; 2D: $^1H–^1H$ COSY, $^1H–^1H$ NOSEY, $^1H–^{13}C$ HSQC, and $^1H–^{13}C$ HMBC) were recorded at 298 K using Bruker AVIII400 (400 MHz), Bruker AV NEO 400 (400 MHz), or Bruker AV NEO 500 (500 MHz) spectrometers. These NMR spectra were also used for assignment of peaks in 1D ^1H NMR spectra. Mass spectra were recorded using a Waters Synapt G2-S mass spectrometer or a Waters Xevo G2-XS mass spectrometer for high resolution MS-ESI or MS-ASAP.

Circular dichroism (CD) spectra were recorded on a Jasco J-1500 CD spectrophotometer with a wavelength accuracy ± 0.2 nm (250 to 500 nm), ± 0.5 nm (500 to 800 nm) and a CD root mean square noise < 0.007 mdeg (500 nm). A quartz cuvette with 1 mm path length was used unless stated otherwise.

UV-vis absorption spectroscopy was performed on a Cary 5000 spectrophotometer, with a wavelength accuracy ≤ 0.08 nm and absorbance accuracy ≤ 0.01 Abs. Scan speed was 100nm/min. Fluorescence spectroscopy was performed on a Jasco FP-8500 spectrofluorometer with emission and excitation wavelength accuracies ± 1.0 nm. The detector base sensitivity is 8500:1. A quartz cuvette with 1 cm path length was used. Slit width is 2.5 nm, and the scan speed was 100 nm/min. All fluorescence

spectra were excited at 400 nm and measurements, as this wavelength was shown by UV-vis absorption spectroscopy to be strongly absorbing for all compounds.

Chiral HPLC studies were performed using a Phenomenex i-Amylose-1 chiral column on an Agilent 1290 Infinity analytical HPLC instrument. The flow rate was 1 mL/minute, and the detection wavelength was 500 nm.

Acyclic compounds which were initially isolated as a regioisomeric mixture and then purified by HPLC were performed using a COSMOSIL Buckyprep Packed Column (10.0 mm I.D. × 250 mm) on an Agilent 1290 Infinity analytical HPLC instrument at a flow rate of 3 mL/minute, with a detection wavelength of 500 nm.

All compounds synthesised have undergone ^{1}H NMR spectroscopy and have shown to be least 95 % pure.

5.2 General procedures

A: Formation of alkyl bromide

The dihydroxy starting material and dibromo alkane were added to a suspension of potassium carbonate in acetone and left to stir at 60 °C for three days. After which, the reaction mixture was left to cool to room temperature and filtered. The filtrate was concentrated *in vacuo* and purified via flash column chromatography (100:0 à 60:40 n-hexane:CH_2Cl_2).

B: Formation of organic azides

Halide substrate and NaN_3 were dissolved in DMF and left to stir at 75 °C for 16 h. The reaction mixture was quenched with H_2O. If a precipitate was formed, the solid product was collected by vacuum filtration, washed with H_2O and left under suction for 15 min to dry. If no precipitate was formed, the reaction mixture was extracted with Et_2O, washed with H_2O (× 4), brine, then dried with $MgSO_4$ and concentrated *in vacuo*.

C: Copper(I)-catalysed Azide-Alkyne Cycloaddition (CuAAC)

Alkyne and organic azide were dissolved in CH_2Cl_2 and degassed by bubbling a stream of N_2 for 15 min. TBTA or THPTA and $Cu(MeCN)_4 \cdot PF_6$ was then sequentially added, and the resulting mixture was left to stir at rt under an atmosphere of N_2 for a specified time, or until reaching completion as monitored by TLC. After which, the reaction mixture concentrated *in vacuo* and purified *via* flash column chromatography.

D: Imidisation of PDA

PDA substrate (1 eq), amine (2.2 eq), $Zn(OAc)_2 \cdot 2H_2O$ (1.5 eq) and imidazole are added to a flask and stirred at 140 °C for 4 hours. The reaction mixture was cooled to 80 °C and 1M HCl was added dropwise. On cooling to rt, the precipitate was collected by vacuum filtration, was with H_2O until neutral, dried in oven or under vacuum, then purified by flash column chromatography.

5.3 Synthesis and Characterisation for Chapter 2

1,7-Dibromo-perylene-3,4,9,10-tetracarboxylic dianhydride[107]

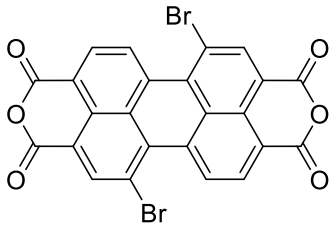

Perylene-3,4,9,10-tetracarboxylic dianhydride (20.0 g, 64.0 mmol, 1 eq) was dissolved in conc H_2SO_4 (300 mL) in a round bottomed flask. *N*-Bromosuccinimide (9.1 g, 79.8 mmol, 1.1 eq) was then added and the reaction flask was stoppered and left to stir at rt for 16 h. After which, additional *N*-bromosuccinimide (9.1 g, 79.8 mmol, 1.1 eq) was added and the flask was again stoppered and left to stir at 80 °C for 1 day. On cooling to rt, the resulting mixture was added onto a large beaker of ice, causing the formation of a red precipitate. Any remaining ice was left to melt, and precipitate was collected by vacuum filtration, washed with H_2O until neutral. The precipitate was dried in the oven overnight to yield a crude mixture of dibromo PDA as a red solid (28.0 g). Its poor solubility in any solvent left it unable to be characterised, and it was subjected to imidization reaction to synthesise **6** without further purification.

N-N-Di(2,6-diisopropylphenyl) 1,7-dibromo-perylene-3,4,9,10-tetracarboxylic diimide[107] 21

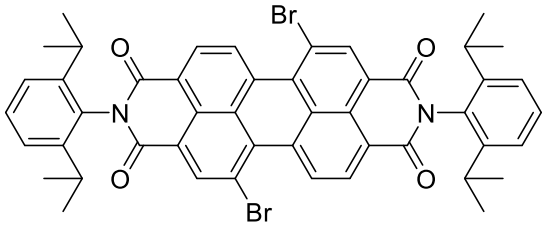

Crude mixture of dibromo PDA (5.90 g, 10.7 mmol, 1 eq) was dissolved in propionic acid (120 mL). 2,6-Diisopropylaniline (4.5 mL, 24 mmol, 2.2 eq) was then added and the reaction mixture was left to stir at 140 °C for four days. On cooling to rt, the resulting mixture was added onto a large beaker of ice, causing the formation of a red precipitate. Any remaining ice was left to melt, and precipitate was collected by vacuum filtration, washed with H_2O until neutral. The red solid was added to CH_2Cl_2 (200 mL), and the resulting suspension was filtered under vacuum, washing with CH_2Cl_2 (3 × 50 mL). The filtrate was concentrated under vacuum and purified by flash column chromatography (SiO_2, 60:40 CH_2Cl_2:n-hexane) to yield dibromo PDI **21** as red solids (2.42 g, 39%).

^{1}H NMR (400 MHz, $CDCl_3$) δ 9.57 (d, *J* = 8.1 Hz, 2H, Ar*H* PDI), 9.03 (s, 2H, Ar*H* PDI), 8.82 (d, *J* = 8.1 Hz, 2H, Ar*H* PDI), 7.53 (t, *J* = 7.8 Hz, 2H, Ar*H* iPr_2-Ar*H*), 7.37 (d, *J* = 7.8 Hz, 4H, iPr_2-Ar*H*), 2.75 (hept, *J* = 7.0 Hz, 4H, C*H* iPr), 1.20 (d, *J* = 7.0 Hz, 24H, $CH(CH_3)_2$ iPr).

MS (ESI): m/z calc. for $C_{48}H_{41}Br_2N_2O_4$ $[M+H]^+$: 869.1418; found 869.1443.

Spectroscopic data is in agreement with literature.[107]

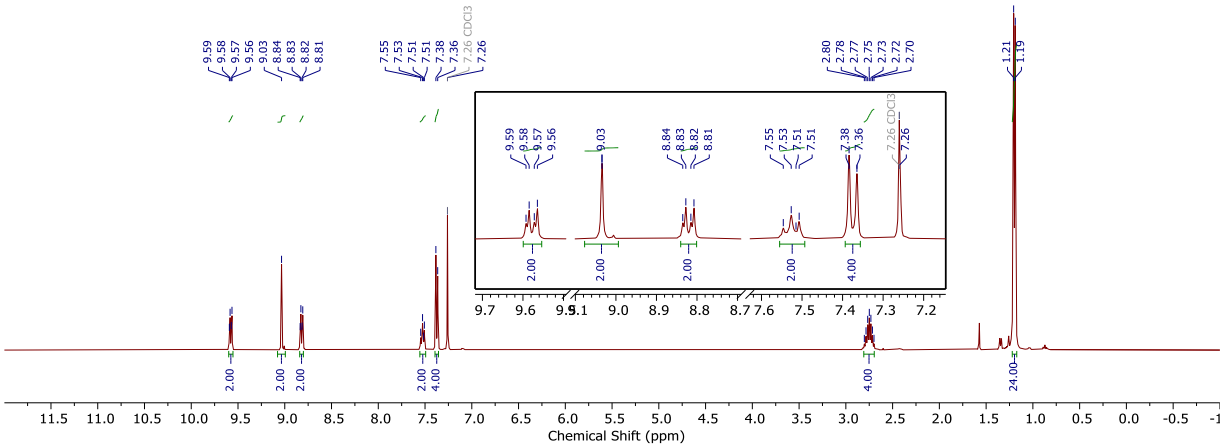

Figure 5.3.1. ^{1}H NMR spectrum of **21** ($CDCl_3$, 298 K, 400 MHz).

N-N-Di(2,6-diisopropylphenyl) 1,7-di((trimethylsilyl)ethynyl)-perylene-3,4,9,10-tetracarboxylic diimide[150] 22

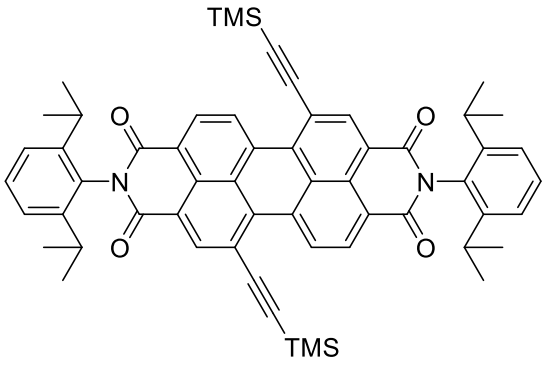

Dibromo PDI **21** (2.40 g, 2.76 mmol, 1 eq) was dissolved in triethylamine (125 mL) and degassed by bubbling a stream of N_2 for 15 min. After which, copper iodide (58.0 mg, 0.303 mmol, 0.11 eq), $PdCl_2(PPh_3)_2$ (116 mg, 0.166 mmol, 0.06 eq), and trimethylsilylacetylene (1.95 mL, 13.8 mmol, 5 eq) was added, and the reacting mixture was left to stir at 60°C for 16 h under an atmosphere of N_2. On cooling to rt, the resulting mixture was quenched with 10M HCl (100 mL). The product was extracted with CH_2Cl_2 (3 × 100 mL), washed with H_2O until neutral, dried with $MgSO_4$ and concentrated *in vacuo*. Purification via flash column chromatography (SiO_2, 60:40 CH_2Cl_2:n-hexane) furnished TMS protected PDI **22** as a red solid (2.28 g, 99%).

^{1}H NMR (400 MHz, $CDCl_3$) δ 10.30 (d, *J* = 8.2 Hz, 2H, Ar*H* PDI), 8.94 (s, 2H, Ar*H* PDI), 8.75 (d, *J* = 8.2 Hz, 2H, Ar*H* PDI), 7.52 (t, *J* = 7.8 Hz, 2H, iPr_2-Ar*H*), 7.37 (d, *J* = 7.8 Hz, 4H, iPr_2-Ar*H*), 2.82 – 2.68 (m, 4H, C*H* iPr), 1.19 (app dd, *J* = 6.8, 1.0 Hz, 24H, CH(CH_3)$_2$ iPr), 0.40 (s, 18H, Si(CH_3)$_3$).

MS (ESI): m/z calc. for $C_{58}H_{59}N_2O_4Si_2$ $[M+H]^+$: 903.4013; found: 903.4020

Spectroscopic data is in agreement with literature.[150]

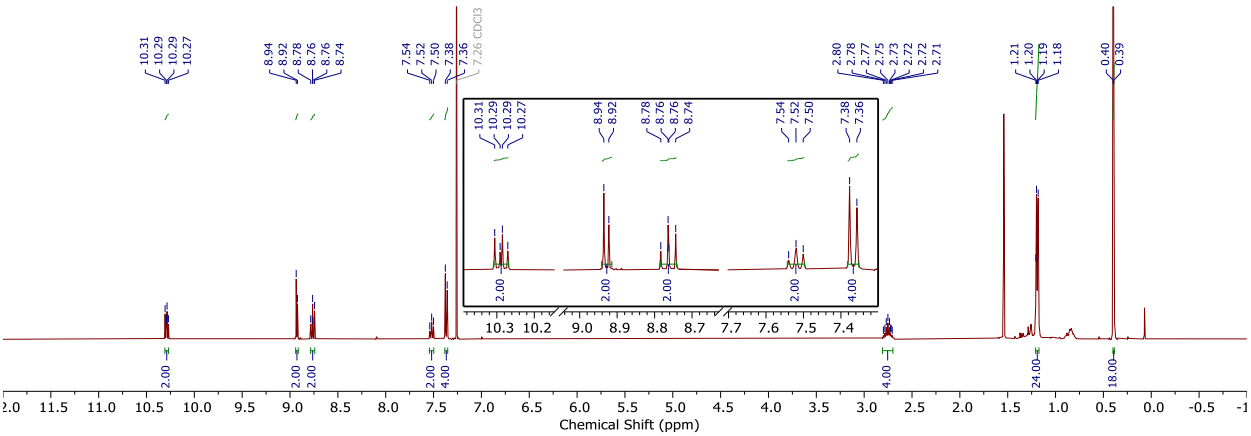

Figure 5.3.2. ^{1}H NMR spectrum of **22** ($CDCl_3$, 298 K, 400 MHz).

N-N-Di(2,6-diisopropylphenyl) 1,7-diethynyl-perylene-3,4,9,10-tetracarboxylic diimide[106] 23

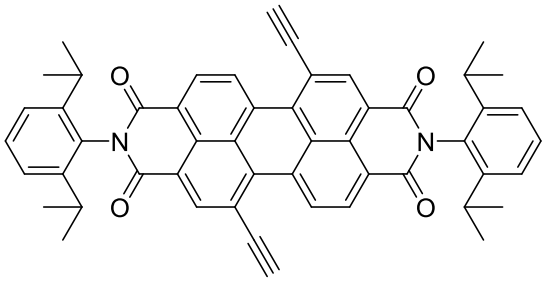

TMS protected PDI **22** (2.28 g, 2.52 mmol, 1 eq) was dissolved in CH_2Cl_2/MeOH (1:1 v/v, 300 mL). Potassium carbonate (1.05 g, 7.57 mmol, 3 eq) was then added and the reaction mixture was stirred at rt for 1 h. After which, the resulting mixture was added to H_2O (200 mL) extracted with CH_2Cl_2, washed with 1 M HCl (200 mL) and H_2O (200 mL). The organic layer was dried with $MgSO_4$ and concentrated *in vacuo* to furnished PDI bisalkyne **23** as a dark red solid (1.93 g, quant.).

^{1}H NMR (400 MHz, $CDCl_3$) δ 10.11 (d, *J* = 8.2 Hz, 2H, Ar*H* PDI), 8.96 (s, 2H, Ar*H* PDI), 8.83 (d, *J* = 8.2 Hz, 2H, Ar*H* PDI), 7.52 (t, *J* = 7.8 Hz, 2H, iPr_2-Ar*H*), 7.37 (d, *J* = 7.8 Hz, 4H, iPr_2-Ar*H*), 3.84 (s, 2H, C≡C*H*), 2.83 – 2.68 (m, 4H, C*H* iPr), 1.19 (d, *J* = 6.8 Hz, 24H, $CH(CH_3)_2$ iPr).

MS (ESI): m/z calc. for $C_{52}H_{43}N_2O_4$ $[M+H]^+$: 759.3223; found 759.3251

Spectroscopic data is in agreement with literature.[106]

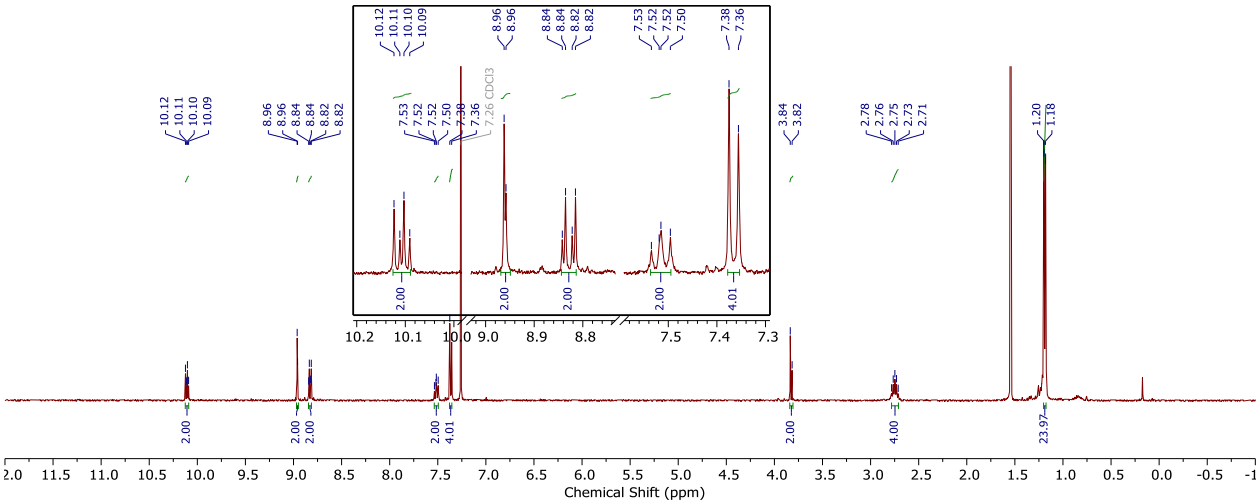

Figure 5.3.3. ^{1}H NMR spectrum of **23** ($CDCl_3$, 298 K, 400 MHz).

2-(allyloxy)ethyl 4-methylbenzenesulfonate 26[151]

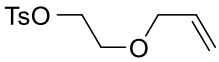

2-(allyloxy)ethan-1-ol (1.00 g, 9.79 mmol, 1 eq) and tosyl chloride (1.87 g, 9.79 mmol, 1 eq) was dissolved in DCM (30 mL). NEt_3 (2.05 mL, 14.7 mmol, 1.5 eq) and a catalytic amount of DMAP was added and the reaction mixture was stirred at rt for 16 h. After which, the resulting mixture was added to H_2O (50 mL), and acidified with 10% citric acid until pH 7 and extracted with CH_2Cl_2, then washed with H_2O (10 mL) and brine (100 mL). The organic layer was dried with $MgSO_4$ and concentrated *in vacuo* to furnished 2-(allyloxy)ethyl 4-methylbenzenesulfonate **26** (1.84 g, 73%).

^{1}H NMR (300 MHz, $CDCl_3$) δ 7.81 (d, *J* = 8.3 Hz, 2H), 7.34 (d, *J* = 7.9 Hz, 2H), 5.82 (ddt, *J* = 17.3, 10.4, 5.6 Hz, 1H), 5.29 – 5.11 (m, 2H), 4.22 – 4.13 (m, 2H), 3.95 (dt, *J* = 5.6, 1.4 Hz, 2H), 3.67 – 3.58 (m, 2H), 2.45 (s, 3H).

MS (ESI): m/z calc. for $C_{12}H_{17}O_4S$ $[M+H]^+$: 257.0769; found 257.0742.

Spectroscopic data is in agreement with literature.[151]

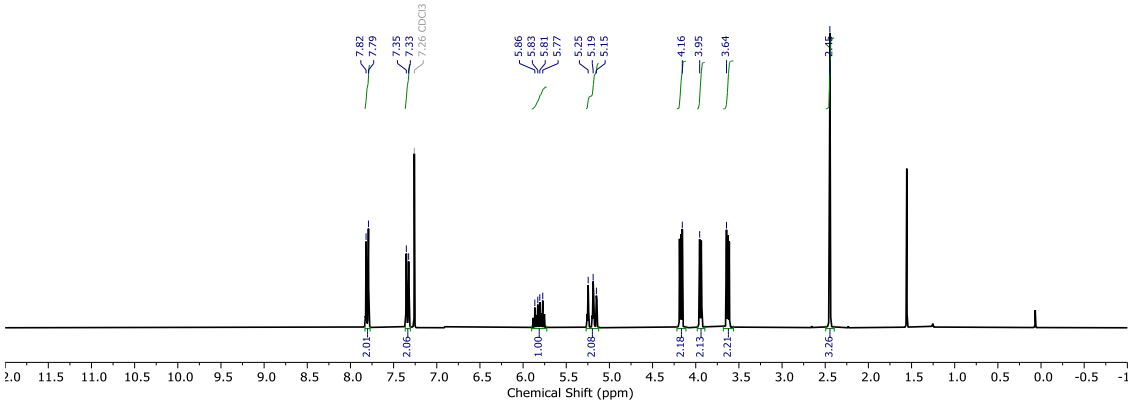

Figure 5.3.4. ^{1}H NMR spectrum of **26** ($CDCl_3$, 298 K, 300 MHz).

3-(2-azidoethoxy)prop-1-ene 27

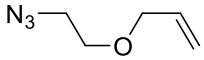

General procedure B was then followed with **26** (1.83 g, 7.16 mmol, 1 eq) and NaN_3 (1.86 g, 28.6 mmol, 4 eq) in DMF (42 mL) to yield azide **27** as a yellow oil that solidified into a cream white solid (0.91 g, quant.).

^{1}H NMR (400 MHz, $CDCl_3$) δ 5.92 (ddt, *J* = 17.2, 10.4, 5.6 Hz, 1H), 5.31 (dq, *J* = 17.3, 1.6 Hz, 1H), 5.25 – 5.17 (m, 1H), 4.04 (dt, *J* = 5.6, 1.4 Hz, 2H), 3.70 – 3.53 (m, 2H), 3.40 (t, *J* = 5.0 Hz, 2H), 1.21 (t, *J* = 7.0 Hz, 1H).

MS (ESI): m/z calc. for $C_5H_{10}N_3O$ $[M+H]^+$: 128.0746; found 128.0776.

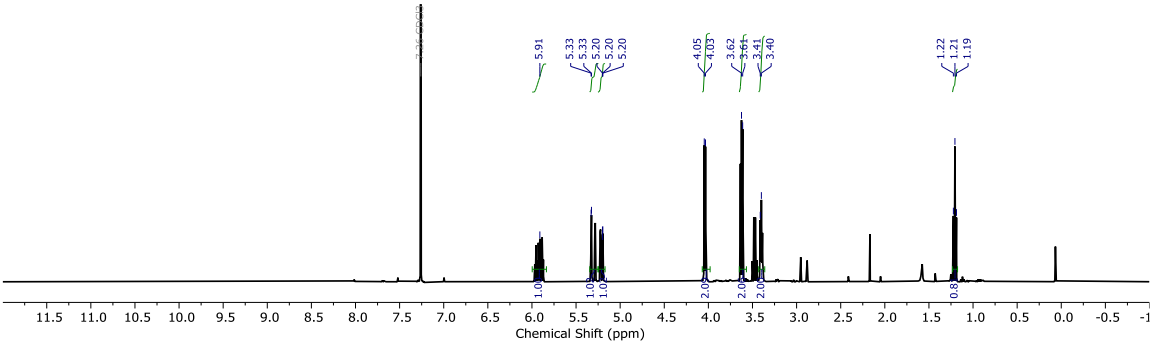

Figure 5.3.5. ^{1}H NMR spectrum of **27** ($CDCl_3$, 298 K, 400 MHz).

PDI Bisalkene 28

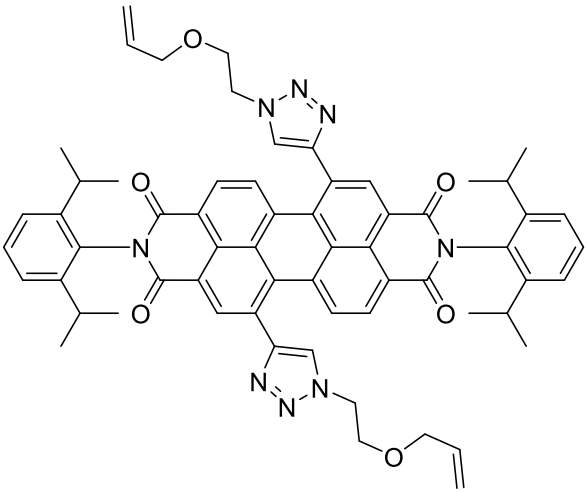

General procedure C was followed with PDI bisalkyne **23** (53.0 mg, 0.698 mmol, 1 eq), azide **27** (47 mg, 3.49 mmol, 5 eq), CH_2Cl_2 (20 mL), TBTA (15 mg, 0.4 eq) and $Cu(MeCN)_4{\cdot}PF_6$ (11 mg, 0.4 eq). The reaction was completed after 16 h and purified by flash column chromatography (SiO_2, 0.4:100 MeOH:CH_2Cl_2) to give **28** as a purple solid (51.0 mg, 72%).

^{1}H NMR (400 MHz, $CDCl_3$) δ 8.83 – 8.66 (m, 2H Ar*H* Ortho PDI), 8.33 (dd, *J* = 9.4, 8.1 Hz, 2H Ar*H* Ortho PDI), 8.03 (d, *J* = 3.9 Hz, 2H Ar*H* Bay PDI), 8.04 – 7.91 (m, 2H, C*H* triazole), 7.55 – 7.43 (m, 2H, iPr_2-Ar*H*), 7.38 – 7.31 (m, 4H, iPr_2-Ar*H*), 5.84 (ddtd, *J* = 17.2, 10.3, 5.7, 3.5 Hz, 2H, C*H* alkene), 5.32 – 5.16 (m, 4H, CH_2 alkene), 4.71 (td, *J* = 5.5, 4.9, 2.2 Hz, 4H, CH_2), 4.04 (ddt, *J* = 5.7, 2.9, 1.4 Hz, 4H, CH_2), 3.91 (dt, *J* = 5.5, 3.7 Hz, 4H, CH_2), 2.82 – 2.66 (m, 4H, CH(CH_3)$_2$ iPr), 1.17 (td, *J* = 7.0, 5.4 Hz, 24H, CH(CH_3)$_2$ iPr).

MS (ESI): m/z calc. for $C_{62}H_{61}N_8O_6$ $[M+H]^+$: 1013.4636; found 1013.4635.

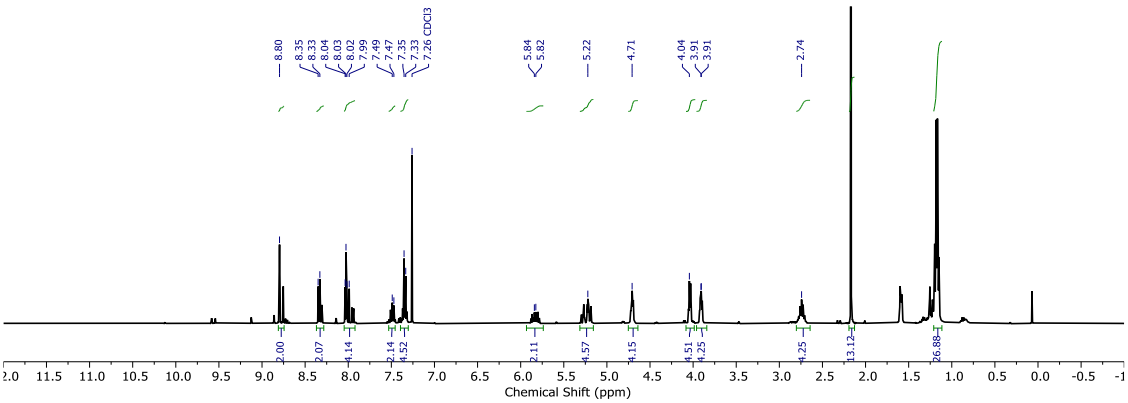

Figure 5.3.6. ^{1}H NMR spectrum of **28** ($CDCl_3$, 298 K, 400 MHz).

1,4-Di(azidomethyl)benzene[152] 31

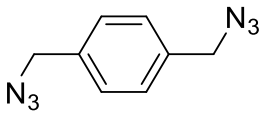

General Procedure B was followed with 1,4-di(chloromethyl)benzene (10.0 g, 57.1 mmol, 1 eq) and NaN_3 (9.20 g, 143 mmol, 2.5 eq) in DMF (20 mL). No precipitation was formed upon quenching with water and thus the reaction mixture was extracted with Et_2O (3 x 100 ML) and washed as mentioned to give a viscous yellow oil which solidified into a white solid upon standing (1.09g, quant).

^{1}H NMR ($CDCl_3$, 400 MHz) δ 7.35 (1H, s, Ar*H*), 4.36 (1H, s, C*H*$_2$).

Spectroscopic data is in agreement with literature.[152]

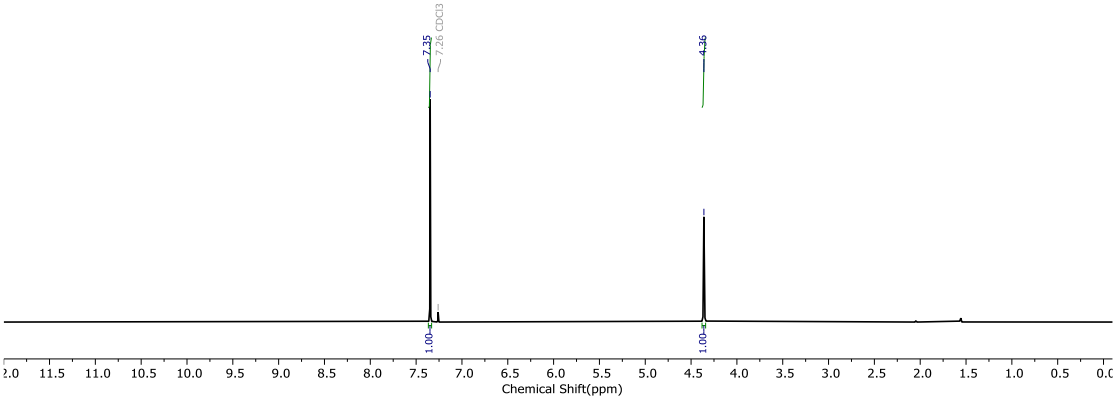

Figure 5.3.7. ^{1}H NMR spectrum of **31** ($CDCl_3$, 298 K, 400 MHz).

(4-(azidomethyl)phenyl)methanamine[153] 32

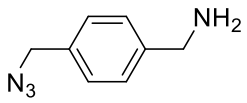

1,4-Di (azidomethyl)benzene **31** (4.00g, 20 mmol, 1 eq) was dissolved in EtOAc (14 mL). 2.5M $HCl_{(aq)}$ (14 mL) was added and the resulting mixture was cooled to 0 °C. PPh_3 (5.53 g, 20 mmol, 1eq) dissolved in EtOAc (14 mL) was added dropwise to the cold mixture, then the mixture was stirred at rt for 16 h. After which, the reaction mixture was poured into a separating funnel along with H_2O (50 mL) and EtOAc (25 mL). The organic layer was discarded and the aqueous layer was washed with CH_2Cl_2 (2 x 50 mL). The aqueous layer was basified to pH 11 with 1 M NaOH and the product was

extracted with $CHCl_3$, which was sequentially dried with $MgSO_4$ and concentrated in vacuo. Purification by flash column chromatography (SiO_2, 1:20 MeOH:CH_2Cl_2) gave a colourless oil **32** which solidified into a white solid upon standing (1.40 g, 65%).

^{1}H NMR ($CDCl_3$, 400 MHz) δ 7.33 (2H, d, *J* = 8.2 Hz, Ar*H*), 7.28 (2H, d, *J* = 8.2 Hz, Ar*H*), 4.31 (2H, s, CH_2), 3.88 (2H, s, CH_2)

MS (ESI): m/z calc. for $C_8H_{11}N_4$ $[M+H]^+$: 163.0905; found 163.0901.

Spectroscopic data is in agreement with literature.[153]

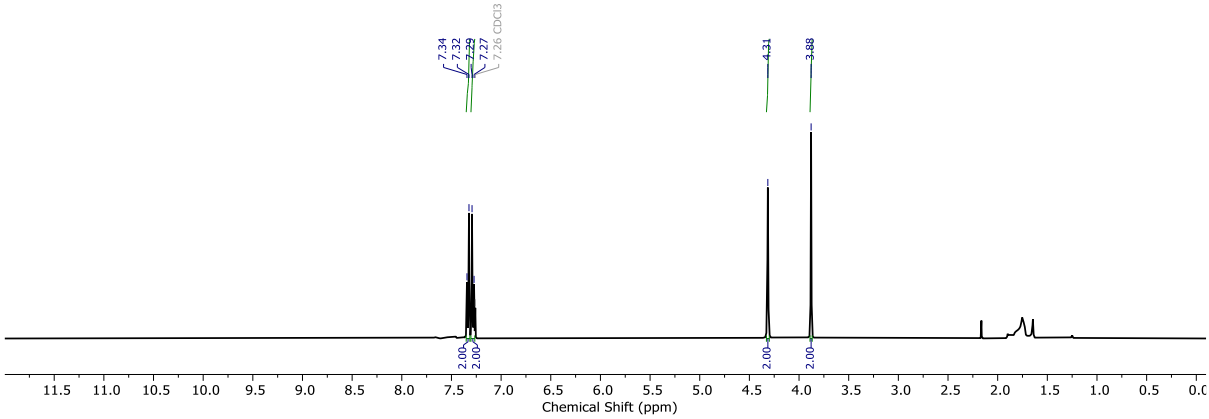

Figure 5.3.8. ^{1}H NMR spectrum of **32** ($CDCl_3$, 298 K, 400 MHz).

tert-butyl (4-(azidomethyl)benzyl)carbamate 33[154]

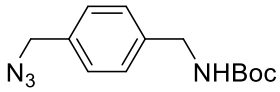

Amine 32 (1.25 g, 7.71 mmol, 1 eq) was dissolved in DCM (27 mL) and stirred with NEt_3 (1.6 mL, 11.6 mmol, 1.5 eq) for 30 mins. After which, $(Boc)_2O$ (1.72 g 7.86 mmol, 1.02 eq) was added and the reaction mixture was stirred for a further 16 h. The reaction mixture was then added to saturated NH_4Cl(aq) and extracted with CH_2Cl_2, washing with H2O and brine. The organic layers were combined and sequentially dried with $MgSO_4$ and concentrated in vacuo. Purification by flash column chromatography (SiO_2, CH_2Cl_2) to give **33** (1.76 g, 87%).

^{1}H NMR (400 MHz, $CDCl_3$) 4.32 (d, J = 5.1 Hz, 4H, C*H*$_2$), 1.46 (s, 9H, C*H*$_3$).

MS (ESI): m/z calc. for $C_{13}H_{19}N_4O_2$ $[M+H]^+$: 263.1430; found 263.1432.

Spectroscopic data is in agreement with literature.[154]

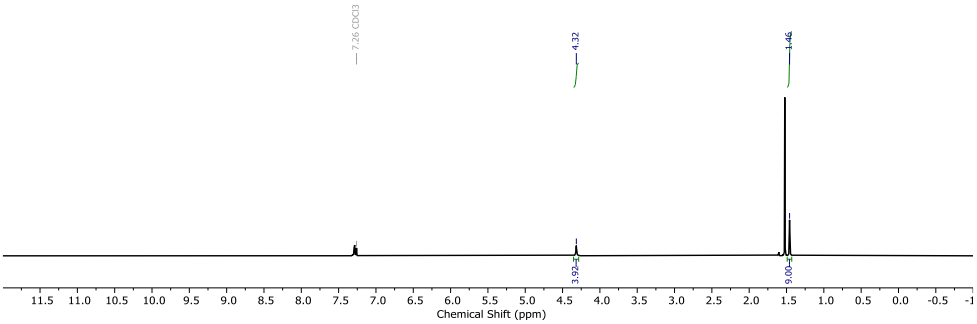

Figure 5.3.9. ^{1}H NMR spectrum of **33** ($CDCl_3$, 298 K, 400 MHz).

PDI Bisamine 34

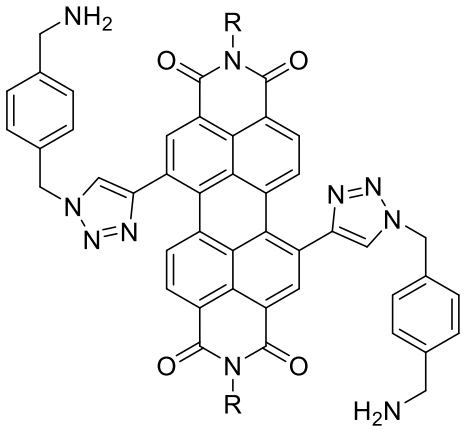

General procedure C was followed with PDI bisalkyne **23** (500 mg, 0.66 mmol, 1 eq), azide **33** (380 mg, 1.45 mmol, 2.2 eq), CH_2Cl_2 (50 mL), TBTA (70 mg, 0.26 mmol, 0.4 eq) and $Cu(MeCN)_4{\cdot}PF_6$ (50 mg, 0.26 mmol, 0.4 eq). The reaction was completed after four days and purified by flash column chromatography (SiO_2, 0.8:100 MeOH:CH_2Cl_2) to a purple solid (410 mg). This product was then dissolved in CH_2Cl_2 (10 mL). TFA (2 mL) was added and the reaction mixture was stirred at rt for 2 h. TFA and CH_2Cl_2 was concentrated in vacuo, and the resulting solid was redissolved in CH_2Cl_2 and added to a saturated solution of $NaHCO_{3(aq)}$ and extracted with CH_2Cl_2 (3 x 100 mL). The organic layers were combined and sequentially dried with $MgSO_4$ and concentrated in vacuo to give PDI bisamine **34** as a purple solid (344 mg, 48%).

^{1}H NMR (400 MHz, $CDCl_3$) δ 8.71 (s, 2H, Ar*H* Ortho PDI), 8.24 (d, *J* = 8.1 Hz, 2H, Ar*H* PDI), 7.93 (d, *J* = 8.1 Hz, 2H, Ar*H* PDI), 7.79 (s, 2H, C*H* triazole), 7.48 (q, *J* = 7.8 Hz, 2H, iPr$_2$-Ar*H*), 7.40 (d, *J* = 8.2 Hz, 4H, iPr$_2$-Ar*H*), 7.36 – 7.32 (m, 8H, Ar*H*), 5.66 (s, 4H, CH_2), 3.89 (s, 4H, CH_2), 2.72 (hept, *J* = 6.9 Hz, 4H, C*H* iPr), 1.17 (t, *J* = 6.6 Hz, 24H, CH(CH_3)$_2$ iPr).

MS (ESI): m/z calc. for $C_{68}H_{63}N_{10}O_4$ $[M+H]^+$: 1083.4956; found 1082.4974.

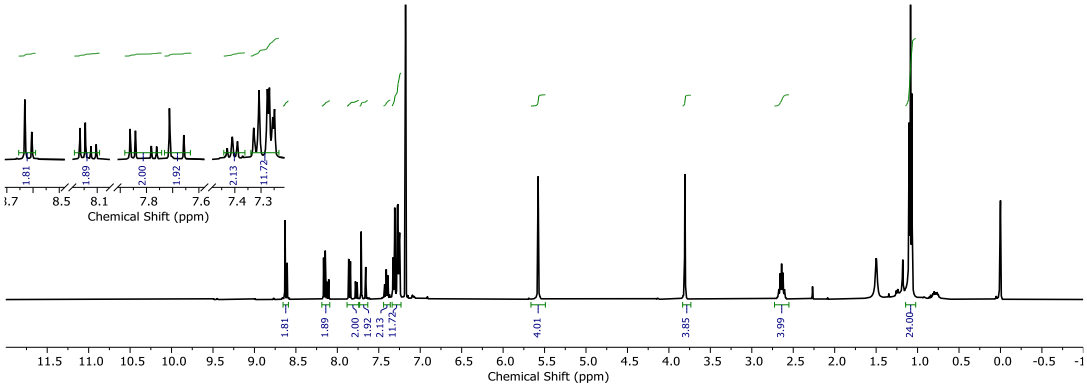

Figure 5.3.10. ^{1}H NMR spectrum of **34** ($CDCl_3$, 298 K, 400 MHz).

Decanedioyl dichloride[155] 36

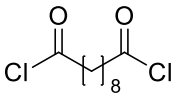

Following a literature procedure,[155] under an inert N_2 atmosphere, decanedioic acid (480 mg, 2.37 mmol, 1 eq) was dissolved in dry DCM (10 mL) and one drop of DMF. Oxalyl chloride (1 mL, 11.7 mmol, 4.9 eq) was then added and the reaction mixture was left to stir at 42 °C for 4 h under an atmosphere of N_2. After which the solvent and excess oxalyl chloride was removed in vacuo, leaving behind decanedioyl dichloride **36** (567 mg, quant.). Due to the instability of the product, **36** was not characterised and was immediately used in the next reaction.

[1,1'-biphenyl]-4,4'-dicarbonyl dichloride 37

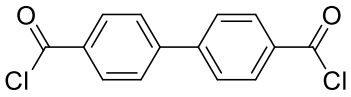

Under an inert N_2 atmosphere, [1,1'-biphenyl]-4,4'-dicarboxylic acid (100 mg, 0.413 mmol, 1 eq) was dissolved in dry DCM (3 mL) and one drop of DMF. Oxalyl chloride (0.17 mL, 1.98 mmol, 4.9 eq) was then added and the reaction mixture was left to stir at 42 °C for 4 h under an atmosphere of N_2. After which the solvent and excess oxalyl chloride was removed in vacuo, leaving behind **37** (115 mg, quant.). Due to the instability of the product, **37** was not characterised and was immediately used in the next reaction.

Tosylated tetraethylene glycol 42

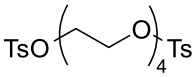

Tetraethylene glycol (5 g, 25.7 mmol, 1eq) and tosyl chloride (9.82 g, 51.5 mmol, 2 eq)was dissolved in DCM (156 mL). Et_3N (10 mL) and a catalytic amount of DMAP was then added, and the resulting mixture was stirred at rt for 3 h. After which, the reaction mixture was added to H_2O and acidified with 10% citric acid to pH 7. The organic layer was extracted with DCM and washed further with H_2O and brine. The organic layers were combined and sequentially dried with $MgSO_4$ and concentrated in vacuo to give Tosylated tetraethylene glycol **42** (9.39g, 36%)

^{1}H NMR (400 MHz, $CDCl_3$) δ 7.72 (ddd, *J* = 8.3, 3.8, 1.8 Hz, 4H, Ar*H* Ts), 7.31 – 7.23 (m, 4H, Ar*H* Ts), 4.13 – 4.05 (m, 4H, CH_2 alkene), 3.68 – 3.52 (m, 8H, CH_2 alkane), 3.56 – 3.43 (m, 10H, CH_2 alkane, C*H* alkene), 2.37 (d, *J* = 2.1 Hz, 6H, CH_3 Ts).

MS (ESI): m/z calc. for $C_{22}H_{31}O_9S_2$ $[M+H]^+$: 503.1331; found 503.1330.

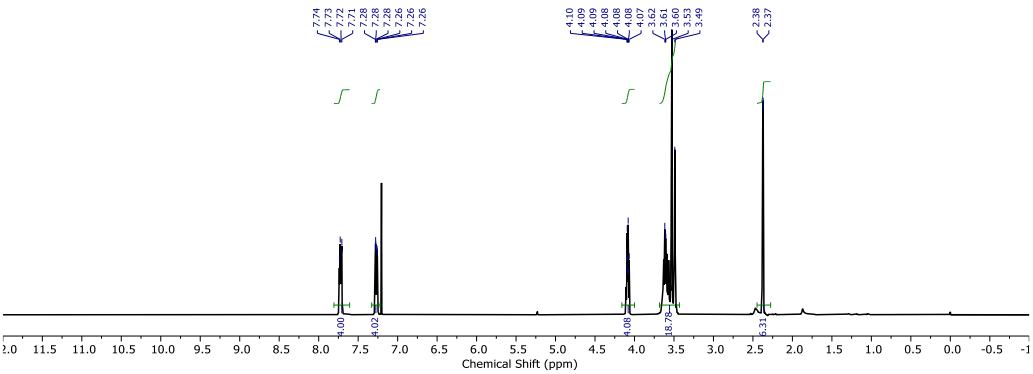

Figure 5.3.11. ^{1}H NMR spectrum of **42** ($CDCl_3$, 298 K, 400 MHz).

Glycol bisazide linker 38

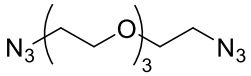

General Procedure B was followed with **42** (8.64 g, 17.2 mmol, 1 eq) and NaN_3 (8.94 g, 138 mmol, 8 eq) in DMF (20 mL). No precipitation was formed upon quenching with water and thus the reaction mixture was extracted with Et_2O (3 x 100 ML) and washed as mentioned to give a viscous yellow oil which solidified into a white solid upon standing (4.20 g, quant.).

^1H NMR (400 MHz, $CDCl_3$) δ 3.74 – 3.62 (m, 12H), 3.39 (t, *J* = 5.0 Hz, 4H).

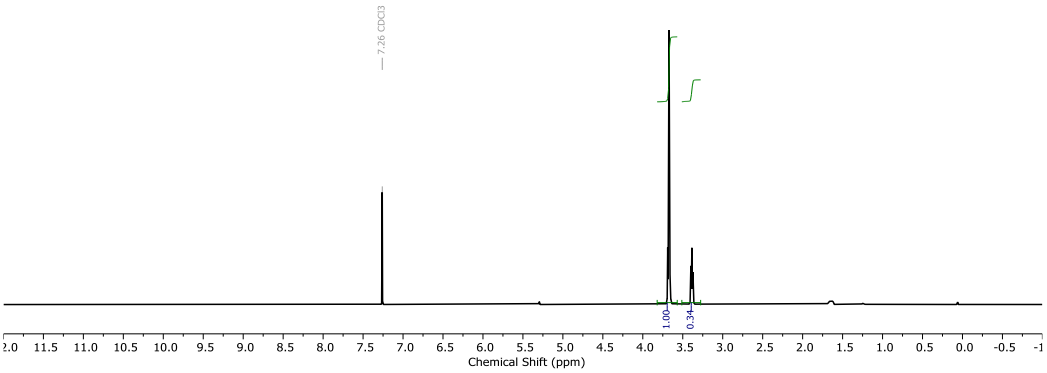

Figure 5.3.12. ^1H NMR spectrum of **38** ($CDCl_3$, 298 K, 400 MHz).

1,5-Di(3-bromopropoxy)naphthalene 43

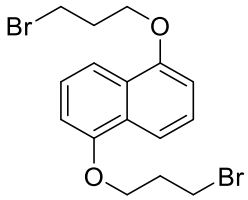

1,3-Dibromopropane (2.5 mL, 25 mmol, 4 eq) was added to a stirring suspension of potassium carbonate (5.18 g, 37.5 mmol, 6 eq) and 1,5-dihydroxynaphthalene (1 g, 6.24 mmol, 1 eq) in acetone (210 mL). The resulting mixture was left to stir at 60 °C for 3 days. Upon cooling to room temperature, the reaction mixture was filtered and the filtrate was concentrated *in vacuo* and then purified by flash column chromatography (SiO_2, 3:7 Hexanes:CH_2Cl_2) to yield an off-white solid **43** (128 mg, 5.1%).

^{1}H NMR ($CDCl_3$, 300 MHz) δ 7.83 (2H, d, *J* = 8.7 Hz, Ar*H*), 7.37 (2H, t, *J* = 8.0 Hz, Ar*H*), 6.87 (2H, d, *J* = 7.6 Hz, Ar*H*), 4.28 (4H, t, *J* = 5.7 Hz, CH_2), 3.71 (4H, t, *J* = 6.5 Hz, CH_2), 2.47 (4H, p, *J* = 6.1 Hz, CH_2).

MS (ESI): m/z calc. for $C_{16}H_{19}Br_2O_2$ $[M+H]^+$: 402.9653; found 402.9693.

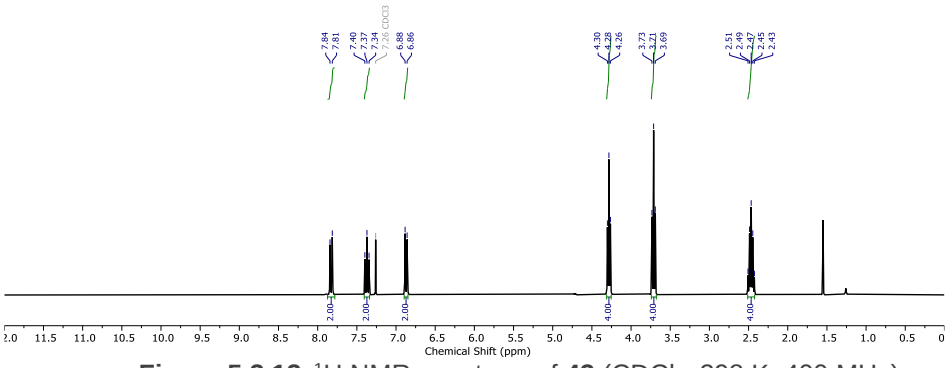

Figure 5.3.13. ^{1}H NMR spectrum of **43** ($CDCl_3$, 298 K, 400 MHz).

1,5-Di(3-azidopropoxy)naphthalene 39

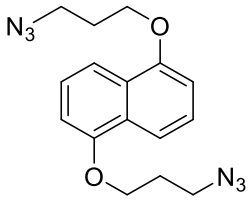

General Procedure A was followed with dibromo **43** (120 mg, 0.298 mmol, 1 eq) and NaN_3 (48.5 mg, 0.746 mmol, 2.5 eq) in DMF (10 mL) to yield a white solid **39** (98 mg, quant.).

^{1}H NMR ($CDCl_3$, 400 MHz) δ 7.83 (2H, dd, *J* = 8.2, 0.8 Hz, Ar*H*), 7.37 (2H, dd, *J* = 8.2, 7.7 Hz, Ar*H*), 6.85 (2H, dd, *J* = 7.7, 0.8 Hz, Ar*H*), 4.23 (4H, t, *J* = 5.9 Hz, CH_2), 3.63 (4H, t, *J* = 6.7 Hz, CH_2), 2.26 – 2.14 (4H, m, CH_2)

MS (ESI): m/z calc. for $C_{16}H_{19}N_6O_2$ $[M+H]^+$: 327.1491; found 327.1489.

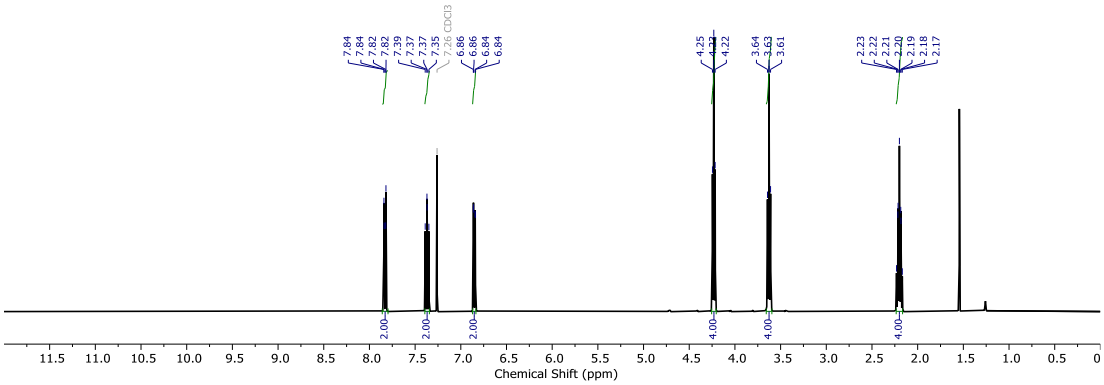

Figure 5.3.14. ^{1}H NMR spectrum of **39** ($CDCl_3$, 298 K, 400 MHz).

1,4-Di(4-bromobutoxy)benzene[156] 44

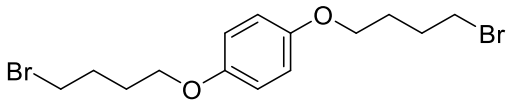

1,4-Dibromobutane (0.87 mL, 7.32 mmol, 3.5 eq) was added to a stirring suspension of potassium carbonate (1.5 g, 10.93 mmol, 5.3 eq) and hydroquinone (227 mg, 2.06 mmol, 1 eq) in acetone (60 mL). The resulting mixture was left to stir at 60 °C for three days. Upon cooling to room temperature, the reaction mixture was filtered, and the filtrate was concentrated *in vacuo* to an orange oil. The oil was diluted in n-hexane (50 mL) and filtered again, washing with more n-hexane (2 × 10 mL). The filtrate was set aside overnight in the fridge to crystallise. The off-white crystals were collected, and the mother liquor was concentrated *in vacuo*, redissolved in a minimal amount of hot ethanol, and set aside overnight to yield a second crop of off-white crystals. These crystals were combined with the first batch to yield **44** (199 mg, 25%).

^{1}H NMR (400 MHz, $CDCl_3$) δ 6.81 (s, Ar*H*, 4H), 3.94 (t, *J* = 6.1 Hz, 4H, CH_2), 3.49 (t, *J* = 6.6 Hz, 4H, CH_2), 2.10 – 1.99 (m, 4H, CH_2), 1.97 – 1.85 (m, CH_2, 4H). Spectroscopic data is in agreement with literature.[156]

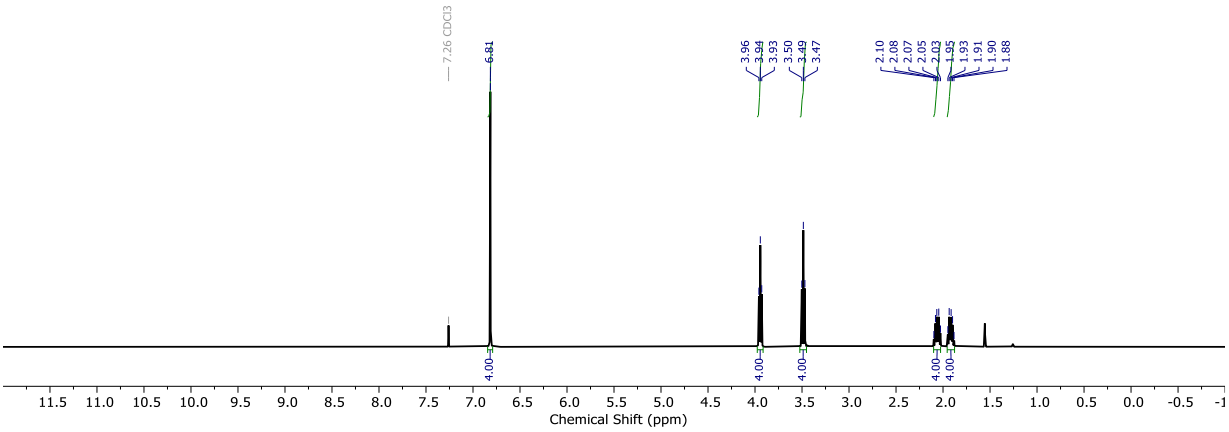

Figure 5.3.15. ^{1}H NMR spectrum of **44** ($CDCl_3$, 298 K, 400 MHz).

1,4-Di(4-azidobutoxy)benzene[157] 40

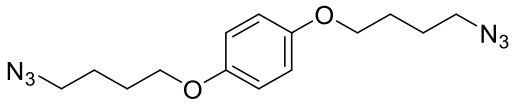

General procedure **B** was followed with dibromo **44** (199 mg, 0.524 mmol, 1 eq) and NaN_3 (85.1 mg, 1.31 mmol, 2.5 eq) in DMF (10 mL) to yield azide **40** an off-white solid (160 mg, quant.)

^{1}H NMR (400 MHz, $CDCl_3$) δ 6.83 (s, 4H, Ar*H*), 3.94 (t, *J* = 5.8 Hz, 4H, CH_2), 3.36 (t, *J* = 6.5 Hz, 4H, CH_2), 1.95 – 1.71 (m, CH_2, 8H).

MS (ASAP): m/z calc. for $C_{14}H_{21}N_6O_2$ $[M]^+$: 304.1648; found 304.1650.

Spectroscopic data is in agreement with literature.[157]

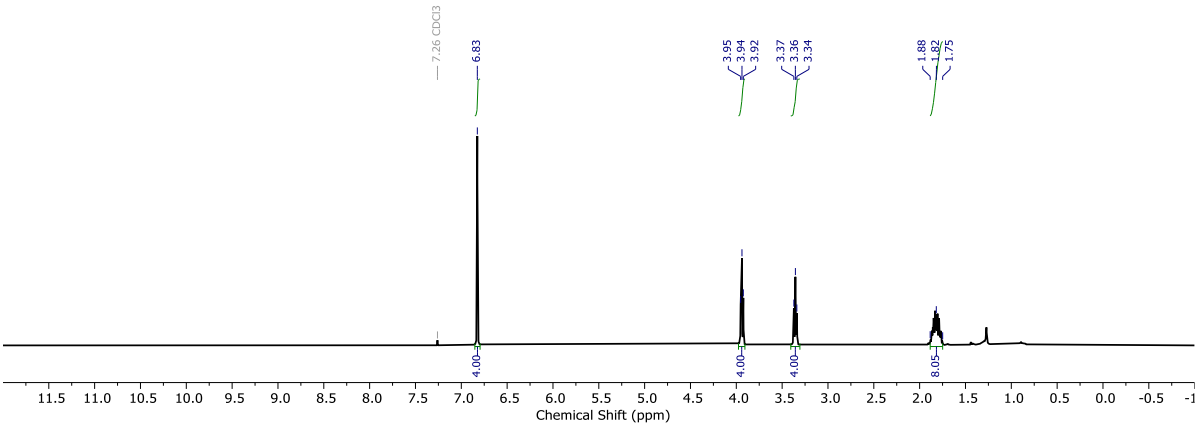

Figure 5.3.16. ^{1}H NMR spectrum of **40** ($CDCl_3$, 298 K, 400 MHz).

1,4-Di(6-azidohexoxy)benzene 41

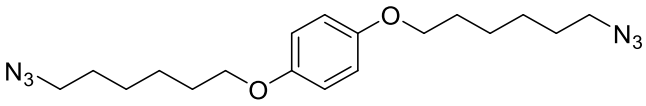

General procedure **A** was followed with hydroquinone (1.00 g, 9.08 mmol, 1 eq), 1,6-dibromohexane (14 mL, 90.8 mmol, 10 eq), potassium carbonate (7.53 g, 54.5 mmol, 6 eq) in acetone (20 mL), to yield 1,4-di(6-bromohexoxy)benzene **45** as a white solid (3.13 g, 79%).

General procedure **B** was then followed with dibromo **45** (3.12 g, 7.15 mmol, 1 eq) and NaN_3 (1.16 g, 17.9 mmol, 2.5 eq) in DMF (50 mL) to yield azide **41** as a yellow oil that solidified into a cream white solid (2.55 g, 99%).

^{1}H NMR (400 MHz, $CDCl_3$) δ = 6.82 (s, 4H, Ar*H*), 3.91 (t, *J* = 6.4 Hz, 4H, CH_2), 3.28 (t, *J* = 6.9 Hz, 4H, CH_2), 1.77 (dq, *J* = 7.7, 6.3 Hz, 4H, CH_2), 1.63 (p, *J* = 7.0 Hz, 4H, CH_2), 1.55 – 1.38 (m, 8H, CH_2).

MS (ASAP): m/z calc. for $C_{18}H_{28}N_6O_2$ $[M]^+$: 360.2274; found 360.2284

Spectroscopic data is in agreement with literature.[157]

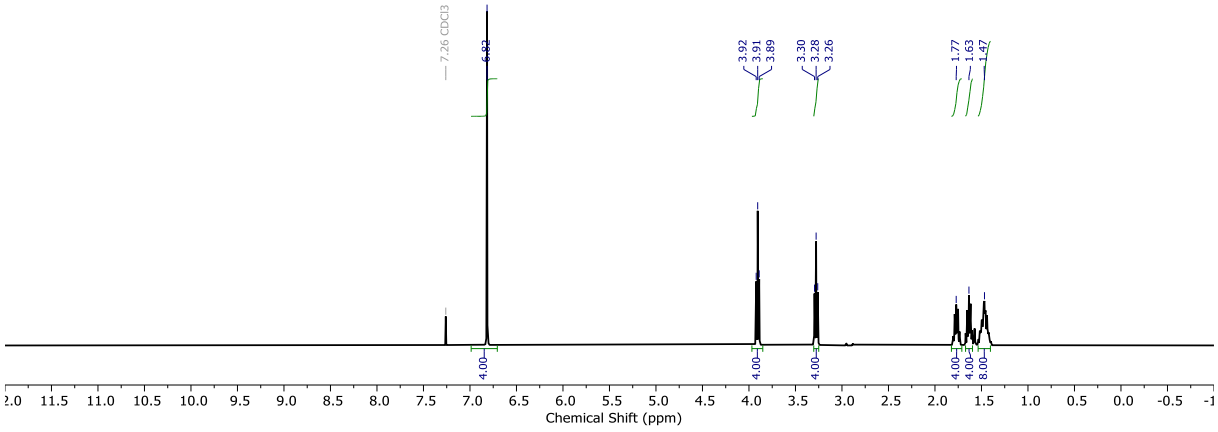

Figure 5.3.17. ^{1}H NMR spectrum of **41** ($CDCl_3$, 298 K, 400 MHz).

1,5-Dipropoxynapthalene PDI macrocycle 46

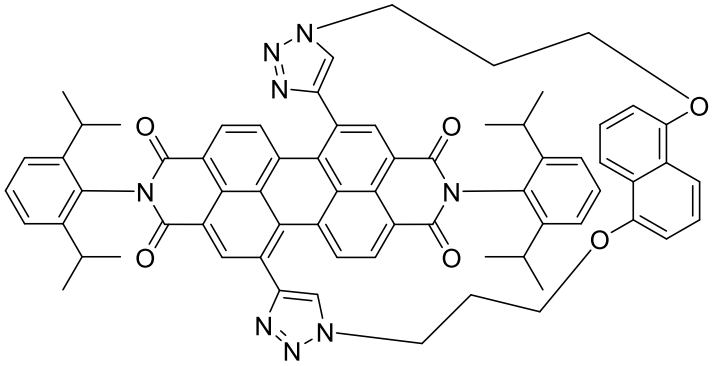

General Procedure C was followed with PDI bisalkyne **23** (102 mg, 0.134 mmol, 1 eq), 1,5-di(3-azidopropoxy)naphthalene **39** (44 mg, 0.134 mmol, 1 eq), CH_2Cl_2 (220 mL), TBTA (30 mg, 0.053, 0.4 eq) and $Cu(MeCN)_4$-PF_6 (20mg, 0.053, 0.4 eq). Reaction was completed after 4 days and purified by flash column chromatography (SiO2, 0.4:100 MeOH:CH_2Cl_2) to give macrocycle **46** a purple solid (35 mg, 24%).

^{1}H NMR ($CDCl_3$, 400 MHz) δ 9.05 (2H, s, Ar*H* Ortho PDI), 8.35 (2H, d, *J* = 8.1 Hz, Ar*H* Ortho PDI), 8.17 (2H, d, *J* = 8.1 Hz, Ar*H* Bay PDI), 7.50 (2H, t, *J* = 7.8 Hz, iPr_2-Ar*H*), 7.39 – 7.31 (4H, m, iPr_2-Ar*H*), 7.21 (2H, d, *J* = 8.4, Ar*H* para-naphthalene), 7.00 (2H, s, C*H* triazole), 6.69 (2H, dd, *J* = 8.4, 7.7 Hz, ArH meta-naphthalene), 6.22 (2H, d, *J* = 7.7 Hz, ortho-naphthalene), 4.95 (2H, ddd, *J* = 14.0, 8.1, 3.0 Hz, $OCH_2CH_2CH_AH_BN$), 4.61 (2H, ddd, *J* = 14.0, 7.1, 3.5 Hz, $OCH_2CH_2CH_AH_BN$), 4.06 (2H, br s, $OCH_AH_BCH_2CH_2N$), 3.61 (2H, t, *J* = 9.8 Hz, $OCH_AH_BCH_2CH_2N$), 2.83 (2H, hept, *J* = 6.9 Hz, C*H* iPr), 2.73 (2H, hept, *J* = 6.9 Hz, C*H* iPr), 2.56 (2H, app tdd, *J* = 10.1, 6.9, 3.4 Hz, $OCH_2CH_AH_BCH_2N$), 2.47 – 2.36 (2H, m, $OCH_2CH_AH_BCH_2N$), 1.22 (6H, d, *J* = 7.0 Hz, $CH(CH_3)_2$ iPr), 1.19 (6H, d, *J* = 7.0 Hz, $CH(CH_3)_2$ iPr), 1.17 (6H, d, *J* = 5.9 Hz, $CH(CH_3)_2$ iPr), 1.15 (6H, d, *J* = 5.9 Hz, $CH(CH_3)_2$ iPr).

^{13}C NMR ($CDCl_3$, 101 MHz) δ 163.5, 163.3, 153.3, 147.5, 145.9, 145.4, 135.1, 134.4, 133.5, 130.5, 130.3, 129.9, 129.7, 129.2, 129.0, 128.6, 125.8, 125.2, 124.9, 124.5, 124.1, 122.9, 122.4, 113.8, 104.6, 65.3, 48.8, 29.6, 29.3, 29.1, 24.2, 24.1, 24.0

MS (MALDI): m/z calc. for $C_{68}H_{61}N_8O_6$ $[M+H]^+$: 1085.471; found 1085.695

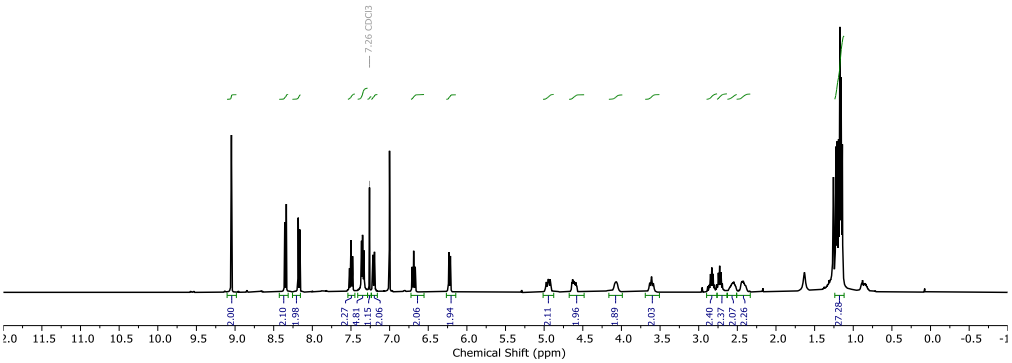

Figure 5.3.18. ^{1}H NMR spectrum of **41** ($CDCl_3$, 298 K, 400 MHz).

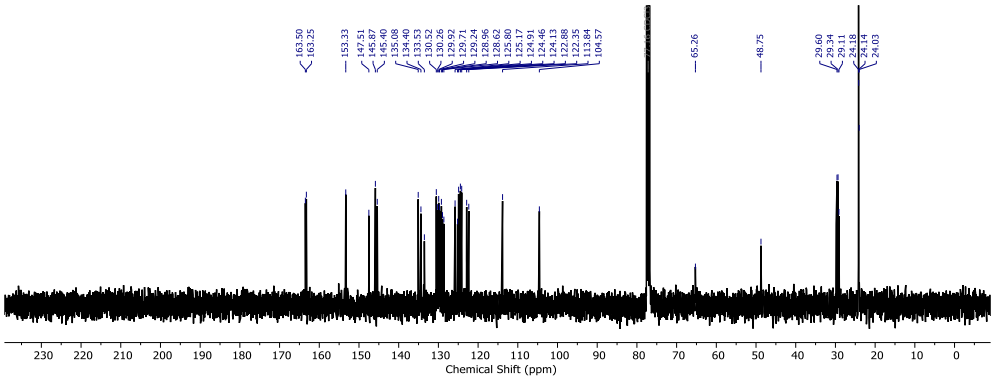

Figure 5.3.19. ^{13}C NMR spectrum of **47** ($CDCl_3$, 298 K, 101 MHz).

1,4-Di(4-butoxy)benzene PDI macrocycle 47

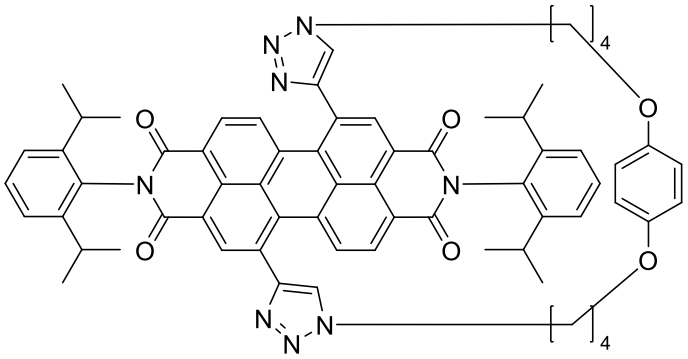

The general procedure C above was followed with PDI bisalkyne **23** (120 mg, 0.158 mmol, 1 eq), 1,4-di(4-azidobutoxy)benzene **40** (48.1 mg, 0.158 mmol, 1 eq), CH_2Cl_2 (260 mL), TBTA (33.5 mg, 0.0633 mmol, 0.4 eq) and $Cu(MeCN)_4 \cdot PF_6$ (23.6 mg, 0.0633 mmol, 0.4 eq). The reaction was completed after four days and purified by flash column chromatography (SiO_2, 0.4:100 MeOH:CH_2Cl_2) to give macrocycle **47** as a purple solid (27 mg, 24%).

^{1}H NMR ($CDCl_3$, 400 MHz) δ 8.84 (2H, s, Ar*H* Ortho PDI), 8.38 (2H, d, *J* = 8.0 Hz, Ar*H* Ortho PDI), 8.27 (2H, d, *J* = 8.0 Hz, Ar*H* Bay PDI), 8.01 (2H, s, C*H* triazole), 7.50 (2H, t, *J* = 7.7 Hz, iPr$_2$-Ar*H*), 7.35 (4H, app dd, *J* = 7.7, iPr$_2$-Ar*H*), 6.11 (4H, s, Ar*H* oxybenzene), 4.63 (2H, ddd, *J* = 14.0, 8.5, 3.7 Hz, O$(CH_2)_3$CH_AH$_B$N), 4.54 (2H, ddd, *J* = 14.0, 6.8, 3.7 Hz, O$(CH_2)_3$CH$_A$*H*$_B$N), 3.36 – 3.23 (4H, m, OC$H_2(CH_2)_3$N), 2.85 (2H, hept, *J* = 6.9 Hz, C*H* iPr), 2.71 (2H, hept, *J* = 6.7 Hz, C*H* iPr), 2.23 – 2.02 (4H, m, OCH$_2$C$H_2(CH_2)_2$N), 1.77 – 1.55 (4H, m, O$(CH_2)_2$CH_2CH$_2$N), 1.24 (1H, d, *J* = 6.9 Hz, CH(C$H_3)_2$ iPr), 1.22 (2H, d, *J* = 6.9 Hz, CH(C$H_3)_2$ iPr), 1.16 (3H, d, *J* = 6.7 Hz, CH(C$H_3)_2$ iPr), 1.24 (1H, d, *J* = 6.7 Hz, CH(C$H_3)_2$ iPr)

^{13}C NMR (101 MHz, $CDCl_3$) δ 163.5, 163.3, 152.3, 147.5, 147.0, 145.8, 145.6, 135.0, 134.6, 133.4, 130.5, 130.1, 129.9, 129.7, 129.5, 129.4, 128.5, 124.4, 124.1, 123.5, 122.8, 122.4, 114.7, 77.5, 77.2, 76.8, 66.3, 50.3, 29.8, 29.5, 29.3, 25.8, 24.2, 24.2, 24.1, 24.0.

MS (ESI): m/z calc. for $C_{66}H_{63}N_8O_6$ $[M+H]^+$: 1063.4871; found 1063.4869

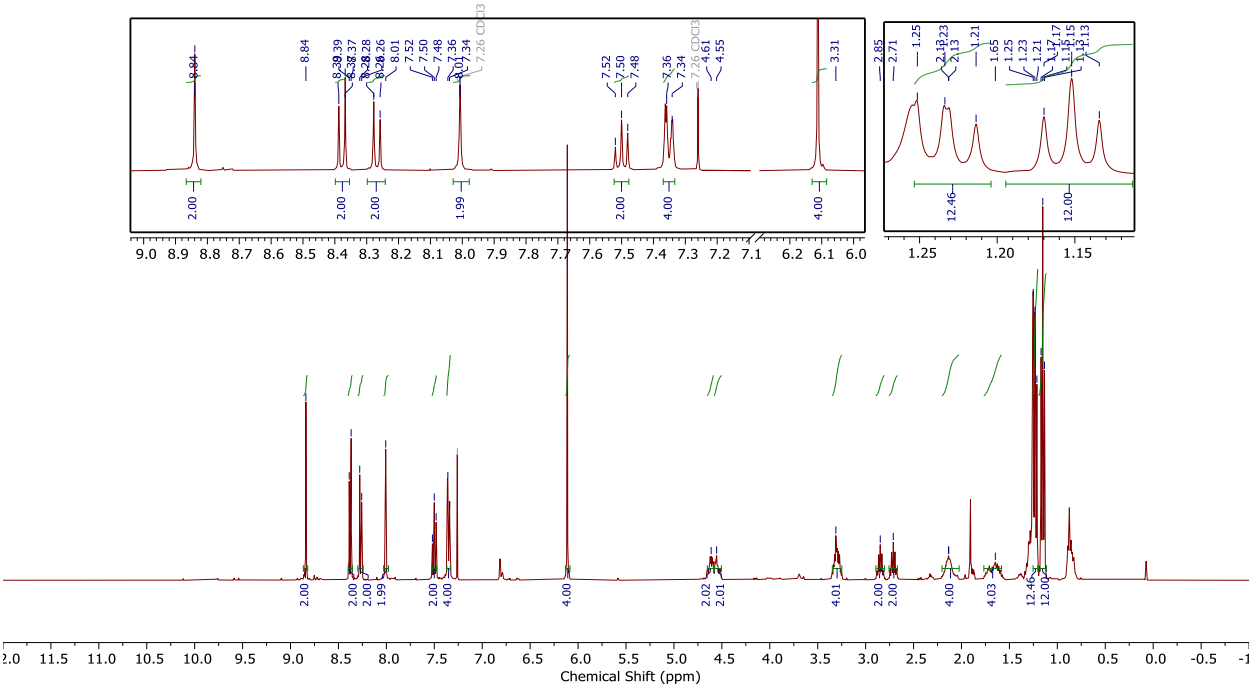

Figure 5.3.20. ^{1}H NMR spectrum of **47** ($CDCl_3$, 298 K, 400 MHz).

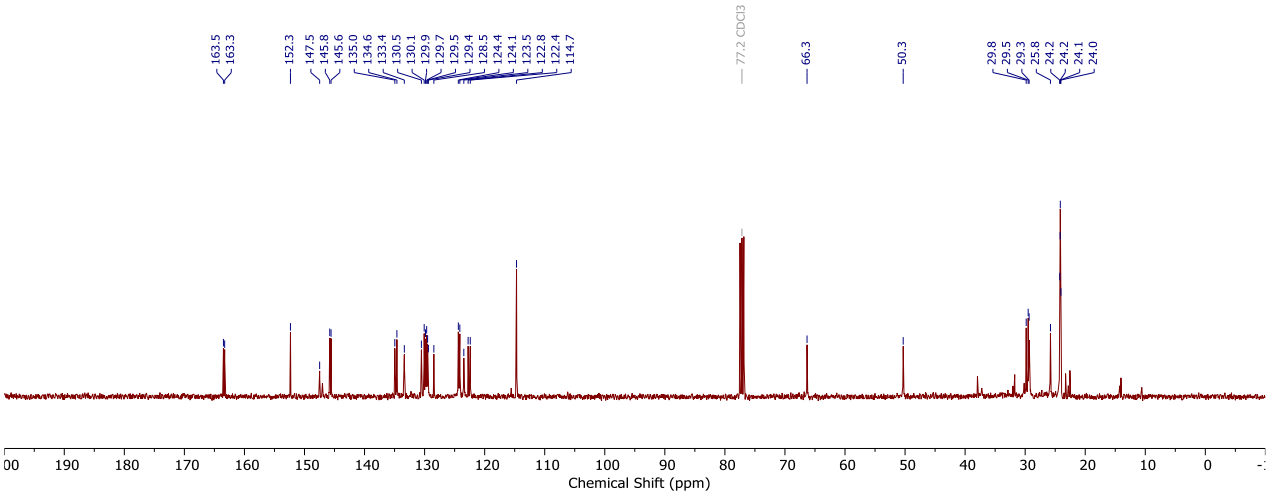

Figure 5.3.21. ^{13}C NMR spectrum of **47** ($CDCl_3$, 298 K, 101 MHz).

1,4-Di(6-hexoxy)benzene PDI macrocycle 48

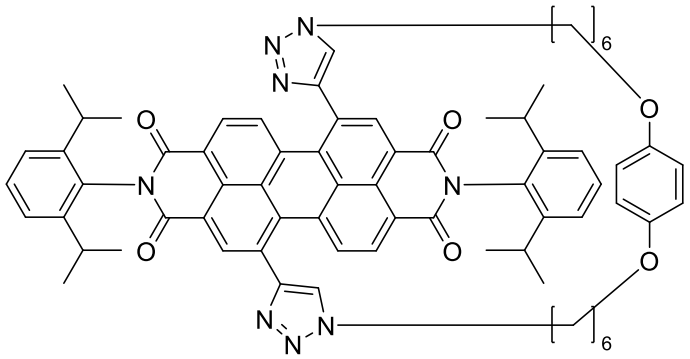

General procedure C was followed with PDI bisalkyne **23** (150 mg, 0.198 mmol, 1 eq), 1,4-di(6-azidohexoxy)benzene **41** (75.0 mg, 0.198 mmol, 1 eq), CH_2Cl_2 (600 mL), TBTA (45 mg, 79.1 µmol, 0.4 eq) and $Cu(MeCN)_4{\cdot}PF_6$ (30 mg, 79.1 µmol, 0.4 eq). The reaction was completed after four days and purified by flash column chromatography (SiO_2, 0.4:100 MeOH:CH_2Cl_2) to give macrocycle **48** a purple solid (33.7 mg, 23%).

^{1}H NMR (400 MHz, $CDCl_3$) δ 8.74 (s, 2H, Ar*H* Ortho PDI), 8.37 (d, *J* = 8.1 Hz, 2H, Ar*H* Ortho PDI), 8.15 (d, *J* = 8.1 Hz, 2H, Ar*H* Bay PDI), 7.65 (s, 2H, C*H* triazole), 7.49 (t, *J* = 7.8 Hz, 2H, iPr$_2$-Ar*H*), 7.37 – 7.31 (m, 4H, iPr$_2$-Ar*H*), 6.19 (s, 4H, Ar*H* oxybenzene), 4.64 (ddd, *J* = 13.9, 7.5, 3.9 Hz, 2H, NCH_AH_B), 4.48 (ddd, *J* = 13.9, 8.1, 3.9 Hz, 2H, NCH_AH_B), 3.60 – 3.37 (m, 4H, OCH_2), 2.79 (p, *J* = 6.8 Hz, 2H, C*H* iPr), 2.68 (d, *J* = 6.9 Hz, 2H, C*H* iPr), 2.22 – 2.04 (m, 2H NCH$_2$CH_AH_B), 2.04 – 1.87 (m, 2H, NCH$_2$CH$_A$$H_B$), 1.72 – 1.25 (m, 12H, CH_2), 1.21 (d, *J* = 6.8 Hz, 6H, CH(CH_3)$_2$ iPr), 1.18 (d, *J* = 6.8 Hz, 6H, CH(CH_3)$_2$ iPr), 1.15 (d, *J* = 6.9 Hz, 6H, CH(CH_3)$_2$ iPr), 1.13 (d, *J* = 6.9 Hz, 6H, CH(CH_3)$_2$ iPr).

^{13}C NMR (101 MHz, $CDCl_3$) δ 163.5, 163.2, 152.6, 147.5, 145.8, 145.7, 135.8, 135.1, 133.8, 130.5, 129.9, 129.7, 129.5, 129.3, 129.0, 124.4, 124.2, 122.7, 122.7, 122.2, 114.7, 67.4, 49.9, 29.3, 29.3, 29.1, 28.2, 24.6, 24.4, 24.3, 24.3, 24.2, 24.1.

MS (ESI): m/z calc. for $C_{70}H_{71}N_8O_6$ $[M+H]^+$: 1119.5497; found 1119.5502

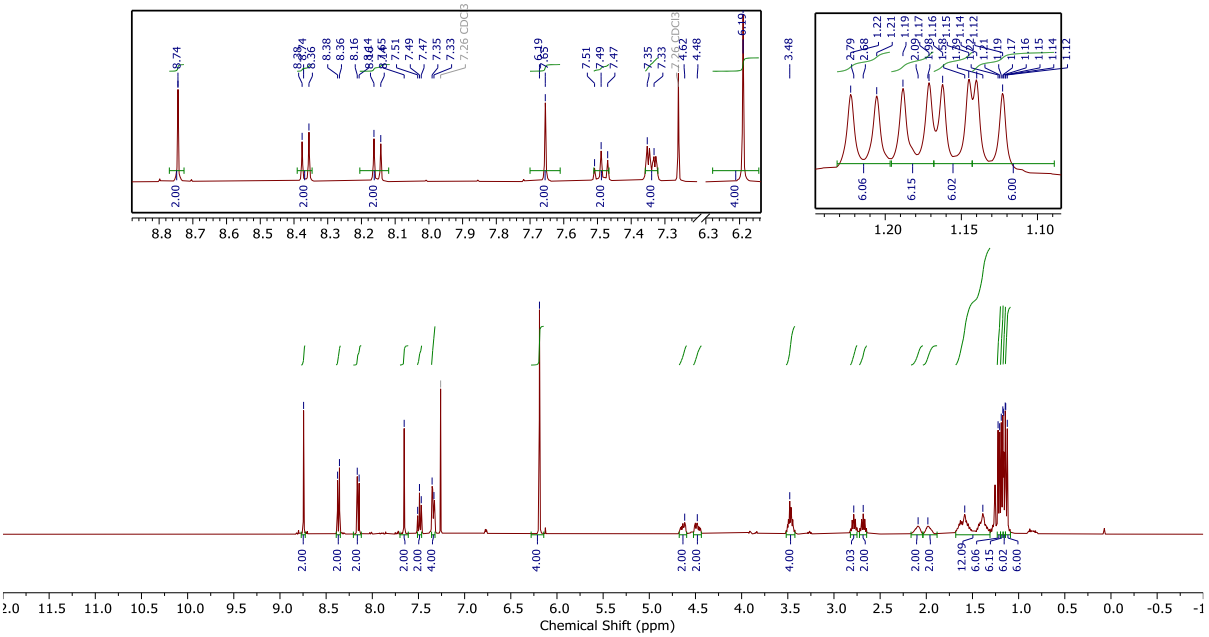

Figure 5.3.22. ^{1}H NMR spectrum of **48** ($CDCl_3$, 298 K, 400 MHz).

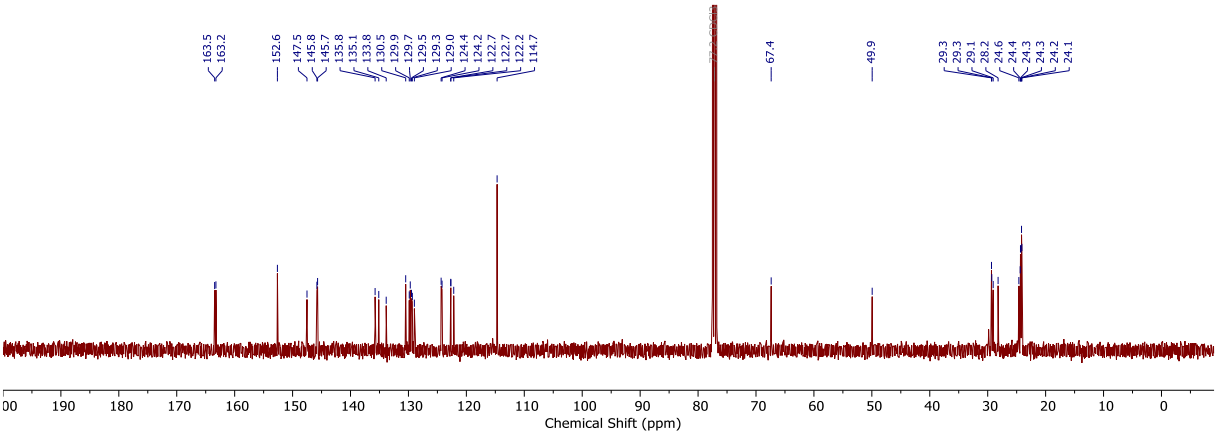

Figure 5.3.23. ^{13}C NMR spectrum of **48** ($CDCl_3$, 298 K, 101 MHz).

1,5-Dipropoxynapthalene PDI acyclic variant 49

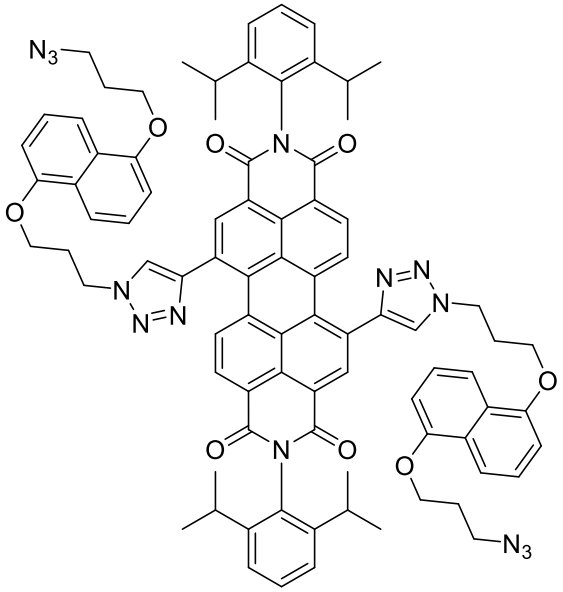

General Procedure C was followed with PDI bisalkyne **23** (42 mg, 55.3 μmol, 1 eq), 1,5-di(3-azidopropoxy)naphthalene **39** (127 mg, 0.387 mmol, 7 eq), CH_2Cl_2 (3 mL), TBTA (12 mg, 22 μmol, 0.4 eq) and $Cu(MeCN)_4$-PF_6 (8.3mg, 22 μmol, 0.4 eq). Reaction was completed after 24 h and purified by flash column chromatography (SiO2, 0.4:100 MeOH:CH_2Cl_2) to give **49** as a purple solid (31.1 mg, 40%).

^{1}H NMR ($CDCl_3$, 400 MHz) δ 8.69 (2H, s, Ar*H* PDI), 8.32 (2H, d, *J* = 8.1 Hz, Ar*H* PDI), 7.96 (2H, d, *J* = 8.1 Hz, Ar*H* PDI), 7.90 – 7.77 (6H, m, C*H* triazole, naphthalene), 7.50 (2H, t, *J* = 7.8 Hz, iPr_2-Ar*H*), 7.40 – 7.30 (8H, m, iPr_2-Ar*H*, naphthalene), 6.90 – 6.78 (4H, m, naphthalene), 4.87 (4H, t, *J* = 6.7 Hz, CH_2), 4.25 (4H, t, *J* = 5.5 Hz, CH_2), 4.19 (4H, t, *J* = 5.9 Hz, CH_2), 3.59 (4H, td, *J* = 6.7, 1.8 Hz, CH_2), 2.81 – 2.61 (8H, m, CH_2, C*H* iPr), 2.16 (4H, app pd, *J* = 6.4, 2.0 Hz, CH_2), 1.17 (24H, d, *J* = 6.9 Hz, CH(CH_3)$_2$ iPr).

^{13}C NMR (101 MHz, $CDCl_3$) δ 163.6, 163.4, 163.4, 163.3, 154.4, 153.9, 148.1, 147.9, 145.8, 136.2, 135.7, 135.3, 134.9, 134.2, 134.1, 130.5, 130.3, 130.1, 129.9, 129.5, 129.4, 129.3, 129.1, 126.8, 126.6, 125.6, 125.4, 124.3, 122.9, 122.8, 122.8, 122.6, 122.5, 114.9, 114.1, 105.7, 77.5, 77.2, 76.8, 64.9, 64.3, 64.2, 48.6, 48.0, 30.2, 29.8, 29.3, 29.3, 29.0, 24.2, 24.1.

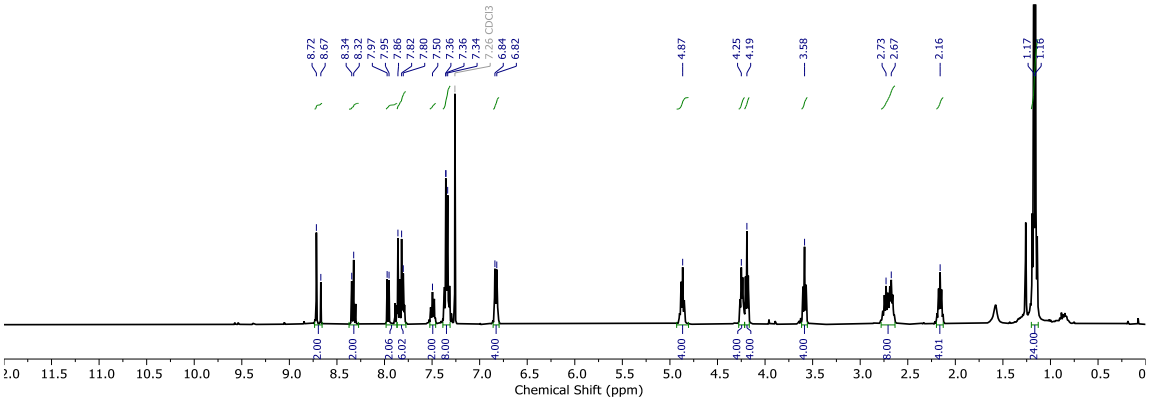

Figure 5.3.24. ^{1}H NMR spectrum of **48** ($CDCl_3$, 298 K, 400 MHz).

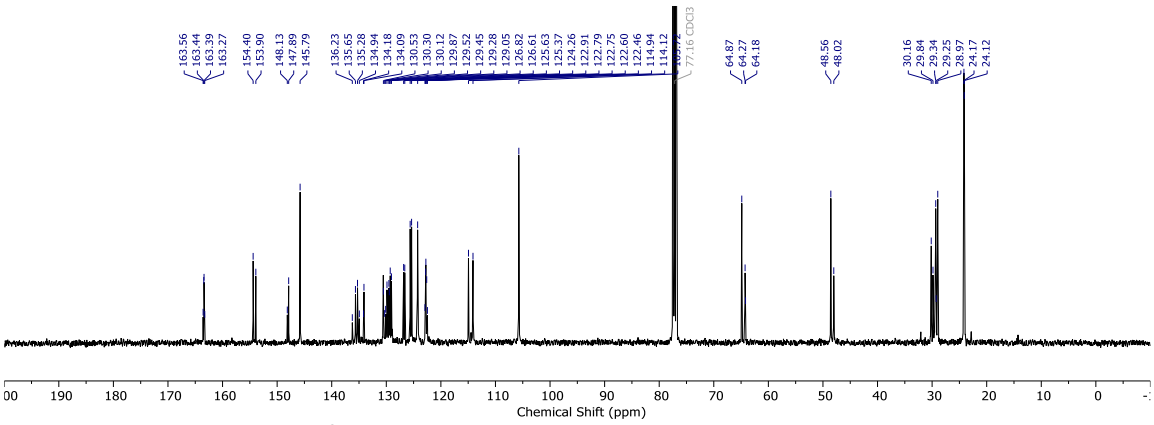

Figure 5.3.25. ^{13}C NMR spectrum of **48** ($CDCl_3$, 298 K, 101 MHz).

1,4-Di(6-hexoxy)benzene PDI acyclic control 50

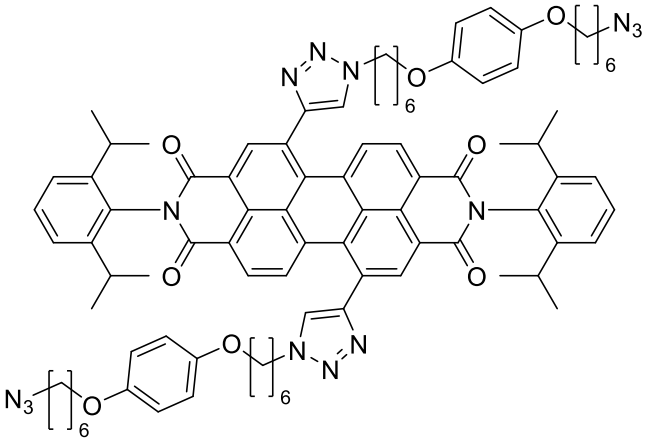

General Procedure C was followed with PDI bisalkyne **23** (50 mg, 0.0659 mmol, 1 eq), 1,4-di(6-azidohexoxy)benzene **41** (237 mg, 0.659 mmol, eq), CH_2Cl_2 (15 mL), THPTA (11.5 mg, 26.4 μmol, 0.4 eq) and $Cu(MeCN)_4{\cdot}PF_6$ (9.82 mg, 26.4 μmol, 0.4 eq). The reaction was completed after three days and purified by flash column chromatography (SiO_2, 0.4:100 MeOH:CH_2Cl_2) to give PDI **3** as a purple solid (66 mg, 68%). The 1,7 and 1,6 regioisomers were separated by HPLC (Buckyprep, 2:60:38 IPA:n-hexane:CH_2Cl_2).

^{1}H NMR (400 MHz, $CDCl_3$) δ 8.75 (s, 2H, Ar*H* Ortho PDI), 8.34 (d, *J* = 8.1 Hz, 2H, Ar*H* PDI), 8.00 (d, *J* = 8.1 Hz, 2H, Ar*H* PDI), 7.88 (s, 2H, C*H* triazole), 7.50 (t, *J* = 7.9 Hz, 2H, iPr$_2$-Ar*H*), 7.35 (d, *J* = 7.9 Hz, 4H, iPr$_2$-Ar*H*), 6.83 – 6.73 (m, 8H, Ar*H* oxybenzene), 4.54 (t, *J* = 7.1 Hz, 4H, CH_2), 3.91 (t, *J* = 6.2 Hz, 4H, CH_2), 3.84 (t, *J* = 6.4 Hz, 4H, CH_2), 3.27 (t, *J* = 6.9 Hz, 4H, CH_2), 2.74 (p, *J* = 6.8 Hz, 4H, C*H* iPr), 2.07 (p, *J* = 7.3 Hz, 4H, CH_2), 1.85 – 1.69 (m, 8H, CH_2), 1.66 – 1.25 (m, 20H, CH_2), 1.17 (d, *J* = 6.8 Hz, 24H, CH(CH_3)$_2$ iPr).

^{13}C NMR (126 MHz, $CDCl_3$) δ 163.5, 163.5, 153.3, 153.2, 147.9, 145.8, 135.7, 135.3, 134.1, 130.6, 130.5, 129.9, 129.6, 129.5, 129.5, 129.1, 124.3, 122.8, 122.6, 122.1, 115.5, 115.5, 68.5, 68.3, 51.5, 50.9, 30.5, 29.9, 29.4, 29.4, 29.3, 28.9, 26.7, 26.4, 25.8, 25.7, 24.2, 24.1.

MS (ESI): m/z calc. for $C_{88}H_{99}N14O_8$ $[M+H]^+$: 1479.777; found 1479.7783

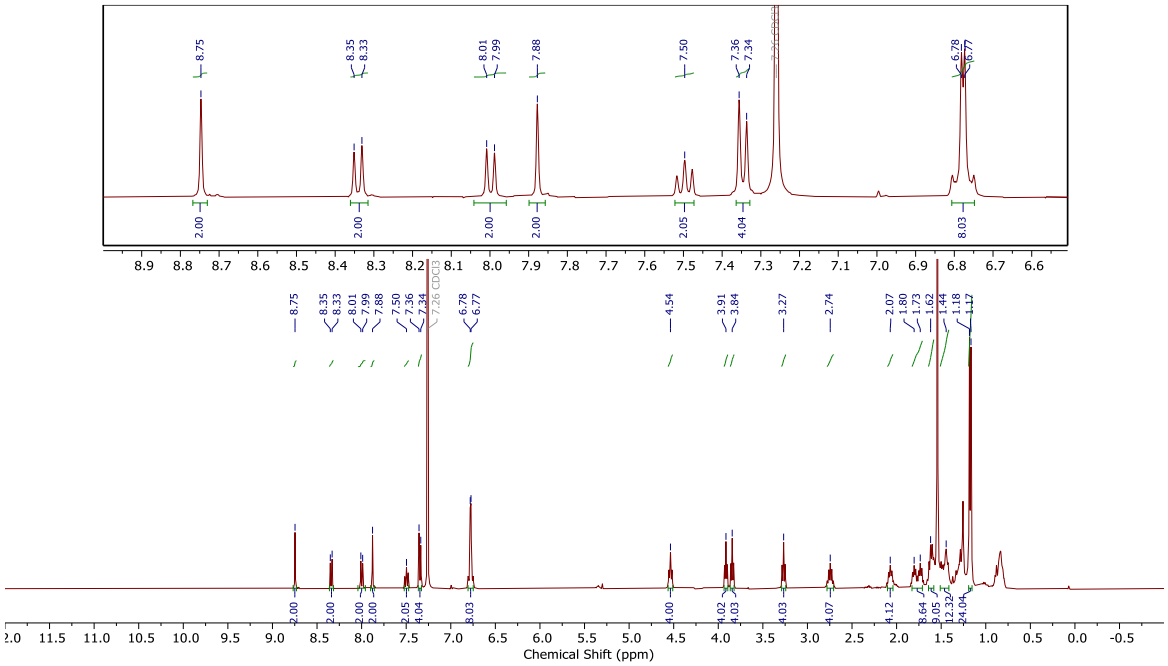

Figure 5.3.26. ^{1}H NMR spectrum of **50** ($CDCl_3$, 298 K, 400 MHz).

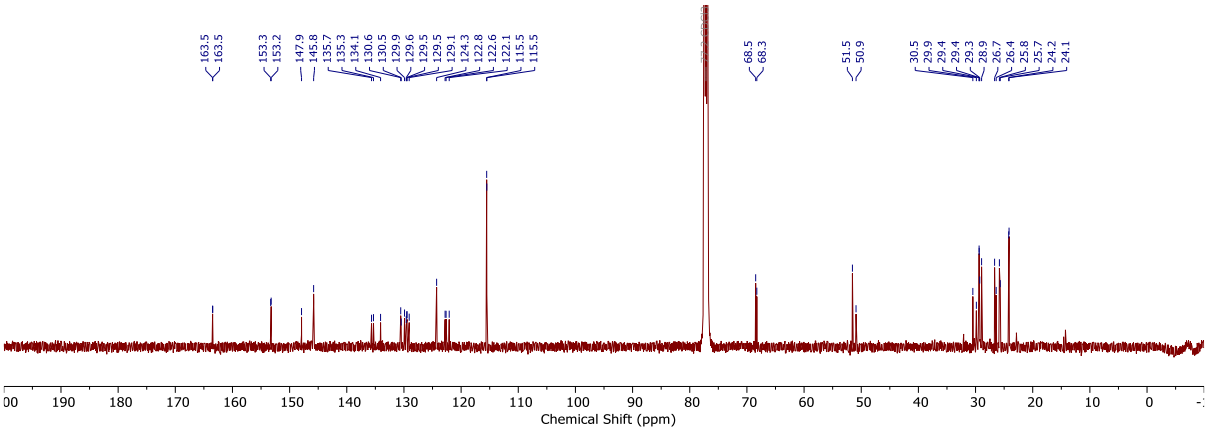

Figure 5.3.27. ^{13}C NMR spectrum of **50** ($CDCl_3$, 298 K, 101 MHz).

Dihexyl triazole PDI acyclic control 51

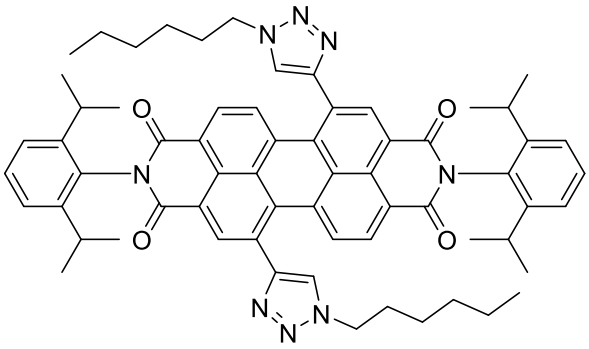

General Procedure C was followed with PDI bisalkyne **23** (50 mg, 65.9 µmol, 1 eq), 1-azidohexane (58.7 mg, 461 µmol, 7 eq), CH_2Cl_2 (260 mL), TBTA (9.82 mg, 26.4 µmol, 0.4 eq) and $Cu(MeCN)_4 \cdot PF_6$ (14.0 mg, 26.4 µmol, 0.4 eq). The reaction was completed after two days and purified by flash column chromatography (SiO_2, 0.4:100 MeOH:CH_2Cl_2) to give PDI **51** as a purple solid (45 mg, 67%). The 1,7 and 1,6 regioisomers were separated by HPLC (Buckyprep, 2:38:60 IPA:n-hexane:CH_2Cl_2) as outlined above.

^{1}H NMR (400 MHz, $CDCl_3$) δ 8.76 (s, 2H, Ar*H* Ortho PDI), 8.34 (d, *J* = 8.1 Hz, 2H, Ar*H* Ortho PDI), 8.01 (d, *J* = 8.1 Hz, 2H, Ar*H* Bay PDI), 7.88 (s, 2H, C*H* triazole), 7.50 (t, *J* = 7.8 Hz, 2H, iPr_2-Ar*H*), 7.35 (d, *J* = 7.8 Hz, 4H, iPr_2-Ar*H*), 4.52 (t, *J* = 7.2 Hz, 4H, NCH_2), 2.74 (p, *J* = 6.8 Hz, 4H, C*H* iPr), 2.02 (p, *J* = 7.3 Hz, 4H, NCH_2CH_2), 1.47 – 1.31 (m, 12H, CH_2), 1.17 (d, *J* = 6.8 Hz, 24H, $CH(CH_3)_2$ iPr), 0.90 (t, *J* = 6.9 Hz, 6H, CH_2CH_3).

^{13}C NMR (101 MHz, $CDCl_3$) δ 163.3, 163.3, 145.7, 135.5, 135.2, 134.0, 130.4, 130.4, 129.7, 129.5, 129.4, 128.9, 124.1, 122.6, 122.5, 50.9, 31.1, 30.4, 29.2, 26.2, 24.0, 24.0, 22.4, 14.0.

MS (ESI): m/z calc. for $C_{64}H_{69}N_8O_4$ $[M+H]^+$: 1013.5442; found 1013.5493.

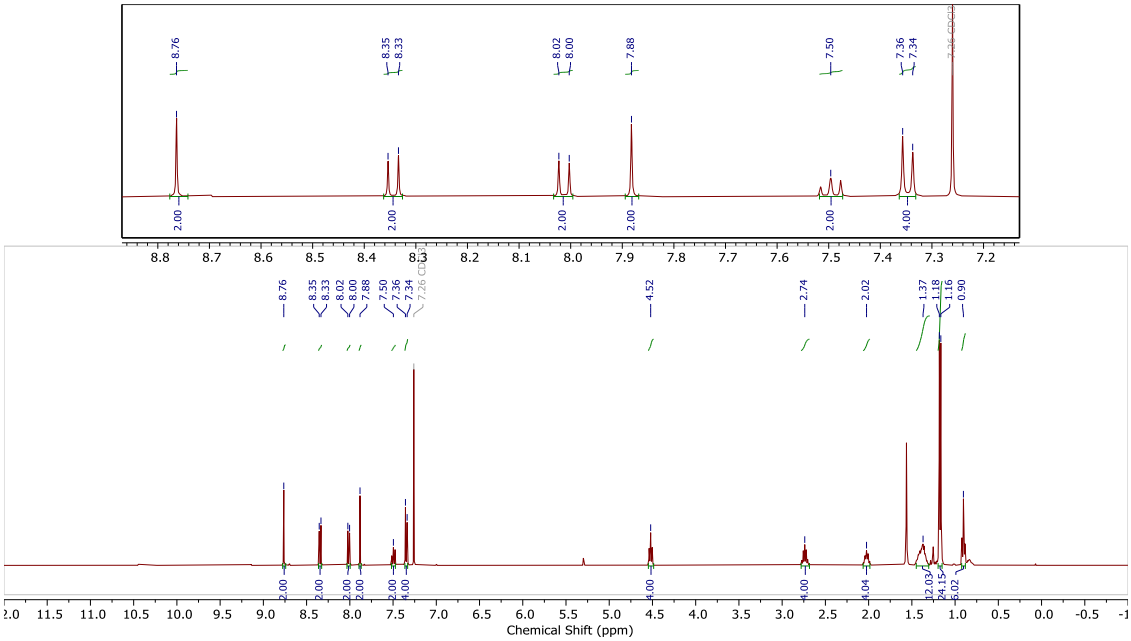

Figure 5.3.28. ^{1}H NMR spectrum of **51** ($CDCl_3$, 298 K, 400 MHz).

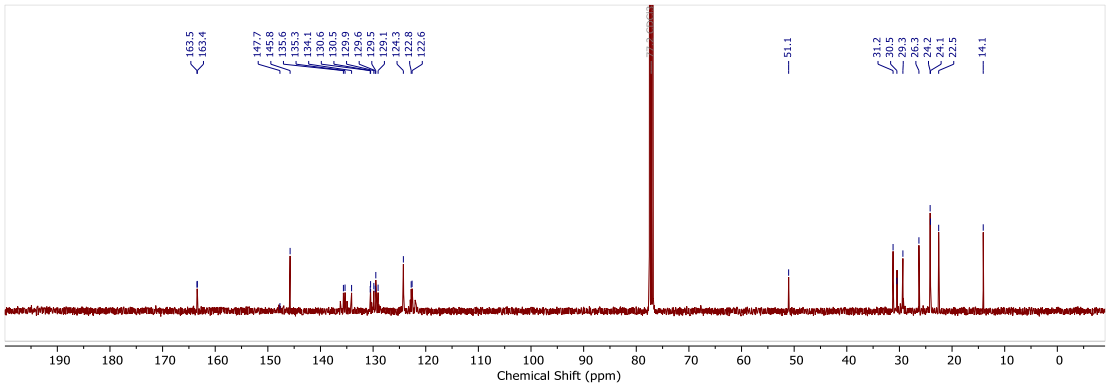

Figure 5.3.29. ^{13}C NMR spectrum of **51** ($CDCl_3$, 298 K, 101 MHz).

1,5-Di(3-bromopropylamino)naphthalene 52

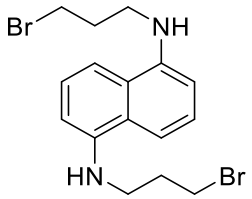

1,3-Dibromopropane (20 mL, 190 mmol, 30 eq) was added to a stirring solution of triethylamine (6.0 mL, 43 mmol, 7 eq) and 1,5-diaminonaphthalene (1 g, 6.24 mmol, 1 eq) in acetonitrile (50 mL). The resulting mixture was left to stir at room temperature for 3 days. After which, the reaction mixture was filtered and the filtrate was concentrated *in vacuo*, then purified by flash column chromatography (SiO_2, 3:7 Hexanes:CH_2Cl_2) to yield an off-white solid **52** (440 mg, 17%).

^{1}H NMR ($CDCl_3$, 400 MHz) δ 7.35 (2H, dd, *J* = 8.5, 7.7 Hz, C(3)*H*), 7.20 (2H, d, *J* = 8.5 Hz, C(2)*H*), 6.68 (2H, d, *J* = 7.7 Hz, C(4)*H*), 4.47 (1H, s, N*H*), 3.60 (4H, t, *J* = 6.4 Hz, BrCH_2), 3.53 (4H, t, *J* = 6.6 Hz, NCH_2), 2.32 (4H, p, *J* = 6.5 Hz, BrCH_2CH_2);

^{13}C NMR ($CDCl_3$, 101 MHz) δ 143.6 (*C*(1)), 125.6 (*C*(3)), 124.1 (*C*(4a)), 109.0 (*C*(2)), 104.6(*C*(4)), 42.3 (Br*C*H_2), 31.8 (BrCH_2*C*H_2), 31.4 (N*C*H_2).

MS (ESI): m/z calc. for $C_{16}H_{21}Br_2N_2$ $[M+H]^+$: 397.9993; found 398.0000.

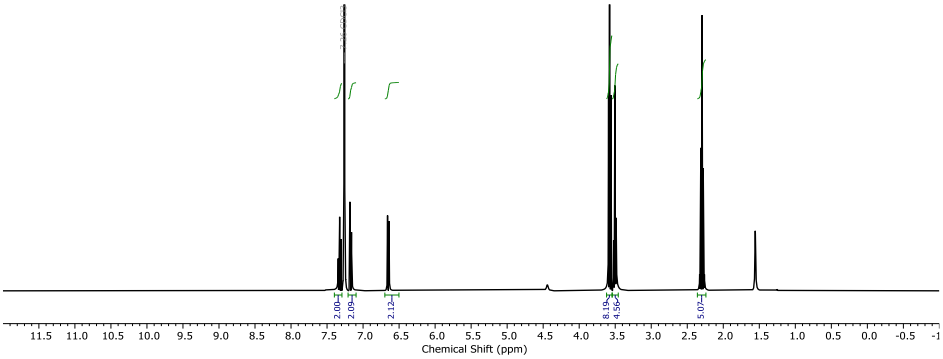

Figure 5.3.30. ^{1}H NMR spectrum of **52** ($CDCl_3$, 298 K, 400 MHz).

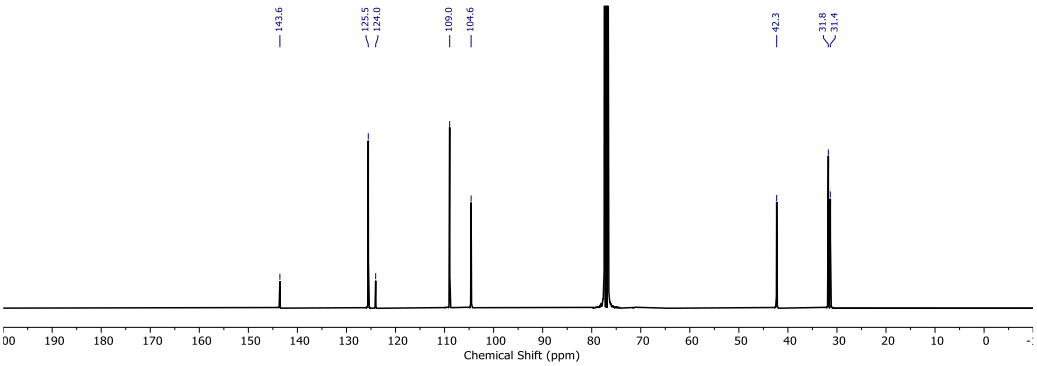

Figure 5.3.31. ^{13}C NMR spectrum of **52** ($CDCl_3$, 298 K, 101 MHz).

1,5-Di(3-azidopropylamino)naphthalene 53

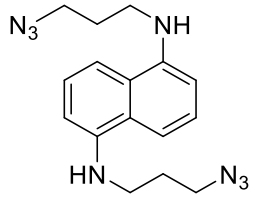

General Procedure B was followed with dibromo **52** (426 mg, 1.06 mmol, 1 eq) and NaN_3 (173 mg, 2.66 mmol, 2.5 eq) in DMF (40 mL) to yield an off-white solid **53** (305 mg, 88%).

^{1}H NMR ($CDCl_3$, 400 MHz) δ 7.33 (2H, dd, *J* = 8.5, 7.6 Hz, C(3)*H*), 7.18 (2H, d, *J* = 8.5 Hz, C(2)*H*), 6.62 (2H, d, *J* = 7.6 Hz, C(4)*H*), 4.45 (2H, s, N*H*), 3.51 (4H, t, *J* = 6.5 Hz, N_3CH_2), 3.41 (4H, t, *J* = 6.7 Hz, $NHCH_2$), 2.03 (4H, p, *J* = 6.6 Hz, $NHCH_2CH_2$);

^{13}C NMR ($CDCl_3$, 101 MHz) δ 143.8 (*C*(1)), 125.7 (*C*(3)), 124.2 (*C*(4a)), 109.1 (*C*(2)), 104.6 (*C*(4)), 49.8 (N_3CH_2), 41.7 ($NHCH_2$), 28.6 ($NHCH_2CH_2$).

MS (ESI): m/z calc. for $C_{16}H_{21}N_8$ $[M+H]^+$: 324.1811; found 324.1802.

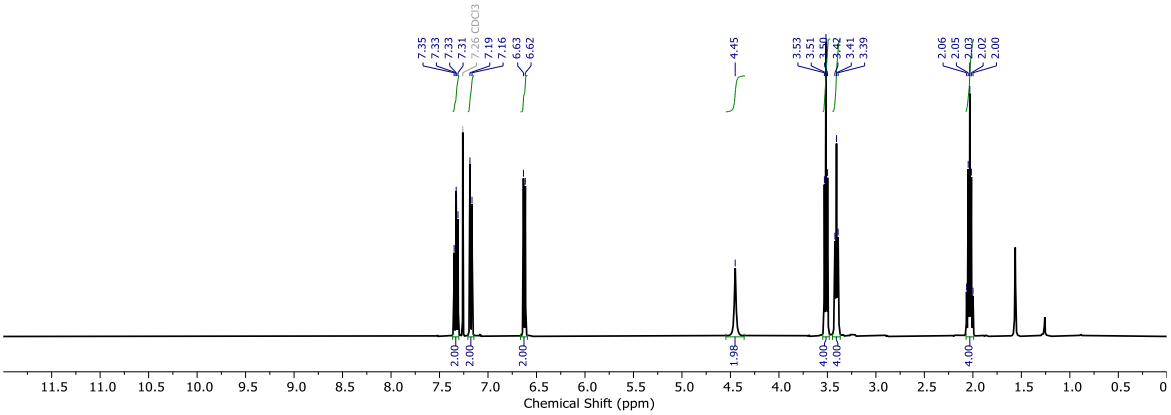

Figure 5.3.32. ^{1}H NMR spectrum of **53** ($CDCl_3$, 298 K, 400 MHz).

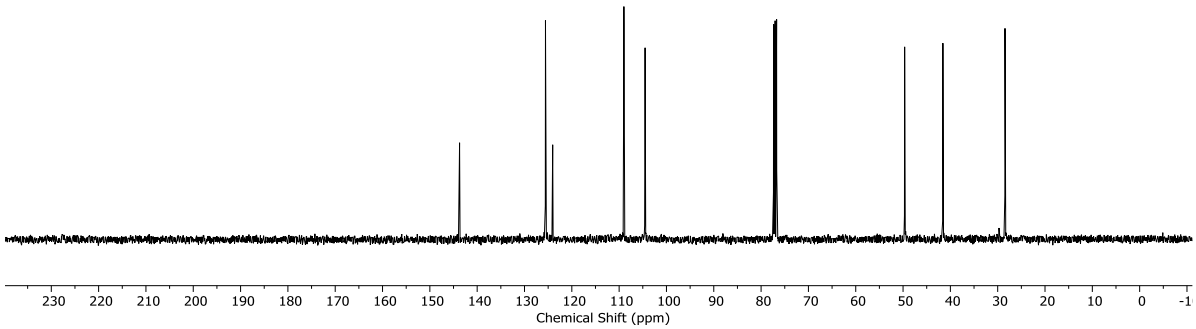

Figure 5.3.33. ^{13}C NMR spectrum of **53** ($CDCl_3$, 298 K, 101 MHz).

1,5-Dipropylaminonapthalene PDI macrocycle 54

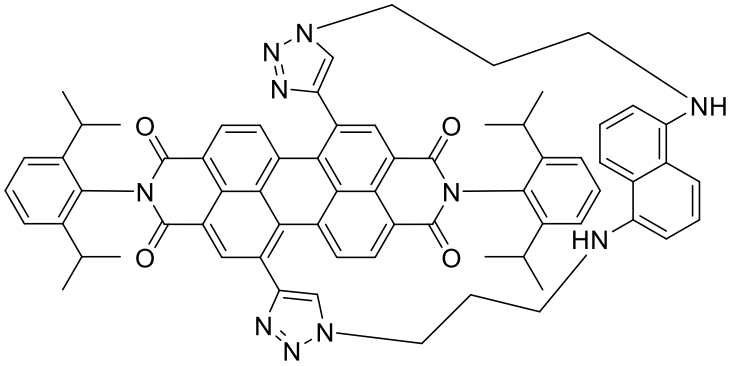

General Procedure C was followed with PDI bisalkyne **23** (100 mg, 0.132 mmol, 1 eq), 1,5-di(3-azidopropylamino)naphthalene **53** (43 mg, 0.132 mmol, 1 eq), CH_2Cl_2 (260 mL), TBTA (30 mg, 0.053, 0.4 eq) and $Cu(MeCN)_4$-PF_6 (20mg, 0.053, 0.4 eq). Reaction was completed after 4 days and purified by flash column chromatography (SiO2, 0.5:100 MeOH:CH_2Cl_2) to give macrocycle **54** a purple solid (25.2 mg, 21%).

^{1}H NMR ($CDCl_3$, 400 MHz) δ 9.08 (2H, s, Ar*H* Ortho PDI), 8.35 (2H, d, *J* = 8.0 Hz, Ar*H* Ortho PDI), 8.22 (2H, d, *J* = 8.0 Hz, Ar*H* Bay PDI), 7.50 (2H, t, *J* = 8.0 Hz, iPr_2-Ar*H*), 7.34 (4H, d, *J* = 8.0,Hz, iPr_2-Ar*H*), 7.21 (2H, s, C*H* triazole), 6.68 – 6.52 (4H, Ar*H* naphthalene), 6.04 (2H, d, *J* = 7.1 Hz, Ar*H* naphthalene), 4.82 (2H, ddd, *J* = 14.6, 8.6, 3.4 Hz, $NHCH_2CH_2CH_AH_BN$), 4.58 (2H, d, *J* = 14.6 Hz, $NHCH_2CH_2CH_AH_BN$), 3.75 (2H, br s, N*H*), 3.29 (2H, app d, *J* = 13.3 Hz, $NHCH_AH_BCH_2CH_2N$), 2.98 (2H, app t, *J* = 11.1 Hz, $NHCH_AH_BCH_2CH_2N$), 2.83 (2H, p, *J* = 6.8 Hz, C*H* iPr), 2.74 (2H, p, *J* = 6.8 Hz, C*H* iPr), 2.36 (2H, d, *J* = 7.7 Hz), 2.31 – 2.22 (4H, m, $NHCH_2CH_2CH_2N$), 1.20 (6H, d, *J* = 6.3 Hz, $CH(CH_3)_2$ iPr), 1.17(6H, d, *J* = 6.3 Hz, $CH(CH_3)_2$ iPr), 1.16 (12H, d, *J* = 6.3 Hz, $CH(CH_3)_2$ iPr).

^{13}C NMR (101 MHz, $CDCl_3$) δ 163.6, 163.3, 147.5, 145.9, 145.4, 142.7, 135.1, 134.5, 133.5, 130.6, 130.2, 129.9, 129.8, 129.2, 129.1, 128.7, 125.0, 124.9, 124.4, 124.4, 124.1, 122.9, 122.4, 109.7, 104.9, 49.3, 41.8, 29.8, 29.5, 29.3, 28.4, 24.2, 24.1, 24.0.

MS (ESI): m/z calc. for $C_{68}H_{63}N_{10}O_4$ [M+H]+: 1083.4956; found 1083.4957.

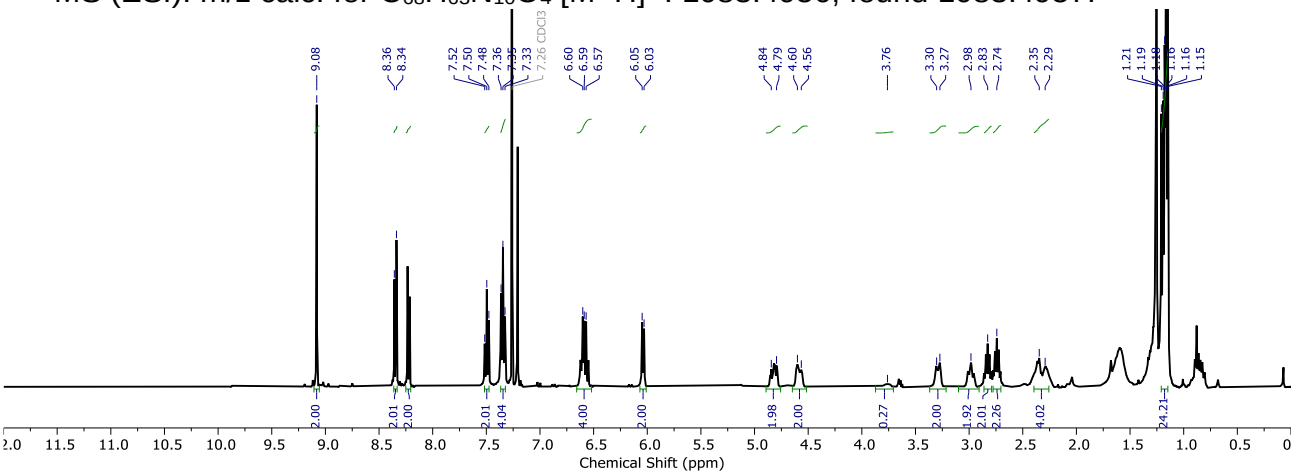

Figure 5.3.34. ^{1}H NMR spectrum of **54** ($CDCl_3$, 298 K, 400 MHz).

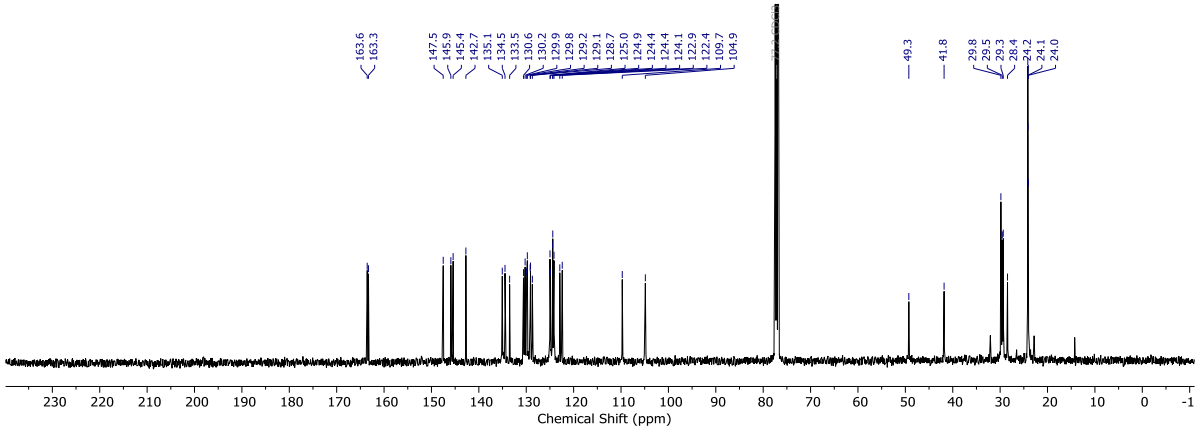

Figure 5.3.35.^{13}C NMR spectrum of **54** ($CDCl_3$, 298 K, 101 MHz).

1,5-Dipropylaminonapthalene PDI acyclic variant 55

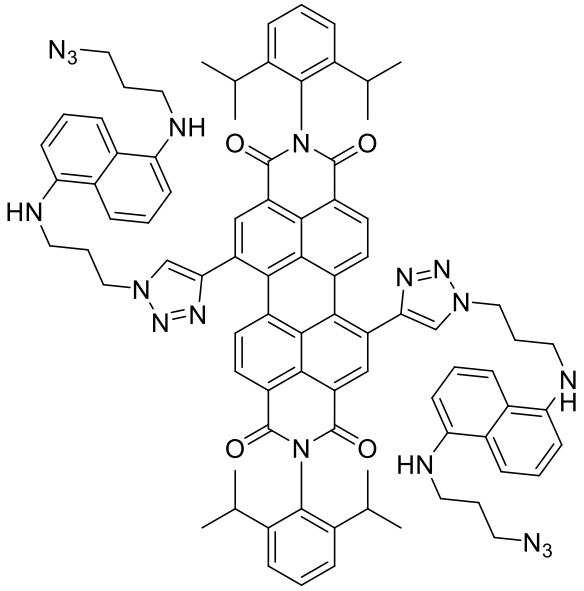

General Procedure C was followed with PDI bisalkyne **23** (50 mg, 65.9 μmol, 1 eq), 1,5-di(3-azidopropylamino)naphthalene **53** (150 mg, 0.462 mmol, 7 eq), CH_2Cl_2 (3 mL), TBTA (14 mg, 24 μmol, 0.4 eq) and $Cu(MeCN)_4$-PF_6 (10 mg, 24 μmol, 0.4 eq). Reaction was completed after 24 h and purified by flash column chromatography (SiO2, 0.5:100 MeOH:CH_2Cl_2) to give **55** as a purple solid (45.0 mg, 49%).

^{1}H NMR ($CDCl_3$, 400 MHz) δ 8.74 (2H, s, Ar*H* PDI), 8.33 (2H, d, *J* = 8.1 Hz), 7.98 (2H, d, *J* = 8.1 Hz), 7.83 (2H, s, C*H* triazole), 7.50 (2H, t, *J* = 8.1 Hz, iPr_2-Ar*H*), 7.35 (4H, d, *J* = 8.1 Hz, iPr_2-Ar*H*), 7.25 – 7.10 (8H, m, Ar*H* naphthalene), 6.55 (4H, dt, *J* = 7.5, 3.6 Hz, Ar*H* naphthalene), 4.70 (4H, dt, *J* = 9.9, 6.9 Hz, triazole-NCH_2), 4.54 (4H, s, N*H*), 3.46 (4H, td, *J* = 6.5, 1.7 Hz, N_3CH_2), 3.43 – 3.35 (4H, m, triazole-$NCH_2CH_2CH_2$NH), 3.35 – 3.25 (4H, m, $N_3CH_2CH_2CH_2$NH), 2.75 (4H, hept, *J* = 7.0, 6.8 Hz, C*H* iPr), 2.44 (4H, app q, *J* = 6.7 Hz, triazole-$NCH_2CH_2CH_2$NH), 1.96 (4H, pd, *J* = 6.6, 1.7 Hz, $N_3CH_2CH_2CH_2$NH), 1.18 (6H, d, *J* = 6.8 Hz, $CH(CH_3)_2$ iPr), 1.16 (6H, d, *J* = 7.0 Hz, $CH(CH_3)_2$ iPr)

^{13}C NMR (101 MHz, $CDCl_3$) δ 163.6, 163.4, 148.3, 147.9, 145.8, 145.7, 143.9, 143.8, 143.3, 136.1, 135.6, 135.2, 134.9, 134.0, 130.5, 130.5, 130.2, 129.9, 129.5, 129.4, 129.2, 129.0, 125.9, 125.5, 125.4, 124.3, 124.2, 124.1, 124.1, 122.7, 122.6, 109.7,

109.0, 104.8, 104.6, 49.7, 48.6, 41.6, 40.7, 29.8, 29.6, 29.5, 29.3, 29.3, 28.5, 24.2, 24.1, 24.1.

MS (MALDI): *m/z* calc. for $C_{84}H_{82}N_{18}O_4$ [M]+: 1406.6766; found 1406.6844.

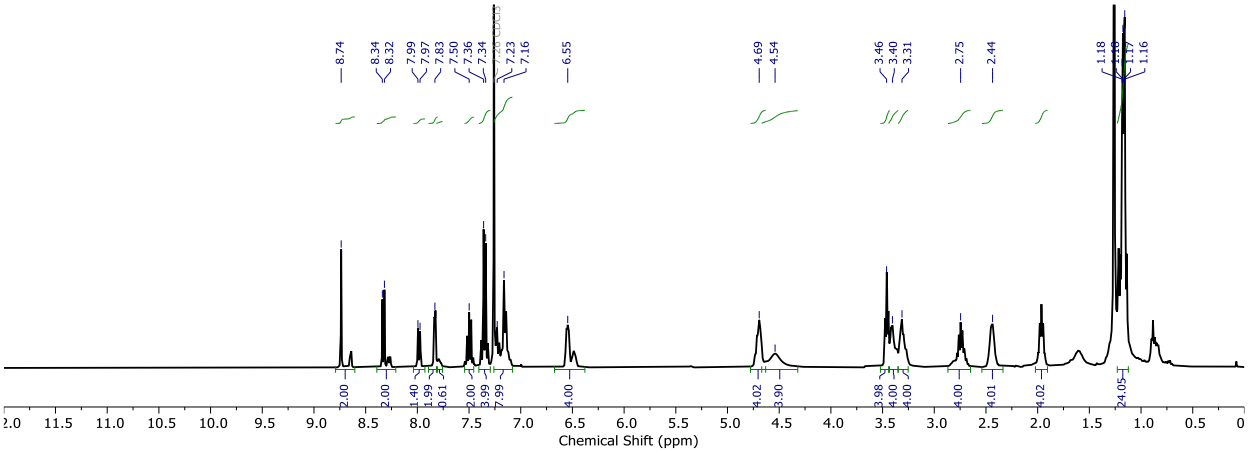

Figure 5.3.36. ^{1}H NMR spectrum of **54** ($CDCl_3$, 298 K, 400 MHz).

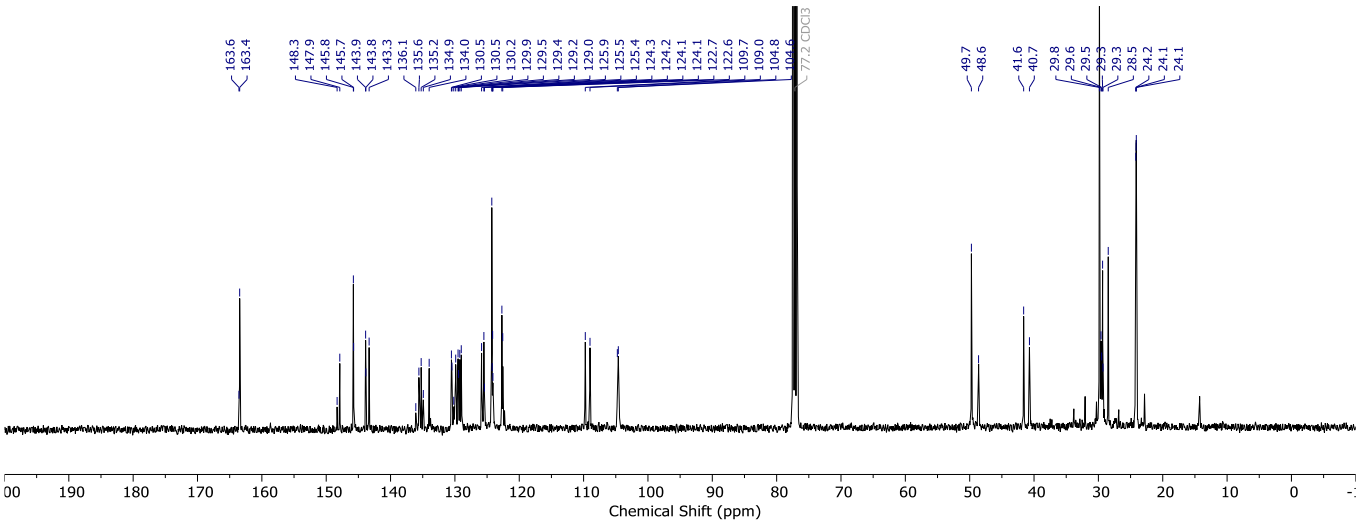

Figure 5.3.37. ^{13}C NMR spectrum of **54** ($CDCl_3$, 298 K, 101 MHz)

N-*N*-Di(2,6-diisopropylphenyl) 1,7-di(1-hexyl-3-methyl-1,2,3-triazol-3-ium-4-yl)-perylene-3,4,9,10-tetracarboxylic diimide·2PF_6 56

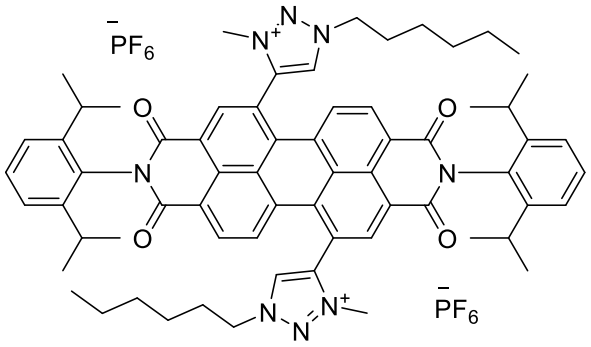

PDI **51** (90.0 mg, 0.0888 mmol, 1 eq) was dissolved in $CHCl_3$ (15 mL) and the solution was degassed with N_2 for 15min. After which, methyl triflate (0.5 mL, 4.44 mmol, 50 eq) was added and the reaction mixture was stirred at rt for 2 days in the dark under N_2. After this time, the reaction was quenched with MeOH (5 mL) and saturated $NaHCO_3$ (20 mL). The resulting mixture was extracted with DCM, dried, and concentrated *in vacuo*, then recrystalised in $CHCl_3$/Hexanes/MeCN (20:20:1 v/v) to furnish **55** red crystals (97 mg, 81%). The anions were exchanged for PF_6^- following the same procedure as **73** (*vide infra*).

Alternatively, PDI **51** was dissolved in MeI in a sealed pressure tube and left to stir at 80 °C for 4 days. The excess MeI was removed in vacuo and the crude mixture was purified by preparative TLC (SiO_2, 5% MeOH in DCM).

^{1}H NMR (CD_3CN, 400 MHz) δ 8.97 (2H, s), 8.71 (2H, s), 8.53 (2H, d, *J* = 8.0 Hz), 7.85 (2H, d, *J* = 8.2 Hz), 7.53 (2H, t, *J* = 7.8 Hz), 7.40 (4H, d, *J* = 7.7 Hz), 4.73 (4H, s), 2.89 – 2.74 (4H, m), 2.45 (16H, s), 1.12 (24H, dd, *J* = 6.9, 2.3 Hz).

^{13}C NMR (101 MHz, CD_3CN) δ 147.1, 134.2, 131.6, 130.8, 129.3, 125.2, 55.7, 31.7, 29.8, 29.7, 26.4, 24.2, 24.1, 23.1, 14.2.

MS (ESI): *m*/*z* calc. for $C_{66}H_{74}N_8O4^{2+}$ $[M+H]^{2+:}$ 521.2911; found 521.2975.

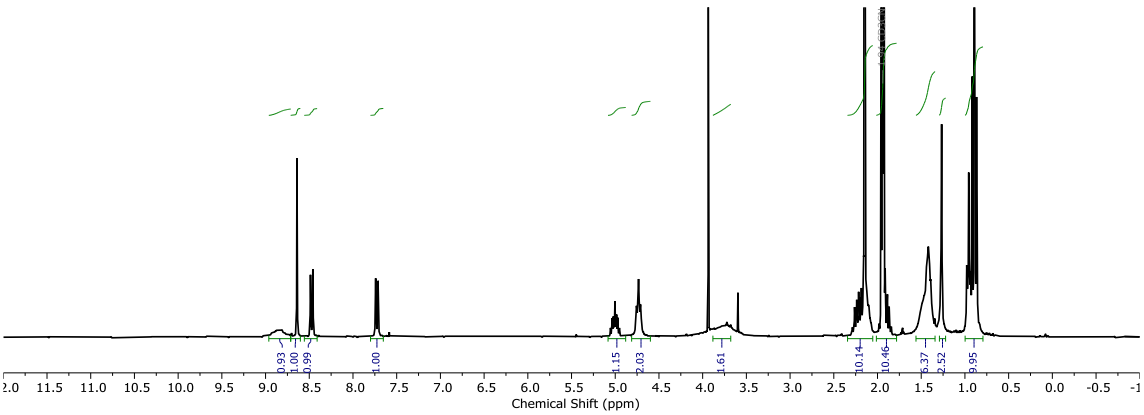

Figure 5.3.38. ^{1}H NMR spectrum of **56** ($CDCl_3$, 298 K, 400 MHz).

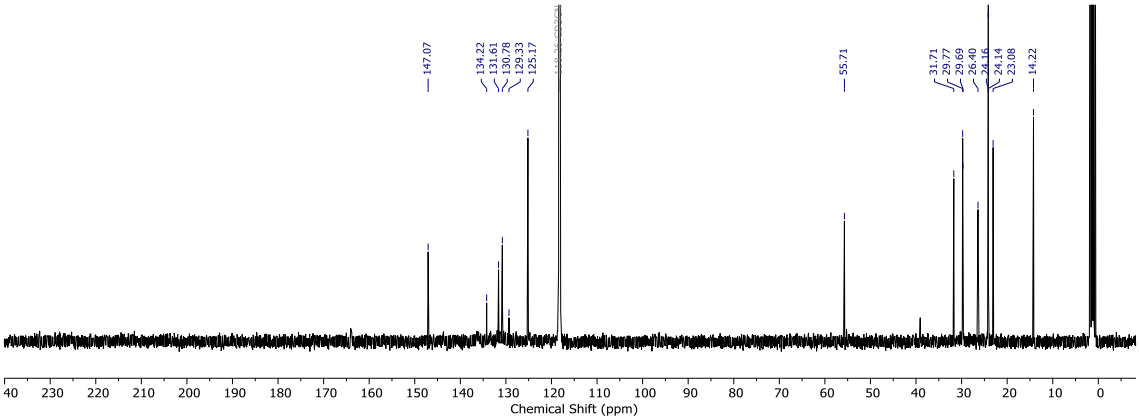

Figure 5.3.39. ^{13}C NMR spectrum of **56** ($CDCl_3$, 298 K, 101 MHz).

5.4 Synthesis and Characterisation for Chapter 3

4-Azidobutan-1-amine 59

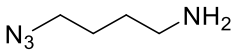

1,4-Dibromobutane (1.00 mL, 8.34 mmol, 1 eq) and NaN_3 (1.56 g, 20.9 mmol, 2.5 eq) were dissolved in DMF (3 mL) and left to stir at 70 °C for 16 h. The reaction mixture was quenched with H_2O (100 mL) and extracted with Et_2O (3 x 100 mL), washed with H_2O (4 x 100 mL), and brine (100 mL). EtOAc (50 mL) was added to the organic layer and was dried with $MgSO_4$ and Et_2O was removed under vacuo, leaving 1,4-diazidobutane in a solution of EtOAc. Due to the explosive nature of high nitrogen to carbon ratio of the organic azide, EtOAc was not removed from the product and was put onto the next step without characterisation.

2.5M $HCl_{(aq)}$ (5.6 mL) was added to the previous EtOAc solution of 1,4-diazidobutane of 2.5M and the resulting mixture was cooled to 0 °C. PPh_3 (2.19 g, 20 mmol, 1 eq) dissolved in EtOAc (5.6 mL) was added dropwise to the cold mixture, then the mixture was stirred at rt for 16 h. After which, the reaction mixture was poured into a separating funnel along with H_2O (50 mL) and EtOAc (25 mL). The organic layer was discarded, and the aqueous layer was washed with CH_2Cl_2 (2 x 50 mL). The aqueous layer was basified to pH 11 with 1 M NaOH and the product was extracted with CH_2Cl_2 (3 x 100 mL), which was sequentially dried with $MgSO_4$ and concentrated in vacuo to give **59** as a colourless oil (0.741 g, 78%).

^{1}H NMR ($CDCl_3$, 400 MHz) δ 3.29 (2H, t, *J* = 6.9 Hz, CH_2), 2.73 (2H, t, *J* = 6.9 Hz), 1.72 – 1.59 (2H, m), 1.59 – 1.46 (2H, m).

Spectroscopic data is in agreement with literature.[158]

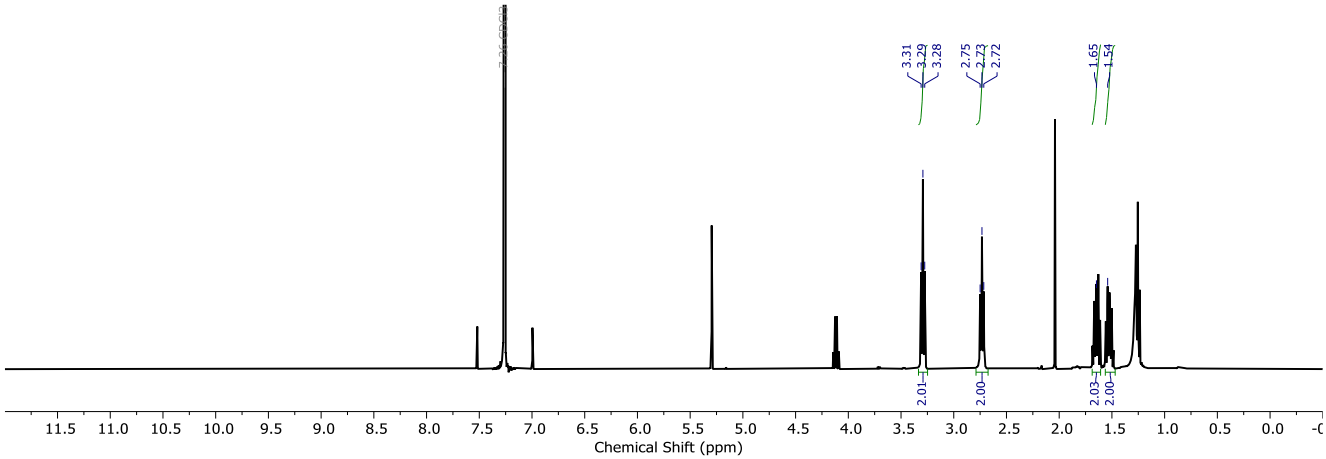

Figure 5.4.1. ^{1}H NMR spectrum of **54** ($CDCl_3$, 298 K, 400 MHz).

N-N-Di(4-(azidomethyl)benzyl) 1,6,7,12-tetrachloro-perylene-3,4,9,10-tetracarboxylic diimide 60

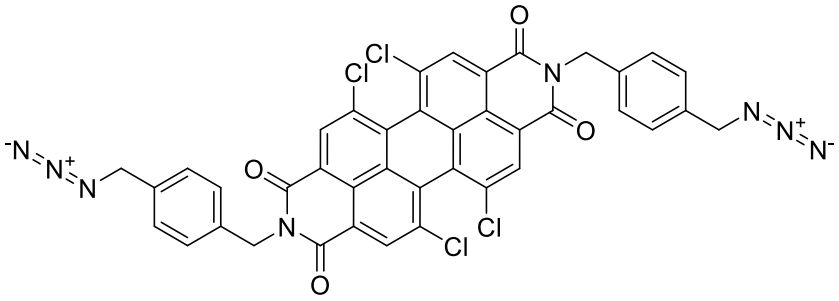

General Procedure D was followed with 1,6,7,12-tetrachloro-perylene-3,4,9,10-tetracarboxylic dianhydride $PDICl_4$ (1 g, 1.89 mmol, 1 eq), (4-(azidomethyl)phenyl)methanamine **32** (673 mg, 4.15 mmol, 2.2 eq), $Zn(OAc)_2{\cdot}2H_2O$ (621 mg, 2.83 mmol, 1.5 eq), imidazole (6 g) and quenched with 1M HCl (100 mL) and purified by flash column chromatography (SiO_2, 60:40 CH_2Cl_2:Hexanes) to yield Spectroscopic data is in agreement with literature. as a red solid (892 mg, 58%).

^{1}H NMR ($CDCl_3$, 400 MHz) δ 8.68 (4H, s, Ar*H* PDI), 7.57 (3H, d, *J* = 8.3 Hz, Ar*H* Xylyl), 7.27 (3H, d, *J* = 8.3 Hz, Ar*H* Xylyl), 5.39 (4H, s, CH_2), 4.28 (4H, s, CH_2)

MS (MALDI): *m/z* calc. for $C_{40}H_{20}Cl_4N_8O_4$ [M]+: 816.0362; found 816.0542

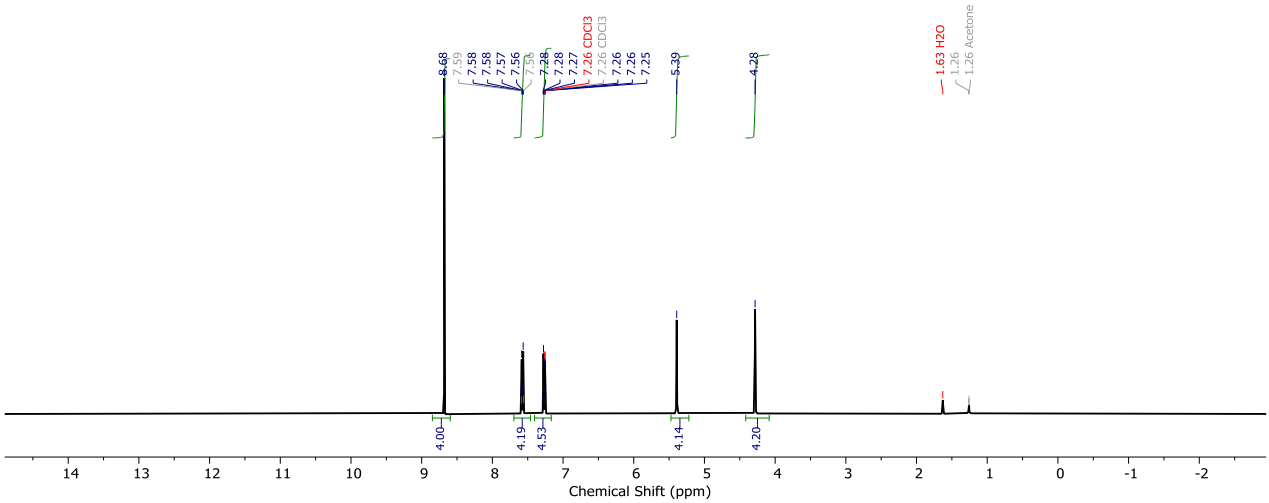

Figure 5.4.2. ^{1}H NMR spectrum of **54** ($CDCl_3$, 298 K, 400 MHz).

N-N-Di(4-azidobutyl) 1,6,7,12-tetrachloro-perylene-3,4,9,10-tetracarboxylic diimide 61

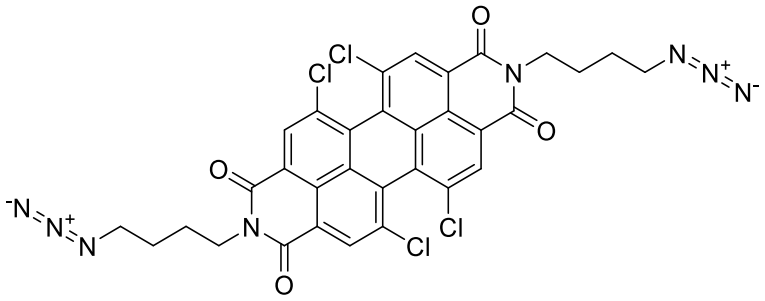

General Procedure D was followed with 1,6,7,12-tetrachloro-perylene-3,4,9,10-tetracarboxylic dianhydride $PDICl_4$ (200 mg, 0.377 mmol, 1 eq), 4-azidobutan-1-amine **59** (290 mg, 2.57 mmol, 6.8 eq), $Zn(OAc)_2 \cdot 2H_2O$ (170 mg, 0.755 mmol, 2 eq), imidazole (1.6 g) and quenched with 1M HCl (100 mL) and purified by flash column chromatography (SiO_2, 80:20 CH_2Cl_2:Hexanes) to yield **61** as a red solid (90.4 mg, 33%).

^{1}H NMR ($CDCl_3$, 400 MHz) δ 8.i66 (4H, s, Ar*H*), 4.24 (4H, t, *J* = 7.0 Hz, CH_2), 3.37 (4H, t, *J* = 7.0 Hz, CH_2), 1.90 – 1.80 (4H, m, CH_2), 1.78 – 1.67 (4H, m, CH_2).

MS (MALDI): *m*/*z* calc. for $C_{32}H_{20}Cl_4N_8O_4$ [M]+: 720.0362; found 720.0601

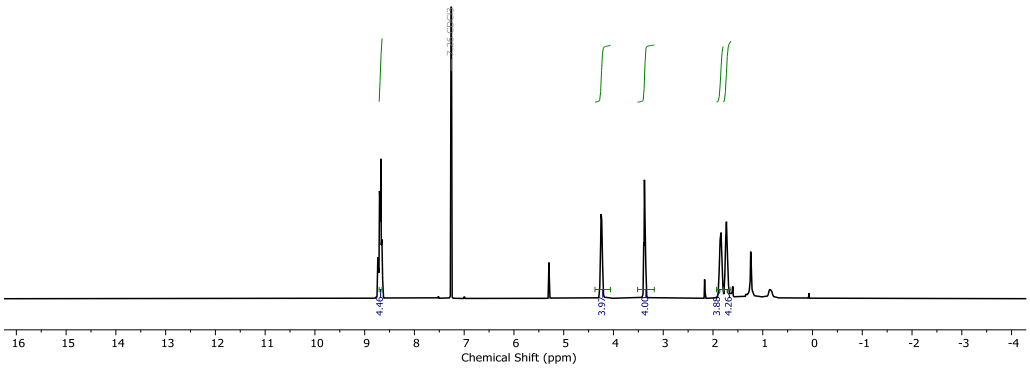

Figure 5.4.3. ^{1}H NMR spectrum of **54** ($CDCl_3$, 298 K, 400 MHz).

XBOX-PDICl$_4$-Xylyl-PDI macrocycle 62

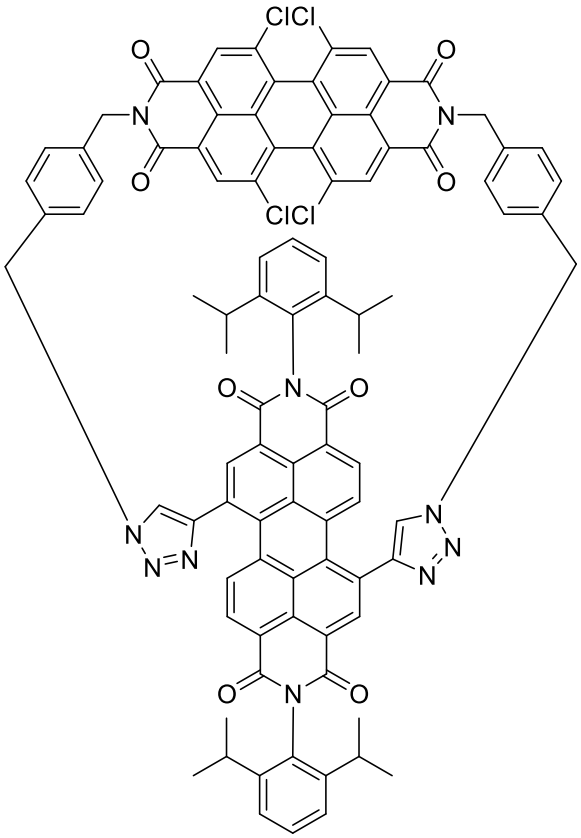

General Procedure B was followed with PDI(alkyne) **23** (195 mg, 0.257 mmol, 1 eq), PDI(azide) **60** (200 mg, 0.257 mmol, 1 eq), TBTA (56 mg, 0.4 eq), Cu(MeCN)4–PF_6 (40 mg, 0.4 eq) and CH_2Cl_2 (800 mL). Reaction was completed after 4 days and purified via flash column chromatography (SiO_2, 0.4:100 MeOH:CH_2Cl_2) to give macrocycle **62** as a red solid (21 mg, 5%).

^{1}H NMR (400 MHz, $CDCl_3$) δ 8.69 (s, 2H, Ar*H* ortho PDI), 8.63 (s, 2H, Ar*H* ortho PDI), 8.40 (s, 2H, Ar*H* ortho PDI), 8.25 (d, *J* = 8.1 Hz, 2H, Ar*H* PDI), 8.04 (d, *J* = 8.0 Hz, 2H, Ar*H* PDI), 7.72 (s, 2H, C*H* triazole), 7.54 (d, *J* = 8.3 Hz, 4H, Ar*H* linker), 7.50 (t, *J* = 7.9 Hz, 4H, Ar*H* linker), 7.34 (ddd, *J* = 7.7, 6.3, 1.5 Hz, 4H, iPr$_2$-Ar*H*), 7.28 (obs d, 2H, iPr$_2$-Ar*H*), 5.70 (d, *J* = 14.8 Hz, 2H, CH_AH$_B$), 5.65 (d, *J* = 13.4 Hz, 2H, CH$_A$$H_B$), 5.46 (d, *J* = 14.8 Hz, 2H, CH_AH$_B$), 5.18 (d, *J* = 13.3 Hz, 2H, CH$_A$$H_B$), 2.75 – 2.56 (m, 4H, C*H* ^{i}Pr), 1.20 – 1.09 (m, 24H, CH_3).

^{13}C NMR (101 MHz, $CDCl_3$) δ 163.3, 163.2, 162.3, 161.6, 147.7, 145.7, 145.7, 138.4, 135.7, 135.5, 135.0, 134.9, 133.9, 133.6, 133.3, 132.9, 131.4, 130.9, 130.4, 130.3,

129.9, 129.3, 129.2, 129.0, 128.9, 128.7, 128.6, 124.2, 123.3, 123.2, 123.1, 122.7, 122.5, 121.6, 54.8, 42.8, 29.8, 29.3, 24.3, 24.1, 24.1.

MS (MALDI): *m/z* calc. for $C_{92}H_{62}Cl_4N_{10}O_8$ [M]+: 1574.3506; found 1574.3516

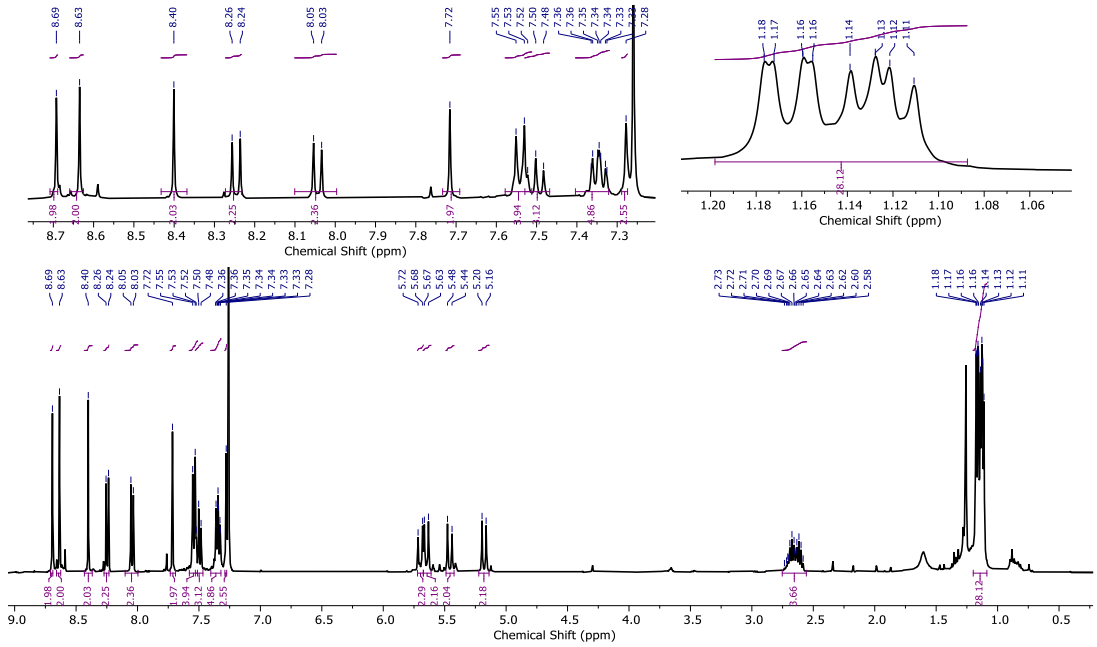

Figure 5.4.4.. ^{1}H NMR spectrum of **62** ($CDCl_3$, 298 K, 400 MHz).

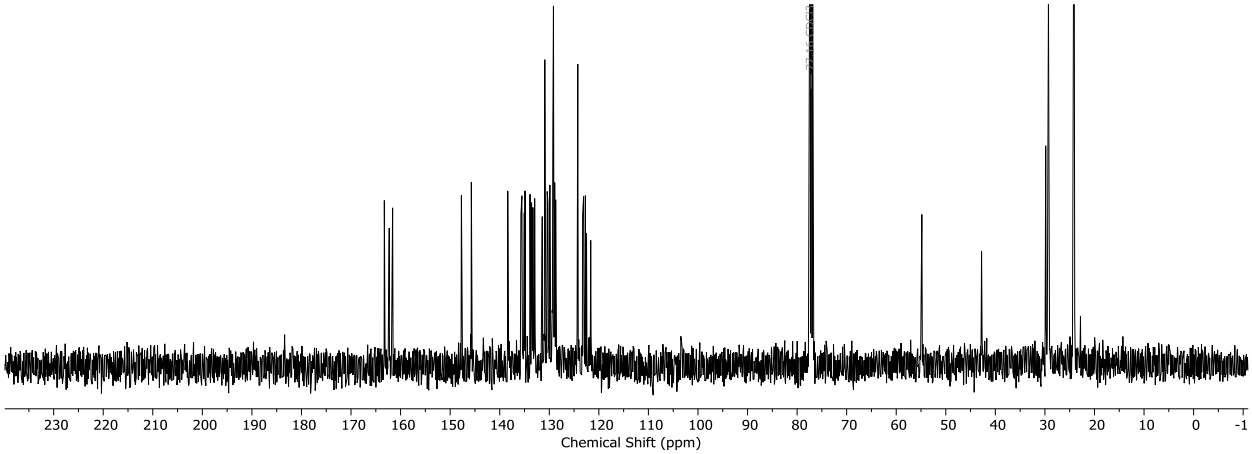

Figure 5.4.5.^{13}C NMR spectrum of **62** ($CDCl_3$, 298 K, 400 MHz).

XBOX-PDICl$_4$-Butyl-PDI macrocycle 63

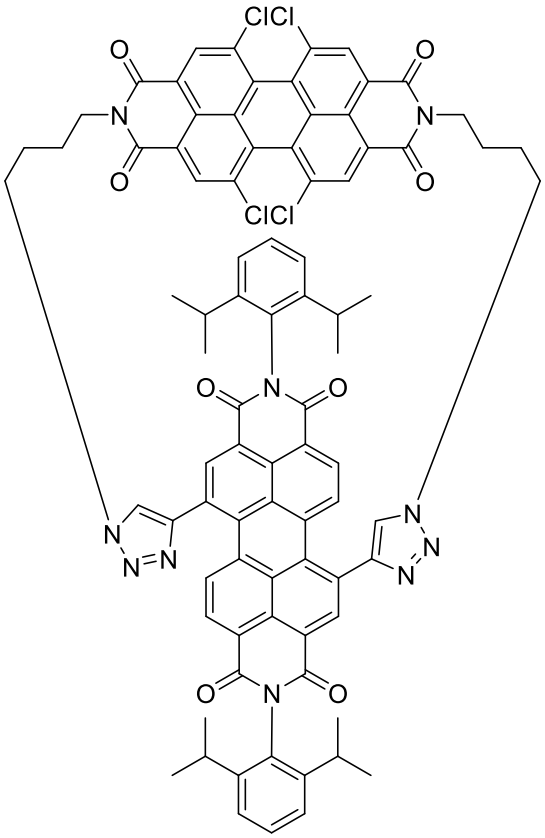

General Procedure B was followed with PDI(alkyne) **23** (105 mg, 0.138 mmol, 1 eq), PDI(azide) **61** (100 mg, 0.138 mmol, 1 eq), TBTA (30 mg, 0.4 eq), Cu(MeCN)$_4$–PF$_6$ (20 mg, 0.4 eq), CH_2Cl_2 (230 mL). Reaction was completed after 4 days and purified via flash column chromatography (SiO_2, 0.4:100 MeOH:CH_2Cl_2) to give macrocycle **63** as a red solid (8 mg, 4%).

^{1}H NMR (300 MHz, $CDCl_3$) δ 8.57 (s, 2H, Ar*H* ortho PDI), 8.47 (s, 2H, Ar*H* ortho PDI), 8.06 (d, *J* = 8.1 Hz, 2H, Ar*H* PDI), 7.93 (s, 2H, Ar*H* ortho PDI), 7.89 (s, 2H, C*H* trz), 7.54 (t, *J* = 7.7 Hz, 2H, Ar*H* linker), 7.44 (dd, *J* = 7.9, 1.6 Hz, 2H Ar*H* linker), 7.38 (d, *J* = 8.1 Hz, 2H, Ar*H* PDI), 7.34 (dd, *J* = 7.7, 1.6 Hz, 2H, Ar*H* linker), 4.64 (d, *J* = 13.8 Hz, 2H, CH_2), 4.43 (t, *J* = 12.5 Hz, 2H, CH_2), 4.14 (t, *J* = 13.1 Hz, 2H, CH_2), 3.95 (d, *J* = 13.4 Hz, 2H, CH_2), 3.64 (t, *J* = 6.6 Hz, 2H, CH_2), 3.03 (p, *J* = 6.9 Hz, 2H, C*H* ^{i}Pr), 2.75 – 2.62 (m, 2H, CH_2), 2.42 – 2.31 (m, 2H, CH_2), 1.59 (br s, 2H, CH_2), 1.46 (d, *J* = 6.8 Hz, 6H, CH_3), 1.33 (d, *J* = 6.9 Hz, 6H, CH_3), 1.17 (d, *J* = 6.8 Hz, 6H, CH_3), 1.09 (d, *J* = 6.9 Hz, 6H, CH_3).

^{13}C NMR (101 MHz, $CDCl_3$) δ 163.7, 163.6, 163.3, 162.1, 146.3, 146.0, 145.7, 134.9, 134.5, 133.9, 133.1, 132.7, 132.5, 131.3, 130.7, 130.6, 130.2, 129.8, 129.2, 129.0, 128.7, 128.2, 127.8, 124.7, 124.4, 124.2, 124.1, 123.9, 123.4, 122.6, 122.0, 52.2, 40.7, 32.1, 29.9, 29.5, 29.3, 29.2, 24.8, 24.1, 22.8, 14.3.

MS (MALDI): *m/z* calc. for $C_{84}H_{62}Cl_4N_{10}O_8$ [M]+: 1478.3506; found 1478.3911.

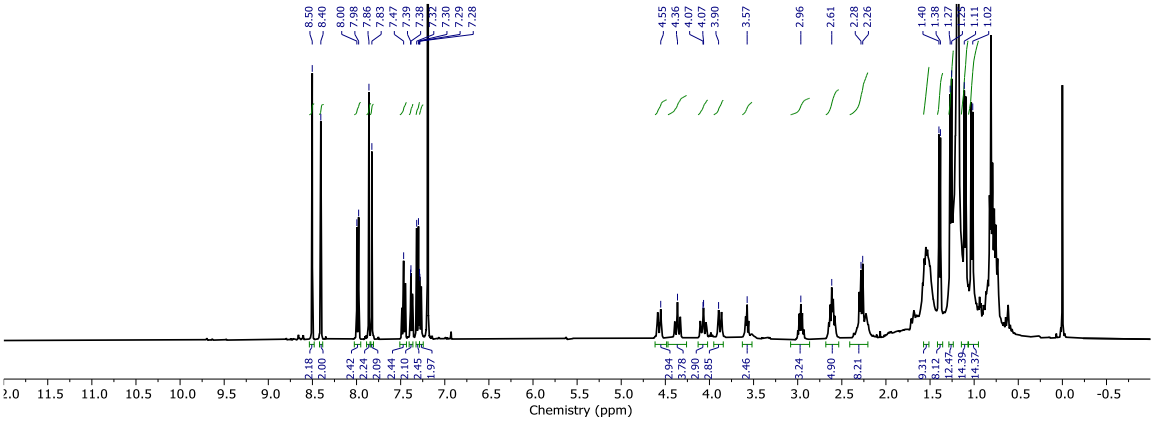

Figure 5.4.6 ^{1}H NMR spectrum of **62** ($CDCl_3$, 298 K, 400 MHz).

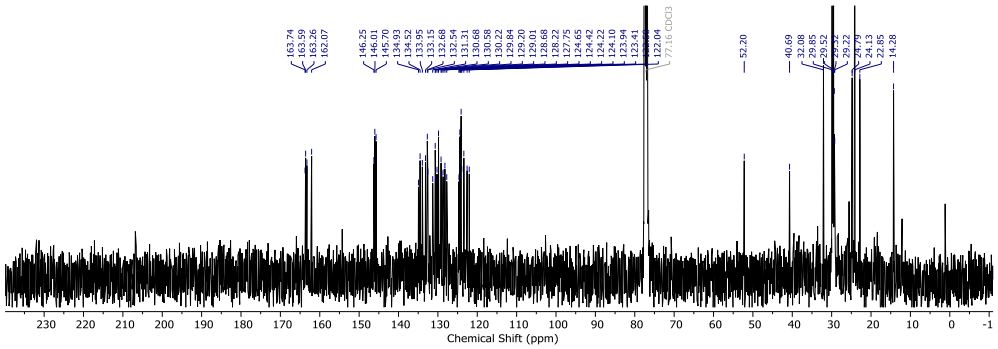

Figure 5.4.7. ^{13}C NMR spectrum of **62** ($CDCl_3$, 298 K, 101 MHz).

Pyrrolidine PDI 60

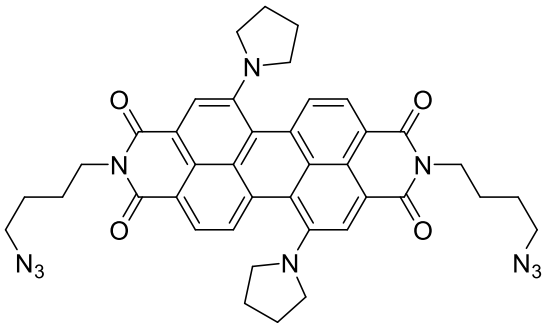

$PDApy_2$ (50 mg, 0.094 mmol, 1 eq) was stirred together with azide **59** (54 mg, 0.471 mmol, 5 eq) in toluene (3 mL) for 4 days at 115° C. Upon cooling, the crude reaction mixture was directly purified by via flash column chromatography (SiO_2, 0.4:100 MeOH:CH_2Cl_2) to give **60** as a green solid (8 mg, 4%).

^{1}H NMR (400 MHz, $CDCl_3$) δ 8.49 (s, 2H, Ar*H* PDI), 8.44 (d, *J* = 8.1 Hz, 2H, Ar*H* PDI), 7.72 (d, *J* = 8.0 Hz, 2H, Ar*H* PDI), 4.28 (t, *J* = 7.2 Hz, 4H), 3.76 (s, 4H), 3.37 (t, *J* = 6.9 Hz, 4H), 2.85 (s, 4H), 2.05 (d, *J* = 35.9 Hz, 12H), 1.88 (p, *J* = 7.2 Hz, 4H), 1.75 (p, *J* = 6.9 Hz, 4H).

Pillar(1,4-Bis(4-azidobutoxy)[1]-dimethyl[4])arene 63

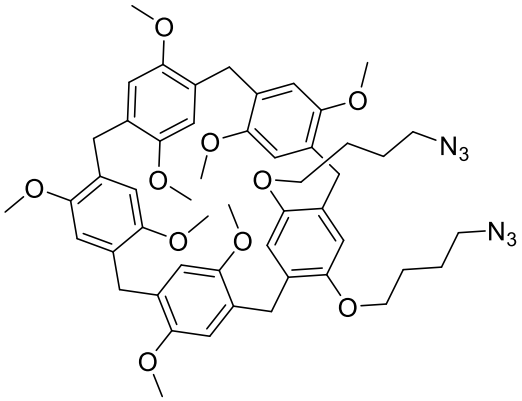

General Procedure B was followed with dibromo **62** (200 mg, 0.201 mmol, 1 eq) and NaN_3 (33 mg, 0.504 mmol, 2.5 eq) in DMF (10 mL) to yield a sticky clear and colourless oil which solidified into a white solid upon standing **63** (185 mg, quant.).

^{1}H NMR ($CDCl_3$, 400 MHz) δ 6.81 (2H, s, Ar*H*), 6.79 (2H, s, Ar*H*), 6.78 (2H, s, Ar*H*), 6.76 (2H, s, Ar*H*), 6.71 (2H, s, Ar*H*), 3.82 (4H, t, *J* = 6.1 Hz, CH_2), 3.79 – 3.74 (10H, m,

OCH_3, CH_2), 3.68 (12H, app s, J = 0.8 Hz, OCH_3), 3.65 (6H, s, OCH_3), 3.64 (6H, s, OCH_3), 3.03 (4H, dt, J = 7.2, 4.5 Hz, CH_2), 1.66 (4H, app q, J = 6.9 Hz, CH_2).

Pillar[5]arene PDI macrocycle 64

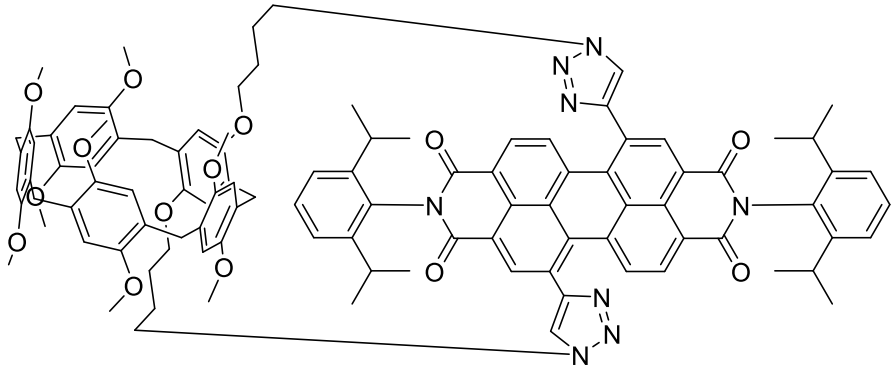

General Procedure B was followed with dialkynyl **23** (184 mg, 0.242 mmol, 1 eq), pillar[5]arene **63** (222 mg, 0.242 mmol, 1 eq), CH_2Cl_2 (500 mL), TBTA (51 mg, 0.097 mmol, 0.4 eq) and Cu(MeCN)$_4$-PF_6 (36 mg, 0.097 mmol, 0.4 eq). Reaction was completed after 4 days and purified by flash column chromatography (SiO_2, 0.4:100 MeOH:CH_2Cl_2) to give an macrocycle 64 a purple solid (102 mg, 25%).

^{1}H NMR ($CDCl_3$, 400 MHz) 8.87 (2H, s, ArH PDI), 8.42 (2H, d, J = 8.0 Hz, ArH bay), 8.36 (2H, d, J = 8.0 Hz, ArH ortho), 8.30 (2H, s, ArH triazole), 7.49 (3H, t, J = 7.8 Hz, iPr$_2$-ArH), 7.38 (2H, dd, J = 7.8, 1.5 Hz, iPr$_2$-ArH), 7.33 (3H, dd, J = 7.8, 1.5 Hz, iPr$_2$-ArH), 6.74 (2H, s, ArH pillararene), 6.71 (2H, s, ArH pillararene), 6.61 (2H, s, ArH pillararene), 6.36 (2H, s, ArH pillararene), 6.23 (2H, s, ArH pillararene), 4.73 (2H, ddd, J = 14.1, 8.1, 2.8 Hz, O(CH$_2$)$_3$CH_AH$_B$N), 4.42 (2H, ddd, J = 14.1, 8.8, 2.6 Hz, O(CH$_2$)$_3$CH$_A$$H_B$N), 3.71 (4H, d, J = 11.8 Hz, ArCH_2Ar pillararene), 3.70 (2H, s, ArCH_2Ar pillararene), 3.65 (obscured, OCH_AH$_B$(CH$_2$)$_3$N), 3.64 (6H, s, OCH_3 pillararene), 3.63 (6H, s, OCH_3 pillararene), 3.49 (obscured, OCH$_A$$H_B$(CH$_2$)$_3$N), 3.46 (2H, d, J = 13.1 Hz, ArCH_2Ar pillararene), 3.41 (6H, s, OCH_3 pillararene), 3.38 (6H, s, OCH_3 pillararene), 3.23 (2H, d, J = 13.1 Hz, ArCH_2Ar pillararene), 2.97 (2H, app p, J = 6.9 Hz, CH iPr), 2.61 (2H, app p, J = 6.9 H, CH iPr), 2.30 – 2.18 (2H, m, OCH$_2$CH_AH$_B$ (CH$_2$)$_2$N), 2.08 – 1.95 (2H, m, OCH$_2$CH$_A$$H_B$ (CH$_2$)$_2$N), 1.69 (2H, dt, J = 13.4, 6.8 Hz, O(CH$_2$)$_2$CH_AH$_B$CH$_2$N), 1.55 (2H, dt, J = 13.4, 6.9 Hz, O(CH$_2$)$_2$CH$_A$$H_BCH_2$N), 1.34 (6H,

d, *J* = 6.8 Hz, CH(C*H*$_3$)$_2$ iPr), 1.30 (6H, d, *J* = 6.8 Hz, CH(C*H*$_3$)$_2$ iPr), 1.12 (6H, d, *J* = 6.8 Hz, CH(C*H*$_3$)$_2$ iPr), 1.10 (6H, d, *J* = 6.8 Hz, CH(C*H*$_3$)$_2$ iPr).

^{13}C NMR (101 MHz, $CDCl_3$) δ 163.71, 162.96, 150.93, 150.89, 150.82, 150.66, 150.09, 148.92, 147.31, 146.05, 145.50, 135.03, 134.53, 133.02, 130.80, 129.86, 129.82, 129.40, 128.93, 128.70, 128.47, 128.18, 127.72, 126.37, 124.39, 124.16, 122.87, 122.66, 122.51, 114.48, 113.76, 113.72, 113.57, 113.26, 65.94, 56.06, 55.95, 55.71, 55.51, 49.79, 29.87, 29.64, 29.49, 29.41, 29.30, 24.98, 24.92, 24.45, 24.29, 24.17, 24.01.

MS (MALDI): m/z calc. for $C_{103}H_{103}N_8O_{14}$ $[M+H]^+$: 1676.763; found 1676.189

***P*-2,2'-bis(3-bromopropoxy)-1,1'-binaphthalene[159] *P*-65-3**

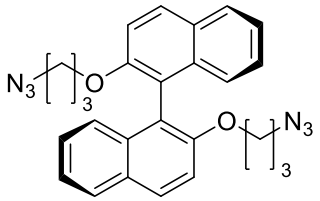

General procedure **A** was followed with ***P***-BINOL (1.00 g, 3.49 mmol, 1 eq), 1,3-dibromopropane (5.3 mL, 52.4 mmol, 15 eq), potassium carbonate (2.90 g, 21.0 mmol, 6 eq) in acetone (10 mL), to yield ***P*-65-3** as a colourless oil (0.945 g, 51%). The major side product was identified to be the [1+1] macrocyclic adduct. The dibromide ***P*-65-3** was further reacted to form the diazide ***P*-66-3** without further characterization.

***P*-2,2'-bis(4-bromobutoxy)-1,1'-binaphthalene[159] *P*-65-4**

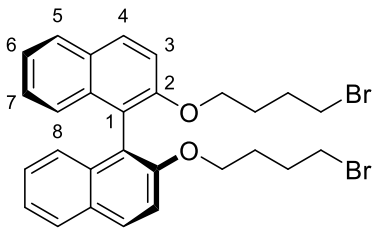

General procedure **A** was followed with ***P***-BINOL (1.00 g, 3.49 mmol, 1 eq), 1,4-dibromobutane (6.3 mL, 52.4 mmol, 15 eq), potassium carbonate (2.90 g, 21.0

mmol, 6 eq) in acetone (10 mL), to yield ***P*-65-4 a** as a colourless oil (0.702 g, 36%). The major side product was identified to be the [1+1] macrocyclic adduct. The dibromide ***P*-65-4** was further reacted to form the diazide ***P*-66-4** without further characterization.

^{1}H NMR (400 MHz, $CDCl_3$) δ 7.95 (d, *J* = 9.0 Hz, 2H, C(4)*H*), 7.87 (dd, *J* = 8.2, 1.0 Hz, 2H, C(5)*H*), 7.41 (d, *J* = 9.0 Hz, 2H, C(3)*H*), 7.33 (ddd, *J* = 8.2, 6.6, 1.0 Hz, 2H, C(6)*H*), 7.22 (ddd, *J* = 8.3, 6.6, 1.0 Hz, 2H, C(7)*H*), 7.16 (dd, *J* = 8.3, 1.0 Hz, 2H, C(8)*H*), 4.04 (ddd, *J* = 9.4, 6.5, 4.8 Hz, 2H, OCH_AH$_B$), 3.93 (ddd, *J* = 9.4, 6.9, 4.8 Hz, 2H, OCH$_A$$H_B$), 2.91 (td, *J* = 6.8, 2.4 Hz, 4H, BrCH_2), 1.64 – 1.48 (m, 4H, CH_2), 1.45 – 1.32 (m, 4H, CH_2).

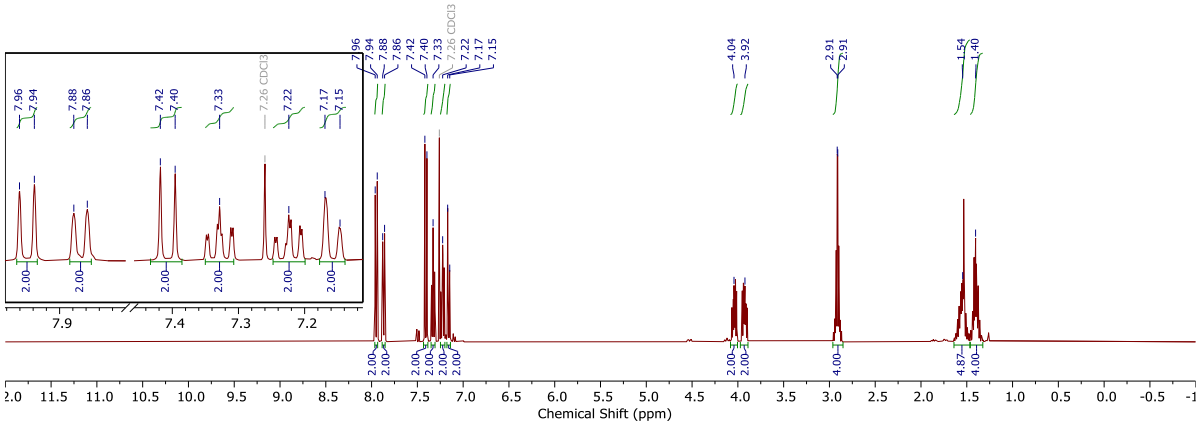

Figure 5.4.8. ^{1}H NMR spectrum of ***P*-65-4** ($CDCl_3$, 298 K, 400 MHz).

***P*-2,2'-bis((6-bromohexyl)oxy)-1,1'-binaphthalene[160] *P*-65-6**

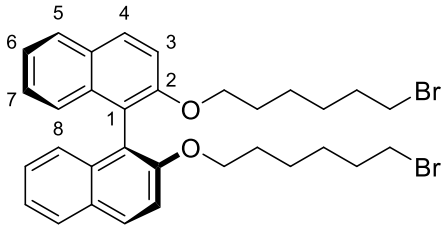

General procedure **A** was followed with ***P*-BINOL** (1.00 g, 3.49 mmol, 1 eq), 1,6-dibromohexane (8.1 mL, 52.4 mmol, 15 eq), potassium carbonate (2.90 g, 21.0 mmol, 6 eq) in acetone (10 mL), to yield ***P*-65-6** as a colourless oil (1.47g, 69%). The major side product was identified to be the [1+1] macrocyclic adduct.

The reaction was repeated with its enantiomer ***M***- to yield ***M*-65-6** with matching results and spectroscopic data.

^{1}H NMR (400 MHz, $CDCl_3$) δ = 7.94 (d, *J* = 8.9 Hz, 2H, C(4)*H*), 7.86 (dd, *J* = 8.3, 1.2 Hz, 2H, C(5)*H*), 7.41 (d, *J* = 8.9 Hz, 2H, C(3)*H*), 7.32 (ddd, *J* = 8.3, 6.5, 1.0 Hz, 2H, C(6)*H*), 7.21 (ddd, *J* = 8.2, 6.5, 1.2 Hz, 2H, C(7)*H*), 7.16 (ddd, *J* = 8.2, 1.0, 0.5 Hz, 2H, C(8)*H*), 4.08 – 3.94 (m, 2H, OCH_AH_B), 3.88 (ddd, *J* = 9.3, 7.1, 5.4 Hz, 2H, OCH_AH_B), 3.15 (t, *J* = 7.0 Hz, 4H, BrCH_2), 1.54 – 1.45 (m, 4H, CH_2), 1.45 – 1.32 (m, 4H, CH_2), 1.05 (dtt, *J* = 9.0, 6.8, 3.2 Hz, 4H, CH_2), 0.90 – 0.75 (m, 4H, CH_2).

Spectroscopic data is in agreement with literature.[160]

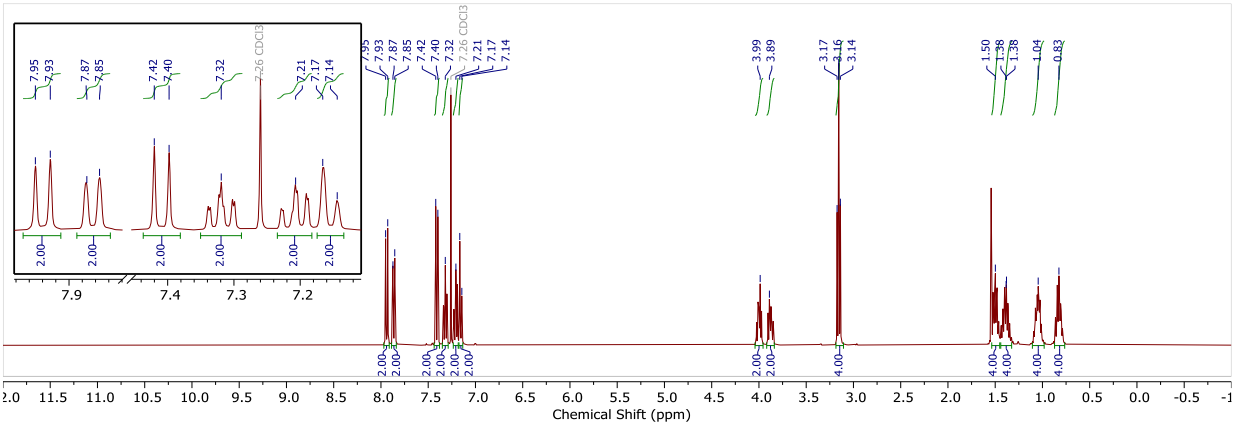

Figure 5.4.9. ^{1}H NMR spectrum of ***P*-65-6** ($CDCl_3$, 298 K, 400 MHz).

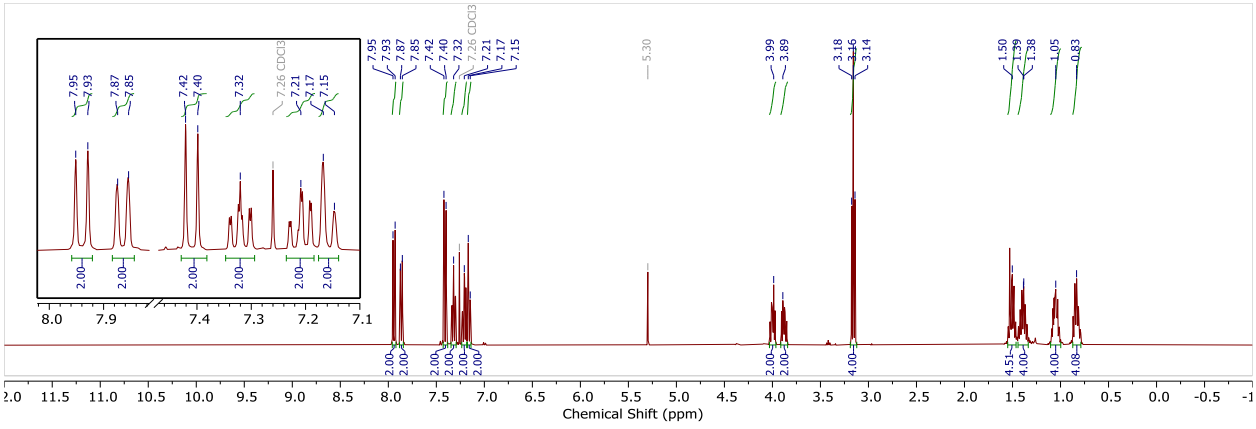

Figure 5.4.10. ^{1}H NMR spectrum of ***M*-65-6** ($CDCl_3$, 298 K, 400 MHz).

P-2,2'-bis(3-azidopropoxy)-1,1'-binaphthalene *P*-66-3

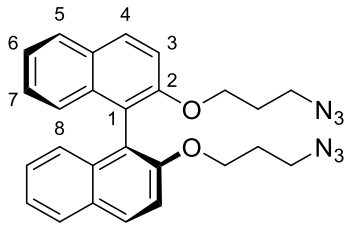

General procedure **B** was followed with dibromo ***P*-65-3** (680 mg, 1.22 mmol, 1 eq) and NaN_3 (200 mg, 3.06 mmol, 2.5 eq) in DMF (10 mL) to yield ***P*-66-3** as a yellow oil that solidified into a cream white solid (575 mg, 97%).

1H NMR (300 MHz, $CDCl_3$) δ 8.02 – 7.93 (m, 2H), 7.88 (dt, *J* = 8.3, 1.0 Hz, 2H), 7.41 (d, *J* = 9.0 Hz, 2H), 7.35 (ddd, *J* = 8.1, 6.6, 1.5 Hz, 2H), 7.29 – 7.22 (m, 3H), 7.18 (ddt, *J* = 8.4, 1.5, 0.8 Hz, 2H), 4.07 (ddd, *J* = 9.5, 6.2, 4.8 Hz, 2H), 3.96 (ddd, *J* = 9.5, 6.9, 4.8 Hz, 2H), 2.81 – 2.60 (m, 4H), 1.63 (qt, *J* = 6.2, 4.8 Hz, 4H).

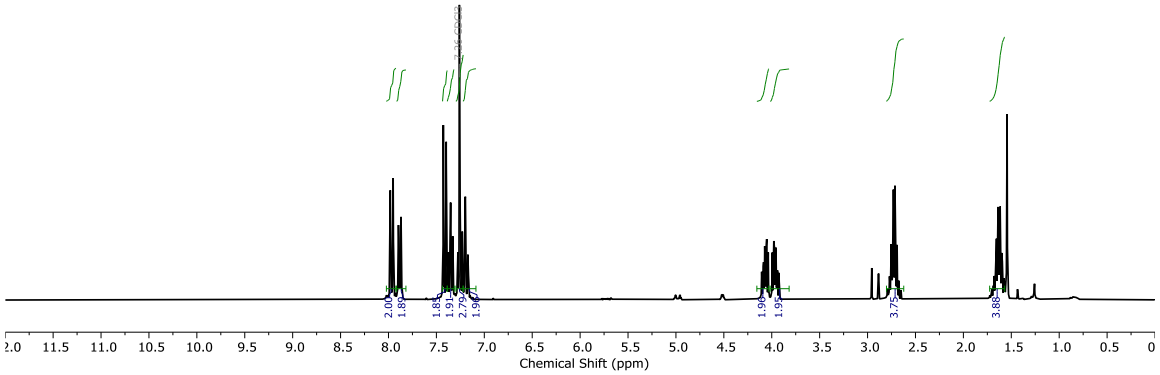

Figure 5.4.11. ^{1}H NMR spectrum of ***P*-204-3** ($CDCl_3$, 298 K, 400 MHz).

P-2,2'-bis(4-azidobutoxy)-1,1'-binaphthalene *P*-66-4

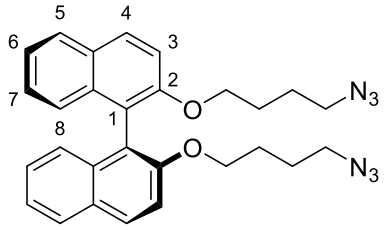

General procedure **B** was followed with dibromo ***P*-200-4** (680 mg, 1.22 mmol, 1 eq) and NaN_3 (200 mg, 3.06 mmol, 2.5 eq) in DMF (10 mL) to yield ***P*-204-4** as a yellow oil that solidified into a cream white solid (575 mg, 97%).

^{1}H NMR (400 MHz, $CDCl_3$) δ 7.96 (d, *J* = 9.0 Hz, 2H, C(4)*H*), 7.88 (d, *J* = 8.0 Hz, 2H, C(5)*H*), 7.41 (d, *J* = 9.0 Hz, 2H, C(3)*H*), 7.34 (ddd, *J* = 8.0, 6.5, 1.3 Hz, 2H, C(6)*H*), 7.23 (ddd, *J* = 8.1, 6.6, 1.3 Hz, 2H, C(7)*H*), 7.17 (dd, *J* = 8.1, 1.3 Hz, 2H, C(8)*H*), 4.02 (ddd, *J* = 9.3, 6.6, 4.9 Hz, 2H, OCH_AH_B), 3.91 (ddd, *J* = 9.4, 7.0, 4.8 Hz, 2H, OCH_AH_B), 2.74 (app td, *J* = 7.0, 3.3 Hz, 4H, N_3CH_2), 1.46 (ttd, *J* = 14.2, 7.0, 4.9 Hz, 4H, CH_2), 1.18 – 1.07 (m, 4H, CH_2).

^{13}C NMR (101 MHz, $CDCl_3$) δ 154.4, 134.2, 129.5, 129.5, 128.1, 126.4, 125.5, 123.8, 120.9, 115.9, 69.3, 50.8, 26.5, 25.5.

MS (ASAP): m/z calc. for $C_{28}H_{28}N_6O_2$ $[M]^+$: 480.2274; found 480.2283.

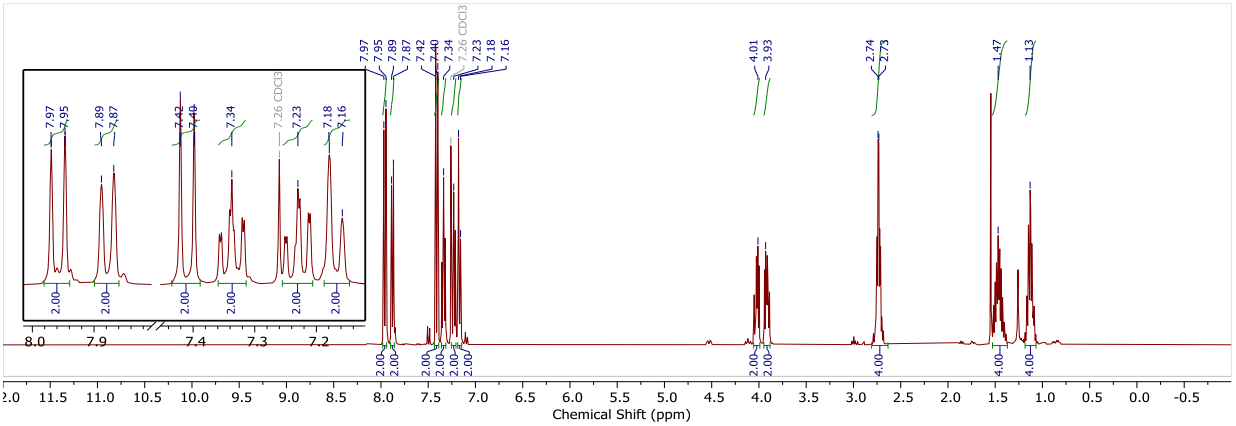

Figure 5.4.12. ^{1}H NMR spectrum of ***P*-66-4** ($CDCl_3$, 298 K, 400 MHz).

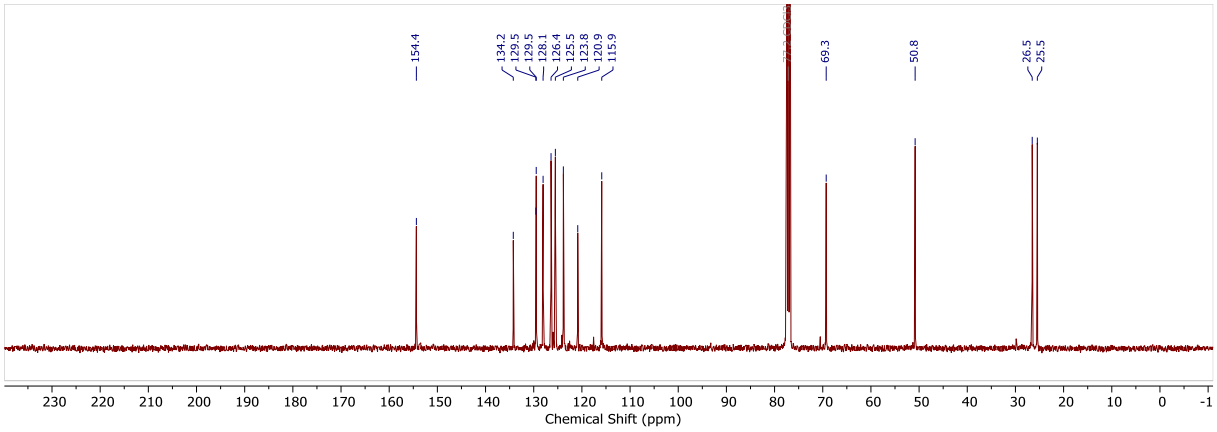

Figure 5.4.13. ^{13}C NMR spectrum of ***P*-66-4** ($CDCl_3$, 298 K, 101 MHz).

***P*-2,2'-bis((6-azidohexyl)oxy)-1,1'-binaphthalene *P*-66-6**

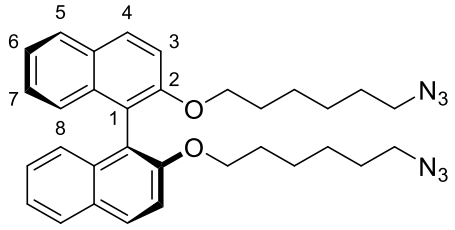

General procedure **B** was followed with dibromo ***P*-65-6** (1.47 g, 2.40 mmol, 1 eq) and NaN_3 (390 mg, 6.00 mmol, 2.5 eq) in DMF (20 mL) to yield ***P*-66-6** as a yellow oil (1.29 g, quant.).

The reaction was repeated with its enantiomer ***M*-65-6** to yield ***M*-66-6** with near identical results and spectroscopic data.

^{1}H NMR (400 MHz, $CDCl_3$) δ 7.94 (d, *J* = 8.9 Hz, 2H, C(4)*H*), 7.86 (dd, *J* = 8.3, 1.1 Hz, 2H, C(5)*H*), 7.41 (d, *J* = 8.9 Hz, 2H, C(3)*H*), 7.32 (ddd, *J* = 8.3, 6.5, 1.4 Hz, 2H, C(6)*H*), 7.21 (ddd, *J* = 8.1, 6.5, 1.1 Hz, 2H, C(7)*H*), 7.16 (dd, *J* = 8.1, 1.4 Hz, 2H, C(8)*H*), 4.00 (dt, *J* = 9.3, 5.8 Hz, 2H, OCH_AH$_B$), 3.88 (ddd, *J* = 9.3, 7.0, 5.5 Hz, 2H, OCH$_A$$H_B$), 3.00 (t, *J* = 7.1 Hz, 4H, N_3CH_2), 1.45 – 1.32 (m, 4H, OCH_2CH_2), 1.31 – 1.19 (m, 4H, NCH_2CH_2), 0.99 (dddd, *J* = 13.5, 11.3, 6.8, 2.4 Hz, 4H, $N(CH_2)_2$CH_2), 0.90 – 0.77 (m, 4H, $O(CH_2)_2$CH_2).

^{13}C NMR (101 MHz, $CDCl_3$) δ 154.6, 134.3, 129.5, 129.2, 128.0, 126.2, 125.6, 123.7, 121.0, 116.1, 69.7, 51.3, 29.3, 28.6, 26.2, 25.3.

MS (ASAP): m/z calc. for $C_{32}H_{37}N_6O_2$ $[M+H]^+$: 537.2978; found 537.2974

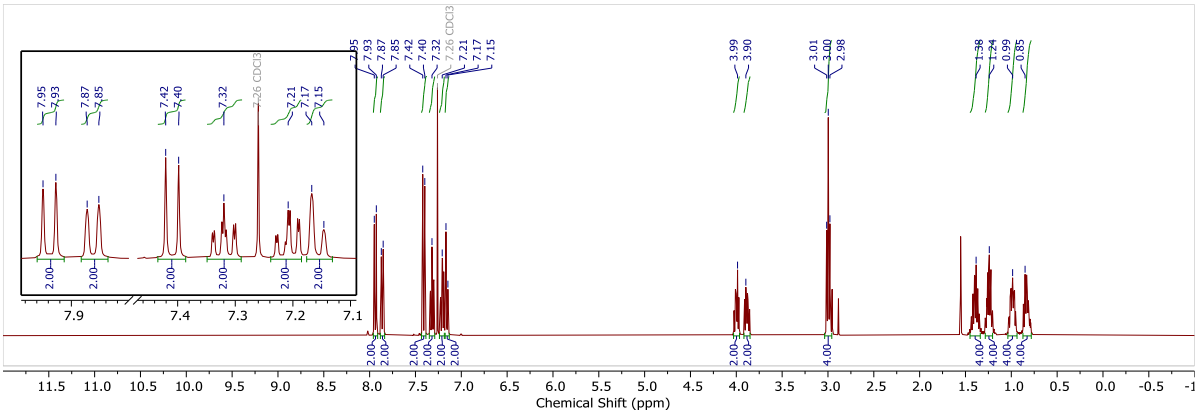

Figure 5.4.14. ^{1}H NMR spectrum of ***P*-66-6** ($CDCl_3$, 298 K, 400 MHz).

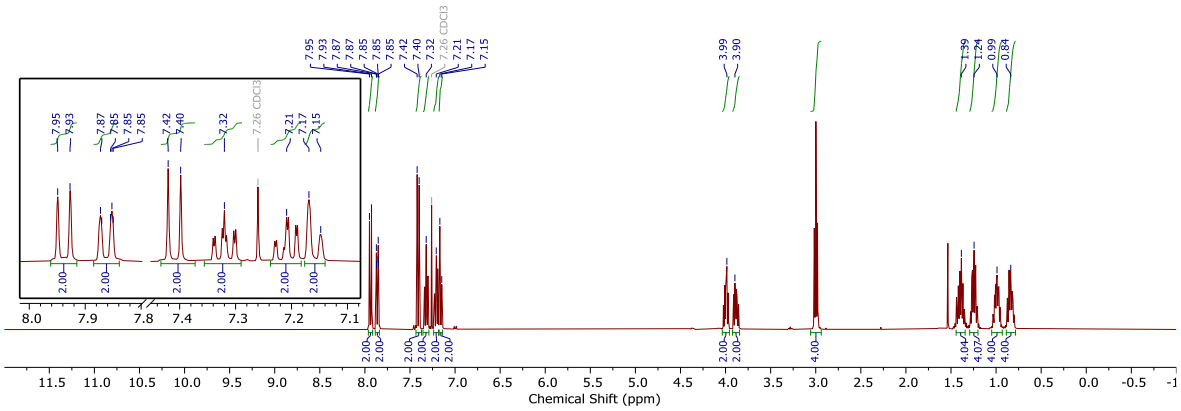

Figure 5.4.15. ^{1}H NMR spectrum of ***M*-66-6** ($CDCl_3$, 298 K, 400 MHz).

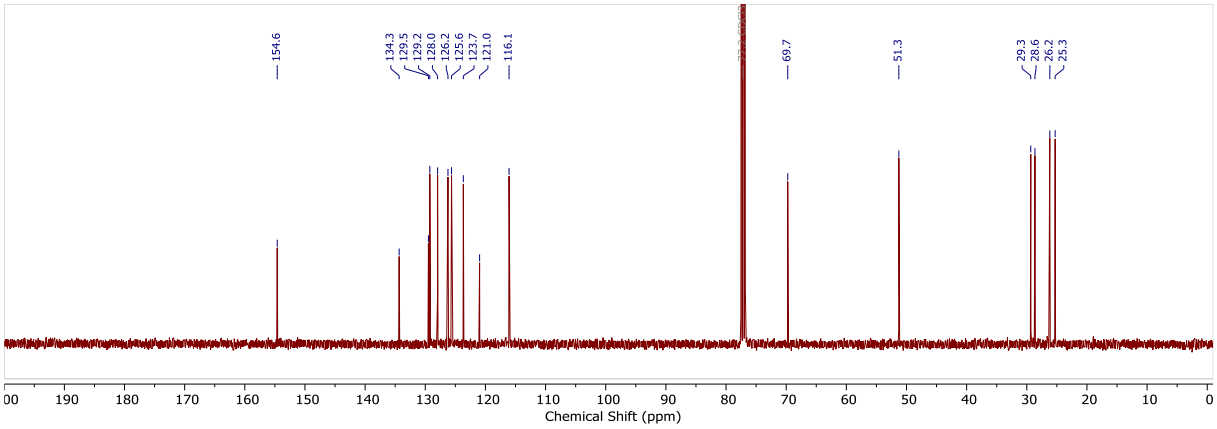

Figure 5.4.16. ^{13}C NMR spectrum of ***P*-66-6** ($CDCl_3$, 298 K, 101 MHz).

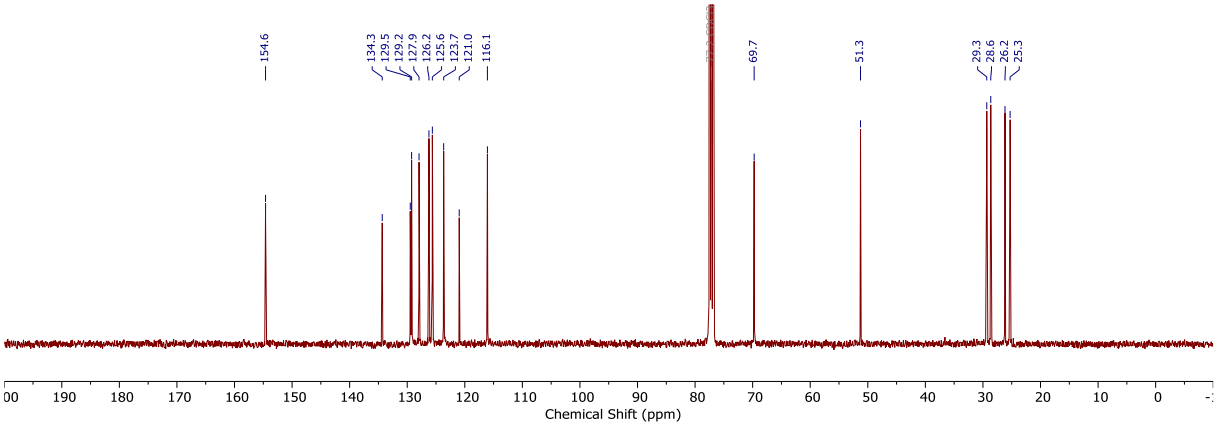

Figure 5.4.17. ^{13}C NMR spectrum of ***M*-66-6** ($CDCl_3$, 298 K, 101 MHz).

***P*-2,2'-bis((8-azidooctyl)oxy)-1,1'-binaphthalene *P*-66-8**

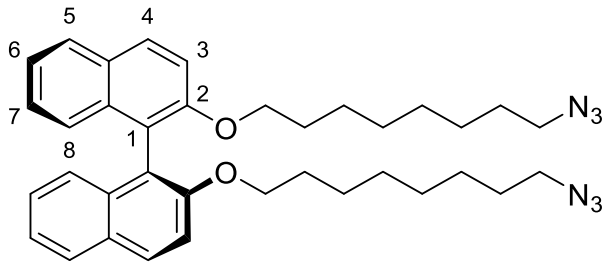

General procedure **A** was followed with ***P***-BINOL (1.00 g, 3.49 mmol, 1 eq), 1,8-dibromooctane (9.7 mL, 52.4 mmol, 15 eq), potassium carbonate (2.90 g, 21.0 mmol, 6 eq) in acetone (10 mL), to yield ***P*-65-8** as a colourless oil (2.00 g, 86%). The major side product was identified to be the [1+1] macrocyclic adduct.

General procedure **B** was followed with dibromo ***P*-65-8** (2.00 g, 2.99 mmol, 1 eq) and NaN_3 (486 mg, 7.48 mmol, 2.5 eq) in DMF (30 mL) to yield ***P*-66-8** as a yellow oil (1.77 g, quant.).

^{1}H NMR (400 MHz, $CDCl_3$) δ 7.92 (d, *J* = 9.0 Hz, 2H, C(4)*H*), 7.85 (dd, *J* = 8.2, 1.3 Hz, 2H, C(5)*H*), 7.40 (d, *J* = 9.0 Hz, 2H, C(3)*H*), 7.30 (ddd, *J* = 8.2, 6.6, 1.4 Hz, 2H, C(6)*H*), 7.20 (ddd, *J* = 8.2, 6.6, 1.3 Hz, 2H, C(7)*H*), 7.15 (dd, *J* = 8.2, 1.4 Hz, 2H, C(8)*H*), 3.97 (dt, *J* = 9.3, 6.2 Hz, 2H, OCH_AH$_B$), 3.89 (dt, *J* = 9.3, 6.4 Hz, 2H, OCH$_A$$H_B$), 3.21 (t, *J* = 7.0 Hz, 4H, N_3CH_2), 1.55 – 1.47 (m, 4H, NCH$_2$CH_2), 1.44 – 1.32 (m, 4H, OCH$_2$CH_2),

1.22 – 1.12 (m, 4H, $N(CH_2)_2CH_2$), 1.10 – 0.92 (m, 8H, CH_2), 0.89 (ddd, *J* = 14.2, 7.9, 4.4 Hz, 4H, $O(CH_2)_2CH_2$).

^{13}C NMR (101 MHz, $CDCl_3$) δ 154.7, 134.4, 129.4, 129.2, 127.9, 126.2, 125.7, 123.5, 120.9, 116.0, 69.9, 51.6, 29.5, 29.0, 28.9, 26.6, 25.6.

MS (ASAP): m/z calc. for $C_{36}H_{44}N_6O_2$ $[M+H]^+$: 593.3604; found 593.3614

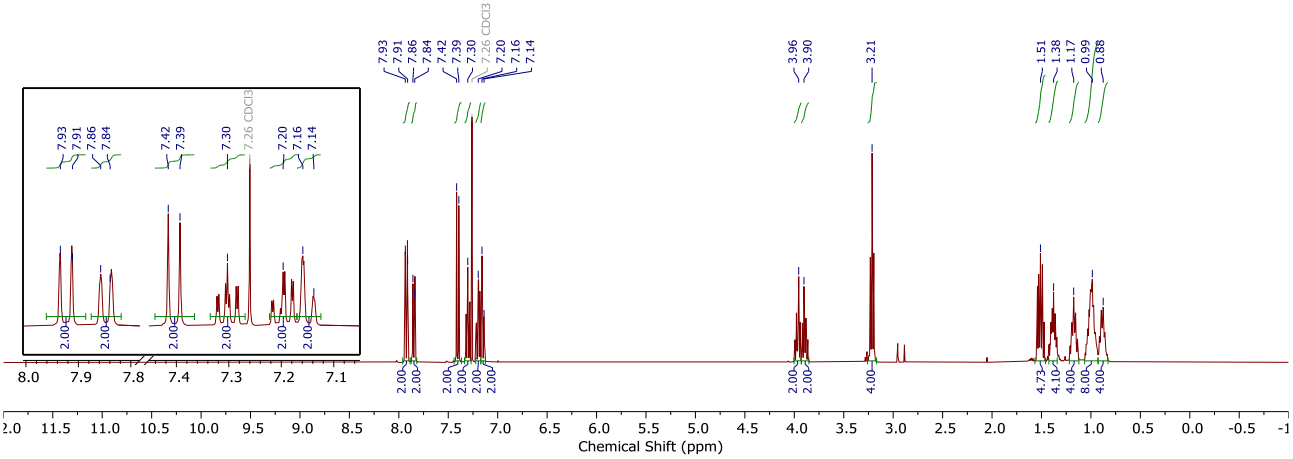

Figure 5.4.18. ^1H NMR spectrum of ***P*-66-8** ($CDCl_3$, 298 K, 400 MHz).

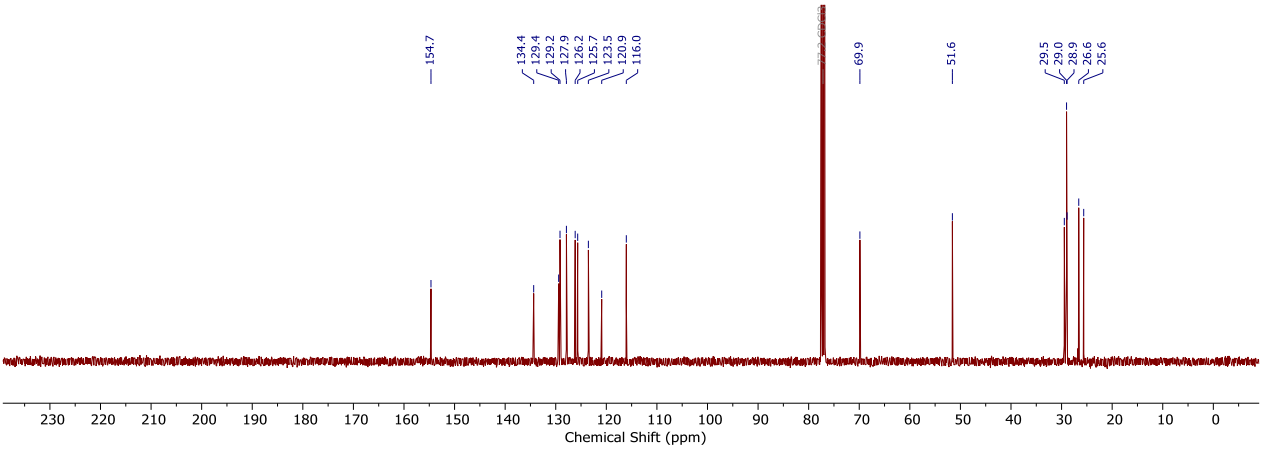

Figure 5.4.19. ^{13}C NMR spectrum of ***P*-66-8** ($CDCl_3$, 298 K, 101 MHz).

***P*-BINOL butyl PDI macrocycle 67-4**

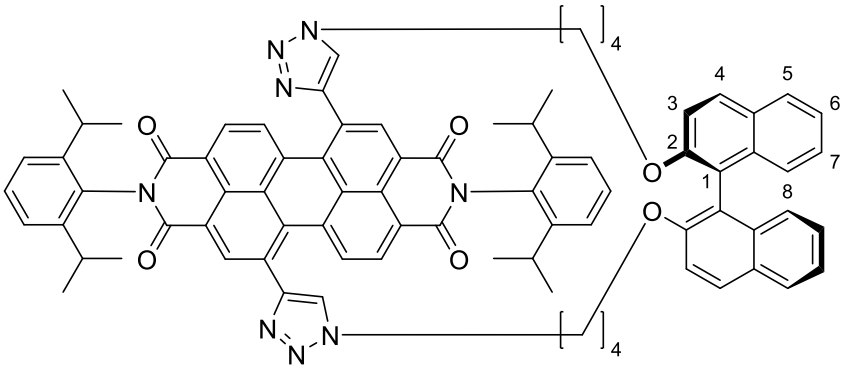

The general procedure above followed with PDI bisalkyne **23** (100 mg, 0.132 mmol, 1 eq), ***P***-2,2'-bis((4-azidobutyl)oxy)-1,1'-binaphthalene **66-4** (63.3 mg, 0.132 mmol, 1 eq), CH_2Cl_2 (600 mL), THPTA (23 mg, 52.7 µmol, 0.4 eq) and $Cu(MeCN)_4{\cdot}PF_6$ (20 mg, 52.7 µmol, 0.4 eq). The reaction was completed after six days and purified by flash column chromatography (SiO_2, 0.4:100 à 0.6:100 MeOH:CH_2Cl_2), then by preparative TLC (SiO_2, 1:100 MeOH:CH_2Cl_2) to give the two diastereomers of the macrocycle ***PM*-67-4** and ***PP*-67-4** as purple solids (2.0 mg, 2%; 2.0 mg, 2%).

Diastereomer 1, ***PM*-67-4**:

^{1}H NMR (500 MHz, $CDCl_3$) δ 9.36 (s, 2H, Ar*H* Ortho PDI), 8.65 (d, *J* = 8.0 Hz, 2H, Ar*H* Ortho PDI), 8.48 (d, *J* = 8.0 Hz, 2H, Ar*H* Bay PDI), 7.55 – 7.48 (m, 4H, iPr_2-Ar*H*, C(5)*H*), 7.36 (app ddd, *J* = 11.8, 7.8, 1.4 Hz, 4H, iPr_2-Ar*H*), 7.30 – 7.26 (obs m, 2H, C(6)*H*), 7.24 (s, 2H, C*H* triazole), 7.18 (ddd, *J* = 8.4, 6.8, 1.3 Hz, 2H, C(7)*H*), 7.10 (d, *J* = 9.0 Hz, 2H, C(4)*H*), 7.07 (dd, *J* = 8.4, 1.1 Hz, 2H, C(8)*H*), 6.77 (d, *J* = 9.0 Hz, 2H, C(3)*H*), 4.54 (ddd, *J* = 13.9, 7.9, 3.5 Hz, 2H, NCH_AH_B), 3.83 (ddd, *J* = 13.9, 7.5, 3.1 Hz, 2H, NCH_AH_B), 3.73 (ddd, *J* = 9.7, 7.7, 3.6 Hz, 2H, OCH_AH_B), 3.52 – 3.41 (m, 2H, OCH_AH_B), 2.81 (dh, *J* = 13.7, 6.8 Hz, 4H, C*H* iPr), 1.22 (d, *J* = 6.9 Hz, 6H, CH(CH_3)$_2$ iPr), 1.21 (d, *J* = 6.9 Hz, 6H, CH(CH_3)$_2$ iPr), 1.19 (d, *J* = 6.9 Hz, 6H, CH(CH_3)$_2$ iPr), 1.12 (d, *J* = 6.9 Hz, 6H, CH(CH_3)$_2$ iPr), 1.39 – 0.98 (m, 4H, CH_2).

^{13}C NMR (126 MHz, $CDCl_3$) δ 163.5, 163.0, 153.8, 147.2, 145.8, 145.4, 134.8, 134.4, 133.7, 132.5, 130.4, 129.8, 128.9, 128.6, 127.5, 126.5, 125.4, 124.3, 124.2, 124.1, 123.2, 122.8, 122.3, 120.3, 115.5, 69.2, 50.5, 29.7, 29.4, 29.3, 26.1, 24.1, 24.1, 24.0, 24.0.

MS (ESI): m/z calc. for $C_{80}H_{71}N_8O_6$ $[M+H]^+$: 1239.5497; found 1239.5510

Diastereomer 2, ***PP*-67-4**:

^{1}H NMR (500 MHz, $CDCl_3$) δ 9.17 (s, 2H, Ar*H* Ortho PDI), 8.43 (d, *J* = 8.0 Hz, 2H, Ar*H* Ortho PDI), 8.38 (d, *J* = 8.0 Hz, 2H, Ar*H* Bay PDI), 7.69 (dd, *J* = 8.1, 1.4 Hz, 2H, C(5)*H*), 7.64 (d, *J* = 9.0 Hz, 2H, C(4)*H*), 7.51 (t, *J* = 7.8 Hz, 2H, iPr_2-Ar*H*), 7.36 (app ddd, *J* = 7.8, 4.4, 1.4 Hz, 4H, iPr_2-Ar*H*), 7.29 – 7.23 (obs m, 2H, C(6)*H*), 7.18 (ddd, *J* = 8.4, 6.7, 1.4 Hz, 2H, C(7)*H*), 7.15 (s, 2H, C*H* triazole), 7.06 (dd, *J* = 8.4, 1.1 Hz, 2H, C(8)*H*), 7.01 (d, *J* = 9.0 Hz, 2H, C(3)*H*), 4.50 (dt, *J* = 14.2, 4.7 Hz, 2H, NCH_AH_B), 4.12 (ddd, *J* = 14.2, 10.6, 3.6 Hz, 2H, NCH_AH_B), 3.84 (td, *J* = 9.5, 5.3 Hz, 2H, OCH_AH_B), 3.54 (ddd, *J* = 9.5, 8.4, 6.6 Hz, 2H, OCH_AH_B), 2.82 – 2.70 (m, 4H, C*H* iPr), 1.64 – 1.57 (obs m, 2H, $NCH_2CH_AH_B$), 1.52 – 1.43 (obs m, 2H, $NCH_2CH_AH_B$), 1.21 (d, *J* = 6.8 Hz, 6H, $CH(CH_3)_2$ iPr), 1.19 (d, *J* = 6.8 Hz, 6H, $CH(CH_3)_2$ iPr), 1.18 (d, *J* = 6.8 Hz, 6H, $CH(CH_3)_2$ iPr), 1.17 (d, *J* = 6.8 Hz, 6H, $CH(CH_3)_2$ iPr), 1.24 – 1.08 (m, 4H, OCH_2CH_2).

^{13}C NMR (126 MHz, $CDCl_3$) δ 163.6, 163.2, 153.9, 147.3, 145.9, 145.5, 134.9, 134.5, 133.8, 132.7, 130.6, 130.0, 129.1, 128.7, 127.6, 126.7, 125.6, 124.4, 124.3, 124.3, 123.3, 122.9, 122.4, 120.5, 115.6, 69.4, 50.6, 29.9, 29.5, 29.4, 26.3, 24.3, 24.2, 24.2, 24.1.

MS (ESI): m/z calc. for $C_{80}H_{71}N_8O_6$ $[M+H]^+$: 1239.5497; found 1239.5508

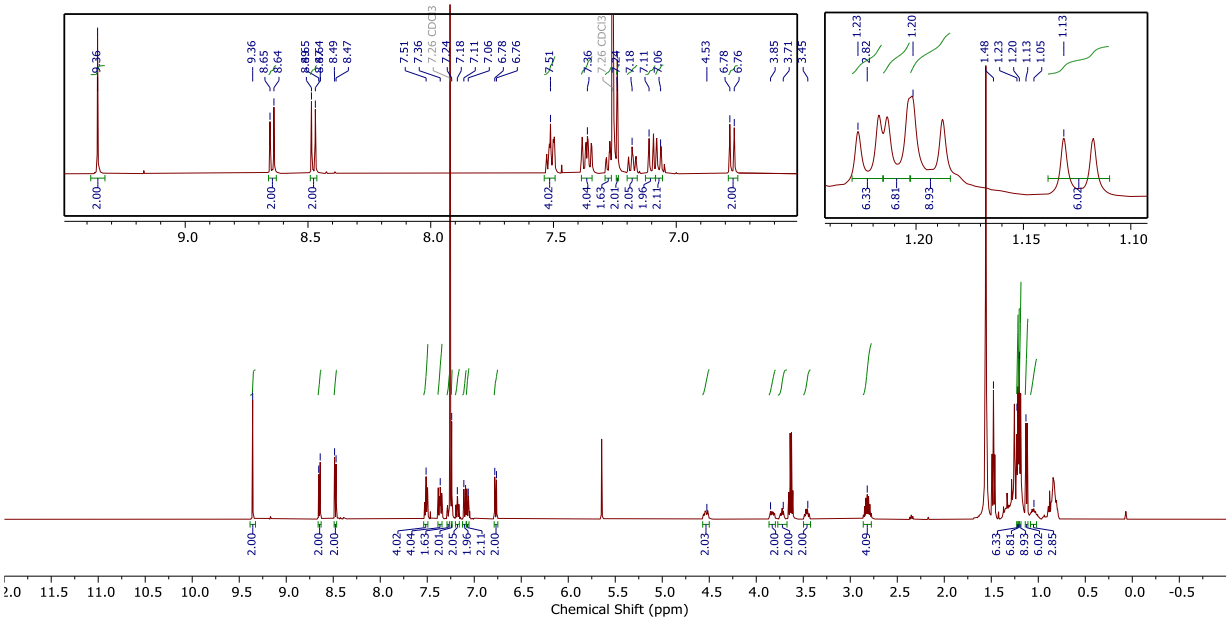

Figure 5.4.20. ^{1}H NMR spectrum of ***PM*-67-4** ($CDCl_3$, 298 K, 500 MHz).

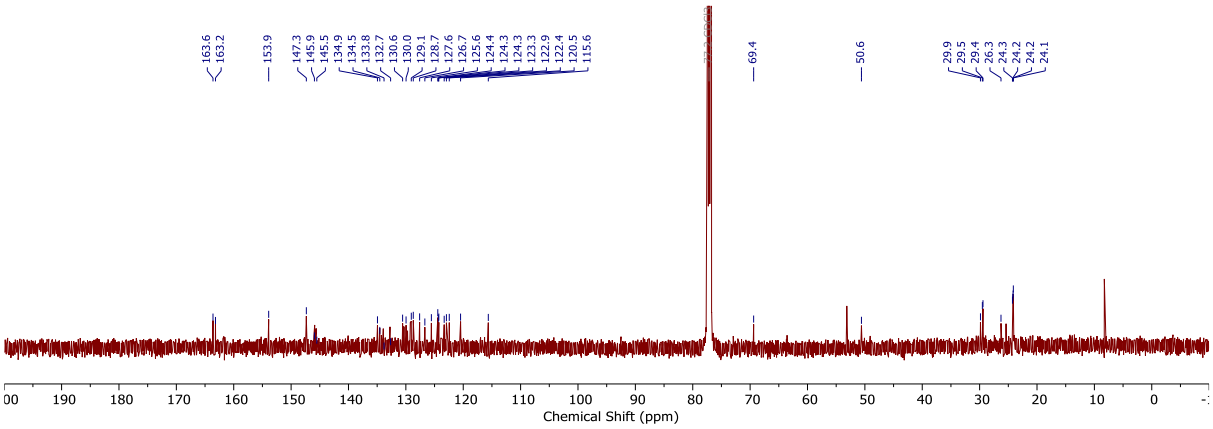

Figure 5.4.21. ^{13}C NMR spectrum of ***PM*-67-4** ($CDCl_3$, 298 K, 126 MHz).

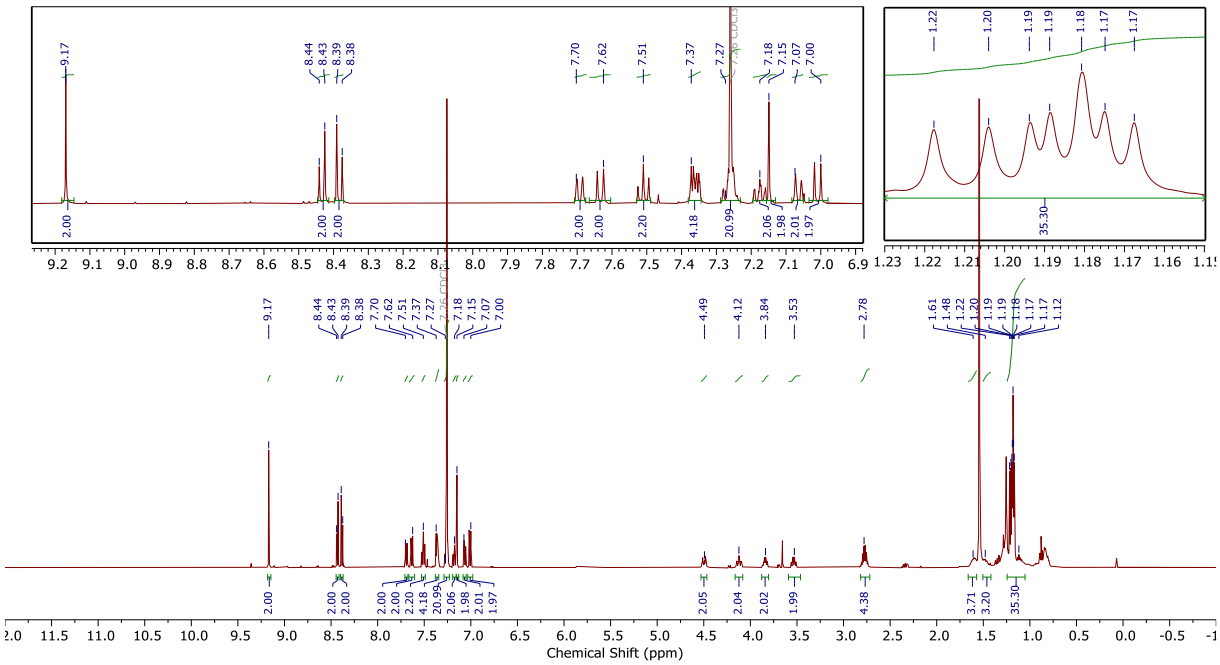

Figure 5.4.22. ^{1}H NMR spectrum of ***PP*-67-4** ($CDCl_3$, 298 K, 500 MHz).

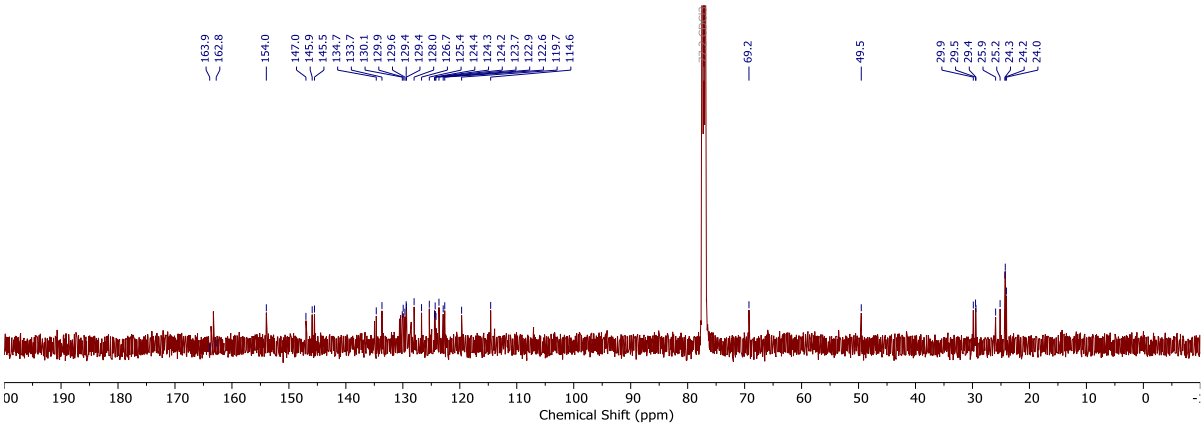

Figure 5.4.23. ^{13}C NMR spectrum of ***PP*-67-4** ($CDCl_3$, 298 K, 126 MHz).

***P*-BINOL hexyl PDI macrocycle 67-6**

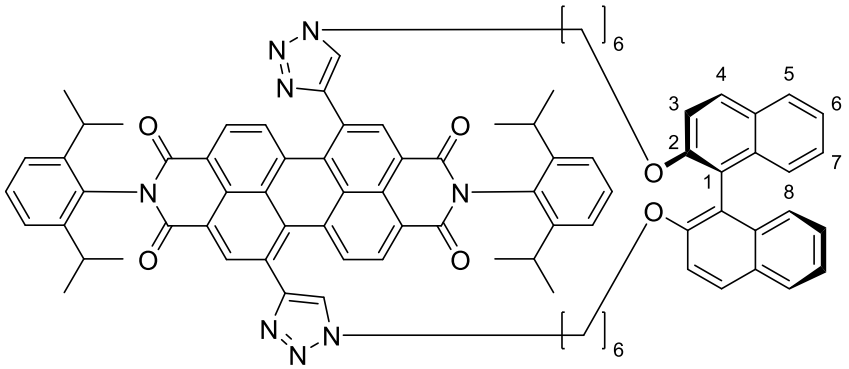

The general procedure above was followed with PDI bisalkyne **23** (113 mg, 0.149 mmol, 1 eq), ***P***-2,2'-bis((6-azidohexyl)oxy)-1,1'-binaphthalene ***P*-66-6** (80.0 mg, 0.149 mmol, 1 eq), CH_2Cl_2 (680 mL), TBTA (31 mg, 59.6 µmol, 0.4 eq) and $Cu(MeCN)_4{\cdot}PF_6$ (22 mg, 59.6 µmol, 0.4 eq). The reaction was completed after four days and purified by flash column chromatography (SiO_2, 0.5:100 MeOH:CH_2Cl_2) to give two diastereomers of macrocycle ***PM*-67-6** and ***PP*-67-6** as purple solids. Diastereomer 1 ***PM*-67-6** did not require any further purification (54.0 mg, 42%), whilst diastereomer 2 ***PP*-67-6** was further purified by preparative TLC (SiO_2, 1:100 MeOH:CH_2Cl_2) (isolated 4.3 mg, 3.3%, calculated yield from crude NMR 11%). The ratio of diastereomers 1 and 2 are calculated to be 4:1 by ^{1}H NMR spectroscopy of the crude product (see Section 3.4).

The reaction was repeated with its enantiomer ***M*-66-6** to yield ***MP*-67-6** and ***MM*-67-6** with near identical results and spectroscopic data (excluding CD and chiral HPLC).

Diastereomer 1 ***PM*-67-6**:

^{1}H NMR (400 MHz, $CDCl_3$) δ 9.14 (s, 2H, Ar*H* Ortho PDI), 8.55 (d, *J* = 8.1 Hz, 2H, Ar*H* Ortho PDI), 8.47 (d, *J* = 8.1 Hz, 2H, Ar*H* Bay PDI), 7.49 (t, *J* = 7.8 Hz, 2H, iPr_2-Ar*H*), 7.41 – 7.34 (m, 4H, iPr_2-Ar*H*, C(5)*H*), 7.29 (dd, *J* = 7.8, 1.4 Hz, 2H, iPr_2-Ar*H*), 7.26 – 7.22 (m, 2H, C(6)*H*), 7.21 (s, 2H, C*H* triazole), 7.15 (ddd, *J* = 8.3, 6.7, 1.4 Hz, 2H, C(7)*H*), 7.00 (dd, *J* = 8.3, 1.2 Hz, 2H, C(8)*H*), 6.95 (d, *J* = 9.0 Hz, 2H, C(4)*H*), 6.79 (d, *J* = 9.0 Hz, 2H, C(3)*H*), 4.53 (ddd, *J* = 13.6, 6.1, 4.1 Hz, 2H, NCH_AH$_B$), 3.78 (ddd, *J* = 13.6, 9.6, 3.5 Hz, 2H, NCH$_A$$H_B$), 3.74 – 3.68 (m, 2H, OCH_AH$_B$), 3.58 – 3.46 (m, 2H,

OCH_AH_B), 2.79 (p, *J* = 6.8 Hz, 2H, C*H* iPr_A), 2.62 (p, *J* = 6.8 Hz, 2H, C*H* iPr_B), 1.99 – 1.71 (m, 2H, $NCH_2CH_AH_B$), 1.50 (obs dq, *J* = 6.6, 3.0 Hz, 2H, $NCH_2CH_AH_B$), 1.20 (app t, *J* = 6.8 Hz, 12H, $CH(CH_3)_2$ iPr_A), 1.02 (d, *J* = 6.8 Hz, 6H, $CH(CH_3)_2$ iPr_B), 0.96 (d, *J* = 6.8 Hz, 6H, $CH(CH_3)_2$ iPr_B) 1.30 – 0.57 (obs m, 12H, CH_2).

^{13}C NMR (101 MHz, $CDCl_3$) δ 163.5, 163.2, 154.0, 146.9, 145.9, 145.5, 135.9, 135.0, 134.0, 133.3, 130.6, 130.4, 130.2, 129.9, 129.6, 129.5, 129.1, 128.9, 128.3, 127.3, 126.3, 125.6, 124.4, 124.2, 124.0, 123.2, 123.1, 122.3, 120.4, 115.0, 69.1, 49.7, 29.8, 29.4, 28.8, 28.6, 24.6, 24.2, 24.2, 24.1, 24.0.

MS (ESI): m/z calc. for $C_{84}H_{79}N_8O_6$ $[M+H]^+$: 1295.6123; found 1295.6139

Diastereomer 2 ***PP*-67-6**:

^{1}H NMR (500 MHz, $CDCl_3$) δ 8.97 (s, 2H, Ar*H* Ortho PDI), 8.30 (d, *J* = 8.0 Hz, 2H, Ar*H* Ortho PDI), 7.88 (d, *J* = 8.0 Hz, 2H, Ar*H* Bay PDI), 7.71 (d, *J* = 8.1 Hz, 2H, C(5)*H*), 7.61 (d, *J* = 9.1 Hz, 2H, C(4)*H*), 7.51 (t, *J* = 7.8 Hz, 2H, iPr_2-Ar*H*), 7.37 (dd, *J* = 8.0, 1.4 Hz, 2H, iPr_2-Ar*H*), 7.34 (dd, *J* = 7.9, 1.4 Hz, 2H, iPr_2-Ar*H*), 7.29 (td, *J* = 8.1, 6.5, 1.3 Hz, 2H, C(6)*H*), 7.14 (td, *J* = 8.4, 6.5, 1.3 Hz, 2H, C(7)*H*), 6.92 (d, *J* = 8.4 Hz, 2H, C(8)*H*), 6.66 (d, *J* = 9.1 Hz, 2H, C(3)*H*), 5.87 (s, 2H, C*H* triazole), 4.28 (dt, *J* = 13.6, 3.9 Hz, 2H, NCH_AH_B), 3.10 (ddd, *J* = 10.5, 7.0, 2.9 Hz, 2H, OH_AH_B), 2.92 (ddd, *J* = 13.6, 11.5, 2.8 Hz, 2H, NCH_AH_B), 2.75 (p, *J* = 6.9 Hz, 2H, C*H* iPr), 2.67 (p, *J* = 6.8 Hz, 2H, C*H* iPr), 2.51 (ddd, *J* = 10.5, 8.4, 2.7 Hz, 2H, OH_AH_B), 1.89 – 1.69 (m, 2H, $NCH_2H_AH_B$), 1.38 – 1.27 (obs m, 2H, $NCH_2H_AH_B$), 1.24 (d, *J* = 6.8 Hz, 6H, $CH(CH_3)_2$ iPr), 1.19 (d, *J* = 6.8 Hz, 6H, $CH(CH_3)_2$ iPr), 1.15 (d, *J* = 6.8 Hz, 12H, $CH(CH_3)_2$ iPr), 1.20 – 1.07 (obs m, 2H, CH_2) 1.03 – 0.78 (obs m, 2H, CH_2), 0.39 (dt, *J* = 12.5, 4.6 Hz, 2H, CH_2), 0.34 – 0.25 (m, 2H, CH_2), 0.22 – 0.11 (m, 4H, CH_2).

^{13}C NMR (126 MHz, $CDCl_3$) δ 163.3, 163.2, 153.1, 146.7, 146.1, 145.0, 135.4, 135.3, 134.8, 133.7, 130.6, 130.5, 130.0, 130.0, 129.8, 129.5, 129.2, 129.1, 128.6, 128.0,

126.8, 125.4, 124.6, 124.3, 124.2, 124.1, 122.4, 122.3, 119.6, 113.6, 65.4, 47.1, 29.9, 29.7, 29.4, 28.6, 27.7, 24.2, 24.1, 24.1, 24.0, 22.6, 21.0.

MS (ESI): m/z calc. for $C_{84}H_{79}N_8O_6$ $[M+H]^+$: 1295.6123; found 1295.6139.

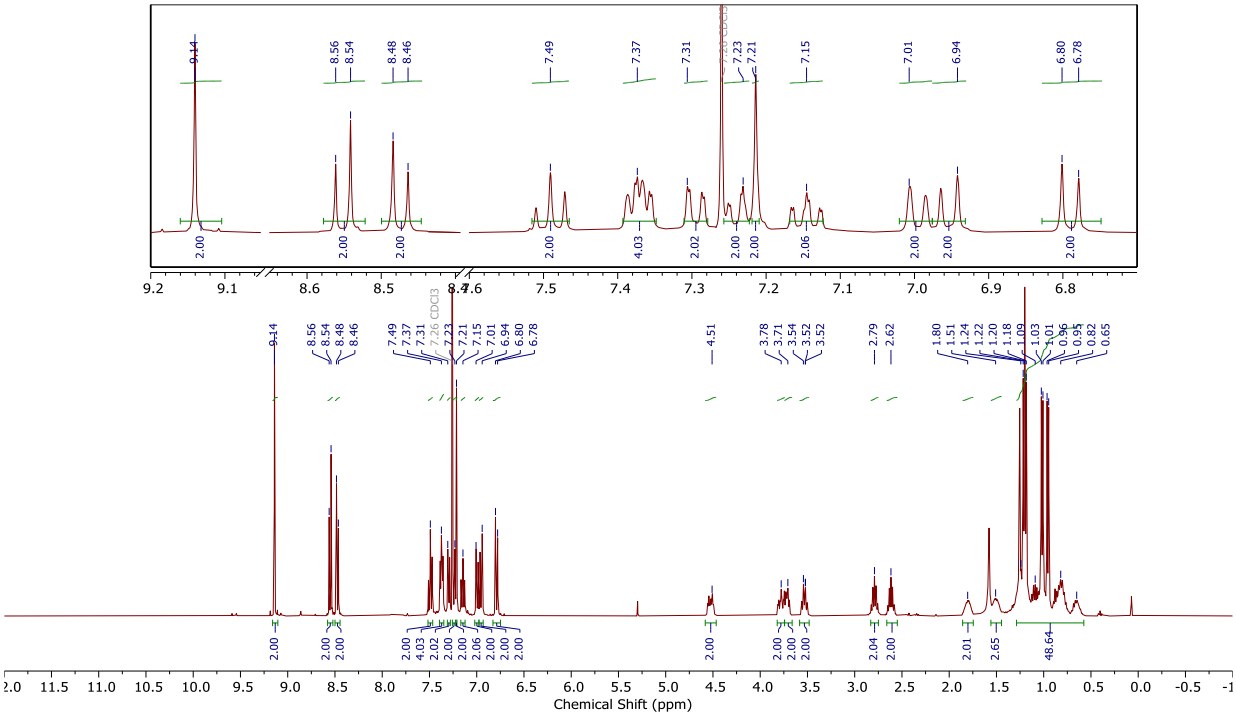

Figure 5.4.24. ^{1}H NMR spectrum of ***PM*-67-6** ($CDCl_3$, 298 K, 400 MHz).

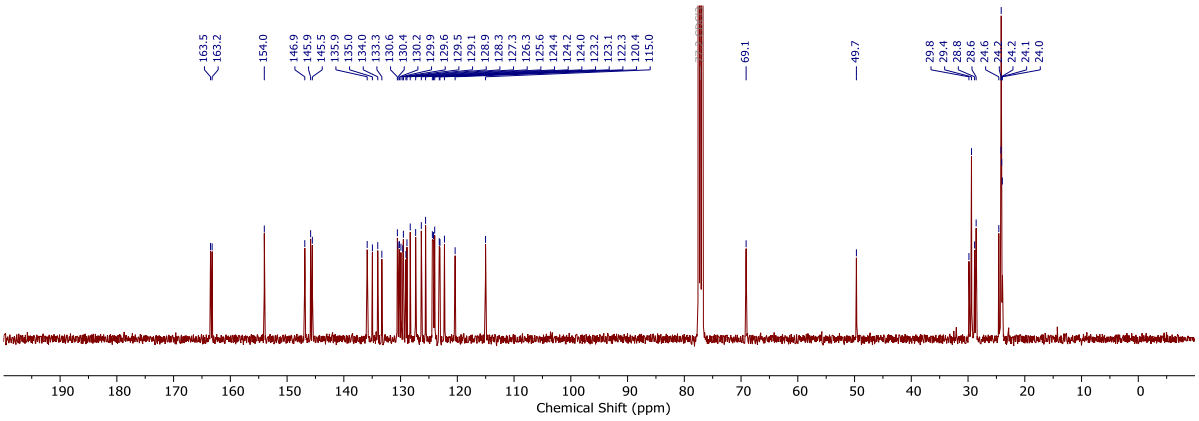

Figure 5.4.25. ^{13}C NMR spectrum of ***PM*-67-6** ($CDCl_3$, 298 K, 101 MHz).

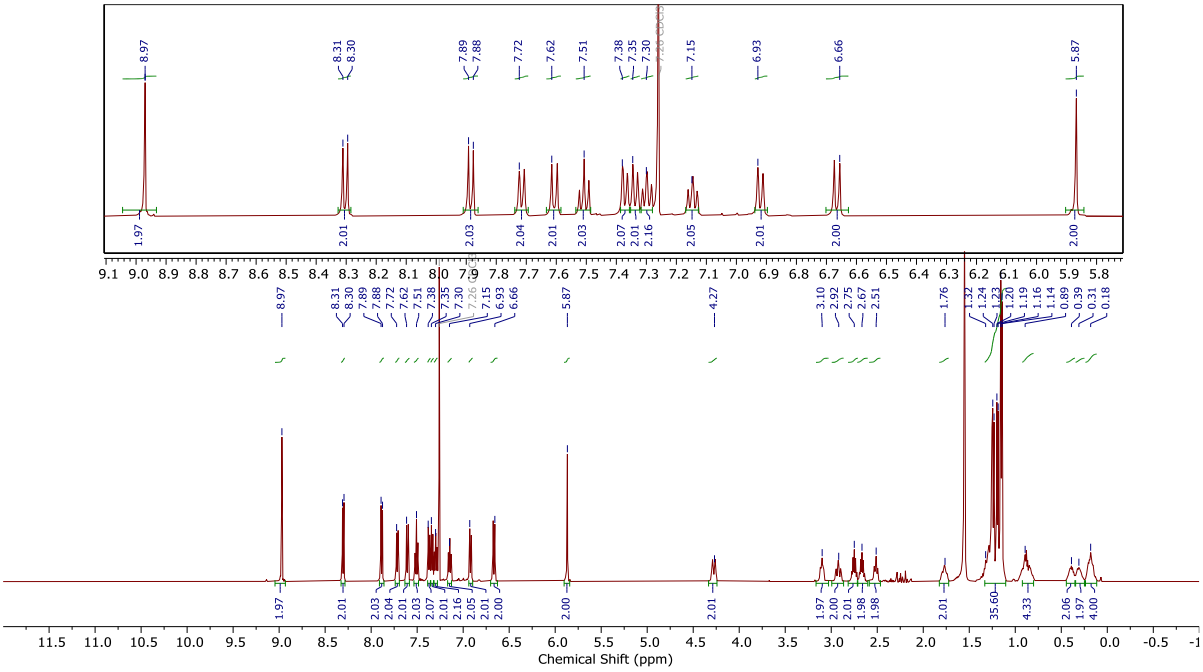

Figure 5.4.26. ^{1}H NMR spectrum of ***PP*-67-6** ($CDCl_3$, 298 K, 500 MHz).

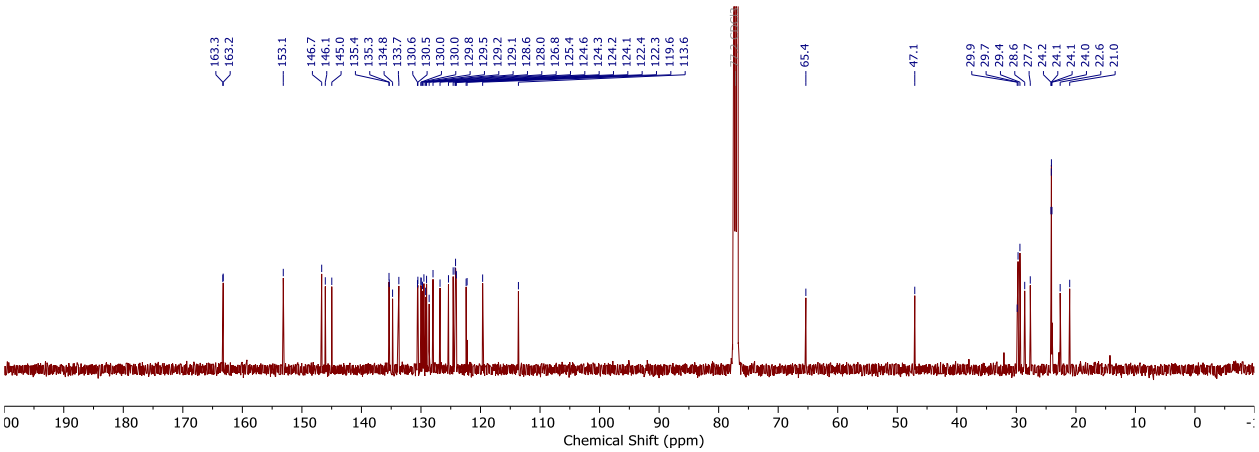

Figure 5.4.27. ^{13}C NMR spectrum of ***PP*-67-6** ($CDCl_3$, 298 K, 126 MHz).

***P*-BINOL octyl PDI macrocycle 67-8**

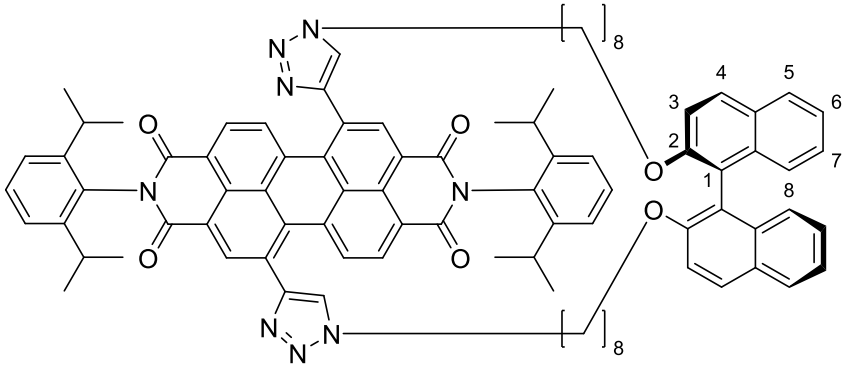

The general procedure above was followed with PDI bisalkyne **23** (150 mg, 198 µmol, 1 eq), ***P***-2,2'-bis((8-azidooctyl)oxy)-1,1'-binaphthalene ***P*-66-8** (117 mg, 198 µmol, 1 eq), CH_2Cl_2 (900 mL), TBTA (35 mg, 79 µmol, 0.4 eq) and $Cu(MeCN)_4 \cdot PF_6$ (30 mg, 79 µmol, 0.4 eq). The reaction was completed after four days and purified by flash column chromatography (SiO_2, 0.5:100 MeOH:CH_2Cl_2) to give a mixture of two diastereomers of macrocycle ***PM*-67-8** and ***PP*-67-8** (80 mg, 33%). This mixture was separated by preparative TLC (SiO_2, 1:100 MeOH:CH_2Cl_2), where despite appearing as a single band on TLC, extracting the top 10% and bottom 10% respectively gives the diastereomer of macrocycle ***PM*-67-8** (isolated 3.4 mg, 1.4%, calculated yield from mixture in NMR 17%) and ***PP*-67-8** (isolated 2.7 mg, 1.1%, calculated yield from mixture in NMR 17%) as purple solids. The ratio of diastereomers is calculated to be 1:1 by ^{1}H NMR spectroscopy of the crude product (see Section 3.4).

Diastereomer 1 ***PM*-67-8**:

^{1}H NMR (400 MHz, $CDCl_3$) δ 8.94 (s, 2H, Ar*H* Ortho PDI), 8.45 (d, *J* = 8.1 Hz, 2H, Ar*H* Ortho PDI), 8.26 (d, *J* = 8.1 Hz, 2H, Ar*H* Bay PDI), 7.63 (s, 2H, C*H* triazole), 7.52 (dd, *J* = 8.0, 1.1 Hz, 2H, C(5)*H*), 7.49 (t, *J* = 7.8 Hz, 2H, iPr_2-Ar*H*), 7.43 (d, *J* = 8.9 Hz, 2H, C(4)*H*), 7.35 (dd, *J* = 8.0, 1.4 Hz, 2H, iPr_2-ArH_AH_B), 7.31 (dd, *J* = 7.8, 1.4 Hz, 2H, iPr_2-ArH_AH_B), 7.20 (ddd, *J* = 8.1, 6.7, 1.2 Hz, 2H, C(6)*H*), 7.11 (ddd, *J* = 8.4, 6.7, 1.1 Hz, 2H, C(7)*H*), 7.01 (obs dd, *J* = 8.4 Hz, 1.2, 2H, C(8)*H*), 7.00 (d, *J* = 8.9 Hz, 2H, C(3)*H*), 4.54 (dt, *J* = 13.5, 5.5 Hz, 2H, NCH_AH_B), 4.39 (dt, *J* = 13.5, 6.5 Hz, 2H, NCH_AH_B), 3.71

– 3.61 (m, 2H, OH_AH_B), 3.55 (dt, *J* = 9.3, 6.4 Hz, 2H, OH_AH_B), 2.74 (h, *J* = 6.7 Hz, 2H, C*H* iPr_A), 2.60 (p, *J* = 6.7 Hz, 2H, C*H* iPr_B), 1.19 (d, *J* = 6.8 Hz, 6H, CH(CH_3)$_2$ iPr_A), 1.16 (d, *J* = 6.8 Hz, 6H, CH(CH_3)$_2$ iPr_A), 1.06 (d, *J* = 6.8 Hz, 6H, CH(CH_3)$_2$ iPr_B), 0.99 (d, *J* = 6.8 Hz, 6H, CH(CH_3)$_2$ iPr_B), 1.84 – 0.52 (obs m, 24H, CH_2).

^{13}C NMR (101 MHz, $CDCl_3$) δ 163.4, 163.3, 154.5, 147.4, 145.8, 145.7, 135.6, 135.2, 134.2, 133.8, 130.5, 130.5, 129.9, 129.9, 129.7, 129.6, 129.2, 129.0, 128.7, 127.5, 126.1, 125.7, 124.3, 124.2, 123.5, 123.0, 122.8, 122.2, 116.0, 50.6, 32.1, 29.8, 29.4, 29.2, 28.2, 27.7, 25.2, 25.0, 24.1, 24.0, 22.8.

MS (ESI): m/z calc. for $C_{88}H_{86}N_8O_6Na$ $[M+Na]^+$: 1373.6569; found 1373.6609

Diastereomer 2 ***PP*-67-8**:

^{1}H NMR (400 MHz, $CDCl_3$) δ 9.02 (s, 2H, Ar*H* Ortho PDI), 8.34 (d, *J* = 8.0 Hz, 2H, Ar*H* Ortho PDI), 8.19 (d, *J* = 8.0 Hz, 2H, Ar*H* Bay PDI), 7.73 (br d, *J* = 8.8 Hz, 4H, C(4)*H*, C(5)*H*), 7.50 (t, *J* = 8.2 Hz, 2H, iPr_2-Ar*H*), 7.41 (s, 2H, C*H* triazole), 7.38 – 7.31 (m, 4H, iPr_2-Ar*H*), 7.25 – 7.23 (obs ddd, *J* = 8.6, 6.7, 1.2 Hz, 2H, C(6)*H*), 7.14 (ddd, *J* = 8.3, 6.7, 1.3 Hz, 2H, C(7)*H*), 7.10 (d, *J* = 9.1 Hz, 2H, C(3)*H*), 7.03 (dd, *J* = 8.3, 1.2 Hz, 2H, C(8)*H*), 4.45 (dt, *J* = 13.3, 6.4 Hz, 2H, NCH_AH_B), 4.36 (dt, *J* = 13.3, 6.1 Hz, 2H, NCH_AH_B), 3.56 (dt, *J* = 9.5, 6.5 Hz, 2H, OCH_AH_B), 3.50 (dt, *J* = 9.5, 6.5 Hz, 2H, OCH_AH_B), 2.81 – 2.66 (m, 4H, C*H* iPr_A), 1.86 – 1.70 (m, 4H, , OCH_2H_2), 1.18 (d, *J* = 6.9 Hz, 6H, CH(CH_3)$_2$ iPr), 1.18 (d, *J* = 7.1 Hz, 6H, CH(CH_3)$_2$ iPr), 1.16 (d, *J* = 7.1 Hz, 6H, CH(CH_3)$_2$ iPr), 1.14 (d, *J* = 6.9 Hz, 6H, CH(CH_3)$_2$ iPr), 1.68 – 0.52 (obs m, 20H, CH_2)

^{13}C NMR (101 MHz, $CDCl_3$) δ 163.2, 163.1, 154.1, 147.2, 145.6, 145.5, 135.4, 135.0, 134.0, 133.8, 130.3, 129.8, 129.7, 129.7, 129.5, 129.4, 129.3, 129.2, 128.9, 128.8, 127.6, 126.1, 125.5, 124.3, 124.0, 123.6, 122.7, 122.6, 121.9, 120.6, 119.8, 115.6, 50.1, 31.9, 29.2, 29.2, 29.1, 28.2, 27.4, 25.1, 24.8, 24.1, 24.0.

MS (ESI): m/z calc. for $C_{88}H_{86}N_8O_6Na$ $[M+Na]^+$: 1373.6569; found 1373.6609

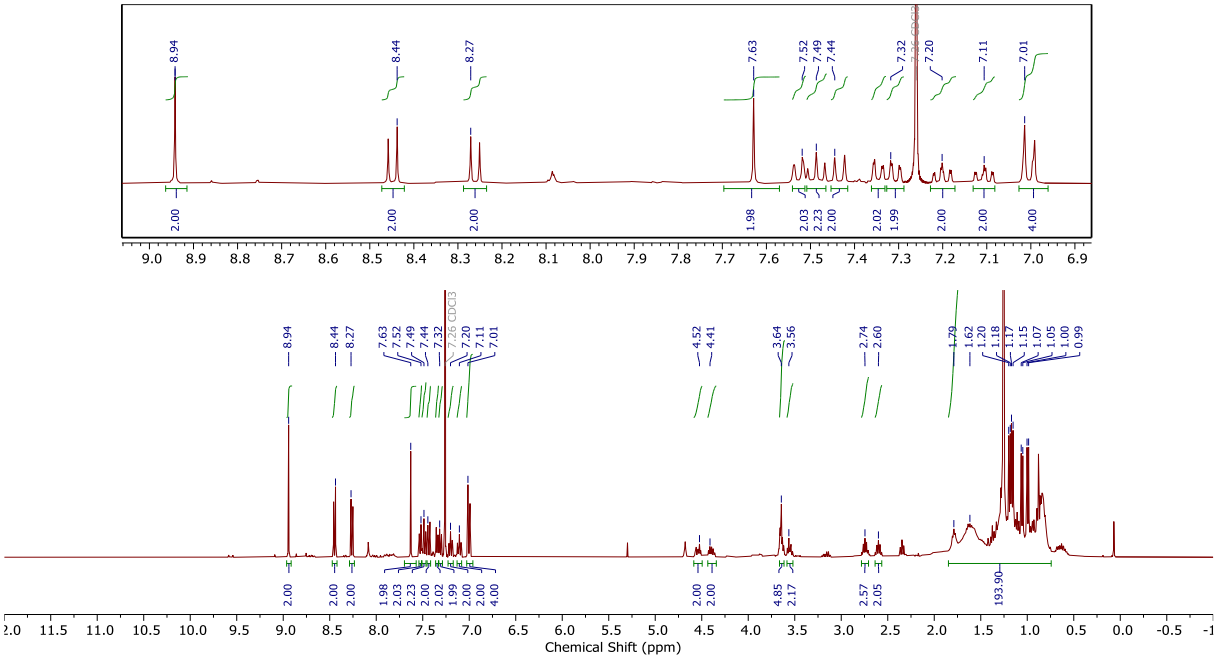

Figure 5.4.28. ^{1}H NMR spectrum of ***PM*-67-8** ($CDCl_3$, 298 K, 400 MHz).

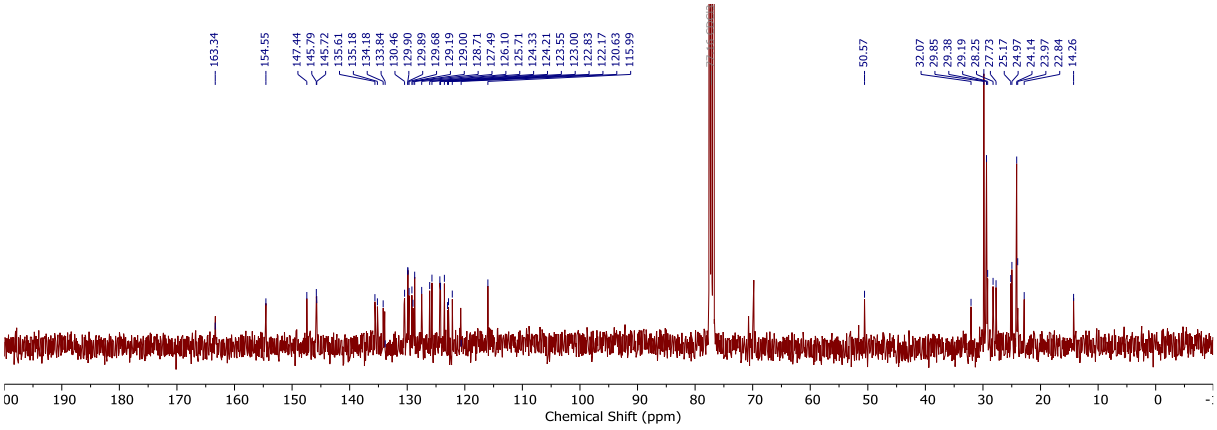

Figure 5.4.29. ^{13}C NMR spectrum of ***PM*-67-8** ($CDCl_3$, 298 K, 101 MHz).

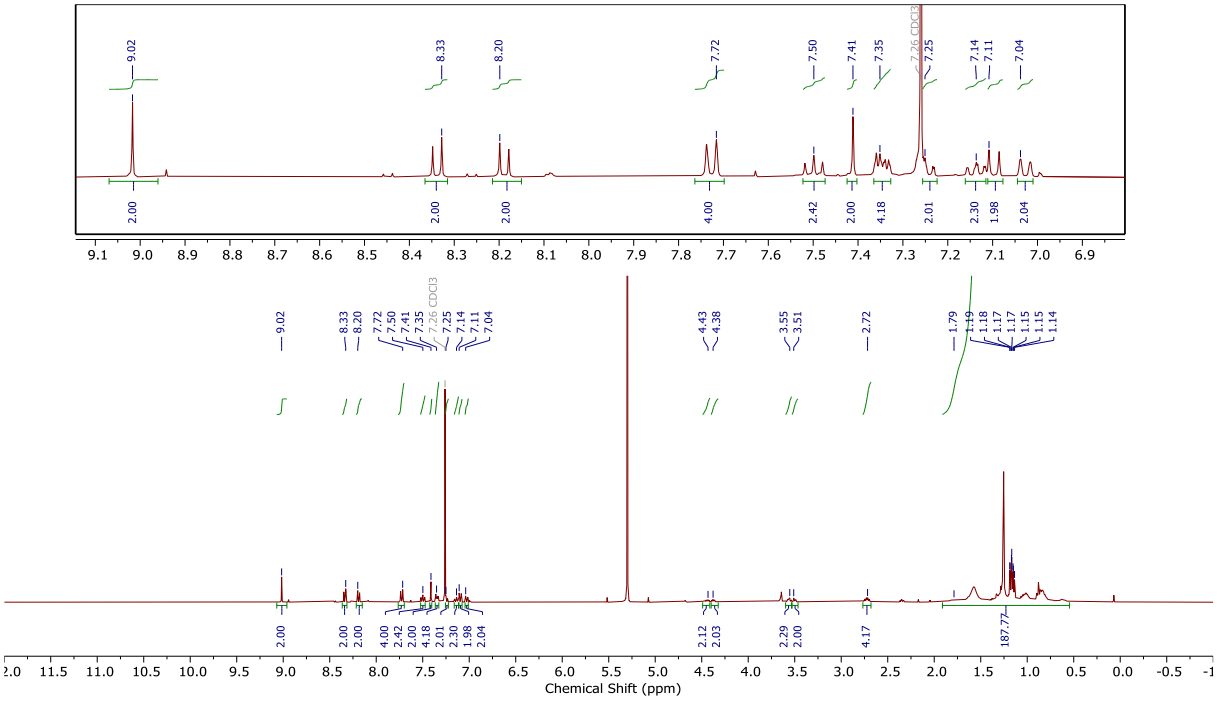

Figure 5.4.30. ^{1}H NMR spectrum of ***PP*-67-8** ($CDCl_3$, 298 K, 400 MHz).

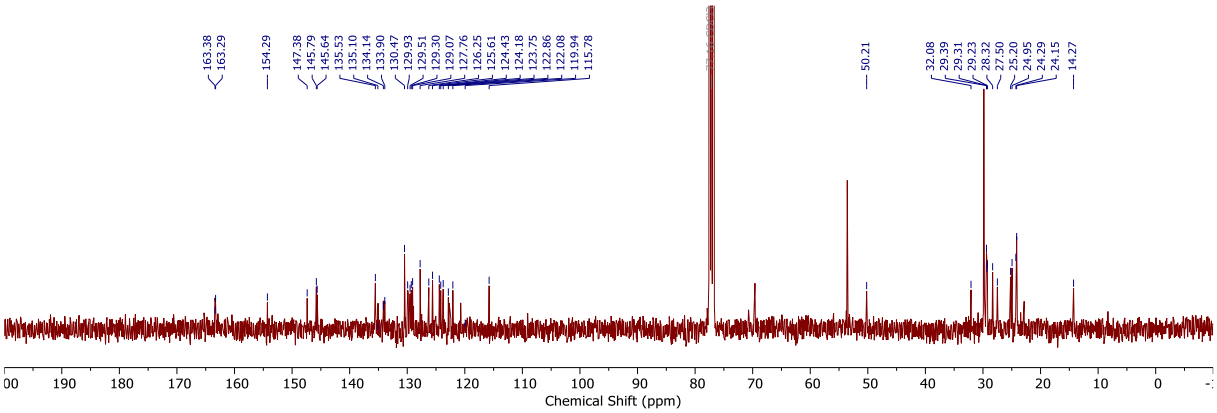

Figure 5.4.31. ^{13}C NMR spectrum of ***PP*-69-8** ($CDCl_3$, 298 K, 101 MHz).

P-BINOL hexyl PDI acyclic control 68

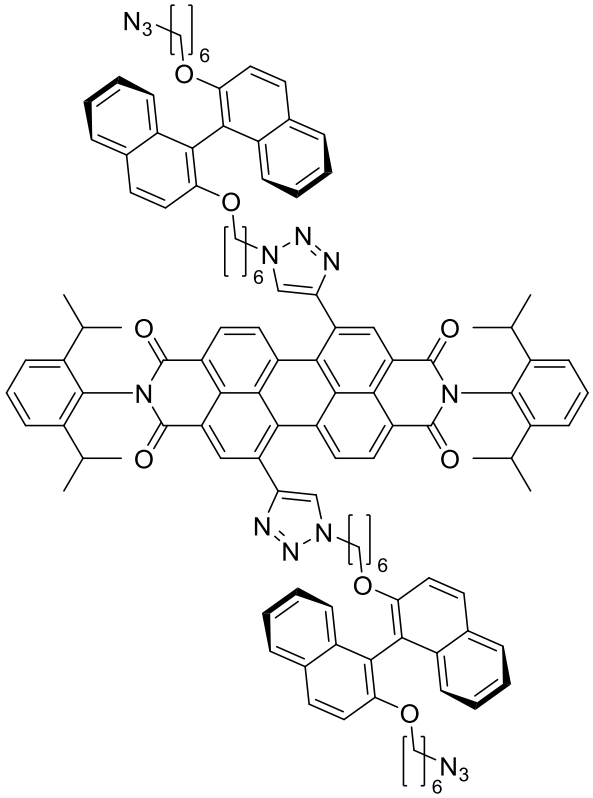

General Procedure B was followed with PDI bisalkyne **23** (53 mg, 69.8 µmol, 1 eq), (*M*)-2,2'-bis((6-azidohexyl)oxy)-1,1'-binaphthalene **66-6** (375 mg, 0.698 mmol, 10 eq), CH_2Cl_2 (20 mL), THPTA (11.7 mg, 26.5 µmol, 0.4 eq) and $Cu(MeCN)_4$-PF_6 (8.30 mg, 26.5 µmol, 0.4 eq). Reaction was completed after 1 day and purified by flash column chromatography (SiO_2, 0.4:100 → 0.6:100 MeOH:CH_2Cl_2) to give PDI **68** as a purple solid (34 mg, 27%). The 1,7 and 1,6 regioisomers were separated by HPLC (Buckyprep, 2:60:38 IPA:n-hexane:CH_2Cl_2).

^{1}H NMR (400 MHz, $CDCl_3$) δ 8.75 (s, 2H, Ar*H* PDI), 8.35 (d, *J* = 8.1 Hz, 2H), 7.98 (d, *J* = 8.1 Hz, 2H), 7.93 – 7.87 (m, 12H), 7.84 (d, *J* = 8.1 Hz, 4H), 7.64 (s, 2H), 7.54 – 7.47 (m, 4H), 7.43 – 7.38 (m, 10H), 7.35 (d, *J* = 7.7 Hz, 6H), 7.30 (ddd, *J* = 8.1, 6.7, 1.3 Hz, 6H), 7.25 – 7.07 (m, 24H), 4.22 – 4.07 (m, 8H), 4.07 – 3.80 (m, 18H), 2.97 (t, *J* = 7.1 Hz, 9H), 2.75 (ddt, *J* = 19.8, 13.1, 6.8 Hz, 9H), 1.67 – 1.58 (m, 8H), 1.50 – 1.28 (m, 14H), 1.28 – 1.09 (m, 65H), 1.07 – 0.88 (m, 15H), 0.87 – 0.74 (m, 11H).

^{13}C NMR (101 MHz, $CDCl_3$) δ 163.5, 163.4, 154.7, 147.9, 145.8, 135.7, 135.4, 134.9, 134.4, 134.3, 130.5, 130.3, 129.9, 129.5, 129.4, 129.3, 129.2, 128.0, 126.3, 125.7, 124.3, 123.7, 122.8, 122.6, 122.1, 121.1, 120.7, 116.1, 115.9, 69.7, 69.5, 51.2, 50.4, 30.0, 29.5, 29.3, 29.1, 28.6, 26.1, 25.7, 25.2, 24.9, 24.1.

MS (ESI): m/z calc. for $C_{116}H_{115}N_{14}O_8$ $[M+H]^+$: 1831.9022; found 1831.8977

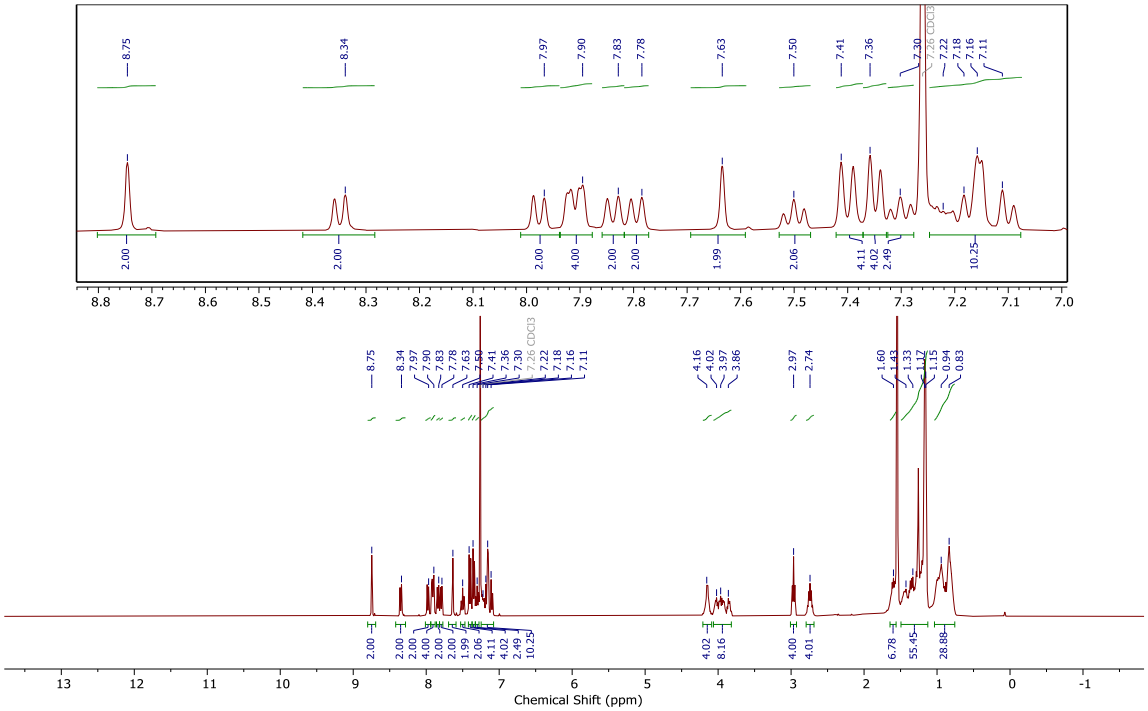

Figure 5.4.32. ^{1}H NMR spectrum of **68** ($CDCl_3$, 298 K, 400 MHz).

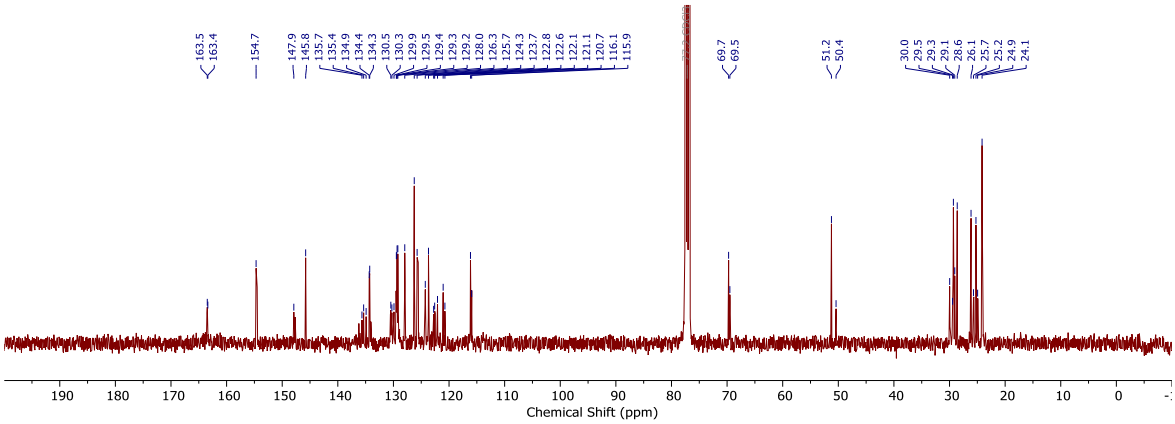

Figure 5.4.33. ^{13}C NMR spectrum of **68** ($CDCl_3$, 298 K, 101 MHz).

5.5 Synthesis and Characterisation for Chapter 4

3,5-di-tert-butylaniline 69

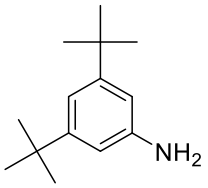

3,5-Di-*tert*-butylbenzoic acid (5 g, 21.3 mmol) was dissolved in a suspension of $CHCl_3$ (15 mL) and H_2SO_4 (15 mL) and stirred at 45 °C. Then NaN_3 (1.50 g, 23.1 mmol, 1.1 eq) was very slowly added to the reaction mixture behind a blast shield over the course of an hour, done in this way to prevent the formation of the highly explosive HN_3. After stirring for five hours at 45 °C, the reaction was worked up and basified with KOH to yield 3,5-tert-butyl aniline **69** (3.44 g, 79%).

Spectroscopic data is in agreement with literature.[161]

N-(6-Bromohexyl)-3,5-di-tert-butylaniline 70

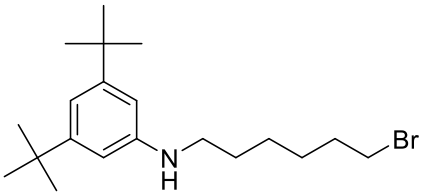

1,6-Dibromohexane (6.00 mL, 39.0 mmol, 10 eq) was added to a stirring solution of 3,5-di-tert-butylaniline **69** (800 mg, 3.90 mmol, 1 eq) in acetonitrile (15 mL). The resulting mixture was left to stir at 70 °C for 2 days. After which, the reaction mixture was cooled to rt and was added H_2O (100 mL) and DCM (100 mL). The resulting mixture was extracted with DCM (50 mL x 3) and the combined organics were dried with $MgSO_4$, filtered, and concentrated *in vacuo*. The resulting yellow oil was purified by flash column chromatography (SiO_2, 2:8 → 8:2 Hexanes:CH_2Cl_2) to yield a colourless oil **70** (1.30, 91%).

^{1}H NMR ($CDCl_3$, 400 MHz) δ 6.80 (1H, t, *J* = 1.7 Hz, Ar*H*), 6.48 (2H, d, *J* = 1.7 Hz, Ar*H*), 3.58 (1H, br s, N*H*), 3.42 (2H, t, *J* = 6.8 Hz, CH_2), 3.13 (2H, t, *J* = 7.0 Hz, CH_2), 1.89 (2H, p, *J* = 6.8 Hz, CH_2), 1.65 (2H, p, *J* = 7.1 Hz, CH_2), 1.56 – 1.42 (4H, m, CH_2), 1.30 (18H, s, CH_3).

MS (ESI): m/z calc. for $C_{20}H_{35}BrN$ $[M+H]^+$: 369.1854; found 369.1875.

N-(6-Azidohexyl)-3,5-di-tert-butylaniline 72

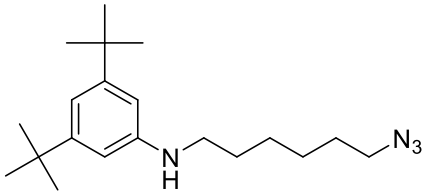

Halide substrate **70** (610 mg, 1.66 mmol, 1 eq), and NaN_3 (216 mg, 3.31 mmol, 2 eq) were dissolved in DMF (10 mL) and left to stir at 75 °C for 16 h. The reaction mixture was quenched with H_2O. The reaction mixture was extracted with Et_2O, washed with H2O (x 4), brine, then dried with $MgSO_4$ and concentrated under vacuo, to yield a colourless oil **11** (547 mg, quant.)

^{1}H NMR ($CDCl_3$, 400 MHz) δ 6.80 (1H, d, *J* = 1.6 Hz, Ar*H*), 6.48 (2H, d, *J* = 1.6 Hz, Ar*H*), 3.46 (1H, br s, N*H*), 3.29 (2H, t, *J* = 6.8 Hz, CH_2), 3.14 (2H, t, *J* = 7.0 Hz, CH_2), 1.71 – 1.57 (4H, m, CH_2), 1.51 – 1.41 (4H, m, CH_2), 1.31 (18H, s, CH_3).

MS (ESI): m/z calc. for $C_{20}H_{35}N_4$ $[M+H]^+$: 331.2783; found 331.2763.

N-(6-Azidohexyl)-3,5-di-tert-butylbenzenaminium hexafluorophosphate 73

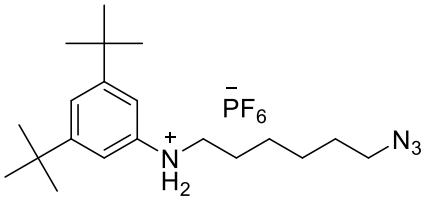

2M HCl in Et_2O (8 mL) was added to a solution of amine **72** (600 mg, 1.82 mmol) in Et_2O (4 mL) and the resulting solution was stirred for 1 h at rt. After which, the solvent and HCl were removed *in vacuo*, then washed with sat. NH_4PF_6 twice, extracting with $CHCl_3$ with each washing. The combined organics was concentrated *in vacuo*, then purified by recrystallisation in $CHCl_3$/hexane to yield a white solid **73** (801 mg, 93%).

^{1}H NMR (300 MHz, $CDCl_3$) δ 7.44 (d, *J* = 1.6 Hz, 1H, Ar*H*), 7.19 (d, *J* = 2.1 Hz, 2H, Ar*H*), 3.35 (s, 2H, CH_2), 3.22 – 3.07 (m, 2H, CH_2), 1.77 – 1.66 (m, 2H, CH_2), 1.54 – 1.40 (m, 2H, CH_2), 1.31 (q, *J* = 3.2 Hz, 2H, CH_2), 1.24 (br s, 2H, CH_2).

Rotaxane 74 and Axle 75

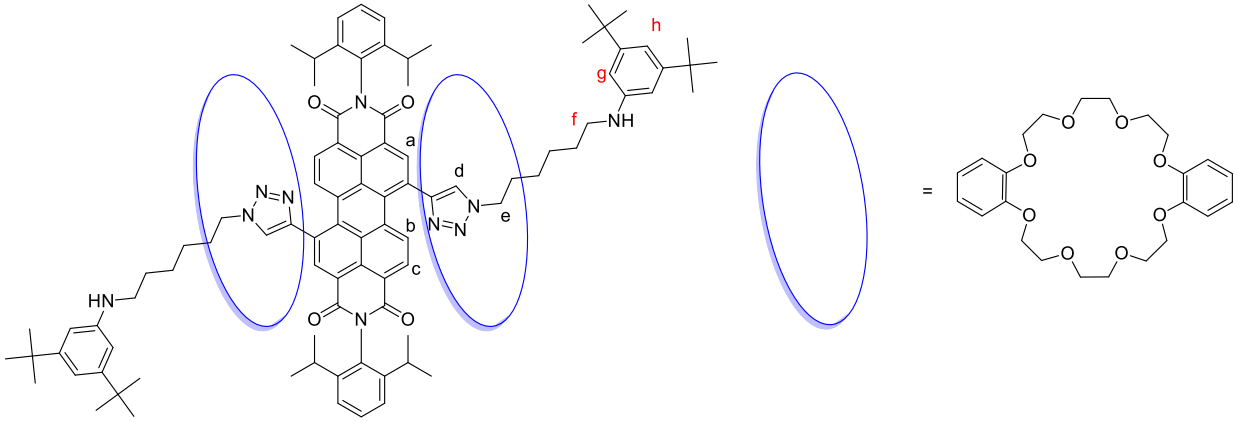

Alkyne **23** (90.0 mg, 0.119 mmol, 1 eq), organic azide **73** (226 mg, 0.474 mmol, 4 eq) and DB24C8 **3** (532 mg, 1.19 mmol, 10 eq) was dissolved in CH_2Cl_2 and degassed by bubbling a stream of N_2 for 15 min. THPTA (20 mg) and $Cu(MeCN)_4$–PF_6 (10 mg) was then sequentially added, and the resulting mixture was left to stir at rt under an atmosphere of N_2 for a specified time, or until reaching completion as monitored by TLC. After which, the reaction mixture concentrated *in vacuo* and purified via flash column chromatography (SiO_2, 0.1:1:99 → 0.1:5:95 NEt_3:MeOH:DCM). The purple solid was redissolved in minimum amount of CH_2Cl_2 and purified again twice by preparative TLC (Plate 1: SiO_2, 0.1:1:99 NEt_3:MeOH:DCM. Plate 2: SiO_2, 0.1:6:4 NEt_3:Hexane:Acetone). A small base wash was performed by dissolving in minimal volume of CH_2Cl_2, then addition of NEt_3 (0.1 mL), then washed with H_2O (2 x 5 mL) to yield a purple solid (4.1 mg, 0.5%).

^{1}H NMR (400 MHz, $CDCl_3$) δ 8.95 (s, 2H), 8.39 (s, 2H), 8.17 (d, *J* = 8.1 Hz, 2H), 8.13 (d, *J* = 8.1 Hz, 2H), 7.57 – 7.42 (m, 2H), 7.38 (d, *J* = 7.8 Hz, 4H), 6.75 (t, *J* = 1.7 Hz, 2H), 6.66 (dt, *J* = 7.4, 3.8 Hz, 8H), 6.59 (dd, *J* = 6.0, 3.5 Hz, 8H), 6.40 (d, *J* = 1.6 Hz, 4H), 5.17 – 5.04 (m, 4H), 4.21 – 4.04 (m, 17H), 4.04 – 3.87 (m, 9H), 3.87 – 3.71 (m, 8H), 3.68 – 3.45 (m, 12H), 2.95 – 2.73 (m, 8H), 2.34 (d, *J* = 9.2 Hz, 5H), 1.41 – 1.32 (m, 1H), 1.25 (d, *J* = 6.8 Hz, 29H).

MS (ESI): m/z calc. for $C_{140}H_{176}N_{10}O_{20}$ $[M+2H]^{2+}$: 1159.1543; found 1159.1510.

There is not sufficient material for ^{13}C NMR spectroscopy.

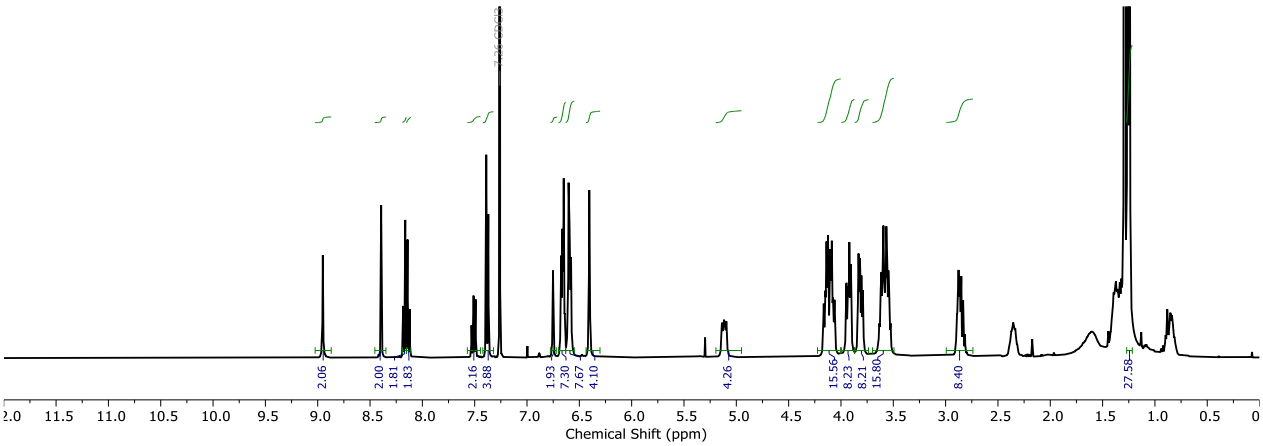

Figure 5.5.1. ^{1}H NMR spectrum of **74** ($CDCl_3$, 298 K, 400 MHz).

Axle 75 was similarly made with PDI bisalkyne **23** (60.0 mg, 0.079 mmol, 1 eq), organic azide **73** (151 mg, 0.316 mmol, 4 eq), THPTA (20 mg) and $Cu(MeCN)_4$–PF_6 (10 mg) then purified via flash column chromatography (SiO_2, 0.1:0.5:99.5 NEt_3:MeOH:DCM). The purple solid was redissolved in minimum amount of CH_2Cl_2 and purified again twice by preparative TLC (Plate 1: SiO_2, 0.1:0.5:99.5 NEt_3:MeOH:DCM. Plate 2: SiO_2, 0.1:7:3 NEt_3:Hexane:Acetone) to yield a purple solid (2.3 mg, 0.4%).

^{1}H NMR (400 MHz, $CDCl_3$) δ 8.77 (s, 2H), 8.35 (d, *J* = 8.1 Hz, 2H), 8.01 (d, *J* = 8.1 Hz, 2H), 7.88 (s, 2H), 7.58 – 7.40 (m, 2H), 7.35 (d, *J* = 7.8 Hz, 4H), 6.77 (t, *J* = 1.6 Hz, 2H), 6.45 (d, *J* = 1.7 Hz, 4H), 4.53 (t, *J* = 7.2 Hz, 4H), 3.15 (t, *J* = 6.9 Hz, 4H), 2.74 (p, *J* = 6.8 Hz, 4H), 2.06 (p, *J* = 7.3 Hz, 5H), 1.67 (q, *J* = 6.9 Hz, 5H), 1.53 (ddt, *J* = 23.0, 12.0, 6.0 Hz, 3H), 1.28 – 1.12 (m, 77H).

^{13}C NMR (101 MHz, $CDCl_3$) δ 163.7, 163.5, 152.7, 147.8, 145.8, 135.7, 135.4, 135.0, 134.2, 130.5, 129.9, 129.5, 129.1, 124.2, 122.6, 122.5, 50.9, 35.1, 31.4, 30.2, 29.8, 29.3, 27.8, 26.2, 24.1, 22.8.

MS (ESI): m/z calc. for $C_{140}H_{176}N_{10}O_{20}$ $[M+2H]^{2+}$: 1418.8712; found 1418.8694.

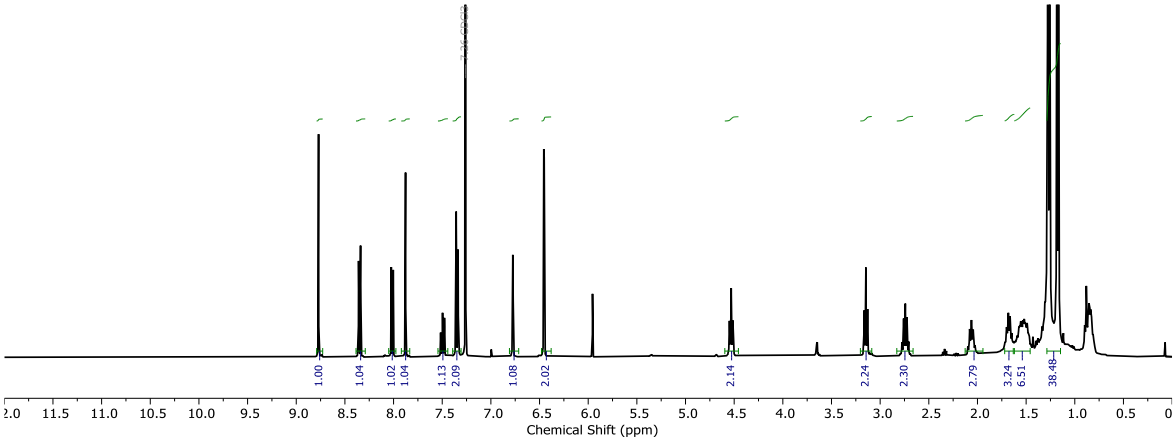

Figure 5.5.2. ^{1}H NMR spectrum of **75** ($CDCl_3$, 298 K, 400 MHz).

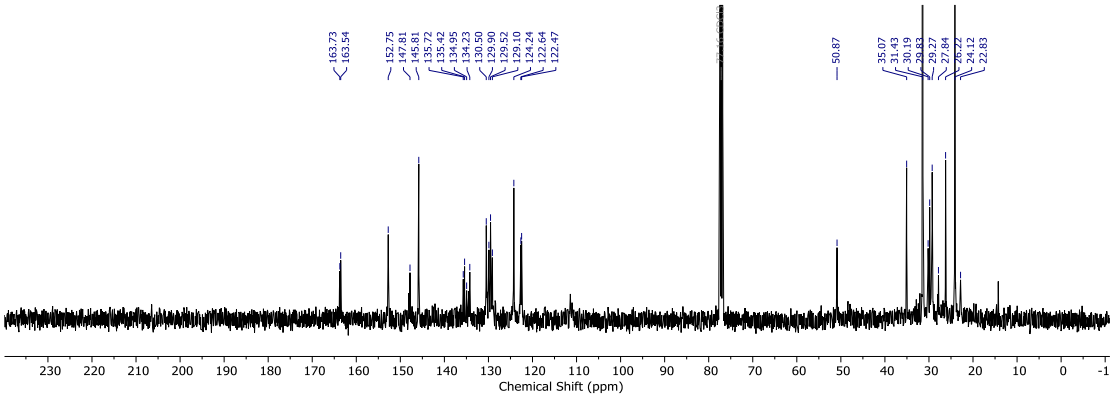

Figure 5.5.3. ^{13}C NMR spectrum of **75** ($CDCl_3$, 298 K, 101 MHz).

BINOL macrocycle 76

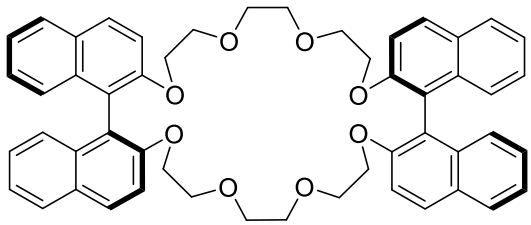

P-BINOL, glycol 77 and ^{t}BuOK dissolved in THF and stirred in the dark under N_2 at 70 °C for 1 week. After cooling to room temperature, THF was removed in vacuo. H_2O and DCM was then added to the reaction mixture. The organic layer was washed with H_2O, then dried with $MgSO_4$ and concentrated under vacuo. The crude solids purified via flash column chromatography (SiO_2, 5% Et_2O in DCM).

^{1}H NMR (400 MHz, $CDCl_3$) δ 7.96 – 7.90 (m, 4H), 7.85 (dt, *J* = 8.6, 0.9 Hz, 4H), 7.45 (d, *J* = 9.1 Hz, 4H), 7.29 (ddd, *J* = 8.1, 6.7, 1.2 Hz, 4H), 7.18 (ddd, *J* = 8.2, 6.7, 1.3 Hz, 4H), 7.06 (ddt, *J* = 8.5, 1.4, 0.8 Hz, 4H), 4.38 (ddd, *J* = 11.4, 8.0, 2.6 Hz, 4H), 4.02 (ddd, *J* = 11.6, 4.1, 2.7 Hz, 4H), 3.72 (ddd, *J* = 11.5, 4.1, 2.6 Hz, 4H), 3.63 (ddd, *J* = 11.6, 8.0, 2.7 Hz, 4H), 3.55 – 3.47 (m, 5H), 3.46 – 3.38 (m, 4H).

Spectroscopic data is in agreement with literature.[162]

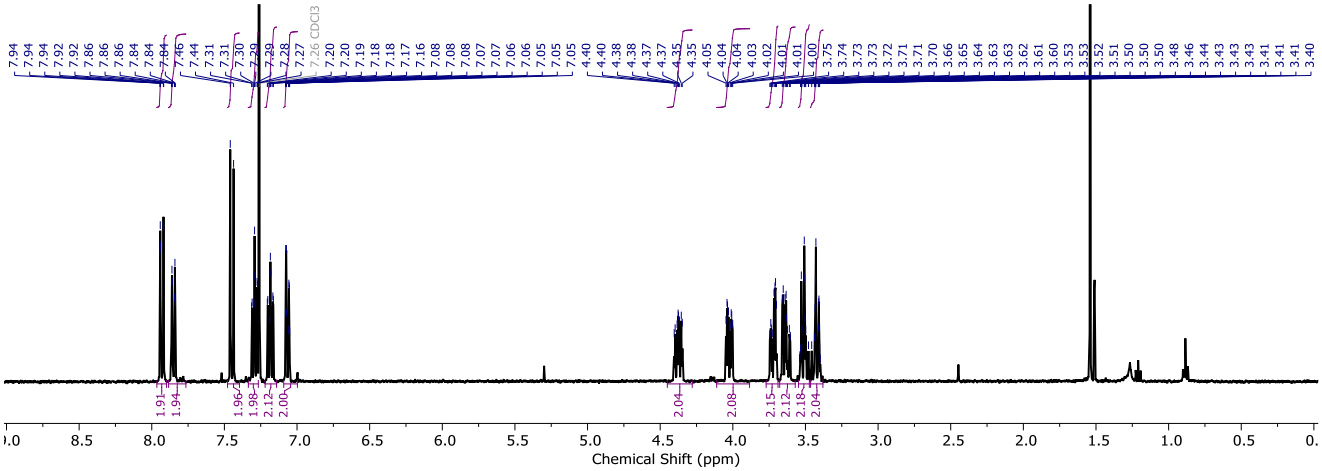

Figure 5.5.4. ^{1}H NMR spectrum of **76** ($CDCl_3$, 298 K, 400 MHz).

5.6 X-ray Crystallography

Crystals of macrocycle **47**, suitable for single crystal X-ray diffraction, were grown from a solution of **47** dissolved in $CHCl_3$, with slow diffusion of n-hexane (antisolvent).

Here, Jennifer Robertson mounted and performed the crystallography, and Georgia R. F. Orton processed and solved the crystallographic data.

Single Crystal X-Ray Diffraction (SCXRD): Data were collected using a Rigaku Synergy-S dual source with a PhotonJet-S X-ray source and a HyPix-6000 detector. Data were collected at 100 K through the use of an Oxford Cryosystems cryostream device. Data were collected and processed using CrysAlis PRO171.42.49. The structures were solved by direct methods using ShelXT and refined with ShelXL using a least squares method.[163] Olex2 software was used as the solution, refinement and analysis program.[164]

Positional disorder is modelled for one of the straps between the PDI and hydroquinone moieties (carbon atoms C52 – C60 and oxygen atom O5). The occupancies of the two sites were refined and constrained to sum to unity with values of 0.85 and 0.15 respectively. All atoms were refined with anisotropic displacement parameters with the exception of carbon atom C42B and oxygen atom O5B which form part of the low occupancy (part 2) disordered strap which could not be modelled satisfactorily anisotropically. The ADPs of carbons C55B, C56B, C57B, C58B, C59B, C60B of the low occupancy part of the disordered strap were constrained to be equal (EADP) as the shift would not settle if the ADPs of these atoms were only restrained to be similar. Hydrogen atoms were geometrically placed and refined using a riding model.

The occupancy of the chloroform residue (Cl1-3, C67, H67) was allowed to freely refine and settle before being fixed at 0.83. Although evidence for additional molecules of chloroform was seen in the electron density map, these disordered solvent molecules could not be sensibly modelled, so the structure was treated with a Solvent Mask,

implemented by Olex. A solvent mask was calculated, and 580 electrons were found in a volume of 1784 $Å^3$ in 1 void per unit cell. This is consistent with the presence of 2.5 chloroform molecules per Asymmetric Unit which account for 580 electrons per unit cell. Figures were produced using CrystalMakerX.

Crystal Data for macrocycle **47** $C_{66}H_{62}N_8O_6$**.** 0.83 $CHCl_3$: monoclinic, space group P2/n, a = 14.39140(10) Å, b = 14.94010(10) Å, c = 33.6959(2) Å, α = 90°, β = 91.1850(10)°, γ = 90°, V = 7243.37(8) $Å^3$, Z = 4, *T* = 100.00(10) K, μ(Cu Kα) = 1.369 mm^{-1}, *Dcalc* = 1.066 g/cm^3, 134698 reflections measured (5.916° ≤ 2Θ ≤ 156.862°), 14866 unique (R_{int} = 0.0433, R_{sigma} = 0.0229) which were used in all calculations. The final R_1 was 0.0829 (I > 2σ(I)) and wR_2 was 0.2357. Deposited cif number: 2249179.

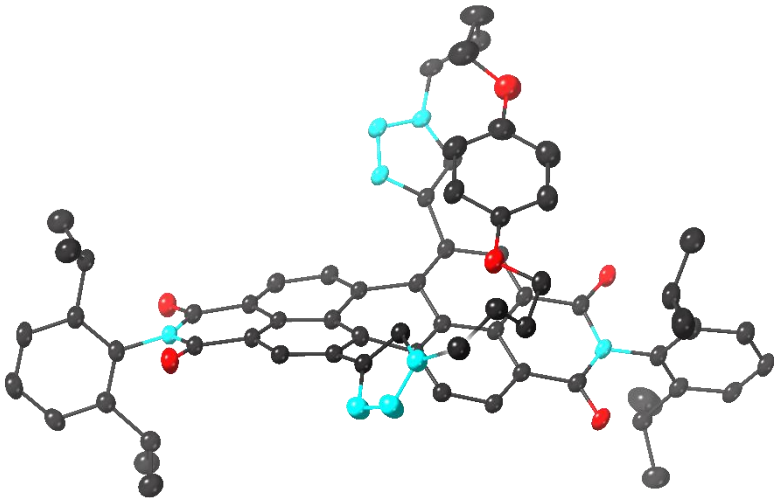

Asymmetric unit of macrocycle **47** with all non-hydrogen atoms represented by ellipsoids at the 50% probability level. Hydrogen atoms omitted for clarity (C, dark grey; O, red; N, blue).

5.7 Density Functional Theory Calculations

The calculations below were calculated by Prof Martijn Zwijnenburg from University College London.

Conformer searches for macrocycles **47**, **67-4** and **47-6** were performed using the combination of the CREST code[112] and the GFN2-xTB semiempirical tight-binding DFT-method.[113] The lowest energy conformers found using CREST were subsequently reoptimized by means of full DTF using the B97-3c composite scheme.[165] Solvation effects in the DFT calculations were described using the COSMO (toluene, chloroform) implicit solvation models.[166] Vertical excitation and circular dichroism spectra of the DFT optimised conformers were calculated by single point calculations using the combination of the ωB97x[167] density functional and the def2-SVP basis-set.[168] Finally, harmonic frequencies were calculated for both the GFN2-xTB (lowest conformers only) and B973c optimised structures to verify that these optimised structures have no imaginary frequencies and, as expected, correspond to minima on their respective potential energy surfaces. All DFT calculations are performed using Turbomole 7.5.[169]

5.7.1 Conformer Searches

The lowest energy conformer for macrocycle ***M*-47** as found in the GFN2-xTB CREST conformer search is shown below. This conformer agrees with the X-ray crystal structure of macrocycle **47** shown in (***M*** atropisomer), thereby supporting this method and thus our predictions for macrocycles **67-4,6** below.

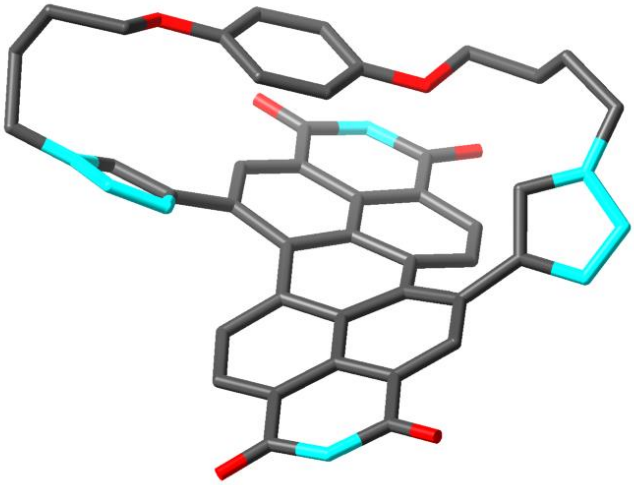

***M*-47**

Figure 5.7.1. Lowest energy conformer for macrocycle ***M*-47**, as found in the GFN2-xTB conformer search. For clarity, hydrogen atoms and the 2,6-diisopropylphenyl imide substituents have been removed from the structure.

The lowest energy conformer for macrocycles **67-4** and **67-6**, found using the same GFN2-xTB CREST conformer search as for ***M*-47**, are shown below. The conformer search returned in all cases only homochiral conformers (i.e., ***PP*/*MM*-67-4** and ***PP*/*MM*-67-6**), even when a full conformer search was performed using the heterochiral structure as input, such that heterochiral conformers must lie at least of the order of 20-30 kJ mol^{-1} higher in energy.

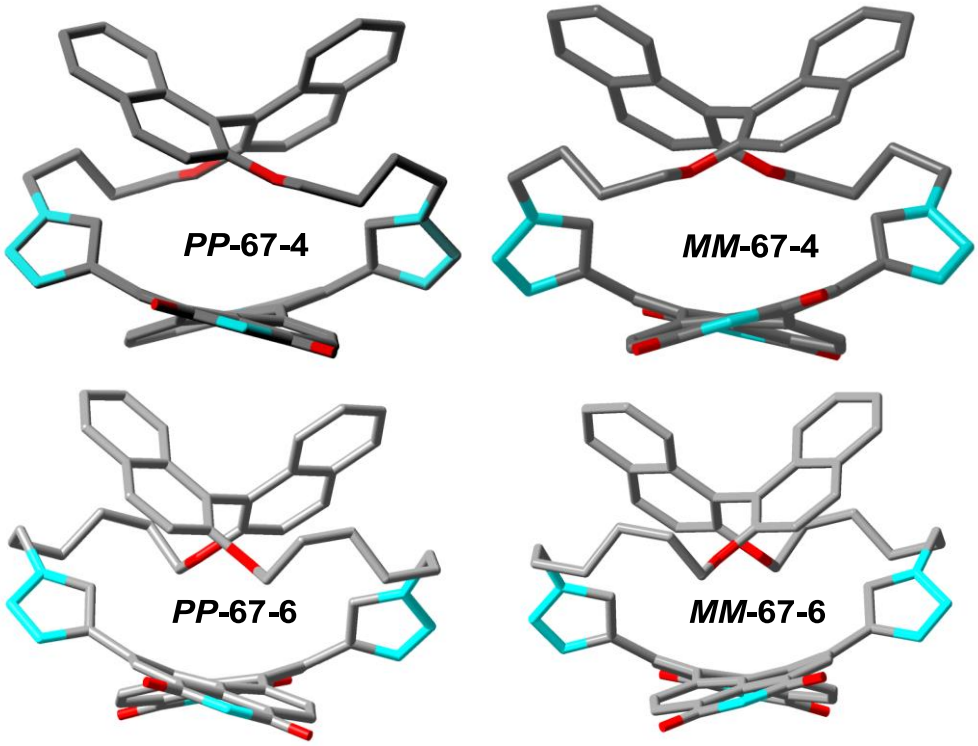

Figure 5.7.2. Lowest energy conformer for macrocycles **67-4** and **67-6**, as found in the GFN2-xTB conformer search. For clarity, hydrogen atoms and the 2,6-diisopropylphenyl imide substituents have been removed from these structures.

Using the lowest energy conformer ***PP*-67-6** as a starting point, a conformer for ***PM*-67-6** was manually constructed (***PM*-67-6***). Then, a constrained conformer search starting from ***PM*-67-6*** was used to obtain our best attempt in achieving the lowest energy conformer of ***PM*-67-6**. These conformers, which are not guaranteed to be the lowest energy ***PM*-67-6** conformer, are predicted to lie 79 and 65 kJ mol^{-1} respectively above the ***MM*/*PP*-67-6** lowest energy structure (B97-3c/$CHCl_3$). Thus, the lowest energy heterochiral conformer must inclusively lie in the energy window between 20 and 65 kJ mol^{-1} above the homochiral conformer.

5.7.2 Predicted Circular Dichroism Spectra

The predicted circular dichroism spectra of the lowest energy conformer of macrocycles ***MM*-67-4** and ***PP*-67-4** (Table A1) and ***MM*-67-6** and ***PP*-67-6** (Table A2). The lowest energy transitions are given since they are exclusive to the PDI chromophore. These predicted CD spectra were used to assign the experimental CD spectra of macrocycles **67-4** and **67-6**. Note that in all cases the predicted CD spectrum is blue-shifted relative to the experimental spectra, which is a side-effect of the range-separated functional used.

	Excitation energy / eV (wavelength / nm)	**Rotary strength / 10^{-40} erg cm^3**	
		***MM*-67-6**	***PP*-67-6**
1	2.57 (482)	+137	−136
2	3.63 (341)	+81	−81
3	3.71 (334)	+26	-26
4	3.88 (319)	−107	+107
5	3.89 (318)	-99	+99
6	4.14 (300)	-6	+6

Table 5.7.1: CD spectra precited for ***MM*-67-4** and ***PP*-67-4** using ϖB97x/def2-SVP.

	Excitation energy / eV (wavelength / nm)	**Rotary strength / 10^{-40} erg cm^3**	
		***MM*-67-6**	***PP*-67-6**
1	2.53 (490)	+186	−186
2	3.61 (343)	+123	−123
3	3.75 (331)	−71	+71
4	3.87 (321)	−163	+163
5	3.90 (318)	-38	+38
6	3.95 (314)	+8	-8

Table 5.7.2: CD spectra precited for ***MM*-67-6** and ***PP*-67-6** using ϖB97x/def2-SVP.

Tables 5.7.3 and 5.7.4 give the predicted CD spectra for ***PM*-67-6*** and ***PM*-67-6**, which show in line with experiment that the sign of the ***PM*** structure (PDI-only region) is opposite to that of the ***PP*** structure, while the magnitude is reduced. The conformers of ***PM*-67-6*** and ***PM*-67-6** are provided as a .xyz file in the 'Macrocycle Structures' folder.

	Excitation energy / eV (wavelength / nm)	Rotary strength / 10^{-40} erg cm^3
		PM*-67-6
1	2.51 (493)	+162
2	3.62 (342)	+90
3	3.87 (321)	−104
4	3.90 (318)	−95
5	4.08 (304)	-3
6	4.20 (295)	-4

Table 5.7.3: CD spectrum predicted for *PM*-67-6* using ϖB97x/def2-SVP.

	Excitation energy / eV (wavelength / nm)	Rotary strength / 10^{-40} erg cm^3
		***PM*-67-6**
1	2.56 (484)	+76
2	3.55 (349)	+7
3	3.66 (338)	+50
4	3.85 (322)	−11
5	3.95 (314)	−83
6	4.05 (306)	−7

Table 5.7.4: CD spectrum predicted for *PM*-67-6 using ϖB97x/def2-SVP.

6 Conclusions

The aim of the work described in this thesis was to develop novel configurationally stable PDIs by integrating these twisted dyes into macrocycles and rotaxanes.

In the context of rotaxanes, the strategy of using mechanical bonding to arrest PDI atropoisomer interconversion is unprecedented. In the context of chirally locked PDI-based macrocycles, these systems have been reported before, albeit in a limited number. However, π-π templation and stereoselectivity are missing in the current scope of their synthesis, in part because the macrocyclic strap is unable to form non-covalent interactions with the PDI. Therefore, the general macrocycle designs developed in this thesis sought to engineer interactions between the π-donor strap and the π-acceptor PDI, which were used to improve yields and ultimately afford diastereoselectivity.

The project commenced in Chapter Two with the design and synthesis of a series of novel chirally-locked PDI-based macrocycles that explore a range of linker lengths and macrocyclisation chemistries. This established the use of CuAAC ‘click’ chemistry to prepare bis-triazole PDI-based macrocycles, which underpinned the remaining work in this thesis. While initial synthetic attempts yielded only [2+2] or larger macrocycles, the successful formation of mono-PDI [1+1] macrocycles in reasonable macrocyclisation yields were realised by reducing ring-strain and introducing π-electron donors into the linkers (e.g. **46**, **47**, **48**, and **54**). The notable absence of such π-π interactions in the acyclic variants (**51**, **49**, **50**, and **55)** demonstrated the importance of the preorganised macrocyclic framework.

Chapter Three developed the synthesis of chiral PDI macrocycles that contained a second chiral aromatic unit in the linker, either a PDI (**62** and **63**), a pillar[5]arene macrocycle (**64**), or a BINOL group (**67**). These systems were used to develop the stereoselective synthesis of PDI-based macrocycles, by exploring kinetic templation

arising from the non-covalent interactions between the PDI unit and the chiral linker. A diastereoselective synthesis was achieved with both a chirally dynamic (i.e. pillar[5]arene) and a chirally locked (i.e. BINOL) strap, indicating that chiral information is transferred during in the transition state of the macrocyclisation reaction. Indeed, the synthesis of the BINOL-PDI macrocycle was investigated using the Curtin-Hammett principle and revealed the potential for non-covalent interactions between the aromatic units to direct the outcome of the dynamic kinetic resolution.[132]

The significant progress towards a configurationally stable PDI through mechanical bonding is described in Chapter Four. Here, the synthesis of a novel PDI-based [3]rotaxane (**74**) containing a two-station axle and two dibenzo-24-crown-8 macrocycle components was described. Chiral HPLC revealed that positioning the macrocycles in close proximity to the twisted PDI unit slows down PDI atropisomer interconversion. Unfortunately, chiral resolution of this [3]rotaxane was not possible, most likely due to the dynamic nature of the [3]rotaxane shuttle. However, the pH dependent shuttling behaviour was used to evidence hydrogen bonding and/or donor–acceptor π–π interactions between the crown ethers and the bis-triazole PDI. These interactions meant that the position of the macrocycles on the axle could be easily detected by UV-vis absorption spectroscopy.

Overall, these results demonstrate that macrocyclisation and rotaxanation are highly promising strategies for reducing the rate of PDI atropisomer interconversion, with the former leading to configurationally stable chiral chromophores. Chiral locking opens the door to stereoselective PDI synthesis and indeed a dynamic kinetic resolution is realised using templating non-covalent interactions between the chiral components within the macrocyclic architecture.[132] Therefore, the concepts established in this thesis could be used to design and prepare new chiral PDIs, including through stereoselective syntheses, functional materials with applications in chiral recognition,[142] sensing,[74] and for the absorption and/or emission of circularly polarised light.[75]

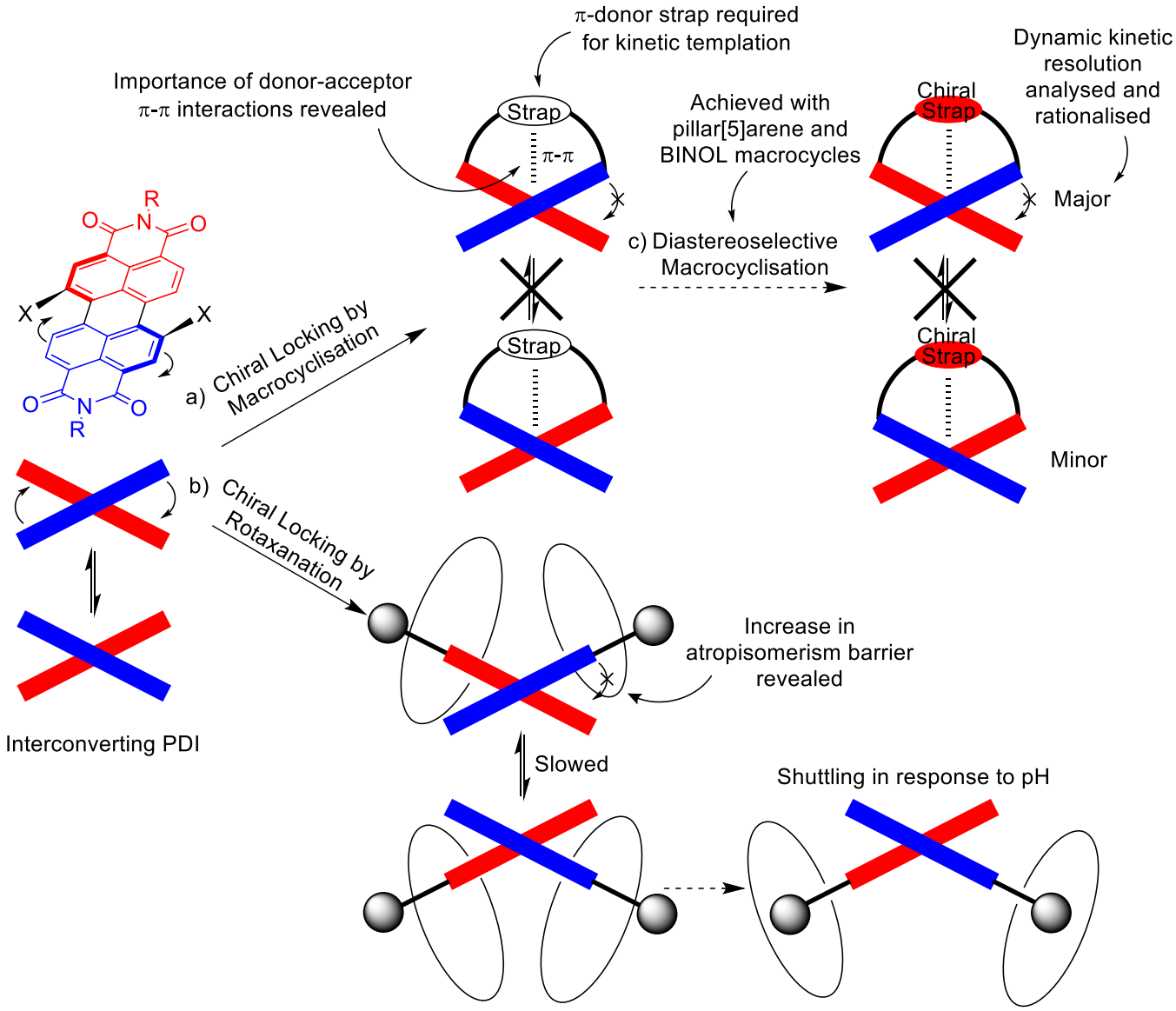

Figure 6.1. Illustration of the key results in this thesis, including the successful chiral locking of PDI molecules by macrocyclisation (a) and slowing of racemisation by rotaxanation (b), where the former is expanded by developing a diastereoselective macrocyclization (c).

Appendix

A) Photophysical Spectra in Toluene

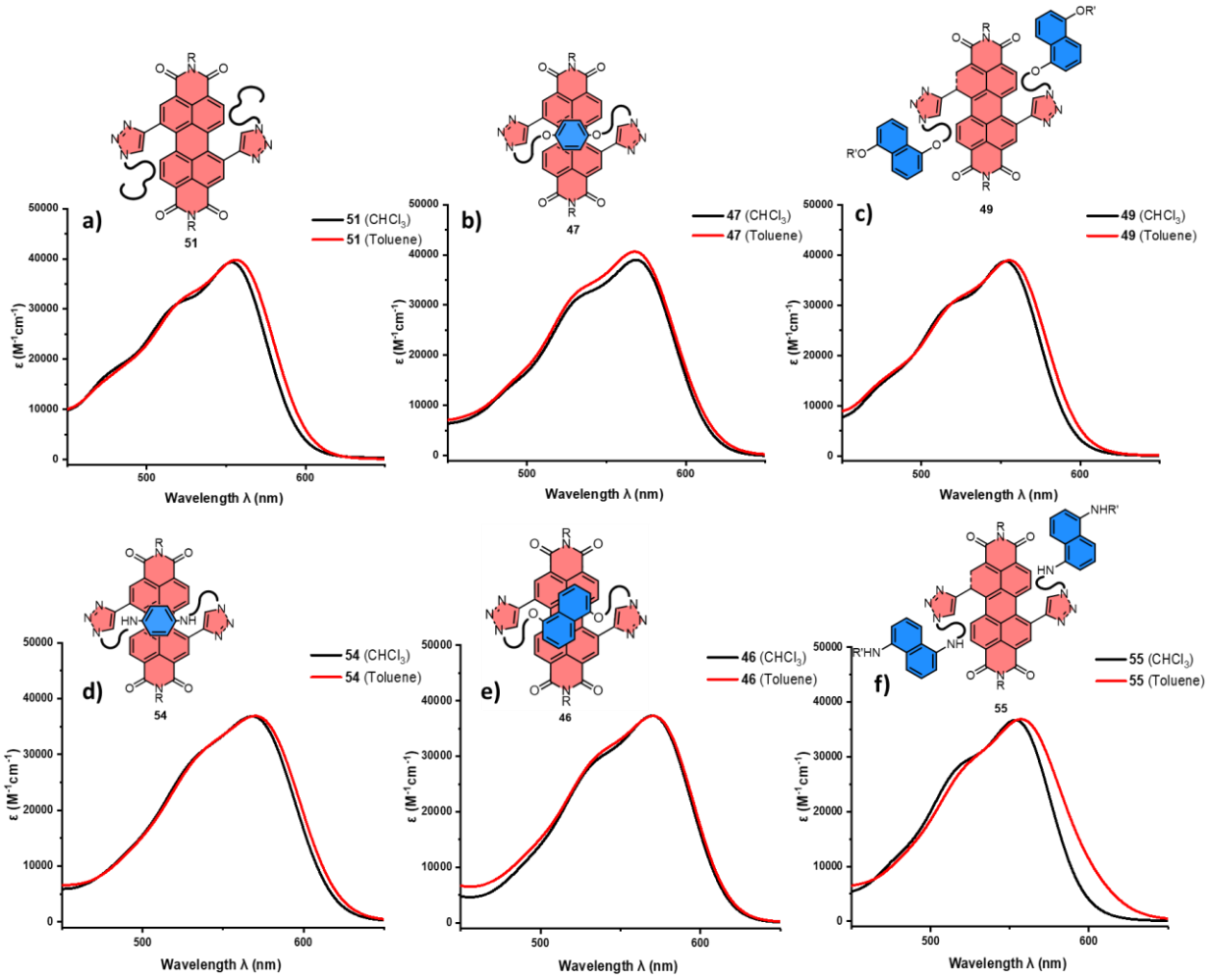

Figure AA. UV-vis absorption spectra of compounds a) **51**, b) **47**, c) **49**, d) **54**, e) **46**, and f) **55**, showing minimal changes in their spectra in different solvents ($CHCl_3$ and toluene). All spectra were recorded in $CHCl_3$ (black) or toluene (red) at a concentration of 26 µM in a quartz cuvette with 1 cm path length.

B) HT data from CD spectroscopy

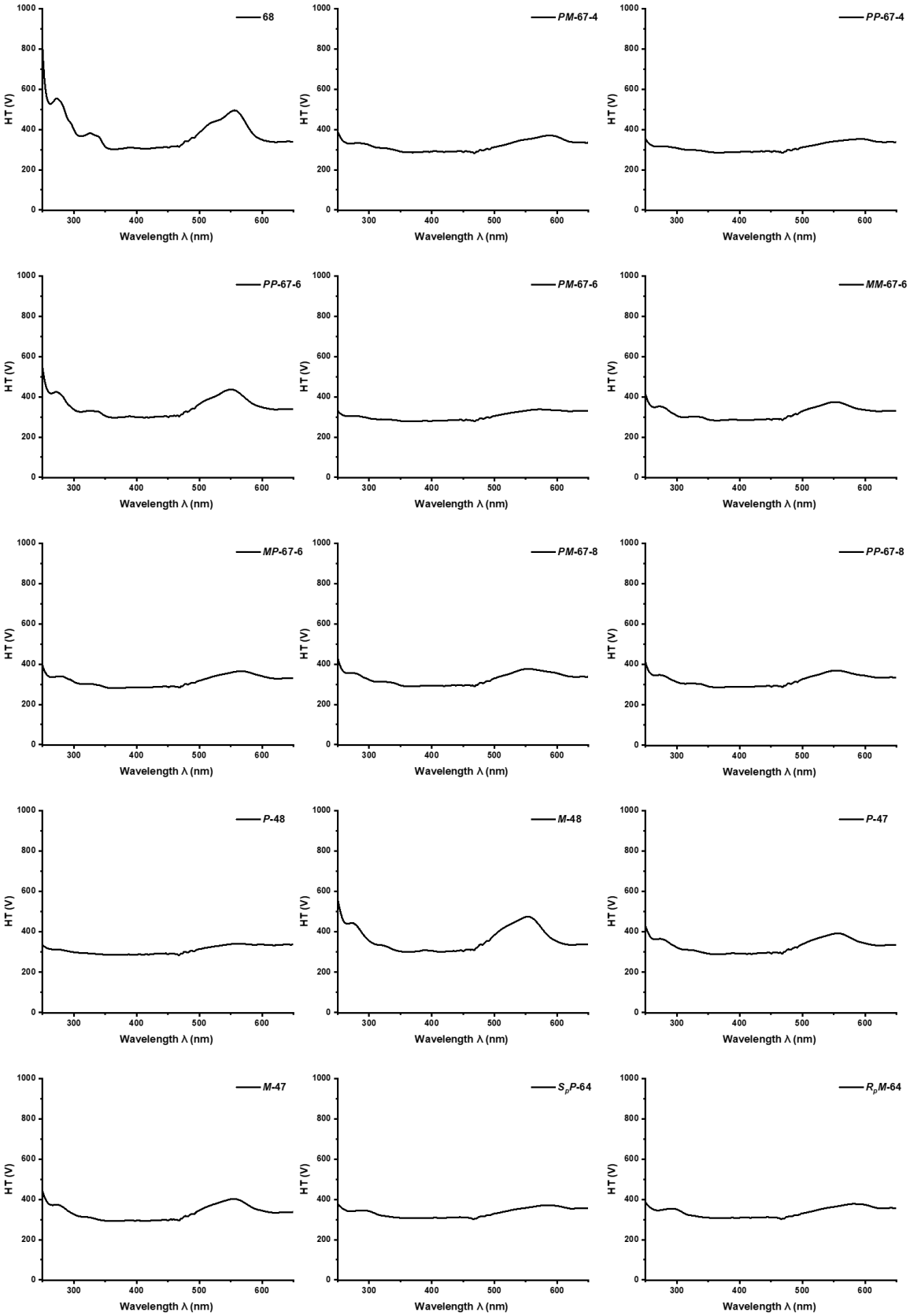

Figure AB. HT data from CD spectroscopy of various compounds.

C) Further Details from Figure 4.7

The purification of [3]rotaxane **74** and axle **75** proved to be challenging. It should be noted that silica gel flash chromatography was undergone with an eluent system containing a small mixture of NEt_3 (**74:** DCM:MeOH:NEt_3 95:5:0.1; **75:** DCM:MeOH:NEt_3 99.5:0.5:0.1) to deprotonate the products, and also to prevent partial protonation of the products from the silica gel. This greatly improved the tightness of the product bands as it travels down the column. Whilst this method was able to remove excess ammonium stopper group, [2]rotaxane, and other unidentified side products; excess DB24C8, TBTA, as well as the 1,6-regioisomers were unable to be removed from neither [3]rotaxane **74** nor axle **75**.

Initial attempts to remove TBTA involved washing with Et_2O and then recrystallisation, but this yielded no pure material, even when the products were protonated by washing with 2M HCl. Note that the protonation state of both [3]rotaxane **74** and axle **75**, despite being impure, was able to be confirmed by ^1H NMR spectroscopy. Ultimately, TBTA was able to be removed by two successive preparative TLC plates (SiO_2, **74:** DCM:MeOH:NEt_3 98.8:0.7:0.5; **75:** DCM:MeOH:NEt_3 99:0.5:0.5), where only the very bottom of the product band was taken as it was least contaminated with TBTA. Unfortunately, this method leaves behind too much products on the preparative TLC plates, especially considering that these products were still contaminated with DB24C8 and 1,6-regioisomers.

It should be noted that when CuAAC was attempted without TBTA, only starting material and decomposition products remained after one week. Fortunately, CuAAC can be accelerated in the presence of a base,[ref] in which NEt_3 was added to the reaction to achieve the axle **75** after one day. This method was not feasible in the synthesis of the rotaxane as this deprotonated the stopper group, which caused DB24C8 to be dethreaded prior to reaction. Instead, it was discovered that tris((1-hydroxy-propyl-1H-1,2,3-triazol-4-yl)methyl)amine (THPTA) could be used as a ligand instead of TBTA. This successfully achieved both axle **75**

and rotaxane **74** in similar yields to that of TBTA, in which the THPTA could be easily removed by aqueous work up due to its water solubility.

Next, to remove the 1,6-regioisomer, after many unsuccessful attempts at purification by flash column chromatograph or preparative TLC with different solvents ratios, including DCM, $CHCl_3$, MeOH, Et_2O, and EtOAc; rotaxane **74** was able to be purified by preparative TLC (SiO_2, Toluene:Acetone:NEt_3 84.5:15:0.5). However, the purification of **75** by preparative TLC with the same solvents merely dropped the amount of 1,6- regioisomers from 33% to 30%, as calculated by ^1H NMR spectroscopy. Preparative TLC under acidic conditions (SiO_2, DCM:MeOH:MeCOOH 99:0.5:0.5) proved to yield better results, dropping the amount of 1,6-regioisomer to 9%. Whilst successive preparative TLC would likely reduce this unwanted regioisomer to an undetectable amount, the loss of product in these preparative TLC plates warrants a more efficient and sustainable method in achieving regio-purity.

It was discovered that $PDIBr_2$ **21**, a precursor to PDI bisalkyne **23** (*vide supra*, Section 2.2.1), was able to be purified on scale by preparative HPLC using a COSMOSIL Buckyprep Packed Column. The conditions used were optimised in a similar methodology as described in Section 2.4, where ultimately the 1,7- regioisomer were successfully separated by elution with 1:2:1 n-hexane:CH_2Cl_2:IPA mixture. This was then further reacted as described in Section 2.2.1 to achieve pure 1,7-PDI bisalkyne **23**, and then further reacted by CuAAC with THPTA and $Cu(MeCN)_4{-}PF_6$, to yield [3]rotaxane **74** and axle **75**.

Finally, to remove DB24C8, after many further unsuccessful attempts at purification by flash column chromatograph or preparative TLC with different solvents ratios, both [3]rotaxane **74** and axle **75** were able to be purified by two successive preparative TLCs (74 - Plate 1: SiO_2, 0.1:1:99 NEt_3:MeOH:DCM. Plate 2: SiO_2, 0.1:6:4 NEt_3:Hexane:Acetone. 75 - Plate 1: SiO_2, 0.1:0.5:99.5 NEt_3:MeOH:DCM. Plate 2: SiO_2, 0.1:7:3 NEt_3:Hexane:Acetone). Whilst the calculated yields (by ^1H NMR spectroscopy)

of [3]rotaxane **74** and axle **75** were 20% and 59% respectively, the isolated yields after these plates were 0.4% and 0.5% respectively.

References

[1] M. Meselson, F. W. Stahl, *Cold Spring Harbor Symposia on Quantitative Biology* **1958**, *23*, 9-12.
[2] R. Jaenicke, *Biochemistry* **1991**, *30*, 3147-3161.
[3] P. A. v. d. Merwe, S. J. Davis, *Annual review of immunology* **2003**, *21*, 659-684.
[4] G. M. Whitesides, J. P. Mathias, C. T. Seto, *Science* **1991**, *254*, 1312-1319.
[5] J. M. Lehn, *Angew Chem. Int. Ed. Engl.* **1990**, *29*, 1304-1319.
[6] J. Stoddart, *Annual Reports Section" B"(Organic Chemistry)* **1988**, *85*, 353-386.
[7] J. F. Stoddart, *Angew. Chem. Int. Ed* **2017**, *56*, 11094.
[8] J.-M. Lehn, *Chemical Society Reviews* **2007**, *36*, 151-160.
[9] H.-J. Schneider, *Angew. Chem. Int. Ed.* **2009**, *48*, 3924-3977.
[10] a) S. Z. Godse, S. Mohini, S. M. Patil, R. Saudagar, *Journal of Advanced Pharmacy Education & Research Oct-Dec* **2013**, *3*; b) R. E. Babine, S. L. Bender, *Chem. Rev.* **1997**, *97*, 1359-1472.
[11] P. R. Ashton, T. T. Goodnow, A. E. Kaifer, M. V. Reddington, A. M. Z. Slawin, N. Spencer, J. F. Stoddart, C. Vicent, D. J. Williams, *Angew Chem. Int. Ed. Engl.* **1989**, *28*, 1396-1399.
[12] V. S. Sharma, A. S. Sharma, N. K. Agarwal, P. A. Shah, P. S. Shrivastav, *Molecular Systems Design & Engineering* **2020**, *5*, 1691-1705.
[13] D. F. Veber, S. R. Johnson, H.-Y. Cheng, B. R. Smith, K. W. Ward, K. D. Kopple, *Journal of Medicinal Chemistry* **2002**, *45*, 2615-2623.
[14] S. Dong, B. Zheng, F. Wang, F. Huang, *Acc. Chem. Res.* **2014**, *47*, 1982-1994.
[15] C. Wang, L. Xu, Z. Jia, T.-P. Loh, *Chinese Chemical Letters* **2024**, *35*, 109075.
[16] J. Mallinson, I. Collins, *Future medicinal chemistry* **2012**, *4*, 1409-1438.
[17] S. Mena-Hernando, E. M. Pérez, *Chemical Society Reviews* **2019**, *48*, 5016-5032.
[18] S. J. Rodgers, C. Y. Ng, K. N. Raymond, *J. Am. Chem. Soc.* **1985**, *107*, 4094-4095.
[19] R. Hoss, F. Vögtle, *Angew Chem. Int. Ed. Engl.* **1994**, *33*, 375-384.
[20] K. Goto, in *Comprehensive Supramolecular Chemistry II* (Ed.: J. L. Atwood), Elsevier, Oxford, **2017**, pp. 61-71.
[21] M. Asakawa, W. Dehaen, G. L'Abbé, S. Menzer, J. Nouwen, F. M. Raymo, J. F. Stoddart, D. J. Williams, *J. Org. Chem.* **1996**, *61*, 9591-9595.
[22] A. Xie, B. Liu, J. E. Hall, S. L. Barron, D. A. Higgins, *Langmuir* **2005**, *21*, 4149-4155.
[23] a) C. Schaack, A. M. Evans, F. Ng, M. L. Steigerwald, C. Nuckolls, *J. Am. Chem. Soc.* **2021**, *144*, 42-51; b) E. Kozma, M. Catellani, *Dyes Pigm.* **2013**, *98*, 160-179.
[24] P. Cheng, X. Zhao, X. Zhan, *Accounts of Materials Research* **2022**, *3*, 309-318.
[25] J.-P. Sun, A. D. Hendsbee, A. J. Dobson, G. C. Welch, I. G. Hill, *Organic Electronics* **2016**, *35*, 151-157.
[26] a) F. Würthner, *Chem. Commun.* **2004**, 1564-1579; b) M. Sun, K. Müllen, M. Yin, *Chemical Society Reviews* **2016**, *45*, 1513-1528; c) A. Nowak-Król, K. Shoyama, M. Stolte, F. Würthner, *Chem. Commun.* **2018**, *54*, 13763-13772; d) C. Yan, S. Barlow, Z. Wang, H. Yan, A. K. Y. Jen, S. R. Marder, X. Zhan, *Nature Reviews Materials* **2018**, *3*, 18003; e) H. Langhals, *Heterocycles* **1995**, *40*, 477-500.
[27] F. Würthner, C. Thalacker, S. Diele, C. Tschierske, *Chem. Eur. J.* **2001**, *7*, 2245-2253.
[28] J. Idé, R. Méreau, L. Ducasse, F. Castet, Y. Olivier, N. Martinelli, J. Cornil, D. Beljonne, *The Journal of Physical Chemistry B* **2011**, *115*, 5593-5603.
[29] A. Syamakumari, A. P. H. J. Schenning, E. W. Meijer, *Chem. Eur. J.* **2002**, *8*, 3353-3361.
[30] Z. Chen, B. Fimmel, F. Würthner, *Organic & Biomolecular Chemistry* **2012**, *10*, 5845-5855.
[31] P. Osswald, F. Würthner, *J. Am. Chem. Soc.* **2007**, *129*, 14319-14326.
[32] V. Dehm, Z. Chen, U. Baumeister, P. Prins, L. D. A. Siebbeles, F. Wuerthner, *Org. Lett.* **2007**, *9*, 1085 - 1088.
[33] Y. Hou, Z. Zhang, S. Lu, J. Yuan, Q. Zhu, W.-P. Chen, S. Ling, X. Li, Y.-Z. Zheng, K. Zhu, M. Zhang, *J. Am. Chem. Soc.* **2020**, *142*, 18763-18768.
[34] P. Tinnefeld, J. Hofkens, D.-P. Herten, S. Masuo, T. Vosch, M. Cotlet, S. Habuchi, K. Müllen, F. C. De Schryver, M. Sauer, *ChemPhysChem* **2004**, *5*, 1786-1790.
[35] S. Betzold, S. Herbst, A. A. P. Trichet, J. M. Smith, F. Würthner, S. Höfling, C. P. Dietrich, *ACS Photonics* **2018**, *5*, 90-94.
[36] W. E. Ford, P. V. Kamat, *The Journal of Physical Chemistry* **1987**, *91*, 6373-6380.

[37] Y. Takashima, Y. Fukui, M. Otsubo, N. Hamada, H. Yamaguchi, H. Yamamoto, A. Harada, *Polymer Journal* **2012**, *44*, 278-285.
[38] E. Aksoy, A. Danos, C. Li, A. Monkman, C. Varlıklı, *Turkish Journal of Science and Technology* **2022**, *17*, 11-21.
[39] M. M. Safont-Sempere, P. Osswald, M. Stolte, M. Grüne, M. Renz, M. Kaupp, K. Radacki, H. Braunschweig, F. Würthner, *J. Am. Chem. Soc.* **2011**, *133*, 9580-9591.
[40] C. Kohl, T. Weil, J. Qu, K. Müllen, *Chem. Eur. J.* **2004**, *10*, 5297-5310.
[41] a) R. Singh, S. R. Suranagi, J. Lee, H. Lee, M. Kim, K. Cho, *Scientific Reports* **2018**, *8*, 2849; b) H. Hu, Y. Li, J. Zhang, Z. Peng, L.-k. Ma, J. Xin, J. Huang, T. Ma, K. Jiang, G. Zhang, W. Ma, H. Ade, H. Yan, *Advanced Energy Materials* **2018**, *8*, 1800234; c) J. Zhang, Y. Li, J. Huang, H. Hu, G. Zhang, T. Ma, P. C. Y. Chow, H. Ade, D. Pan, H. Yan, *J. Am. Chem. Soc.* **2017**, *139*, 16092-16095.
[42] A. Lv, S. R. Puniredd, J. Zhang, Z. Li, H. Zhu, W. Jiang, H. Dong, Y. He, L. Jiang, Y. Li, W. Pisula, Q. Meng, W. Hu, Z. Wang, *Advanced Materials* **2012**, *24*, 2626-2630.
[43] M. Marchini, A. Gualandi, L. Mengozzi, P. Franchi, M. Lucarini, P. G. Cozzi, V. Balzani, P. Ceroni, *Phys. Chem. Chem. Phys.* **2018**, *20*, 8071-8076.
[44] a) F. Glaser, C. Kerzig, O. S. Wenger, *Angew. Chem. Int. Ed.* **2020**, *59*, 10266-10284; b) N. A. Romero, D. A. Nicewicz, *Chem. Rev.* **2016**, *116*, 10075-10166.
[45] Y. Gao, H. Xu, S. Zhang, Y. Zhang, C. Tang, W. Fan, *Organic & Biomolecular Chemistry* **2019**, *17*, 7144-7149.
[46] I. Ghosh, *Physical Sciences Reviews* **2019**, *4*.
[47] a) I. Ghosh, T. Ghosh, J. I. Bardagi, B. König, *Science* **2014**, *346*, 725-728; b) L. Zeng, T. Liu, C. He, D. Shi, F. Zhang, C. Duan, *J. Am. Chem. Soc.* **2016**, *138*, 3958-3961; c) H.-X. Gong, Z. Cao, M.-H. Li, S.-H. Liao, M.-J. Lin, *Org. Chem. Front.* **2018**, *5*, 2296-2302.
[48] a) D. Gosztola, M. P. Niemczyk, W. Svec, A. S. Lukas, M. R. Wasielewski, *The Journal of Physical Chemistry A* **2000**, *104*, 6545-6551; b) A. Seegerer, P. Nitschke, R. M. Gschwind, *Angew. Chem. Int. Ed.* **2018**, *57*, 7493-7497; c) C. J. I. V. Zeman, S. Kim, F. Zhang, K. S. Schanze, *J. Am. Chem. Soc.* **2020**, *142*, 2204-2207.
[49] a) T. Chand, L. Khamari, D. Chopra, S. Mukherjee, M. Kapur, *Chem. Eur. J.* **2022**, *28*, e202200723; b) J. van Herrikhuyzen, A. Syamakumari, A. P. H. J. Schenning, E. W. Meijer, *J. Am. Chem. Soc.* **2004**, *126*, 10021-10027; c) N. Chen, J. Lu, D. Wang, C. Zheng, H. Wu, H. Zhang, D. Gao, *Macromolecules* **2018**, *51*, 80-90.
[50] R. K. Dubey, N. Westerveld, E. J. R. Sudhölter, F. C. Grozema, W. F. Jager, *Org. Chem. Front.* **2016**, *3*, 1481-1492.
[51] W. Qiu, S. Chen, X. Sun, Y. Liu, D. Zhu, *Org. Lett.* **2006**, *8*, 867-870.
[52] F. Würthner, V. Stepanenko, Z. Chen, C. R. Saha-Möller, N. Kocher, D. Stalke, *J. Org. Chem.* **2004**, *69*, 7933-7939.
[53] a) Y. Yang, Y. Wang, Y. Xie, T. Xiong, Z. Yuan, Y. Zhang, S. Qian, Y. Xiao, *Chem. Commun.* **2011**, *47*, 10749-10751; b) Z. Yuan, J. Li, Y. Xiao, Z. Li, X. Qian, *J. Org. Chem.* **2010**, *75*, 3007-3016; c) E. E. Beauvilliers, M. R. Topka, P. H. Dinolfo, *RSC Advances* **2014**, *4*, 32866-32875.
[54] H.-Y. Tsai, C.-W. Chang, K.-Y. Chen, *Molecules* **2014**, *19*, 327-341.
[55] L. Fan, Y. Xu, H. Tian, *Tetrahedron Lett.* **2005**, *46*, 4443-4447.
[56] R. K. Dubey, A. Efimov, H. Lemmetyinen, *Chemistry of Materials* **2011**, *23*, 778-788.
[57] Y. Shibano, H. Imahori, C. Adachi, *J. Phys. Chem. C* **2009**, *113*, 15454-15466.
[58] M.-J. Lin, B. Fimmel, K. Radacki, F. Würthner, *Angew. Chem. Int. Ed.* **2011**, *50*, 10847-10850.
[59] N. Zink-Lorre, E. Font-Sanchis, Á. Sastre-Santos, F. Fernández-Lázaro, *Org. Chem. Front.* **2017**, *4*, 2016-2021.
[60] C. Zhao, Y. Zhang, R. Li, X. Li, J. Jiang, *J. Org. Chem.* **2007**, *72*, 2402-2410.
[61] B. A. Jones, M. J. Ahrens, M.-H. Yoon, A. Facchetti, T. J. Marks, M. R. Wasielewski, *Angew. Chem. Int. Ed.* **2004**, *43*, 6363-6366.
[62] Y. Li, L. Tan, Z. Wang, H. Qian, Y. Shi, W. Hu, *Org. Lett.* **2008**, *10*, 529-532.
[63] a) M. Queste, C. Cadiou, B. Pagoaga, L. Giraudet, N. Hoffmann, *New Journal of Chemistry* **2010**, *34*, 2537-2545; b) Q. Yan, D. Zhao, *Org. Lett.* **2009**, *11*, 3426-3429.
[64] G. Goretzki, E. S. Davies, S. P. Argent, J. E. Warren, A. J. Blake, N. R. Champness, *Inorganic Chemistry* **2009**, *48*, 10264-10274.

[65] a) G. Fang, X. Bi, *Chemical Society Reviews* **2015**, *44*, 8124-8173; b) S.-L. Shi, S. L. Buchwald, *Nature chemistry* **2015**, *7*, 38-44; c) J. E. Hein, V. V. Fokin, *Chemical Society Reviews* **2010**, *39*, 1302-1315.
[66] C. D. Schmidt, N. Lang, N. Jux, A. Hirsch, *Chem. Eur. J.* **2011**, *17*, 5289-5299.
[67] a) Z. Xie, V. Stepanenko, K. Radacki, F. Würthner, *Chemistry–A European Journal* **2012**, *18*, 7060-7070; b) Y. Huang, J. Wang, H. Zhai, L. Zhu, Z. Wei, *Soft Matter* **2014**, *10*, 7920-7924; c) G. Echue, I. Hamley, G. C. Lloyd Jones, C. F. Faul, *Langmuir* **2016**, *32*, 9023-9032.
[68] a) A. Li, X. Zhang, S. Wang, K. Wei, P. Du, *Org. Lett.* **2023**, *25*, 1183-1187; b) M. Weh, A. A. Kroeger, K. Shoyama, M. Grüne, A. Karton, F. Würthner, *Angew. Chem. Int. Ed.* **2023**, *62*, e202301301.
[69] a) R. J. Phipps, G. L. Hamilton, F. D. Toste, *Nature chemistry* **2012**, *4*, 603-614; b) Y. Zhang, J. Deng, K. Pan, *Macromolecules* **2018**, *51*, 8878-8886.
[70] S. G. Davies, A. M. Fletcher, P. M. Roberts, J. E. Thomson, A. Yeung, *Tetrahedron* **2019**, *75*, 130694.
[71] Z.-X. Wang, Y. Tu, M. Frohn, J.-R. Zhang, Y. Shi, *J. Am. Chem. Soc.* **1997**, *119*, 11224-11235.
[72] a) E. Francotte, W. Lindner, *Chirality in Drug Research*, John Wiley & Sons, Weinheim, Germany, **2007**; b) V. Andrushko, N. V. Andrushko, *Stereoselective synthesis of drugs and natural products*, John Wiley & Sons, Inc., Hoboken, NJ, **2013**; c) T. T. Talele, *J. Med. Chem.* **2020**, *63*, 13291-13315.
[73] M. T. Miller, *Trans Am Ophthalmol Soc* **1991**, *89*, 623-674.
[74] a) T. Hirao, S. Kishino, T. Haino, *Chem. Commun.* **2023**, *59*, 2421-2424; b) M. Quan, X. Y. Pang, W. Jiang, *Angew Chem. Int. Ed. Engl.* **2022**, *61*, e202201258; c) L. Pu, *Acc. Chem. Res.* **2012**, *45*, 150-163; d) Z. Chen, Q. Wang, X. Wu, Z. Li, Y. B. Jiang, *Chem. Soc. Rev.* **2015**, *44*, 4249-4263.
[75] a) M. C. Carreno, A. Enriquez, S. Garcia-Cerrada, M. J. Sanz-Cuesta, A. Urbano, F. Maseras, A. Nonell-Canals, *Chem. Eur. J.* **2008**, *14*, 603-620; b) J. Wade, F. Salerno, R. C. Kilbride, D. K. Kim, J. A. Schmidt, J. A. Smith, L. M. LeBlanc, E. H. Wolpert, A. A. Adeleke, E. R. Johnson, J. Nelson, T. Mori, K. E. Jelfs, S. Heutz, M. J. Fuchter, *Nat. Chem.* **2022**, *14*, 1383-1389; c) C. Liu, J. C. Yang, J. W. Y. Lam, H. T. Feng, B. Z. Tang, *Chem. Sci.* **2022**, *13*, 611-632; d) J. R. Brandt, F. Salerno, M. J. Fuchter, *Nat. Rev. Chem.* **2017**, *1*, 0045; e) T. Ikai, K. Oki, S. Yamakawa, E. Yashima, *Angew Chem. Int. Ed. Engl.* **2023**, *62*, e202301836; f) J. Crassous, M. J. Fuchter, D. E. Freedman, N. A. Kotov, J. Moon, M. C. Beard, S. Feldmann, *Nat. Rev. Mater.* **2023**, *8*, 365-371.
[76] L. Pu, *Acc. Chem. Res.* **2012**, *45*, 150-163.
[77] a) R. J. Phipps, G. L. Hamilton, F. D. Toste, *Nat. Chem.* **2012**, *4*, 603-614; b) J. M. Ovian, P. Vojackova, E. N. Jacobsen, *Nature* **2023**, *616*, 84-89; c) S. Das, C. Zhu, D. Demirbas, E. Bill, C. K. De, B. List, *Science* **2023**, *379*, 494-499.
[78] J. L. García Ruano, J. Alemán, I. Alonso, A. Parra, V. Marcos, J. Aguirre, *Chem. Eur. J.* **2007**, *13*, 6179-6195.
[79] J. Karolin, L. B. a. Johansson, U. Ring, H. Langhals, *Spectrochim. Acta, Part A* **1996**, *52A*, 747-753.
[80] P. Osswald, F. Wuerthner, *J. Am. Chem. Soc.* **2007**, *129*, 14319-14326.
[81] M.-J. Lin, M. Schulze, K. Radacki, F. Wuerthner, *Chem. Commun.* **2013**, *49*, 9107-9109.
[82] Y. El-Azizi, J. E. Zakarian, L. Bouillerand, A. R. Schmitzer, S. K. Collins, *Advanced Synthesis & Catalysis* **2008**, *350*, 2219-2225.
[83] X. Shang, I. Song, H. Ohtsu, Y. H. Lee, T. Zhao, T. Kojima, J. H. Jung, M. Kawano, J. H. Oh, *Advanced Materials* **2017**, *29*, 1605828.
[84] P. Osswald, M. Reichert, G. Bringmann, F. Würthner, *J. Org. Chem.* **2007**, *72*, 3403-3411.
[85] a) E. E. Neuteboom, S. C. J. Meskers, P. A. van Hal, J. K. J. van Duren, E. W. Meijer, R. A. J. Janssen, H. Dupin, G. Pourtois, J. Cornil, R. Lazzaroni, J.-L. Brédas, D. Beljonne, *Journal of the American Chemical Society* **2003**, *125*, 8625-8638; b) E. E. Neuteboom, P. A. van Hal, R. A. J. Janssen, *Chem. Eur. J.* **2004**, *10*, 3907-3918.
[86] W. Wang, A. D. Shaller, A. D. Q. Li, *Journal of the American Chemical Society* **2008**, *130*, 8271 - 8279.
[87] P. Osswald, M. Reichert, G. Bringmann, F. Wuerthner, *J. Org. Chem.* **2007**, *72*, 3403-3411.
[88] Z. Xie, F. Wuerthner, *Org. Lett.* **2010**, *12*, 3204-3207.

[89] M. M. Safont-Sempere, V. Stepanenko, M. Lehmann, F. Wuerthner, *J. Mater. Chem.* **2011**, *21*, 7201-7209.
[90] M. M. Safont-Sempere, P. Osswald, K. Radacki, F. Wuerthner, *Chem. Eur. J.* **2010**, *16*, 7380-7384, S7380/7381-S7380/7323.
[91] M. M. Safont-Sempere, P. Osswald, M. Stolte, M. Gruene, M. Renz, M. Kaupp, K. Radacki, H. Braunschweig, F. Wuerthner, *J. Am. Chem. Soc.* **2011**, *133*, 9580-9591.
[92] M. Ball, B. Fowler, P. Li, L. A. Joyce, F. Li, T. Liu, D. Paley, Y. Zhong, H. Li, S. Xiao, F. Ng, M. L. Steigerwald, C. Nuckolls, *J. Am. Chem. Soc.* **2015**, *137*, 9982-9987.
[93] M. Xue, Y. Yang, X. Chi, X. Yan, F. Huang, *Chem. Rev.* **2015**, *115*, 7398-7501.
[94] J. F. Stoddart, *Chemical Society Reviews* **2009**, *38*, 1802-1820.
[95] X. Ma, Q. Wang, D. Qu, Y. Xu, F. Ji, H. Tian, *Advanced Functional Materials* **2007**, *17*, 829-837.
[96] A. Rescifina, C. Zagni, D. Iannazzo, P. Merino, *Current Organic Chemistry* **2009**, *13*, 448-481.
[97] W. Yang, Y. Li, H. Liu, L. Chi, Y. Li, *Small* **2012**, *8*, 504-516.
[98] C. Saiz, A. Slawin, A. Carmichael, D. Haddleton, A. Brouwer, W. Buma, G. Wurpel, S. León, F. Zerbetto, **2005**.
[99] a) J. J. Gassensmith, S. Matthys, J. J. Lee, A. Wojcik, P. V. Kamat, B. D. Smith, *Chemistry–A European Journal* **2010**, *16*, 2916-2921; b) T. D. Nguyen, H.-R. Tseng, P. C. Celestre, A. H. Flood, Y. Liu, J. F. Stoddart, J. I. Zink, *Proceedings of the National Academy of Sciences* **2005**, *102*, 10029-10034.
[100] J. Baggerman, D. C. Jagesar, R. A. Vallée, J. Hofkens, F. C. De Schryver, F. Schelhase, F. Vögtle, A. M. Brouwer, *Chemistry–A European Journal* **2007**, *13*, 1291-1299.
[101] E. Jamieson, F. Modicom, S. Goldup, *Chemical Society Reviews* **2018**, *47*, 5266-5311.
[102] G. Bottari, D. A. Leigh, E. M. Pérez, *J. Am. Chem. Soc.* **2003**, *125*, 13360-13361.
[103] A. H. G. David, R. Casares, J. M. Cuerva, A. G. Campaña, V. Blanco, *J. Am. Chem. Soc.* **2019**, *141*, 18064-18074.
[104] a) M. Weh, J. Ruhe, B. Herbert, A. M. Krause, F. Würthner, *Angew Chem. Int. Ed. Engl.* **2021**, *60*, 15323-15327; b) M. M. Safont-Sempere, P. Osswald, K. Radacki, F. Würthner, *Chem. Eur. J.* **2010**, *16*, 7380-7384; c) M. M. Safont-Sempere, P. Osswald, M. Stolte, M. Grüne, M. Renz, M. Kaupp, K. Radacki, H. Braunschweig, F. Würthner, *J. Am. Chem. Soc.* **2011**, *133*, 9580-9591; d) A. Li, X. Zhang, S. Wang, K. Wei, P. Du, *Org. Lett.* **2023**, *25*, 1183-1187.
[105] M. C. Heffern, L. M. Matosziuk, T. J. Meade, *Chem. Rev.* **2014**, *114*, 4496-4539.
[106] H. Kang, W. Jiang, Z. Wang, *Dyes Pigm.* **2013**, *97*, 244-249.
[107] A. H. Endres, M. Schaffroth, F. Paulus, H. Reiss, H. Wadepohl, F. Rominger, R. Kramer, U. H. Bunz, *J. Am. Chem. Soc.* **2016**, *138*, 1792-1795.
[108] C. Janiak, *J. Chem. Soc., Dalton trans.* **2000**, 3885-3896.
[109] C. A. Hunter, J. K. M. Sanders, *J. Am. Chem. Soc.* **1990**, *112*, 5525-5534.
[110] a) T. A. Barendt, L. Ferreira, I. Marques, V. Felix, P. D. Beer, *J. Am. Chem. Soc.* **2017**, *139*, 9026-9037; b) P. Spenst, A. Sieblist, F. Würthner, *Chem. Eur. J.* **2017**, *23*, 1667-1675; c) P. Spenst, F. Würthner, *Angew Chem. Int. Ed. Engl.* **2015**, *54*, 10165-10168; d) Z. Wang, X. Gou, Q. Shi, K. Liu, X. Chang, G. Wang, W. Xu, S. Lin, T. Liu, Y. Fang, *Angew Chem. Int. Ed. Engl.* **2022**, *61*, e202207619.
[111] K. E. Brown, W. A. Salamant, L. E. Shoer, R. M. Young, M. R. Wasielewski, *The Journal of Physical Chemistry Letters* **2014**, *5*, 2588-2593.
[112] P. Pracht, F. Bohle, S. Grimme, *Phys. Chem. Chem. Phys.* **2020**, *22*, 7169-7192.
[113] C. Bannwarth, S. Ehlert, S. Grimme, *J. Chem. Theory Comput.* **2019**, *15*, 1652-1671.
[114] K. Jackowska, M. Skompska, E. Przyłuska, *Journal of Electroanalytical Chemistry* **1996**, *418*, 35-39.
[115] G. Zhao, X. Yan, Y. Dai, J. Xiong, Q. Zhao, X. Wang, H. Yu, J. Gao, N. Zhang, M. Hu, J. Yang, *Small* **2024**, *20*, 2306071.
[116] N. Rehmat, I. V. Kurganskii, Z. Mahmood, Q. L. Guan, J. Zhao, Y. H. Xing, G. G. Gurzadyan, M. V. Fedin, *Chem. Eur. J.* **2021**, *27*, 5521-5535.
[117] E. I. Rogers, D. S. Silvester, D. L. Poole, L. Aldous, C. Hardacre, R. G. Compton, *J. Phys. Chem. C* **2008**, *112*, 2729-2735.
[118] P. R. Somani, S. Radhakrishnan, *Materials chemistry and physics* **2003**, *77*, 117-133.
[119] a) F. S. Menke, B. Wicher, V. Maurizot, I. Huc, *Angew Chem. Int. Ed. Engl.* **2023**, *62*, e202217325; b) M. Liu, L. Zhang, T. Wang, *Chem. Rev.* **2015**, *115*, 7304-7397.
[120] R. L. Furlan, S. Otto, J. K. Sanders, *Proc. Natl. Acad. Sci. U.S.A.* **2002**, *99*, 4801-4804.

[121] a) F. S. Menke, B. Wicher, V. Maurizot, I. Huc, *Angew. Chem. Int. Ed.* **2023**, *62*, e202217325; b) Y. Zuo, X. Liu, E. Fu, S. Zhang, *Angew Chem. Int. Ed. Engl.* **2023**, *62*, e202217225.
[122] *Macrocyclic and Supramolecular Chemistry: How Izatt–Christensen Award Winners Shaped the Field*, John Wiley & Sons, **2016**.
[123] a) V. Marti-Centelles, M. D. Pandey, M. I. Burguete, S. V. Luis, *Chem. Rev.* **2015**, *115*, 8736-8834; b) M. A. Casadei, C. Galli, L. Mandolini, *J. Am. Chem. Soc.* **2002**, *106*, 1051-1056.
[124] P. Osswald, F. Würthner, *Chem. Eur. J.* **2007**, *13*, 7395-7409.
[125] T. A. Barendt, W. K. Myers, S. P. Cornes, M. A. Lebedeva, K. Porfyrakis, I. Marques, V. Félix, P. D. Beer, *J. Am. Chem. Soc.* **2020**, *142*, 349-364.
[126] a) P. Osswald, F. Würthner, *J. Am. Chem. Soc.* **2007**, *129*, 14319-14326; b) S. R. LaPlante, P. J. Edwards, L. D. Fader, A. Jakalian, O. Hucke, *ChemMedChem* **2011**, *6*, 505-513; c) M. Mancinelli, G. Bencivenni, D. Pecorari, A. Mazzanti, *Eur. J. Org. Chem.* **2020**, *2020*, 4070-4086; d) J. P. Heeb, J. Clayden, M. D. Smith, R. J. Armstrong, *Nat. Protoc.* **2023**, *18*, 2745-2771.
[127] K. Du, P. Demay-Drouhard, K. Samanta, S. Li, T. U. Thikekar, H. Wang, M. Guo, B. van Lagen, H. Zuilhof, A. C. H. Sue, *J. Org. Chem.* **2020**, *85*, 11368-11374.
[128] N. L. Strutt, D. Fairen-Jimenez, J. Iehl, M. B. Lalonde, R. Q. Snurr, O. K. Farha, J. T. Hupp, J. F. Stoddart, *J. Am. Chem. Soc.* **2012**, *134*, 17436-17439.
[129] T. Ogoshi, K. Kitajima, T. Aoki, S. Fujinami, T.-a. Yamagishi, Y. Nakamoto, *J. Org. Chem.* **2010**, *75*, 3268-3273.
[130] L. Meca, D. Reha, Z. Havlas, *J. Org. Chem.* **2003**, *68*, 5677-5680.
[131] a) S. E. Penty, M. A. Zwijnenburg, G. R. F. Orton, P. Stachelek, R. Pal, Y. Xie, S. L. Griffin, T. A. Barendt, *J. Am. Chem. Soc.* **2022**, *144*, 12290-12298; b) M. Ball, B. Fowler, P. Li, L. A. Joyce, F. Li, T. Liu, D. Paley, Y. Zhong, H. Li, S. Xiao, F. Ng, M. L. Steigerwald, C. Nuckolls, *J. Am. Chem. Soc.* **2015**, *137*, 9982-9987; c) G. Ouyang, J. Ruhe, Y. Zhang, M. J. Lin, M. Liu, F. Würthner, *Angew Chem. Int. Ed. Engl.* **2022**, *61*, e202206706; d) I. Solymosi, S. Krishna, E. Nuin, H. Maid, B. Scholz, D. M. Guldi, M. E. Perez-Ojeda, A. Hirsch, *Chem. Sci.* **2021**, *12*, 15491-15502.
[132] A. Yeung, M. A. Zwijnenburg, G. R. F. Orton, J. H. Robertson, T. A. Barendt, *Chemical Science* **2024**, *15*, 5516-5524.
[133] a) J. I. Seeman, *Chem. Rev.* **2002**, *83*, 83-134; b) J. I. Seeman, *J. Chem. Educ.* **1986**, *63*, 42.
[134] a) P. Beak, A. Basu, D. J. Gallagher, Y. S. Park, S. Thayumanavan, *Acc. Chem. Res.* **1996**, *29*, 552-560; b) G. Fodor, R. V. Chastain, D. Frehel, M. J. Copper, N. Mandava, E. L. Gooden, *J. Am. Chem. Soc.* **2002**, *93*, 403-413.
[135] A. K. Yudin, *Chem. Sci.* **2015**, *6*, 30-49.
[136] a) S. Amano, M. Esposito, E. Kreidt, D. A. Leigh, E. Penocchio, B. M. W. Roberts, *J. Am. Chem. Soc.* **2022**, *144*, 20153-20164; b) L. Binks, S. Borsley, T. R. Gingrich, D. A. Leigh, E. Penocchio, B. M. W. Roberts, *Chem* **2023**, *9*, 2902-2917; c) M. Alvarez-Perez, S. M. Goldup, D. A. Leigh, A. M. Slawin, *J. Am. Chem. Soc.* **2008**, *130*, 1836-1838.
[137] D. C. Patel, R. M. Woods, Z. S. Breitbach, A. Berthod, D. W. Armstrong, *Tetrahedron: Asymmetry* **2017**, *28*, 1557-1561.
[138] S. J. Howell, P. R. Ashton, N. Spencer, D. Philp, *Org. Lett.* **2001**, *3*, 353-356.
[139] A. Mateo Alonso, R. Horcajada, H. J. Groombridge, R. Chudasama Nee Mandalia, M. Motevalli, J. H. Utley, P. B. Wyatt, *Org. Biomol. Chem.* **2005**, *3*, 2832-2841.
[140] S. Anderson, H. L. Anderson, J. K. M. Sanders, *Acc. Chem. Res.* **1993**, *26*, 469-475.
[141] a) K. Uehara, H. Kano, K. Matsuo, H. Hayashi, M. Fujiki, H. Yamada, N. Aratani, *Chemphotochem* **2021**, *5*, 974-978; b) L. A. de Ceuninck van Capelle, J. M. Macdonald, C. J. T. Hyland, *Org. Biomol. Chem.* **2021**, *19*, 7098-7115.
[142] a) S. M. Wang, Y. F. Wang, L. Huang, L. S. Zheng, H. Nian, Y. T. Zheng, H. Yao, W. Jiang, X. Wang, L. P. Yang, *Nat. Commun.* **2023**, *14*, 5645; b) G. A. Hembury, V. V. Borovkov, Y. Inoue, *Chem. Rev.* **2008**, *108*, 1-73.
[143] a) P. Waelès, C. Clavel, K. Fournel-Marotte, F. Coutrot, *Chemical science* **2015**, *6*, 4828-4836; b) B. Riss-Yaw, J. Morin, C. Clavel, F. Coutrot, *Molecules* **2017**, *22*, 2017.
[144] F. Coutrot, *ChemistryOpen* **2015**, *4*, 556-576.
[145] H. R. Wessels, H. W. Gibson, *Tetrahedron* **2016**, *72*, 396-399.
[146] H. Kawai, A. Kusuda, S. Mizuta, S. Nakamura, Y. Funahashi, H. Masuda, N. Shibata, *Journal of Fluorine Chemistry* **2009**, *130*, 762-765.

[147] M. H. Ngai, P. Y. Yang, K. Liu, Y. Shen, M. R. Wenk, S. Q. Yao, M. J. Lear, *Chem. Commun.* **2010**, *46*, 8335-8337.
[148] T. R. Chan, R. Hilgraf, K. B. Sharpless, V. V. Fokin, *Org. Lett.* **2004**, *6*, 2853-2855.
[149] P. S. Ghosh, A. D. Hamilton, *Chem. Eur. J.* **2012**, *18*, 2361-2365.
[150] M. Bagui, T. Dutta, H. Zhong, S. Li, S. Chakraborty, A. Keightley, Z. Peng, *Tetrahedron* **2012**, *68*, 2806-2818.
[151] G. Zhang, S. Jiang, Y. Gao, F. Sun, *Journal of Materials Science* **2017**, *52*, 9931-9945.
[152] G. Zhang, L. Fang, L. Zhu, D. Sun, P. G. Wang, *Bioorganic & Medicinal Chemistry* **2006**, *14*, 426-434.
[153] C.-S. Kwan, R. Zhao, M. A. Van Hove, Z. Cai, K. C.-F. Leung, *Nat. Commun.* **2018**, *9*, 497.
[154] P. Mukherjee, L. J. Leman, J. H. Griffin, M. R. Ghadiri, *J. Am. Chem. Soc.* **2018**, *140*, 15516-15524.
[155] R. Sarkar, E. B. Gowd, S. Ramakrishnan, *Polymer Chemistry* **2020**, *11*, 4143-4154.
[156] Q. Lin, Y. Q. Fan, P. P. Mao, L. Liu, J. Liu, Y. M. Zhang, H. Yao, T. B. Wei, *Chem. Eur. J.* **2018**, *24*, 777-783.
[157] A. Qin, C. K. W. Jim, W. Lu, J. W. Y. Lam, M. Häussler, Y. Dong, H. H. Y. Sung, I. D. Williams, G. K. L. Wong, B. Z. Tang, *Macromolecules* **2007**, *40*, 2308-2317.
[158] Q. Ma, H. Yang, J. Hao, Y. Tan, *Journal of Dispersion Science and Technology* **2012**, *33*, 639-646.
[159] C. Gao, S. Silvi, X. Ma, H. Tian, A. Credi, M. Venturi, *Chem. Eur. J.* **2012**, *18*, 16911-16921.
[160] Y. Zhou, D. Zhang, L. Zhu, Z. Shuai, D. Zhu, *J. Org. Chem.* **2006**, *71*, 2123-2130.
[161] L. Ochmann, M. Fuhrmann, F. J. Gössl, A. Makaveev, P. R. Schreiner, *Org. Lett.* **2022**, *24*, 6968-6972.
[162] A. Grün, É. Kőszegi, I. Bitter, *Tetrahedron* **2004**, *60*, 5041-5048.
[163] G. M. Sheldrick, *Acta Crystallogr. A* **2015**, *71*, 3-8.
[164] O. V. Dolomanov, L. J. Bourhis, R. J. Gildea, J. A. K. Howard, H. Puschmann, *J. Appl. Crystallogr.* **2009**, *42*, 339-341.
[165] J. G. Brandenburg, C. Bannwarth, A. Hansen, S. Grimme, *J. Chem. Phys.* **2018**, *148*, 064104.
[166] A. Klamt, G. Schüürmann, *J. Chem. Soc., Perkin Trans. 2* **1993**, 799-805.
[167] J. D. Chai, M. Head-Gordon, *J. Chem. Phys.* **2008**, *128*, 084106.
[168] F. Weigend, R. Ahlrichs, *Phys. Chem. Chem. Phys.* **2005**, *7*, 3297-3305.
[169] a) F. Furche, R. Ahlrichs, C. Hättig, W. Klopper, M. Sierka, F. Weigend, *Wiley Interdiscip. Rev. Comput. Mol. Sci.* **2013**, *4*, 91-100; b) S. G. Balasubramani, G. P. Chen, S. Coriani, M. Diedenhofen, M. S. Frank, Y. J. Franzke, F. Furche, R. Grotjahn, M. E. Harding, C. Hattig, A. Hellweg, B. Helmich-Paris, C. Holzer, U. Huniar, M. Kaupp, A. Marefat Khah, S. Karbalaei Khani, T. Muller, F. Mack, B. D. Nguyen, S. M. Parker, E. Perlt, D. Rappoport, K. Reiter, S. Roy, M. Ruckert, G. Schmitz, M. Sierka, E. Tapavicza, D. P. Tew, C. van Wullen, V. K. Voora, F. Weigend, A. Wodynski, J. M. Yu, *J. Chem. Phys.* **2020**, *152*, 184107.